



**THESE DE DOCTORAT DE L'UNIVERSITE PIERRE ET
MARIE CURIE**

Spécialité :
Astrophysique des hautes énergies
Ecole Doctorale : Particules, Noyaux et Cosmos

Presentée par
Boutayeb BOUHOU

Pour obtenir le grade de
DOCTEUR de L'UNIVERSITÉ PIERRE ET MARIE CURIE

Sujet de thèse:

**Recherche conjointe d'ondes gravitationnelles et de
neutrinos cosmiques de haute énergie avec les détecteurs
VIRGO-LIGO et ANTARES**

soutenue le 19 décembre 2012

devant le jury composé de:

| | |
|------------------------|-----------------------|
| M. E. Chassande-Mottin | Co-directeur de thèse |
| M. A. Kouchner | Directeur de thèse |
| Mme. A. Margiotta | Rapporteur |
| Mme. F. Marion | Rapporteur |
| M. A. Meregaglia | Examineur |
| M. J.P. Tavernet | Président du jury |

CONTENTS

| | |
|--|----------|
| Introduction | 1 |
| 1 Multimessenger astronomy | 7 |
| 1.1 High-energy neutrino astronomy | 7 |
| 1.1.1 First steps | 7 |
| 1.1.2 Cosmic rays and neutrinos | 8 |
| 1.1.3 Neutrinos as cosmic probes | 15 |
| 1.1.4 Astrophysical sources of high-energy neutrinos | 17 |
| 1.2 Gravitational waves | 27 |
| 1.2.1 Basics of gravitational-wave theory | 27 |
| 1.2.2 Phenomenology of gravitational waves | 29 |
| 1.2.3 Astrophysical sources of gravitational waves | 32 |
| 1.3 Joint sources of gravitational waves and high-energy neutrinos | 35 |
| 1.3.1 Core-collapse supernovae with mildly relativistic jet | 36 |
| 1.3.2 Other sources | 37 |
| 1.3.3 Time delay between gravitational wave and high-energy neutrino emissions | 37 |

CONTENTS

| | | |
|----------|--|-----------|
| 2 | Neutrino telescopes | 43 |
| 2.1 | Summary | 43 |
| 2.2 | Neutrino telescopes | 43 |
| 2.2.1 | General principles | 43 |
| 2.2.2 | Neutrino interactions | 44 |
| 2.2.3 | Propagation of the neutrinos in the Earth | 46 |
| 2.2.4 | Propagation of the muons in water and rocks | 47 |
| 2.2.5 | Detection principle | 49 |
| 2.2.6 | Overview of the past and current detectors | 51 |
| 2.3 | The ANTARES neutrino telescope | 54 |
| 2.3.1 | Detector design | 55 |
| 2.3.2 | ANTARES coordinates | 56 |
| 2.3.3 | Background noise at the ANTARES site | 57 |
| 2.3.4 | Physical background: atmospheric muons and neutrinos | 58 |
| 2.3.5 | Trigger and DAQ systems | 60 |
| 2.3.6 | Detector calibration and electronics | 61 |
| 2.4 | Data quality | 63 |
| 2.5 | Simulation chain | 64 |
| 2.5.1 | Simulation of high-energy neutrinos | 64 |
| 2.5.2 | Simulation of atmospheric muons | 66 |
| 2.5.3 | Simulation of the Cherenkov light | 68 |
| 2.5.4 | Generation of the optical background | 69 |
| 2.5.5 | MC run by run approach | 69 |
| 2.6 | Track reconstruction algorithm | 69 |
| 2.6.1 | In-situ reconstruction algorithm | 70 |
| 2.6.2 | Off-line reconstruction algorithm | 73 |

| | | |
|--------------|---|----------------|
| 3 | Gravitational-wave interferometric detectors | 81 |
| 3.1 | Summary | 81 |
| 3.2 | Detection principle | 81 |
| 3.3 | The Virgo detector | 82 |
| 3.4 | Response of a gravitational wave interferometer | 83 |
| 3.5 | Astrophysical reach of a gravitational wave detector | 85 |
| 3.6 | Worldwide network of gravitational wave detectors | 88 |
| 3.6.1 | Source positioning | 88 |
| 3.6.2 | Sensitivities reached so far and coordinated data takings | 89 |
| 3.7 | Analysis of gravitational wave data | 89 |
| 3.7.1 | Wavelets and time-frequency analysis | 91 |
| 3.7.2 | Multi-detector analysis | 92 |
| 3.7.3 | Sensitivity estimate | 94 |
| 3.7.4 | Data analysis methods to search for gravitational wave bursts | 95 |
| 4 | GW+HEN analysis of 5L-S5/VSR1 | 101 |
| 4.1 | Summary | 101 |
| 4.2 | High energy neutrino triggered search procedure | 101 |
| 4.3 | Selection of High Energy Neutrino candidates | 103 |
| 4.3.1 | The ANTARES data and Monte Carlo sample | 103 |
| 4.3.2 | Event selection criteria | 104 |
| 4.4 | High energy neutrino horizon | 112 |
| 4.4.1 | Angular resolution and angular search window | 114 |
| 4.4.2 | List of neutrino candidates | 118 |
| 4.5 | Coincidence with gravitational waves | 120 |
| 4.5.1 | Gravitational wave event analysis | 120 |
| 4.5.2 | GW search optimization | 124 |

CONTENTS

| | | |
|----------|--|------------|
| 4.5.3 | Low-frequency and high-frequency GW analyses | 125 |
| 4.5.4 | Binomial test | 125 |
| 4.6 | GW+HEN joint search results | 126 |
| 4.6.1 | Individual GW searches | 126 |
| 4.6.2 | GW upper limits | 127 |
| 4.7 | Astrophysical implications | 130 |
| 4.7.1 | Upper limits on joint source populations | 130 |
| 4.7.2 | Comparison of limits with existing estimates | 132 |
| 4.8 | Conclusions | 132 |
| 5 | GW+HEN analysis for 12L–S6/VSR2-3 | 135 |
| 5.1 | Summary | 135 |
| 5.2 | Data set | 135 |
| 5.2.1 | Description of ANTARES data | 135 |
| 5.2.2 | Description of Virgo and LIGO data | 136 |
| 5.2.3 | The ANTARES, the Virgo and the LIGO joint data set | 137 |
| 5.3 | Gravitational wave event generation | 137 |
| 5.3.1 | Skymask coherent WaveBurst pipeline | 138 |
| 5.3.2 | Background estimation | 139 |
| 5.3.3 | Sensitivity estimates | 141 |
| 5.4 | Optimization procedures | 142 |
| 5.4.1 | Model rejection factor and Model discovery potential | 143 |
| 5.5 | Description of the joint optimization strategy | 149 |
| 5.5.1 | Definition of the joint figure-of-merit | 150 |
| 5.5.2 | Joint optimization procedure | 151 |
| 5.5.3 | Dealing with non-stationary backgrounds | 151 |
| 5.6 | Application of the joint optimization procedure | 152 |

| | | |
|---|---|----------------|
| 5.6.1 | Efficiency to HEN | 152 |
| 5.6.2 | Approximation of the GW background | 153 |
| 5.6.3 | Results of the optimization | 155 |
| 5.7 | List of neutrino candidates | 158 |
| 5.8 | Procedure for the event post-processing and joint statistical treatment | 162 |
| 5.8.1 | Statistical characterisation of the neutrino candidates | 163 |
| 5.8.2 | Statistical characterisation of the GW reconstructed events | 165 |
| 5.8.3 | Statistical characterisation of the joint candidates | 167 |
| 5.8.4 | Final test statistic | 169 |
| 5.8.5 | Estimation of the horizon of detection | 170 |
| 5.9 | Conclusion | 171 |
| Conclusions | | 175 |
| A Demonstration of the MRF approximation | | 177 |
| B Coherent WaveBurst statistics | | 183 |
| C List of high energy neutrino candidates for the 2009-2010 data | | 185 |

CONTENTS

INTRODUCTION

High-energy multimessenger astronomy has entered an exciting era with the development and operation of new detectors offering unprecedented opportunities to observe the universe through all kind of cosmic radiations. These includes high-energy (\gg GeV) neutrinos (HENs) and gravitational waves (GWs) which are on the waiting list for a first detection (see e.g. [1, 2] for recent reviews on these subjects). Contrary to high-energy photons (which are absorbed through interactions in the source and by intervening photon backgrounds) and charged cosmic rays (which are deflected by ambient magnetic fields), both HENs and GWs can escape from the sources and travel at the speed of light through magnetic fields and matter without being altered. They are therefore expected to provide important information about the processes taking place in the core of the production sites and they could even reveal the existence of sources opaque to hadrons and photons, that would have remained undetected so far.

No GW nor cosmic HEN have been individually detected so far. The detection of coincident GW and HEN events would hence be a landmark observation confirming the astrophysical origin of both signals. Coincident searches are also a way to enhance the sensitivity of each individual channel by correlating the HEN and GW significances, considering that the two types of detectors have uncorrelated backgrounds.

In this thesis, we investigate the potentials of combining GW and HEN observations. We

CONTENTS

implement and conduct two such analyses using the data of the neutrino telescope ANTARES and the GW interferometric detectors Virgo and LIGO.

The multimessenger approach followed here could improve our understanding of the properties of the astrophysical processes at the origin of both emissions. While GW emission requires relativistic bulk motion of massive objects such as gravitational collapse or merger of compact objects, the production of HEN arises from the interaction of hadrons in relativistic jets. A joint detection would then sign the presence of accelerated hadrons in the source and constrain the progenitor nature thanks to the GW detection.

The results presented in this thesis is the outcome of a collaborative work. We stress our main contributions in the following list below.

First joint search for gravitational wave and high-energy neutrinos using 2007 data

Late 2007, LIGO and Virgo completed a first joint data taking period. During this period, ANTARES was operating in an incomplete configuration with five active detection strings. We report in Chapter 4 on the analysis of this first concomitant data set.

To allow for a short analysis cycle and the rapid obtaining of results, available tools and methods were re-used. The selection of the neutrino candidates relied on the developments done for a point-source search. The HEN candidates were followed-up in the GW observations with the pipeline originally conceived for GW search triggered by gamma-ray bursts. The outcome of this first search has been submitted for publication and has led to several public presentations.

Methodological developments and application to the second search using 2009-2010 data

LIGO and Virgo completed a second joint data taking period during 2009-2010. During this

period, ANTARES was operating in its complete configuration with twelve detection strings. We report in Chapter 5 on the analysis of this second concomitant data set.

A new and more sophisticated neutrino reconstruction algorithm could be used to analyze this data set, providing reduced error boxes and allowing for more neutrinos candidates. We also developed a new GW search algorithm based on an already existing pipeline (coherent WaveBurst) used for the all-sky burst search. This pipeline searches for the GW signal within the neutrino uncertainty and enables a search in the case of availability of only two GW detectors. This pipeline is much faster than the one used in the first search and includes more sources by extending the search up to 2kHz.

Optimization of the joint search sensitivity

The selection of neutrino candidates used in the first search was not fully satisfactory since it was performed regardless of the combined sensitivity. This led to a suboptimal search. We proposed and applied a novel optimization procedure for the selection of neutrino candidates taking into account parameters from both GW and HEN data. This optimization, by maximizing the number of detectable sources, is one of the major contributions of this dissertation.

Selection and characterization of the neutrino candidates

We analysed the ANTARES data and selected a set of neutrino candidates using the optimized cuts. This resulted in a list of 1986 neutrino candidates which we fully characterized in terms of pointing precision and background compatibility. The GW data associated to these neutrino candidates are currently being analyzed.

This thesis is divided into five chapters, structure that reflects the above mentioned contributions. Chapter 1 introduces the main physical concepts associated with GW and HEN along with a description of their joint sources. In Chapters 2 and 3, we give an overview of the experiments and review the data analysis tools. The aim of these three chapters is to bring the

CONTENTS

reader to the forefront present-day research, theoretical and experimental, in the field of both GW and HEN physics. Finally, in Chapters 4 and 5 we give a detailed presentation of the first and second searches respectively.

REFERENCES

- [1] J. K. BECKER, Phys. Rept., 458, 173-246 (2008). [1](#)
- [2] K. RILES, To appear in Progress in Particle and Nuclear Physics (2012). [1](#)

REFERENCES

CHAPTER 1

MULTIMESSENGER ASTRONOMY

1.1 High-energy neutrino astronomy

1.1.1 First steps

Neutrinos are among the most intriguing known elementary particles. Their story started on December 4, 1930, when Wolfgang Pauli postulated the existence of an elusive particle in order to explain the missing amount of energy (and momentum) observed in certain nuclear reactions such as β decays. In mid-1930s papers [1], Enrico Fermi took over Pauli and developed a theory incorporating a neutrino to explain the phenomenology of beta decays. This theory became later the basis of weak interaction physics, but it was only in 1956 that Cowan and Reines directly observed the first neutrinos [2]. Their experiment aimed at detecting the interaction of anti-neutrinos, initially produced in a nuclear reactor, with target protons, according to:

$$\bar{\nu}_e + p \longrightarrow n + e^+ \tag{1.1}$$

This led to the discovery of electron neutrinos (ν_e), more than 25 years after Pauli's proposal. It took even longer to discover the muon neutrinos (ν_μ), which are of most interest in the scope of this dissertation. This second step was achieved in 1962 in Brookhaven by Schwartz and his collaborators [3]. It was known at that time that pions π and kaons K produced in atmospheric showers could decay into a muon μ and a neutrino, and that this neutrino could differ from the electron neutrino. The idea was thus to study the interactions of a neutrino beam created by the disintegrations of pions produced via the interactions of 15 GeV protons on a Beryllium target. Only the neutrinos could pass through the 13 m thick steel shield placed after the target. The interaction of the produced neutrinos could then be studied with a spark chamber. Muons could then be identified in the product of the interactions but no electrons. This was the signature of a new species of neutrino: the muon neutrino.

The existence of a third species of neutrino was anticipated in 1975 after the discovery of tau (τ) leptons in Stanford [4]. But 25 more years were needed to directly observe these ν_τ neutrinos. This was done by the DONUT collaboration [5]. The used neutrino beam was obtained by the interaction of 800 GeV protons onto a Tungsten target, producing charmed mesons, which in turn decayed into ν_τ neutrinos. The identification of tau leptons in the subsequent neutrino interactions was obtained with the scanning of nuclear emulsions, looking for the specific signature of tau decays.

In parallel to the efforts made towards the direct detection of neutrinos produced on Earth, a first step towards a possible neutrino astronomy was made in the 60's with the detection of MeV neutrinos originating from the Sun [6]. The first observation, by the Homestake experiment, was followed by several others using different complementary techniques which enabled to confirm the solar origin of the observed events. At the same time, these observations gave rise to the famous "solar neutrino anomaly", which is now explained by the theory of neutrino oscillations. This extends beyond the scope of the present dissertation, but an overview of the solar neutrino history can be found in [7]. In the same energy range to that of solar neutrinos, or slightly above, the detection on February 23, 1987, of 25 events arriving within 12 seconds from the Supernova 1987A, was another landmark for neutrino astronomy [8].

Both observations have encouraged the development of large neutrino telescopes as we will see in chapter 2 for the detection of the astrophysical neutrinos, and were rewarded by the Nobel Prize in Physics in 2002. But the extremely low cross section of weak interactions (of order $6 \times 10^{-44} \text{cm}^2$ for an MeV energy experiment) and the poor angular resolution at nuclear energies represent major obstacles in extending stellar neutrino astronomy much beyond targets like the Sun and a few nearby supernovae. Without denying the important role of the various effects due to neutrino itself, the primary goal of present (experimental and theoretical) investigations remains the astrophysical sources of neutrinos. At present, their detection is currently being challenged by large neutrino telescopes with best sensitivity in the TeV-PeV range.

Keeping these considerations in mind, we begin this chapter with the puzzling question of the origin of the observed cosmic rays (section 1.1.2). We then focus on the possible sources of high-energy neutrinos (HEN).

1.1.2 Cosmic rays and neutrinos

One of the main motivations for a neutrino astronomy is to better understand the physics of the observed cosmic rays (CR). In particular, there is a hope that the observation of cosmic neutrinos could unveil the origin of the high-energy cosmic rays observed on Earth. In this section, we briefly describe the current knowledge about cosmic rays. We also describe how

1.1.1 High-energy neutrino astronomy

neutrinos could be produced as by-product of the interactions of CR, in the specific cases of atmospheric and cosmogenic neutrinos. The connection in the production mechanism between cosmic rays and astrophysical neutrinos is described in more details in section 1.1.3.

Cosmic rays

Cosmic rays are nuclei and elementary particles originating in the cosmos and reaching the Earth's atmosphere at a rough rate of 10^4 per square meter and per second. Where penetrating the atmosphere, these CR collides the N and O nuclei and produce showers of secondary particles (referred to as atmospheric particles), which can be detected at ground level and even underground. The story of CR began in 1912 when the Austrian physicist Victor Francis Hess published results concluding that there was radiation penetrating the atmosphere from outer space. Later in 1925, Robert Millikan confirmed these observations and termed them "cosmic rays". The relative abundances of the different nuclei is shown in Figure 1.2 while the overall

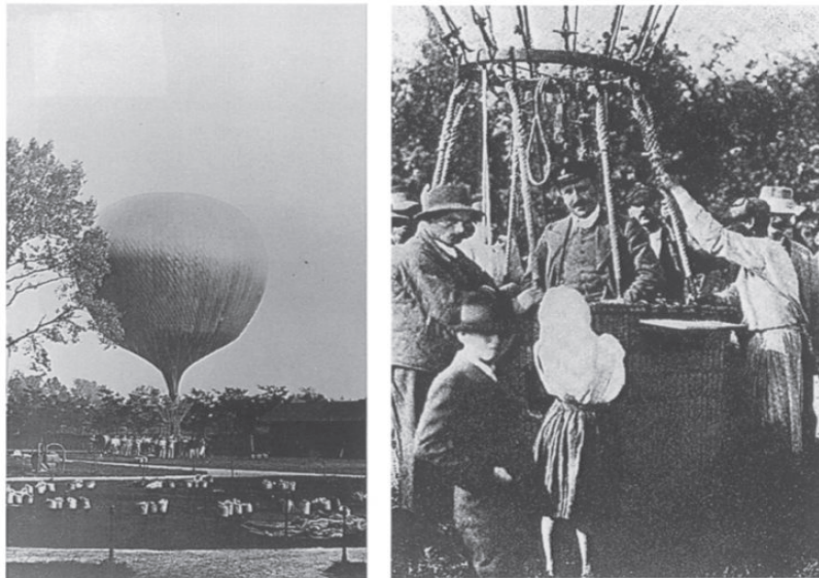


Figure 1.1 – In 1912 (1913), Hess (Klhorster) started his balloon experiments in which he measured the ionisation of the atmosphere with increasing altitude. Left: Preparation of one of his flights. Right: Hess team after one of the successful balloon flights, Especially the flight of August 7, 1912 when V. Hess reached an altitude of 5 km.

spectrum can be seen in Figure 1.3 [9]. The spectrum of cosmic rays varies slightly with the nucleon species, but at the higher energies the chemical composition shows an enrichment with heavier nuclei from the Iron group, as shown in Figure 1.2. Cosmic rays are divided into two classes:

- Primary cosmic rays: are those particles accelerated at astrophysical sources. This in-

CHAPTER 1. MULTIMESSENGER ASTRONOMY

cludes electrons, protons, helium, carbon, oxygen and iron.

- Secondary cosmic rays: are those particles produced in interaction of the primaries with interstellar gas. This includes lithium, beryllium, boron, and (part of) antiprotons and positrons.

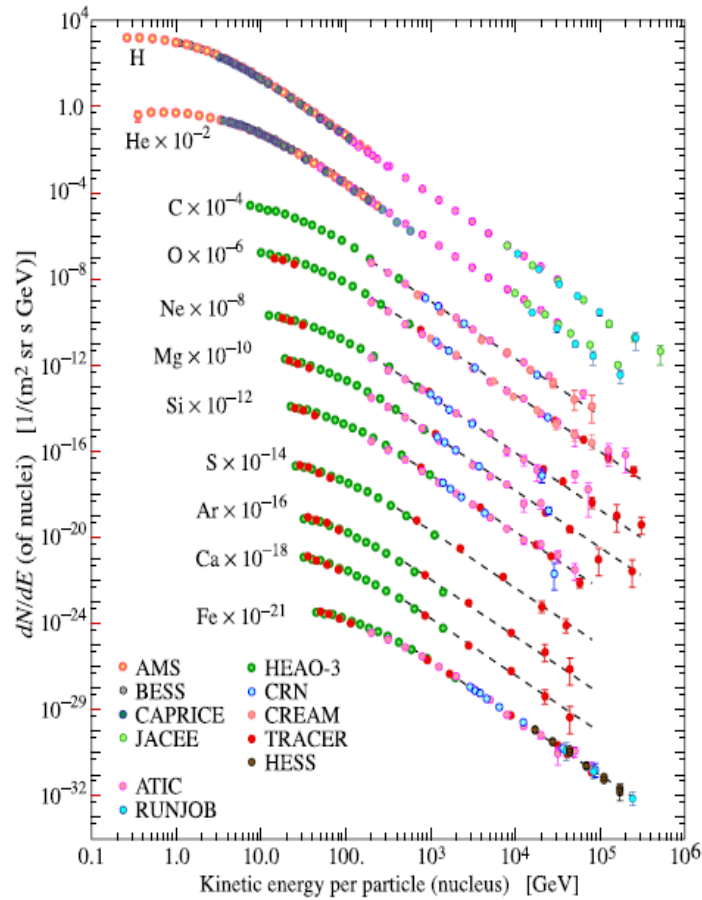


Figure 1.2 – Composition of cosmic rays at different energies. The curves are shown as fluxes of nuclei against energy-per-nucleus. (Source [10])

Perhaps, the most important characteristic of CR is that the observed energy spectra can be well represented by power-law energy distributions. In the first range of these spectra, extending from $\text{GeV}\cdot\text{nucleon}^{-1}$ to $\text{PeV}\cdot\text{nucleon}^{-1}$ the spectrum is an isotropic power law in $E^{-\gamma}$, where $\gamma = 2.7$, usually explained as resulting from *galactic* sources such as supernovae. The second energy interval ranging from $\text{PeV}\cdot\text{nucleon}^{-1}$ to $10 \text{ EeV}\cdot\text{nucleon}^{-1}$ is also an isotropic power law spectrum with an index $\gamma = 3.1$, possibly originating from *extragalactic* sources, such as active galactic nuclei (AGNs) or sources of gamma-ray bursts (GRBs). Both types of sources

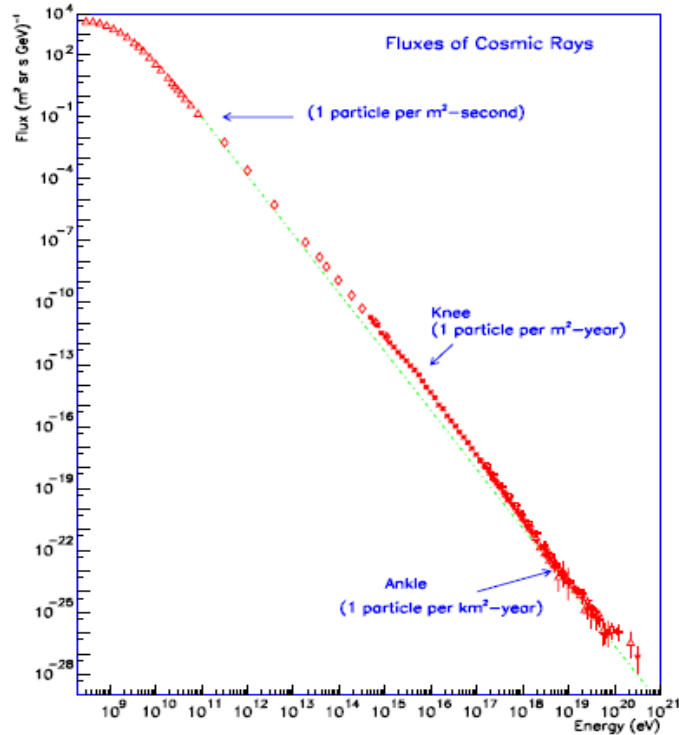


Figure 1.3 – The differential cosmic ray flux versus energy.

are further discussed in section 1.1.4. The region in between these two energy domains (around $\sim 10^{15-16}$ eV) is known as *the knee*, which is poorly understood. Some attempts explain this break as the result of changing propagation characteristics within the galaxy, other as the result of the different production sites.

Beyond 10^{19} eV, where one usually calls the particles "Ultra-High Energy Cosmic Rays" (UHECRs), the spectrum flattens to a slope $\gamma = 2.7$. Particles are also thought to be from extragalactic origin since, at these energies, they cannot be confined magnetically in the Galaxy. The recorded arrival directions are as well nearly isotropic on the sky. The break at $\sim 10^{18-19}$ eV is referred to as the *ankle*. Beyond the ankle, the observed flux seems to vanish. This is compatible with the so called GZK (Greisen-Zatsepin-Kuz'min) effect [11, 12] which predicts a suppression in the spectrum of cosmic rays because of their interaction with diffuse (mainly infrared and microwave) radiations, relics of different stages of the formation of the Universe. As an example, extragalactic protons with energy above the pion production threshold (5×10^{19} eV) lose most of their energy over a distance of about 100 Mpc, small compared to the dimension of the Universe. This implies that cosmic rays can not reach us with an energy of 10^{20} eV unless they originate from a nearby source. This hypothesis remains possible even though there are few sources powerful enough to accelerate particles to such energies at this distance from the

Earth.

The determination of the origin of cosmic rays is also difficult because the arrival directions measured on Earth do not indicate the sources of production. Since they are electrically charged, CR are deflected by interstellar and intergalactic magnetic fields, as opposed to neutrinos. Even at ultra high energy the expected difference between the direction of the source and direction of the particle can reach several degrees. These differences naturally depend on the electric charge carried by cosmic rays, i.e. their composition. This question in the highest energy range remains open. Many experts still favor the hypothesis that highest energy CR are protons, although recent results from the Auger collaboration suggest a transition at around 10^{19} eV, to heavier elements (iron nuclei) [13].

The constraints imposed by the existence of UHECR are related to the size of the potential sources and magnetic field strength prevailing there, which confines charged particles. To acquire a great energy, particles must indeed be confined for some time in the area of acceleration. But the more energetic the particle, the more difficult for magnetic fields (B) to confine it. An upper bound to the maximum energy that can be reached in an acceleration site can be inferred by requiring the Larmor radius ($r_L = E/qBc$) to be smaller than the dimensions of the site, R. The quantities B and R are obtained by the equation:

$$E_{\max} = ZecBR \tag{1.2}$$

As a result of this relationship, only certain types of sources are eligible for particle acceleration beyond 10^{20} eV. They are shown in Figure 1.4. A number of these sources are described in more detail in section 1.1.4, as they are all candidates to neutrino production.

Atmospheric muons and neutrinos

The atmosphere is very rich in particles produced by the interaction of cosmic rays in the air. The vertical flux for different components is shown in Figure 1.5. The most relevant particles for Neutrino Telescopes are atmospheric muons and neutrinos, since they constitute the main physical source of background. The main process responsible for their production is :



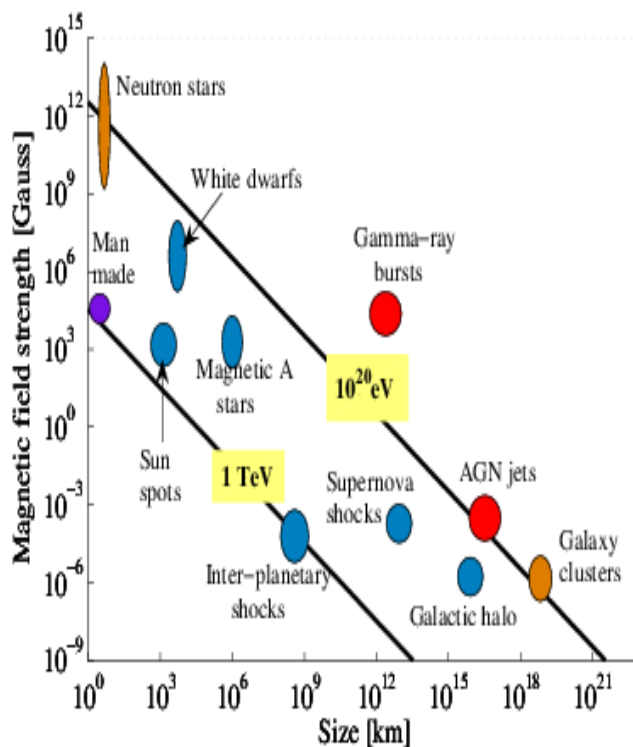


Figure 1.4 – Hillas diagram (from ([14]) representing the type of sites likely to accelerate cosmic rays to extreme energies. The figure shows the size of the potential sources depending on the intensity of magnetic fields estimated in Gauss units (Earth’s magnetic field is of the order of Gauss). To accelerate protons to energies of 1 TeV (10^{20} eV), the sources must lie above the corresponding line. This condition, which is necessary, is not necessarily sufficient: accelerating protons 10^{20} eV in clusters of galaxies, for example, requires an acceleration time larger than the age of the universe. As for neutron stars, they are unlikely candidates because of high energy losses associated with the presence of strong magnetic field.

followed by



Resulting in both muon- and electron-neutrinos. These neutrinos span energies from few MeV to the highest-energy cosmic rays and they are much more abundant at lower energies. Muons are the most numerous charged particles at sea level. They are the remaining of the secondary cosmic rays in the high atmosphere (typically 15 km) and lose about 2 GeV to ionization before reaching the ground. Their energy and angular distributions reflect the convolution of production spectrum, energy loss in the atmosphere and decay [10]. Further discussions on these atmospheric muons and neutrinos follow in section 2.5.

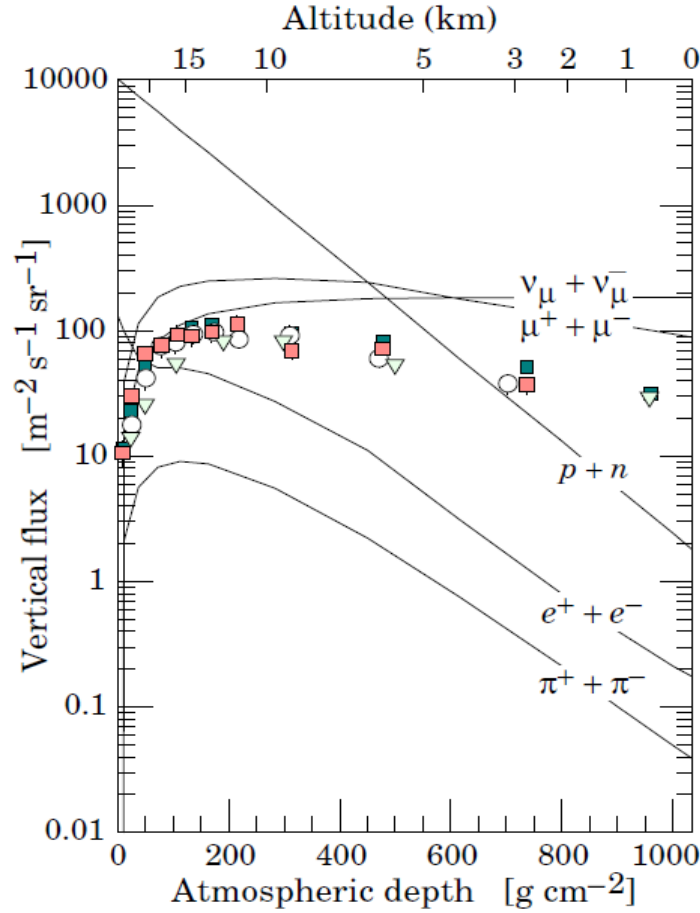


Figure 1.5 – Components of the cosmic rays in the atmosphere with $E > 1\text{GeV}$. The points show measurements of negative muons with energy above 1 GeV. (Source [10])

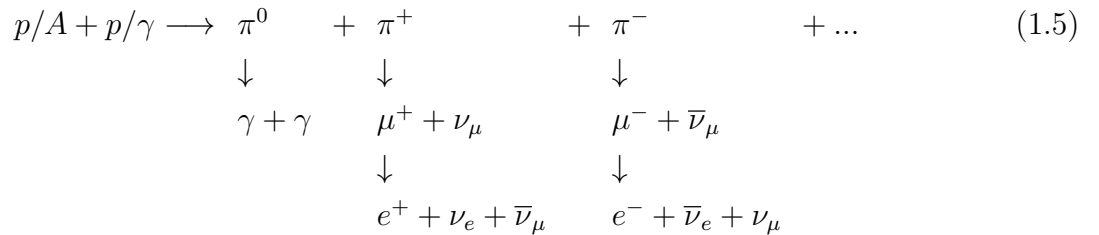
Cosmogenic neutrinos

As previously stated, as they propagate over cosmological distances, UHECRs may interact with the relic photons fields (GZK effect), These interactions generate pions and neutrons, which decay to produce neutrinos of energy greater than 10^{17}eV . The accumulation of these neutrinos over cosmological time is known as the cosmogenic neutrino flux [15, 16]. Although guaranteed sources, the predicted fluxes of cosmogenic neutrinos are low compared with the sensitivity of current neutrino telescopes. Estimates of these fluxes depend mainly on the properties of the primary cosmic ray flux, particularly in terms of composition. Another important parameter is the variation of the intensity of injected flux (or density of sources) as a function of redshift. All of these parameters lead to predictions that differ substantially. The detection of such cosmogenic neutrinos would represent an important step for neutrino astronomy. An accurate measurement of flux would further constrain the composition and the variation of the density

of sources of cosmic rays with redshift.

1.1.3 Neutrinos as cosmic probes

Our current knowledge about astrophysical sources largely rely on observations made using photons (electromagnetic radiation), which are the essential messengers of modern astrophysics. The gamma-ray astronomy (in the TeV range) experienced an unprecedented boom with the advent of new Cherenkov telescopes such as WHIPPLE and more recently HESS. These have demonstrated that TeV photons are actually emitted by number of Galactic and extragalactic sources. The study of these sources has put new constraints on models of cosmic ray production. There is indeed a link between the production of charged cosmic rays and that of photons (or neutrinos) at high energy. Photons and neutrinos can be produced in a beam dump scenario, by the interaction of cosmic rays of high energy with the surrounding matter and background radiation (usually produced by synchrotron radiation of charged particles in magnetic fields) as follows:



In this context, the gamma-rays are produced by the decay of neutral pions (π^0). This production is necessarily linked to that of high-energy neutrinos from the decay of charged pions. Similarly, the existence of cosmic rays of high energy necessarily implies the production of HEN. This is known as the "cosmic ray connection". As such, sources of cosmic rays could be revealed by observing gamma-rays or HEN which, due to their electrical neutrality, travel in a straight line indicating the location of their production area. The high-energy photons can also be produced in a purely electromagnetic process without hadron. This is the "Synchrotron Self Compton" scenario where electrons accelerated to high energy generate photons by synchrotron radiation. These photons are further accelerated to TeV energies by collision with the high energy electrons. Therefore photons alone can not readily discern the electromagnetic processes from the hadronic ones. On the contrary, the detection of neutrinos would be an unambiguous signature for hadronic mechanisms.

The other limitation of high energy photons is their absorption by matter or radiation, which prevents them from escaping dense sources. Besides, when they do escape, high-energy photons are absorbed by interaction with the interstellar radiations (similarly to cosmic rays in the GZK

effect). As an example for PeV photons, the mean free path is typically restricted to dimension of our Galaxy. Photons can therefore hardly be used at high energies for astronomical survey over cosmological distances.

Neutrinos do not suffer these limitations: they are neutral and weakly interacting. Therefore, if they can be detected with sufficiently high statistics, they appear to be ideal candidates for high energy astronomy, providing access to cosmological distances and inner regions of astrophysical sources. This makes of the neutrino a singular probe able to open a window of observation on the sky.

In this sense, HEN astronomy can address a number of fundamental questions in astrophysics and cosmology. Among these are the nature of dark matter (see section 1.1.4), the origin of the cosmic rays, and the extreme physics responsible for gravitational energy release in the most luminous objects in the universe. The work presented in this dissertation focuses on the detection of neutrinos in coincidence with gravitational waves, following the advocated lines of a multimessenger approach.

Theoretical upper bounds to the cosmic neutrino flux

If neutrinos of extragalactic origin have not yet been detected, the link (described in the previous paragraph) between cosmic messengers allows to estimate the diffuse neutrino flux produced by the "cosmic accelerators" [17, 18].

The observable spectrum of cosmic rays provides the most restrictive limit. Bahcall and Waxman (WB) have determined a benchmark cosmic neutrino flux, based on the assumption that the observed cosmic rays above 10^{19} eV are protons produced by extragalactic cosmic accelerators. The calculation is based on the production rate (per unit time, volume, and energy) of these ultra high energy protons estimated at:

$$E_p^2 \frac{dN}{dE_p dV dt} \approx 0.65 \times 10^{44} \phi(z) \text{ erg Mpc}^{-3} \text{ year}^{-1} \quad (1.6)$$

where $\phi(z)$ (with $\phi(0) = 1$) takes into account the evolution of the production rate as a function of redshift (small since following the GZK effect, the protons lose their energy over relatively small distances). The choice, consistent with the Fermi mechanism, of a E^{-2} differential spectrum is motivated by observations of processes involving shocks (relativistic or not).

The production rate given by equation 1.6 enables to infer an upper limit for the production of HEN from extragalactic sources as AGN or GRBs. The underlying assumption is that the rate of energy injected in the form of neutrinos can not exceed that of the associated protons

1.1.1 High-energy neutrino astronomy

even when all are involved in the production of pions (relation 1.5). The resulting limit is:

$$E_\nu^2 \phi_\nu < 2 \times 10^{-8} \xi_z \left[\frac{(E_p^2 \frac{dN}{dE_p dV dt})_{z=0}}{10^{44} \text{ erg/Mpc}^3 \text{ year}} \right] \text{ GeV cm}^{-2} \text{ s}^{-1} \text{ sr}^{-1} \quad (1.7)$$

where ξ_z , of the order of unity, indicates the evolution of the injection rate following the redshift. Such a flux is being challenged by current neutrino telescopes which have therefore entered a quite exciting era.

1.1.4 Astrophysical sources of high-energy neutrinos

In this section we present a selected list of astrophysical sources that are candidates for high-energy neutrino emission. These sources can be sorted into 2 types: *galactic* and *extragalactic*. Based on relation (1.5), estimates of the expected neutrino flux can be achieved relying on the recent observations with gamma-rays with, for example, HESS [19] and FERMI [20]. But these estimates can still vary by orders of magnitude depending on the precise model used to infer them. These estimates of neutrino fluxes at Earth must also be corrected to take into account the flavor mixing occurring during propagation. To the first order, neutrinos are produced in a ratio of flavor (see relation (1.5)) ($\nu_e : \nu_\mu : \nu_\tau = 1 : 2 : 0$) but reach the Earth in the proportions ($\nu_e : \nu_\mu : \nu_\tau = 1 : 1 : 1$).

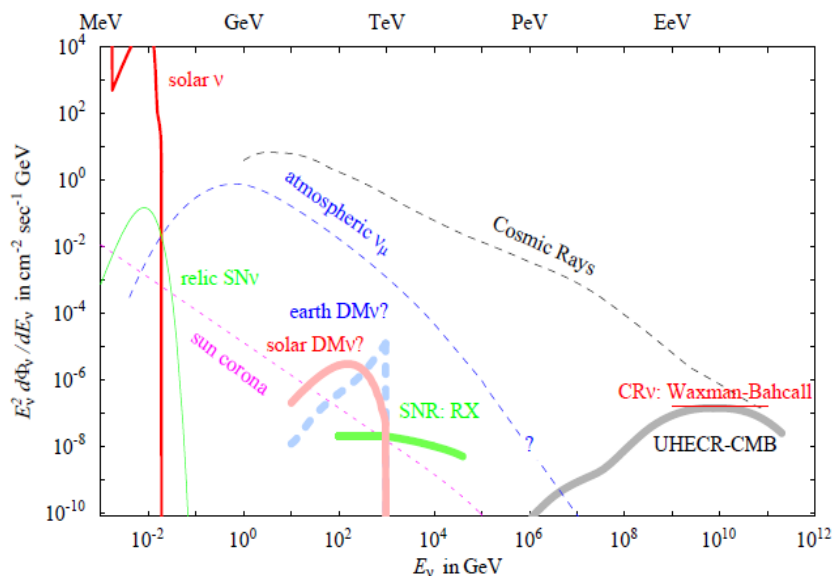


Figure 1.6 – Optimistic astrophysical neutrino fluxes from various sources

Galactic sources

The most promising Galactic sources of neutrinos are briefly reviewed below. Estimates of expected associated neutrino fluxes can be found, for instance, in [21]:

- **Supernova remnants (SNR):** They are the prime candidate sources for accelerating the cosmic rays observed up to $\sim 10^{15}$ eV thanks to the Fermi mechanism. After the explosion of the star, leading to a supernova, ejected particles can be accelerated to high energies. From the death of the star arises a pulsar with a high magnetic field that contribute to the acceleration of particles. The production of (TeV) neutrinos is expected in the collision of cosmic rays *proton/neutron* with the thermal nucleon in the remnant shell which leads to neutral and charged pions π^+/π^0 .

The observation by HESS of the southern sky with γ rays at the TeV and above revealed two particularly bright SNR. The first one is Vela Junior (*RXJ0852.0 – 4622*). The flux of γ was observed in a region extending up to $\sim 2^\circ$. The second is *RXJ1713.7 – 3946*. The observed spectra below 10 TeV look like power laws with hard spectral indices: $\Phi_\gamma = dN_\gamma/dE \propto E^{-\Gamma}$ with $\Gamma \sim 2$, the value suggested by the Fermi acceleration mechanism. Various spectral analyses of these sources seem to favor a hadronic origin for the gamma emissions detected, which could lead to an observable flux for a km-scale neutrino telescope.

The flux of neutrinos can be calculated from the flux of π^+ . First, we get the flux of π from the γ flux, using the π^0 decay and assuming that $\Phi_\pi^+(E) = \Phi_\pi^-(E) = \Phi_\pi^0(E) = \frac{-E d\Phi_\gamma}{2dE}$. Consequently one can deduce the neutrino flux using the $\pi^+ \rightarrow \mu^+ \nu_\mu$ decay:

$$\Phi_{\nu_\mu}(E) = \int_{E/(1-r)}^{\infty} \frac{d\epsilon \Phi_\pi^+(\epsilon)}{(1-r)\epsilon} = \frac{\Phi_\gamma(E/1-r)}{2(1-r)} \quad (1.8)$$

where $r = (M_\mu/M_\pi)^2$.

- **Microquasars:** These objects are binary stellar systems with collimated relativistic jets at radio frequencies. They consist of an accreting compact object, either a black hole or a neutron star, and a companion star. The behavior of these systems resembles, to some extent, that presented by extragalactic quasars, hence the origin of the name. The detection of the microquasar Cygnus X-3 above 100 MeV by both Fermi/LAT and AGILE satellites, together with the short flares from Cygnus X-1 reported by AGILE, confirmed that this class of astrophysical objects are interesting candidates for very high energy gamma-ray observations.

1.1.1 High-energy neutrino astronomy

Microquasars could produce HEN according to two models. In the first model, inhomogeneities in the jet could generate internal shocks accelerating electrons and protons arising in a power law energy spectrum. Accelerated protons could interact with X-ray emitted by the accretion disc or synchrotron photons generated in the jet by the accelerated electrons [22]. Both Synchrotron self-Compton (SSC) and strong external X-ray fields can cool extremely relativistic protons through pion production. However, the protons should be accelerated up to very high energies (10^{16} eV) in the inner jet in order to produce a significant flux of multi-TeV neutrinos. It is not established that microquasars can accelerate particles up to such energies at the base of the jets. The high neutrino fluxes predicted by [23] on the basis of this model for different microquasars are in some cases already ruled out by AMANDA II data, and recently by ANTARES [24].

In the second model [25], high-energy gamma-rays and neutrinos could result in matter interactions: accelerated nuclei of the jet could lose neutrons as a result of photo-decay process in collisions with thermal photons from the accretion disk and the massive star. These neutrons propagating toward the disk and the massive star could generate neutrinos by interacting with matter.

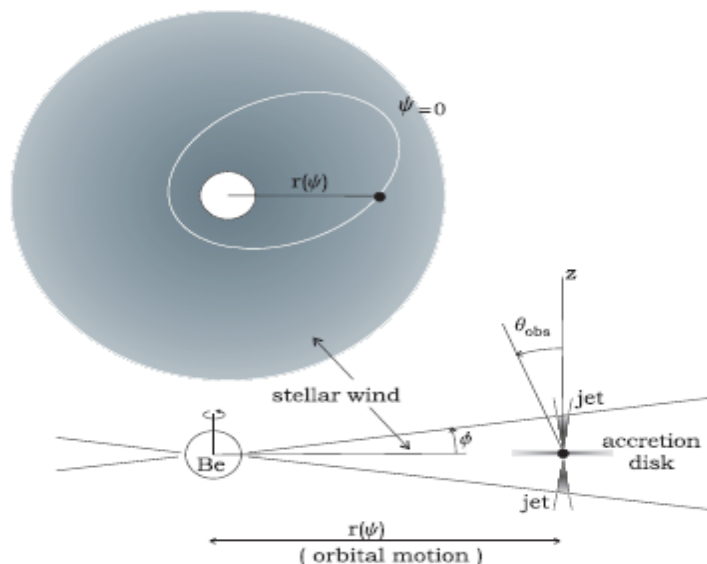


Figure 1.7 – Schematic model of a possible hadronic model of microquasars. (source [26])

- **Soft gamma-ray repeaters (SGRs)** They are X-ray pulsars which have quiescent soft (2–10 keV) periodic X-ray emissions with periods ranging from 5 to 10 s. They exhibit repetitive erratic bursting episodes lasting a few hours each and composed of numerous

very short (\sim ms) pulses. Every once in a while they emit a giant flare in which a short (< 0.5 s) spike of harder radiation is observed; such flares can reach peak luminosities of $\sim 10^{47}$ erg/s, in X-rays and γ -rays. A handful of SGR sources are known, most of them in the Milky Way and one in the Large Magellanic Cloud. Three of them have had hard spectrum (\sim MeV energy) giant flares: one with a luminosity of 10^{40} J/s, the two others being two orders of magnitude weaker.

The favoured *magnetar* model for these objects is a neutron star with a huge magnetic field $B \gtrsim 10^{15}$ G, which is subject to star-quakes that are thought to fracture the rigid crust, causing outbursts. The giant flares result from the formation and dissipation of strong localized currents due to magnetic field rearrangements associated with the quakes, and liberate a high flux of X- and γ -rays. Sudden changes in the large magnetic fields would accelerate protons or nuclei that produce neutral and charged pions in interactions with thermal radiation. These hadrons would subsequently decay into TeV or even PeV energies γ -rays and neutrinos, making flares from SGRs potential sources of HEN.

An alternative model involving a large scale rearrangement of the magnetic field has also been proposed by [27], which allows for huge energy releases, and detectable HEN fluxes from Galactic magnetars even for relatively small HEN efficiencies.

- ***The Galactic centre:*** Since its observation by the HESS telescope in the TeV domain [28] the centre of our Galaxy has become of particular interest for neutrino astronomy. Indeed, initial observations revealed the presence of two bright sources, one in the direction of Sagittarius A* (HESS J1745-290), the supermassive black hole at the centre of the Galaxy, and another one, close to supernova Sgr A East. After subtraction of these intense sources, a more diffuse emission has been observed. This diffuse emission of photons of energy greater than 100 GeV is strongly correlated with molecular clouds [29], suggesting a hadronic origin of the observed γ -rays. The associated neutrino emission could be observed with the next generation of neutrino telescopes to be built in the Northern hemisphere.
- ***Pulsar wind nebulae (PWNe):*** They are ejecta of shocked relativistic particles produced when a pulsar emits a relativistic wind further interacting with its environment. The best known among these sources is the Crab Nebula that harbors an energetic pulsar¹ whose spin-down power manifests itself as a synchrotron-emitting source of energetic particles. Recent discoveries of very high energy γ -ray emission associated with PWNe have

¹A rapidly rotating, highly-magnetized neutron star, which generates coherent beams of radiation along its magnetic poles.

opened a new channel for investigations of the structure and evolution of these objects. It is thought that this emission in the TeV band probably originates from inverse-Compton scattering of ambient soft photons with energetic electrons in the nebula [30]. Nevertheless, hadronic models have been considered in which the emission is associated with the decay of neutral pions produced in collisions of energetic ions with ambient hadronic material [31], of particular interest is Vela X.

Extragalactic sources

We discussed in section 1.1.2 that extragalactic sources could be at the origin of the cosmic rays (CR) at the highest energies $E_{CR} > 10^{18}$ GeV. In this context, several sources are suggested to produce high energy neutrinos:

- **Active galactic nuclei (AGNs):** Active galaxies are galaxies whose center shows increased luminosity with respect to the rest of the galaxy. These galaxies have a concentration of stars, gas and dark matter in the center which make their nucleus active, i.e. gas is being accreted in large quantities and/or stars are being captured, disrupted and swallowed in significant number. AGNs were first observed in 1963 [32] in the radio emission. Some of them are detected in γ -ray range. It has been discovered during the last three decades that these active galaxies have a massive black hole at their center that accretes continuously matter. In the center of the accretion disc, matter is ejected in jet perpendicularly to the accretion disc. Active Galactic nuclei are thought to accelerate electrons in shocks either inside their jets or at the jet termination surface, see Figure 1.8. Certain classes of AGNs (like Blazars) may be capable of accelerating cosmic rays to energies in excess of PeV, which could lead to TeV neutrinos and gamma-rays via photo-meson process. The correlations established by the AUGER collaboration [34] reinforce the hypothesis that AGN could be the source of cosmic rays of ultra high energy, but they are still subject to an intense debate. Searching for neutrinos from known AGN is therefore of particular importance.

An important factor to take into account when predicting neutrino fluxes associated with the observed high-energy gamma rays, for this type of extragalactic sources, is the absorption by the extragalactic background light (EBL). The spectral index of 2.9 observed by the telescope HESS in the case of the blazar 1ES1101 ($z = 0.186$) could, for example, correspond to an index in the source, 1.5 [35], which could therefore lead to a neutrino flux significantly more intense than the gamma flux.

Another feature of blazars is their variability. In the case of PKS2155, an increase of

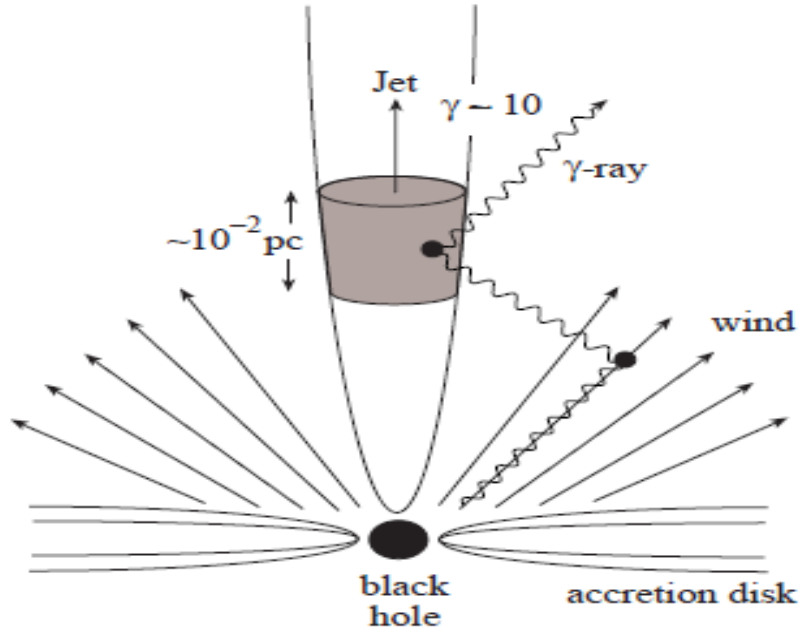


Figure 1.8 – Schematic blazar internal shock scenario. Blazars are a subset of AGNs, that emit high-energy radiation in collimated jets pointing at the Earth. (Source [33])

almost a factor of 100 in the gamma flux has been observed by HESS over a one-hour period [36]. Such a flurry of activity in a short period could allow the detection of neutrinos through the significant reduction of associated background noise. This technique is similar to the one adopted to search for neutrinos from sources of gamma-ray burst (GRB).

- **Unidentified sources:** Finally, it is interesting to note that a number of sources detected by HESS have no observable counterpart in the electromagnetic spectrum. The origin of this type of source is therefore a theoretical challenge. Observation of high energy neutrinos in the direction of these sources could probably help modeling these objects. The detection of these sources without counterpart underlines once more the possibility of detecting previously unknown sources.
- **Starburst Galaxies:** The observation of synchrotron emission in the radio band from some galaxies (where the star formation rate is unusually high) named "starburst galaxies" implies the presence of a few GeV electrons assuming the existence of intense magnetic fields. The presence in these galaxies of many massive stars in formation phase considerably enriches the interstellar medium with matter. So if protons were accelerated together with the electrons (e.g. supernova explosion), this would result in a significant flow of neutrinos by pp interactions (on the order of $dN = 10^{-7}E^{-2}\text{GeV}^{-1}\text{cm}^{-2}\text{s}^{-1}\text{sr}^{-1}$),

detectable by the new generation of neutrino telescopes [37].

- ***Gamma-Ray Bursts (GRBs)***: Gamma-ray Bursts (GRBs) (see Figure 1.9) are detected as an intense and short-lived flash of gamma-rays with energies ranging from tens of keVs to tens of GeVs. The morphology of their light curves is highly variable and typically exhibits millisecond variability, suggesting very compact sources and relativistic expansion. GRBs are divided into two classes depending on the duration of their prompt gamma-ray emission, which appears to be correlated with the hardness of their spectra and are believed to arise from different progenitors: short-hard bursts last less than 1–2 seconds while long-soft bursts can last up to dozens of minutes.

The BATSE detector, launched in 1991 on board the Compton Gamma-Ray Observatory, was the first mission to accumulate observations on more than a thousand GRBs, establishing the isotropy of their sky distribution and characterizing their light curve and broken power-law spectra [38]. The detection of X-ray and optical counterparts pertaining to the afterglow phase of several GRBs, triggered by the first observation of an X-ray transient emission from GRB970228 by the BeppoSAX satellite [39], subsequently confirmed their extragalactic origin by allowing a more accurate localization of the source and a redshift determination. Currently operating GRB missions include *Swift*, hosting a wide-field hard X-ray (15 keV–350 keV) burst alert telescope (BAT) coupled to softer X-ray, ultraviolet and optical telescopes and the GBM on the Fermi Gamma-Ray Space Telescope which focuses on the high-energy (15 keV–300 GeV) emission from GRBs. In the standard picture (see e.g. the review by [40]), the mechanism responsible for the enormous, super-Eddington energy release ($\sim 10^{50} - 10^{52}$ ergs) in the prompt emission and in the afterglow is the dissipation (via internal shocks, magnetic reconnection and external shocks) of bulk kinetic or Poynting flux into highly relativistic particles. The particles are accelerated to a non-thermal energy distribution via the Fermi mechanism in a relativistically expanding fireball ejected by the GRB central engine. The accelerated electrons (and positrons) in the intense magnetic field emit non-thermal photons via synchrotron radiation and inverse Compton scattering.

The plasma parameters inferred from observations to characterize GRB's baryonic fireballs are such that proton acceleration to energies exceeding 10^{20} eV is likely to be possible in these sources. Moreover, the time averaged energy output of GRBs in photons is comparable to the proton energy production rate required to produce the UHECR flux. Therefore, the canonical baryonic fireball also suggests that GRBs are a prime candidate source for the ultra-high-energy cosmic rays (UHECR), observed at energies

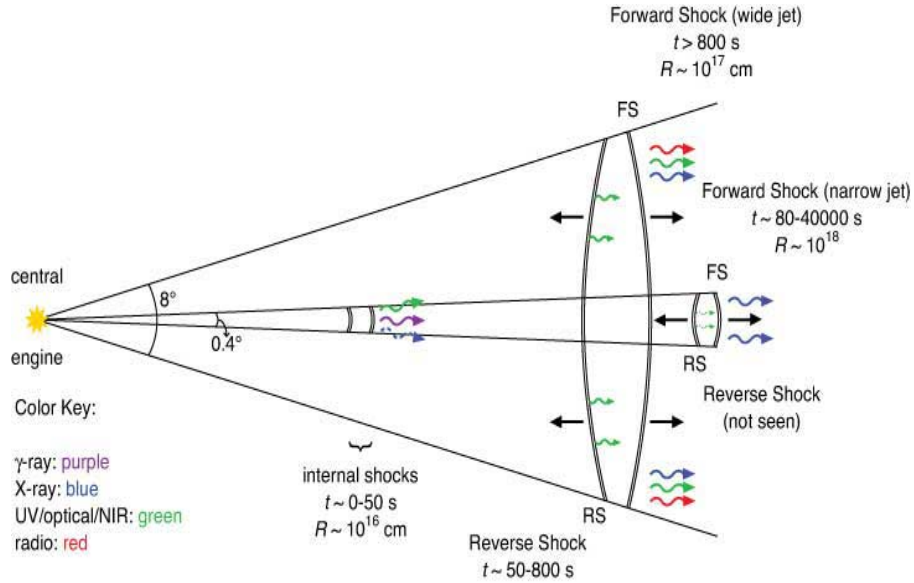


Figure 1.9 – Schematic GRB jet and location of jet photosphere, dissipation (internal shock) and external shock radii.

$E \sim 10^{18} - 10^{20}$ eV. In a baryonic outflow, the internal or external shocks accelerate protons that interact with the gamma-rays and/or other protons inside the fireball producing neutrinos according to the relation 1.5. Such neutrinos are emitted in spatial and temporal coincidence with the GRB prompt electromagnetic signal; their energy is typically in the range \sim TeV to PeV. Neutrinos with higher (up to $\sim 10^{10}$ GeV) energy can also be emitted at the beginning of the afterglow phase, when the outflow is decelerated by external shocks with ambient material and the accelerated protons undergo interactions with the matter outside of the jet [41]. An alternative mechanism for neutrino production in fireballs suggested by [42] involves neutral particles that are picked up by the stream when they acquire a charge, such as a decaying neutron, or, further downstream, a neutral atom that is ionized. Such a particle will be extremely energetic in the jet frame, and immediately attains an energy of a PeV. The associated neutrinos would come within an order of magnitude of that energy (~ 100 TeV), providing a harder spectrum than the one expected from shock acceleration. The sensitivity achieved by neutrino telescopes is such that their observations will allow in a few years to test and distinguish between GRB models with different physics, and to constrain the physical parameters of such models. The current non-detection of neutrinos by IceCube [43] (see also Chapters 4 and 5) already questions the viability of models in which ultra high energy cosmic rays are the decay products of neutrons that have escaped the fireball with high energy. The

current upper limit is still consistent with the "standard" (i.e., following [44]) predictions of neutrino emission from GRB fireballs.

Gamma-Ray Burst diffuse flux of Waxman-Bahcall

As stated in the previous section, GRBs are considered to be produced from the collapse of stars or the merger of compact objects with the central object being a black hole (or in case of the magnetar model a fast rotating high-mass neutron star which eventually collapses into a black hole). During the collapse the release of high amounts of gravitational energy during a short time in a small volume leads to an explosion or expansion.

Waxman and Bahcall calculated an upper bound for the diffuse flux [45] of muon-neutrinos produced in GRBs. The shape of this flux is the result of relatively general considerations depending on the photon and proton spectra. The observed spectra can be parametrized as following. First one needs to specify the proton spectrum:

$$N_p(E_p) = N_{p,0} E_p^{-2} \cdot \exp \left[- \left(\frac{E_p}{\epsilon_{p,max}} \right) \right]; \quad E_p \leq \epsilon_{p,max} \quad (1.9)$$

where $\epsilon_{p,max}$ is the proton maximum energy. Its value is derived from comparison of acceleration time and synchrotron loss time. $N_{p,0}$ is the normalization of the spectrum. The photon spectrum $N_\gamma(E)$ is derived from observed GRB photon spectra and is parametrized by the Band function:

$$N_\gamma(E_\gamma) = N_{\gamma,0} \begin{cases} E_\gamma^{-1} & \text{if } \epsilon_{\gamma,min} \leq E_\gamma < \epsilon_{\gamma,b} \\ \epsilon_{\gamma,b} E_\gamma^{-2} & \text{if } \epsilon_{\gamma,b} \leq E_\gamma < \epsilon_{\gamma,max} \\ 0 & \text{else} \end{cases}$$

where $N_{\gamma,0}$ is the normalisation factor. The break energy $\epsilon_{\gamma,b}$ is retrieved from the photon spectrum of a burst. The energy $\epsilon_{\gamma,max}$ is the maximum photon energy, and $\epsilon_{\gamma,min}$ is the lower energy cut-off of the photon spectrum.

Using these spectra Waxman and Bahcall (WB) derived a power-law spectrum of the muon-neutrino at Earth:

$$E_{\nu_\mu}^2 dN_{\nu_\mu}(E_{\nu_\mu})/dE_{\nu_\mu} = N_{\nu_\mu,0} \begin{cases} \epsilon_{\nu_\mu,b}^{-1} E_{\nu_\mu} & \text{if } E_{\nu_\mu} \leq \epsilon_{\nu_\mu,b} \\ 1 & \text{if } \epsilon_{\nu_\mu,b} \leq E_{\nu_\mu} < \epsilon_{\nu_\mu,s} \\ \epsilon_{\nu_\mu,s} E_{\nu_\mu}^{-2} & \text{if } E_{\nu_\mu} \geq \epsilon_{\nu_\mu,s} \end{cases}$$

The first break of the WB spectrum $\epsilon_{\nu_\mu,b} = 10^{14}$ eV is connected to the break in the photon spectrum $\epsilon_{\gamma,b}$ via the energetics of the Δ -resonance. It is determined through the minimal

energy necessary to produce a $\Delta(1232)$ -resonance in the shock fronts of the bursts.

$$E_\gamma E_p \geq \frac{m_\Delta^2 - m_p^2}{2(1 - \cos(\theta_{p\gamma}))} \quad (1.10)$$

where m_Δ and m_p are the rest mass of the Δ -resonance and the proton respectively. We now need an approximation of how much energy is passed from the parent protons to the neutrinos (after pion decay). It is possible to estimate the fraction of energy $f_\pi = 0.2$ passed on from the protons to the pions. In the subsequent decay of the pions about 1/4 of the pion energy is transformed into neutrinos:

$$\begin{aligned} E_{\nu_\mu} &= \frac{1}{4} f_\pi E_p \\ &= \frac{1}{20} \cdot \frac{m_\Delta^2 - m_p^2}{2(1 - \cos(\theta_{p\gamma}))} E_\gamma \end{aligned} \quad (1.11)$$

This result then has to be boosted to the observer's frame as well as shifted due to cosmological effects to obtain the observed values:

$$E_{\nu_\mu} = \frac{\Gamma^2}{(1+z)^2} \cdot \frac{1}{20} \cdot \frac{m_\Delta^2 - m_p^2}{2(1 - \cos(\theta_{p\gamma}))} E_\gamma \quad (1.12)$$

Using the numerical values given in [46] for the proton mass, $m_p = 0.94$ GeV, and the Δ -mass, $m_\Delta = 1.23$ GeV, leads to:

$$\epsilon_{\nu_\mu, b} = 7.10^5 \cdot \frac{\Gamma^2}{(1+z)^2} \epsilon_{\gamma, b} \text{ GeV} \quad (1.13)$$

The second energy break of the WB spectrum at $\epsilon_{\nu_\mu, s} = 10^{16}$ eV in the neutrino spectrum results from the fact that pions lose energy at very high energy due to synchrotron radiation. It can be obtained by considering synchrotron cooling of the pions. To calculate the energy of this break one has to compare the particle life time τ to the synchrotron loss time t_{syn} .

Some exotic sources

Another hypothetical source of HEN is related to the presence of dark matter in the universe. It was first in 1933 that Zwicky pointed out that a possibly significant amount of mass was missing from observations [47]. The bulk of this dark matter is non-baryonic. One of the candidates is the neutralino, a stable and neutral particle in the minimal standard super-symmetric model. The Galaxy would lie in a halo consisting of these particles, which would, *inter alia*, help explain the anomalous behavior of the distribution of the velocities of visible objects (constant speed

of about 220 km/s regardless of the distance to the center of the Galaxy).

Subject to the Kepler's laws, like any other massive object, these particles revolve with the same average speed. Under the influence of gravity, the neutralinos get trapped at the center of massive bodies, such as the Sun and the Galactic center, where they can annihilate. In this scenario, neutrinos would emerge as by product of the annihilations. The discovery potential of a neutrino telescope like ANTARES for such dark matter particles is discussed, for example, in [48].

1.2 Gravitational waves

Einstein's theory of General Relativity introduces the concept of a dynamical and deformable space-time. The dynamics result from the interaction between space-time and its matter contents. In short, "spacetime tells matter how to move; matter tells spacetime how to curve" [49].

General Relativity describes Gravity as a direct effect of space-time curvature. It predicts that the equations of space-time can give rise to radiative solutions, called *gravitational waves*. Gravitational waves (GW) are ripples in the metric of spacetime that propagate at the speed of light.

Here, we give an introduction to GWs in section 1.2.1 and their phenomenology in section 1.2.2. We present in section 1.2.3 the potential astrophysical sources.

1.2.1 Basics of gravitational-wave theory

In the theory of General Relativity, gravitation is described as a geometrical effect connected to the curvature of space-time. The geometry of space-time is defined by a metric g which determines the distance ds of neighbouring events taking place at space-time coordinates x^α ($\alpha = 0, 1, 2, 3$) and $x^\alpha + dx^\alpha$. We have

$$ds^2 = g_{\mu\nu} dx^\mu dx^\nu \quad (1.14)$$

where Einstein's summation convention in use here implies the summation over indices μ and $\nu = 0, 1, 2, 3$. The metric g used in the above equation through its components $g_{\mu\nu}$ describes how intervals are measured in space-time and hence the properties of the gravitational field.

The curvature of space-time is determined by the energy-matter distribution through the Einstein equations

$$G_{\mu\nu} = R_{\mu\nu} - \frac{1}{2}R = \frac{8\pi G}{c^4}T_{\mu\nu} \quad (1.15)$$

CHAPTER 1. MULTIMESSENGER ASTRONOMY

where c is the speed of light, G is the constant of gravitation. The Einstein equations connects the Einstein tensor $G_{\mu\nu}$ which describes the dynamics of space-time geometry and is directly connected to the metric g to the stress-energy tensor $T_{\mu\nu}$ which describes the matter and energy source distribution.

The Einstein equations form a set of 10 non-linear partial differential equations. Finding a solution to those equations is difficult in general. Approximated solutions can be found in the weak field approximation, where the metric results from a small perturbation of the Minkowski metric $\eta_{\mu\nu} = \text{diag}(-1, 1, 1, 1)$ of special relativity associated to flat space-time

$$g_{\mu\nu} = \eta_{\mu\nu} + h_{\mu\nu} \quad (1.16)$$

where the term $h_{\mu\nu}$ represents a small (tensor) perturbations with $|h_{\mu\nu}| \ll 1$. In this case, the Einstein equations can be linearized. Applying the Lorentz gauge condition, we get

$$\left(\nabla^2 - \frac{1}{c^2} \frac{\partial^2}{\partial t^2} \right) h_{\mu\nu} = 0 \quad (1.17)$$

This is the wave equation. If the propagation direction be z , the solutions are

$$h_{\mu\nu} = \Re \{ \varepsilon_{\mu\nu} \exp(\omega t - kz) \} \quad (1.18)$$

where $\omega = kc$ and $\varepsilon_{\mu\nu}$ is a 4×4 symmetric matrix of constants.

This implies the existence of oscillatory wave-like solutions to Einstein's equations: *gravitational waves* (GW). They are predicted to propagate at speed of light.

The freedom to choose a coordinate frame allows us to select one where $h_{\mu\nu}$ is transverse traceless (also referred to as "TT gauge"). In this frame, $\varepsilon_{\mu\nu} = h_+ \varepsilon_{\mu\nu}^+ + h_\times \varepsilon_{\mu\nu}^\times$ can be linearly decomposed into two independent polarization tensors $\varepsilon_{\mu\nu}^+$ and $\varepsilon_{\mu\nu}^\times$ which define the "+" (plus) and "×" (cross) polarizations respectively.

$$\varepsilon_{\mu\nu}^+ = \begin{bmatrix} 0 & 0 & 0 & 0 \\ 0 & 1 & 0 & 0 \\ 0 & 0 & -1 & 0 \\ 0 & 0 & 0 & 0 \end{bmatrix} \quad \varepsilon_{\mu\nu}^\times = \begin{bmatrix} 0 & 0 & 0 & 0 \\ 0 & 0 & 1 & 0 \\ 0 & 1 & 0 & 0 \\ 0 & 0 & 0 & 0 \end{bmatrix}. \quad (1.19)$$

This shows that GW have two independent polarizations.

1.2.2 Phenomenology of gravitational waves

Effect of gravitational waves on matter

Equations (1.18) and (1.19) show that a GW modulates the distance between two nearby objects at the wave frequency ω with opposite sign in the plane *transverse* to the direction of propagation.

This is a *differential strain* effect which is illustrated in Figure 1.10 over a ring of free falling test masses submitted to gravity only. We also see that the effect of the + and \times polarization is the same except a rotation of 45° degrees.

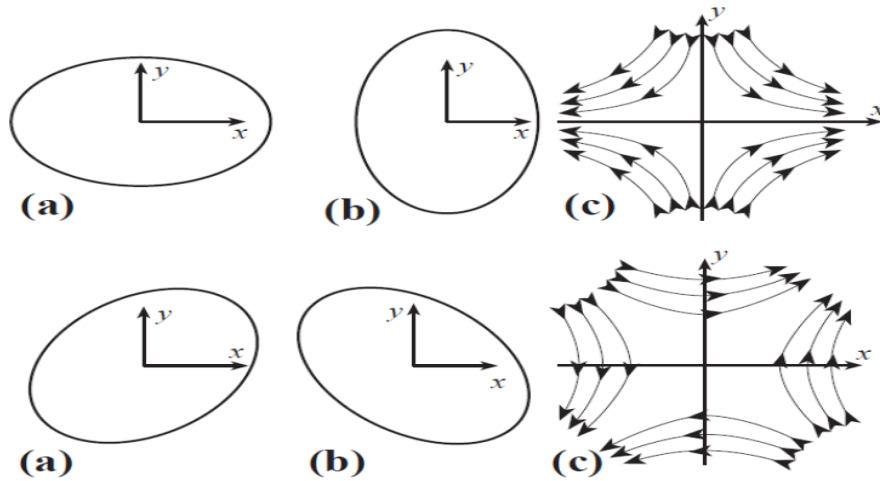


Figure 1.10 – Deformation of a ring of freely falling test masses due to an impinging GW which propagates in the direction normal to the plane of the ring. (a and b top) effect of the “+” polarization. (a and b bottom) effect of the \times polarization. (c top) the field lines corresponding to the + polarization (The arrows show the direction of the field). (c bottom), the field lines corresponding to the \times polarization.

Production of gravitational waves—Quadrupole formula

Electromagnetic (EM) waves are produced by accelerated charges. Similarly, GW are produced by accelerated masses. The lowest non-vanishing term in the multipole expansion of the source distribution is the quadrupole, since the dipole vanishes due to the conservation of momentum. This is a major difference with respect to EM waves (which are dominated by the dipole). The emission of GW are thus associated to variations of the quadrupolar moment tensor of the mass distribution defined by

$$Q_{ij}(t) = \frac{1}{c^2} \int T_{00}(t, x) x_i x_j d^3x \quad (1.20)$$

where T_{00} is the time component of the stress-energy tensor which is directly connected to the energy density and hence source rest-mass density. Clearly, a spherically symmetric system

CHAPTER 1. MULTIMESSENGER ASTRONOMY

cannot emit GW as its quadrupole does not vary. The so-called *quadrupole formula* obtained in the far field and slow motion approximation ($v \ll c$), connects the GW amplitude to the quadrupole moments defined in Equation (1.20). We have

$$h_{ij} = \frac{2G}{r c^4} \frac{\partial^2}{\partial t^2} Q_{ij}(t - r/c) \quad (1.21)$$

where r is the distance from the observer to the source. This shows that GW are a *radiation* as its amplitude decreases inversely with the distance r to the source.

The leading factor $G/c^4 \approx 8.3 \times 10^{-45} \text{ s}^2/\text{m}/\text{kg}$ is extremely small. To generate GW of sufficient amplitude to be detectable, it has to be compensated by very large variations of Q .

These variations have typical magnitude $\ddot{Q} \sim (mv^2)_{\text{non-sph}}$ which is twice the non-spherical part of the kinetic energy inside the source. Let us denote the source characteristic radius R and ϵ the degree of asymmetry of the mass distribution and let us assume that the source evolves over the characteristic time scale T . We then get the estimate $\ddot{Q} \approx \epsilon m R^2 / T^2$. Applying this estimate to systems at the human scale, we see that they are unable to reach a sufficient \ddot{Q} .

This implies that GW cannot be generated in a laboratory. The sources must involve very massive, dense, relativistic systems and are therefore necessarily high-energy astrophysical processes. To get typical estimates, let us consider a system formed of two compact stars (such as, a neutron-star binary). A detailed discussion of this system as a GW source will be given later in section 1.2.3. For such a source, the above estimate yields $\ddot{Q} \sim m(\Omega R)^2 \sim m^{5/3} \Omega^{2/3}$ using 3rd Kepler's law. For a binary neutron-star system with $m = 1.4M_\odot$ located at $r = 10$ Mpc and orbiting at $\Omega/(2\pi) \sim 100$ Hz, the above estimate gives $h \sim 10^{-21}$. This corresponds to the detectability limits of current GW detectors (as explained in detail in chapter 3).

A consequence of the estimates provided in this section is that GW are produced by the coherent relativistic bulk motion of large mass distributions. This radically differs from EM waves generally produced in Nature by the individual and incoherent motion of charges (atoms or electrons). While EM waves (and neutrino emission) are sensitive to the micro-physics, GW carries information about the global dynamics of the source.

Radiated GW energy

It is interesting to calculate the energy radiated by a GW away from the source. The GW energy flux (per unit time and unit area) is defined by [50]

$$F_{GW} = \frac{c^3}{16\pi G} \langle \dot{h}_+^2(t) + \dot{h}_\times^2(t) \rangle \quad (1.22)$$

where \dot{x} designates the time derivative and where the average $\langle \cdot \rangle$ operates over several periods. This averaging is necessary and arises from the impossibility to define the energy of a gravitational field locally in General Relativity.

For example, the energy flux of a sinusoidal, linearly polarized wave of amplitude H_+ and angular frequency ω is

$$F_{GW} = \frac{c^3}{32\pi G} \omega^2 H_+^2 \quad (1.23)$$

Assuming a frequency of $\omega/(2\pi) = 100$ Hz and amplitude $H_+ = 10^{-21}$, one obtains a flux of 3.3 mW/m^2 (or equivalently 3.3 erg/s/cm^2). This is a considerable energy for astrophysical standard candles. For instance, it is eight orders of magnitude larger than the Crab pulsar luminosity in the ~ 10 keV band.

The GW radiated energy is obtained with

$$E_{GW} = D_L^2 \int d\Omega \int_T F_{GW}(t) dt \quad (1.24)$$

where D_L is the luminosity distance of the source from the detector, Ω is the solid angle and F_{GW} is measured at the detector.

Indirect evidence of existence

In 1993, the physicists Russel Hulse and Joseph Taylor has been awarded the Nobel Prize in Physics for their experimental observations in 1974. These observations consisted in following the evolution of the orbit of the binary pulsar PSR1913+16 as shown in Figure 1.11 [51, 52]. This system is composed of two neutron stars, of which one is a pulsar and the other is dark, bound in an orbit with period $P \sim 7hr45min$.

Hulse and Taylor used their timing measurements of the pulses to infer the details of the orbital motion. The number of pulses received each second increases when the pulsar is moving towards us and is close to its periastron and vice-versa. These observations of the pulse emitted by the pulsar evidenced the orbital decay $dP/dt < 0$ of the binary (about 40 seconds over 30 years). This implies that the system loses energy.

The measured decay is in remarkably close agreement ($\sim 0.2\%$) [52] with the predictions of General Relativity assuming that the system essentially loses energy by radiating GW away. This provided an indirect evidence for the existence of GW.

Since the discovery of PSR1913+16, other binary pulsars have been detected which includes PSR B1534+12 and PSR J0737-3039A/B [53]. All those newly discovered systems exhibit the same orbital decay as PSR1913+16.

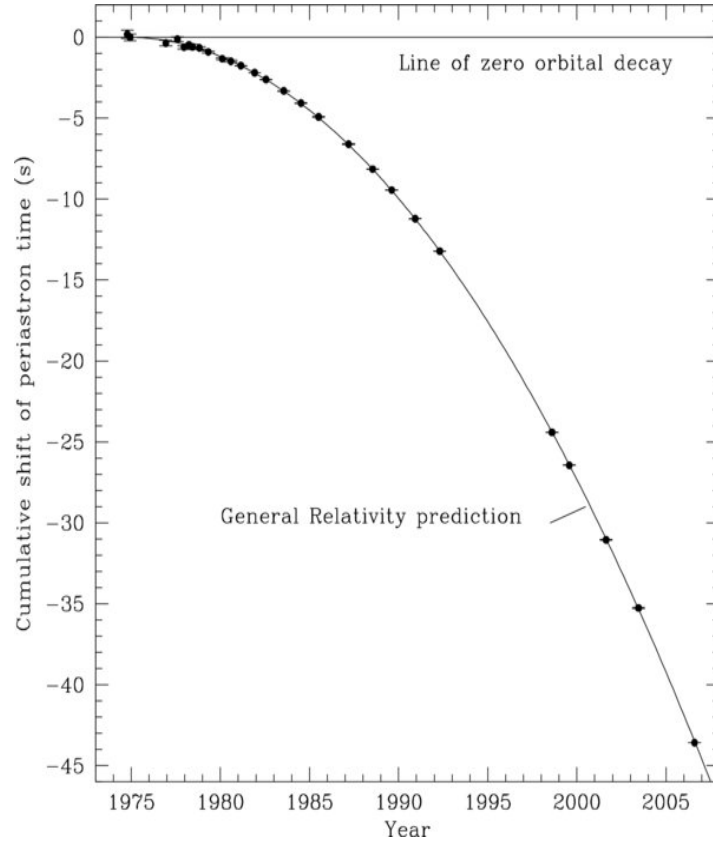


Figure 1.11 – Cumulative shift of the periastron time for PSR 1913+16 from 1975 to 2007. The continuous curve shows the predictions from the General Relativity. The observations are shown with as points with measurement error bars.

1.2.3 Astrophysical sources of gravitational waves

Astrophysical sources of gravitational radiation can be divided into two categories: *permanent* and *transient* sources.

Permanent sources includes *periodic sources* and *stochastic backgrounds*. We refer to periodic sources as sources that emit periodic GW continuously. They are related to isolated rotating neutron stars with some degree of asymmetry (characterized by the ellipticity of the star) that may be due to accretion or pressure from internal magnetic fields for instance. If there is a sufficient degree of asymmetry, such a system is expected to emit a monochromatic GW at twice the rotation period. The wave amplitude is weak (much lower than the noise floor of current detectors). However, since it is permanent, it can be integrated over a long duration. Stochastic GW backgrounds can have an astrophysical or a cosmological origin. Astrophysical backgrounds result from the incoherent superposition of many GW from unresolved faint sources located in the Galaxy or in the nearby Universe. Current cosmological models also predict the existence

of a relic stochastic background from the very early phase of the Universe history. Both types of backgrounds are stochastic GW signals and require at least two detectors in operation to be detected (by the measurement of an excess of correlation).

This thesis focuses on transient sources as they are potentially connected to the emission of high-energy neutrinos. This section discusses into more detail the potential astrophysical sources of transient GW.

Coalescing compact binaries

A large fraction of stars are in binary systems. If both components of the binary end up forming compact bodies (neutron star or black hole) and if their orbit is sufficient tight, the resulting system will eventually coalesce after losing a considerable amount of energy through GW emission. The coalesce of neutron-star and/or black-hole binaries similar to the Hulse-Taylor binary mentioned previously is often considered the most promising source.

During the inspiralling phase where the two bodies are far apart, the dynamics of such a system (and hence the expected GW waveform) can be predicted with great accuracy by using post-Newtonian expansions [54, 55].

The GW signature consists in a *chirp* signal whose frequency sweeps toward high values according to a power law at first order (see Figure 1.12). A substantial amount of energy is radiated in the following phase when the two bodies merge into a black-hole. In this highly relativistic phase, the perturbative treatment of binary dynamics is not valid anymore and one has to resort to numerical simulations. The process is concluded by the ring-down phase during which the resulting distorted black-hole radiates away its asymmetry down to equilibrium.

During the whole coalescence process, a stellar-mass binary with equal masses radiates away of the order of a percent of its rest mass [56]. This corresponds to a GW amplitude of $h \sim 10^{-21}$ observable at Earth for a system located at 10 Mpc as estimated above in section 1.2.2. More precise estimates of the detectability horizon can be obtained: GW detectors can ideally observe those binary systems up to a distance of ~ 30 Mpc and ~ 440 Mpc for initial and advanced detectors respectively.

Although binary systems are fairly common, only a small fraction eventually forms a compact binary that is sufficiently tight to coalesce in less than the Hubble time. A survey of population estimates [57] gives a “realistic” rate of one neutron star–neutron star coalescence² per 10,000 year per galaxy equivalent in size to the Milky Way. When converted into a rate of *detectable* coalescences, the above horizons lead to ~ 0.02 events per year with the first generation of (initial) detectors and to ~ 40 events for the second generation (advanced). Large

²Similar rates are obtained for the other types of systems mixing neutron-stars and/or black-holes.

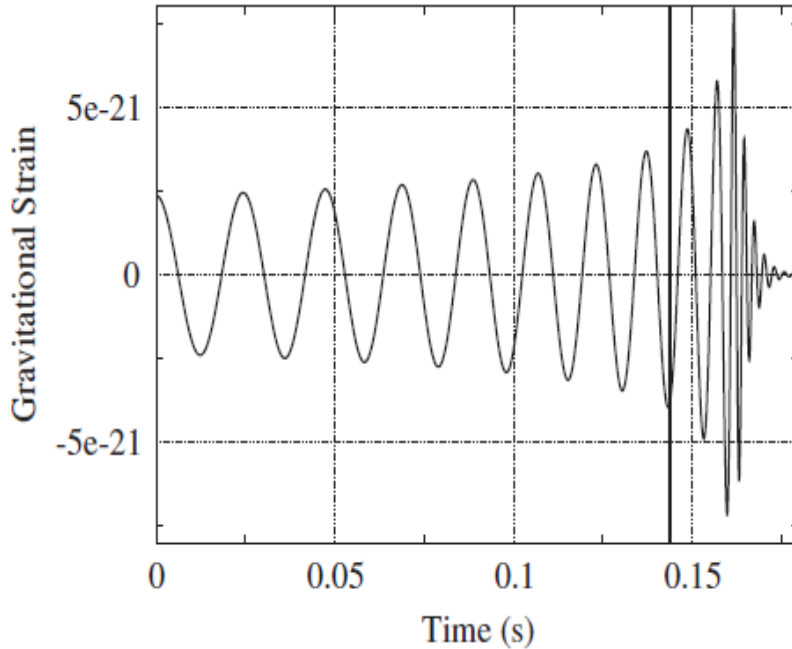


Figure 1.12 – Example of a GW chirp waveform from coalescing compact binaries.

error bars are attached to those estimates reflecting the weakness of the observation constraints we have about those systems. The above stated rates can be 10 times smaller or larger in the “pessimistic” or “optimistic” scenarios respectively.

It is suspected that binary coalescences could be the progenitors of at least a fraction of the short-hard gamma-ray bursts. The “realistic” rates presented above are corroborated by the ones derived from that assumption [57].

Core collapse supernova

Gravitational stellar-core collapse is another potential source of GW if some degree of non-axisymmetry is exhibited during this process. The simulations required to make reliable predictions of the emission levels are very challenging as they have to incorporate many physical ingredients including relativistic magneto-hydrodynamics and a detailed treatment of neutrino transport and nuclear iterations [58]. The current realistic estimate of the amount of radiated GW energy is of order $10^{-7}M_{\odot}$ and corresponds approximately [59] to a distance reach of order ~ 10 kpc with the initial detectors, ~ 100 kpc with the advanced detectors. The detectable sources are therefore located in the Galaxy.

A few mechanisms have been suggested in which GW emission associated with gravitational core-collapses is enhanced. This is connected to the collapse of very massive star associated with high rotation rate possibly due to accretion. In that case, bar or fragmentation instabilities

1.1.3 Joint sources of gravitational waves and high-energy neutrinos

[60, 61] may lead to the emission of order $10^{-2}M_{\odot}$ in GW, leading to similar detectability horizons as the coalescing binaries of neutron-stars. This astrophysical scenario may also be at the heart of long-soft GRB.

Star quakes

Several observations indicate that neutron stars may experiment large stress during the course of their life. Although “ordinary” neutron stars are characterized by extremely strong surface magnetic fields ($\sim 10^{12}$ G), many magnetars appear to have fields 100-1000 times stronger, implying enormous pent-up magnetic energy. Soft gamma ray repeaters (SGRs) and anomalous X-ray pulsars (AXPs) are different observational manifestations of the same underlying system with a highly magnetized star which sporadically converts magnetic field energy into radiation [62].

The sudden release of the magnetic energy may also excite to some extent the fundamental or f -modes of the star, which radiate GW with damping times of ~ 200 ms.

Detailed predictions about the GW amplitude are difficult to obtain. An upper-limit of $\sim 10^{49}$ erg on the maximum *total* energy release in an SGR giant flare can be derived from one of the most optimistic models (see [63]), of a giant flare associated with a global reconfiguration of the internal magnetic field. Similarly, [64] estimated a maximum total energy release of $\sim 10^{48}$ - 10^{49} ergs in a fraction of the parameter space, within the model originally proposed by [63].

1.3 Joint sources of gravitational waves and high-energy neutrinos

In the previous sections, we described models for the single production of GWs or HENs. In this section, we discuss plausible sources of both GW and HEN emissions. We will see that some of the scenarios leading to joint emissions are tightly connected to gamma-ray bursts (GRBs) [65].

GW emission requires relativistic bulk motion of massive objects such as gravitational collapse or merger of compact objects. Production of HEN requires the formation of a fireball and ejection of relativistic particles with some hadronic load. These two requirements restricts the wide range of sources presented so far. The list of plausible sources gives a global and coherent picture of the astrophysical scenarios from both GW and HEN perspectives. When applicable, we will also mention their connection to observations in the electromagnetic spectrum. Note however, that will be especially interested in the sources that are *not* observed electromagnet-

ically. This may be due to the source opacity (which often arises in the dense media considered here). This may be also due to observational limitations. For instance, a significant fraction of GRBs are missed by current observatories. Swift/BAT and Fermi/GBM miss about 90 % and 40 % of all GRBs respectively. This is due to the limited fields of view, technical downtime, and orbital passes through the South Atlantic Anomaly.

1.3.1 Core-collapse supernovae with mildly relativistic jet

One of the promising sources are core-collapse supernovae (CCSN) with mildly relativistic jet [66]. There are evidence for the existence of such jets, observed in radio [67].

The HEN emission for this source is somewhat related to the fireball model for (long) GRB presented in section 1.9. In this model, a jet of plasma is ejected at relativistic velocity. Relying on the assumption that protons are accelerated in the jet through Fermi acceleration in internal shocks, pp and $p\gamma$ interactions will produce kaons (K) and pions (π). In these two interactions (non-thermal) neutrinos of TeV energy can be produced through the decay of charged pions and kaons [66, 68]. The charged π^\pm and K^\pm are expected to follow the proton spectrum falling as E^{-2} . About 20% of the proton energy is converted into the produced neutrinos. An ejected mass with a kinetic energy of 3×10^{51} erg and a Lorentz factor of 3 at 10 Mpc would generate ~ 30 neutrino events detected in a km^3 detector [68] which translates to order of few events in ANTARES.

GW emission associated to the gravitational collapse of massive star was already discussed in section 1.2.3. We mentioned that the presence of a high rotation rate (due to accretion for instance) may develop bar-mode instability thus leading to enhanced GW emission. [69] quote upper limits of $P_{max} = 10^{53}$ erg/s at $f = 1$ kHz. If the bar remains coherent for ~ 100 cycles, this conducts to a GW emitted energy of order $10^{-2}M_\odot$. Under the (unlikely) assumption of extreme rotation, [70] predicts the formation of fragments ($< 1M_\odot$) leading to the emission of an inspiral-like GW chirp. If we estimate that order of one percent of the rest-mass is emitted during merger, we again get a GW emitted energy of order $10^{-2}M_\odot$, this time at frequencies of few hundred Hz.

If core collapse supernovae may lead to significant GW and HEN emission, they may also be faint or undetectable electromagnetically. Mildly relativistic jets might not be powerful enough to break out the star hydrogen envelope [68]. This is usually referred to as the “choked GRB” model. Without an emerging jet, the X-ray, optical, IR, and radio afterglows typical of GRB would also be absent. Also, core collapse of massive star may not lead systematically to SN shock breakout. For instance, some of the nearby GRBs (e.g., GRB060505 or GRB060614) miss a supernova. Even if the process succeeds in yielding a supernova, it may not be observable.

1.1.3 Joint sources of gravitational waves and high-energy neutrinos

A significant fraction (up to 15 % with 10 Mpc) of supernovae are missed optically in the local Universe because of selection effects and dust extinction.

Choked GRBs may be at the extreme end of a (potentially large) local population of faint long-soft GRBs. A subclass of GRBs with luminosities lower by a few orders of magnitude than typical luminosities has been identified. Less luminous than typical long GRBs, “low-luminosity GRBs”, are discovered at much smaller distances (SN 1998bw at redshift $z = 0.0085$, about 40 Mpc away from Earth, SN 2003lw at $z = 0.105$, and SN 2006aj at $z = 0.033$). The event rate per unit volume of those type of events has been estimated to be more than one order of magnitude larger than that of conventional long GRBs.

1.3.2 Other sources

Short-hard GRBs are thought to be driven by NS–NS or NS–BH mergers [71, 72]. As discussed in section 1.2.3, coalescing binaries are expected to emit GWs that are detectable to large distances ([73, 74]), ~ 30 Mpc with the initial versions of LIGO and Virgo. Much less is known about the HEN emission from those systems. If the binary merger is associated to a GRB, this implies the presence of an ultrarelativistic jet. If there is significant baryon loading in the jet, this should eventually conduct to the production of HEN.

Other potential galactic sources of GW+HEN joint emission can be considered in this work. Such sources are Soft Gamma Repeaters (SGRs) which are X-ray pulsars with soft gamma-ray bursting activity. According to the magnetar model, SGRs may be associated with star-quakes. The deformation of the star during the outburst could produce GWs (see section 1.2.3), while HENs could potentially emerge from hadron-loaded flares (see section 1.1.4).

A more exotic class of sources are cosmic strings, topological defects formed during phase transitions in the early Universe. Emission of gravitational waves is considered the main channel for cosmic string loops to decay. In particular, cosmic string cusps appear to be potential sources of gravitational waves due to the very large Lorentz factor achieved when they contract. Cosmic strings and topological defects in general are also of interest to high energy neutrino astronomy as they can produce particles, including neutrinos, up to the Planck scale [75].

1.3.3 Time delay between gravitational wave and high-energy neutrino emissions

The scenarios evoked in the previous sections are connected to GRBs. GRBs provide an interesting astrophysical scenario where the delay between GW and HEN emissions can be characterized. A conservative estimate of this delay determines the baseline duration over which GW and HEN are declared in coincidence. A statistical estimate has been obtained in [76] based

on GRBs mainly observed by BATSE, Swift and Fermi LAT. In this article, we considered the duration of the different emission processes to constrain the size of the time search window. Figure 1.13 summarizes the assumptions and modelling of [76]. This leads to an upper bound on the size of $\Delta t_{GW+HEN} = [-500s, +500s]$ the time search window. The latter is conservative enough to encompass most theoretical models of GW and HEN emissions for GRBs. This time window will be used in both analyses presented in this work, see Chapters 4 and 5 for further details.

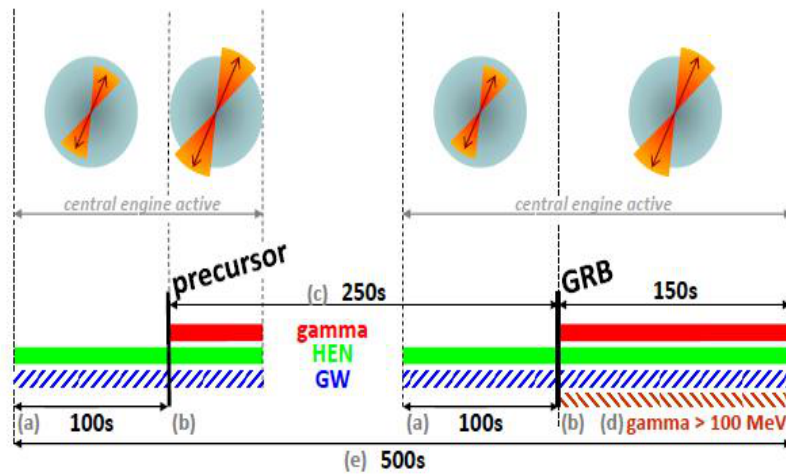


Figure 1.13 – Overview of the GRB emission processes and GW/HEN time search window. (a) Active central engine before the relativistic jet has broken out of star; (b) Active central engine with relativistic jet broken out of star; (c) Delay between onset of precursor and main burst; (d) Duration corresponding to 90% of GeV photon emission; (e) Time span of central engine activity. Possible GW/HEN emission between the precursor and the main GRB (no emission is shown on the figure) has no effect on the estimated time window. Overall, the considered processes allow for a maximum of 500s between the observation of a HEN and a GW transient, setting the time search window to $[-500s; 500s]$. (Adapted from [76])

REFERENCES

- [1] E. FERMI, Z. Phys. 88 (1934) and Nuovo Cim. 11 (1934). 7
- [2] C.L COWEN ET AL, Science, 124, 103 (1956). 7
- [3] G. DANBY ET AL, Phys. Rev. Lett. 9, 36, (1962); 7
- [4] M. L. PERL ET AL, Phys. Rev. Lett 35, 1489, (1975). 8
- [5] K. KODAMA ET AL, Phys. Lett. B, 504, 218-224, (2001). 8
- [6] B.T. CLEVELAND ET AL., Astrop. Jour. 496 505 (1998). 8
- [7] J. N. BAHCALL AND R. DAVIS, PASP, 112, 770, 429-433, (2000). 8
- [8] THE KAMIOKANDE II COLLABORATION, Phys. Rev. Lett. 58 1490 (1987) and Phys. Rev. D38 448 (1988). 8
- [9] M. S. LONGAIR, newblock High-energy astrophysics, Cambridge University Press (2011). 9
- [10] J. BERINGER ET AL, Phys. Rev. D86, 010001 (2012). 10, 13, 14
- [11] K. GREISEN, Phys. Rev. Lett. 16, 748 (1966). 11
- [12] G. T. ZATSEPIN AND V. A. KUZMIN, JETP Lett. 4, 78 (1966). 11
- [13] J. ABRAHAM ET AL, Phys. Rev. Lett. 104:091101, (2010). 12
- [14] E. WAXMAN, NIM A 827, 15c-25c (2009). 13
- [15] D. ALLARD, e-Print: arXiv:1111.3290 (2011). 14
- [16] G. DECERPRIT, D. ALLARD, A&A, 535, A66 (2011). 14
- [17] E. WAXMAN AND J. N. BAHCALL, Phys. Rev. D 59 023002 (1999). 16

REFERENCES

- [18] K. MANNHEIM, R.J. PROTHEROE AND J.P. RACHEN, Phys. Rev. D 63 (2001). 16
- [19] <http://www.mpi-hd.mpg.de/hfm/HESS/>. 17
- [20] <http://fermi.gsfc.nasa.gov/> 17
- [21] W. BEDNAREK ET AL, New Astron. Rev. 49 (2005). 18
- [22] A. LEVINSON AND E. WAXMAN, Phys. Rev. Lett., 87, 171101 (2001). 19
- [23] C. DISTEFANO, Astrophys. J., 575:378-383, (2002). 19
- [24] S. GALATA, PhD thesis, Université Aix-Marseille (2012). 19
- [25] W. BEDNAREK, Astrophys. J. 631 466 (2005). 19
- [26] H. R. CHRISTIANSEN ET AL, Phys. Rev. D73, 063012, (2006). 19
- [27] D. EICHLER, MNRAS, 335, 883, (2003). 20
- [28] F. AHARONIAN ET AL, Astron. Astrophys. 425 13-17, (2004). 20
- [29] F. AHARONIAN ET AL, Nature 439 695 (2006). 20
- [30] F. AHARONIAN, ET AL, A&A 448, L43 (2006). 21
- [31] D. HORNS ET AL, A&A 451, L51-L54 (2006). 21
- [32] C. HAZARD ET AL, Nature 197 1037-1039 (1963). 21
- [33] F. HALZEN, astro-ph/0506248 (2005). 22
- [34] J. ABRAHAM ET AL, Science 318, 938-943 (2007). 21
- [35] F. AHARONIAN ET AL, Nature 440, 1018 (2006). 21
- [36] W. BENBOW ET AL, Proceedings of the 30th ICRC, Merida, Mexique, (2007). 22
- [37] A. LOEB AND E. WAXMAN, JCAP 0605 003 (2006). 23
- [38] W. S. PACIESAS ET AL, Astrophys. J. Supp., 122, 465-495, (1999). 23
- [39] E. COSTA ET AL, Nature, 387, 783-785, (1997). 23
- [40] T. PIRAN, Rev. Mod. Phys. 76, 1143-1210, 2004. 23
- [41] E. WAXMAN AND J. N. BAHCALL, Astrophys. J., 541, 707-711, (2000). 24
- [42] A. LEVINSON AND D. EICHLER, Astrophys. J., 594, L19-L22, (2003). 24
- [43] R. ABBASI ET AL, Nature 484 351-354 (2012). 24

-
- [44] E. WAXMAN AND J. N. BAHCALL, Phys. Rev. Lett 78, 2292-2295, (1997). 25
- [45] J. N. BAHCALL AND E. WAXMAN, Phys. Rev. D64, 023002 (2001). 25
- [46] PARTICLE DATA GROUP, Phys. Let. B 592 1 (2004). 26
- [47] F. ZWICKY, Helv. Phys. Acta, 6-110 (1933). 26
- [48] G. LIM, PhD thesis, University of Amsterdam (2012). 27
- [49] J. WHEELER, K. FORD, newblock Geons, Black Holes, & Quantum Foam: a life in physics, W. W. Norton, New York, (1998). 27
- [50] M. MAGGIORE, newblock Gravitational Waves Volume 1. Theory and Experiments, Oxford University Press, (2007). 30
- [51] R. A. HULSE J. H. TAYLOR, Astrophys. J., 195, L51-L53 (1975). 31
- [52] J. M. WEISBERG, D. J. NICE, AND J. H. TAYLOR, Astrophys. J. 722, 1030-1034 (2010). 31
- [53] , <http://arxiv.org/abs/astro-ph/0609417>. 31
- [54] L. BLANCHET, Living Rev. Relat., 5 (2002). 33
- [55] A. BUONANNO ET AL, Phys. Rev. D75, 124018 (2002). 33
- [56] B. S. SATHYAPRAKASH AND B. F. SCHUTZ, Living Rev. Relat, 12 (2009). 33
- [57] J. ABADIE ET AL, Class. Quantum Grav., 27, 173001 (2010). 33, 34
- [58] C. D. OTT, Class. Quantum Grav., 27, 063001 (2009). 34
- [59] P. SUTTON, LSC Technical Paper, P1000041 (2010). 34
- [60] L. F. CHRIS AND C.B. N. KIMBERLY, Living Rev. Relat., 14, 1 (2011). 35
- [61] M. B. DAVIES ET AL., Astrophys. J., 579 L63, (2002). 35
- [62] V. M. KASPI, Proc. Nat. Acad. Sci. 107, 7147 (2010). 35
- [63] K. IOKA, MNRAS, 327, 639-662 (2001). 35
- [64] A. CORSI AND J. B. OWEN, Phys. Rev. D83, 104014 (2011). 35
- [65] S. ANDO ET AL, submitted to Rev. Mod. Phys. arXiv:1203.5192. 35
- [66] S. RAZZAQUE ET AL, Mod. Phys. Lett., 20, A2351 (2005). 36
- [67] Z. PARAGI ET AL, Nature 463, 516-518 (2010). 36

REFERENCES

- [68] S. ANDO AND J. F. BEACOM, *Phys. Rev. Lett.*, 95, 061103 (2005). [36](#)
- [69] C. FRYER AND K. NEW, *Living Rev. Relat.*, 14, 1 (2011). [36](#)
- [70] M. DAVIES ET AL, *Astrophys. J.*, 579, L63 (2002). [36](#)
- [71] W. H. LEE, AND E. RAMIREZ-RUIZ, *New J. Phys.*, 9, (2007). [37](#)
- [72] Z. B. ETIENNE ET AL., *Phys. Rev. D*79, 044024 (2009). [37](#)
- [73] É. É. FLANAGAN AND S. A. HUGHES, *Phys. Rev. D*57, 4535-4565 (1998). [37](#)
- [74] S. KOBAYASHI AND P. MÉSZÁROS, *Astrophys. J.*, 589, 861-870, (2003). [37](#)
- [75] T. DAMOUR AND A. VILENKIN, *Phys. Rev. Lett.* 85, 3761-3764 (2000). [37](#)
- [76] B. BRUNY ET AL, *Astropart. Phys.*, 35, 1-7 (2011). [37](#), [38](#)

CHAPTER 2

NEUTRINO TELESCOPES

2.1 Summary

With the advent of a new generation of observatories including the ANTARES neutrino telescope observational astrophysics is entering a new era. The ANTARES neutrino telescope gives access to new and unexplored observations of the Universe complementary to the standard photon-based astronomy. This chapter gives an introduction to the neutrino astronomy from an instrumental point-of-view ranging from the general detection principles to the description of the instruments currently in operation. We focus in the most part of this chapter on the ANTARES instrument.

2.2 Neutrino telescopes

2.2.1 General principles

The detection rate $T(E_{\min}, \theta)$ of charged leptons l (e, μ, τ) produced by neutrino interactions around the detector can be obtained by convoluting the incoming neutrino flux dN/dE_ν and the detection probability of these neutrinos:

$$T(E_{\min}, \theta) = \int_{E_{\min}} P_{\nu \rightarrow l}(E_\nu, E_{\min}) P_{\text{trans}}(\theta, E_\nu) \frac{dN}{dE_\nu} dE_\nu \quad (2.1)$$

where $P_{\text{trans}}(\theta, E_\nu)$ is the transmissivity coefficient of a neutrino through the Earth and $P_{\nu \rightarrow l}(E_\nu, E_{\min})$ is the probability that a neutrino of energy E_ν creates a detectable lepton of energy greater or equal to E_{\min} . This latter probability can be written as :

$$P_{\nu \rightarrow l} = \mathcal{N} \int_{E_{\min}}^{E_\nu} dE_l \frac{d\sigma}{dE_l} R_l(E_l, E_{\min}) \quad (2.2)$$

CHAPTER 2. NEUTRINO TELESCOPES

where \mathcal{N} is the Avogadro number, $\frac{d\sigma}{dE_l}$ is the interaction cross section as a function of the neutrino energy and $R_l(E_l, E_{min})$ is the path length of the produced lepton. In the case of a muon ($l = \mu$), this distance can be much greater than the detector size, contrarily to electrons and τ which are respectively absorbed or quickly desintegrated. This explains why the detection of muon neutrinos is favoured over the other flavors ("golden" channel). However, neutrino telescopes are also sensitive to electron and tau neutrinos and can in principle discriminate between flavors: tau-neutrino with energies $\geq 1PeV$ can indeed travel several meters before decaying producing a second shower, while electron-neutrino yields an electron which produces an electromagnetic shower.

In the following, we will concentrate on muon neutrino interactions and describe into more details the different terms of relation 2.2.

2.2.2 Neutrino interactions

After penetrating the Earth, the neutrino is subject to interactions with electrons and nuclei of atoms and molecules that constitute the rock, the sea or the ice. Neutrinos interact through only the weak interaction and have a small cross section ($10^{-38}cm^2$ at 1 GeV) [1]. Interactions at higher energy ($E_\nu > 10GeV$) are dominated by deep inelastic scattering onto atomic nuclei. When they interact, neutrinos are subject to two main ¹ interaction processes: charged current (CC) interaction or neutral current (NC) interaction. While the former consists in an exchange of charged boson W^\pm , the second involves the exchange of a neutral boson Z^0 (see Figure 2.1 for illustration):

$$\begin{aligned}\nu_l(\bar{\nu}_l) + N &\longrightarrow l^-(l^+) + X \\ \nu_l + N &\longrightarrow \nu_l + X\end{aligned}\tag{2.3}$$

where l stands for any kind of leptons (e, μ, τ), $N \equiv \frac{n+p}{2}$ can be seen, for simplicity, as an isoscalar nucleon and X represents the hadronic products of the interaction. In the following we concentrate on the CC interaction which produces a charged lepton that will be later detected.

The differential cross section of the neutrino for this process can be expressed in terms of the parton distribution functions as follow [2, 3]:

$$\frac{d^2\sigma}{dxdy} = \frac{2G_F^2 M_N E_\nu}{\pi} \left(\frac{M_W^2}{Q^2 + M_W^2} \right)^2 [xq(Q^2, x) + x\bar{q}(Q^2, x)(1-y)^2]\tag{2.4}$$

where:

¹we will not treat here the Glashow resonance $\bar{\nu}_e \rightarrow W \rightarrow X$

- G_F is the Fermi constant.
- Q is the invariant momentum transfer.
- M_N and M_W are the nucleon and the intermediate-boson masses.
- $\nu = E_\nu - E_l$ is the fraction of energy carried by the boson in the laboratory frame.
- $x = \frac{Q^2}{2M_N\nu}$ and $y = \frac{\nu}{E_\nu}$ are the Bjorken scaling factors.
- $q(Q^2, x)$ and $\bar{q}(Q^2, x)$ represent the parton distribution functions (PDFs) describing the quark and anti-quark content of nucleon.

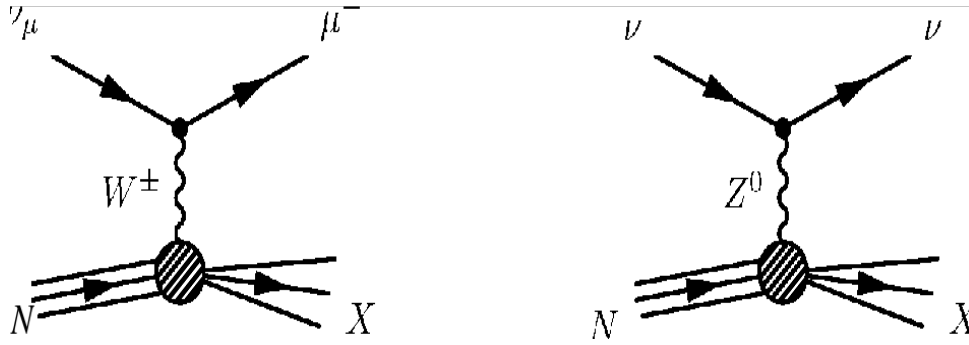


Figure 2.1 – Feynman diagram representation of the CC (left) and NC (right) interactions

Figure 2.2 left and right show the cross section of the ν and $\bar{\nu}$ interaction respectively. At energies $E_\nu > 10\text{GeV}$ the cross section increases linearly with energy while it follows a $\sigma \propto E_\nu^{0.4}$ relation at energies $E_\nu > 1\text{PeV}$. These different regimes arise from the non negligible value of Q^2 at high energy with respect to the mass propagator.

For muon neutrino interactions, the angle between the direction of the initial neutrino and the out-going muon in the charged-current channel is very small, the muon track and the parent neutrino are almost collinear. The angular difference between the direction of the primary ν_μ and the induced μ can be approximated by [4]:

$$\langle \theta_{\mu\nu} \rangle \approx \frac{0.7^\circ}{(E_\nu/\text{TeV})^{0.6}} \quad (2.5)$$

During the propagation in the medium the muon track is further deflected as the muon undergoes multiple scattering. The mean angular deviation between the initial muon direction and

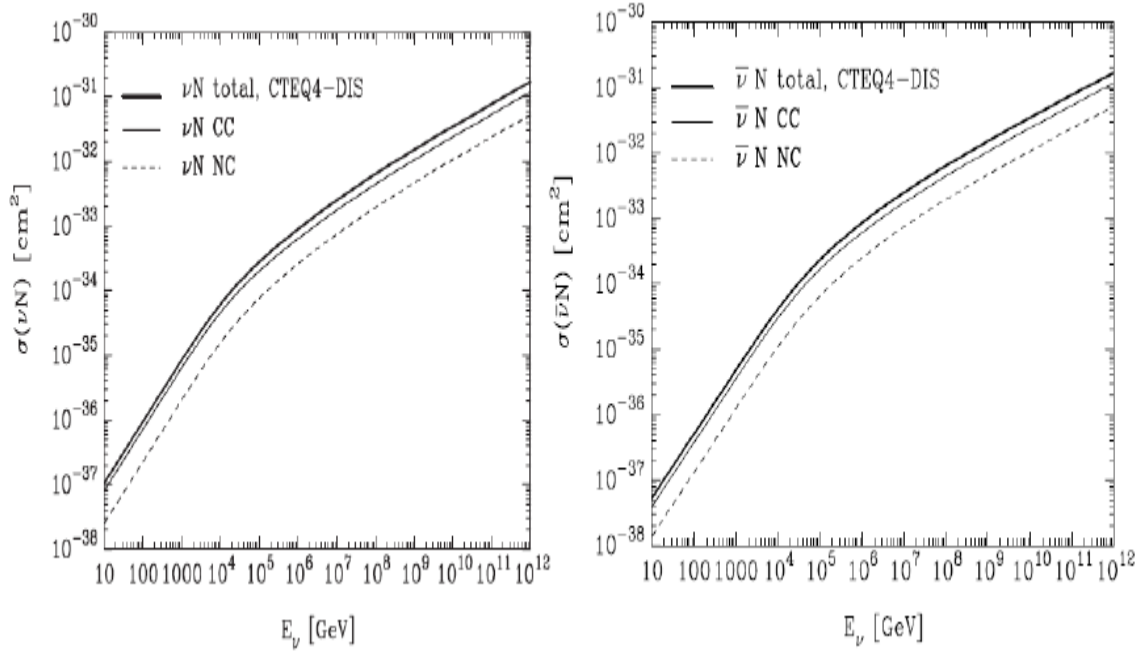


Figure 2.2 – The ν - N (left) and the $\bar{\nu}$ - N (right) cross section interaction as function of the energy

the direction after passing a distance x in the medium is described by [5]:

$$\Delta\theta_{ms} = \frac{13.6 \text{ MeV}}{E_\mu} z \sqrt{\frac{x}{X_0}} \left[1 + 0.038 \ln \left(\frac{x}{X_0} \right) \right] \quad (2.6)$$

where X_0 is the radiation length² of the medium and $\Delta\theta_{ms}$ is given in radians and z is the charge number of the incident particle. The deviations due to the multiple scattering described by Equation (2.6) are generally smaller than the scattering angle in Equation (2.5). Therefore this allows the produced muon to somewhat preserve the original direction of the muon-neutrino. Indeed for neutrino energies larger than 1 TeV, the muon track is aligned with the incident neutrino within a degree. At higher energies ($\geq 10 \text{ TeV}$) the kinematics effects start to be negligible and the biggest uncertainty in the direction estimation comes from the calibration (timing and positioning) of the detector (see section 2.3.6).

2.2.3 Propagation of the neutrinos in the Earth

At high energies, as the cross section increases, neutrinos can be absorbed. Typically, the Earth becomes opaque to neutrinos at 70 TeV where the interaction length becomes comparable to the diameter of the Earth.

²For hadronic projectiles, the strong interactions also contribute to multiple scattering.

To quantify this effect, we take into account the profile of the earth density shown in Figure 2.3 [2]. Using this profile, 10 different layers whose density depends on the distance from the centre of the Earth are considered. The probability of a neutrino traveling a distance L (referred to as transmissivity coefficient Equation (2.2)), not to be absorbed, can be written in units of water-equivalent-length as:

$$P_{trans}(L) = e^{-\frac{L(\theta)}{\lambda}} \quad (2.7)$$

where $\lambda = 1/(\mathcal{N}\sigma_{tot})$ is the free mean path taking into account the total cross section. Figure 2.4 shows the absorption coefficient $(1 - P_{trans})$ as a function of energy and zenith angle in the Earth. These plots show that the absorption for neutrinos crossing horizontally a small amount of matter is negligible. Thus high energy neutrino telescopes are sensitive to high energy neutrinos ($> PeV$) mostly in that directions.

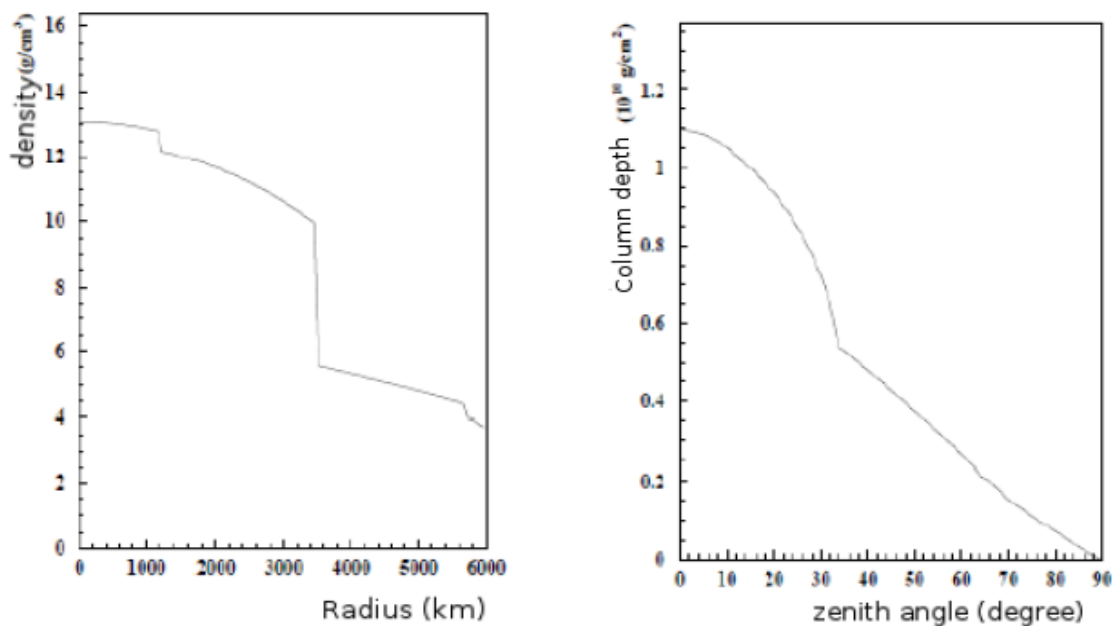


Figure 2.3 – Left: Density profile of the Earth according to the Preliminary Earth Model. Right: Thickness of the Earth as a function of the angle of incidence of the incoming neutrinos

2.2.4 Propagation of the muons in water and rocks

Depending on their energy and during their propagation in water or rock, muons lose energy due to various processes (see Figure 2.5). For $E_\mu < 1$ TeV the dominant process is the ionization, which can be described as a continuous process. At higher energies, muon lose their energy via stochastic phenomena such as bremsstrahlung, pair production and photonuclear interactions.

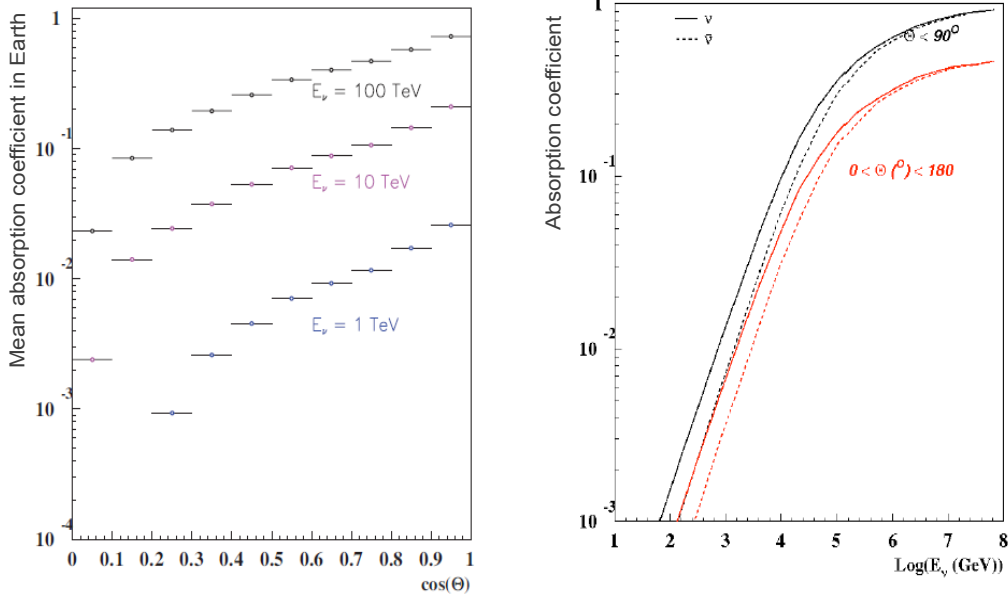


Figure 2.4 – Left: Mean absorption effect on neutrinos of energies: 1, 10 and 100 TeV as a function of the zenith angle θ_ν . Right: Absorption coefficient for upgoing neutrinos (black) and for the two hemisphere (red) as function of energy

- **Ionisation:** The continuous energy loss of muons passing through a medium at relatively low energy transfers to atomic electrons, ionising the material along the muon path. The energy loss is calculated using the Bethe-Bloch formula.
- **Bremsstrahlung:** In the electric field of a nucleus or atomic electrons, muons can radiate high energy photons.
- **Pair Production:** A muon can radiate a virtual photon which, again in the electric field of a nucleus, can convert into a real e^+e^- pair.
- **Photonuclear Interaction:** A muon can radiate a virtual photon which directly interacts with a nucleus in the muon propagation medium. The average energy loss for this process increases almost linearly with energy, and at TeV muon energies constitutes about 10% of the energy loss rate.

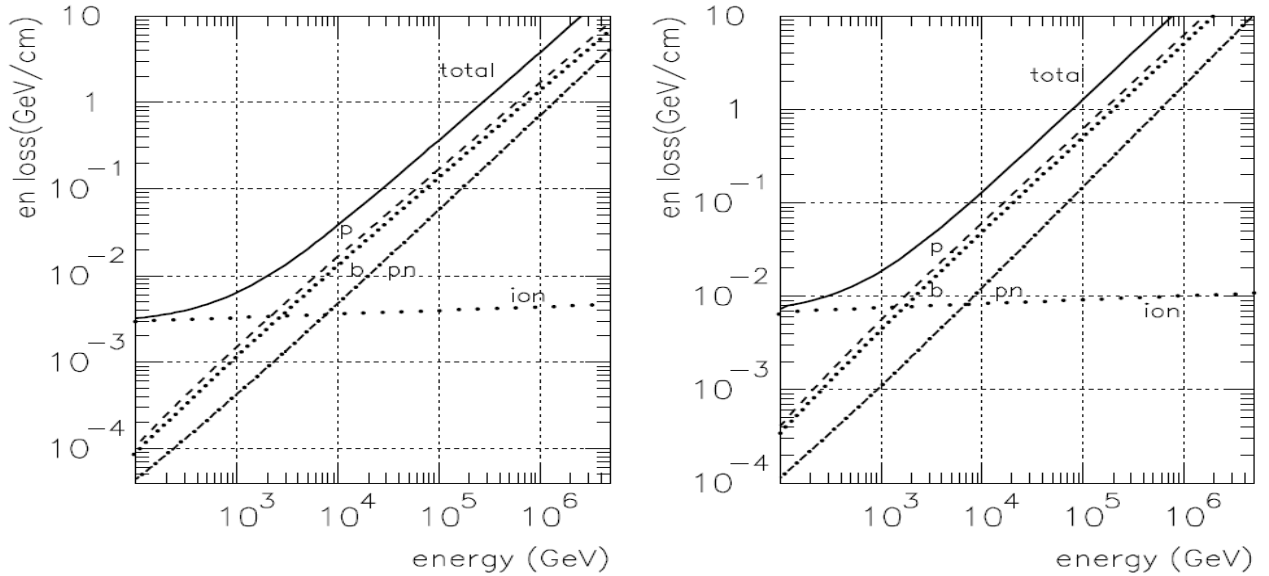


Figure 2.5 – Total and partial energy losses for muons in water (left) and standard rock (right) as a function of muon energy. Total energy loss : solid line; pair production (p): dashed line; bremsstrahlung (b): dotted line; photomuclear interaction (pn): dot-dashes; ionization (ion): large dots

The global contribution of all these processes to the mean energy loss of muons is given by [6]:

$$\left\langle -\frac{dE}{dx} \right\rangle = a(E) + b(E)E \quad (2.8)$$

where E is the total energy, $a(E)$ is the contribution due to ionization and $b(E)$ is due to the radiative processes. Both terms $a(E)$ and $b(E)$ are slowly varying functions of E at high energies. At low energies (<1 TeV) the dominant term comes from the ionization. In the approximation of a and b constant, the mean free path of a muon of energy E_μ until it reaches an energy E_{min} can be written as:

$$R_\mu(E_\mu, E_{min}) = \int_{E_{min}}^{E_\mu} \frac{1}{\left\langle \frac{dE}{dX} \right\rangle} dE \approx \frac{1}{b} \ln \frac{(a/b) + E_\mu}{(a/b) + E_{min}} \quad (2.9)$$

This gives an estimate of the distances which can be travelled by the muons. Nevertheless, in the high energy regime, the stochastic radiative processes enjoin to use Monte Carlo simulations to better reproduce the high energy losses. (see section 2.5).

2.2.5 Detection principle

Neutrino telescopes use sea water or ice as a detection medium to observe cosmic neutrinos. In parallel, these media act as a shield for down going particles of atmospheric origin, since muons

CHAPTER 2. NEUTRINO TELESCOPES

and neutrinos are the only particles able to reach deep underground or underwater. Other atmospheric and cosmic particles have either a short lifetime or a short interaction length and can not survive long in dense media.

A small fraction of the incoming high energy neutrino flux interacts, (following Equation (2.1)), with the nucleons that make up the matter (water, ice and rock) surrounding the detector. The induced muon-neutrino produces a relativistic muon, with a Lorentz factor $\beta > 1/n$. During its propagation, the muon produces an amount of Cherenkov light, see Figure 2.6 [7]. The Cherenkov radiation propagates in a cone whose opening angle θ_c depends on the particle velocity as:

$$\cos\theta_c = \frac{1}{\beta n_{water}} \quad (2.10)$$

with $n_{water} = 1.35$ for a wavelength of 450 nm and $\beta=1$, this formula leads to $\theta_c = 42^\circ$. The emitted number of photons per unit of length x and wavelength λ (Equation (2.11)) increases with frequency [8]:

$$\frac{d^2 N_\gamma}{dx d\lambda} = \frac{2\pi\alpha Z^2}{\lambda^2} \left(1 - \frac{1}{\beta^2 n_{water}^2}\right) \quad (2.11)$$

where α is the fine structure constant, Z the charge of the particle causing the emission and λ the wavelength of the emitted photons. Most part of photons is then produced in the ultraviolet region of the electromagnetic spectrum. Integrating Equation (2.11) between 300 nm and 600 nm, for which Cherenkov light contributes most to the signal from a muon, yields a quantity of $\simeq 350$ photons emitted per centimeter of the track.

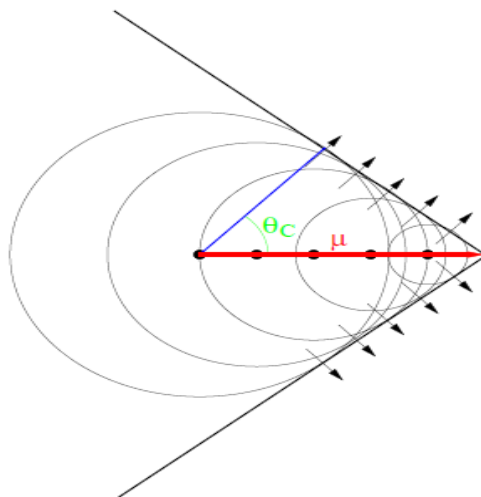


Figure 2.6 – Illustration of the Cherenkov effect. Local distortions of the charge configuration in the medium lead to the emission of electromagnetic waves. Individual contributions along the track (red line) interfere constructively on the envelope which forms a cone. Cherenkov photons (blue line) are emitted under the characteristic angle θ_C .

2.2.6 Overview of the past and current detectors

The BAIKAL neutrino telescope

The BAIKAL experiment [9] is a German-Russian collaboration. The detector is deployed at a depth of about 1km in the Siberian Baikal Lake. The experiment has been running since 1993, when three detection strings were immersed and put into operation. Since 1998 the detector was expanded to 18 strings with a total of 192 optical modules (OMs) (NT-200 detector). The detector is arranged around a central unit with the main electronic block and a calibration laser on the top of the layout that provides the support structures for the 18 strings which are distributed on a circular geometry with a radius of 22 m. Each of the strings measures 68.5 m. This setup was extended in 2005 by three additional strings of 200 m length with 36 PMTs at a distance of 100 m (NT-200+) to the detector center in order to increase the effective area for showers. Compared to neutrino telescopes in deep sea, the Baikal setup offers several advantages. Firstly, the operation in fresh water naturally reduces the background contributions from ^{40}K decays. Secondly, the maintenance of the detector is greatly alleviated by the possibility to use the frozen sea surface as a basis for deployment and recovery operations. The main disadvantages are the reduced absorption length of the water in Lake Baikal and the relatively low depth which leads to a larger atmospheric muon background compared to deep-sea telescopes.

The collaboration published the first limit on the neutrino diffuse flux from the Southern hemisphere using 1038 days of data [10]. The limit $dN/dE < 8.1 \cdot 10^{-7} E^{-2} GeV^{-1} cm^{-2} s^{-1} sr^{-1}$ is obtained in the range of energy $20 TeV \leq E \leq 50 PeV$.

In order to further improve the sensitivity to cosmic signals, the collaboration envisages the enhancement of the telescope towards a Gigaton detector. An R&D and prototyping phase has started in this view.

The Antarctica neutrino telescopes

AMANDA: The AMANDA experiment [11] (Antarctica Muon and Neutrino Detector Array) started in 1990. It is located near the Scott-Amundsen South Pole station in Antarctica Ice. The experiment in its final configuration (AMANDA-II) consists of 19 strings immersed in the glacial ice at a depth ranging from 1500 m to 2000 m, carrying 677 OMs. Each OM is a glass pressure vessel, which contains an 8-inches hemispherical PMT and its electronics. AMANDA-B10, the inner core of 302 OMs placed on 10 strings, has been operating since 1997. The high level of light scattering at that depth limits considerably the performance of the detector. This affects especially the angular resolution that remains above few degrees. The optical

CHAPTER 2. NEUTRINO TELESCOPES

absorption length in the ice is typically 110 m at 400 nm with a strong wave-length dependence. The ice parameters vary strongly with depth due to horizontal ice layers, i.e. variations in the concentration of impurities which reflect past geological events and climate changes.

The AMANDA-II has been switched off early 2009 to allow for the extension to km-scale experiment IceCube. With 7 years of data taking, AMANDA-II collected a statistics of 6595 neutrino candidates and measured the spectrum of atmospheric neutrinos up to energies two orders of magnitude higher than in the previous experiments.

IceCube: The IceCube Neutrino Observatory is the successor of the AMANDA neutrino telescope. Construction of the IceCube Neutrino Observatory began at the geographic South Pole in the 2004-05 austral summer and was completed during the 2010-11 austral summer. IceCube consists of two parts: IceTop, a surface air shower array [12, 13], and IceCube, a muon and neutrino telescope [14] installed deep in the ice. The final configuration consists of 86 strings (IC86) of over 1000m length separated by 125m, with 5800 PMTs. Each string is comprised of light sensors called Digital Optical Modules (DOMs), which detect Cherenkov photons emitted by relativistic charged particles passing through ice. Each DOM is a spherical, pressure-resistant glass shell containing a 25 cm diameter Hamamatsu photomultiplier tube (PMT), a mu-metal grid for magnetic shielding of the PMT, and electronics for operation and control of the PMT as well as amplification, digitization, filtering, and calibration.

Each IceCube string is associated with an IceTop station, which consists of two cylindrical ice Cherenkov tanks separated by 10 m. Each tank has an inner diameter of 1.82 m, is 1.3 m high, and contains two down-facing DOMs, with center-to-center spacing of 58 cm, frozen in optically clear ice 90 cm in depth.

A large amount of data has already been acquired with smaller configurations throughout the installation period (IC22, IC40, IC59, IC79 and IC86), where for example IC22 denotes the 22-string configuration. Using the data from IC40, the atmospheric neutrino spectrum in the northern hemisphere has been measured up to 100 TeV. No point sources have been identified in a set of more than 10^5 neutrino candidates from both hemispheres. Searches for transient sources have set stringent limits on neutrino emission from gamma-ray bursts, and are now accompanied by an extensive neutrino-triggered follow-up program. A very large statistics of cosmic ray events has revealed an anisotropy in the cosmic ray flux at the 10^{-3} level in the 10-100TeV range. While no source of extra-terrestrial neutrinos has been found yet, the physics results obtained so far illustrate the very good performance of the detector.

Some of recent results published by the IceCube collaboration at the moment of writing this thesis can be found in [12, 15–17].

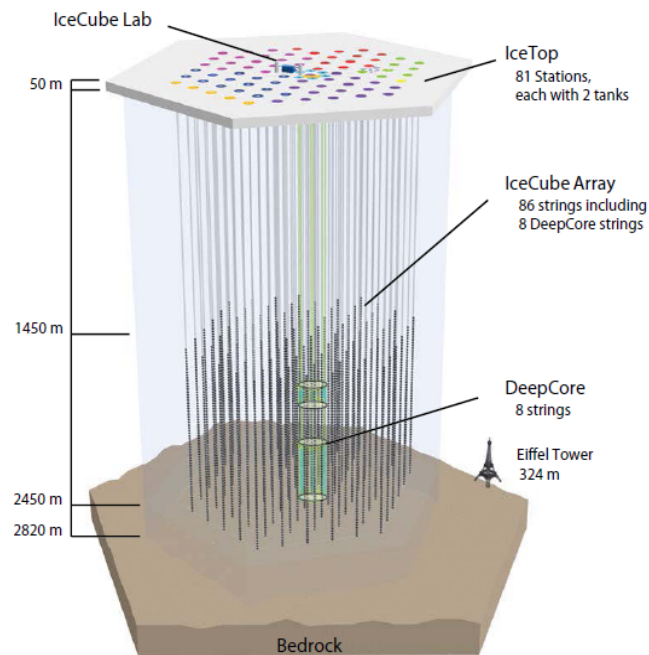


Figure 2.7 – The IceCube detector with its components DeepCore and IceTop in the final configuration (December 2010)

The Mediterranean neutrino telescopes

NESTOR: The Greek NESTOR (Neutrino Extended Submarine Telescope with Oceanographic Research) collaboration [18] initiated the first project for a neutrino telescope in the Mediterranean sea at a site located 18 km off the coast of Pylos at a depth of 4000 m. The chosen telescope design uses tower-like rigid support structures instead of flexible mooring strings. These towers consist of 12 layers made up of six arms each, which are laid out in a star-shaped form. On each of these arms one upward and one downward looking 13" PMT are mounted. A prototype version of a tower storey has been tested in 2003, and first atmospheric muon data were recorded. Some recent results from the NESTOR collaboration are published in [19].

NEMO: The Italian NEMO (Neutrino Mediterranean Observatory) project [20] has focused on research and design studies for a future km-scale detector in the Mediterranean sea. The NEMO design concept features a flexible tower structure of horizontal bars of 15 m length which are connected by ropes. At each end of the bars two PMTs are mounted, one looking downwards, the other one in the horizontal direction. The detection towers can be deployed as a compact object together with a socket and self unfurl in the sea. After the unfolding, adjacent bars are aligned perpendicular to each other. NEMO published results from a sample of data recorded in January 2007 [21].

The KM3NET neutrino telescope: The KM3NeT consortium [22] is a joint effort of the ANTARES (see next section), NEMO and NESTOR collaborations to construct a cost-effective next generation telescope of cubic-km size. The geometry of the detector [23] consists of a three-dimensional array of OMs attached to vertical structures (Detection Units, DUs). An array of DUs constitutes a detector building block. Several building blocks form the full detector of about 300 DUs. A DU, which is anchored to the sea floor and kept upright by a submerged buoy, could consist of horizontal bars equipped with 2 OMs, one at each end. Alternatively, vertical strings with single optical module could be a simpler design. This should be decided by the end of 2012. The DUs will anyway be connected to shore by an electro-optical cable, and the OMs will consist of 31 3-inch PMTs housed inside a 17-inch pressure-resistant glass sphere covering almost a 4π field of view.

2.3 The ANTARES neutrino telescope

The ANTARES neutrino telescope [24] is an underwater neutrino detector deployed in the Mediterranean Sea at a depth of 2500 m offshore from Toulon (France) for a design lifetime of about 10 years. It is the most sensitive high energy neutrino observatory studying the Southern Hemisphere, including the Galactic Center 2/3 of the time. The ANTARES field of view has a sky coverage of 3.5π sr (see Figure 2.8).

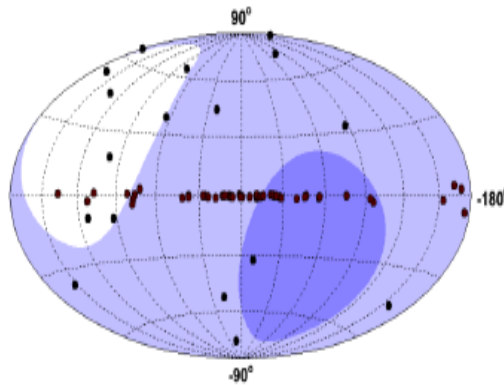


Figure 2.8 – Sky coverage of the ANTARES neutrino telescope. The blue area is seen 100% of the time by ANTARES while it is completely blind to the white area.

The ANTARES neutrino telescope consists of twelve lines with a sensitive area for high energy muons of more than 0.05 km^2 for $E \geq 100 \text{ TeV}$. Its construction started with the installation of the first lines in 2006, and has been completed on May 30, 2008. The full structure is a three-dimensional array of photo-multipliers (PMT). In addition, a special instrumentation

line (IL), mostly dedicated to environmental studies, was put in operation in January 2008. This makes of the ANTARES detector an interesting observatory for Earth science, oceanographic and acoustic studies. The ANTARES Collaboration is a joint effort of about 29 laboratories from 8 countries (France, Germany, Italy, Morocco, the Netherlands, Romania, Russia and Spain).

2.3.1 Detector design

A detailed description of the ANTARES neutrino telescope is given in [24]. The basic elements of the detector are the optical modules (OMs). The later is the assembly of a pressure resistant glass sphere of diameter 43 cm housing a photomultiplier tube and the electronics needed to provide the necessary high voltage [25]. An exhaustive study of PMTs was carried out during the R&D phase, started in 1990, which led to the selection of the 10" Hamamatsu R7081-20 model. Three OMs make up a floor and five floors are grouped to form a sector. One string comprises five sectors.

The layout of the detector consists in a 3-dimensional array of optical modules (OMs) supported by flexible vertical strings anchored to the seabed with the Bottom String Socket (BSS) and are held vertical by a buoy at the top. A schematic overview of the detector string is shown in Figure 2.9. The PMTs are oriented downwards with an angle of 45° below the equator. This orientation gives high efficiency for tracks between upward vertical and horizontal directions, and minimize the effects due to the biofouling. The latter is caused by the adhesion of microorganisms, mostly bacteria, on the external surface.

The detector is operating since 2008 in its complete configuration of 12 strings with 25 floors (75 OMs by string). Eleven strings have a nominal configuration while the twelfth string is equipped with 20 storeys and completed by devices dedicated to acoustic detection. Thus, the total number of the OMs installed in the detector is 885. The strings are about 450m long and separated from each other by at least 60 meters. The distance between two adjacent floors is 14.5m. All strings are connected to a main junction box, which provides the connection to the 40km long cable to the shore station. All the electronics for one storey are housed in a pressure resistant titanium container making up the so-called Local Control Module (LCM). A photon that hits the photo-cathode of a PMT can induce an electrical signal on the anode. If the amplitude of the signal exceeds a certain voltage threshold corresponding typically to 0.3 photo-electron, the signal is read out and digitized by a custom designed front-end chip. Every OM is read out by an electronics board housed in the LCM carrying a pair of Analogue Ring Samplers (ARS). The later provides the time and amplitude of the signal, both essential to reconstruct the muon track direction and estimate its energy (section 2.6). Each sector

contains a Master Local Control Module (MLCM), that collects the data produced in the floors of a sector and sends them to the main junction box.

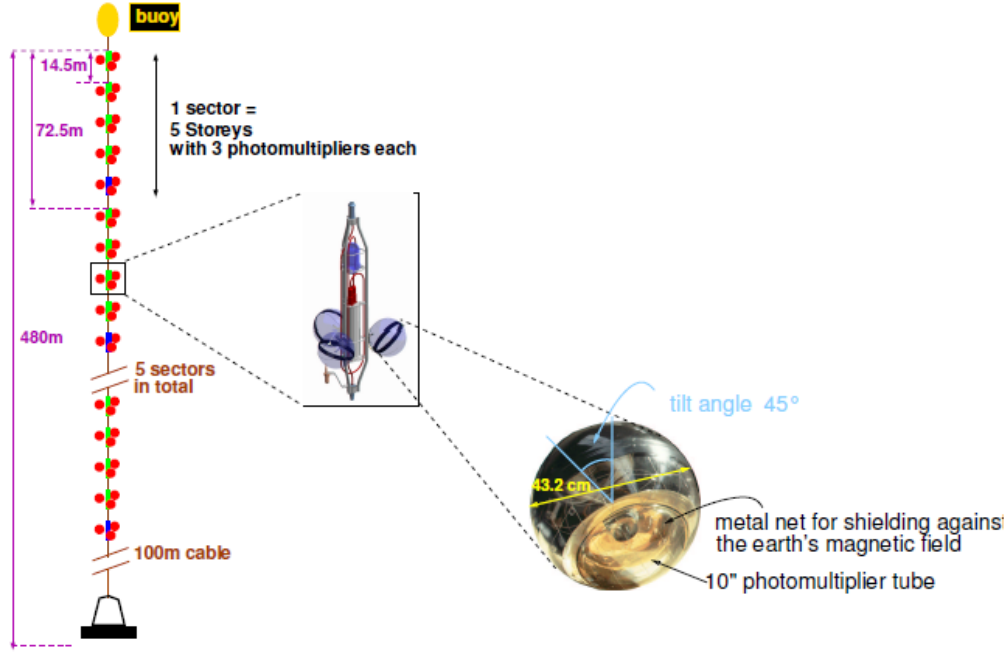


Figure 2.9 – A schematic view of ANTARES string.

2.3.2 ANTARES coordinates

The geographic site of ANTARES neutrino telescope is located at Latitude $42^{\circ}47.935'N$ and Longitude $6^{\circ}09.942'E$. The convention for the detector coordinate system (UTM grid) [26, 27], shown in Figure 2.10, is a right-handed system with the x-axis pointing toward the East, the y-axis to the North and the z-axis parallel to the detector line going upwards. The origin is defined on the center of the detector on the sea floor. The direction of the particle track is defined by two angles:

- The angle θ is measured from the positive z-axis in a range $[0, \pi]$. Upgoing events have $\theta \leq 90^{\circ}$, $\theta_{\uparrow} = 0^{\circ}$, $\theta_{\rightarrow} = 90^{\circ}$ and $\theta_{\downarrow} = 180^{\circ}$.
- The azimuthal angle ϕ is measured from the positive x-axis and it increases counterclockwise towards the positive y-axis (East→North). ϕ is measured in a range $[-\pi, \pi]$.

To find the zenith of the source, θ should be rotated by 180° in space: $\text{zenith} = 180^{\circ} - \theta$. Elevation (also called altitude) can be used to denote the position of the source and is defined as "zenith - 90° ".

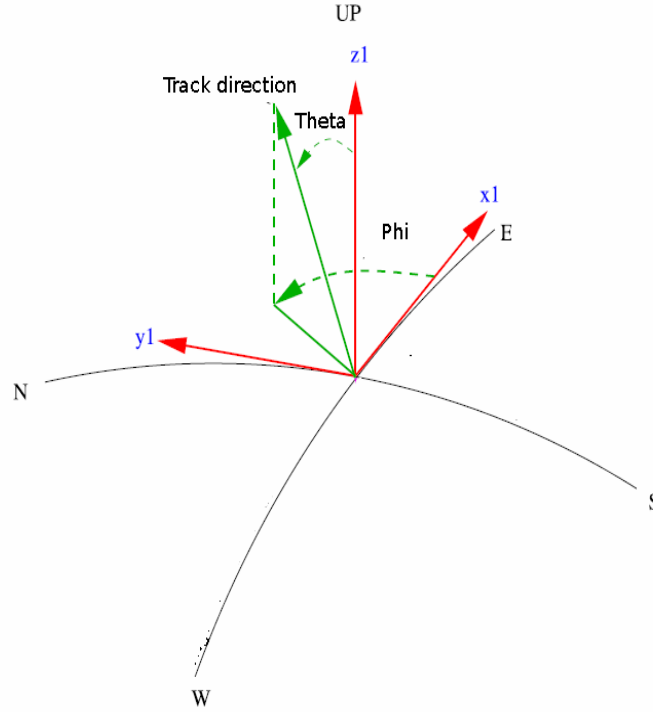


Figure 2.10 – Coordinate system of ANTARES

2.3.3 Background noise at the ANTARES site

Optical background: bioluminescence and ^{40}K

The Cherenkov radiation from ν -induced muons is not the only light at the depth of the ANTARES site. Background light is produced by the decay of radioactive potassium-40 (^{40}K) and marine microorganisms (bioluminescence). The latter being enhanced in periods of high sea current. Figures 2.11 and 2.12 shows some examples of the sea current and the PMT rates. The ^{40}K decays into two channels:



The first decay channel (β decay) is the dominant decay mode of ^{40}K with a probability of 0.89. The average kinematic energy of the emitted electron is 1.12 MeV, enough to produce

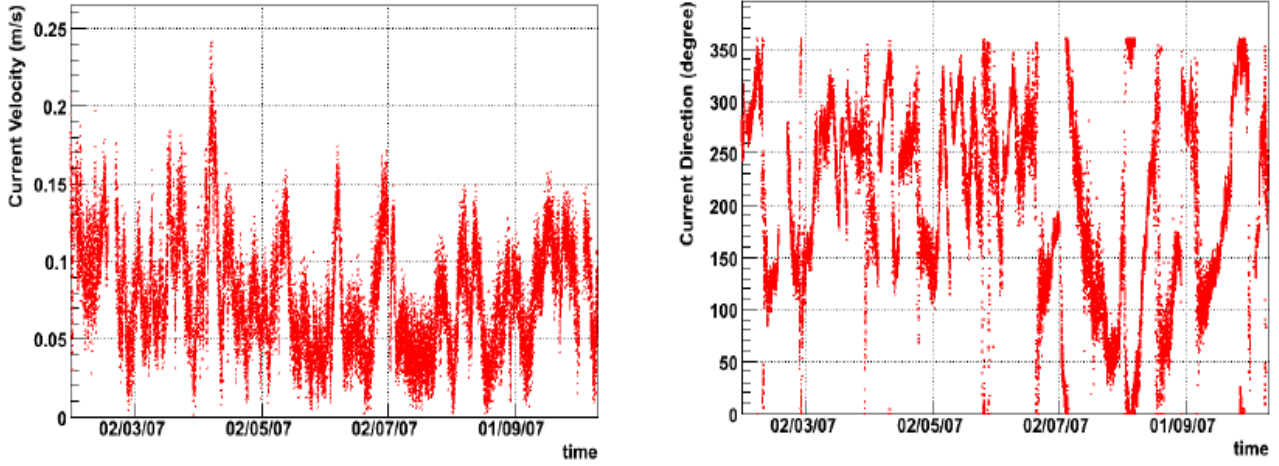


Figure 2.11 – Sea current velocity (left) and direction (right) in the ANTARES zone during the period going from February to November 2007.

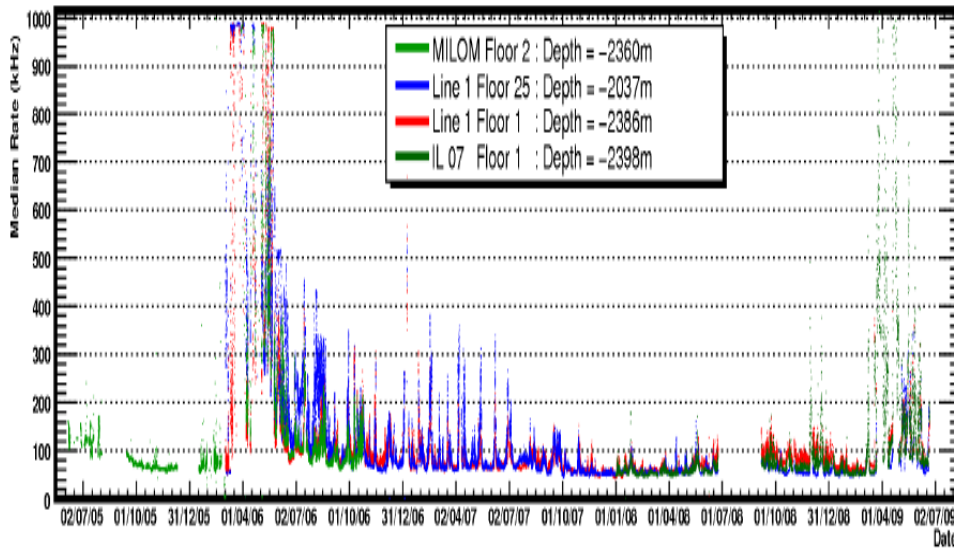


Figure 2.12 – Median single PMT background rates at different depth levels, monitored over four years of operation from 2005 and 2009.

Cherenkov light in water. The decay of the ^{40}K contribute to the PMT rates by a stable rate of around 30 kHz. In the second decay mode, the Cherenkov light comes from the Compton scattering of the 1.4 MeV photon emitted in the desexcitation of the ^{40}Ar .

2.3.4 Physical background: atmospheric muons and neutrinos

Cosmic ray interactions in the Earth’s atmosphere above the detector produce energetic atmospheric muons (see section 1.1.2). When the muon energy is high enough, they can travel large

2.2.3 The ANTARES neutrino telescope

distances and reach the detector from above. The aim to build the detector in deep sea is to use the water as a shield against the flux of those downward going atmospheric muons. However, upward going atmospheric muons can not travel through the Earth. Everything a part from the desired cosmic neutrinos is considered as background in the detector and should be discarded with filtering algorithms and dedicated predefined cuts in order to increase the sensitivity to cosmic neutrinos. However, upward going atmospheric neutrinos are an irreducible background in the detector. Their flux is several orders of magnitude smaller than atmospheric muons as it is shown in Figure 2.13. As cosmic neutrinos have hard spectrum ($\frac{dN}{dE} \propto E^{-2}$) [28], in contrast with the atmospheric neutrinos ($\frac{dN}{dE} \propto E^{-3.7}$) [29], the neutrino energy could be used to eliminate atmospheric neutrinos (this will be discussed in Chapter 4).

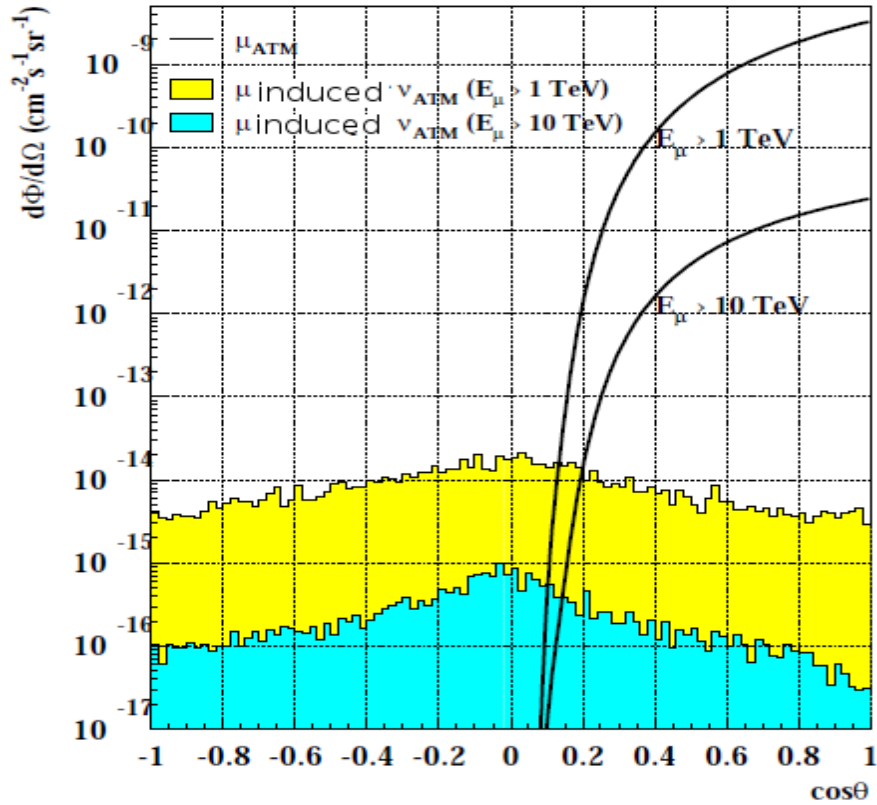


Figure 2.13 – Flux of atmospheric muons and muon induced by atmospheric neutrinos at 2300m water equivalent depth. In the downgoing direction ($\cos\theta > 0$) the atmospheric muon flux is about 10^6 times higher than the neutrino-induced muon flux. The maximum near $\cos\theta=0$ in the neutrino induced muon spectrum reflects the increased probability of meson decay close to the horizon.

2.3.5 Trigger and DAQ systems

Data acquisition

The overall data rate being too heavy to be fully written on disk, filtering algorithms must be applied on-line to discard as much as possible the background and save as much as possible the signal events. Several filtering algorithms can be applied depending on the optical background rate, but the basic idea is to search in all directions a time sequence of hits compatible with the passing of a relativistic particle emitting Cherenkov radiation. This is done on shore with a trigger elaborated to process all data coming from the detector in quasi real time [30]. These hits are causally related in time and position, while time-position of hits produced by ^{40}K decays or bioluminescence are uncorrelated (caused by random processes).

The aim of the trigger is to select correlated hits in the ARS data stream for digitization³, readout and transfer to the on-line data processing system on shore. Once the signal has been digitized in the ARS, it is sent to the Data Acquisition (DAQ) board for storage. The DAQ board collects data and sends them to the shore via an Ethernet port. Then, the characteristics of the hits are evaluated in order to discard most background hits, resulting in reduction of data rate by a factor of at least 10^4 . Off-shore, the ARS data are organized in data frames. All frames that belong to the same time window are sent to the same processor in the processing farm, as sketched in Figure 2.14. The program buffers the frames in a queue to handle transmission delays in the network. When all frames of a particular time window have been collected, they are passed to the trigger algorithm. The complete collection of frames is referred to as a *time slice*. The time and charge of all hits in the data are determined using the known calibration constants of the detector (see section 2.3.6).

Trigger algorithms

The first level of trigger is a simple threshold of about 0.3 photo-electron⁴ (pe) equivalent charge applied to the analog signal of the PMT. The corresponding digital data (time and charge) are then referred to as L0 hits.

The detection of two coincident photons by the same PMT generally results in a single hit with a charge that corresponds to $\simeq 2$ pe. This is unlikely to happen as the result of random background hits, which are mainly produced by single photons and consequently have a charge that corresponds to a single pe. Therefore, the second level of trigger (L1) searches for hits with a large charge (greater than 3 pe or 10 pe depending on the detector's configuration), or

³Because of the length of the optical link to the shore, electrical signals cannot be transmitted in analog form, thus they must be formatted by the ARS.

⁴Equivalent to 45mV.

alternatively for coincidence of hits in the same storey (but different OMs) within 20 ns, (i.e. local coincidence of L0 hits). The time window of 20 ns accommodates the difference in OM positions, uncertainties in the time calibration and some light scattering.

The two most frequently used algorithms both uses L1 hits as a starting point:

- The 3N trigger looks for causality relations in space-time between different "L1 hits" in $\pm 2.2\mu\text{s}$ time window⁵, roughly corresponding to the muon transit time across the detector. A minimum of 5 L1 hits (so at least 10 pe) in coincidence is required to write the event on disk, that is the overall L0 hits sequence during the $\pm 2.2\mu\text{s}$ time window. The efficiency of the trigger (for the 12 line configuration) rapidly grows with the number of pe in the event. It reaches almost 100% for 40 detected photo-electrons. The purity of this filtering is evaluated at 90% by Monte Carlo simulations.
- The T3 filtering [31] condition can be added in case of low optical background. This algorithm is more open and therefore accepts more background hits, but allows for more efficient shower recognition. Instead of looking for hits that are causally connected, one searches for a T3 trigger cluster within a time window of $\pm 2\mu\text{s}$. A T3 trigger cluster is defined as the occurrence of at least 2 L1 hits in two consecutive storeys within a coincidence time window. This time window is 100 ns in the case that the two storeys are adjacent, and 200 ns in the case of next to adjacent storeys.

In this context, it is important to mention that only the 3N trigger will be used in the results obtained with 2007 data presented in Chapter 4. However, in the results obtained with 2009-2010 data presented in Chapter 5 we use the T3 and 3N triggers.

2.3.6 Detector calibration and electronics

The precision on the muon track reconstruction (i.e., its time and its direction) requires a precise measurement of the arrival time of the photon, the position of the PMTs, the charge of the hits and the threshold voltage for the readout of the PMTs by associated front end electronics. These PMTs have been calibrated on-shore prior to the deployment. Below, we concentrate on the *in-situ* calibration system of the time and the PMT position. For the threshold and charge calibration, see for example [32].

Time calibration

ANTARES is designed to achieve an angular resolution smaller than 0.3° for muons above 10 TeV. This pointing accuracy is closely related to the precision in the determination of the

⁵More precisely $2.2\mu\text{s}$ before the time of the first L1 hit up to $2.2\mu\text{s}$ after the last L1 hit.

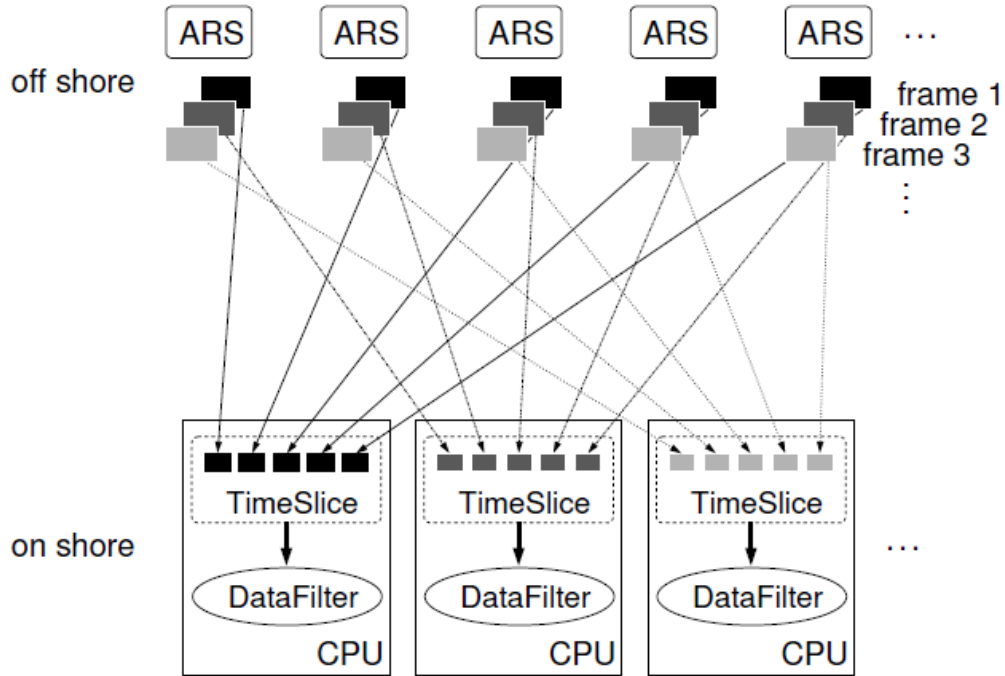


Figure 2.14 – A schematic view of the data collection on shore.

arrival time of the Cherenkov photons at the PMTs. Thus, a time calibration of the detector is necessary [33]. The calibration system includes a 20 MHz reference master clock on shore, LEDs installed inside each OM and Optical Beacons (OBs), equipped with LED or laser devices. The clock system provides a common signal to synchronize the readout of the OMs. Signal received from shore are converted and decoded by an electronics board inside the LCM and are then distributed over an electrical bus to the ARS chips. The relative offset of each local clock can be measured by using a calibration signal sent by the master clock and echoed back. The clock system assigns an absolute event time with a GPS master clock synchronization accuracy of $100 \mu s$.

The optical beacon system is used to calibrate the relative offsets between the PM tubes. Four blue (472 nm) LED beacons on storeys 2, 9, 15 and 21 of each detector line and two green (592 nm) laser beacons on the BSS of L7 and L8 are used for this purpose. The LED beacons are used for intra-line calibration purposes while the laser beacon, being much more powerful and able to illuminate all the lines, is used for inter-line calibration. An initial set of time offsets is determined in the laboratory prior to deployment. After deployment, these values may change due to different factors such as temperature changes or stresses in the cables. Using the optical beacon system they are monitored every month and readjusted as necessary. A

second calibration system consisting of a blue (470 nm) LED inside each OM is used to measure time offsets between the PM tube photo-cathode and the read-out electronics. Internal LED and optical beacon measurements reveal less than 0.5 ns contribution of the electronics to the photon arrival time resolution. Thus, time resolution is dominated by the transit time spread of the PM tubes which is about 1.5 ns, and light scattering and chromatic dispersion, which depends on the distance travelled by the photon. The calibration system just described provides a relative time calibration of better than 1 ns.

Position calibration

The optical modules are hanged to strings that are freely floating in the sea water. Thus, orientations and positions of each PMT should be measured at every moment to enable their monitoring. This is done, every two minutes, by an acoustic system which is set up on the BSS of each string. A pulse of frequency 40-60 kHz is sent by an acoustic transmitter held on the BSS and is received by the hydrophones situated on each sector along the line allowing a real time localization in space of the OMs by triangulation. The orientation of each optical module frame is measured by a compass and a tilt-meter located inside the LCM container. Together, measurements from the tilt-meters, compasses and acoustic system provide a measurement of the relative position of the OMs with an accuracy of 10-20 cm [34].

2.4 Data quality

The selection of data is based on some quality criteria. Each run is tagged by some quality parameters that are stored in the ANTARES data base. The main flags are the 'SCAN' and the Quality-Basic (QB) flags. The former allows to check the run setup of each run as some of them are not write-protected in the database thus they may have been modified during the data taking. In this analysis we select all physics runs which have run setup protected against writing " $SCAN \neq 1$ ". The second parameter allows to define some crude criteria in order to determine the quality of the data. It can take the following values (1, 2, 3 and 4), where each number stands for:

- QB = 1 : Defined to perform a basic selection, minimum requirement for a run to be included in the analysis.
- QB = 2 : It requires that at least 80% of the OMs expected to work at the time of the run are effectively working.

- QB = 3 : It requires a mean baseline rate over all active PMT ≤ 120 kHz AND a burst fraction $\leq 40\%$.
- QB = 4 : Same condition on baseline as in QB = 3 AND a burst fraction $\leq 20\%$.

The baseline rate, in kHz, represents the most probable counting rate of a given OM computed from the rate distributions (number of hits divided by the frame duration) in each PMT over the whole (typically few hours long) run. For one PMT the baseline is extracted from a gaussian fit on the left part of the distribution of the rates measured every 15 mn. The burst fraction, in percent, corresponds to the fraction of time during which the OM counting rates are larger than 20 % above the baseline rate [35].

For the analysis of 2007 (2009-2010) data presented in Chapter 4 (Chapter 5) we require a minimum QB value of 3 (1). Requirements about the external conditions (e.g. baseline, burst fraction and sea current), the configuration and behaviour of the detector during a given run (e.g. number of active units, L1 thresholds, alignment), and the properties of the run itself (e.g. duration, number of slices, trigger rates) can also be taken into account for the selection of runs.

2.5 Simulation chain

Simulation tools are one of the main ingredients needed to assess the performances of the detector. The simulation chain basically starts with the physics processes occurring in the atmosphere, Earth and underground, that can lead to the production of some detectable light in the detector, taking into account the probability of each process to occur. It also mimics the detector response to these processes. The particles that are simulated are the atmospheric muons and neutrinos induced by interactions of cosmic rays with the Earth's atmosphere, and cosmic neutrinos.

2.5.1 Simulation of high-energy neutrinos

These particles are generated using the program GENHEN [36]. The code generates a flux of neutrinos with uniformly distributed directions, within a zenith angle range $[\theta_{min}, \theta_{max}]$ and according to an arbitrary user input spectrum $E_\nu^{-\Gamma}$. The choice adopted in this work is $\theta \in [0, \pi]$, $\Gamma = 1.4$ and $E_\nu \in [10^2, 10^8] GeV$. GENHEN first generates the neutrino position, direction and energy. Neutrino interactions are simulated with LEPTO [37] for deep inelastic scattering (DIS) and RSQ [38] for resonant and quasi-elastic scattering (QES). The secondary particles resulting from the interaction that are able to produce detectable light are stored

for further usage. We introduce a volume within which the Cherenkov light is generated (see section 2.5.3), named *the can*. A schematic view of the can is shown in Figure 2.15.

The simulated flux of neutrinos arriving at the Earth is given per units of energy dE , solid angle $d\Omega$, area dS and time dt by the following relation:

$$\frac{d\Phi_\nu^{sim}}{dE_\nu d\Omega dS dt} = \frac{N_{total}}{t_{gen} V_{gen} I_\theta I_E E^\Gamma} \frac{1}{\sigma(E_\nu) \rho N_A} \frac{1}{P_{Earth}(E_\nu, \theta_\nu)} \quad (2.14)$$

where:

- N_{total} is the total number of generated events.
- Γ is the generation spectral index.
- $t_{gen}(s)$ is the arbitrary duration covered by the simulation.
- $V_{gen}(m^3)$ is the total generation volume of the Cherenkov light (in water equivalent units in this case)
- I_E is the energy phase space factor. It depends on the Γ chosen value:

$$I_E = \begin{cases} \frac{E_{max}}{E_{min}} & \text{if } \Gamma = 1 \\ \frac{E_{max}^{1-\Gamma} - E_{min}^{1-\Gamma}}{1 - \Gamma} & \text{otherwise} \end{cases}$$

- $I_\theta(sr) = 2\pi \times (\cos(\theta_{max}) - \cos(\theta_{min}))$ is the angular phase space factor corresponding to the specified range of $\cos(\theta_\nu)$.
- $\sigma(E_\nu)(m^2)$ is the charged current neutrino interaction cross-section.
- $\rho N_A(m^{-3})$ the number of target nucleons per unit volume.
- $P_{Earth}(E_\nu, \theta_\nu)$ is the probability of transmission through the Earth for a neutrino of given E_ν and θ_ν .

For a given flux model $\frac{d\Phi_\nu^{model}}{dE_\nu d\Omega dS dt}$ each event is reweighted by the ratio of two fluxes at the point (E_ν, θ_ν) . That is, the event weight is defined as follow:

$$w_{event} = \frac{d\Phi_\nu^{model}}{dE_\nu d\Omega dS dt} \times \left(\frac{d\Phi_\nu^{sim}}{dE_\nu d\Omega dS dt} \right)^{-1} \quad (2.15)$$

The same sample of neutrinos, initially generated following a $E^{-1.4}$ spectrum, can be re-weighted using any user specified spectrum by assigning a different weight to each event, w_{event} . Three weighting parameters are introduced in the ANTARES convention of Monte Carlo simulations [39]. First, the weight $w1$ contains the projected area of the can onto the plane perpendicular to the neutrino direction. Second, the weight $w2$, is equal to $\frac{N_{total}}{t_{gen}} \times \left(\frac{d\Phi_{\nu}^{sim}}{dE_{\nu}d\Omega dS dt} \right)^{-1} \times F$, where F is the number of second per year. It has units $\text{GeV} \cdot \text{m}^2 \cdot \text{sr} \cdot \text{s} \cdot \text{year}^{-1}$. Third, the global weight $w3$ equivalent to w_{event} , is defined as follows:

$$w3 = w2 \times \frac{d\Phi_{\nu}^{model}}{dE_{\nu}d\Omega dS dt} \quad (2.16)$$

where $\frac{d\Phi_{\nu}^{model}}{dE_{\nu}d\Omega dS dt}$ is the differential flux of neutrinos before penetrating the Earth, in unit of $\text{GeV}^{-1} \cdot \text{m}^{-2} \cdot \text{sr}^{-1} \cdot \text{s}^{-1}$. The global weight $w3$ has unit of year^{-1} which can be understood as "rate" per year.

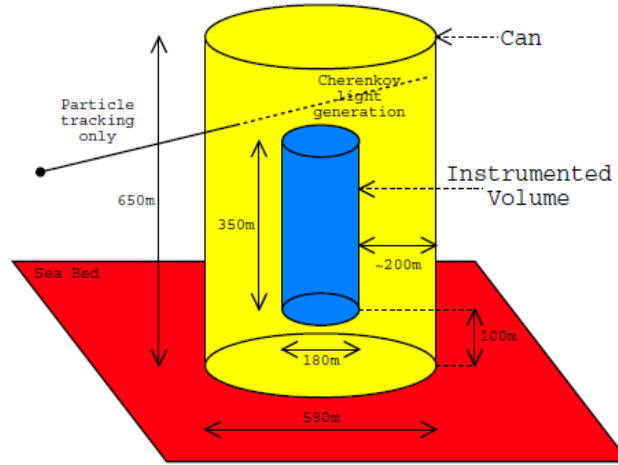


Figure 2.15 – Schematic view of the can, surrounding the instrumented volume.

2.5.2 Simulation of atmospheric muons

Apart from neutrinos, only atmospheric muons, as secondaries from hadronic showers, with energies typically above 500 GeV (1TeV) at the sea level can reach the detector (at a depth larger than 2000 m) for zenith angle $< 60^\circ$ ($> 60^\circ$) while the others are absorbed. The surviving events at sea level are characterized by a certain energy, direction and muon multiplicity. ANTARES Collaboration uses two independent approaches to simulate this atmospheric muon background:

Full simulation package: The program named CORSIKA⁶ [40] is used to simulate high energetic primary cosmic radiation (protons, α particles and heavier nuclei) interactions in the atmosphere and the propagation of the secondary particles to sea level. Most of the particles emerging from these interactions are pions and kaons. The primary cosmic ray flux is generated following a diffuse flux $dN/dE \propto E^{-\Gamma}$ which allows a later re-weighting with a user specified flux model. CORSIKA offers the choice of the cosmic ray flux and their model of interactions in the atmosphere. To minimize the CPU time, the ANTARES collaboration has chosen to split the flux of the primary cosmic rays into 5 groups including the most abundant particles: proton, helium, carbon, magnesium and iron nuclei in an energy range from few TeV to 10^2 PeV and zenith range from 0° to 85° . Secondary particles such as photons, leptons, mesons and nuclei are also propagated to sea level. The development of the hadronic shower in the atmosphere is simulated with the QGSJET01 model [41]. In the analysis presented in chapter 4 we use the Battistoni parametrization of the primary cosmic rays [42]. CORSIKA allows to compare at each step the results of the simulation with data from other experiments which permits a well control of the systematics.

For the propagation of muons from sea level to the detector, the ANTARES collaboration uses the MUSIC⁷ package [43]. MUSIC takes into account the interaction processes of muons with matter, i.e. bremsstrahlung, multiple scattering, ionization and pair production (see section 2.2.4). The energetic losses of muons can be modeled by the formula Equation (2.8). Ionization can be considered as a continuous process. As such, it is treated identically over the whole energy range, while the other processes are treated differently when a huge energy loss is induced. Energy losses are thus split into two parts: continuous energy losses (calculated with the Bethe-Bloch formula) and stochastic losses. These latter processes are taken into account when the fraction of energy lost by the muon is greater than $10^{-3}E$. In MUSIC, muons are deflected by the three processes quoted above except ionization.

Fast simulation package: This program named MUPAGE⁸ [44] is based on a predefined parametrization of muon flux measured by several experiments. The parameters include the depth (from 1.5 km to 5 km, the zenith angle θ and, for muon showers, the multiplicity m and the distance of each muon with respect to the direction of the shower). The parametrization has been extracted from the full simulation package HEMAS [45, 46] and the hadronic interaction models were simulated using the DPMJet model [47]. MUPAGE generates events for a user specified data acquisition time, in such a way that no further weighting is needed. This

⁶COsmic Ray SIMulation for KAscade

⁷MUon SIMulation Code

⁸Atmospheric MUons from PArametric formulas: a fast GEnerator for neutrino telescopes

simulation provides the best data/MC agreement, hence it is used for the results presented in the Chapter 5.

2.5.3 Simulation of the Cherenkov light

The propagation of muons and electrons in water results in the emission of Cherenkov photons. Those are simulated using KM3 [48] and GEASIM codes. The former simulates the propagation of muons using the MUSIC package, the light and secondary particles emitted by these muons. The latter, generates the hits at the OMs by means of a full GEANT (version 3.21) simulation of photon production. In contrast of KM3, GEASIM neglects the photon scattering, thus it assumes their direction as a straight line. This assumption makes GEASIM faster than KM3. Hereafter we concentrate on the KM3 code which simulates the Cherenkov light from muons and electromagnetic showers in three steps:

1. **GEN**: includes a complete GEANT3 simulation of the Cherenkov light. It generates photons produced from short muon track segment (typically one meter) and electromagnetic showers. The Cherenkov photons (direct and scattered) are traced individually through water until absorption takes place. Their positions and times are recorded at concentric spheres of various radii centered on the origin of emission. The program output consists of some tables containing all the photons recorded at each spherical shell.
2. **HIT**: uses the output tables described above to create the hit distributions at the OMs for muon track segments and electron showers. The photon probabilities are computed taking into account the optical properties (absorption and scattering length and refractive index) measured at the ANTARES site [49]. Positions and times of arrival of photons at each OM are stored and used to convert the hit probability into photo-electron number using Poisson statistics. During this step, the orientation of the PMT with respect to the track direction, the position of the lines are taken into account.
3. **KM3MC**: At this level, the propagation of the muons already generated at the can surface is performed. It takes as input the detector description and uses the photon tables to calculate the number of photo-electrons produced in each PMT and their arrival time. Segments of about 1m are examined step by step taking into account the energy losses of the muon. If the energy lost by the muon is greater than the mean energy lost by ionization an electromagnetic shower is produced along the segment. This electromagnetic shower is treated independently using the table of electrons.

Both GEN and HIT programs are run only once to generate the relevant tables of OM hit

probabilities. These tables are then stored on disk for subsequent use by KM3MC which is the program the end-user is most likely to use.

2.5.4 Generation of the optical background

The ANTARES neutrino telescope is located in an environment of high optical background produced by ^{40}K and bioluminescence at rates of about 100kHz per OM. The triggerEfficiency program [50] generates the background hits at the OMs according to the rates found in the raw data files. Then, it applies the same trigger criteria as for data to select candidate events in the Monte Carlo samples.

2.5.5 MC run by run approach

Recently the ANTARES collaboration has adopted a new Monte Carlo simulation approach in order to reproduce more realistic conditions of data taking following a run-by-run strategy [51]. The input information (run setup, mean rates, position and orientation of OMs, time and charge calibrations, ARS threshold and run duration) are taken from the data themselves and plugged into the simulation. This approach calls the simulation codes described in section 2.5.

Practically, 5×10^8 neutrinos are simulated using GENHEN package in the energy range of 100 GeV and 100 PeV. To simulate downgoing atmospheric muons we generate one tenth of the statistics of the corresponding data run using MUPAGE. The run-by-run MC simulation approach is used in the analysis described in Chapter 5.

2.6 Track reconstruction algorithm

The track reconstruction consists of finding values for the free parameters in the assumed model which most likely caused the outcome of the measurement. In the case of muon track reconstruction, the basic model is a straight line passing through the detector along which a muon moves with the speed of light producing a Cherenkov light on its way as shown in Figure 2.16 (right). The reconstruction takes a set of PMT hits within the three OMs on each storey of each string and deduces the best set of values for the track parameters that are, at a given time t_0 , the position $\vec{p} = (x, y, z)$ and direction $\vec{d} = (\sin(\theta)\cos(\phi), \sin(\theta)\sin(\phi), \cos(\theta))$ of the muon. By convention, the time t_0 is defined as the time when the muon passes through the plane perpendicular to its direction and containing the centre of gravity of the detector (see Figure 2.16 on the left).

The muon trajectory is then characterized by $N_{parameters} = 5$ independent parameters that must be estimated by a given reconstruction algorithm. In practice, an analytical expression

which connects the photon arrival times t_i^{th} to the track parameters is used:

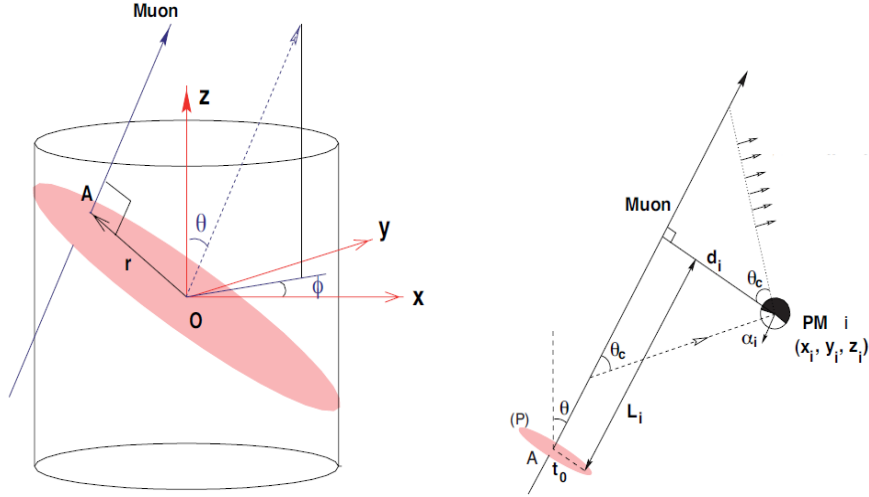


Figure 2.16 – Schematic view of the reconstruction strategy. Left: the geometrical description of the *can* and the coordinates used for the reconstruction. Right: the geometrical structure of the muon track induced by a muon-neutrino: definition of variables.

$$t_i^{th} = t_0 + t_{trans} + t_{trav} \quad (2.17)$$

where t_{trans} is the time it takes for the muon to reach the point where the light is emitted and t_{trav} is the time it takes for the photon to travel from that point to the OM. Using Figure 2.16 it follows:

$$t_{trans} = \frac{L_i}{c} - \frac{d_i}{c \tan(\theta_c)}$$

$$t_{trav} = \frac{d_i}{v_g \sin(\theta_c)}$$

where c is the velocity of light in vacuum and v_g is the group speed in water [52].

In the following we describe the two main reconstruction algorithms adopted by the ANTARES collaboration and used in this thesis. These methods assume that only a single muon crosses the detector. Therefore atmospheric muon bundles will be worse reconstructed and consequently removed by quality cut criteria.

2.6.1 In-situ reconstruction algorithm

The fast reconstruction algorithm called BBfit [53], convenient for the online use has been developed as a robust reconstruction method, which produces reliable results without precise

2.2.6 Track reconstruction algorithm

positioning calibration. Its strict hit selection leads to an accurate up-down separation while keeping a good efficiency. In BBfit, the exact geometry of the detector is ignored: the detector lines are straight (i.e lines are supposed unaffected by the sea current) and the 3 OMs of each storey are considered as a single OM centered onto the string. Thus, the hits altitude corresponds to the altitude of the optical modules.

As the first step, time and charge calibration (see section 2.3.6) is applied, the calibrated hit times and amplitudes being given in units of nano-seconds and photo-electrons (pe) respectively. For the selection of hits the algorithm uses the same criteria as those of the T3 trigger (see section 2.3.5). The algorithm requests a coincidence of 2 "L1 hits" in two adjacent floors (next-to-adjacent floors) within 80 ns (160 ns). Then, all hits of the same floor, in coincidence within 20 ns, are merged into one single hit. The time of the merged hit is the earliest time of the participating hits, and the charge is the combined charge of all merged hits. These merged hits are used for the reconstruction. The quality of the reconstruction is measured by a modified- χ^2 function, given by the Equation (2.18):

$$\chi^2 = \frac{Q}{N_{dof}} \quad (2.18)$$

where $N_{dof} = N_{hit} - N_{parameters}$ is the degrees of freedom, N_{hit} is the number of merged hits used in the fit, and

$$Q = \sum_{i=1}^{N_{hit}} \left[\frac{\Delta t^2}{\sigma_i^2} + \frac{q(q_i)d(d_{fit})}{\langle q \rangle d_0} \right] \quad (2.19)$$

where σ_i is the timing error introduced to take into account the applied geometrical approximation and the occasional presence of late hits from small angle scattering or from electromagnetic processes. Its value is set to 10 ns for $q_i > 2.5$ pe and to 20 ns otherwise. The first term is a time residual, it exploits the difference time $\Delta t = (t_\gamma - t_i)$ between the hit time t_i and the expected arrival time of the photons t_γ from the muon track. The second term exploits the fact that an accumulation of storeys with high charges is expected on each detector line at its point of closest approach to the track. It depends on the measured amplitude q_i and the theoretical distances traveled by the detected photon d_{fit} . The chosen form gives an empirical penalty to the combination of high charge and large distance. The term $q(q_i) = q_0 q_i / \sqrt{q_0^2 + q_i'^2}$ is the amplitude of the hit corrected for the angular acceptance of the floor, i.e. $q' = 2q_i / (\cos(\theta_\alpha) + 1)$, where θ_α is the inclination of the photon track to the detector line, with an artificial saturation at 10pe. The term $d(d_{fit}) = \sqrt{d_{fit}^2 + d_1^2}$ is protected against small distance travelled by photons. One can assume the constant $q_0 d_1$ to be around $50m \times \text{photoelectron}$ since the intensity

of the Cherenkov light decreases with the distance. The product $q.d$ is divided by the average corrected amplitude $\langle q \rangle$, calculated from all hits which have been selected for the fit, to compensate for the fact that more energetic tracks or showers will produce more light at the same distance. The normalization d_0 balances the weight between the two terms. The value of d_0 has been chosen to be 50m, which is motivated by the fact that at this distance the typical signal in a PMT which points straight into the Cherenkov light front is of the order of one photoelectron.

The same quantity defined in Equation (2.18) is used to estimate a track or a shower (bright point) reconstruction parameters. The two cases differ in the way of calculating the expected arrival time of the photon at the PMT.

In the BBfit algorithm, events are split into four kinds: track reconstructed with a single line, track reconstructed with multiple lines, shower reconstructed with a single line and shower reconstructed with multiple lines. In the case of a single line reconstruction the azimuth information is lost leading to the estimate of only four parameters.

The azimuth degeneracy: In the case of tracks reconstructed using only two detector lines, an ambiguity is introduced on the reconstructed azimuth angle of the track, ϕ_{rec} . Thus two muon tracks are reconstructed both having the same zenith angle but different azimuth angle. The distribution of the hit times of the true track and of the track obtained by mirror symmetry with respect to the plane connecting the two lines, are identical. An illustration of this degeneracy is shown in Figure 2.17. The azimuth of the reconstructed original and mirror tracks are connected in the following way: $\phi_{mirror} = 2\phi_{lines} - \phi_{track}$, where ϕ_{lines} is the azimuth angle of the plane connecting the two lines.

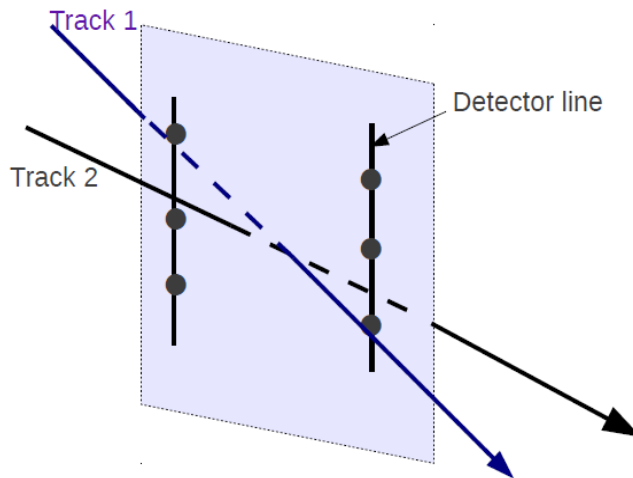


Figure 2.17 – Illustration of the azimuth degeneracy

The version of BBfit used in this thesis is *v3r6*. In this version we added the coordinates of the mirror track (named hereafter $\text{track}(\phi_{\text{mirror}})$) in addition to the original one (named hereafter $\text{track}(\phi_{\text{track}})$). Previous versions provided only one solution randomly chosen among the two mirror tracks. This additional information permits to compare the *best* = $\text{Min}(\text{track}(\phi_{\text{track}}), \text{track}(\phi_{\text{mirror}}))$ and the *random* (the one chosen randomly among the two solutions) track. Further details are presented in Chapter 4.

The choice between the tracks cannot be based on the χ^2 value since it is the same for both solutions. Thus to resolve the azimuth degeneracy, an intermediate reconstruction step was later introduced to BBfit. It consists of a temporary selection of all (raw) hits with time residuals less than 30ns for both tracks, over the whole detector. The sum of the charges of the two sets of selected hits is calculated and the track corresponding to the highest value is considered to be the correct one. The results presented in this thesis were completed before the implementation of this degeneracy breaking.

Bright point: When an electromagnetic or a hadronic shower is produced, it develops itself over a distance small compared to the spacing between detection storeys. As a consequence, light appears as if it was emitted isotropically from a bright point, and expanding with a velocity v_g . The four bright point parameters are therefore defined by the position of the emission point $\vec{P} = (x_0, y_0, z_0)$ and the emission time t_0 . The spherical envelop of the light can then be fitted based on the simple relation:

$$v_g(t_i - t_0) = \sqrt{(x_i - x_0)^2 + (y_i - y_0)^2 + (z_i - z_0)^2}$$

where t_i are the hit times, x_i, y_i the fixed horizontal positions of the lines and z_i the altitude of the PMT fired by the hit i .

The χ^2 of Equation 2.18 is then referred to as $b\chi^2$. Both the track χ^2 and the bright point $b\chi^2$ are used in the selection criteria of the final events to reject background: well reconstructed muons have a good χ^2 but poor $b\chi^2$ in contrast of background events.

2.6.2 Off-line reconstruction algorithm

A second more sophisticated and complex algorithm for the reconstruction of muon tracks, so-called Aafit, is based on the maximum likelihood method. Its full description is given in [54]. It consists of several stages:

Pre-selection of hits: This step allows to keep as much as possible hits that are most likely originating from a muon. The hits selected should verify the causality criterion given by the

following relation:

$$\Delta t_{ij} \leq \frac{d_{ij}}{v_g} + 20ns \quad (2.20)$$

where Δt_{ij} is the time difference between a hit i and the hit j with the largest amplitude, and d_{ij} is the distance between the OMs of the two hits. Hits with larger time differences cannot be related to the same muon, unless they have a residual larger than the safety factor 20ns [55], which is unlikely.

In order to reduce the impact of PMT afterpulses on the reconstruction, all the hits selected on the same OM using Equation (2.20) are merged within a time window of 300ns.

Pre-fit: The reconstruction procedure starts from a linear pre-fit based on the L1 hits, in order to provide a robust starting point for the further fitting procedure. At this stage, Aafit assumes that the hits occur on points that are located on the muon track, which allows to derive analytically a starting point from the minimization of the χ^2 , although with a poor precision.

M-estimator fit: The M-estimators are a broad class of functions that allow parameter estimation even when the probability distribution that defines the problem is not exactly known. They are referred to as robust estimators when the result is insensitive to small variations of the underlying distribution assumed. The robustness of the M-estimator fit allows better estimate of a set of track parameters, using the residual Δt_i , and reduces the influence of outlier hits.

The output parameters of the prefit are used as seed in the M-estimator fit procedure which considers a sub-set of hits within 100m around the track estimated by the prefit and within a time window $\pm 150ns$ of the photon arrival times or a charge $\geq 2.3pe$. The function that is maximized to estimate the track parameters is:

$$M = \sum_i \lambda \left(-2\sqrt{1 + A_i \frac{(t_i - t_i^{th})^2}{2}} \right) - (1 - \lambda) f_{ang}(\alpha_i) \quad (2.21)$$

where A_i is the hit amplitude, f_{ang} is the angular acceptance of the PMT as a function of the incident angle of the photon (with respect to the PMT axis) α_i . The λ parameter is set to 0.05 as the result of a Monte Carlo based optimization.

The maximum likelihood fit: The final fit procedure uses the principle of Maximum Likelihood (ML). It evaluates the theoretical arrival time of the photon at the OM i , t_i^{th} . Thus the time residual $\Delta t_i = t_i - t_i^{th}$, between the measured time and the expected time of the photon, is used to calculate the probability that the photon comes from the track. The track fitter searches for event direction for which the likelihood \mathcal{L} takes maximum value. Under the

2.2.6 Track reconstruction algorithm

muon-like event assumption the following likelihood is calculated:

$$\mathcal{L} = \prod_i P(t_i | t_i^{th}) \quad (2.22)$$

Here $P(t_i | t_i^{th})$ is the statistical probability of observing t_i with the expectation of t_i^{th} . The probability of a hit with a certain residual Δt_i is described by a Probability Density Function (PDF). This PDF is a combination of a signal PDF and a background PDF. The first step

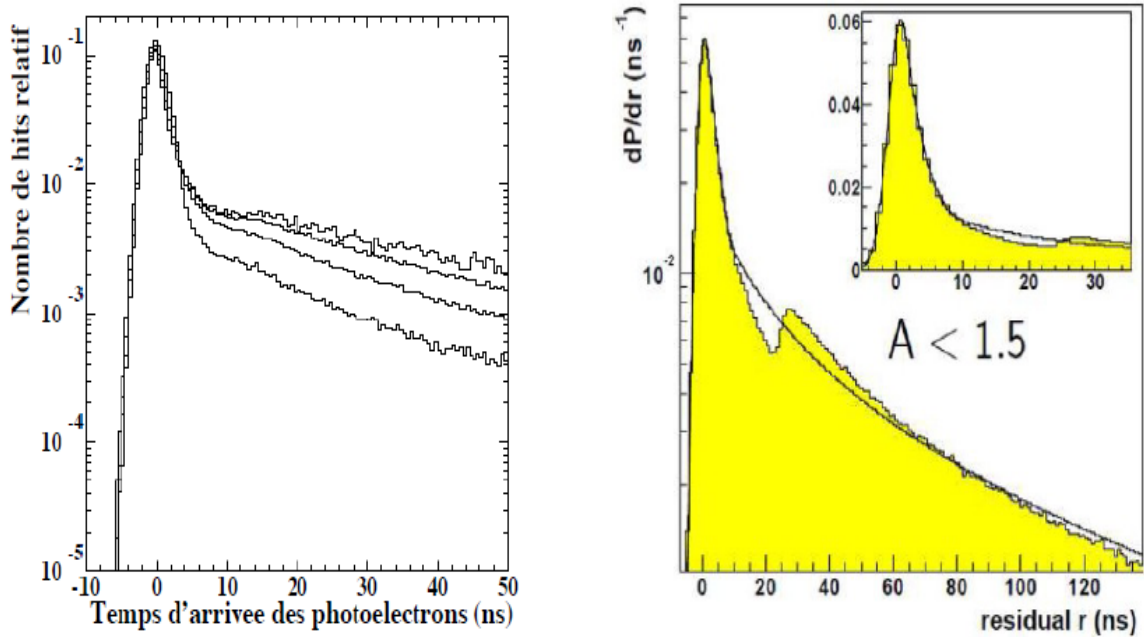


Figure 2.18 – Distributions of the time residuals used in the ML fit. Left: The curves correspond to four different muon energies, from the top to the bottom: 250, 50, 10 and 2 TeV. These PDFs do not take into account the background hits. The one used in the fit is the one for 10 TeV events. Right: An example of the full PDF used in final ML fit step for hit amplitudes < 1.5 pe. In yellow the histogram obtained by the Monte Carlo, the solid line is the parametrization used by the likelihood fit

of the ML fit is done using a signal only PDF as shown in Figure 2.18 (left). It takes into account the smearing on the hit times introduced by the transit time spread of the PMTs, which impacts the width of the peak around zero, and the scattering of light in water, which causes the long tail at positive values. An unphysical tail is present at values < -5 ns, which was introduced to render the PDF differentiable at negative values. In this step hits with residual $\Delta t_i \in [-0.5R, R]$, where R is the root mean square of the residuals used in the M-estimator, are taken into account. Hits that are part of a coincidence or that have an amplitude larger than 2.5 pe are also selected.

The M-estimator and ML fit steps are repeated 9 times with some initial parameters inferred

from the pre-fit. Four starting points are obtained by rotating the pre-fit track by 25° . The rotation is done around the track point which is closest to the center of gravity of the selected hits. Four more trials are obtained by translating the starting point of the track by ± 50 m in the direction $\vec{d} \times \hat{z}$ (where \vec{d} is the track direction) and by ± 50 m in the direction of \hat{z} . Among the 9 trials, the track with the best likelihood is stored. The number of the trials, N_{comp} , giving rise to compatible solutions (i.e with direction within 1° similar to the stored one) is used later in the analysis, as quality selection criterion.

The final fit uses an improved PDF using hits with time residual of ± 250 ns (in order to add background hits), local coincidences and hits with amplitude larger than 2.5pe. An example of distribution of this PDF is shown in Figure 2.18 (right). At the output, the algorithm provides two quality parameters of the track. The first given by:

$$\Lambda = \frac{\log \mathcal{L}}{N_{dof}} + 0.1(N_{comp} - 1) \quad (2.23)$$

where $N_{dof} = (N_{hits} - N_{parameters})$ is the number of degrees of freedom used in the fit. The second term acts as an ad hoc reward for fits with $N_{comp} > 1$. The second quality parameter is the angular error estimate, β , of the reconstructed track. This quality parameter is obtained from the fit of the likelihood and is given by:

$$\beta = \sqrt{\sigma_\theta^2 + \sin^2 \theta \sigma_\phi^2} \quad (2.24)$$

where σ_θ and σ_ϕ are the error estimates of the track's zenith and azimuth angles respectively. The use of these quality parameters for the event selection is studied in Chapter 5 for the data recorded during the 2009-2010 data taking period.

REFERENCES

- [1] K.F GRIEDER, Cosmic Rays At Earth, Researcher's Reference Manual and Data Book, Elsevier (2001). [44](#)
- [2] R. GANDHI ET AL, Phys. Rev., D58, 093009, (1998). [44](#), [47](#)
- [3] R. GANDHI ET AL, Astropart. Phys., 5, 81110, (1996). [44](#)
- [4] J. G. LEARNED AND K. MANNHEIM, Annu. Rev. Nucl. Part. Sci, 50, 679-749 (2000). [45](#)
- [5] PARTICLE DATA GROUP, European Physics Journal C, 3, 144 (1998). [46](#)
- [6] P. H. BARRETT ET AL, Rev. Mod. Phys. 24, 133178 (1952). [49](#)
- [7] P. CERENKOV, CRAc. Sci. U.S.S.R. 8, 451 (1934). [50](#)
- [8] J. D. JACKSON, John Wiley and Sons, Inc (1998). [50](#)
- [9] G. V. DOMOGATSKY, Nucl. Phys. Proc. Suppl. 91, 438 (2001). [51](#)
- [10] V. AYNUTDINOV ET AL, NIMA 602 (2009). [51](#)
- [11] E. ANDRES ET AL, Astropart. Phys. 13, 1-20 (2000). [51](#)
- [12] H. KOLANOSKI ET AL, ePrint: arXiv:1209.5610 (2012). [52](#)
- [13] R. ABBASI ET AL, Astrophys. J. Lett. 689, L65 (2008). [52](#)
- [14] J. AHRENS ET AL, Proc. of the 27th International Cosmic Ray Conference, Hamburg Germany, 1237 (2001). [52](#)
- [15] R. ABBASI ET AL, Nature 484, 351-354 (2012). [52](#)
- [16] R. ABBASI ET AL, ePrint: arXiv:1208.4861 (2012). [52](#)
- [17] S. BÖSER ET AL, ePrint: arXiv:1205.6405 (2012). [52](#)

REFERENCES

- [18] G. AGGOURAS ET AL, Nucl. Phys. Proc. Suppl., 151, 279 (2006). 53
- [19] L. K. RESVANIS, J. Phys. Conf. Ser. 39, 447 (2006). 53
- [20] C. DISTEFANO ET AL, Astrophys. Space Sci., 309, 415-420 (2007). 53
- [21] C. DISTEFANO ET AL, Nucl. Phys. Proc. Suppl., 190, 109-114 (2009). 53
- [22] U. F. KATZ, NIM A567, 457-461 (2006). 54
- [23] KM3NET COLLABORATION, available on <http://www.km3net.org/TDR/TDRKM3NeT.pdf>. 54
- [24] J.A. AGUILAR ET AL, NIM A 656 11-38 (2011). 54, 55
- [25] M. AMRAM ET AL, NIM A484 369-383 (2002). 55
- [26] P. VERNIN, ANTARES internal note, ANTARES-SOFT-2008-002 (2008). 56
- [27] P. VERNIN, ANTARES internal note, ANTARES-SOFT-2007-018 (2007). 56
- [28] E. WAXMAN AND J. BAHCALL, Phys. Rev. D 59 (1998). 59
- [29] G. D. BARR ET AL, Phys. Rev. D70 023006 (2004). 59
- [30] J.A. AGUILAR ET AL, NIM A570 107 (2007). 60
- [31] J. CARR ET AL, ANTARES internal note, ANTARES-SOFT-2007-016 (2007). 61
- [32] A. KOUCHNER, HDR, Université Paris Diderot (2009). 61
- [33] J.A. AGUILAR ET AL, Astropart. Phys. 34 539-549 (2011). 62
- [34] A. M. BROWN ET AL, Proceedings of the 31st ICRC, Łódź, Poland (2009), e-Print: arXiv:0908.0814. 63
- [35] S. ESCOFFIER, ANTARES internal note, ANTARES-SITE/2005-001 (2005). 64
- [36] D. BAILEY, ANTARES internal note, ANTARES-SOFT-2002-004 (2002). 64
- [37] G. INGELMAN ET AL, Computer Phy. Communications 101, 108-134 (1997). 64
- [38] G. D. BARR, PhD thesis, University of Oxford (1987). 64
- [39] J. BRUNNER, ANTARES internal note, ANTARES-SOFT-1999-003 (1999). 66
- [40] D. HECK ET AL, CORSIKA: a Monte Carlo code to simulate extensive air showers, TIB Hannover (1998). 67
- [41] G. BOSSARD ET AL, Phys. Rev. D 63, 054030 (2001). 67

- [42] G. BATTISTONI ET AL, Nucl. Phys. B (Proc. Suppl.) 70 367-370 (1999); Astropart. Phys. 12 315-333 (2000). [67](#)
- [43] P. ANTONIOLI ET AL, Astropart. Phys., 7, 357368 (1997). [67](#)
- [44] G. CARMINATI ET AL, Comput. Phys. Commun., 179: 915923 (2008). [67](#)
- [45] E. SCAPPARONE, arXiv/physics.9902043 (1998). [67](#)
- [46] Y. BECHERINI ET AL, Astropart. Phys., 25, 113 (2006). [67](#)
- [47] J. RANFT, Phys. Rev. D51 (1995) 64 (2000). [67](#)
- [48] D. BAILEY, ANTARES internal note, ANTARES-SOFT-2002-006 (2002). [68](#)
- [49] S. ADRIÁN-MARTÍNEZ ET AL, Astropart. Phys., 35, 552557 (2012). [68](#)
- [50] M. DE JONG, ANTARES-SOFT-2009-001 (2009). [69](#)
- [51] C. RIVIÈRE, ANTARES internal note, ANTARES-PHYS-2012-001 (2012). [69](#)
- [52] L. A. KUZMICHEV, NIM A482, 304 (2002). [70](#)
- [53] J.A. AGUILAR ET AL, Astropart. Phys. 34 652662 (2011). [70](#)
- [54] A. HEIJBOER, PhD thesis, Universiteit van Amsterdam (2004). [73](#)
- [55] S. GALATA, PhD thesis, Université Aix-Marseille (2012). [74](#)

REFERENCES

CHAPTER 3

GRAVITATIONAL-WAVE INTERFEROMETRIC DETECTORS

3.1 Summary

After the detailed review of neutrino astronomy with the ANTARES neutrino telescope given in the previous chapter, we review in this chapter the observational astrophysics possible with the gravitational wave detectors such as Virgo and LIGO. This chapter first gives an introduction to gravitational-wave astronomy from an instrumental point-of-view ranging from the general detection principles to the description of the instruments currently in operation. Being LIGO and Virgo very similar we will focus on the Virgo detector. The main part of this chapter offers an introduction to the analysis techniques for gravitational wave (GW) data.

3.2 Detection principle

The idea of using interferometry to detect gravitational waves was first proposed by two Russian theorists, M. Gertsenshtein and V.I. Pustovoit in 1962 [1]. The applicability of this idea was thoroughly studied by R. Weiss [2] and further by D. Drever [3] leading to the general design followed in today's instruments.

As we have seen in section 1.2.1, gravitational wave exerts a strain on space-time. It thus affect the distances between freely falling test particles. The idea is to sense this deformation thanks to ultra-precise laser interferometry. Let us consider a Michelson-type interferometer in which two laser beams propagate along two orthogonal arms of lengths L_1 and L_2 . An impinging GW is equivalent to a relative displacement of the end mirrors of the interferometer (used as test masses) $\delta\ell \equiv L_1 - L_2$. This is related to the GW amplitude $h = \delta\ell/L$ where L is the interferometer arm length. The relative displacement of the test masses induces a

CHAPTER 3. GRAVITATIONAL-WAVE INTERFEROMETRIC DETECTORS

phase shift between the two interfering beams, measurable at the interferometer output with a photodetection. Three fundamental noises limit the accuracy of this measurement:

- **Seismic noise:** is a *displacement noise* which results from the vibration of the ground below the instrument. The noise comes from the global and large-scale motion of the tectonic plates (including the *micro-seismic* dominated by the interaction of the plates with ocean waves) and from the local anthropic activity. Seismic noise rises rapidly toward low frequencies and limits the sensitivity below 10 Hz. The seismic noise is reduced using suspension systems, as the Virgo *super-attenuator* (see section 3.3).
- **Thermal noise:** is also a *displacement noise* which originates from the Brownian motion of the atoms that compose the mirrors and their suspensions. To reduce this noise both are made of material with a high mechanical quality factor. This noise limits the sensitivity in the frequency band around 100 Hz (where the sensitivity is maximum) and therefore limits the observational horizon of the instrument.
- **Shot noise** is a *sensing noise* which results from the quantum fluctuation of light. Those fluctuations can be interpreted as fluctuations in the phase shift at the photo-detector, thus they can mimic the GWs. The effect of the shot noise is reduced by increasing the number of photons in the interferometer. This is why high-power lasers are used and light is “recycled” thanks to the technique of power recycling. Several kilo-Watts of light power is stored in the initial GW interferometers.

The impact of those three noises can be reduced to reach the accuracy of $h_{noise} \sim 10^{-21}$. Several instruments have reached this objective after many years of preparation and construction involving a large number of scientists and engineers coming from many countries. We will describe the Virgo detector in more details in the next section. A next generation of instruments is under way and expected for 2015. The objective is a ten-fold improvement of the sensitivity over the first (and current) generation of instruments. This increases the accessible volume of the Universe (and hence the number of detectable sources) by a factor of 1000.

3.3 The Virgo detector

The Virgo interferometer [4] has been built by a collaboration between France and Italy. It is located near Pisa, Italy. The vertex of the Virgo detector is at elevation 53.238 m and at geographic coordinates 43°37'53"N and 10°30'16"E.

3.3.4 Response of a gravitational wave interferometer

In short, Virgo consists in two orthogonal kilometeric arms (3 km) illuminated by a laser source. The laser is a Nd:YAG with a wavelength $\lambda_L = 1064$ nm and output power $P \sim 10$ W in the initial Virgo design. An initial resonating optical cavity called *mode cleaner* performs both spatial filtering (“mode cleaning”) and frequency stabilization of the input beam. The cleaned laser beam is sent to the beam splitter which separates the light into two identical beams directed to the two arms. To increase the optical path length the interferometer arms are replaced by Fabry-Perot resonating optical cavities. A simplified scheme of Virgo interferometer is shown in Figure 3.1. The relative position of the mirrors of the cavity is controlled so that the light after one round-trip is coherent in phase with the in-coming light from the beam splitter. The equivalent number of round trips or *finesse* is determined by the transmissivity and reflectivity of the input mirrors as well as by their optical losses. The finesse is about 50 in the initial Virgo design. The light beam propagates in an ultra-vacuum system to protect it from air density fluctuations. The two beams recombine and interfere at the beam splitter. The interferometer is tuned on the *dark fringe* by a control system which adjusts the position of the end mirrors accordingly. In the absence of GWs, the small fraction of light power that constitutes the dark fringe goes to a photo-detector that measures its intensity, while all the light that circulates in the arms (bright fringe) is reflected by the beam-splitter back toward the laser. Here, a semi-reflective *power-recycling* mirror feeds the bright fringe back into the interferometer in phase with in the in-coming light from the main laser.

In summary, Virgo is composed of six main mirrors (four large input and end mirrors, the beam splitter and the power recycling mirror) [5] and four resonating optical cavities (mode cleaner, two in the arms and the power recycling cavity). The main optics in the arms are mirrors of 350mm diameter, 100mm thickness and 20kg mass.

All the mirrors are suspended to a specific seismic isolation system, called *super-attenuator* [6]. At its heart is a chain of pendulums, each stage of which provides good attenuation of the vertical and horizontal ground vibrations. The overall attenuation is more than 10^{10} at frequencies ≤ 10 Hz.

3.4 Response of a gravitational wave interferometer

The response h of the interferometer to an impinging GW with polarization h_+ and h_\times can be written as

$$h = F_+(\theta, \phi, \psi)h_+ + F_\times(\theta, \phi, \psi)h_\times \quad (3.1)$$

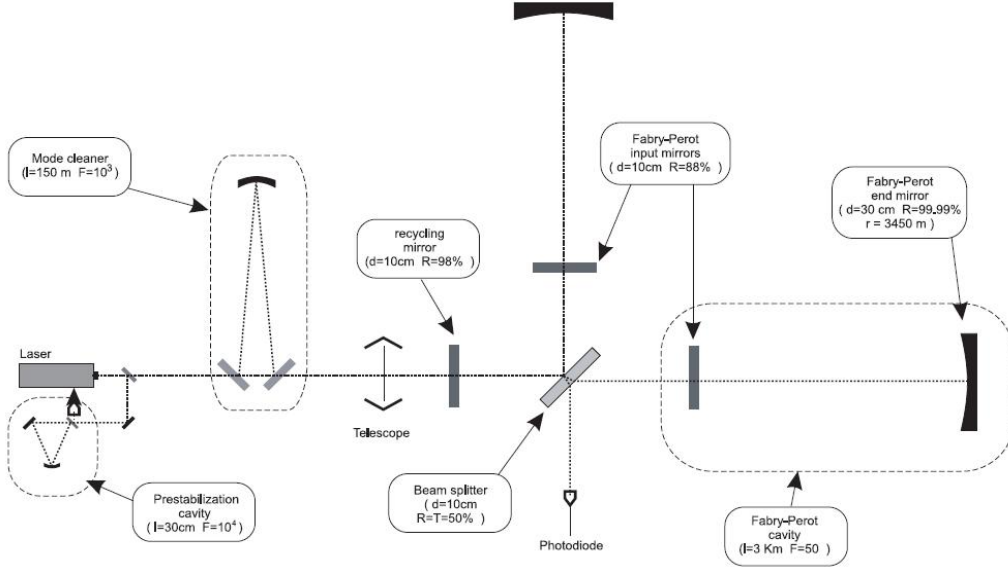


Figure 3.1 – The basic optical scheme of Virgo

where the antenna pattern F_+ and F_\times are equal to

$$\begin{aligned} F_+(\theta, \phi, \psi) &= \frac{1}{2}(1 + \cos^2 \theta) \cos 2\phi \cos 2\psi - \cos \theta \sin 2\phi \sin 2\psi \\ F_\times(\theta, \phi, \psi) &= \frac{1}{2}(1 + \cos^2 \theta) \cos 2\phi \cos 2\psi + \cos \theta \sin 2\phi \sin 2\psi \end{aligned} \quad (3.2)$$

and are functions of the three angles θ , ϕ and ψ defined as follows. Let the Cartesian frame (x, y, z) have the origin on the beam-splitter and the arms of interferometer are along the x and y axes. The propagation plane of the GW is characterized by the frame (x', y', z') . In the prime coordinates the propagation of the GW coincides with the z' axis. Its sky location is defined by the polar angles θ and ϕ with respect to (x, y, z) , see Figure 3.2. The polarization angle ψ is between the projection of the x arm onto the plane orthogonal to the direction of propagation and the x' axis.

The antenna pattern F_+ and F_\times in Equations (3.2) encode the detector angular sensitivity (see Figure 3.3). Generally speaking, GW detectors have a very wide aperture and are hence non-directional. We see that the GW detector is blind to certain directions for any value for ψ , i.e., for $\phi = \pm\pi/4$ and $\theta = \pi/2$. This corresponds to the two bisectors of the detector arms. Conversely, the response $F_+^2 + F_\times^2$ is maximum for $\theta = 0$ or π i.e, a GW coming from the zenith.

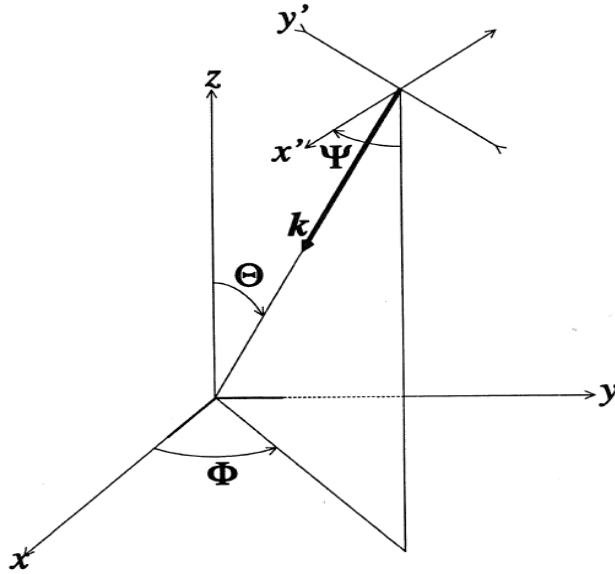


Figure 3.2 – The coordinate system used in Virgo in the computation of the antenna pattern functions. The origin coincides with beam-splitter and along the x and y axes. A rotation by an angle θ around y axis and ϕ around z axis brings the (x', y', z') frame onto the (x, y, z) frame

3.5 Astrophysical reach of a gravitational wave detector

An approximate yet realistic estimate of the astrophysical reach of GW detectors can be obtained by considering isotropic monochromatic source of GW [7]. We start from the expression of the GW flux and GW radiated energy given in Equations (1.22) and (1.24) respectively in section 1.2.2.

For monochromatic source emitting at frequency f_0 , we have

$$F_{GW} \approx \frac{\pi c^3}{4GT} f_0^2 h_{rss}^2 \quad (3.3)$$

where $h_{rss}^2 \equiv \int_T h_+^2(t) + h_\times^2(t) dt$. Here we integrated over the duration T which corresponds to the entire duration of the considered GW transient.

Assuming that the source is isotropic, we get from Equation (1.24)

$$E_{GW} = \frac{\pi^2 c^3}{G} D_L^2 f_0^2 h_{rss}^2 \quad (3.4)$$

CHAPTER 3. GRAVITATIONAL-WAVE INTERFEROMETRIC DETECTORS

More realistically, the emission pattern may be linear (e.g., supernova core collapse)

$$h_+(t) \sim \sin^2 \iota s(t) \quad (3.5)$$

$$h_\times(t) \sim 0 \quad (3.6)$$

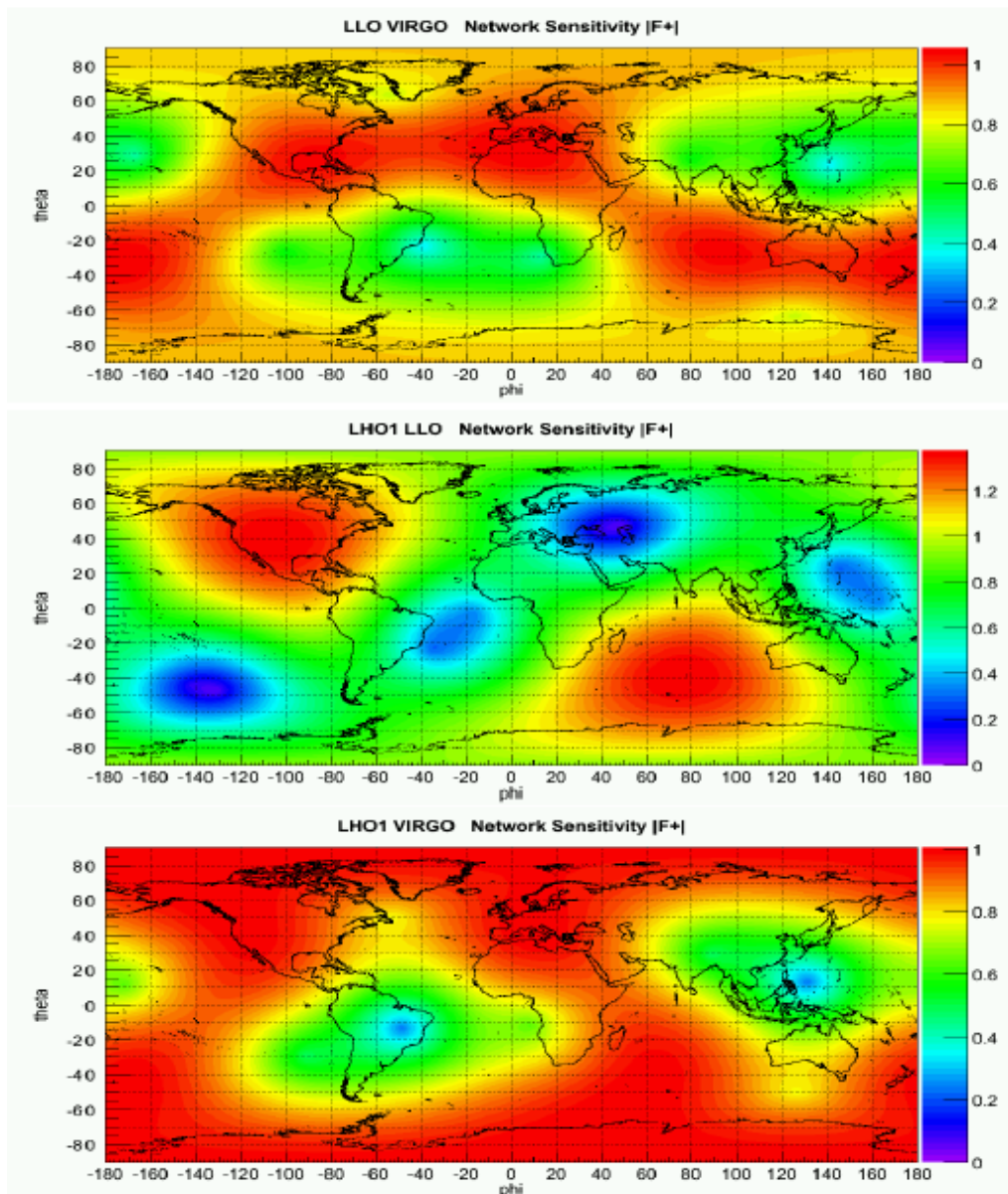


Figure 3.3 – The module of the plus component of the network antenna pattern considering the three couples of detectors: H1L1, H1V1, L1V1. The area which network are more sensitive (red colour) increase with respect to the single detector case. This immediately shows the advantage of using more than one detector.

3.3.5 Astrophysical reach of a gravitational wave detector

or elliptical (e.g., binary mergers)

$$h_+(t) \sim (1 + \cos^2 \iota)/2A \cos \Phi(t) \quad (3.7)$$

$$h_\times(t) \sim \cos \iota A \sin \Phi(t) \quad (3.8)$$

In that case, it is easy to show that the Equation (3.4) holds

$$E_{GW} = \alpha \frac{\pi^2 c^3}{G} D_L^2 f_0^2 h_{rss}^2 \quad (3.9)$$

with a rescaling factor α in section 1.2.2 whose value depends on the polarization pattern. We have $\alpha = 8/15$ and $\alpha = 2/5$ for linear and elliptical polarization respectively.

Let ρ define the signal-to-noise ratio (SNR),

$$\rho^2 \equiv \int \frac{|H(f)|^2}{S(f)} df \quad (3.10)$$

where $H(f)$ is the Fourier transform of the detector response $h(t) = F_+ h_+(t) + F_\times h_\times(t)$ as defined in Equation (3.1). $S(f)$ is the two-sided noise power spectral density.

For monochromatic sources, it is easy to show that

$$\rho^2 \approx \beta^2 \frac{h_{rss}^2}{S(f_0)} \quad (3.11)$$

where $\beta^2 = F_+^2 + F_\times^2$, $\beta^2 = F_+^2 \sin^2 \iota$ and $\beta^2 = F_+^2 ((1 + \cos^2 \iota)/2)^2 + F_\times^2 \cos^2 \iota$ for the isotropic, linear and elliptical emission patterns respectively as defined in Equations (3.5) and (3.7).

Combining Equations (3.11) and (1.24), we finally get

$$E_{GW} = \frac{\alpha}{\beta^2} \frac{\pi^2 c^3}{G} D_L^2 f_0^2 S(f_0) \rho^2 \quad (3.12)$$

It can be checked numerically that $\alpha/\beta^2 \approx 2$ for all polarization cases [7].

Consider a burst source that releases $E_{gw} = 10^{-2} M_\odot$ (which is the typical order-of-magnitude for mergers of stellar-mass compact objects) at frequency $f = 50$ Hz where Virgo sensitivity is $S^{1/2}(f) \approx 8 \times 10^{-23} / \text{Hz}^{1/2}$. By inverting the above Equation (3.12), we can compute that this source is detectable with SNR $\rho = 10$ at $D_L \sim 11$ Mpc. This is compatible with the distance estimates for the horizon of binary mergers (see reference [8]).

3.6 Worldwide network of gravitational wave detectors

The first generation of interferometric GW detectors includes a total of five large-scale instruments. The French-Italian project Virgo presented earlier. The US-based Laser Interferometer Gravitational-Wave Observatory (LIGO), which includes three kilometer-scale instruments located in Livingston, Louisiana and Handford, Washington (the latter hosts two interferometers in the same vacuum enclosure). GEO, a German-British detector in operation near Hannover, Germany (see Figure 3.4).



Figure 3.4 – Geographic location of the interferometric detectors. This world map displays the location of the four sites of the first generation detectors (LIGO H and L, Virgo and GEO).

3.6.1 Source positioning

GW detectors are non-imaging instruments with a nearly omni-directional response. Source localization therefore requires multiple detectors, in order to use the measured time delay between detectors as well as the amplitude of the measured signal in each detector to triangulate a sky location. Several methods of localization have been investigated. The timing accuracy of a GW signal can be written as [9]:

$$\sigma_t \sim \frac{1}{2\pi\sigma_f\rho} \quad (3.13)$$

where σ_f is the effective bandwidth of the source and ρ is the SNR. For nominal values $\sigma_f = 100$ Hz and $\rho = 8$, timing accuracies are of the order of 0.1 ms. This can be compared to the light travel time between detectors (10–30 ms for the LIGO-Virgo network) to deduce the angular uncertainty for the triangulation of times of arrival. For example, for a binary coalescence signal at the threshold of detectability, [9] estimates a best-case localization of 20 deg² (90% containment), and a typical localization of twice this. Additional constraints provided by other

instruments with a better angular accuracy such as HEN telescopes can therefore significantly help improving the source localization.

3.6.2 Sensitivities reached so far and coordinated data takings

In 2007, LIGO and Virgo have concluded an agreement which includes the data sharing and coordination of their data takings. The first joint data taking is the LIGO fifth Science Run (or S5) and the first Virgo Science Run (or VSR1). The former started on November 4th, 2005 and ran until October 1, 2007; and the later began on May 18, 2007 until Sep 30, 2007. A second joint data taking with enhanced detectors, S6/VSR2-3, began on 7 July 2009 and ended on 20 October 2010.

We show in Figures 3.5 and 3.6 the strain sensitivity that these detectors reached during S5/VSR1 and S6/VSR2-3 respectively.

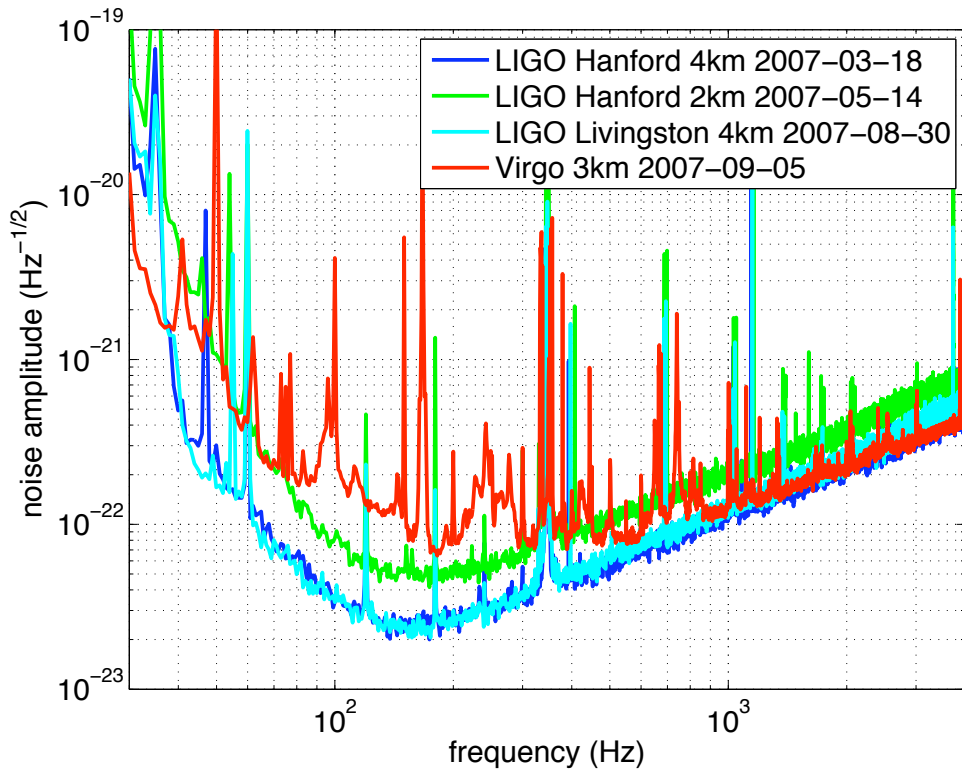


Figure 3.5 – Typical Virgo and LIGO sensitivity curves during the joint science run S5/VSR1

3.7 Analysis of gravitational wave data

The output of a GW detector is a time series which contains the response to an impinging GW $h(t)$ and the instrumental noise $n(t)$. The astrophysical sources are expected to be rare

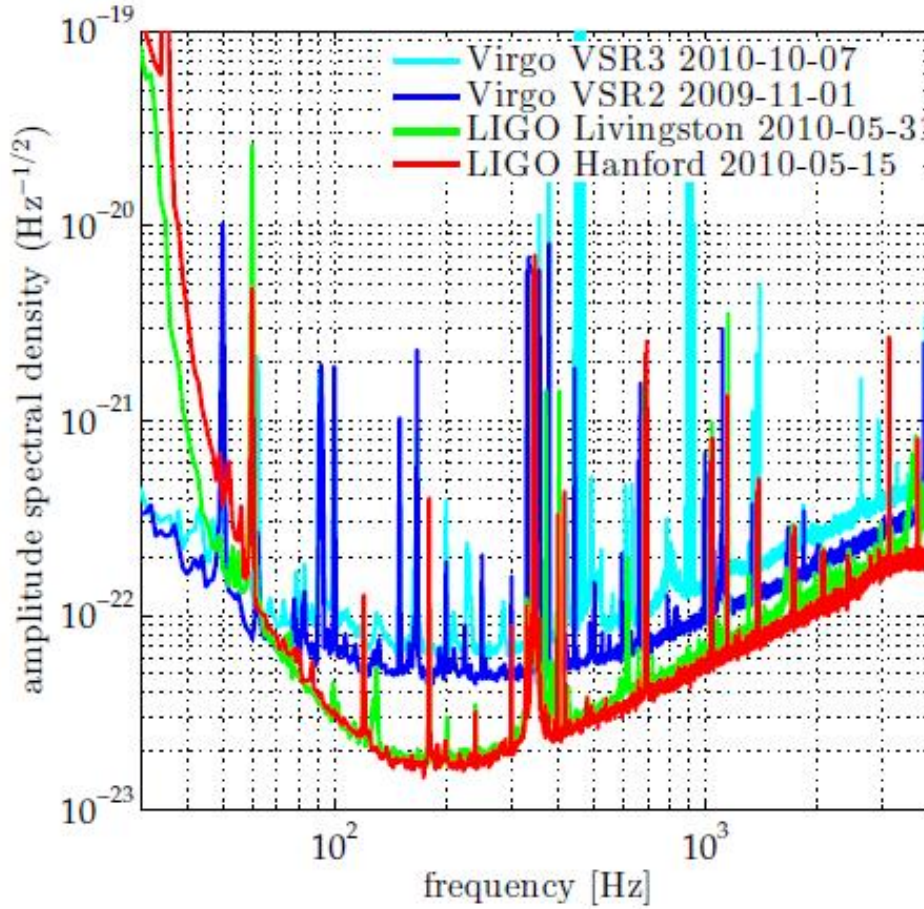


Figure 3.6 – Typical Virgo and LIGO sensitivity curves during the joint science run S6/VSR2-3

with signature at the limit of detectability. Efficient signal processing methods are thus required to detect the GW signal at low SNR.

Two distinct cases can be considered: (i) the GW signal is known to a good accuracy thanks to reliable astrophysical models; (ii) the GW signal is unknown or poorly known. In the first case, it can be shown that under that the noise is stationary and Gaussian, the optimal detection method is the *matched filtering*. Essentially this consists in cross-correlating the data with the expected signal. A detection is made when an excess of correlation is observed. In the second case (unmodelled burst signals), *time-frequency* techniques are used to extract transient signals from the background noise. We considered that the joint sources of GW and HEN falls in the latter category.

In this section, we give a general overview of the methods and techniques used for the detection of GW bursts. We also introduce in the section two algorithms used to search for GW bursts: the *X-pipeline* and *coherent WaveBurst* (cWB). Both those methods have been

used in the context of the joint GW and HEN searches we present in Chapters 4 and 5.

3.7.1 Wavelets and time-frequency analysis

Fourier transform decomposes a signal into its frequency components. The power spectrum provides information about frequency only. The temporal localization is cancelled. A time-frequency distribution is a transform that maps a 1-D signal into a 2-D time-frequency map, which describes the evolution of spectra over time. Each pixel in this map represents the signal power at a given time and frequency.

There exists various ways to produce such representation. Short-term Fourier analysis or wavelet based transforms are the most commonly used. This consists in replacing the Fourier basis composed of long-duration complex exponentials by short duration signals called wavelets concentrated about a given time and frequency. The time-frequency representation results from the projection of the signals on the wavelet basis.

Stationary background noise is associated with a homogeneous wavelet representation while transient signals appears as a localized excess of power. This can be used to detect GW transients by searching for clusters of connected time-frequency pixels (associated with an outstanding power). An example of the time-frequency representation of a transient is given in Figure 3.7.

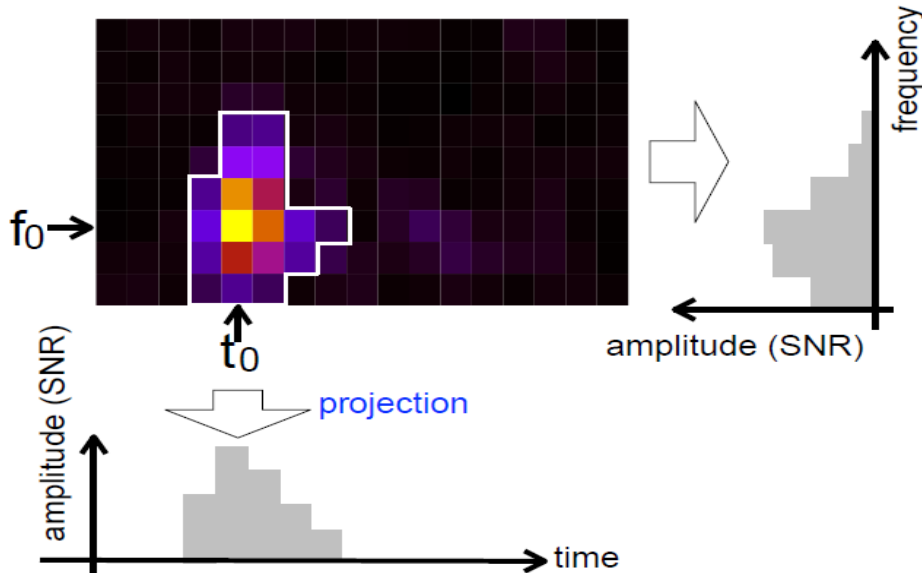


Figure 3.7 – Time-frequency representation and its projection to time- and frequency-axis respectively. (source: [10])

3.7.2 Multi-detector analysis

In the previous section, we described the basic methods used for the analysis of the data stream from a single detector. In the following, we will be interested in aspects specifically related to multiple data streams. The availability of multiple data streams impacts on the way the data are analyzed at different levels.

Coherent analysis of multiple data stream

Coherent excess power methods used to search for unmodelled GW bursts require that the signals received by all detectors are *consistent* in time *and* phase. Concretely this is realized by combining the data streams from multiple detectors, taking into account the antenna response and noise level of each detector so that the sum operates constructively for a GW burst from a given sky direction. The data stream which results from this coherent combination maximises the signal-to-noise ratio (SNR). It is used to produce a time-frequency map of the signal energy (equivalently, the SNR), which is then scanned for transient excursions (or *events*) that may be GW signals. Each event is characterised by a measure of significance, based on energy and/or correlation between detectors, as well as its time-frequency properties. Another outcome from this type of analysis is the probability (pseudo-)distribution over the sky usually referred to *sky map* from which the most likely location of the source can be extracted (see Figure 3.8).

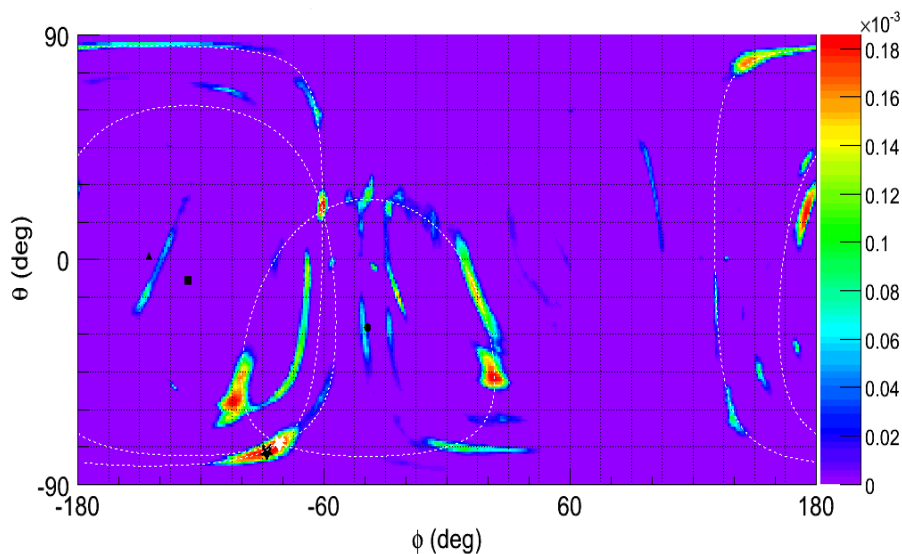


Figure 3.8 – An example of sky map of network statistics for a three detector networks. (source [11])

Mitigation of non-Gaussian/non-stationary noise with multiple data

Fundamental noises presented above are expected to be Gaussian and stationary. However, the real instrument noise is dominated by an overwhelming fraction of non-Gaussian non-stationary noises from various origins. It consists in a large number of transient noise excursions commonly called *glitches*. Glitches are produced by a variety of environmental and instrumental processes, such local seismic noise or saturations in feedback control systems. Since glitches occasionally occur nearly simultaneously in separate detectors by chance, they can mimic a gravitational-wave signal.

The population of glitches are difficult to model. The size and the large complexity of GW detectors makes this modelling even more difficult. GW detectors being extended instruments over kilometers, it is hard to completely isolate them from the outside world and the surrounding anthropic activity. Therefore, the accurate modelling of the non-Gaussian/non-stationary noise background is for now out-of-reach. It has to be mitigated and this can be done at least partially by using multiple data.

It is possible to calculate combinations of the data from multiple detectors where the GW signals from all detectors interfere destructively in the sum. The GW signal thus cancels, but not background glitches. The energy in these “null” stream(s) may be used to reject or down-weight events not consistent with a gravitational wave. The success of such tests depend critically on having several independent detectors of comparable sensitivity. The cross-correlation with auxiliary non-GW sensitive channels (which monitors the global status and environment of the GW detector) provides also an important resource for background rejection.

Use of multiple data for background estimation

We explained earlier that the accurate modelling of non-Gaussian non-stationary noise is out-of-reach. The remaining part of the glitches that cannot be identified by the coherent techniques described in the previous section constitutes the dominating background noise in burst searches. This background has to be estimated. However, GW signals cannot be turned off: the detectors cannot be shielded from them. Therefore, we don't have “noise-only” data at disposal for background estimation.

Nevertheless, the background can be estimated thanks to the availability of multiple data streams by time shifting one detector's data with respect to the others by a delay much longer than the time-of-flight between detectors. Time shifts only leave triggers due to random coincidences in detector noise and erase the contribution from real GW signals. By repeating the analysis many times with different time-shifts, we get an accurate estimate of the rate of background events.

3.7.3 Sensitivity estimate

We test the performance of the search algorithms by repeatedly adding fake gravitational wave signals to the raw data stream and estimating the detection efficiency of each “injected” waveform models. The astrophysical origin and waveform morphology, of the gravitational wave bursts we search for in this work are a priori unknown. A broad range of signal waveforms were considered for the analysis of 2007 data presented in Chapter 4. These include astrophysically-motivated waveforms as well as ad-hoc waveforms. The list of test signals includes:

- ***Sine-Gaussian waveforms*** both linearly polarized

$$h_+(t + t_0) = h_0 \exp(-t^2/(4\tau^2)) \cos(2\pi f_0 t) \quad (3.14)$$

$$h_\times(t + t_0) = 0 \quad (3.15)$$

or circularly polarized

$$h_+(t + t_0) = \frac{1 + \cos^2 \iota}{2} h_0 \exp(-t^2/(4\tau^2)) \cos(2\pi f_0 t) \quad (3.16)$$

$$h_\times(t + t_0) = \cos \iota h_0 \exp(-t^2/(4\tau^2)) \sin(2\pi f_0 t). \quad (3.17)$$

The latter case mimics at least qualitatively the expected GW emission from the final part (merger and ringdown) of the coalescence of a neutron-star and/or black-hole binary. It also provides a reasonable model for the GW emission from some of the extreme scenarios considered for core-collapse supernovae described in section 1.3.1.

In the above equations, f_0 is the central frequency, t_0 is the central time and the decay time $\tau \equiv Q/(\sqrt{2\pi}f)$. Q is the effective number of cycles of the waveforms with values ranging from 2 to 100.

- ***White noise bursts*** are bandpassed random time-series of selected duration with independent polarization amplitudes. White noise bursts can be considered as a limiting case: their waveform does not help to distinguish them from the detector noise. The only discriminant property used to detect them is that they are correlated signatures in the various detector data.
- ***Ring-down waveforms*** are expected from processes like f-modes of NS, or during the ring-down of newly formed BH/NS during the post merger phase after coalescence, or produced in SN star-quakes related to Soft Gamma Repeaters (SGR). They are characterized by their frequency f_0 , duration τ or Q (similarly to SG) and polarization. They

have the following expression:

$$h_+(t + t_0) = \sin(2\pi f_0 t) \exp(-t/\tau) \quad (3.18)$$

$$h_\times(t + t_0) = \cos(2\pi f_0 t) \exp(-t/\tau) \quad (3.19)$$

Figure 3.9 illustrates the various families of waveforms injected into data for simulation studies in time and time-frequency domain.

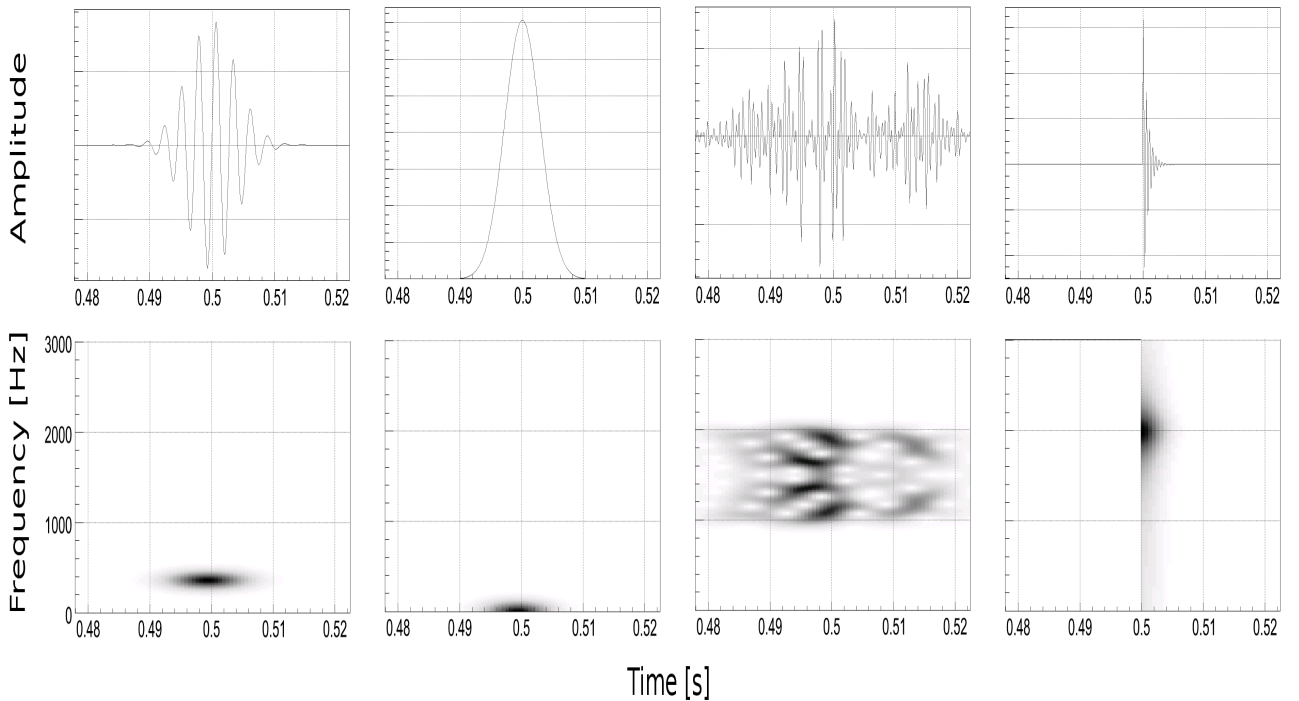


Figure 3.9 – Representation of waveforms in the time domain (top row) and a time-frequency domain (the bottom row). From left to right: a 361 Hz $Q = 9$ sine-Gaussian, a $\tau = 4.0$ ms Gaussian waveform, a white noise burst with a bandwidth of 1000-2000 Hz and characteristic duration of $\tau = 20$ ms and, finally, a ringdown waveform with a frequency of 2000 Hz and $\tau = 1$ ms. (source: [13])

3.7.4 Data analysis methods to search for gravitational wave bursts

The X-pipeline algorithm

X-pipeline is an analysis algorithm for interferometric gravitational wave detection. It deals with unmodelled gravitational wave bursts associated with external astrophysical triggers such as gamma rays or neutrinos. The X-pipeline processes data *coherently* from an arbitrary network of GW detectors in the frequency band 64-500 Hz.

For a specific time and direction, the X-pipeline reads the appropriate GW data and Fourier transforms it. Then for each specified direction it makes a time-frequency map of the time-series data, and computes the different statistics for each time-frequency bin, mainly coherent energies. After that, the X-pipeline looks at a fixed percentage (e.g. 1%) of bins with the highest value of the detection statistics (measured coherent energy) and marks those bins as black bins, see Figure 3.10. Black bins that share a common side are grouped together into clusters which are considered a candidate detection event [12].

X-pipeline algorithm is used, with a slightly modifications that will be discussed later, in this work to analyse the ANTARES, LIGO and Virgo data from 2007. Results are presented in Chapter 4.

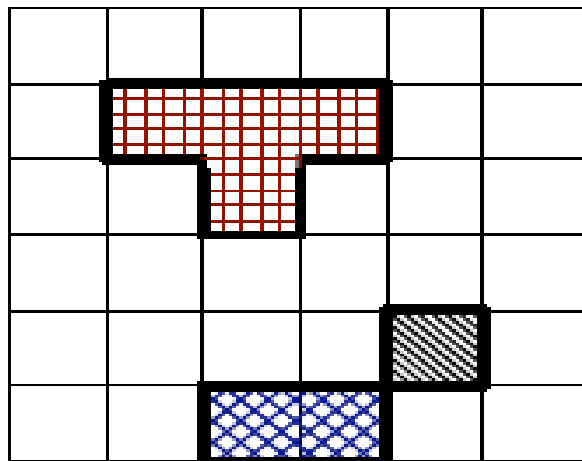


Figure 3.10 – A time frequency map with "black" pixels grouped into 3 clusters. Nearest-neighbor black pixels (those that share an edge) are grouped into a single cluster. Each cluster in this image is denoted by a different color and hatching pattern. (Source [12])

The coherent WaveBurst algorithm (cWB)

coherent WaveBurst (cWB) [14, 15] is, in contrast with the X-pipeline, an un-triggered (all-sky) search algorithm for detecting gravitational wave burst. It uses the constraint likelihood approach [16] to construct a least-squares fit of the two GW polarizations to the combined data from a network of detectors in the frequency band 64-5000 Hz. The cWB analysis is performed in several steps. First, detector data is decomposed into a time-frequency representation and then whitened and conditioned to remove narrow-band noise features. Events are identified by clustering time-frequency pixels with significant energy which is coherent among detectors and characterized using test statistics derived from a constrained (regulated) likelihood (which is also a measure of the signal energy detected in the network and is calculated as described

in [16]). Two statistics are computed by cWB. The first is a network correlation coefficient net_{cc} , which is a measure of the degree of correlation between the detectors. The second is the coherent network amplitude ρ and is proportional to the signal-to-noise ratio. The latter is used to rank events within a homogeneous sub-period.

A triggered version of cWB, named *skymask coherent WaveBurst* (s-cWB), has been developed and used in the analysis presented in Chapter 5. Further details about the s-cWB are discussed in Chapter 5.

CHAPTER 3. GRAVITATIONAL-WAVE INTERFEROMETRIC DETECTORS

REFERENCES

- [1] E. GERTSENSHTEIN AND V. I. PUSTOVOIT, Soviet Physics JETP 43, 605-607 (1962). 81
- [2] R. WEISS, Quarterly Progress Report, Research Laboratory of Electronics, MIT 105: 54 (1972). 81
- [3] P. SAULSON, Fundamentals of Interferometric Gravitational Wave Detectors, World Scientific, (1994). 81
- [4] F. ACERNESE ET AL, Class. Quantum Grav. 25, 114045 (2008). 82
- [5] F. BEAUVILLE, Virgo Technical Paper, VIR-NOT-ROM-1390-262. 83
- [6] F. ACERNESE ET AL, Astropart. Phys. 33, 182-9 (2010). 83
- [7] P. J. SUTTON, LSC Technical Paper, P1000041. 85, 87
- [8] J. ABADIE ET AL, e-Print, arXiv:1203.2674 [gr-qc] (Mar. 2012). 87
- [9] S. FAIRHURST, New J. Phys., 11, 123006, (2009). 88
- [10] H. RYOTA ET AL, 12th GWDAW (Gravitational Wave Data Analysis Workshop), arXiv:0804.0296 [gr-qc] (2008). 91
- [11] <http://www.ligo.org/science/GW100916/>. 92
- [12] P. J. SUTTON ET AL, New J. Phys. 12 053034 (2010). 96
- [13] J. ABADIE ET AL, Phys. Rev. D 85, 122007 (2012). 95
- [14] S. KLIMENKO ET AL, Class. Quantum Grav. 25, 114029, (2008). 96
- [15] M. DRAGO, PhD thesis, Università degli Studi di Padova (2010). 96
- [16] S. KLIMENKO ET AL, Phys. Rev. D 72, 122002 (2005). 96, 97

REFERENCES

CHAPTER 4

GW+HEN ANALYSIS OF 5L-S5/VSR1

4.1 Summary

In this chapter we present the first joint search for gravitational-wave bursts associated with high energy neutrinos. Contrarily to the analysis presented in chapter 5, this first search was not jointly optimized: we used the neutrino candidate list obtained for a point source search and looked for possible concomitant, both in time and direction, GW signal using an algorithm specially designed for this kind of *triggered* searches. In this chapter, we describe the method used for this first search and take special care to the description of the neutrino candidate selection using the 2007 data set of ANTARES, LIGO and VIRGO detectors. All detectors were running in their initial sensitivity: ANTARES was running in 5-lines (5L) configuration; LIGO and VIRGO were just finishing their first science runs (S5) and (VSR1) respectively. The outcome of this first search is submitted for publication in the Astrophysical journal [1] and has led to several public presentations [2]. No significant coincident events were observed. We placed limits on the density of joint HEN+GW emission events in the local universe, and compare them with densities of merger and core-collapse events.

4.2 High energy neutrino triggered search procedure

The outline of the proposed search procedure [3–6] is shown in diagram 4.1. The GW+HEN joint search is performed by combining GW and HEN data using a *triggered* analysis [7, 8]. Using the latter, the search for GW signals is then restricted to an astrophysically motivated range of arrival times around the neutrino time and in its estimated direction. Compared to a classical method where GW signals are searched for with random arrival time, triggered searches can be run with a lower event detection threshold thanks to the reduction in the volume of analyzed data. This leads to a higher detection probability at a fixed false alarm probability

and better limits in the absence of detection. Similarly, the *a priori* knowledge of the source direction allows for searching only a small part of the sky and vetoing candidate events at times not consistent with the expected GW arrival time. In fact, the number of accidental coincidences between GW detectors decreases as the size of the search window decreases. This part of the sky is referred to as *angular search window* (or ASW) and is described in section 4.4.1. Thus, the use of an external trigger can be a very effective tool for a successful search of GW signals.

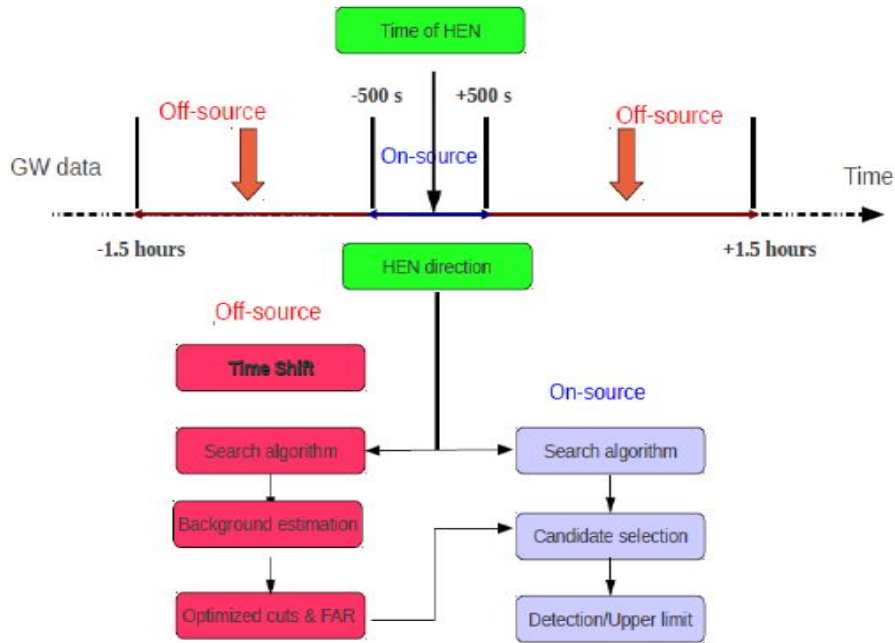


Figure 4.1 – Schematic flow diagram of a HEN-triggered search for GWs. Each neutrino candidate (with its time and directional information) provided by ANTARES acts as an external trigger for the GW algorithm, which searches the combined GW data flow from all active interferometers (ITFs) for a possible concomitant signal. The size of the spatial search window is related to the angular accuracy associated to each HEN candidate. The background estimation and the optimization of the selection strategy are performed using time-shifted data from the off-source region in order to avoid contamination by a potential GW signal. Once the search parameters are tuned, the box is opened and the analysis is applied to the on-source data set.

In the present analysis, the external trigger is a neutrino candidate provided by ANTARES. The neutrino candidate, used as input for the GW+HEN joint search, is characterized by a set of parameters: its sky position \vec{d} , as given by the direction of the reconstructed muon track, the associated (and possibly direction-dependent) point-spread function of the detector (PSF), the neutrino arrival time, which defines the trigger time t_0 , and the range of possible time delays (positive and negative) Δt between the neutrino signal and the associated GW signal, which is astrophysically motivated, as discussed in section 1.3.3. The latter quantity is referred to as the *on-source* window for the neutrino; this is the time interval which is searched

for GW candidate signals. To estimate the significance of the resulting GW candidates, the background rate has to be approximated using time-shift analysis as described in section 3.7.2. This background study is performed in an *off-source* window (shown in red on the diagram of Figure 4.1) around the time of the neutrino candidates.

The GW data used in this thesis are the LIGO S5 runs and VIRGO VSR1 runs (see section 3.2). These data are selected from periods where the detectors H1, H2, and V1 were in science mode, i.e. usable for the detection of GW. The LIGO fifth "science run" (S5) ranges from November 4, 2005 until September 30, 2007 [9, 10]. Over one year of science-quality data were collected with all three LIGO interferometers in simultaneous operation at their design sensitivity, with duty factors of 75%, 76%, and 65% for H1, H2, and L1 respectively. The Virgo detector started its first science run, VSR1 [11], on May 18, 2007. The Virgo duty factor over VSR1 was 78%. The GW data used in this analysis cover the period between January 27 and September 30, 2007.

4.3 Selection of High Energy Neutrino candidates

4.3.1 The ANTARES data and Monte Carlo sample

The 5L data sample of ANTARES ranges from January 27 to December 4, 2007 [12]. This analysis is restricted to the data taking period overlapping with the science runs of VIRO and LIGO detectors: January 27 to September 30, 2007.

The ANTARES sample is composed of the so-called silver runs selected by data quality criteria applied on all runs. The silver data set is obtained by accepting a baseline rate up to 120 kHz and a burst fraction up to 40% (cf paragraph 2.4). For each detector configuration at least 80% of OMs are required to be active over the full run. This means that among 375 channels a minimum of 300 OMs were active during the 5L period. Taking into account all the above mentioned criteria and the 20% dead time present in the on-line trigger at that period [13, 14], the remaining active time is $T_{obs} = 104$ days. The final common observation time, considering the duty cycle of the LIGO-Virgo detectors, reduces to $T_{obs}^{com} = 91.36$ days. The events are triggered with the $3N$ filter (section 2.3.5). The raw data are processed with the BBfit *v3r6* (section 2.6.1). The set of calibration used for these data are shown in the table 4.1.

In the following we will distinguish between events reconstructed with 2-lines (2L) and those reconstructed with 3-lines and more (3L+). This distinction comes from the presence of two mirror tracks in the case of events reconstructed with 2L, for BBfit *v3r6*. As mentioned in

| first run → last run | Calibration set |
|----------------------|-----------------|
| 25700 → 27640 | 2007:L5:V4.0 |
| 27729 → 29763 | 2007:L5:V4.1 |

Table 4.1 – Calibration sets used to calibrate data

section 2.6.1 this version allows access to both mirror tracks. This is a crucial improvement for the present triggered search as it allows to reduce the size of the search window and consequently the background rate. This improvement is illustrated in section 4.4.1

Various Monte Carlo files are simulated as described in section 2.5. In this thesis the neutrino sample is simulated by GENHEN and weighted according to the Bartol flux for atmospheric neutrinos and an E^{-2} spectrum for cosmic neutrinos. The sample of atmospheric muons is simulated with CORSIKA and weighted with the Battistoni flux. All the MC files used in this analysis are processed by TriggerEfficiency with the 3N trigger. In Figure 4.2 we show the distributions of the nadir angle θ (as introduced in section 2.3.2) for data and MC samples. The colour code of the nadir distributions is the following:

- Turquoise curve: the MC truth for down-going atmospheric muons, which have been simulated within $90^\circ \leq \theta \leq 180^\circ$.
- Red curve: the reconstructed θ for MC atmospheric muons.
- Green curve: the MC truth for atmospheric neutrinos, which have been simulated in the range $0^\circ \leq \theta \leq 90^\circ$.
- Blue curve: the reconstructed θ for MC atmospheric neutrinos.
- Black curve: data.

The red curve extends over the whole range of θ in contrast of MC truth, showing that the majority of events with $\theta \leq 90^\circ$ are atmospheric muons misreconstructed as up-going. Cuts based on the above parameters will be studied in the next section to remove these misreconstructed muons and select a sample of data with optimized discovery potential.

4.3.2 Event selection criteria

The first step of the selection is to keep only upgoing tracks:

cut 1: $\theta \leq 90^\circ$

4.4.3 Selection of High Energy Neutrino candidates

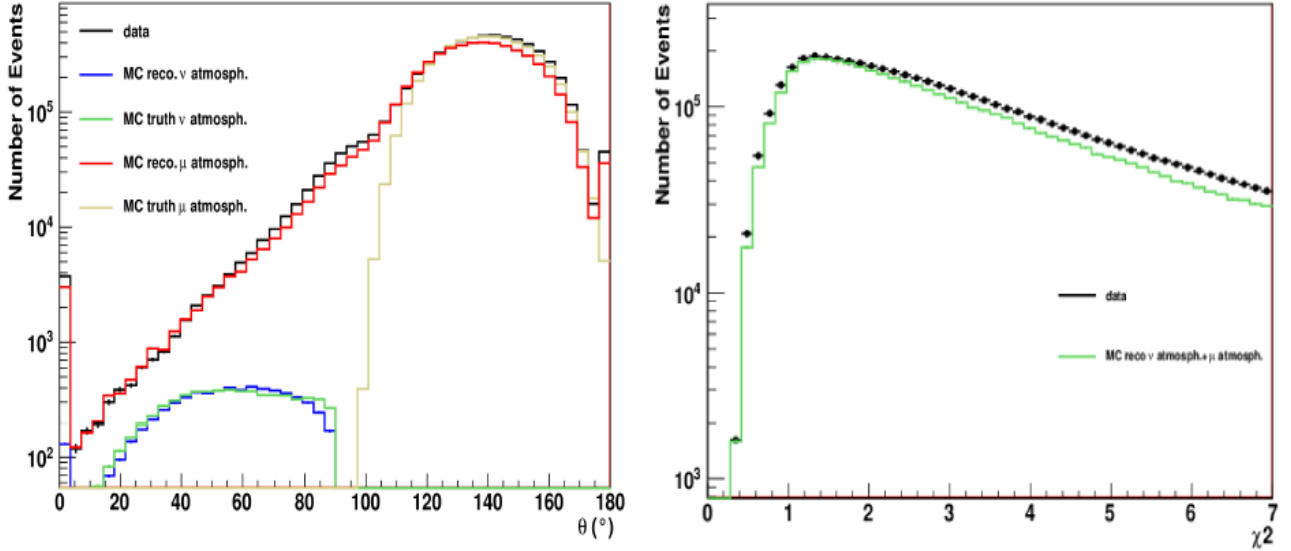


Figure 4.2 – Left: distributions of nadir θ for the data and MC. The colour code is explained in the text. We see that part of the atmospheric muons are reconstructed as upgoing while they are downgoing. Those are known as *misreconstructed* atmospheric muons. Right: distribution of the track χ^2 for data and MC including all the reconstructed events.

The subsequent steps are motivated by the will to distinguish remaining misreconstructed atmospheric muons from the desired muons originating from the interaction of upgoing neutrinos around the detector. The parameters used for this selection are the quality parameters χ^2 , $b\chi^2$ presented in section 2.6.1, whose distributions are illustrated in Figure 4.3.

After selecting the events passing the cuts, it is easy to compute with the MC simulations, the effective surface that represents the detector sensitivity for the given set of cuts. The neutrinos effective area is defined as the ratio of the rate of selected events to the neutrino flux at Earth:

$$A_{\nu}^{eff}(E_{\nu}, \theta) = \frac{N_{sel}}{N_{gen}} \times V_{generation}(E_{\nu}, \theta) \times (\rho \cdot N_A) \times \sigma(E_{\nu}) \times P_{Earth}(E_{\nu}, \theta) \quad (4.1)$$

Where N_{sel} and N_{gen} stand for the selected and generated events respectively. While, $V_{generation}$, ρ , N_A , P_{Earth} were introduced in section 2.5. For illustration purposes, we show in Figure 4.9 the neutrino effective area as function of neutrino energy.

In the present analysis, the final cuts on χ^2 and $b\chi^2$ are derived in such a way to maximize the chances to discover a point-like source of HEN following the prescriptions detailed in [15, 16]. The objective is to maximize the so-called discovery potential. In order to do so we minimize the model discovery factor (MDF) that is defined, for a point source at declination δ , emitting

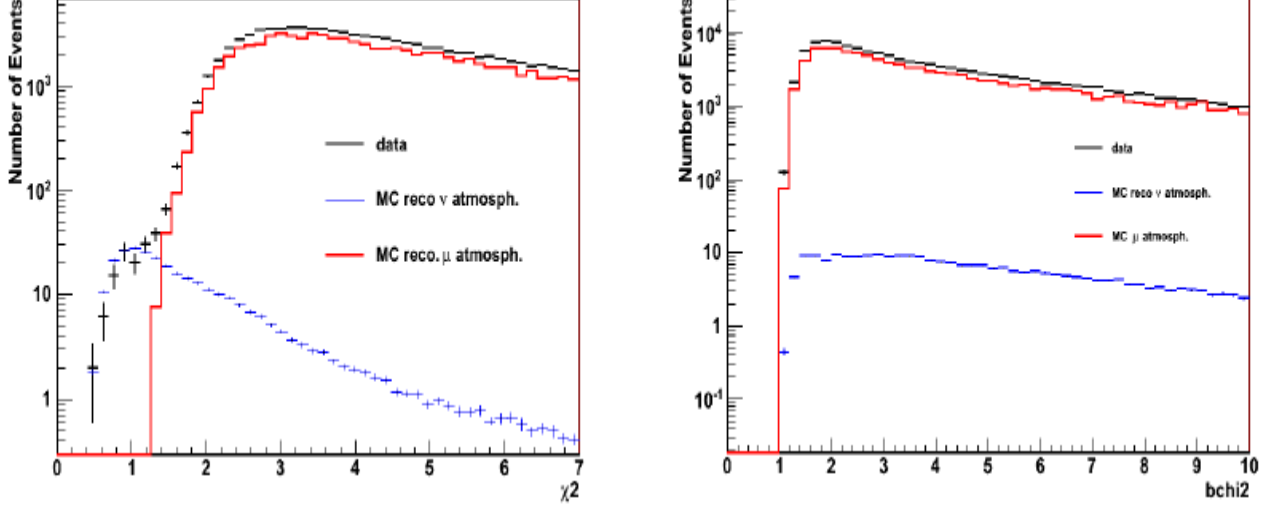


Figure 4.3 – Distributions of the track χ^2 (left) and the bright point $b\chi^2$ for Data and MC including all the events reconstructed as upgoing.

a power law flux with spectral index γ , as:

$$E^\gamma \frac{d\Phi(\delta)}{dEdSdt} = \frac{N_{sig}(\delta)}{A_{eff}(\delta) \times \Delta t \times \int_{E_{min}}^{E_{max}} E^{-\gamma} dE} \quad (4.2)$$

where:

- $N_{sig}(\delta)$ is the average expected number of signal events needed to have a 50% probability to make a discovery at the 5σ level.
- $A_{eff}(\delta)$ is the effective area as defined by Equation (4.1).
- Δt is the live time of selected runs.
- $[E_{min}; E_{max}]$ is the simulated events energy range.

Several combinations of values were tried for the maximization of the discovery potential:

- χ^2 : 1.4, 1.6, 1.8, 2.0, 2.2, 2.4, 2.6.
- $b\chi^2$: 1.0, 1.4, 1.8, 2.2, 2.6.

Examples are shown in Figure 4.4 for a variety of cuts on χ^2 and for different nadir angle ranges, applying a cut on $b\chi^2 \geq 1.8$. Figure 4.5 shows other examples for 2 other cuts on $b\chi^2$.

4.4.3 Selection of High Energy Neutrino candidates

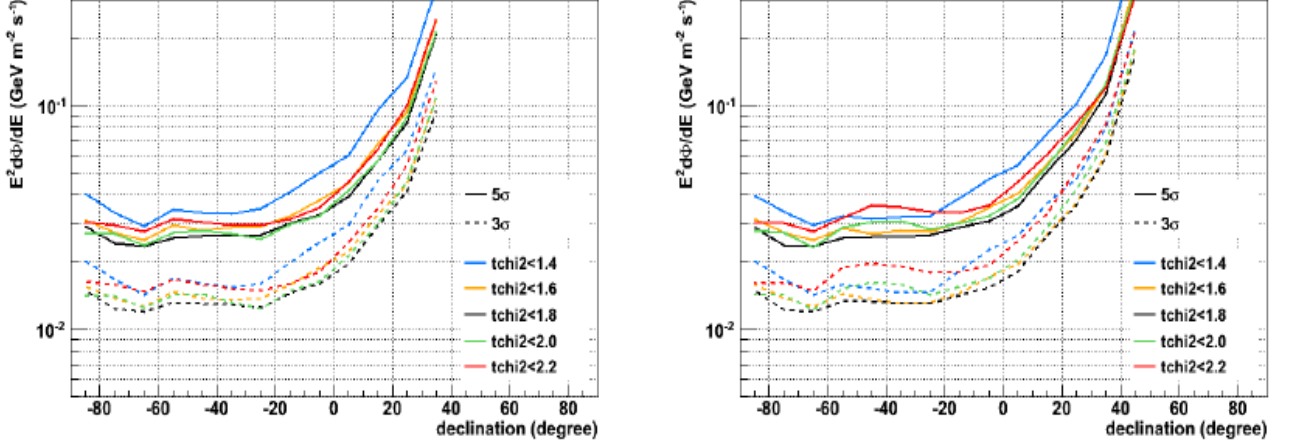


Figure 4.4 – Model discovery factor, for different values of χ^2 (labeled "tchi2" in the legend), for $b\chi^2 \geq 1.8$ and $\theta \leq 80^\circ$ (left), $\theta \leq 90^\circ$ (right). (Source [16])

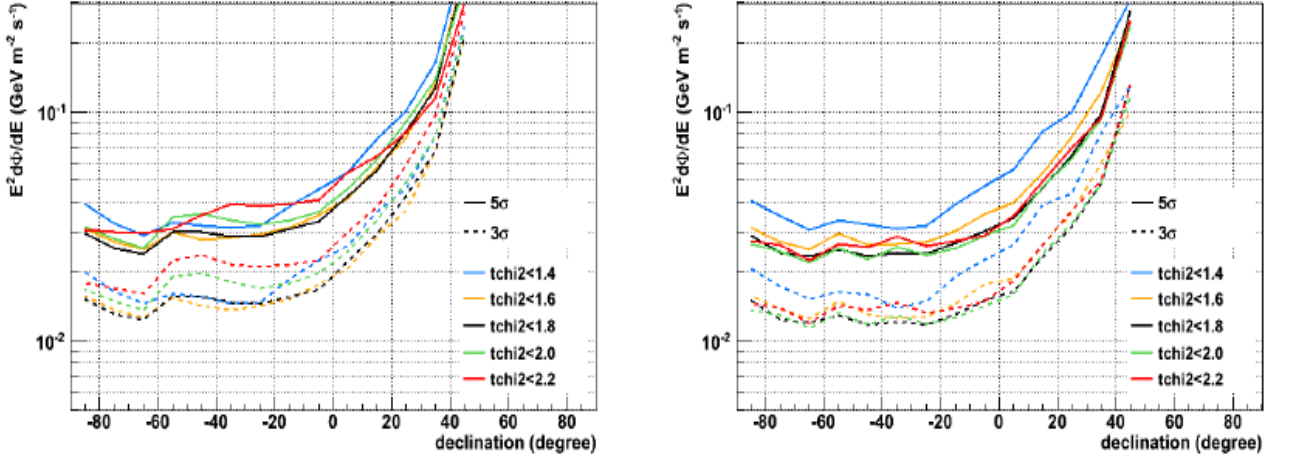


Figure 4.5 – Model discovery factor, for different values of χ^2 (labeled "tchi2" in the legend), for $\theta \leq 90^\circ$ and $b\chi^2 \geq 1.0$ (left), then $b\chi^2 \geq 2.6$ (right). (Source [16])

At this stage the following cuts $\theta \leq 90^\circ$, $\chi^2 \leq 1.8$ and $b\chi^2 \geq 2.2$ yield one of the best discovery potentials for a large declination band. However, applying these cuts implies a relatively high contamination of atmospheric muons close to the horizon, i.e. $80^\circ < \theta \leq 90^\circ$. To reduce this contamination it has been decided to apply a tighter χ^2 cut in this specific nadir θ range. Thus, the final chosen cuts are:

cut 2: $b\chi^2 \geq 2.2$. This cut is illustrated in Figure 4.6. This rejects events from large electromagnetic showers likely to appear in downgoing muon bundles.

cut 3: Further cuts are applied on the track depending on the arrival direction of the candidate: $\chi^2 \leq 1.8$ when $\theta \leq 80^\circ$ and $\chi^2 \leq 1.4$ when $80^\circ \leq \theta \leq 90^\circ$. Figure 4.7 illustrates the discrimination power of these cuts for both nadir ranges.

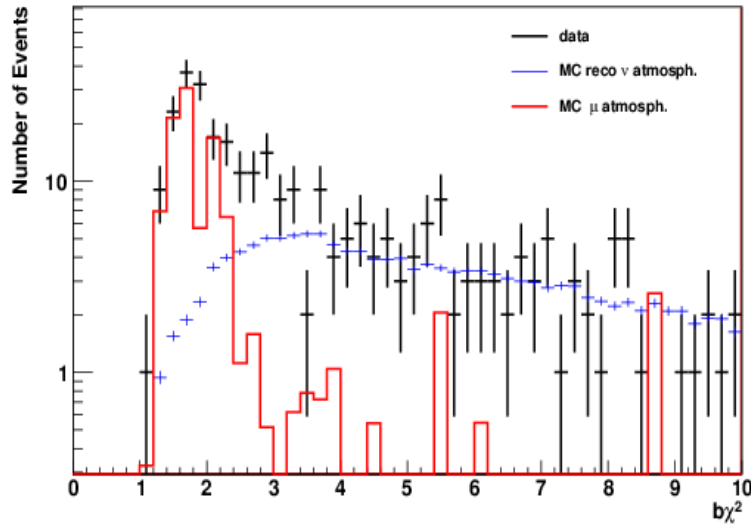


Figure 4.6 – Bright point fit distributions for up-going events for data and MC where **cut 3** has been applied. Since a bright point is a point-like light source which emits a isotropic light flash at a given moment, events with a very good bright-points fit are not retained as they are not compatible with a muon track. This is more likely to happen with mis reconstructed atmospheric muons.

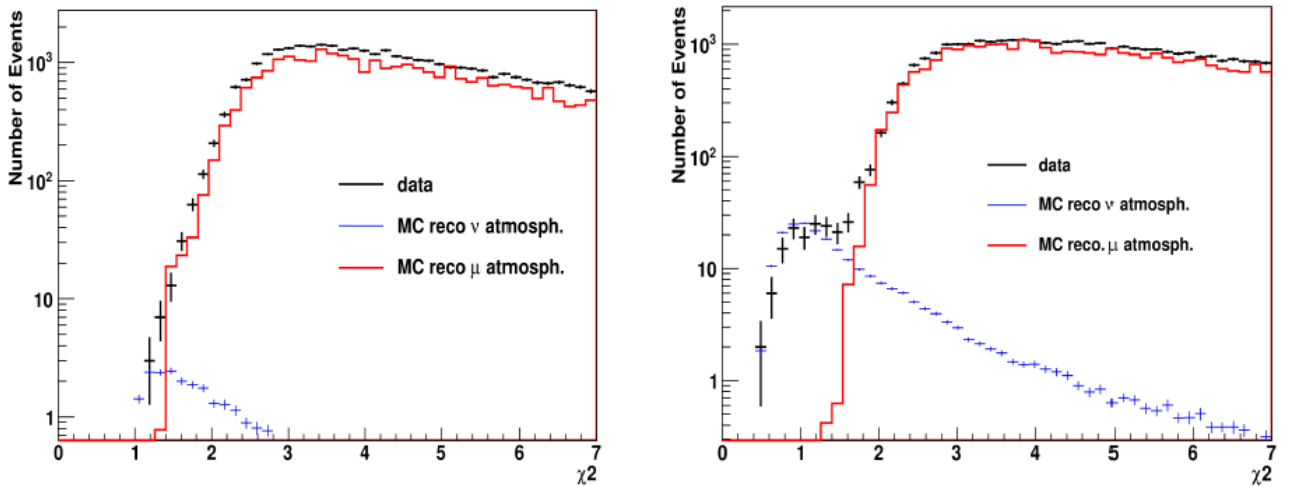


Figure 4.7 – Quality distributions of the track fit for up-going events for data and MC in the range of $\theta \leq 80^\circ$ (right) and in the range $80^\circ \leq \theta \leq 90^\circ$ (left). The cut on $b\chi^2 \geq 2.2$ is applied in both cases.

4.4.3 Selection of High Energy Neutrino candidates

In this section we have described a set of cuts derived from MC sample to discriminate between the true neutrino signal and the background of atmospheric muons. We have shown that using two quality fit values $\chi^2 \leq 1.8$ when $\theta \leq 80^\circ$, and $\chi^2 \leq 1.4$ when $80^\circ \leq \theta \leq 90^\circ$ allows to cut out most misreconstructed upward going muons. The percentage of remaining atmospheric muons (or contamination) in the final data sample is estimated to be roughly less than 20%.

Figures 4.8 shows the distributions of the nadir angle and the sine of the declination for the events selected with the final cuts, which are globally consistent with the MC expectations.

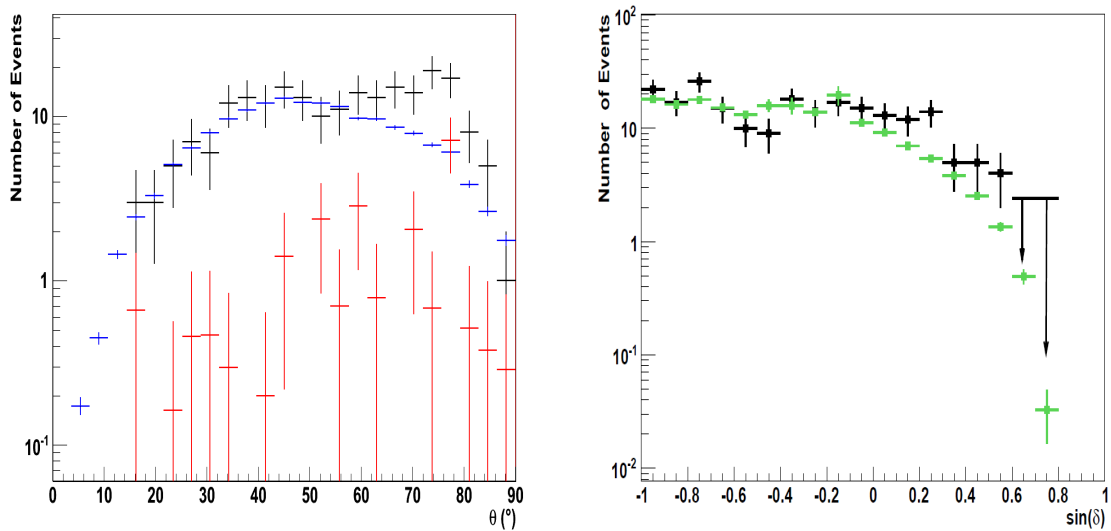


Figure 4.8 – Left: θ distributions for data and MC samples (blue: atmospheric neutrinos, red: atmospheric muons). Right: distributions of the sine of the declination for data (black) and MC (green: total atmospheric background). All cuts are applied.

The corresponding effective surface, as defined by Equation (4.1) is shown on Figure 4.9 as a function of the neutrino energy. To characterize further the potential physics yield of the selected sample, we define the sensitivity as the median 90% upper limit obtained over an ensemble of simulated experiments with zero-signal assumption. The sensitivity of the HEN search has been quantified for the whole 5 line data period. It depends on the declination of the potential source. Figure 4.10 shows the sensitivity for the search using the selection criteria described above and assuming an E^{-2} spectrum. From the curve it's shown that the best sensitivity is estimated to be $E^2 \frac{dN}{dE} \approx 10^{-6} \text{ GeV cm}^{-2} \text{ s}^{-1}$.

In the next section, we discuss into details the angular accuracy that can be expected applying the present cuts. This angular accuracy not only depends on the reconstruction parameters, but also on the energy of the selected events. We discussed in chapter 1 that

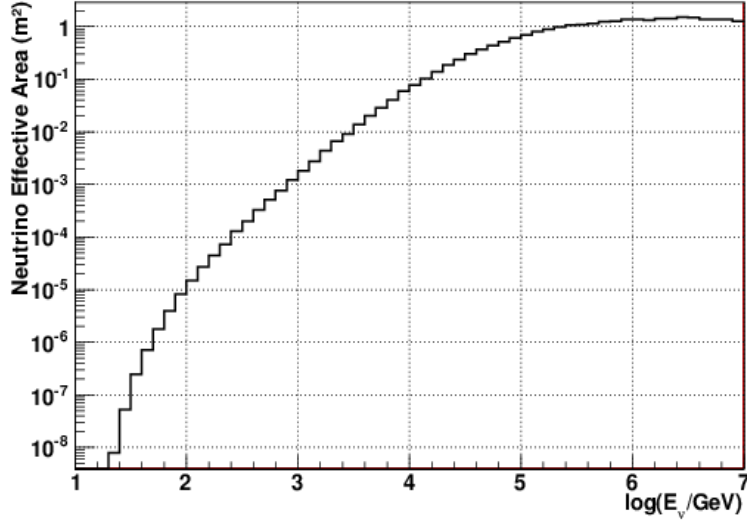


Figure 4.9 – The effective area for neutrinos as a function of the neutrino energy. The sensitivity of the detector for up-going neutrinos increases with energy due to the rise of neutrino cross-section. Above an energy of 1 PeV the sensitivity saturates at about 1 m^2 as the increasing neutrino cross-section and the Earth absorption cancel out.

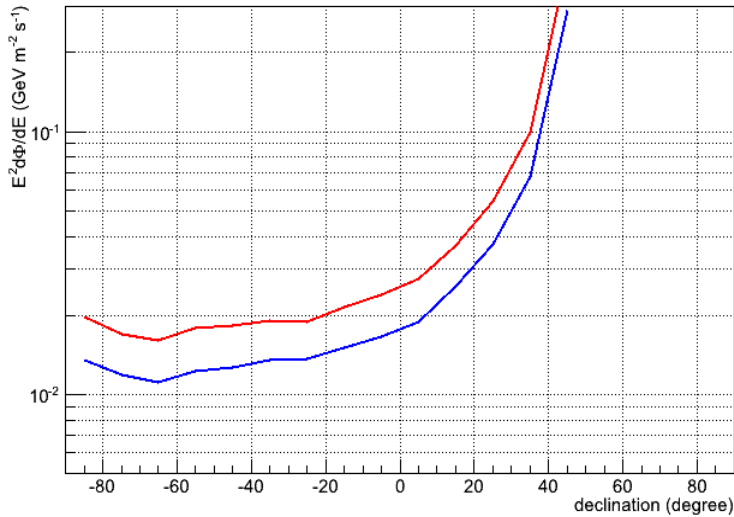


Figure 4.10 – Sensitivity, after applying all the above described cuts, for the whole 5Line period (blue) and for the GW+HEN joint time of observation (red).

the energy of the high energy neutrino, when correctly reconstructed, can indeed be a good indicator of whether the candidate is of cosmic or atmospheric origin. This is illustrated with the present sample in Figure 4.11.

4.4.3 Selection of High Energy Neutrino candidates

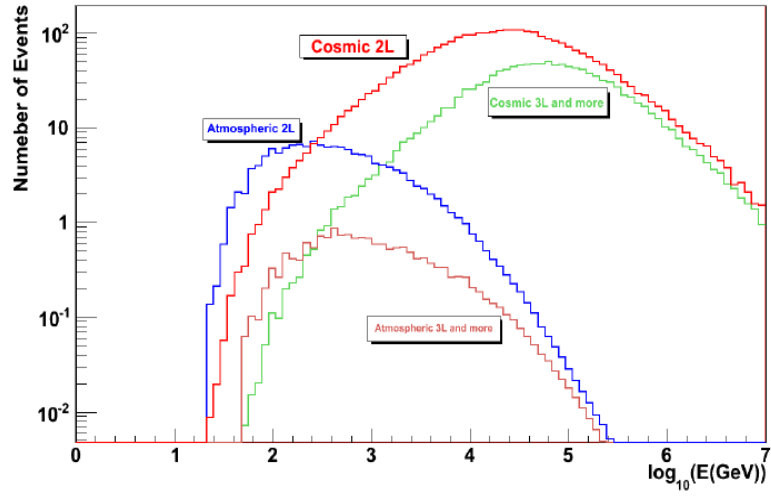


Figure 4.11 – Distributions of energy for atmospheric and cosmic (according to an E^{-2} spectrum) neutrinos. The 2L and 3L+ case are presented separately.

The approach used in this analysis is to use the number of hits as an energy estimator of the candidate. Figure 4.12 shows that the number of hits and the MC energy of the neutrino candidate are correlated. On basis of event-by-event selection, we shall associate to each event in the final list an energy (in term of number of hits) in addition to the basic characteristics discussed in section 4.4.2. For illustration purposes the distributions of the number of hits used by the reconstruction for both MC and data, after applying all cuts, are shown in Figure 4.13.

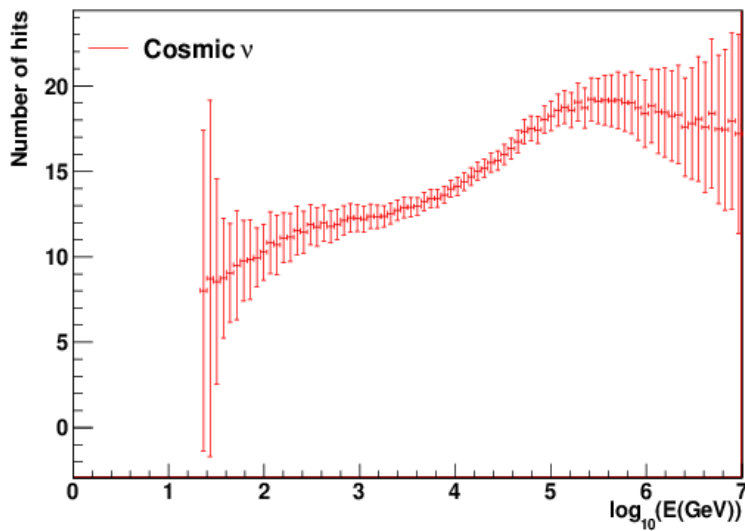


Figure 4.12 – Number of hits versus neutrino energy for cosmic (E^{-2}) neutrinos.

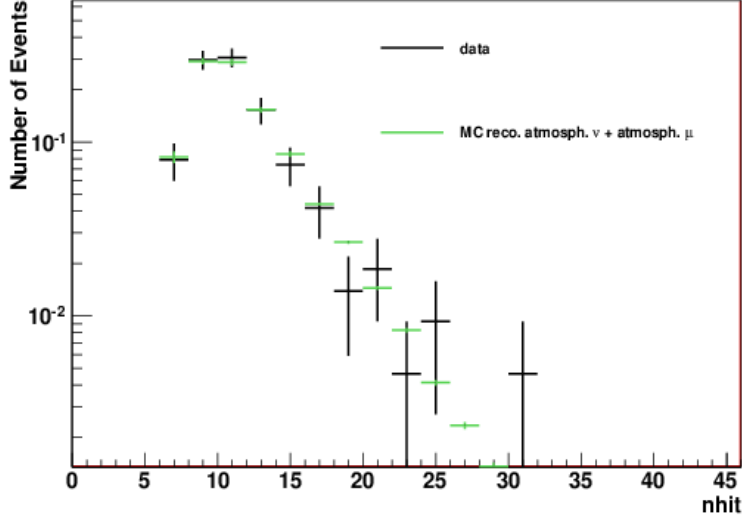


Figure 4.13 – Number of hits used in the fit for up-going events after applying the cuts described in the text.

4.4 High energy neutrino horizon

In this section we estimate the horizon d_ν of the ANTARES neutrino telescope given the cuts presented above and assuming certain models of sources, namely long-GRBs (LGRB) and short-GRBs (SGRB). These models are presented in section 1.9 and the associated neutrino fluxes are plotted in Figure 4.14. The detectability of each kind of source also depends on its distance to the observer.

Let $N_\nu(\theta, \phi, d_\nu)$ be the expected number of detected neutrino events from a source located at a distance d_ν and with local coordinates (θ, ϕ) :

$$N_\nu(\theta, \phi, d_\nu) = \left(\frac{d_s}{d_\nu(\theta, \phi)} \right)^2 T \int_{E_\nu^{min}}^{E_\nu^{Max}} A_\nu^{eff}(E_\nu, \theta, \phi) \times \frac{d\Phi(E_\nu, \theta, \phi)}{dE_\nu} dE_\nu, \quad (4.3)$$

where $A_\nu^{eff}(E_\nu, \theta, \phi)$ is the neutrino effective area of the detector, $\Phi_\nu(E_\nu, \theta, \phi)$ the reference theoretical flux at Earth for a source located at a distance d_s , and T is the average duration of a GRB in the considered model. Note that we have omitted here the redshift energy loss of neutrinos, which is negligible for sources at $z < 1$. Rearranging the Equation (4.3) gives:

$$d_\nu(\theta, \phi, N_\nu) = d_s \sqrt{\frac{\int_{E_\nu^{min}}^{E_\nu^{Max}} A_\nu^{eff}(E_\nu, \theta, \phi) \cdot \frac{d\Phi(E_\nu, \theta, \phi)}{dE_\nu} \cdot dE_\nu}{N_\nu}} \quad (4.4)$$

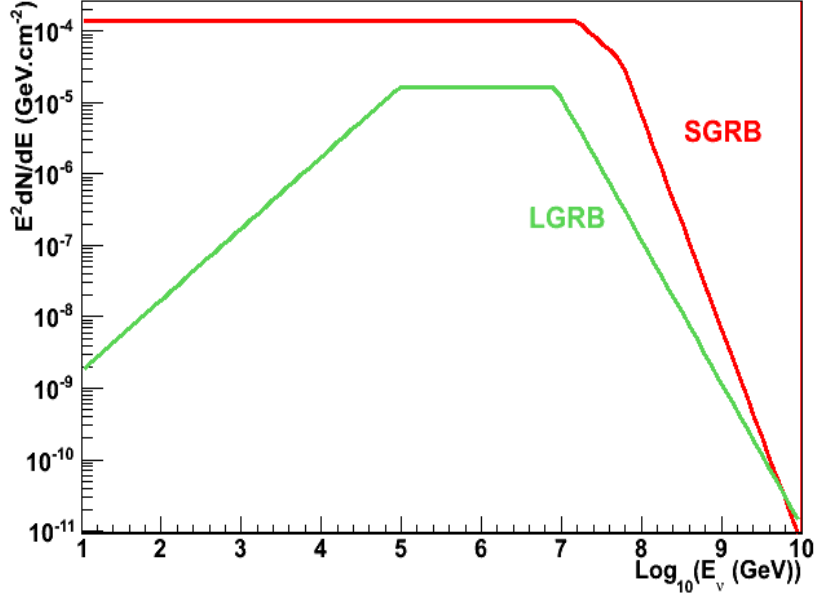


Figure 4.14 – Flux spectrum of LGRB ($z=2$) and SGRB ($z=1$) used in this thesis.

We then define $d_\nu^{50\%}$ as the distance at which the probability to observe at least one event from the considered source is 50%:

$$P(\geq 1|N_\nu) = 1 - P(0|N_\nu) = 50\% \quad (4.5)$$

where N_ν is the number of expected events as given by Equation (4.3) and $P(0|N_\nu)$ follows the Poisson statistics:

$$P(n|N_\nu) = \frac{(N_\nu)^n \exp(-N_\nu)}{n!} ; n > 0 \quad (4.6)$$

The 50% probability corresponds to the value $N_\nu = 0.7$.

Our approach allows the calculation of the HEN horizon on a event-by-event basis. For this we use the effective area $A_\nu^{eff}(E_\nu, \theta, \phi)$ calculated in bins of (θ, ϕ) and of in bins of energy (ranging between $[10, 10^7]$ GeV). We finally compute numerically $d_\nu^{50\%}$ given d_s , using Equation (4.4) and $N_\nu = 0.7$.

For both cases (LGRB and SGRB), we assume $d_s = 21$ Mpc (equivalent to $z = 0.005$). We find in average $d_\nu^{50\%} = 12.4$ Mpc for the former and $d_\nu^{50\%} = 4.3$ Mpc for the latter. The full distributions of $d_\nu^{50\%}$ for the selected sample of neutrinos are shown in Figure 4.15.

Alternatively, we show on Figure 4.16 the probability to observe one event at least, as a

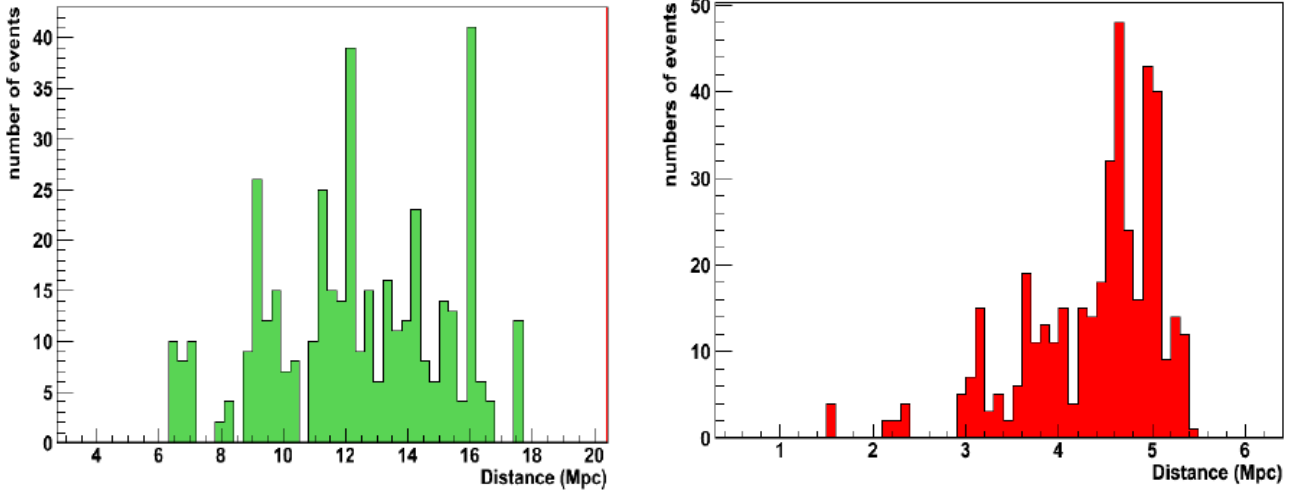


Figure 4.15 – Neutrino horizon calculated for selected sample according to the cuts described in section 4.3.2. On the left is result for long-GRB and on the right for short-GRB.

function of the source distance. This stands for standard LGRB and SGRB. The probability is averaged over all possible locations on the sky.

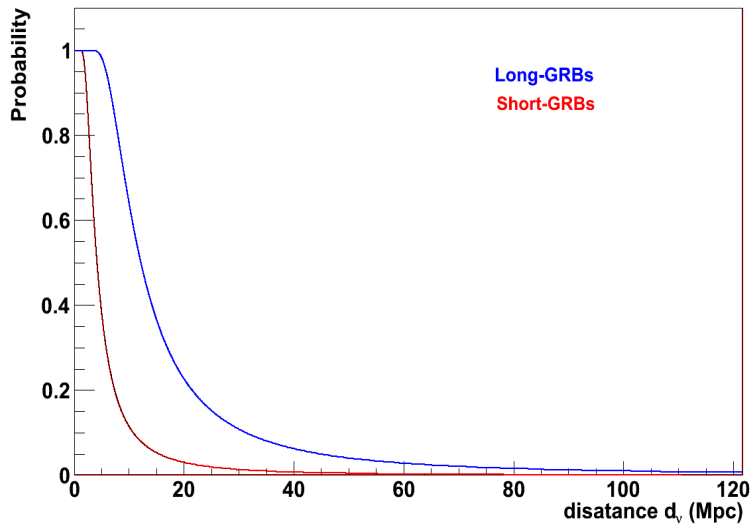


Figure 4.16 – Probability to detect a source as a function of its distance, for LGRB (blue curve) and SGRB (red curve).

4.4.1 Angular resolution and angular search window

The angular resolution is related to the error on the reconstructed track direction. It is defined as the median of the distribution of the space angle ψ between the true neutrino direction and

the reconstructed track and is obtained from MC sample obtained with the cuts defined in the previous section and weighted according to an E^{-2} flux. In the case of events reconstructed with 2 lines, we determine the angular difference of both mirror tracks with respect to the true MC direction. The minimum of those two values, which corresponds to the best track (as defined in section 2.6.1) is used to determine the angular resolution. This method allows to significantly improve the angular resolution as illustrated in Figure 4.17 and sketched in Figure 4.18.

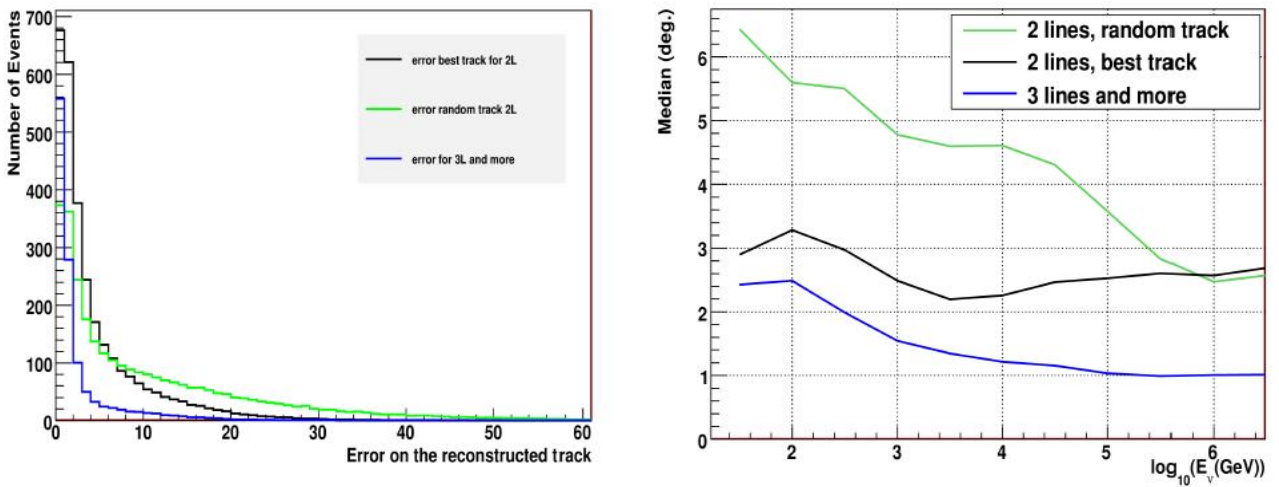


Figure 4.17 – Left: distribution of angular error between the neutrino direction and the reconstructed track for an E^{-2} flux. At low energies the error is dominated by the kinematics of neutrino interactions (see section 2.2.2). The median of this distribution is shown on the right plot as function of the neutrino energy (right). Both plots show the values obtained for the best and random tracks in the case of events reconstructed with 2 lines.

The uncertainty on the neutrino arrival direction has to be accounted for in the GW coherent analysis. This is done by defining, on an event-by-event basis, an angular search window (ASW) and the associated ψ distribution. This distribution is needed by the X-pipeline to compute the significance of an hypothetical signal for the scanned directions inside the ASW. The radius of this window is defined as the 90% (ASW90%) quantile of the ψ distribution. The following method is used to calculate the ASW90%:

- We calculate the ψ distribution for the selected MC sample in bins of declination and number of hits. We create 18 bins in declination range with steps of 10 degrees and, for each bin of declination, we create 16 bins in number of hits with step of 1 hit.
- For each distribution error we compute the 90% quantile of the distribution. The corresponding value is the ASW90%.

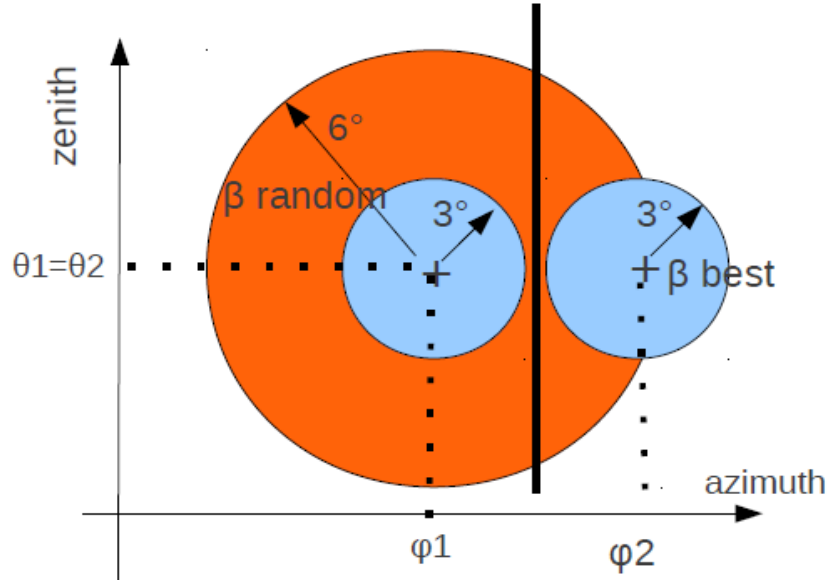


Figure 4.18 – Example (arbitrary values) of the projected angular resolution in local coordinates as obtained for the best (blue) and random (orange) track. The black line illustrates the plane containing the 2 detector lines used for reconstruction.

- We fit the ψ distribution by a log-normal function given by Eq. 4.7:

$$\mathcal{F}(x) = \frac{1}{\sqrt{2}} \frac{e^{-((\ln((x-\theta)/m))^2/2\sigma^2)}}{(x-\theta)\sigma} \quad (4.7)$$

with $x \geq \theta$ and $\sigma \geq 0$. θ is the location parameters, σ is related to the shape of the distribution and m is a scaling parameter.

In Figure 4.19 is shown an example of the ψ distribution fitted by log-normal distribution for a given bin of declination.

The fit is carried out until the 90% quantiles which is the limit radius used for GW searches. The output fit parameters are added to the HEN candidates list (see section 4.4.2).

In the 2L case, the best track distribution is used to determine the ASW90%. This allows for a substantial reduction of the solid angle to be scanned by the GW search algorithm, as can be deduced from the sketch of Figure 4.18. This can be further quantified by computing the ratio R as defined by:

$$R = \frac{\Omega_{best}}{\Omega_{random}} \quad (4.8)$$

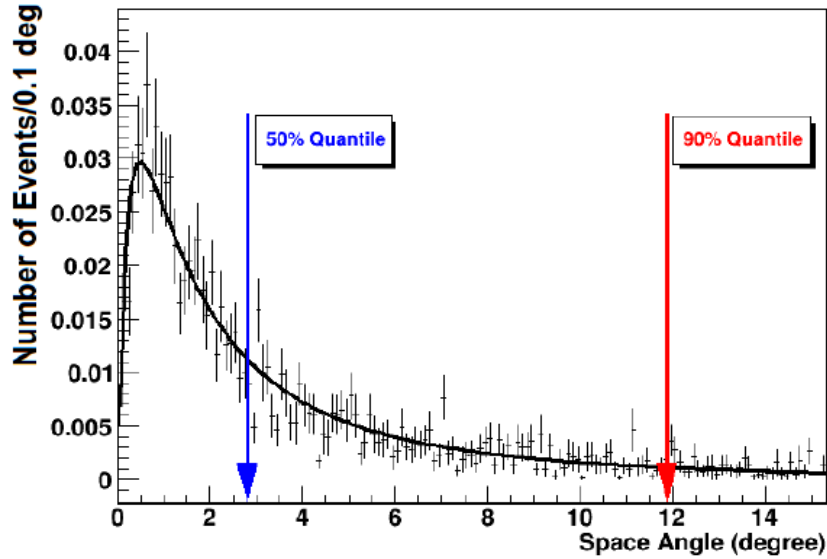


Figure 4.19 – Error distribution on the HEN arrival direction for a bin of declination between -30° and -20° and number of hits=9 together with the fitted log-normal. The arrows indicate the 50th (median) and the 90th (ASW90%) of the distribution.

where

$$\Omega_{best} = 2 \times 2\pi(1 - \cos(ASW90_{best})) \quad (4.9)$$

And

$$\Omega_{random} = 2\pi(1 - \cos(ASW90_{random})) \quad (4.10)$$

are the solid angles associated to the $ASW90_{best}$ and $ASW90_{random}$ respectively. The ratio between the $ASW90_{best}$ and $ASW90_{random}$ is plotted in Figure 4.20. We see from the curve that the size of the best angular search window $ASW90_{best}$ is in average 44.6% of the size of the random one, which justifies our approach.

The ASW50% (median) and ASW90% are plotted in the Figure 4.21. This Figure shows the improvement on the ASW90% derived from the approach described above. A single circular region of radius $ASW90\%=30$ degrees encompasses the two mirror tracks, while the individual mirror tracks are contained in a circular region of radius $ASW90\%=12.5$ degrees. The solid angle to be analyzed is 0.84 sr in the first case while it is $2 \times 0.15 = 0.30$ in the second case. The distinction of the two mirror tracks allows us to reduce the search window by a factor of almost 3. We show also the Point Spread Function (PSF) in Figure 4.22.

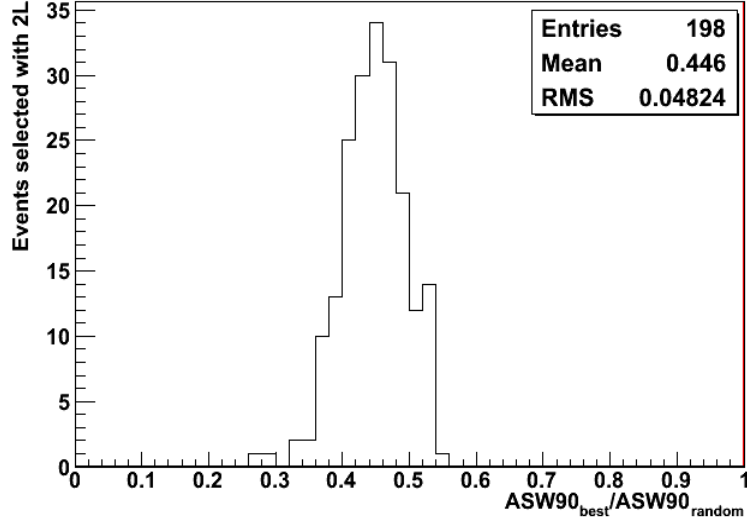


Figure 4.20 – Ratio between $ASW90_{best}$ and $ASW90_{random}$, ignoring any overlap between the search windows associated to each mirror solutions.

4.4.2 List of neutrino candidates

After applying the set of cuts described in the previous sections to the 181 runs corresponding to 104 days equivalent live time to the present analysis period, 414 neutrino candidates remain, which are listed in [17]. In this sample we have separated events reconstructed with exactly 2 lines from those reconstructed with at least 3 lines. This strategy is imposed to take into account the mirror track for events reconstructed with exactly 2 lines. The main informations

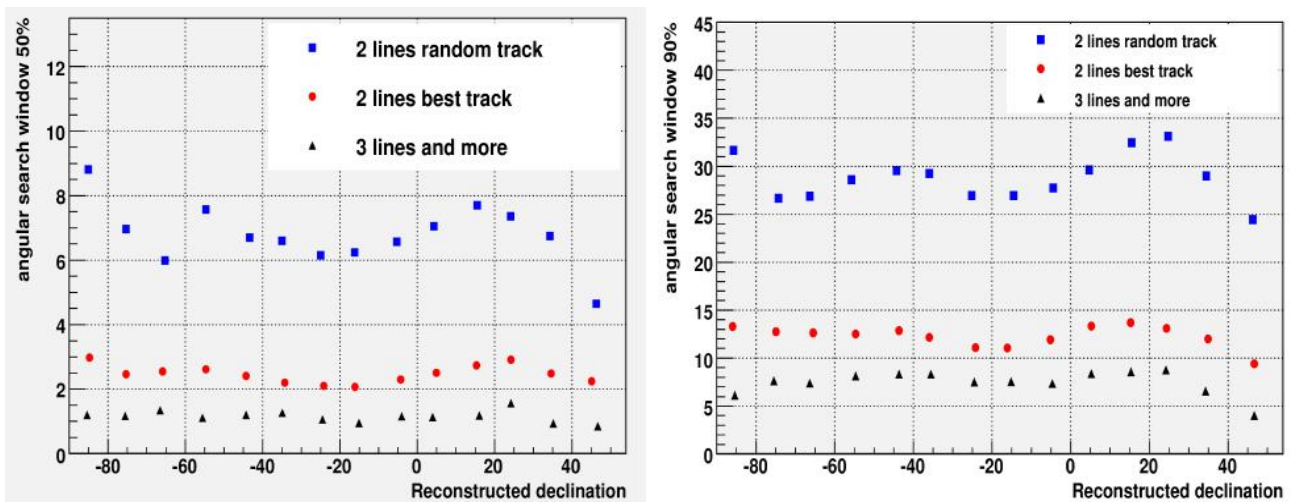


Figure 4.21 – $ASW50\%$ (left) and $ASW90\%$ (right) as function of declination

in the event list correspond to:

- The neutrino arrival time in Julian Day specified for epoch J2000, which is used also for the computation of the celestial coordinates (right ascension and declination). It is the sum of the UTC event time, computed from the start time of the run, and the product of the frame duration and the frame index;
- The equatorial coordinates (α, δ) of each candidate (computed using ConvertCoordinates libraries from the ANTARES local coordinates (θ, ϕ));
- The number of lines and the number of hits used in the fit of the track;
- The angular search windows for both 50% and 90% quantiles;
- The log-normal fit parameters obtained by fitting the angular error distribution in bins of event declination and number of hits, as explained in section 4.4.1.

The equatorial coordinates (α, δ) and the galactic coordinates of the selected candidates are shown in Figures 4.24 and 4.25 respectively. Due to the geographical location of the detector, the part of the sky with declination greater than 48° is always above the horizon and is thus never observed by the ANTARES telescope. In contrast, the part of the celestial sphere with declination below -48° , is always visible. The region in between is visible during some fraction of the day. This visibility factor convoluted to the intrinsic acceptance of the detector is shown in galactic coordinates in the Figure 4.26.

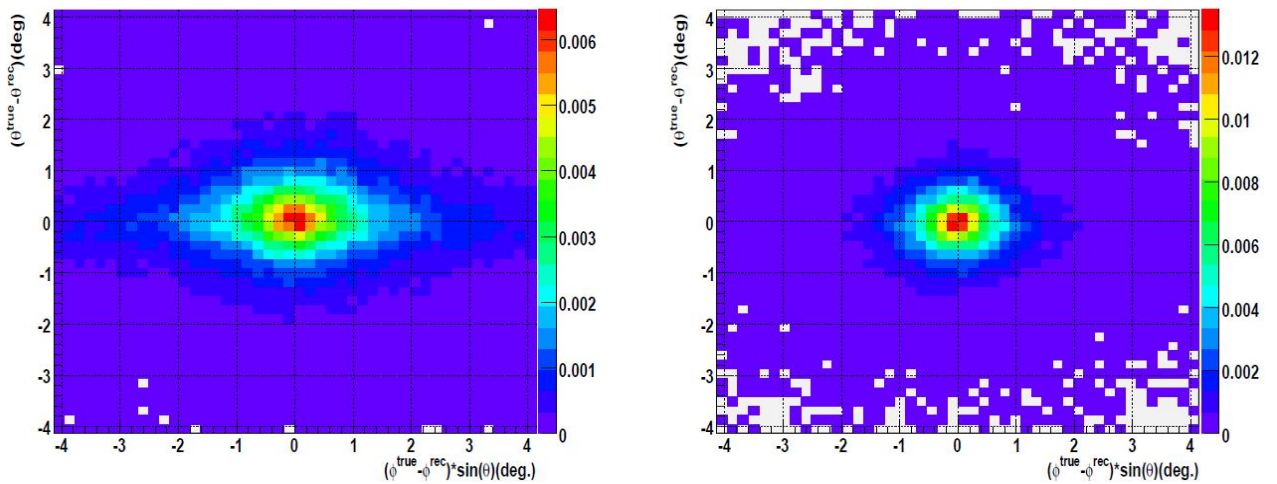


Figure 4.22 – PSF of the ANTARES neutrino telescope, on the left for event selected with 2L (best track) and, on the right for events selected with 3L+.

Of the HEN candidate events, 158 occurred at times when at least two gravitational-wave detectors were operating. Since two or more detectors are required to discriminate GW signals from background noise (as described in section 4.5), in the following we consider only these remaining 158 HEN candidates: 144 2-line events and 14 3-line events. We show in Figure 4.23 the distribution of the ASW90% of these events.

4.5 Coincidence with gravitational waves

4.5.1 Gravitational wave event analysis

Once the list of HEN candidates has been established, they can be fed as external triggers into the X-pipeline to search for GW signals in coincidence with them. The GW dataset used is described in section 4.2. We now concentrate on the preprocessing of the GW dataset using a *coherent triggered* method. The triggered search requires several components provided by the neutrino candidate event, especially time and directional informations. This adopted procedure follows the one used in [18] where the GRB triggers are replaced by neutrino candidates. All the detectors operating at the time of the trigger and passing the data-quality requirements are used in the analysis.

As described in section 4.2 the dataset can be split into two parts: *on-source* and *off-source* data. The former serve to generate GW triggers in coincidence with the neutrino candidates,

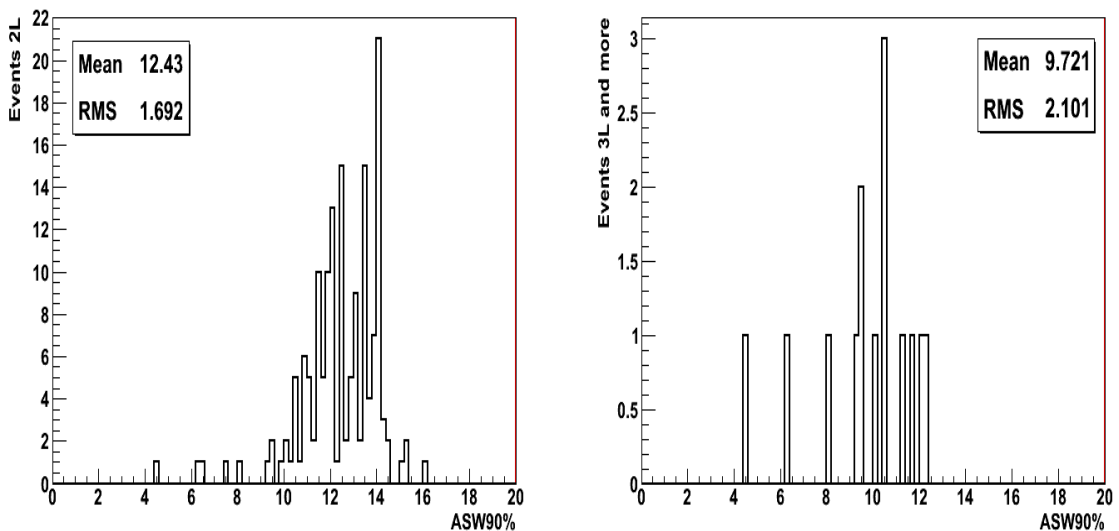


Figure 4.23 – ASW90% of the remaining 158 neutrino candidates. Left: events reconstructed with 2 lines. Right: events reconstructed with at least 3 lines.

4.4.5 Coincidence with gravitational waves

while the latter are used to optimize the search parameters, to measure the expected false alarm rate and to standardize statistics derived from the on-source window. The on-source data consists of a segment from each interferometer data. The data segments are time-delayed according to the sky location being analysed so that a GW signal from that direction would appear simultaneous in each data stream.

In the context of the joint GW+HEN searches, the source emits a collimated jet pointing to Earth. This gives a quite strong indication about the source core dynamics and its orientation. In particular, it is natural to associate this direction to the source angular momentum. This motivates the assumption of a circular polarization of the incoming gravitational wave to separate the signals from noise. While some of the considered source models do not predict a circularly polarized GW, we expect the loss in sensitivity in that case to be relatively small. In addition to the marginalized circular polarization sum, other combinations of the data are constructed. Of particular importance are the “null” combinations designed to cancel out the GW signal from the given sky location; comparison to corresponding incoherent combinations provides powerful tests for identifying events due to background noise fluctuations glitches, as described in [19]. For each combination, the event cluster is assigned a combined energy as the sum of the energy values of its constituent pixels. This defines a first ranking statistics for the events. In addition, GW events are characterized by their duration, central time, bandwidth, and central frequency. Also, a second ranking statistic is computed based on a

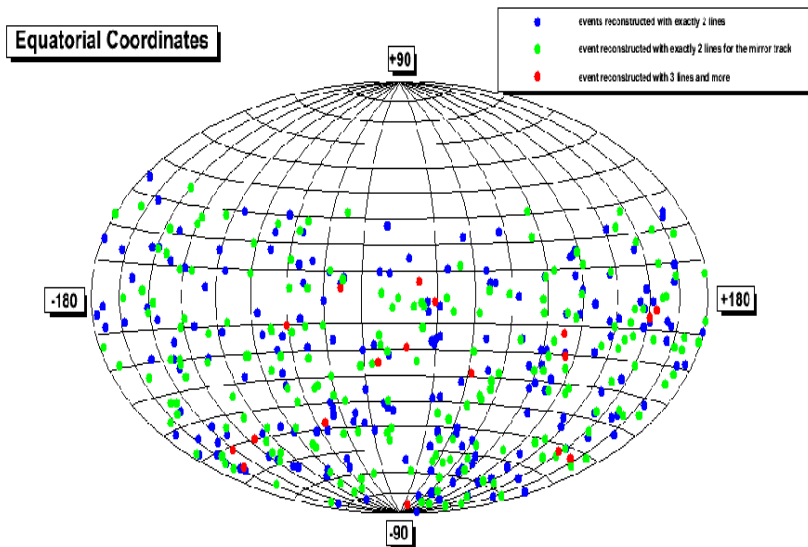


Figure 4.24 – Sky-map showing the reconstructed declination and right ascension of all the selected events. The blue and green dots correspond to the two possible directions of events reconstructed with exactly 2 lines. The red dots represent the coordinates of the events reconstructed with 3 lines and more.

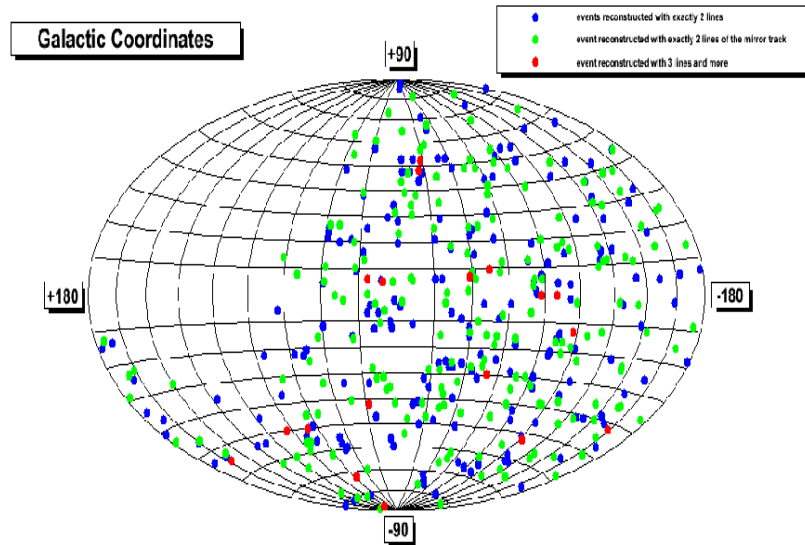


Figure 4.25 – Sky-map showing the selected events in galactic coordinates: The blue and green dots correspond to the two possible directions of events reconstructed with exactly 2 lines. The red dots represent the coordinates of the events reconstructed with 3 lines and more.

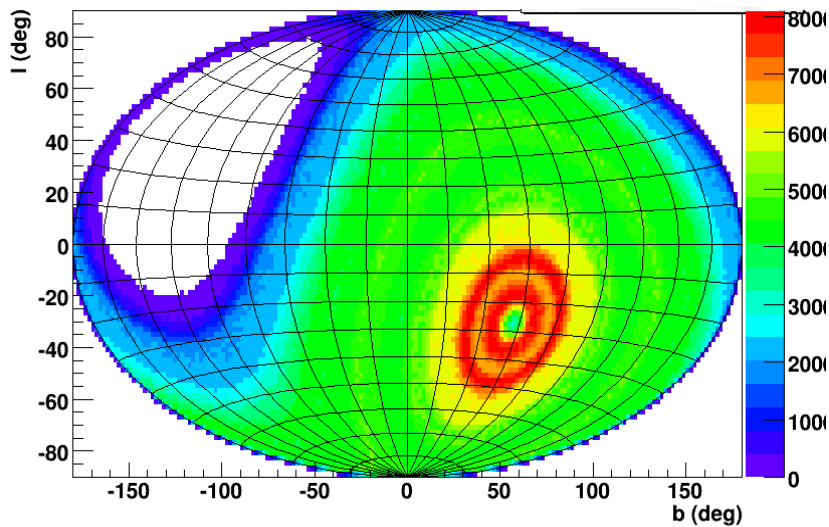


Figure 4.26 – Acceptance of the ANTARES detector in galactic coordinates, taking into account the visibility factor due to the rotational Earth motion. This quantity is the number of detected events for a given (arbitrary) flux. Only the relative values are relevant.

maximum-likelihood analysis of the event assuming a power-law distributed background noise with no assumption on the GW polarization. In practice this statistic is often found to provide signal-noise separation due to the non-Gaussian nature of the GW detector noise.

4.4.5 Coincidence with gravitational waves

The time-frequency (TF) analysis (see section 3.7.1) is repeated for Fourier transform lengths of 1/128, 1/64, 1/32, 1/16, 1/8, 1/4 s, to maximize the sensitivity to GW signals of different durations. It is also repeated over a discrete grid of sky positions covering most of the source sky location probability distribution. A simple regular grid is used here, composed of concentric circles around the best estimate of the neutrino sky location, which covers 90% of the sky location probability distribution (see Figure 4.27). This grid is designed such that the maximum relative timing error between any pair of GW detectors is less than 0.5 ms. Finally, the events are decimated to a rate of 0.25 Hz before being written to disk.

GW triggers are produced independently for each sky position grid point. The detection statistic, written as a log-likelihood ratio between a signal and a background model, is penalized by the probability $\mathcal{F}(\vec{d})$ of the trial sky location being the true one, by adding the logarithm of that probability to the detection statistic. The reconstructed source sky position for a given signal is the sky position for which the trigger has the largest penalized detection statistic. Only that maximal trigger is kept by the analysis of the grid of sky positions.

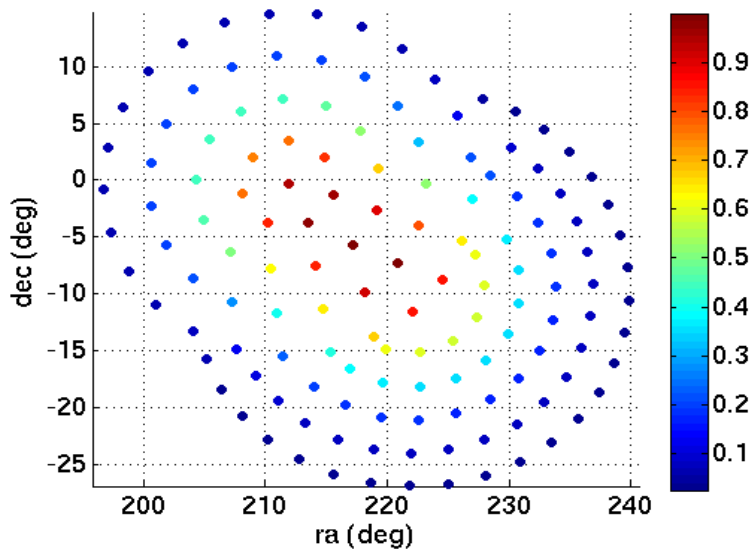


Figure 4.27 – The estimated neutrino locations and their uncertainties may give rise to overlapping regions on the sky. Searching for one point and its mirror image at once. The color bar shows the probability distribution. (Source [20])

The *off-source* window is defined as all data within ± 1.5 hours of the neutrino time, excluding the *on-source* interval. The statistical features in the off-source window are similar to the ones in the on-source window. In order to enlarge the background sample, we also repeat the off-source analysis after applying time shifts of multiples of 6 s to the data from one or more detectors. With such time slides, we were able to produce $O(10^3)$ background trials for

each HEN.

To assess the sensitivity of this joint search, the analysis is repeated with injections of simulated GW signals to the on-source data. The amplitudes and morphologies tested are discussed in section 4.6.2.

4.5.2 GW search optimization

As we stated in section 3.7.2, the sensitivity of searches for gravitational-wave bursts is limited by noise (glitches included). The trigger rejection operates in two steps, namely a data pre-selection followed by a glitch removal procedure. To reduce this background, events that overlap in time within known instrumental and/or environmental disturbances are vetoed. In addition to this, GW consistency tests comparing the coherent and incoherent energies are applied to each event [19]. These tests are applied to the on-source, off-source and injection events. The events failing one or more of these tests are discarded.

The thresholds are optimized by testing a preset range of thresholds and selecting those which give the best overall detection efficiency at a fixed false alarm probability of 1% when applied to a random sample of background and injection events (the on-source events are *not* used; i.e., this is a blind analysis). These tests also determine which of the two ranking statistics discussed in section 4.5 (based on circularly polarized GW energy or power law noise) gives the better detection efficiency. The winner is selected as the final ranking statistic.

Once the thresholds have been fixed, these consistency tests are applied to the on-source events and to the remaining off-source and injection events (those not used for tuning). The surviving on-source event with the largest significance (highest energy or power law statistic) is taken to be the best candidate for a gravitational wave signal and is referred to as the loudest event [21]. All surviving on-source events are assigned a false alarm probability by comparison to the distribution of loudest events from the off-source trials. Any on-source event with probability $p < 0.01$ is subjected to additional checks to try to determine the origin of the event and additional background time slide trials are performed to improve the accuracy of the false alarm probability estimate. After the p values have been determined for the loudest events associated with each of the 158 HEN events, the collective set of p values is tested for consistency with the null hypothesis (no GW signal) using the binomial test, discussed in section 4.5.4. We also set a frequentist upper limit on the strength of gravitational waves associated with each neutrino trigger, as discussed in section 4.6.2.

4.5.3 Low-frequency and high-frequency GW analyses

The analysis procedure described in the previous section has been implemented in the X-PIPELINE. Given our knowledge of possible GW sources discussed in chapter 1, the most likely detectable signals at extra-galactic distances are in the low-frequency band (LF, $f \lesssim 500$ Hz), where the detectors have maximum sensitivity (see Figure 3.5). At the same time, the computational cost of the X-PIPELINE analysis increases at high frequencies. This is due in part to the extra data to be analyzed, but also to the need for finer-resolution sky grids to keep time delay errors much smaller than one GW period. We therefore split the gravitational wave band into two regions: 60-500 Hz and 500-2000 Hz.

The low-frequency band is analyzed for all HEN events. Such a search is computationally feasible while covering the highest-sensitivity region of the GW detectors. However, compact objects such as neutron stars or collapsar cores have characteristic frequencies for GW emission above 500 Hz. Such emissions might be detectable from galactic sources such as soft gamma repeater giant flares, or possibly from nearby galaxies. Since the computational cost in the high-frequency range for all HEN events is prohibitive with the current analysis pipeline, we perform the 500-2000 Hz (high frequency HL) analysis on the 3L+ HEN events only. The 3L+ events are a small subset ($\sim 10\%$) of the total trigger list and have the smallest sky position uncertainties, and therefore the smallest computational cost for processing. To further reduce this cost, we use the same sky grid for the high-frequency search as was used at low frequencies, after determining that the loss of sensitivity is acceptable. The HF analysis is performed independently of the low-frequency analysis (e.g. independent tuning, background estimation) using the identical automated procedure.

4.5.4 Binomial test

A quantitative analysis of the significance of any gravitational-wave event must take into account the trial factor due to the number of neutrino events analyzed. We use the *binomial test* [22], as the statistical method to look for a GW signature associated with individual neutrino candidates. Under the null hypothesis, the false alarm probabilities (FAPs) p for each HEN loudest event are expected to be uniformly distributed between 0 and 1. The binomial test compares the measured p values (in the on-source window) to the null distribution to determine if there is an excess which may have been due to the cumulative effect of weak GW signals.

The binomial test considers a number of events, N_{tail} , among the total number of events in the sample, N , that have to be tested and sorts their probabilities $p_{i \in [1, N_{\text{tail}]}}$ in increasing order (i.e. decreasing significance): $p_1 \leq p_2 \leq p_3 \leq \dots \leq p_N$. For each of these probabilities, p_i , we

compute the cumulative binomial probability $P_{\geq i}(p_i)$ for getting i or more events at least as significant as p_i :

$$\begin{aligned} P_{\geq i}(p_i) &= \sum_{j=i}^N P_j(p_i) \\ &= 1 - \sum_{j=0}^{i-1} P_j(p_i) \end{aligned} \tag{4.11}$$

where $P_j(p_i)$ denotes the probability for getting j successes in N trials:

$$P_j(p_i) = \frac{N!}{(N-j)!j!} p_i^j (1-p_i)^{N-j}. \tag{4.12}$$

and N is the number of neutrino candidates analyzed. The lowest $P_{\geq i}(p_i)$ for $i \in [1, N_{\text{tail}}]$ will point to the most significant deviation from the null hypothesis. To assess the significance of the deviation, we repeat the test using p values drawn from a uniform distribution and count the fraction of such trials which give a lowest $P_{\geq i}(p_i)$ smaller than that computed from the true measured p values.

4.6 GW+HEN joint search results

4.6.1 Individual GW searches

After applying several quality criteria to both the GW and the HEN data a list of neutrino candidates was retained for further search of possible concomitant GW signals. Out of this list, 158 neutrinos (reconstructed with 2L) have been analyzed in the low frequency (LF) range, and 14 (reconstructed with a least 3L) have been analyzed in both the LF and the high frequency (HF) range. We choose N_{tail} to be 5% of N ; i.e., $N_{\text{tail}} = 8$ for the low frequency band and $N_{\text{tail}} = 1$ for the high frequency band.

The smallest FAP was found to be ($p = 0.01$), in the LF range. The corresponding neutrino trigger was localized on the sky by ANTARES telescope in direction $(\alpha, \delta) = (204.4, -13.03)$ on Wed Sep 12, 2007. Additional time shifts totaling 18064 background trials yielded a refined FAP of $p = 0.004$, which is not significant given a trial factor of 158. This event came from the analysis of the H1, H2, and V1 data. Follow-up checks were performed, including checks of detector performance at the time indicated by monitoring programs and operator logs and

scans of data from detector and environmental monitoring equipment to look for anomalous behavior. While these checks did not uncover a physical cause for the event, they did reveal that it occurred during a glitching period in V1. We conclude that we have no clear gravitational wave burst signal associated with any of our sample of 158 neutrino events. The full analysis is therefore consistent with no GW events being present. Figures 4.28 and 4.29 show the cumulative distribution of p -values measured in the LF and HF analyses. In both cases the measured p -values are consistent with the null hypothesis. We also found no candidates in the HF band.

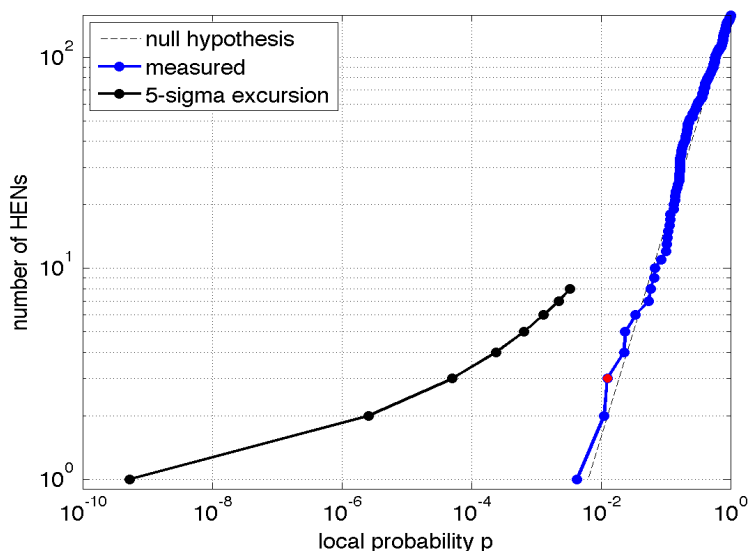


Figure 4.28 – Distribution of observed p values for the loudest GW event associated with each neutrino analysed in the low frequency analysis. The red dot indicates the largest deviation of the low p tail from the uniform distribution null hypothesis; this occurs due to having the three loudest events below $p_3 \sim 0.013$. Deviations this large or larger occur in approximately 64% of experiments under the null hypothesis. The black line shows the threshold for a 5-sigma deviation from the null hypothesis.

4.6.2 GW upper limits

The sensitivity of the GW search is determined by a Monte-Carlo study. For each neutrino trigger, we add simulated GW signals to the on-source data and repeat the analysis described in section 4.5. We consider that the simulated signal is detected if it produces an event louder than the loudest on-source event after all event tests have been applied. We define a 90% confidence level lower limit on the distance to the source as the maximum distance $D_{90\%}$ such that for any distance $D \leq D_{90\%}$ the probability of detection is 0.9 or greater.

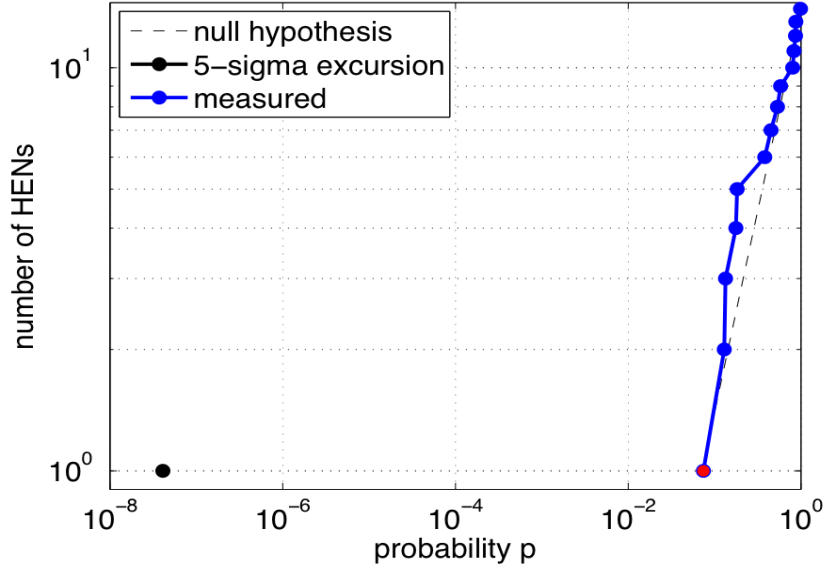


Figure 4.29 – Distribution of observed p values for the loudest GW event associated with each neutrino analysed in the high frequency analysis. The red dot indicates the largest deviation of the low p tail from the uniform distribution null hypothesis; since $N_{\text{tail}} = 1$, this is constrained to occur for p_1 . Deviations this large or larger occur in approximately 66% of experiments under the null hypothesis. The black dot shows the threshold for a 5-sigma deviation from the null hypothesis.

Injected waveforms: We added different burst-type signals to the raw data. The *ad hoc* waveforms are Gaussian-modulated sinusoids already introduced in section 3.7.3:

$$h_+ = \frac{(1 + \cos^2 \iota)}{2} \frac{h_{\text{rss}}}{(2\pi\tau^2)^{\frac{1}{4}}} e^{-\frac{(t-t_0)^2}{4\tau^2}} \cos 2\pi f_0(t - t_0), \quad (4.13)$$

$$h_\times = \cos \iota \frac{h_{\text{rss}}}{(2\pi\tau^2)^{\frac{1}{4}}} e^{-\frac{(t-t_0)^2}{4\tau^2}} \sin 2\pi f_0(t - t_0). \quad (4.14)$$

Here f_0 is the central frequency, t_0 is the central time, and we chose $\tau = 1/f_0$ as the duration. We use central frequencies of 100 Hz, 150 Hz, and 300 Hz for the low-frequency analysis and 554 Hz and 1000 Hz for the high-frequency search. The quantity h_{rss} is the root-sum-square signal amplitude:

$$h_{\text{rss}} \equiv \sqrt{\int h_+^2(t) + h_\times^2(t) dt}. \quad (4.15)$$

This amplitude is related to the total energy E_{GW} in the gravitational-wave burst by:

$$E_{\text{GW}} = \frac{2}{5} \frac{\pi^2 c^3}{G} h_{\text{rss}}^2 f_0^2 D^2. \quad (4.16)$$

This waveform is consistent with the GW emission from a rotating system viewed from an inclination angle ι to the rotational axis. We select the inclination uniformly in $\cos \iota$ with $\iota \in [0^\circ, 5^\circ]$. This corresponds to a nearly on-axis system, such as would be expected for association with an observed long GRB. For astrophysical injections we use the gravitational-wave emission of inspiraling neutron star and black hole binaries, which are widely thought to be the progenitors of short GRBs. Specifically, we use the post-Newtonian model for the inspiral of a double neutron star system with component masses $m_1 = m_2 = 1.35M_\odot$, and the one for a black-hole-neutron-star system with $m_1 = 5M_\odot$, $m_2 = 1.35M_\odot$, as discussed in Chapter 1. We set the component spins to zero in each case. Motivated by estimates of the jet opening angle for short GRBs, we select the inclination uniformly in $\cos \iota$ with $\iota \in [0^\circ, 30^\circ]$.

For each HEN trigger, the injections are distributed uniformly in time over the on-source window. The injection sky positions are selected randomly following the estimated probability distribution (see Eq. 4.7) for the HEN trigger, to account for the uncertainty in the true HEN direction of incidence. The polarization angle (orientation of the rotational axis on the sky) is distributed uniformly. Finally, the amplitude and arrival time at each detector is perturbed randomly to simulate the effect of calibration errors in the LIGO and Virgo detectors.

Exclusion distances: For each waveform type (sine-Gaussians at 100, 150, 300, 554, 1000 Hz, and $1.35M_\odot$ - $1.35M_\odot$ and $5M_\odot$ - $1.35M_\odot$ inspirals), injections are performed over a range of amplitudes. For the inspiral signals, each amplitude corresponds to a well-defined distance. We can associate a physical distance to each amplitude for the sine-Gaussian waveforms as well, by assuming a fixed energy in gravitational waves. For concreteness, we select $E_{\text{GW}} = 10^{-2}M_\odot c^2$. This value corresponds to the optimistic limit of possible gravitational-wave emission by various processes in the collapsing cores of rapidly rotating massive stars [23–26]; more conservative estimates based on 3D simulations have been made in [27–31].

The exclusion distance is defined as the largest distance at which in 90% of the cases the event corresponding to the GW signal would be louder than the loudest on-source event found in the data. For each type of gravitational wave simulated, the distributions of exclusion distances for our neutrino sample are shown in Figures 4.30 and 4.31. For binary neutron star systems of $(1.35 - 1.35)M_\odot$ and black hole - neutron star systems of $(5 - 1.35)M_\odot$ typical distance limits are 5 Mpc and 10 Mpc respectively. For the sine-Gaussian waveforms in the low-frequency band the typical distance limits are between 5 Mpc and 17 Mpc, while for those in the high-frequency band the typical limits are of order 1 Mpc.

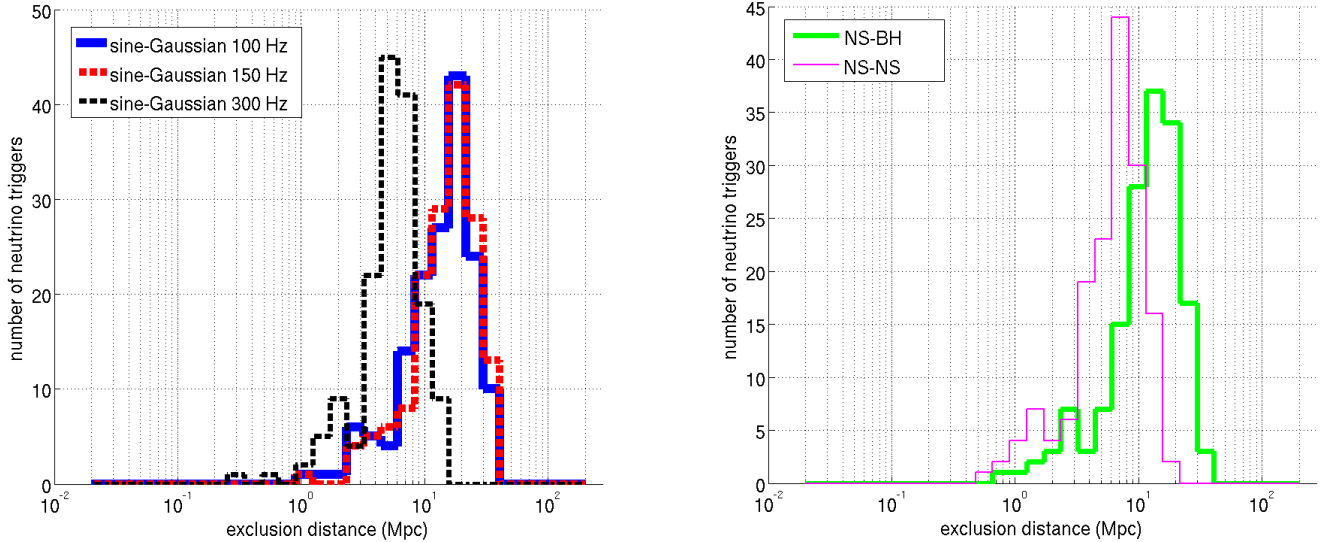


Figure 4.30 – Low-frequency analysis: the left plot is the histogram for the sample of analyzed neutrinos of the distance exclusions at the 90% confidence level for the 3 types of circular sine-Gaussian models considered: 100 Hz, 150 Hz and 300 Hz. A standard siren gravitational wave emission of $E_{GW} = 10^{-2} M_{\odot} c^2$ is assumed. The right plot shows histogram across the sample of analyzed neutrinos of the distance exclusions at the 90% confidence level for the 2 families of binary inspiral models considered: NS-NS and BH-NS.

4.7 Astrophysical implications

4.7.1 Upper limits on joint source populations

The present search for GW and HEN correlations in space and time revealed no evidence for coincident events. In accordance with the Poisson statistics, this implies a 90% confidence level upper limit on the rate of detectable coincidences of $2.3/T_{\text{obs}}^{\text{com}}$, where $T_{\text{obs}}^{\text{com}} \approx 91.36$ days is the duration of coincident observations. This can be expressed as a limit on the rate density (number per unit time per unit volume) $\rho_{\text{GW-HEN}}$ of objects which would yield coincident GW and HEN signals:

$$\rho_{\text{GW-HEN}} V_{\text{GW-HEN}} \leq \frac{2.3}{T_{\text{obs}}}. \quad (4.17)$$

In this expression, $V_{\text{GW-HEN}}$ is the volume of universe probed by the present analysis for typical GW-HEN sources and 2.3 is the in accordance with the a Poisson process. This volume is related to the GW and HEN detection efficiencies as a function of distance, and must be estimated for typical emission models. We take as fiducial sources two classes of objects: the final merger phase of the coalescence of two compact objects (short GRB-like), or the collapse

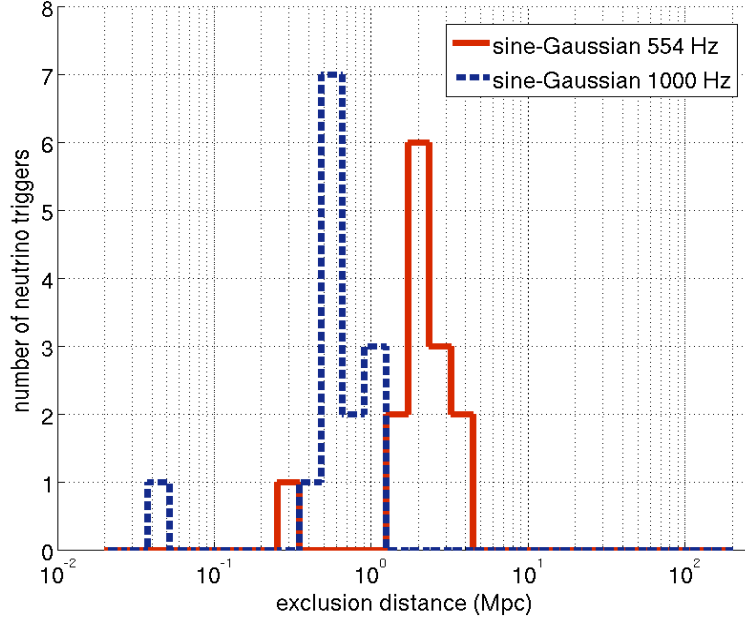


Figure 4.31 – High-frequency analysis: the histogram for the sample of analysed neutrinos of the distance exclusions at the 90% confidence level for the 2 frequencies of circular sine-Gaussian models considered: 554 Hz and 1000 Hz.

of a massive object (long GRB-like), both followed by the emission of a relativistic hadronic jet. The corresponding HEN and GW detection horizons (or exclusion distances) have been estimated respectively in sections 4.4 and 4.6.2. In the case of short GRBs, $d_{HEN} \sim 4.41$ Mpc and $d_{GW} \sim 5$ -10 Mpc depending on the binary masses, while for long GRBs they increase to $d_{HEN} \sim 12.55$ Mpc and $d_{GW} \sim 10$ -20 Mpc (under the optimistic assumption of $E_{GW} = 10^{-2} M_{\odot} c^2$). The effective volume probed by the GW+HEN joint analysis can be written as:

$$V_{GWHEN} = \int_0^{\infty} P_{GWHEN}(r) 2\pi r^2 dr \int_{-\pi/2}^{\pi/2} \epsilon_{HEN}(\delta) \cos \delta d\delta \quad (4.18)$$

where $P_{GWHEN}(r) = P_{HEN}(r) \times P_{GW}(r)$ is the detection probability for a joint emitter and $\epsilon(\delta)$ is the visibility in ANTARES of a source at declination δ . This integral effectively extends until a certain distance $d_{GWHEN} \simeq \min(d_{HEN}, d_{GW})$. As $d_{GW} > d_{HEN}$ for the sources considered hereabove, we approximate $P_{GW}(r)$ by a step function ($P_{GW}(r) = 1$ for $r < d_{GW}$, 0 elsewhere) and fold it with the probability $P_{HEN}(r)$ to detect at least one neutrino from the source (as described in section 4.4 and Figure 4.16). From Eq. 4.17 one can then derive approximate limits on the population density of joint GW+HEN emitters: $\rho_{GW-HEN}^{SGRB} \lesssim 10^{-2} \text{Mpc}^{-3} \text{yr}^{-1}$ for

SGRB-like sources, and $\rho_{\text{GW-HEN}}^{\text{LGRB}} \lesssim 10^{-3} \text{Mpc}^{-3} \text{yr}^{-1}$ for LGRB-like sources.

4.7.2 Comparison of limits with existing estimates

[32, 33] suggest a local rate density of SGRB of $\rho_{\text{SGRB}} \lesssim 10^{-9} \text{Mpc}^{-3} \text{yr}^{-1}$, and the abundance of binary neutron star mergers, their assumed progenitors, is estimated to be $\rho_{\text{NS+NS}} \sim 10^{-6} \text{Mpc}^{-3} \text{yr}^{-1}$ [34], well below the reach of the present search ($\rho_{\text{GW-HEN}}^{\text{SGRB}} \lesssim 10^{-2} \text{Mpc}^{-3} \text{yr}^{-1}$). With $T_{\text{obs}} = 1$ year, an improvement of a factor 10 on the detection distance is required in order to be able to constrain the fraction of mergers producing coincident GW+HEN signals. [32] estimate a total rate of long GRBs of $\rho_{\text{LGRB}} \sim 3 \times 10^{-8} \text{Mpc}^{-3} \text{yr}^{-1}$; these sources are closely related to Type II and Type Ibc core-collapse supernovae. The local rate of SNIbc is $\rho_{\text{SNIbc}} \sim 2 \times 10^{-5} \text{Mpc}^{-3} \text{yr}^{-1}$, whereas $\rho_{\text{SNII}} \sim 2 \times 10^{-4} \text{Mpc}^{-3} \text{yr}^{-1}$, relatively close to the obtained limit $\rho_{\text{GW-HEN}}^{\text{LGRB}} \lesssim 10^{-3} \text{Mpc}^{-3} \text{yr}^{-1}$ under our optimistic assumptions of GW emission in this scenario. A factor 10 only is required in order to constrain the fraction of star collapses producing coincident GW-HEN signals, which translates into a required improvement of 2 on the detection distance.

4.8 Conclusions

In this chapter we have described the first joint GW+HEN search using coincident data taken in 2007 from the ANTARES neutrino telescope and the Virgo/LIGO GW interferometers. The absence of GW triggers in coincidence with a list of preselected HEN candidate events has allowed to establish limits on the rate density $\rho_{\text{GW-HEN}}$ of joint GW+HEN emitting systems. These limits are however not stringent enough to constrain the density of realistic, known candidate GW+HEN progenitors such as binary neutron star mergers or Type II/Ibc core-collapse supernovae. An increased sensitivity can be achieved by performing similar coincidence analyses using other data sets provided by the same instruments. The next chapter presents an improved analysis method applied to the joint data sample collected by ANTARES in its 12L configuration concomitantly with science runs conducted with enhanced Virgo and LIGO interferometers in 2009-2010. This analysis is described in chapter 5.

REFERENCES

- [1] S. ADRIAN-MARTINEZ ET AL, arXiv:1205.3018, (2012). 101
- [2] B. BOUHOUE, Proceedings of the VLVNT11 conference, arXiv:1201.2840 (2011). 101
- [3] T. PRADIER, arXiv:0807.2567v1 (2008). 101
- [4] V. V. ELEWYCK ET AL, Int. J. Mod. Phys. D18:1655-1659, (2009). 101
- [5] B. BOUHOUE ET AL, Proceedings of SF2A'11, G. Alecian et al. Eds, 63-68 (2011). 101
- [6] S. ANDO ET AL, submitted to Rev. Mod. Phys. arXiv:1203.5192. 101
- [7] S. D. MOHANTY ET AL, Class. Quantum Grav. 21 5, S765-S774 (2004). 101
- [8] K. HAYAMA ET AL, Class. Quantum Grav. 24, S681-S688, (2007). 101
- [9] J. ABADIE ET AL, Astrophys. J., 715, 1453-1461 (2010). 103
- [10] J. ABADIE ET AL, Phys. Rev. D 81, 52010 (2010). 103
- [11] F. ARCENESE ET AL, Class. Quantum Grav., 24, S671 (2007). 103
- [12] B. BARET ET AL, ANTARES internal note ANTARS-PHY-2011- (2011). 103
- [13] <http://marantares.in2p3.fr:8080/ANALYSIS/125>, 103
- [14] P. CLAIRE, PhD thesis, Université Paris Diderot, (2009). 103
- [15] G. HALLADJIAN ET AL, ANTARES internal note, ANTARES-PHY-2010-002 (2010). 105
- [16] G. HALLADJIAN ET AL, PhD thesis, Université de la Méditerranée Aix-Marseille II (2010). 105, 107

REFERENCES

- [17] http://antares.in2p3.fr/users/bbouhou/internal/HEN_list_2007_Updated_v2.txt, 118
- [18] B. ABBOTT ET AL, *Astrophys. J.*, 715, 1438 (2010). 120
- [19] M. WAS ET AL, *Phys. Rev. D* 86, 022003 (2012). 121, 124
- [20] I. DI PALMA, Proceedings of TAUP 2011, *J. Phys. Conf. Ser.* 375, 060002 (2012). 123
- [21] P. BRADY ET AL., *Class. Quantum Grav.* 21, S1775 (2004). 124
- [22] B. ABBOTT ET AL, *Phys. Rev. D*, 77, 062004 (2008). 125
- [23] C. FRYER ET AL, *Astrophys. J.*, 565 430-446 (2002). 129
- [24] S. KOBAYASHI AND P. MÉSZÁROS, *Astrophys. J.*, 589 861–870 (2003). 129
- [25] A. L. PIRO AND E. PFAHL, *Astrophys. J.* 658 1173 (2007). 129
- [26] C. FRYER AND K. NEW, *Living Rev. Relat.*, 14 1 (2011). 129
- [27] H. DIMMELMEIER ET AL, *Phys. Rev. D*, 78 065056 (2008). 129
- [28] C. D. OTT, *Class. Quantum Grav.*, 26 063001 (2009). 129
- [29] S. SCHEIDEGGER ET AL, *A&A* 514 A51 (2010). 129
- [30] C. OTT ET AL, *Phys. Rev. Lett*, 106 161103 (2011). 129
- [31] T. TAKIWAKI AND K. KOTAKE, *Astrophys. J.*, 743 1 (2011). 129
- [32] GUETTA, ET AL., *Astropart. Phys.* 20 429-455 (2004). 132
- [33] E. NAKAR, *Phys. Rept.*, 442, 166 (2007). 132
- [34] R. O'SHAUGHNESSY ET AL, *Astrophys. J.*, 716 615 (2010). 132
- [35] G. M. HARRY ET AL, *Class. Quantum Grav.* 27 084006 (2010).
- [36] S. BRACCINI ET AL., *Astropart. Phys.* 23, 557 (2005).
- [37] P. MESZAROS, *Astron. Astrophys. Suppl. Ser.*, 138, 533 (1999).
- [38] G. J. FELDMAN AND R. D. COUSINS, *Phys. Rev. D* 57, 3873 (1998).
- [39] E. WAXMAN, *Lect. Notes Phys.*, 576, 122 (2001).
- [40] J. ABADIE ET AL., *Phys. Rev. D* 81 102001 (2010).
- [41] K. KOTAKE ET AL, *Rep. Prog. Phys.*, 69 971-1143 (2006).

CHAPTER 5

GW+HEN ANALYSIS FOR 12L-S6/VSR2-3

5.1 Summary

We have presented in the previous chapter results from the first joint search for gravitational-wave bursts associated with high energy neutrinos using the ANTARES, the Virgo and the LIGO data from 2007. In this chapter we present results from the analysis of their 2009-2010 data. A new method is proposed. The neutrinos are selected by a joint optimisation procedure taking into account efficiencies to the neutrino and gravitational-wave signals. The neutrinos have been reconstructed with a more sophisticated reconstruction algorithm, labelled Aafit, in contrast of the robust one (Bbfit) used in the previous search (Chapter 4). The search for GW in coincidence with these neutrinos are done using a specific GW search algorithm, labelled skymask-cWB, specifically prepared for this joint search. Below we describe further these data, the search strategies adopted and the final results.

5.2 Data set

5.2.1 Description of ANTARES data

We select from the database 2184 runs from July 7th, 2009 through October 20th, 2010. This list of runs has been selected using data quality (DQ) requirement (see section 2.4). That is, we select all runs with QualityBasic flag greater than 1 ($QB \geq 1$) and runs with run setup "physics". We discard all runs with duration < 5 minutes. Taking into account these DQ criteria we get a duty cycle of 56%. Figure 5.1 shows the distribution of run numbers selected for the analysis. The total observation time (using only neutrino side) is $T \equiv 266$ days.

A Monte Carlo simulation is performed to match the realistic condition of the data taking following the run by run approach (see section 2.5.5). These information (runsetup, mean rates, alignment, high rate veto, run duration) are taken from the data runs themselves and plugged

into the simulation. This method has been adopted recently by the ANTARES collaboration and is used by all ongoing analyses. A total of 5×10^8 neutrinos are simulated using the GENHEN package in the energy range 100 GeV-100 PeV, with an energy spectrum $dN/dE \propto E^{-\gamma}$, where $\gamma = 1.4$, and in all zenith directions. The spectrum used to simulate neutrinos permits a later re-weighting according to a user specified flux. In this analysis the same neutrino sample is weighted differently to be used as atmospheric neutrinos according to the Bartol flux [2] or as astrophysical signal according to the GRB diffuse flux of Waxman and Bahcall [3] (see section 1.1.4) or E^{-2} flux [4]. The simulation of atmospheric muons is performed using Mupage package (see section 2.5). In this analysis we select all the events passing the 3N or T3 trigger's condition (see section 2.3.5). These events are then reconstructed with the Aafit reconstruction algorithm (see section 2.6.2).

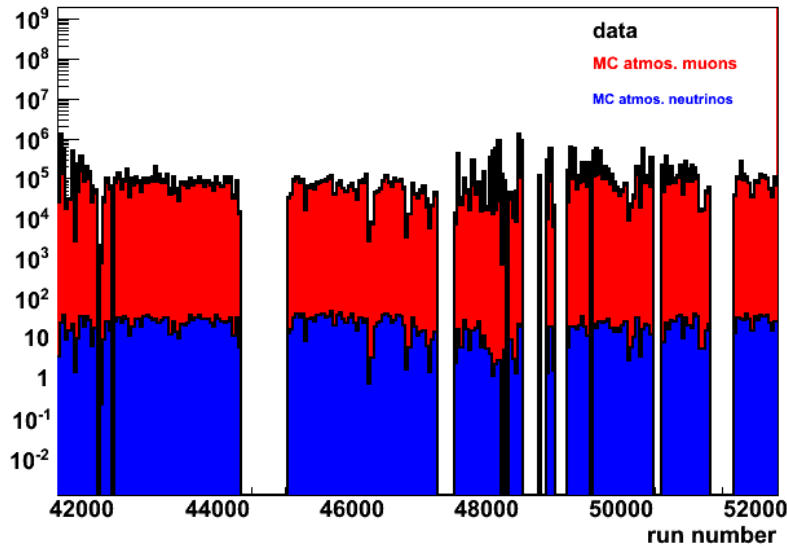


Figure 5.1 – Run numbers that passes the DQ requirements described in the text.

5.2.2 Description of Virgo and LIGO data

The GW data used in this search are the S6-VSR2/3 LIGO-Virgo data. Three detectors participated to this data taking namely LIGO-Livingston (L1), LIGO-Hanford (H1) and Virgo (V1). These data were collected between July 07, 2009 and October 21, 2010. LIGO S6 and Virgo VSR data are divided into four parts:

- Period A (S6A-VSR2): running from Tue July 7, 2009 at 21:00 UTC to Tue Sept. 1, 2009 at 00:00 UTC.

5.5.3 Gravitational wave event generation

- Period B (S6B-VSR2): running from Saturday Sep 26, 2009 12:46:33 UTC, Friday Jan 8, 2010 22:00:00 UTC.
- Period C (S6C) : running from Friday Jan 8, 2010 22:00:00 UTC to Saturday Jun 26, 2010 00:00:00 UTC.
- Period D (S6D-VSR3): running from Saturday Jun 26 2010 00:00:00 UTC to Wednesday Oct 20 2010 15:00:00 UTC.

This search aims at detecting bursts of gravitational waves in the frequency range from 64 Hz to 2 kHz. Note that the detectors are most sensitive at about ~ 200 Hz as can be seen from Figure 5.2. The sensitivity in the selected frequency range is within a factor of 10 of the best sensitivity. Each curve in Figure 5.2 shows the amplitude spectral density as a function of frequency. The vertical "spikes" are from mechanical vibrations in parts of the detector. The sensitivity of a detector can be expressed in terms of the amplitude spectral density, which is the square root of the power spectral density, since the strength of a gravitational wave signal is proportional to the strain induced in the interferometer. We use the calibrated data with LSC tag `LDAS_C02` and the Virgo tag `HrecV2` and `HrecV3`. The calibration uncertainty is estimated to be 20% in amplitude and 10 degrees in phase for LIGO and 5.5% in amplitude and 3 degrees in phase for Virgo. The data quality flags [5] aim at eliminating periods where data have poor quality (some or all of the detectors was particularly noisy e.g., due to internal malfunctioning and/or environmental disturbances).

5.2.3 The ANTARES, the Virgo and the LIGO joint data set

The search requests at least two GW detectors in operation. The concomitant data taking period between S6VSR2/3 and ANTARES 12L goes from July 7th, 2009 up to October 20th 2010 with some in between periods where one or no interferometer (IFO) was in science mode. In this period, the observation time for each IFO network is: 44.7 days (H1L1V1), 33.5 days (H1L1), 23.1 days (L1V1) and 27.4 days (H1V1). The sum of these partial periods gives the total concomitant observation time of $\tau \equiv 128.7$ days.

5.3 Gravitational wave event generation

For this analysis we rely on a new detection pipeline `skymask coherent WaveBurst` which is a variant of the coherent WaveBurst (cWB) pipeline, presented in section 3.7.4 developed for the purpose of this search.

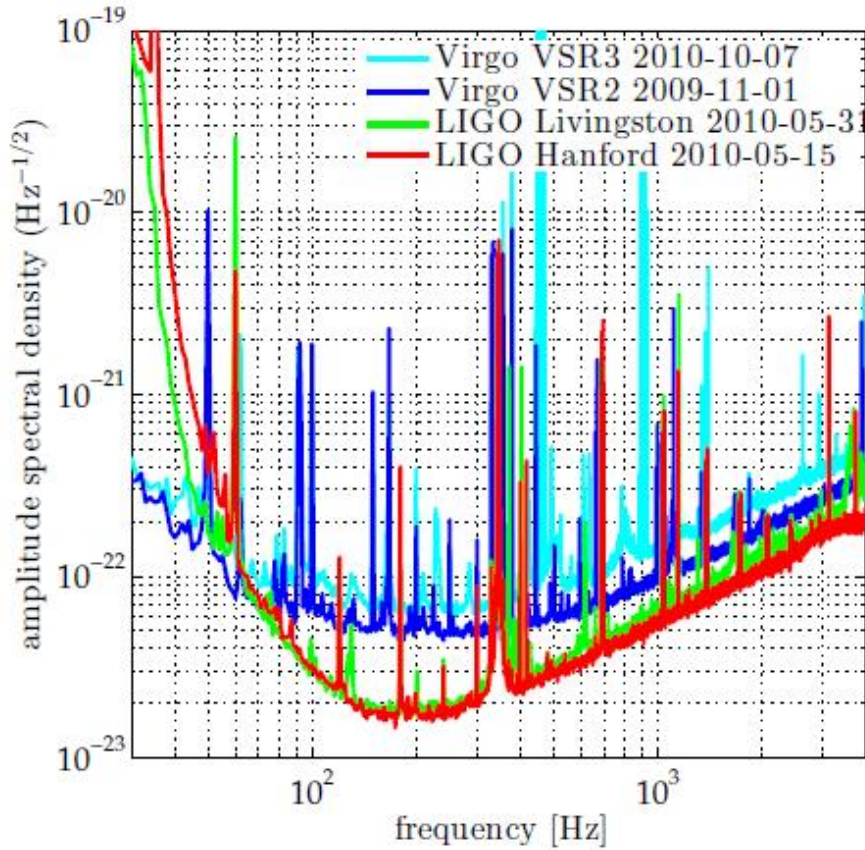


Figure 5.2 – Sensitivity of LIGO-Virgo during the S6-VSR2/3 period.

5.3.1 Skymask coherent WaveBurst pipeline

This pipeline has been developed to overcome limitations of earlier analysis schemes presented in section 3.7.4. In particular, it takes into account the lessons learned from the first ANTARES–LIGO/Virgo joint search (see Chapter 4) [6] based on the X-pipeline algorithm.

Core collapse supernovae being one of the potential source targets, the frequency bandwidth should extend to 2 kHz at least. We also expect many more neutrino candidate for this data set, of the order of $\mathcal{O}(10^3)$, which is an order-of-magnitude increase with respect to the previous analysis. The current implementation of the X-pipeline used for the first search would require a very large computing power to perform the analysis in a realistic time.

This is why we developed “skymask coherent Wave-Burst” (in short, s-cWB) [7], a variant of the cWB pipeline which reconstructs GW events only in an *a priori* sky area specified by a *sky mask*. This enables the analysis of periods with two GW detectors only (see Figure 5.4 for an illustration). We are thus able to cover the whole livetime. This pipeline is also computationally more efficient than the X-pipeline thus enabling the broadband analysis (up to 2 kHz) for order

of thousands of neutrino triggers.

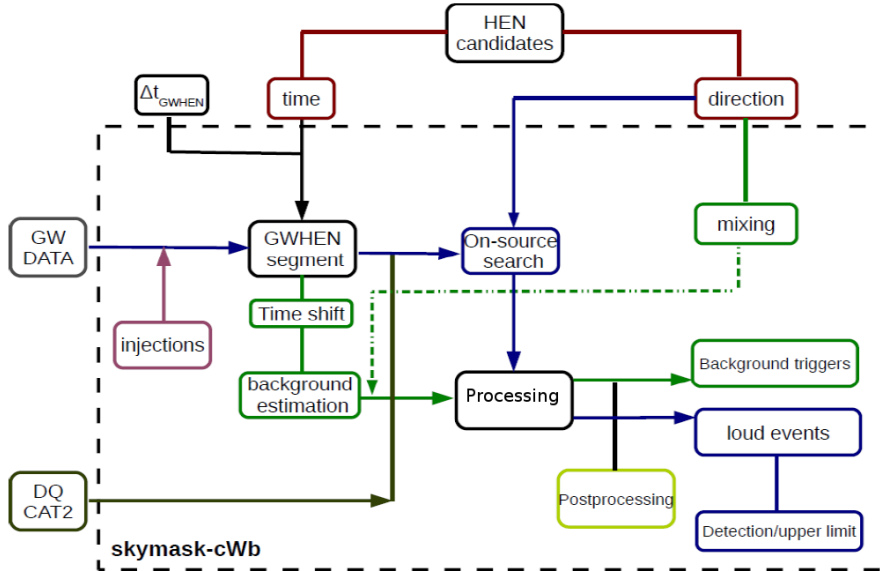


Figure 5.3 – Schematic outline of the GW+HEN 12LS6VSR2-3 analysis pipeline.

As discussed in section 4.2 the time and direction of the neutrino candidates are exploited as input to the s-cWB pipeline. s-cWB selects GW data segments of length ΔT centered about the t_ν , i.e. *on-source* window (see section 4.2). It also takes into account the ASW associated to the direction of the neutrino candidate. The search for GW signal is thus restricted to areas on the sky defined by the provided ASW90% instead of scanning the whole sky. A grid, of same resolution as cWB, i.e. 0.4×0.4 degree, is used within the ASW90% (see section 4.4.1). The neutrino PSF is taken into account as a probability distribution: each event inside this angular search window is weighted according to the PSF. Figure 5.3 shows a schematic view of the s-cWB pipeline used in this analysis. s-cWB defines the same coherent statistics as cWB, the most relevant ones for this study are the network correlation amplitude ρ , the network correlation coefficient net_{cc} and the network energy disbalance net_{ED} . While cuts on net_{cc} and net_{ED} are used to distinguish noise outliers from genuine GW signals, the final event selection is done through a cut over the statistic ρ which characterises the event significance [8]. We refer the reader to appendix B for the mathematical definition of those statistics.

5.3.2 Background estimation

The method used in the cWB for background study is described in [9]. For completeness, we now describe the general principle. We remind that in a coherent analysis such as s-cWB, time delays are applied to each data streams in order to compensate the time taken by the wave to

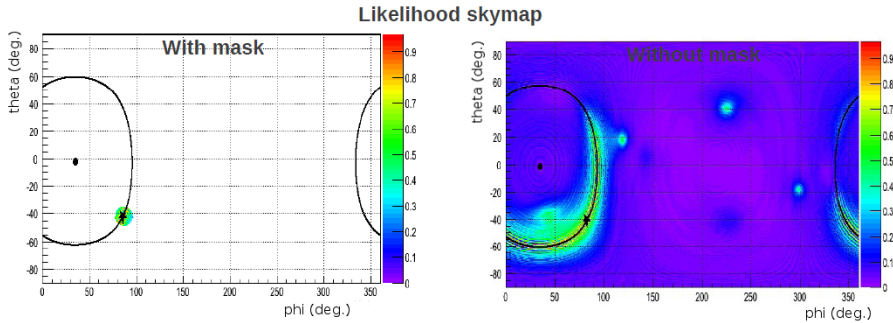


Figure 5.4 – Likelihood skymap of the reconstructed GW events in the case of 2 IFOs, without neutrino skymask (right) and with skymask (left).

propagate from one detector to the other. Thanks to this operation, GW signals from a given source direction are thus aligned in time. The time delays are necessarily smaller than the time-of-flight (at the speed of light) between Virgo and LIGO is about to 27 ms and 10 ms for the Handford and Livingston detector respectively. The method used for background estimation consists in applying additional and non-physical time-shifts to one or more GW data streams as described in section 3.7.2. The time-shifts applied for the background estimation are much larger than the time-of-flight added to the noise auto-correlation time scale (which dominate the sum). These time-shifts erases any correlation between pairs of GW detectors due to any GW signal. The analysis is repeated over several time-shifted data set. The distribution of the resulting events provides an estimate of the experiment background.

In addition to the time-shift analysis s-cWB allows the possibility to estimate background using mixing skymasks and/or combine both methods. While skymask mixing is convenient numerically, we observed that it has limitations because it introduces correlation between trials especially in the case of two-detector network. We consider it as an option for the final analysis. The analysis cuts are tuned based on the estimated background.

We evaluated the background and performance of s-cWB over a simulated neutrino test sample. This study is approximately representative of the final analysis using real neutrino candidate events. The fake neutrino set consisted in 1000 events randomly generated uniformly distributed over the entire sky and during the S6A/VSR2 period. The neutrino localisation uncertainties were chosen to mimick that of 2007 neutrino sample (see chapter 4). We used the modelled 'g'-search which is optimized for circularly polarized GW signals and we disabled regulation. We performed multiple (101) time-shift and (70) skymask mixing experiments between L1, H1 and V1 detectors. This leads to the background estimates presented in Figure 5.5. We adjusted the rejection cuts on net_{cc} and net_{ED} to mitigate the long background tails due to the absence of regulation. For an objective FAR of 10^{-7} Hz we therefore need a selection

cut $\rho \geq \rho_{\text{threshold}} = 3.25$.

5.3.3 Sensitivity estimates

In order to test the performance of the s-cWB we add simulated signals of various amplitudes and waveforms to data (see section 3.7.3). The simulated signals are produced using the Burst-MDC package described in [10].

For each neutrino candidate, we simulate randomly a set of source position according to the PSF. Fake signals are added every ~ 100 seconds mimicking the GW signature from sources at those position. We test the probability of detection and correct recovery for various amplitudes by applying multiplicative factors from weak to strong signals covering the full range from 0 to 100 % efficiency. The resulting data stream is processed identically to the standard analysis.

For each waveform, we evaluate the efficiency for detection as a function of the gravitational wave strain h_{rss} which is the incoherent sum of the “+” and “ \times ” polarizations defined in Equation (4.15), see Figure 5.6. As expected, the efficiencies are essentially 100% for large values of h_{rss} , consistent with noise and thus 0% efficiency for small h_{rss} , and transitioning over a narrow intermediate range of h_{rss} . The resulting curve is empirically fitted by a sigmoid curve in $\log_{10}(h_{rss})$.

We produced the efficiency curves associated to the analysis of the test neutrino sample

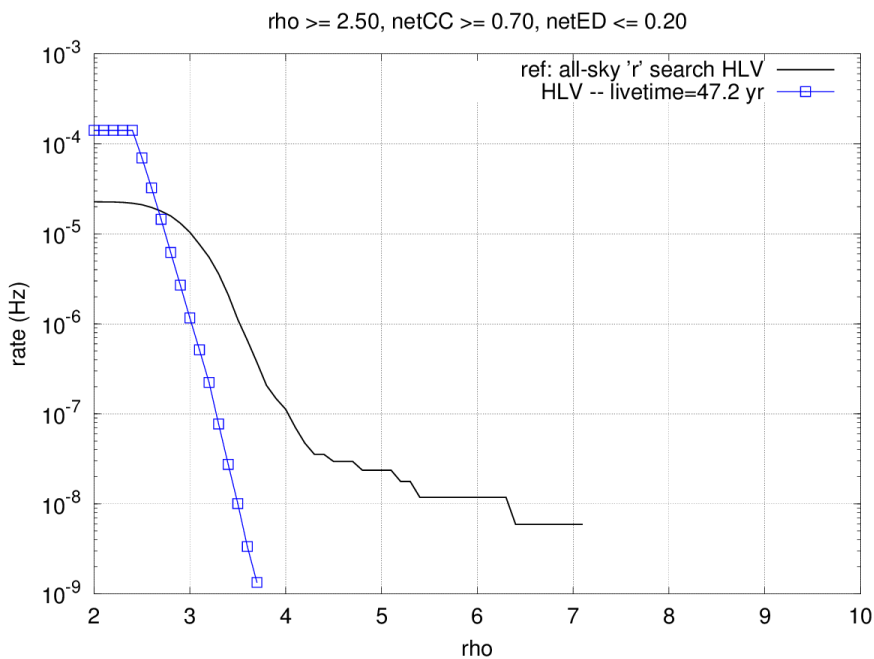


Figure 5.5 – Background estimate for the test neutrino sample as described in the text and considering triple detector network HLV compared to the all sky background for the same data taking.

introduced in the previous section. We performed multiple injections of circularly polarized Sine-Gaussian waveforms as in Equations (3.16) and (3.17) at four different frequencies i.e., 153, 100, 1053 and 1304 Hz. For selection cut corresponding to the FAR = 10^{-7} Hz we get $h_{rss}^{50\%} = 4.1 \times 10^{-22}/\sqrt{\text{Hz}}$ at 153 Hz. This can be compared to the result obtained with the X-pipeline in Chapter 4, namely $h_{rss}^{50\%} = 3 \times 10^{-22}/\sqrt{\text{Hz}}$ at the same frequency and for the same FAR requirement. Despite the absence of the (numerically expensive) event-by-event optimization of the cuts performed by the X-pipeline, the s-cWB performs at a comparable level.

5.4 Optimization procedures

The selection of the neutrino events can, in principle, be based on several approaches. Independently from the GW interferometers, the selection can be made in order to discard as much as possible misreconstructed atmospheric muons (resulting in a high purity sample of atmospheric neutrinos). Another criterion would be to filter the events in order to establish the best possible limit on some putative astrophysical neutrino flux (minimizing the so-called model rejection factor MRF). Reversely one can target a discovery by maximizing the model discovery

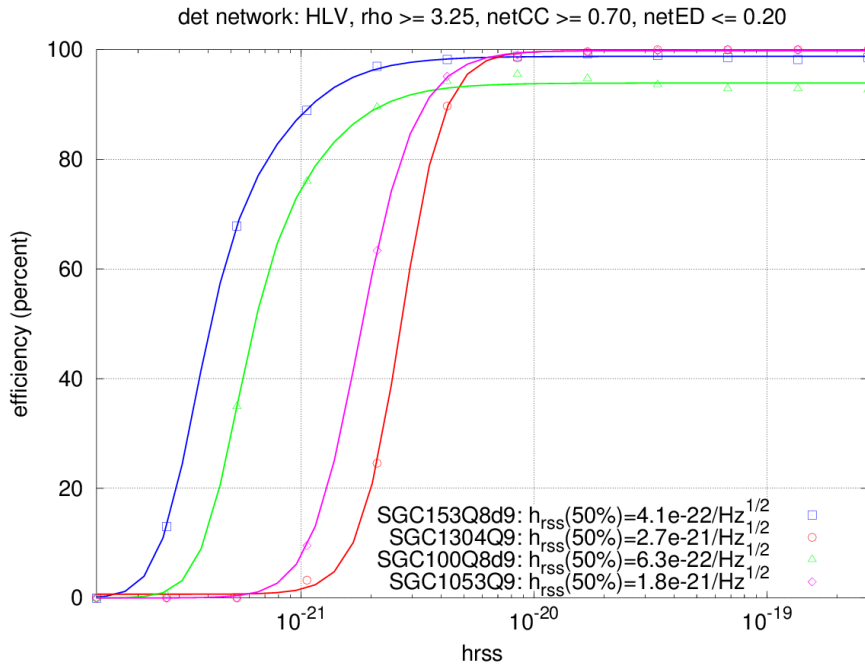


Figure 5.6 – Sensitivity estimate obtained with the test neutrino sample as described in the text and for triple detector network HLIV.

potential MDP (minimizing the model discovery factor MDF) for this particular neutrino flux.

The third approach is completely dependent of the GW interferometers. This approach maximises a joint figure-of-merit (FOM) by combining the individual efficiencies of HEN and GW. FOM relies on our knowledge on the false alarm probability.

In the following subsections, we describe the three latter options. In the all cases, the signal is assumed to be a diffuse flux (as the sources of interest are distributed anywhere in the sky). We use the Waxman-Bahcall flux for unresolved GRBs, since the energy spectrum is supposed to be representative of generic long- and short-GRBs, (see section 1.1.4).

5.4.1 Model rejection factor and Model discovery potential

Model rejection factor (MRF): The model rejection factor (MRF) [11] is used in this search to optimize selection criteria in order to place the best upper limit on the signal from an assumed theoretical model. We use in this work the GRB diffuse flux of Waxman-Bahcall. The computation relies **only on Monte Carlo simulation sample** to estimate the expected background events (n_b) and true neutrino signal events (n_s). The authors in [11] introduce the *average upper limit* at 90% C.L, when $n_s=0$, as follows:

$$\bar{\mu}_{90}(n_b) = \sum_{n_{obs}}^{\infty} \mu_{90}(n_{obs}, n_b) \frac{(n_b)^{n_{obs}}}{n_{obs}!} \exp(-n_b) \quad (5.1)$$

where $\mu_{90}(n_{obs}, n_b)$ is the Feldman-Cousins (F.C) upper limit [12]. That is, the best upper limit is obtained when the ratio between $\bar{\mu}_{90}(n_b)$ and n_s , labeled MRF, is minimum for a set of cuts:

$$MRF(\text{cuts}) = \frac{\bar{\mu}_{90}(n_b(\text{cuts}))}{n_s(\text{cuts})} \quad (5.2)$$

In this work we compute n_b and n_s against the reconstruction quality parameter Λ , introduced in section 2.6.2. It's worth noting that Λ and β are correlated as shown in Figure 5.7 right. We show also in Figure 5.8 distributions of β for upgoing events with and without cutting on Λ . Thus we decide not to use β in the optimisation. The distribution of Λ is shown in Figure 5.9 for only upgoing events. It's extrapolated to high Λ values using a Gaussian distribution.

With a number of background events of order of 10^4 for small Λ , the computation of $\bar{\mu}_{90}(n_{obs}, n_b)$ becomes considerably slow because of F.C. algorithm at high statistics. To speed up the computation time we model the upper limit by an analytical parameterization (see

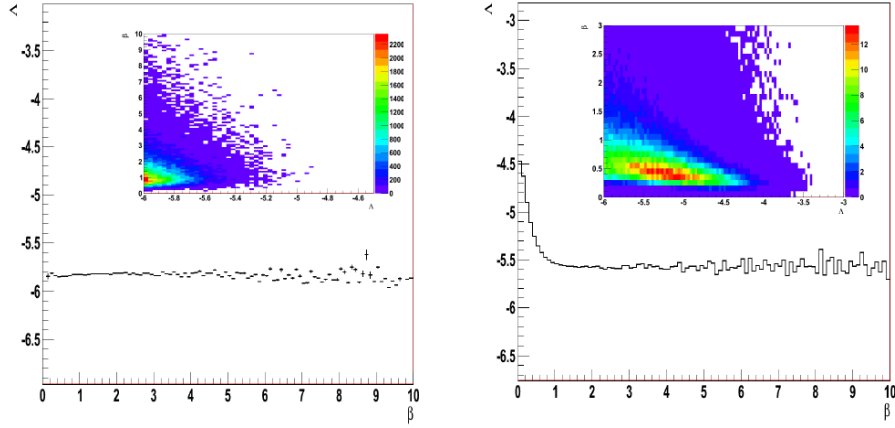


Figure 5.7 – Distribution of Λ as function of β parameter for atmospheric muons (left), for atmospheric neutrinos (right). Only upgoing events are selected.

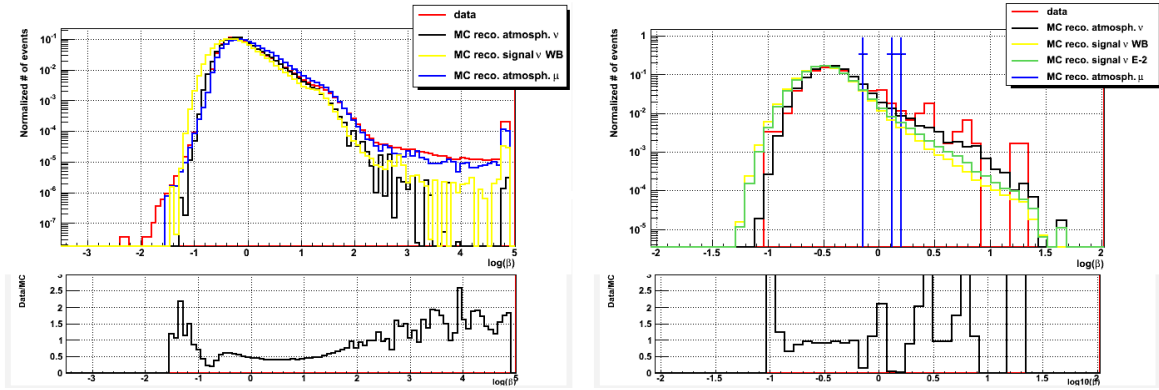


Figure 5.8 – Distributions of β parameter for data and MC without (top) and with (bottom) cut on Λ ($\Lambda > -5$). Only upgoing events are selected.

appendix A for further mathematical details):

$$\tilde{\mu}_Q(n_{obs}, n_b) = \left(\frac{-\sqrt{2} \cdot \text{Erf}^{-1}(2Q - 1) + \sqrt{2 \text{Erf}^{-1}(2Q - 1)^2 + 4n_{obs}}}{2} \right)^2 - n_b \quad (5.3)$$

where Erf is the error function and $Q = 90\%$ is the significance level. In analogy with Equation 5.1, $\tilde{\mu}_Q(n_{obs}, n_b)$ is weighted with its Poisson probability of occurrence. Thus the model rejection factor becomes:

$$M\tilde{R}F(\text{cuts}) = \frac{\tilde{\mu}_{90\%}(n_b(\text{cuts}))}{n_s(\text{cuts})} \quad (5.4)$$

In Figure 5.10 is shown the modified ratio (Equation (5.4)) as function of Λ . We define Λ_{min} in such way the ratio Equation (5.4) is minimum. From the curve 5.10 we find a minimum for

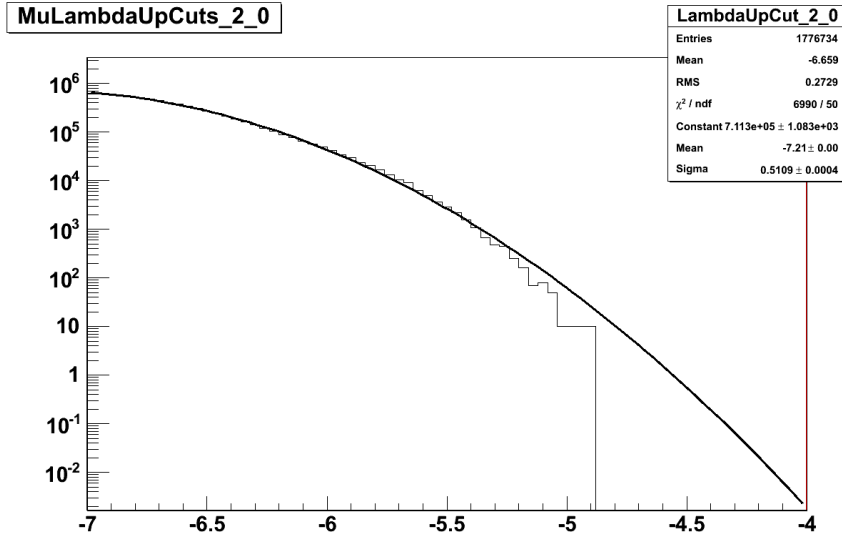


Figure 5.9 – Distribution of the track quality parameter Λ for misreconstructed atmospheric muons. The distribution is fitted by a Gaussian function.

$\Lambda_{min} = -4.1$. The final number of events passing Λ_{min} is ~ 20 events.

Model discovery potential: We report in this section a commonly used technique in high energy astrophysics, the so-called "Model Discovery Potential" (MDP) [13, 14], for optimizing quality cuts in order to maximize the probability of detecting an excursion of $n\sigma$ (a "discovery")

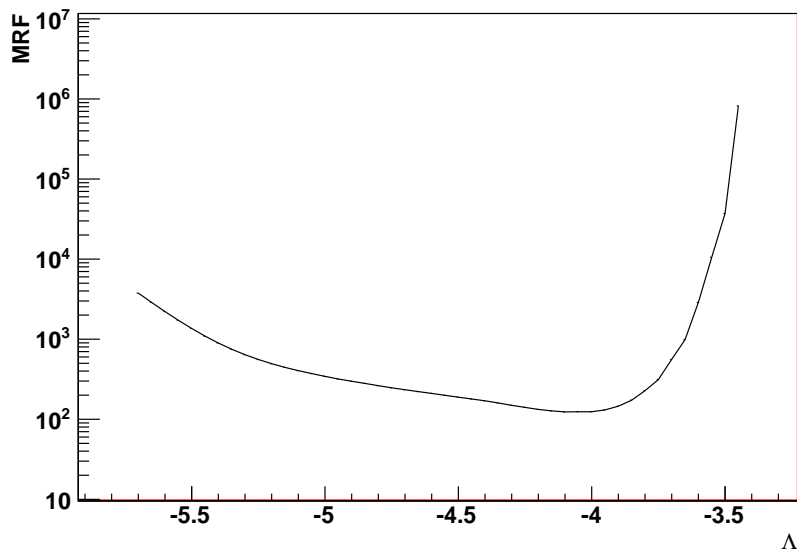


Figure 5.10 – MRF as a function of Λ completed as described in the text. The minimum value is found for $\Lambda = -4.1$

with a given C.L. We introduce n_{crit} the smallest number of events needed to claim a detection at a significance level α . A standard way to quantify this number is to calculate the probability for observing $\geq n_{crit}$ under the background only hypothesis:

$$\begin{aligned} P(\geq n_{crit}|\mu_b) &= \sum_{n=n_{obs}}^{\infty} P(n|\mu_b) \\ &= 1 - \sum_{n=0}^{n_{obs}-1} P(n|\mu_b) \end{aligned} \quad (5.5)$$

If $P(\geq n_{crit}|\mu_b) < 5.73 \times 10^{-7}$ we can report that we have a detection at 5σ level. This probability is called p_{value} , i.e $p = P(\geq n_{crit}|\mu_b)$. Small p_{value} is evidence against null hypothesis. If in addition to n_b a real signal μ_s is assumed then the probability that we would observe at least n_{crit} becomes:

$$\begin{aligned} P(\geq n_{crit}|\mu_b + \mu_s) &= \sum_{n=n_{obs}}^{\infty} P(n|\mu_b + \mu_s) \\ &= 1 - \sum_{n=0}^{n_{obs}-1} P(n|\mu_b + \mu_s) \\ &= 1 - \beta \end{aligned} \quad (5.6)$$

$1 - \beta$ is commonly known as the statistical power. Fixing $(1 - \beta)$ allows to calculate the corresponding value of μ_s for which Equation (5.6) is satisfied, i.e. μ_{lds} . We then define the model discovery factor (MDF) as the ratio between μ_{lds} and μ_s .

$$MDF(\Lambda) = \frac{\mu_{lds}(\Lambda)}{\mu_s(\Lambda)} \quad (5.7)$$

An optimization of the analysis which aims at minimizing the MDF against Λ for a given statistical power and a given significance (C.L.), has to be done numerically. From other side Punzi derived in [14] an analytical parameterization of μ_{lds} by approximation of Poisson distribution by Gaussian one:

$$S_{min} = \frac{cl^2 + 2\sigma\sqrt{n_b} + cl \times \sqrt{cl^2 + 4\sigma\sqrt{n_b} + 4n_b}}{2} \quad (5.8)$$

where σ and cl are the desired *number* of sigmas and C.L respectively (see Figure 5.11). Thus the MDF can be redefined by Equation (5.9):

$$M\tilde{D}F(\Lambda) = \frac{S_{min}}{\mu_s} \quad (5.9)$$

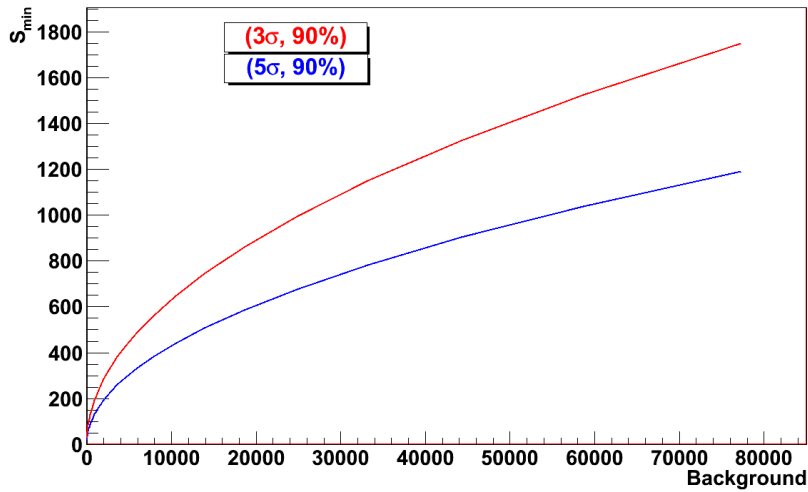


Figure 5.11 – Minimum number of signal events versus number of background events.

A study of MDF for a given (σ, cl) as a function of two reconstruction parameters, Λ and β is shown in Figure 5.12. It shows that the MDF has no clear minimum in the accessible parameter space. We confirm this with a 2D distribution of Λ vs β (insert in color in Figure 5.13), which shows the mean value of Λ for each bin in β . Figure 5.13 left shows that there is no minimum of the MDF as a function of β . On the contrary there is a clear minimum of the MDF as a function of Λ . Thus, we restrict this study to the only Λ parameter.

In this work we minimize Equation (5.9) against Λ . Figure 5.14 shows the result for different number of σ and number of cl . The minimum is obtained for $\Lambda_{min} = -4.9$ and is roughly the same whatever the assumed number of σ and cl . The number of events surviving this cut is ~ 600 .

Figure 5.14 shows a rather flat behaviour of the MDF value against Λ (above -5.5). As a consequence the Λ value found to minimize the MRF is not far from the minimum value of the MDF. However, the optimal MRF cut shows a factor 2 loss in the detectable flux (proportional to the MDF) and the optimal cut for the MDF leads to a 3 times worse flux limit (proportional to the MRF). More over, these two approaches do not take into account the fact that we are

looking for common sources of GW and HEN. We conclude that none of these two approaches, often used in neutrino astrophysics, is fully satisfactory for our purpose. In the following section, we present a new optimization method that takes into account parameters from both GW and HEN data, as opposed to MRF and MDP approaches just described.

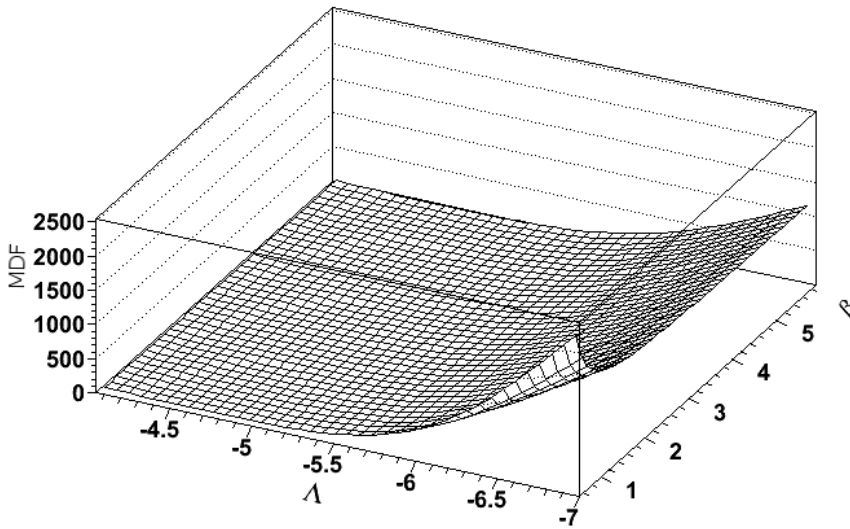


Figure 5.12 – The Model discovery factor in the two parameter space (β , Λ) for (3σ , 90%).

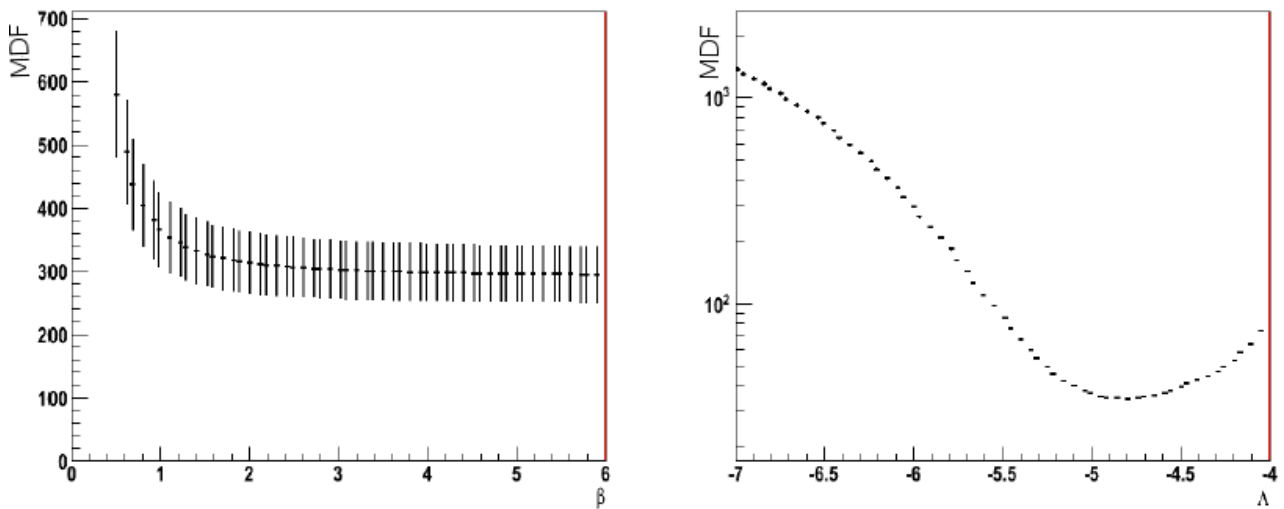


Figure 5.13 – Profile histogram of the MDF on β parameter (Left) and on Λ parameter (right).

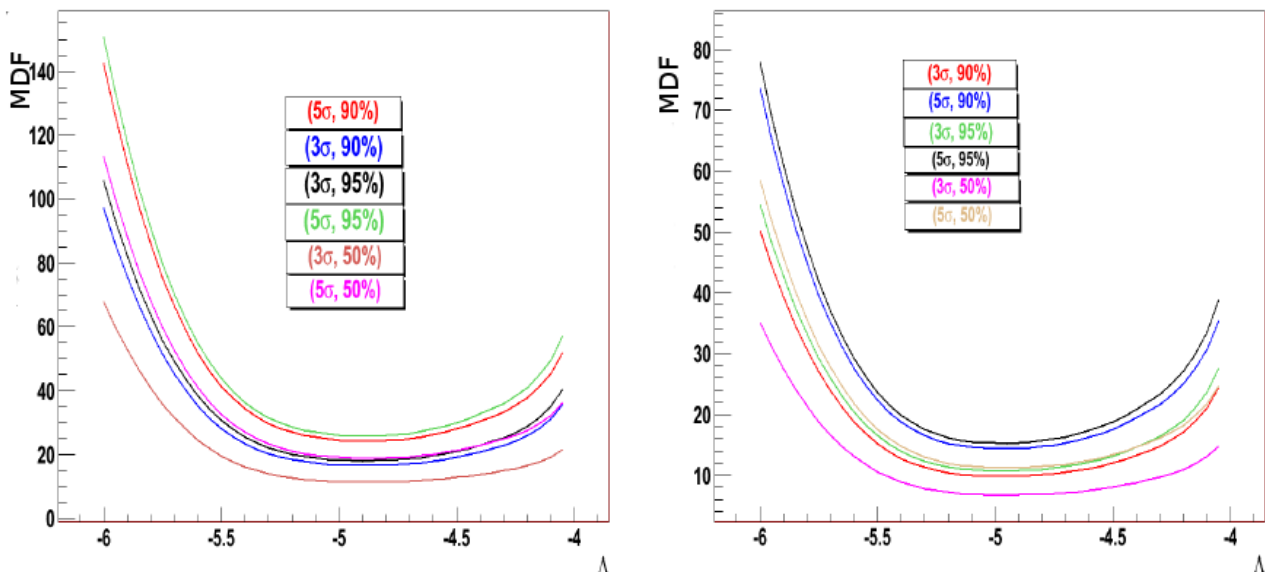


Figure 5.14 – The model discovery factor for different number of σ and cl as function of Λ , for W&B GRB diffuse flux (left) and E^{-2} flux (right). The curves show that the minimum of the MDF is independent of the number of sigma $n\sigma$ and the C.L.

5.5 Description of the joint optimization strategy

The two selection procedures described above are not fully satisfactory since they only apply to the neutrino data and do not take into account the impact of the selection onto the GW search. Such independent selection criteria were used in the previous joint searches of HE neutrinos and GW (see chapter 4) leading to suboptimal searches. Here we propose a novel joint optimization procedure. The idea relies on the simple following arguments:

- The rationale behind the concomitant search is to select as much as possible cosmic neutrino candidates and assess their cosmic nature by the observation of GW in time and space coincidence. In this view, the selection should leave large the efficiency to signal neutrinos which can be defined, by means of Monte Carlo simulations, as the ratio of selected events $N_{selected}$ (after cuts) over triggered events $N_{triggered}$:

$$\epsilon_{\nu}(\text{cuts}) = \frac{N_{selected}}{N_{triggered}} \quad (5.10)$$

The cuts considered here are $\cos\theta_{MC} \geq 0$, $\cos\theta_{rec} \geq 0$. In order to increase ϵ_{ν} , loose cuts must be applied. This also considerably increases the number of selected background events.

- A too high number of these background events will result in an increased number of accidental coincidences FAR for a fixed set of cuts in the GW search. To avoid this situation, such triggered searches, are usually made with a fixed FAR. In order to keep this FAR constant, the higher the number of neutrino candidates to probe, the tighter the cuts should be applied on the GW side, leading to a poorer efficiency $\epsilon_{GW}(E_{GW}, r)$ for a given distance r and a model GW energy release. In other words this leads to a closer horizon for the GW search. In this case the probed distance for GW appears to depend on the neutrino selections cuts and one may write: $D \equiv D(cuts)$.

As a consequence, there should be a trade-off in these two approaches, which allows us to stick to the predefined FAR, with cuts that are optimal for the joint search.

5.5.1 Definition of the joint figure-of-merit

The approach adopted here is to apply the neutrino cuts to maximize the number $\mathcal{N}_{\text{GWHEN}}$ of detectable sources emitting both GW and HEN. Let us assume that the sources are all identical and radiate E_{GW} in GW and emit a fluence φ_ν in HEN. Let us also assume that their population is isotropic so their density per unit time and volume R is a constant. The number of detectable sources is

$$\mathcal{N}_{\text{GWHEN}}(\text{cuts}) = \iint dt d^3\Omega \mathcal{R}(r, t) \epsilon_\nu(\text{cuts}) \epsilon_{GW}(\text{cuts}; E_{GW}, r) \quad (5.11)$$

where $\mathcal{R}(r, t) = R \mathcal{P}(N_\nu > 0 | \varphi_\nu / (4\pi r^2))$ is the density of detectable sources. From Poisson statistics, we get $\mathcal{P}(N_\nu > 0 | \varphi_\nu / (4\pi r^2)) \propto 1/r^2$ in the limit of small fluxes.

The cuts being applied are connected to the methodologies in use for the muon track reconstruction on the HEN side and for the transient detection on the GW side. Those methodologies are detailed in section 5.3 for GW and in section 2.6 for HEN. We will optimize over the cut thresholds applied to the two following parameters: the quality of the muon track reconstruction Λ and a proxy to the signal-to-noise ratio ρ for the HEN and GW, respectively. We obtain

$$\mathcal{N}_{\text{GWHEN}}(\Lambda, \rho_{\text{threshold}}) \propto \int_0^\infty 4\pi r^2 dr \frac{1}{r^2} \epsilon_\nu(\Lambda) \epsilon_{GW}(\rho_{\text{threshold}}; E_{GW}, r) \quad (5.12)$$

where we dropped the useless constants such as the global livetime τ of the experiment which results from the time integral.

The typical shape of $\epsilon_{GW}(\rho_{\text{threshold}}; E_{GW}, r)$ as a function of r for a given threshold and energy E_{GW} presents a rather sharp transition (less than a decade) from 100% to 0% (see e.g., Figures 3 and 4 of [15]). It can be reasonably well approximated by a step-like function with

5.5.5 Description of the joint optimization strategy

the edge placed at the maximum distance $D(\rho_{threshold})$ at which a GW source is detectable, i.e., the GW *horizon*. Equation (5.12) can therefore be re-written as:

$$\mathcal{N}_{\text{GWHEN}}(\Lambda, \rho_{threshold}) \propto \epsilon_\nu(\Lambda) \int_0^{D(\rho_{threshold})} dr \quad (5.13)$$

The parameter $\rho_{threshold}$ sets a cut on the minimal detectable GW amplitude. For a GW “standard candle” emitted a given amount of energy in GW, it is inversely proportional to $D(\rho_{threshold})$. Therefore, we get

$$\mathcal{N}_{\text{GWHEN}}(\Lambda, \rho_{threshold}) \propto \epsilon_\nu(\Lambda) / \rho_{threshold} \quad (5.14)$$

As a conclusion, our aim is to tune the neutrino selection cuts in order to maximize the figure-of-merit given by the ratio $\epsilon_\nu(\Lambda) / \rho_{threshold}$.

5.5.2 Joint optimization procedure

We will now present the procedure for seeking the optimal cuts. Let the false-alarm probability FAP for the combined search be the probability of a fortuitous (time and spatial) coincidence of a GW and HEN background event. We define the working point of the optimization by setting a value for the FAP. Typically, we set FAP to 4.7×10^{-3} (which corresponds to a “ 2σ ” excursion).

We scan the number N of neutrino candidates in the total livetime from a minimum to maximum value (typically from 10^2 to 10^4). There is a one-to-one correspondence between each selected N and a value for Λ . For each value of N , we compute the target GW false-alarm-rate FAR_{GW} from

$$\text{FAR}_{\text{GW}} = \frac{\text{FAP}}{N\Delta T}, \quad (5.15)$$

where ΔT is the duration of the temporal coincidence window (1000s).

We compute the GW background associated to a search triggered by N neutrino candidates. This is obtained thanks to the approximation using the all-sky GW background described in section 5.6.2. We deduce the value of $\rho_{threshold}$ for which the resulting background equals the target FAR_{GW} . At this point, the figure-of-merit defined in Equation (5.14) can be computed. The maximum value leads the optimal cuts for the considered range.

5.5.3 Dealing with non-stationary backgrounds

While an average signal neutrino efficiency $\langle \epsilon_\nu(\Lambda) \rangle$ valid for the full livetime period can be estimated, the GW background rate and sensitivity instead depends on the exact configuration

of the GW detector network which varies with time.

The whole livetime is divided into segments associated to a single configuration. Each period has a respective livetime τ_n such that the total livetime is $\tau = \sum_n \tau_n$. If we denote $f_n = \tau_n/\tau$, the respective livetime fraction, the average number of neutrino candidates falling in the segment n is therefore $N_n = f_n N$. Correspondingly, we divide the time integral in Equation (5.11) running over the whole livetime into segments

$$\mathcal{N}_{\text{GWHEN}}(\text{cuts}) = \sum_n \int_{\tau_n} dt \int d^3\Omega \mathcal{R}(r, t) \epsilon_\nu(\text{cuts}) \epsilon_{\text{GW},n}(\text{cuts}; E_{\text{GW}}, r) \quad (5.16)$$

Following the same steps described in section 5.5.1, we get

$$\mathcal{N}_{\text{GWHEN}}(\Lambda, \rho_{\text{threshold}}) \propto \langle \epsilon_\nu(\Lambda) \rangle \sum_n f_n / \rho_{\text{threshold},n} \quad (5.17)$$

where the thresholds $\rho_{\text{threshold},n}$ corresponds to the false-alarm-rate $\text{FAR}_{\text{GW},n}$ for segment n .

The initial requirement on the FAP defines a global budget that has to be divided among the different segment analysis i.e., $\text{FAP} = \sum_n \text{FAP}_n$. It is natural to split this budget proportionally to the segment livetime, namely $\text{FAP}_n = f_n \text{FAP}$. In this setting, we thus have

$$\text{FAR}_{\text{GW},n} = \frac{\text{FAP}_n}{N_n \Delta T} = \frac{\text{FAP}}{N \Delta T} = \text{constant} \quad (5.18)$$

The overall optimization detailed in section 5.5.2 remains the same with the difference that $1/\rho_{\text{threshold}}$ is now replaced by $\sum_n f_n / \rho_{\text{threshold},n}$.

5.6 Application of the joint optimization procedure

5.6.1 Efficiency to HEN

The first input to the joint optimization described above is the efficiency to neutrino candidates, i.e. ϵ_ν . It is obtained assuming the WB GRB diffuse flux (described in section 1.1.4) by means of MC simulations. The only parameter studied here is the quality of the reconstruction Λ , whose cumulative distributions are shown in Figure 5.15 for atmospheric muons, atmospheric neutrinos, and the studied WB flux of cosmic neutrinos. The MC distributions are compared to the data. The good agreement observed over the full range of Λ values allows us to proceed with the chosen optimization method. This agreement is obtained by applying a scaling factor of 0.8 to the atmospheric muons. Such correction is well within the uncertainty on theoretical

5.5.6 Application of the joint optimization procedure

flux (30%) [16]. The obtained efficiency ϵ_ν is shown in Figure 5.16 as a function of the total number of selected events. The cuts considered here are $\cos\theta_{rec} \geq 0, \cos\theta_{MC} \geq 0$. The first cut ($\cos\theta_{rec} \geq 0$) permits to select events reconstructed as upgoing, while the second cut ($\cos\theta_{MC} \geq 0$) rejects those that are down-going reconstructed as upgoing (misreconstructed events). The inflection in the curves originates where the number of selected neutrino candidates starts to be dominated by misreconstructed atmospheric muons rather than atmospheric neutrinos.

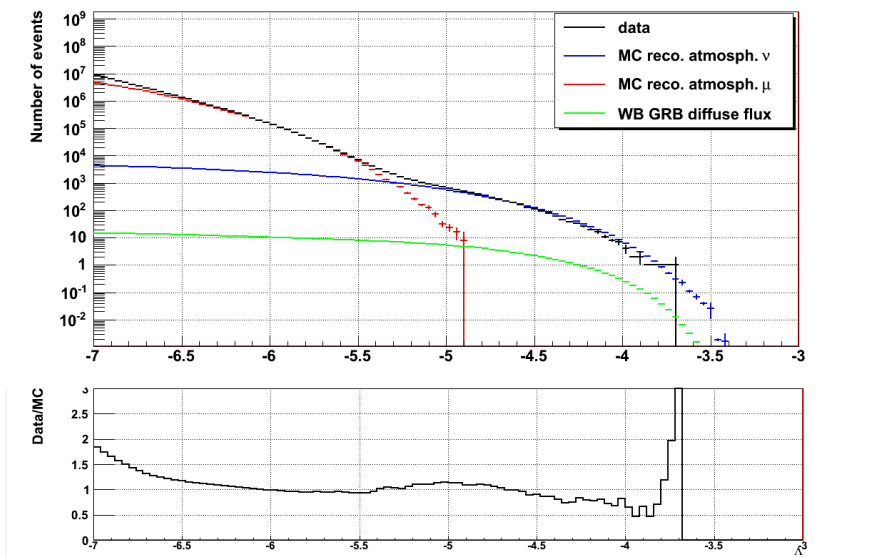


Figure 5.15 – Cumulative distribution of events, for the overall search period, as a function of Λ for the cuts described in the text. Curves of data and MC atmospheric muons and neutrinos are plotted. The distribution corresponding to the WB GRB diffuse flux is shown in green curve

The contamination (by atmospheric muons) and purity (with respect to the atmospheric neutrino sample) are shown as a function of number of neutrinos candidates in Figure 5.17.

5.6.2 Approximation of the GW background

Using s-cWB for the background estimation necessary for the cut optimization would be too much time consuming, due to high number of neutrino trials. Instead, we decided to approximate the background associated to the neutrino candidates by using the all-sky background(s).

If the GW background events are isotropically and Poisson distributed, it is easy to show that the background rate of triggered search should be rescaled by a factor $\sim (\Omega_{GW}^{1/2} + \Omega_{HEN}^{1/2})^2 / (4\pi)$ where Ω_{GW} and Ω_{HEN} are the solid angles under the GW and HEN error-boxes (or PSF) respectively. This factor essentially results from an estimate of the probability that those two error boxes overlap if their central directions is chosen at random. The HEN error box

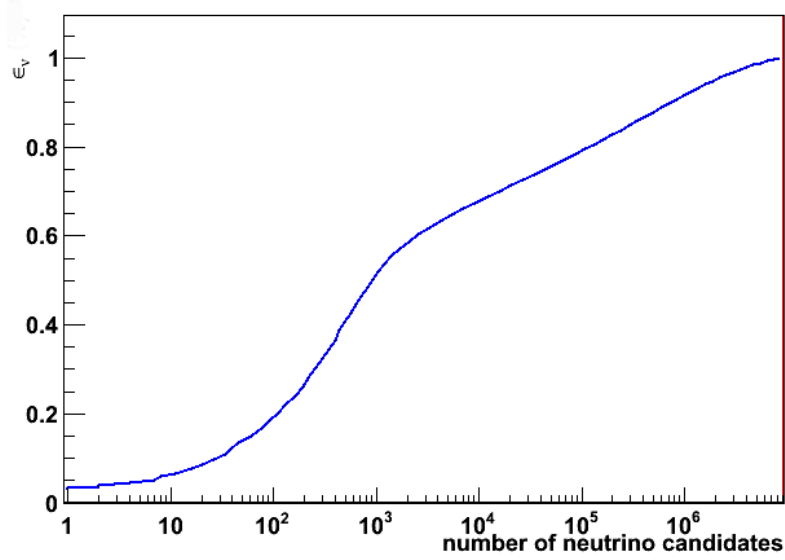


Figure 5.16 – Efficiency to neutrino candidates for WB GRB diffuse flux.

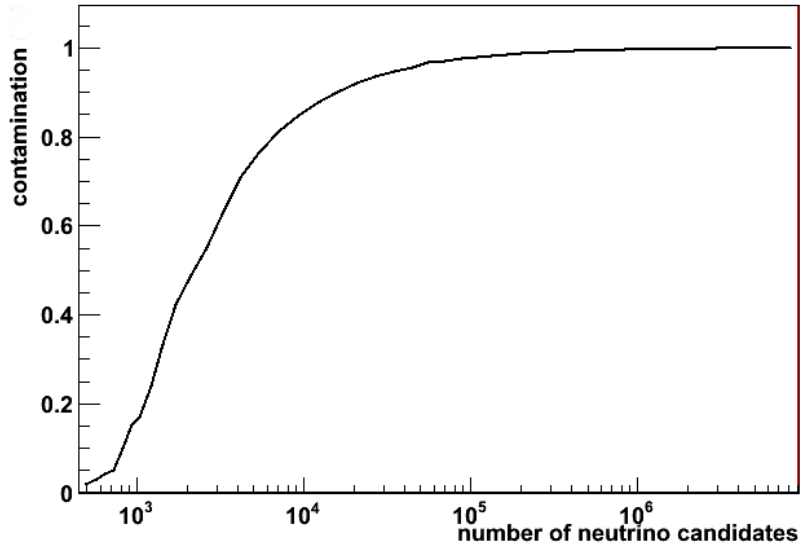


Figure 5.17 – Muon contamination of the neutrino sample for upgoing events in function of the number of candidates.

$\Omega_{HEN}^{1/2} = \sqrt{\pi}ASW90\%$ depends on the cut applied for the muon track reconstruction. In particular, it is a function of Λ and hence of N , the number of neutrino candidate. Ω_{GW} depends on the configuration of the GW detector network. We estimated that on average the sky map of a background event covers about 425 square degrees, which corresponds to a circular

5.5.6 Application of the joint optimization procedure

region of radius about 12 degrees.

We checked this approximation with a Monte-Carlo simulation using a set of GW background triggers obtained for the all-sky S6A/VSR2 analysis. We cross-correlated many times these triggers with a random set of neutrino candidates of variable size. The backgrounds we obtain with this simulation are in rough agreement with the prediction obtained by rescaling the original all-sky background. However an additional factor is necessary to get a good fit of the joint predicted background. This factor estimated heuristically is $\sim aN + b$ where $a \approx 10^{-4}$ and $b \approx 0.5$ and N is the number of neutrino candidates. The result of background distributions is shown in Figure 5.18.

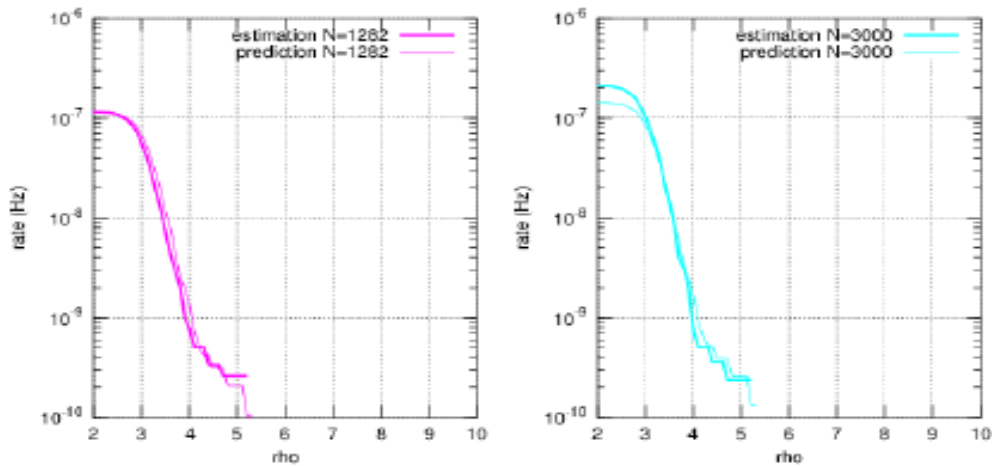


Figure 5.18 – Background distributions of the network correlated amplitude ρ for triggered search obtained by rescaling all-sky backgrounds

5.6.3 Results of the optimization

Study without cut on β

In this section, we summarize the results of the optimization procedure detailed in section 5.5.2. For simplicity, we restricted the optimization to periods with three operating GW detectors which is the most sensitive part of the data set. This corresponds to three separate runs labelled {“S6A/VSR2”, “S6B/VSR2”, “S6D/VSR3”}. This corresponds to the respective live-times $\tau_n = \{6.9 \text{ days}, 13.7 \text{ days}, 24.1 \text{ days}\}$ and livetime percentages $f_n = \{5.36 \%, 10.64 \%, 18.72\% \}$.

We use the approximation scheme described in the previous section 5.6.2 to compute the GW backgrounds for various N . The rescaling uses the neutrino angular window $\text{ASW}^{90\%}$ as a function of Λ parameter as shown in Figure 5.19. We deduce $\rho_{\text{threshold},n}$ and the figure-of-merit

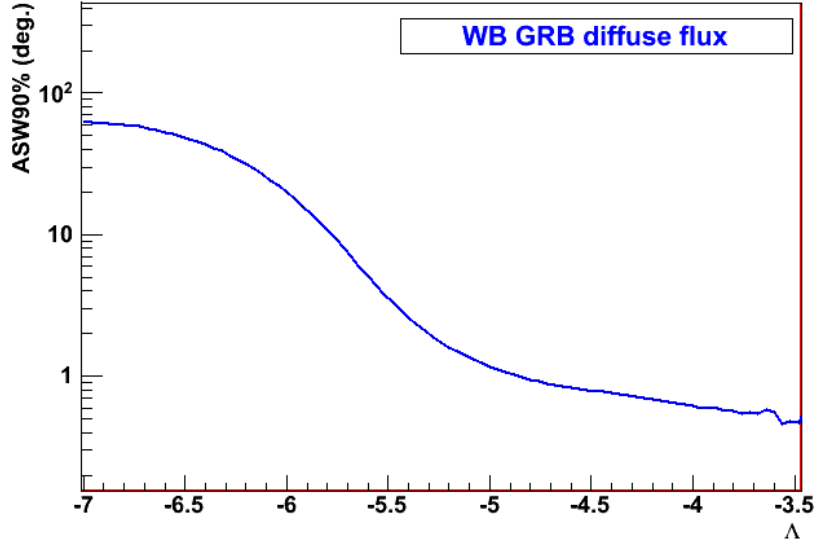


Figure 5.19 – The ASW90% used to estimate the GW background from the all-sky one. No cut on β is applied.

in Equation (5.17). Those quantities are shown as functions of the *total* number N of neutrino candidates (for the entire ANTARES livetime $T \approx 266$ days) in Figure 5.21. This number of neutrinos is taken from the data set and not from the MC sample. As such we are less dependent on the MC simulation and avoid problems of low statistics in the atmospheric muon MC sample. We see in Figure 5.20 that $\rho_{threshold,n}$ increases as a function of N as expected.

The number N of candidates (Λ) for the whole observation time τ that maximises the FOM is 3279 (-5.4). The angular search window is significantly better ASW90% = 2.6 degrees than the one used in 2007 joint search. In addition the efficiency ϵ_ν increases to about 62%.

Study against β parameter

The results presented in the previous section were obtained without any cut on the angular error estimate, β , of the reconstructed track. In this section we present an additional study by considering cuts on β . We choose the following cuts on $\beta < \{0.6^\circ, 1^\circ, 1.4^\circ\}$ (see Figures 5.22).

The table 5.1 shows the atmospheric muon contamination, FOM and total number of candidates corresponding to the optimal $\{\Lambda, \beta\}$ cuts. The best FOM and hence sensitivity is obtained with no cut on β . However increasing the number of candidates leads to serious difficulties. Above of the order of 2000 candidates the estimation of GW background gets at the same time computationally very heavy and more difficult to estimate. Indeed, with growing number of candidates, the GW data segments used to estimate the background ρ distributions will begin

5.5.6 Application of the joint optimization procedure

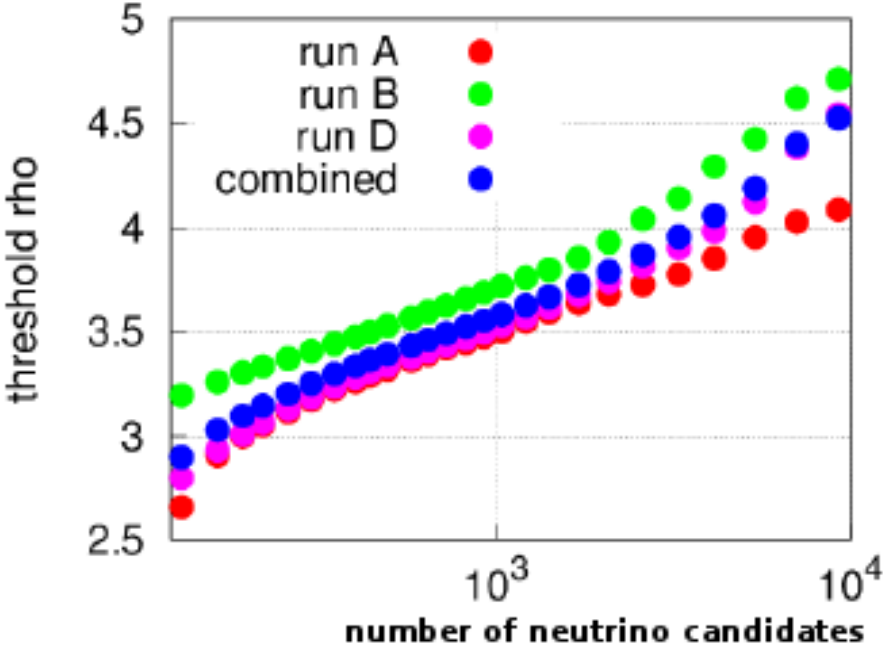


Figure 5.20 – Distributions of ρ as function of the number of neutrino candidates for the different GW data taking periods considered.

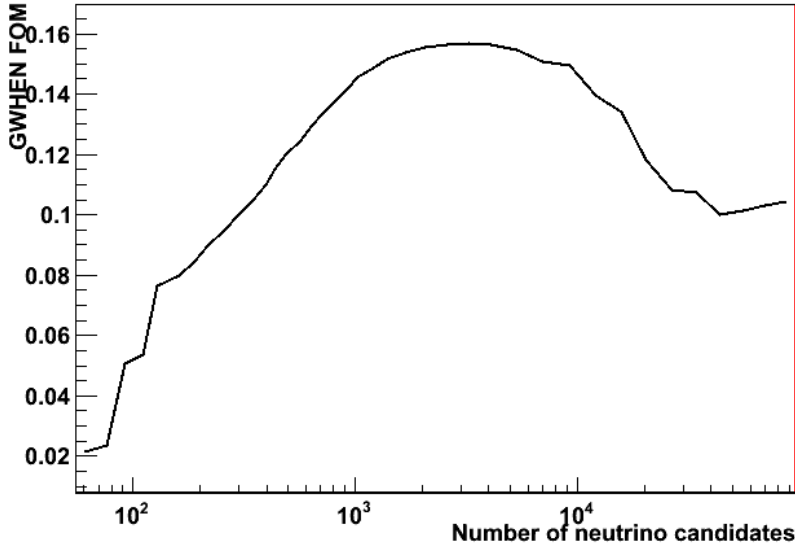


Figure 5.21 – FOM as a function of the number of neutrino candidates N without cut on β .

to overlap and correlation will appear. Given that with a β cut at 1 degree the loss in number of detectable sources (which is proportional to FOM) is just 2% with an affordable number of

candidates, we set the final cut values at $\Lambda > -5.44$ and $\beta < 1$. This can also be qualitatively justified by the fact that the contamination by atmospheric muons grows by 20% between $\beta < 1$ and no β cut. Since meanwhile the neutrino efficiency just marginally grows by 5%, most of the additional neutrino candidates brought by the reduction of the strength of the β cut will be mis-reconstructed atmospheric muons which will just make the GW background estimation more difficult.

| $\Lambda >$ | $\beta <$ | Contamination (%) | ϵ_ν (%) | FOM | ASW90% (deg.) | MC N_ν | Data N_ν |
|-------------|-----------|-------------------|--------------------|--------|---------------|------------|--------------|
| -5.60 | 0.6 | 40.36 | 50 | 0.1358 | 1.3 | 1645 | 1699 |
| -5.44 | 1.0 | 44.24 | 57 | 0.1525 | 1.7 | 1971 | 1986 |
| -5.44 | 1.4 | 57.12 | 60 | 0.1547 | 2.0 | 2717 | 2633 |
| -5.40 | No cut | 63.27 | 62 | 0.1564 | 2.6 | 3224 | 3279 |

Table 5.1 – Results of the joint optimization in term of FOM for each cut on Λ and β .

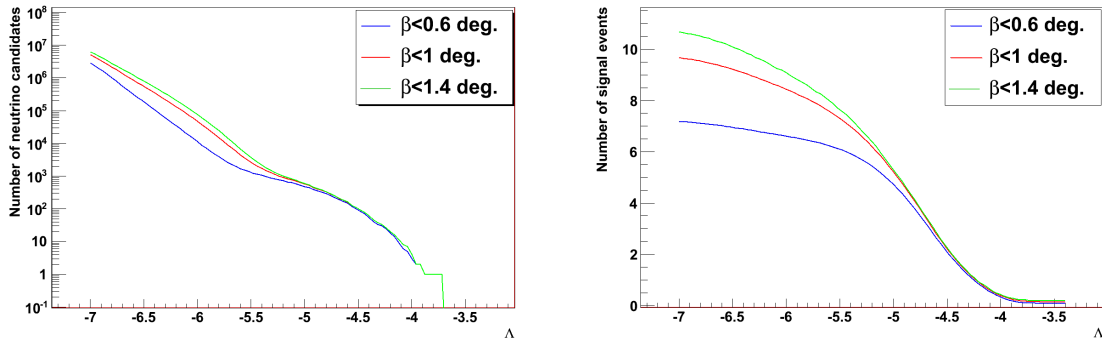


Figure 5.22 – Number of neutrino candidate events (Left) and signal WB GRB diffuse flux events (right) as function of Λ for different cuts on β

We compare Figure 5.25(left) the effective areas obtained with these different cuts and the one obtained with the cuts of the Point Source search ($\Lambda > -5.2$ and $\beta < 1^\circ$). Figure 5.25(right) shows for comparison the ratio between the effective areas obtained in this work to the one obtained with the cuts applied in the search for the point sources [17]. We can see that the final set of cuts of this work gives a gain in effective area between 50% at low energy and almost 20% at high energy.

5.7 List of neutrino candidates

We present in this section the result obtained after applying the optimized cuts described in the previous sections. The list obtained consists in $N = 1986$ neutrino candidates.

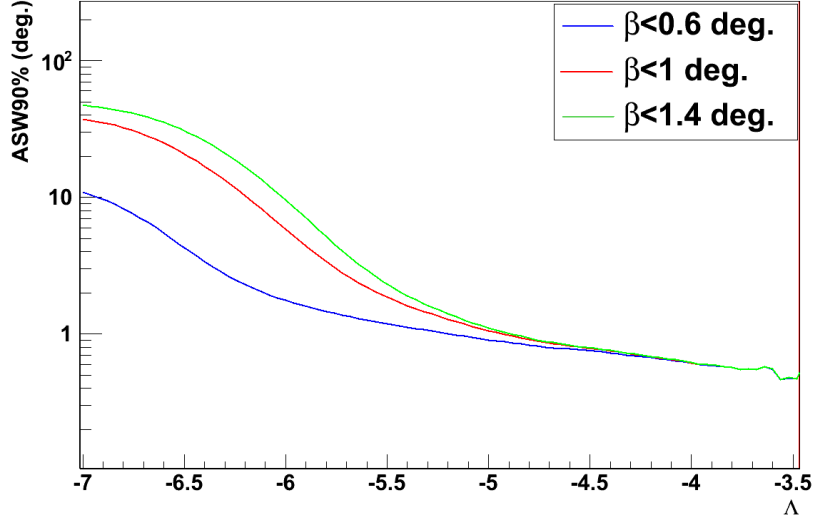


Figure 5.23 – Angular search window ($ASW_{90\%}$) as function of Λ for different cuts on β

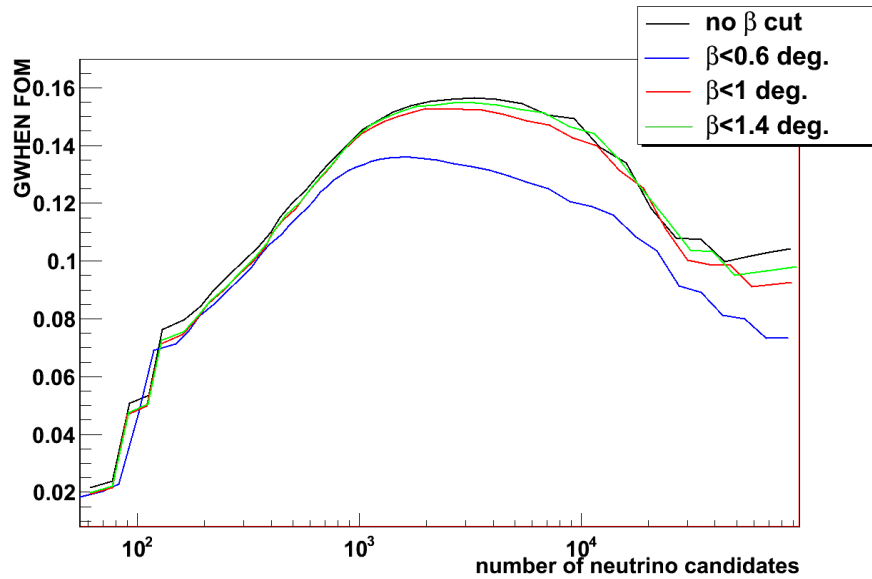


Figure 5.24 – Distribution of GWHEN FOM as a function of the number of neutrino candidates N , for different cuts on beta

The result consists in a list of neutrino candidates. Each of them is characterized by its arrival time, sky direction and associated error box. The following notations are adopted:

- Time t_i is given in Julian Day (or GPS)
- Reconstructed direction of the event $\vec{\mathbf{d}}_i = (\alpha_i, \delta_i)$ is given in equatorial coordinates, i.e. right ascension and declination. The skymap of the selected candidates is shown in Figure

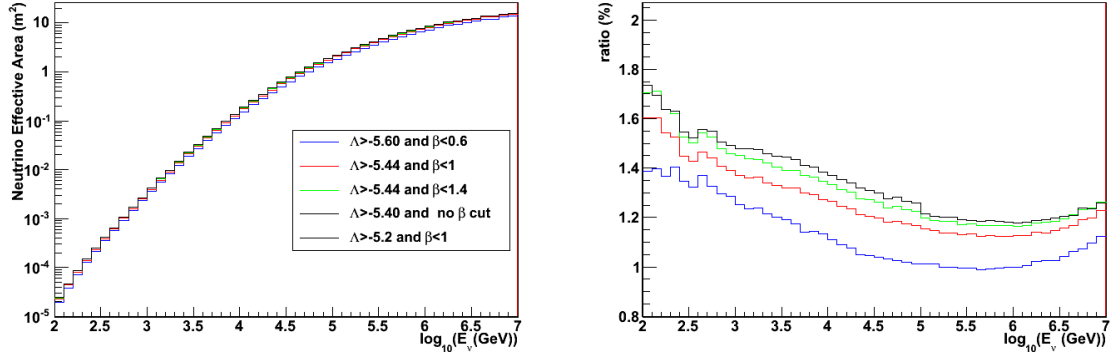


Figure 5.25 – Left: Neutrino effective areas as a function of neutrino energy. Right: ratio between GWHEN effective areas (corresponding to the different cuts in the text) and point-source one (after applying the corresponding cuts) as a function of neutrino energy.

5.26 in equatorial coordinates.

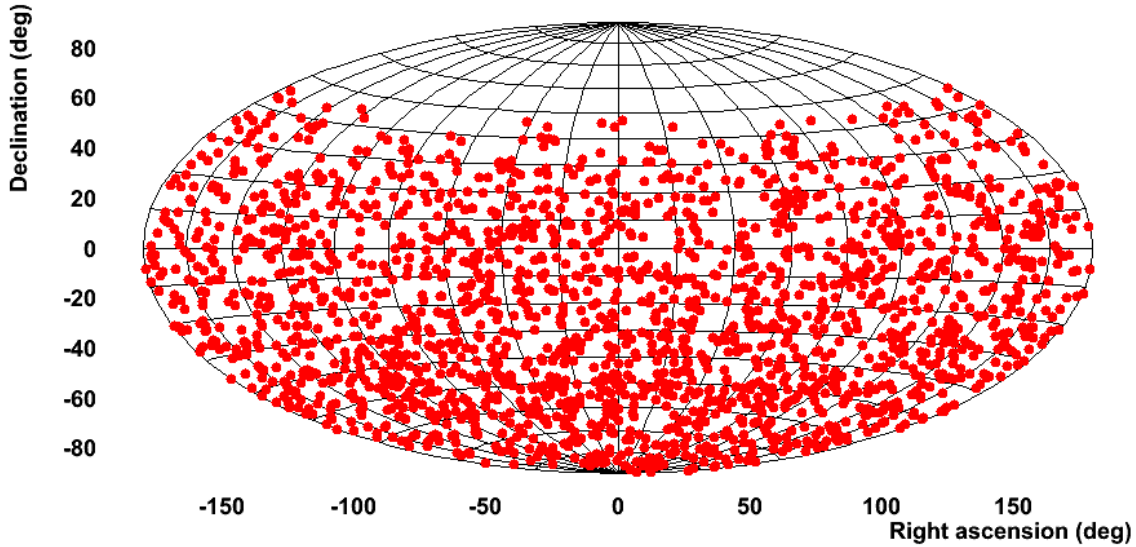


Figure 5.26 – Sky map of the final neutrino candidates selected for the analysis. The sky map is shown in equatorial coordinates.

- Energy estimator, given as the number of hits (or n^{hit}) used in the track fit. The distribution of the number of hits for data and MC is shown in Figure 5.27.
- ASW_{GWHEN}^{90} is a circle on the sky sphere with radius the 90% percentile of the distribution of space angles ψ between the reconstructed muon and the MC neutrino direction. It is computed from MC neutrino ANTARES simulation with the same selection cuts applied

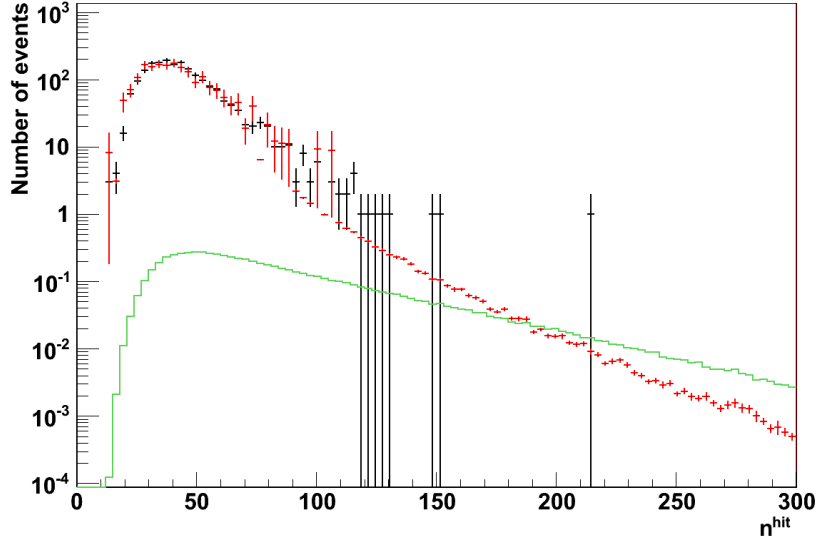


Figure 5.27 – Distribution of the number of hits used as proxy energy in this search. The black curve is the data, the red is the MC atmospheric background and the green is the MC distribution obtained for the WB GRB diffuse flux.

as that for the joint optimization and with an event weighting following the Waxman Bahcall GRB diffuse flux. This distribution is fitted with a log-normal function as defined hereafter:

$$P(\psi) = \frac{1}{\sqrt{2\pi}} \frac{\exp[-\ln(\psi/m)^2/2\sigma^2]}{\sigma\psi} \quad (5.19)$$

where m and σ are respectively the so called scale and shape parameters. It can be linked to the neutrino bi-dimensional point spread function (PSF),

$$\mathcal{F}_i^{\text{HEN}}(\vec{\mathbf{d}}) \equiv P(\vec{\mathbf{d}}|\vec{\mathbf{d}}_i) \propto \frac{1}{\sin(\psi_i(\vec{\mathbf{d}}))} \frac{\exp[-\ln(\psi_i(\vec{\mathbf{d}})/m)^2/2\sigma^2]}{\sigma\psi_i(\vec{\mathbf{d}})} \quad (5.20)$$

where $\psi_i(\vec{\mathbf{d}})$ is the space angle between the directions $\vec{\mathbf{d}}$ and $\vec{\mathbf{d}}_i$. An example of this point spread function can be seen on Figure 5.28.

In practice ASW_{GWHEN}^{90} (or equivalently $\mathcal{F}_i^{\text{HEN}}$), m and σ can depend on several parameters like Λ (see Figure 5.19), the arrival direction of the neutrino, the number of hits, or the angular reconstruction error parameter β . Figure 5.29 shows the median of the space angle distribution as a function of declination. This quantity is to a good approximation independent of the declination and hence its variation with declination will not be used further to characterize events.

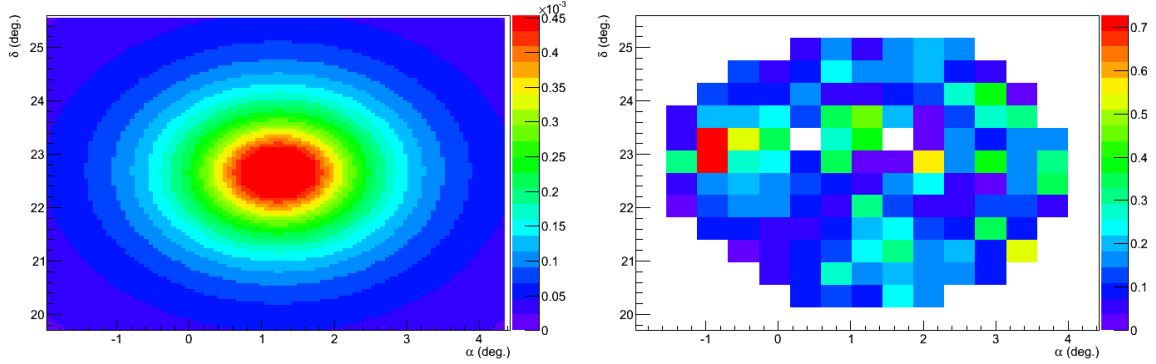


Figure 5.28 – Example of the neutrino PSF (left) and the corresponding GW skymap (right).

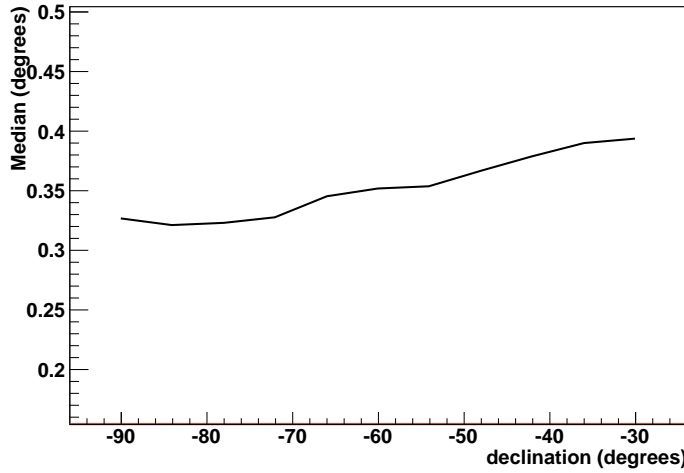


Figure 5.29 – The angular search window for 50% percentile as function of declination.

5.8 Procedure for the event post-processing and joint statistical treatment

The statistical analysis of the outcome of the joint search is based on the original proposal from [18], but different aspects are adapted to cope with the specificities of our study, in particular the use of sky masks (with typical size of a few squared degrees) in s-cWB.

Below we describe the different steps and define the relevant quantities that will be used in the final statistical treatment as well as in the estimation of the sensitivity and discovery power of the search.

The goal is to construct a test statistics based on the characteristics of each neutrino event

5.5.8 Procedure for the event post-processing and joint statistical treatment

and its associated GW trigger and to compute their joint p-value (or equivalently their excess significance) relying on pseudo-experiment realizations of the search with no signal injected. The discovery potential will then be estimated with the same method but using pseudo experiments containing neutrinos following a WB energy spectrum and associated to GW signal injections. The pseudo experiments will be based on the neutrino characteristics and the combined test statistic described in sections 5.8.1 and 5.8.4.

5.8.1 Statistical characterisation of the neutrino candidates

In addition to the neutrino characteristics described above we compute the p-value of the neutrino event, denoted p_i^{HEN} . Since these will be considered independently, atmospheric and potential cosmic neutrinos differ only by their energy spectrum. As shown in Figure 5.30, we will use the simple energy estimator given by the number of hits n^{hit} of the reconstructed track. The p-value, i.e. the probability that the atmospheric background would produce an event with at least the number of hits of the considered event, is defined as:

$$p_i^{\text{HEN}} = \frac{\int_{n_i^{\text{hit}}}^{\infty} P(n^{\text{hit}}) dn^{\text{hit}}}{\int_0^{\infty} P(n^{\text{hit}}) dn^{\text{hit}}} \quad (5.21)$$

where n_i^{hit} is the value corresponding to the event i and P the corresponding probability density function (or equivalently the not normalized distribution).

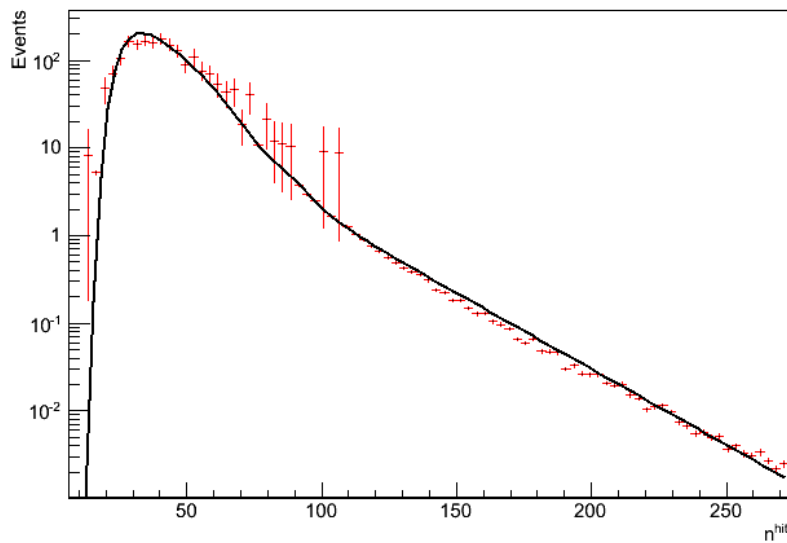


Figure 5.30 – Distribution (modified as described in the text) of n^{hit} together with the function used to fit it and evaluate the corresponding p-values.

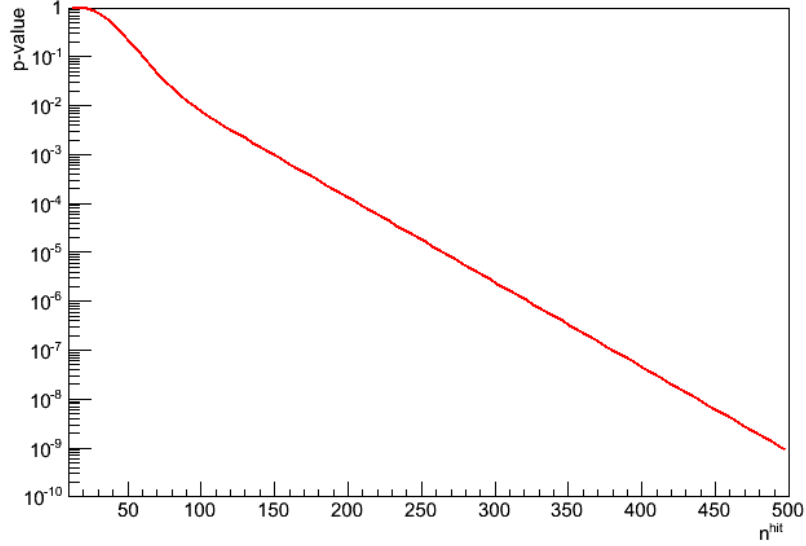


Figure 5.31 – Distribution of the HEN p-value as a function of n^{hit} estimated from MC simulation as defined in equation 5.21.

In practice the computation can be made with Monte Carlo simulations extrapolated to high values of n^{hit} if needed. Considering the overall contamination of atmospheric muons in the final sample (44%) and in order to compensate for the lack of statistics in the atmospheric muon simulation in the $n^{hit} > 100$ region we conservatively choose to apply a penalty factor for the p-values obtained in the $n^{hit} > 100$ region. This is achieved by multiplying the atmospheric neutrino distribution by 1.7 in the considered $n^{hit} > 100$ region. The validity of this approach has been checked by relaxing the cuts and verifying the shape consistency of the muon and neutrino samples. The modified simulated n^{hit} distribution has been fitted with the following function:

$$P_{n^{hit}}(x) = \exp\left(\sum_{n=0}^4 p_n x^n\right) / (1 + \exp(-p_5(x - p_6))) p_7 \exp(p_8 x) \quad (5.22)$$

where p_n , $n \in [0, 8]$ are the fit parameters. The result is presented in Figure 5.30. The p-value as a function of n^{hit} can then be computed by numerical integration and is displayed in Figure 5.31.

Figures 5.32 and 5.33 show the local coordinates of the neutrino triggers together with the fitted functions which will be used to generate the pseudo experiments. The latter also allow us to draw the analysis exposure map, which is presented in Figure 5.34 in galactic coordinates.

5.5.8 Procedure for the event post-processing and joint statistical treatment

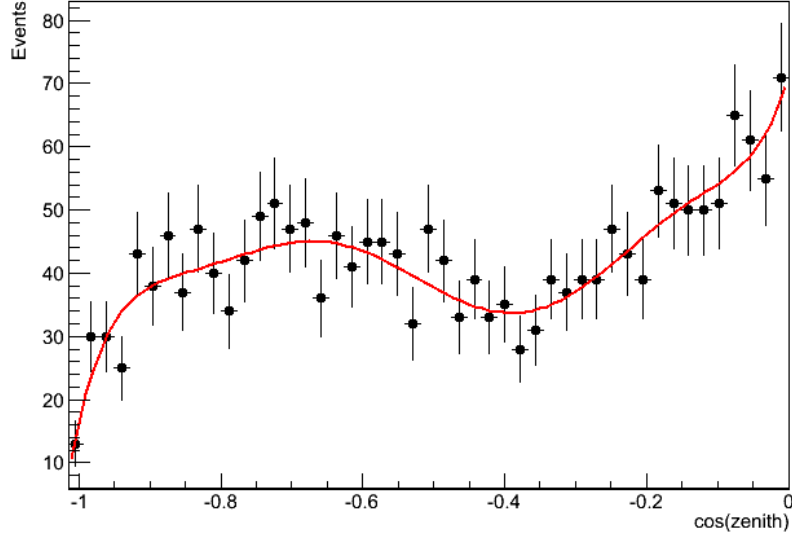


Figure 5.32 – Normalized distribution of the zenith angle for data together with the 7 degree polynomial used to fit it.

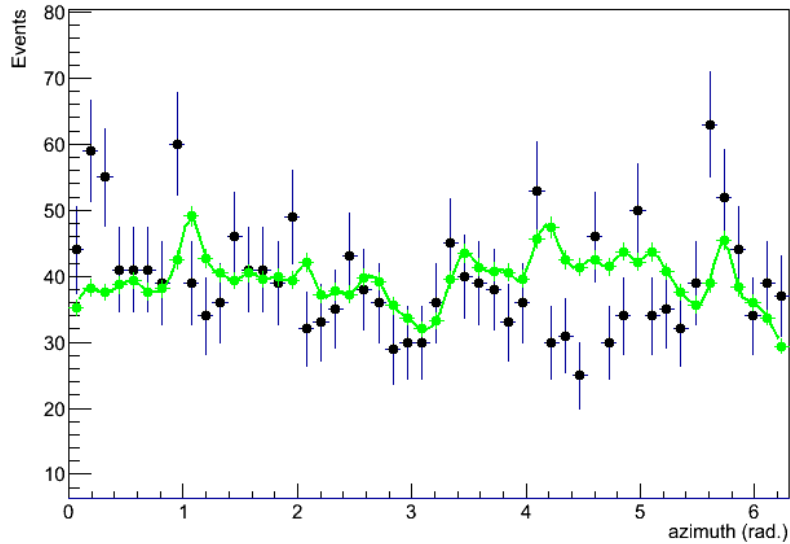


Figure 5.33 – Distribution of the azimuth for data together with the spline function used to parametrize it. This spline has been fitted on the neutrino Monte Carlo simulation (green points).

5.8.2 Statistical characterisation of the GW reconstructed events

For each of the selected neutrino events, s-cWB performs a search for GW around the neutrino time. The whole sky is not scanned but only the region corresponding to ASW90% centered on

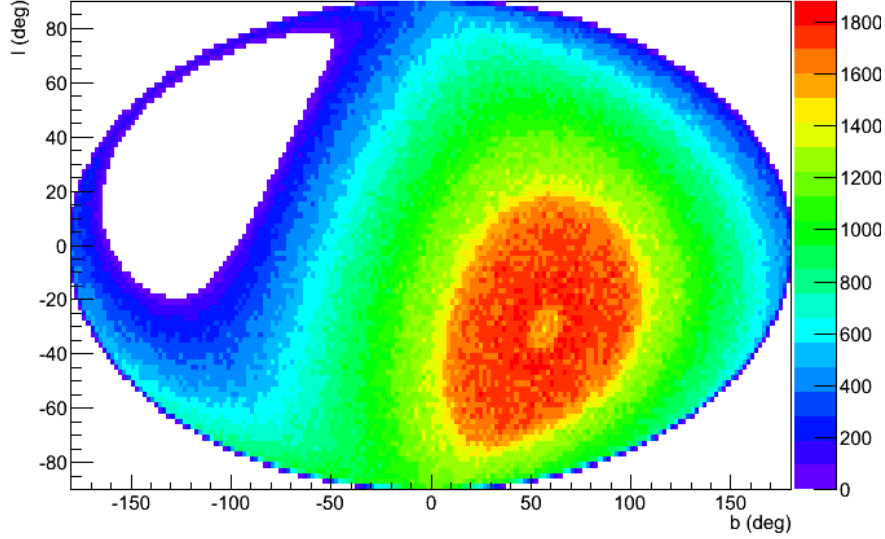


Figure 5.34 – Relative sky exposure map (arbitrary units) of ANTARES corresponding to the selected neutrino sample in Galactic coordinates.

the reconstructed arrival direction of the neutrino $\vec{\mathbf{d}}_0$. For each candidate, s-cWB will provide the GW skymap (SP) labeled hereafter $\mathcal{F}_i^{\text{GW}}(\vec{\mathbf{d}})$ within ASW90% (see Figure 5.28 right for an example). These "sky-maps" will be made of pixels of $0.4^\circ \times 0.4^\circ$ each associated with the probability that a GW is coming from it. The following parameters, of each GW candidate, are provided by the s-cWB. The arrival time, the reconstructed sky location (θ, ϕ) in the Earth fixed frame with $\phi = 0^\circ$ corresponding to the Greenwich Meridian, $\theta = 90^\circ$ corresponding to the equator. Also it provides the value of ρ for each GW candidates. This latter will correspond to a false alarm rate $\text{FAR}_i(\rho_i)$ as defined in sections 5.5.2 and 5.5.3. This will lead to a GW p-value indicating what is the probability that coherently combined GW interferometers background produces an event with at least this value of ρ_i , defined as:

$$p_i^{\text{GW}} = 1 - P(0|\tau_i \times \text{FAR}_i(\rho_i)) \quad (5.23)$$

where τ_i is the duration of the GW interferometers run corresponding to event i (see sections 5.5.2 and 5.5.3). The distributions are computed using $O(10^3)$ background realisations obtained with time shifts. The background distributions ρ of all detector configurations and run periods are presented in Figures 5.35 and 5.36. The corresponding p-value evolution for S6A run is shown in Figure 5.37.

5.5.8 Procedure for the event post-processing and joint statistical treatment

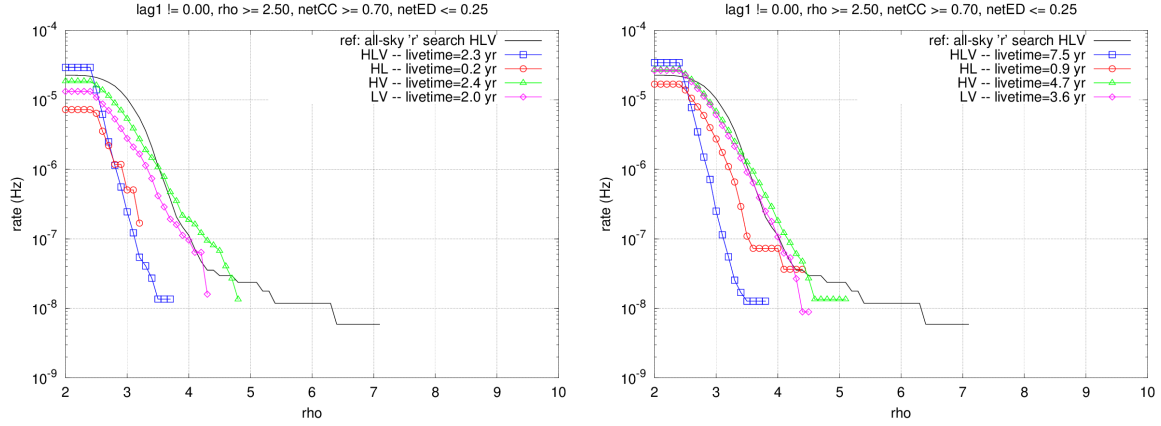


Figure 5.35 – Background estimate of the network correlated amplitude ρ for triggered search. Left: for the S6AVSR2-3 segments. Right: for the S6B segments

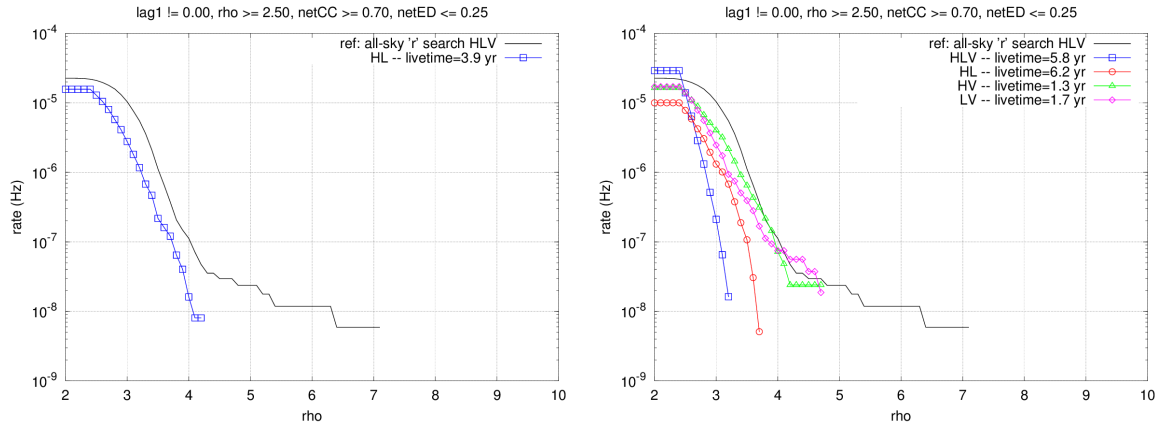


Figure 5.36 – Background estimate of the network correlated amplitude ρ for triggered search. Left: for the S6C segments. Right: for the S6D segments

5.8.3 Statistical characterisation of the joint candidates

The direction of the joint candidate event can be defined as the one maximizing the product of the HEN PSF and the GW SP: $\mathcal{F}_i^{\text{GW}} \times \mathcal{F}_i^{\text{HEN}}$.

The joint directional test statistic will rely on the marginalized likelihood of the joint event which is defined as:

$$\ln(\mathcal{L}_i) = \int \mathcal{F}_i^{\text{GW}}(\vec{x}) \times \mathcal{F}_i^{\text{HEN}}(\vec{x}) d\vec{x} \quad (5.24)$$

Figure 5.38 shows an example of the joint likelihood. Figure 5.39 shows the distribution of P_{bg} of $\ln(\mathcal{L})$ for background estimated with the S6A data for three interferometers together with a Gaussian fit.

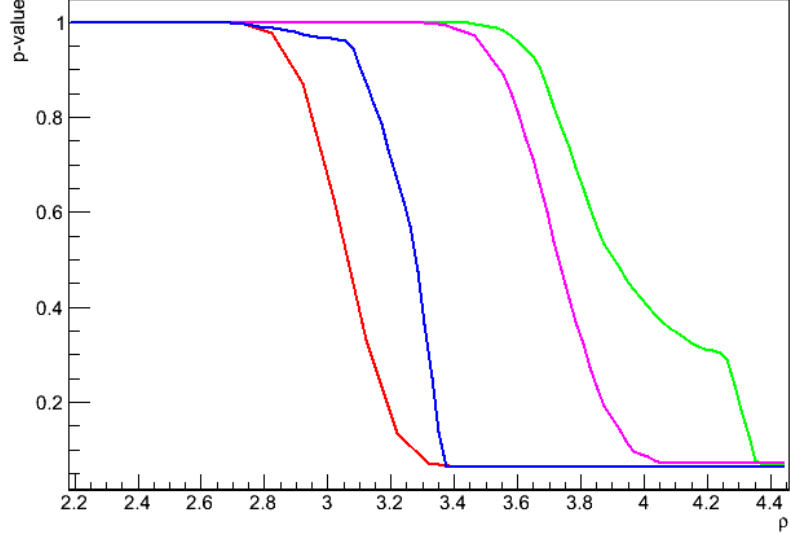


Figure 5.37 – The p-value as a function of ρ corresponding to S6A data and different detector configurations HLV (blue), HL (red), HV (green) and LV (magenta)

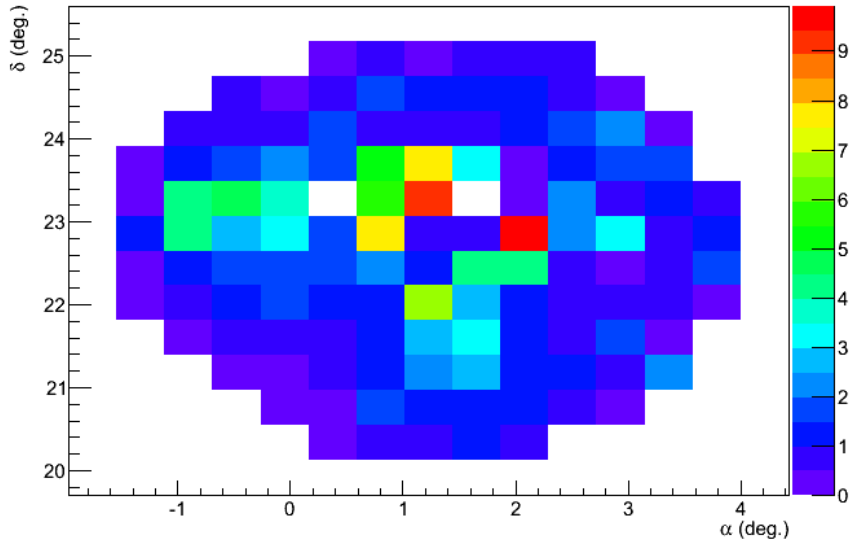


Figure 5.38 – Example of the joint likelihood obtained with the product of GW SP and HEN PSF

The p-value corresponding to the combined PSF-likelihood will be defined as:

$$p_i^{sky} = \int_{\mathcal{L}_i}^{\infty} P_{bg}(\ln(\mathcal{L})) d\mathcal{L} \quad (5.25)$$

5.5.8 Procedure for the event post-processing and joint statistical treatment

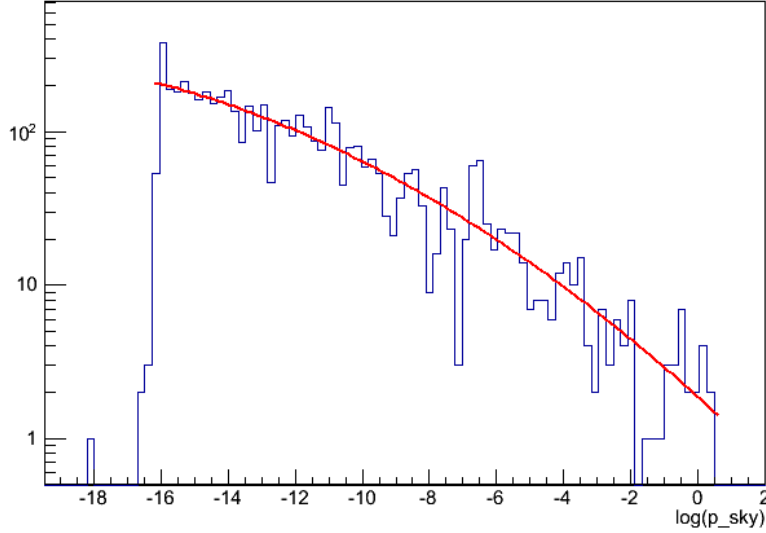


Figure 5.39 – Distribution of $\ln(\mathcal{L})$ for background estimated with the S6A data for the detector network. The red curve corresponds to a Gaussian fit

and is determined by numerical integration of the fitting function. A dedicated fit will be performed for each S6 period and each interferometer configuration independently.

5.8.4 Final test statistic

All these p-values can be combined using Fisher's method [19] to construct a test statistic for each event i :

$$X_i^2 = -2 \ln(p_i^{sky} \times p_i^{GW} \times p_i^{HEN}) \quad (5.26)$$

This variable behaves like a χ^2 with 6 degrees of freedom in case variables are independent. But since this is not guaranteed here and since p^{GW} , p^{HEN} and p^{sky} may not behave as proper p-values (i.e. be independently uniformly distributed in $[0;1]$), the significance of the final outcome of the search will be computed thanks to pseudo-experiment Monte Carlo realisations. In order to do so, the background probability density function of X^2 will be fitted for each S6 period and interferometer configuration. Figure 5.40 shows, for the particular case of S6A run and 3 interferometers configuration, the background distribution of the X^2 variable. It has been fitted with a "scaled χ^2 " with 6 degrees of freedom and a general Γ distribution. The two functions obey to the following formula:

$$f(x; k; \theta) = \frac{1}{\theta^k} \frac{1}{\Gamma(k)} x^{k-1} e^{-x/\theta} \quad (5.27)$$

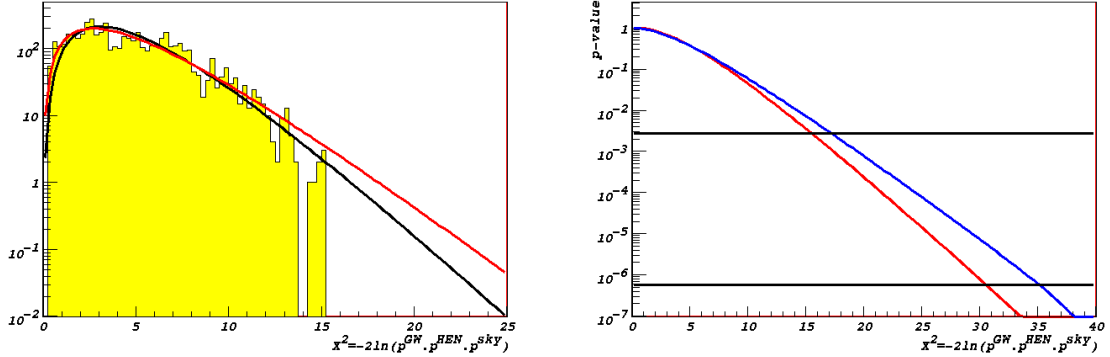


Figure 5.40 – Left: Background distribution of the X^2 for S6A with three interferometers. The black line is the scaled χ^2 and the red one the Γ distribution (see text). Right: corresponding p-value evolution of the Γ distribution (red) and scaled χ^2 (blue) together with lines corresponding to 3 (upper) and 5 (lower) sigma confidence levels.

The scaled χ^2 distribution has $k=3$ (from the 6 degrees of freedom), free θ (the scale parameter) and the fit gives a χ^2 per degree of freedom of 8.2. The general Γ distribution has both parameters free and the fit gives a slightly worse χ^2 per degree of freedom of 8.5. However, given the corresponding p-values evolution, displayed on the right panel of Figure 5.40, the most conservative choice for the pseudo experiments generation is the Γ distribution. The final result of the search will be the p-value of its most significant event i and is defined as:

$$p^{\text{GWHEN}} = \int_{\text{Max}(X_i^2)}^{\infty} P_{bg}(\text{max}(X^2)) dX^2 \quad (5.28)$$

where the probability density function $P_{bg}(\text{max}(X^2))$ is the result of Monte Carlo simulation of pseudo experiments of 1986 joint triggers.

5.8.5 Estimation of the horizon of detection

The detection horizon $D_{50\%}^{\text{HEN}}$ and $D_{50\%}^{\text{GW}}$ of each detector for a given model can be defined as the maximum distance for which there is at least a 50% chance probability that the signal would be detected. The common GW+HEN horizon will thus be:

$$D^{\text{GWHEN}} = \text{Min}(D_{50\%}^{\text{HEN}}, D_{50\%}^{\text{GW}})$$

On the HEN side the horizon corresponds to the maximum distance at which there is a 50% chance probability to have at least one neutrino detected in ANTARES. On the GW side, the procedure is to generate a list of neutrinos with only one having the characteristics of a signal (i.e. with a WB n^{hit} distribution as shown by the green curve in Figure 5.27). This neutrino

has to be associated with a p_i^{GW} corresponding to an injected signal. This is repeated many times and the probability of detection will be the ratio of the number of realisations where $\max(X_i^2)$ has a p-value lower than the threshold fixed at the end of last section. This detection power will correspond to the intensity of the GW injected in the data. An other interesting quantity would be to inject more and more signal neutrinos at a fixed GW signal intensity and see when the probability is above 50 percent. Once the GWHEN horizon is determined source population limit estimates will be set following the reasoning of section 4.7.

5.9 Conclusion

In this chapter we have described the second GW+HEN joint analysis using coincident data taken in 2009-2010 from the ANTARES neutrino telescope and the Virgo/LIGO GW interferometers. In particular we have detailed the methods specifically developed for this search. The joint optimisation procedure on GW and HEN data has led to a list of 1986 neutrino candidates maximizing the number of detectable joint sources. These neutrino events have been completely characterized with the main parameters needed for the coincidence search with GW (see section 5.7). Of these neutrino events, 775 candidates are associated with 2 or 3 interferometer configuration (i.e., HLV: 303, HV: 147, LV: 135 and HL: 190 neutrino candidates).

At the time of submission of this document, the analysis was not completed, some GW data processing being still necessary before launching the pseudo-experiment Monte Carlo simulations needed to set the final joint results. However, all technical steps and ingredients were well defined and presented in this chapter. The final results will be presented in a dedicated paper.

The analysis presented in this chapter has been obtained with improved algorithms and detectors with respect to the analysis of the 2007 data. The global improvement gain expected on the upper limit of population density of common HEN and GW emitters is estimated as follows:

- A gain of a factor 1.4 arises from the observation time (91.36 days and 128.7 days for 2007 and 2009-2010 data respectively).
- A gain of a factor ~ 5 comes from the improvement of the neutrino effective area with respect to 2007 analysis. Indeed, the horizon is imposed by ANTARES and the effective area of the detector has been multiplied by 3 leading to a gain of factor $\sqrt{3}$ on the distance and hence $\sqrt{3^3} \sim 5$ on the volume.

This implies a net improvement by a factor ~ 7 with respect to what is presented in section [4.7.1](#).

REFERENCES

- [1] C. RIVIÈRE, ANTARES internal note, ANTARES-PHYS-2012-001 (2012).
- [2] V. AGRAWAL ET AL, Phys. Rev. D, 53, 13141323 (1996). 136
- [3] J. N. BAHCALL AND E. WAXMAN, Phys. Rev. D64, 023002 (2001). 136
- [4] D. GUETTA ET AL, Astropart. Phys. 20: 429-455 (2004). 136
- [5] https://www.lsc-group.phys.uwm.edu/bursts/public/runs/s6/dqv/category_definer/H1L1V1-S6A_BURST_ALLSKY_OFFLINE-930960015-5011200.xml. 137
- [6] S. ADRIAN-MARTINEZ ET AL, arXiv: <http://arxiv.org/abs/1205.3018>, (2012). 138
- [7] B. BOUHOU ET AL, Poster at the Gravitational Wave Physics and Astronomy Workshop, Hanover (2012). 138
- [8] J. ABADIE ET AL, Phys. Rev., D81, 102001 (2010). 139
- [9] M. DRAGO, PhD thesis, Università degli Studi di Padova. 139
- [10] <http://www.gravity.phys.uwm.edu/cgi-bin/cvs/viewcvs.cgi/matapps/src/simulation/BurstMDC/documentation/?cvsroot=lscsoft>. 141
- [11] G. C. HILL AND K. RAWLINS, Astropart. Phys., 19, 393-402 (2003). 143
- [12] G. J. FELDMAN AND R. D. COUSINS, Phys. Rev. D57, 3873-3889 (1998). 143
- [13] G. C. HILL ET AL, Oxford Physics, PHYSTAT2005 Proceedings (2006). 145
- [14] G. PUNZI, SLAC, PHYSTAT2003 Proceedings (2003). 145, 146
- [15] J. ABADIE ET AL., Phys. Rev. D 85 122007, (2012). 150
- [16] G. D. BARRET AL, Phys. Rev. D74, 094009 (2006). 153

REFERENCES

- [17] S. ADRIÁN-MARTÍNEZ ET AL, *Astropart. J.* 743: L14, (2012). [158](#)
- [18] B. BARET ET AL, *Phys. Rev. D*85, 103004 (2012). [162](#)
- [19] R. A. FISHER, Statistical Methods for Research Workers, Oliver and Boyd (Edinburgh), (1925). [169](#)

CONCLUSIONS

By pioneering with the combination of two non-photonic observations, gravitational waves and high-energy neutrinos, this thesis work initiated a new domain in multimessenger astronomy. We designed and assembled a complete pipeline allowing for the combined analysis of ANTARES and LIGO/Virgo data.

We did this in two steps. A first search was conducted on concomitant data taken during 2007. No significant coincident event was detected. This resulted in upper limits on the source population (including potential photon-dark or obscured sources only accessible through GW and HEN observations). To allow rapid progresses, we essentially relied on pre-existing analysis tools. Once the search completed, we identified the limitations and issues of those tools. This has led us to develop new and more sensitive analysis tools that are better suited to the observations at hand. These tools are now integrated in a new pipeline which we applied in the context of a second search using 2009-2010 data currently in progress. The improvements brought to this second search includes a new neutrino selection strategy relying on a combined figure of merit, which maximizes the number of common observable sources.

Some of the methodologies proposed here could be developed in other contexts, and even beyond the GW and HEN context. For instance, the pipeline skymask coherent WaveBurst could serve as a basis to other types of “triggered” GW follow-up burst searches (e.g., in coincidence with gamma-ray bursts). Another example is the optimization scheme which is fairly generic and may be used to optimize the other types of joint searches combining GW or HEN with other cosmic messengers (gamma-rays for instance).

The pathfinder developments done in this thesis pave the way for future collaborations involving the next generation of detectors. These projects include KM3NeT, the future km^3 neutrino telescope in the Mediterranean sea and the second generation of interferometric GW

Conclusions

detectors (advanced LIGO and advanced Virgo). The sensitivity of those instruments will be significantly improved with respect to their predecessors. There are reasonable chances that they will lead to actual observation in their respective channel.

APPENDIX A

DEMONSTRATION OF THE MRF APPROXIMATION

We follow Neymann's construction of confidence interval to have an estimation of the upper limit in case the computing time of Feldman Cousin limit is prohibitive. For a normal distribution, the probability that a measurement n_{obs} falls within the interval $[\mu + c, \mu + d]$, where μ is the mean and $c < 0$, is equivalent to the probability that a measurement μ falls within the interval $[n_{obs} - d, n_{obs} - c]$. Thus we write:

$$\begin{aligned} P(\mu + c_Q \leq n_{obs} \leq \mu + d) &= P(n_{obs} - d \leq \mu \leq n_{obs} - c_Q) \\ &= Q \\ &= erf(d) - erf(c_Q) \end{aligned} \tag{A.1}$$

where erf is the error function and Q is the significance level.

$$erf(x) \equiv \frac{1}{\sqrt{2\pi}} \int_{-\infty}^x e^{-t^2/2} dt \tag{A.2}$$

If $d \equiv \infty$

$$\begin{aligned} Q &= erf(\infty) - erf(c_Q) \\ &= 1 - erf(c_Q) \\ \Rightarrow c_Q &= erf^{-1}(1 - Q) \end{aligned} \tag{A.3}$$

DEMONSTRATION OF THE MRF APPROXIMATION

From Eqs. A.1 and A.3 we write:

$$\mu \leq n_{obs} - erf^{-1}(1 - Q) \quad (\text{A.4})$$

Thus,

$$\mu_{max} = n_{obs} - erf^{-1}(1 - Q) \quad (\text{A.5})$$

Using the following relation [1]:

$$erf\left(\frac{x}{\sigma}\right) = \frac{1}{2} + \frac{1}{2}Erf\left(\frac{x}{\sqrt{2}\sigma}\right) \quad (\text{A.6})$$

where σ is the standard deviations and Erf is given by:

$$Erf(x) = \frac{2}{\sqrt{\pi}} \int_0^x e^{-t^2} dt \quad (\text{A.7})$$

we find that:

$$\mu_{max} = n_{obs} - \sqrt{2\mu}Erf^{-1}(1 - 2Q) \quad (\text{A.8})$$

we can also write $\mu_{max} = n_s + n_b$ where n_s and n_b are the number of signal and background events respectively. We put $x = \sqrt{\mu_{max}} > 0$, thus

$$x^2 + \sqrt{2}Erf^{-1}(2Q - 1)x - n_{obs} = 0 \quad (\text{A.9})$$

resolving this equation we find:

$$\begin{aligned} x &= \frac{-\sqrt{2}Erf^{-1}(1 - 2Q) + \sqrt{2(Erf^{-1}(1 - 2Q))^2 + 4n_{obs}}}{2} \\ &= \sqrt{n_s + n_b} \end{aligned} \quad (\text{A.10})$$

Finally:

$$n_s \equiv \tilde{\mu}_Q(n_{obs}, n_b) = \left[\frac{-\sqrt{2}Erf^{-1}(2Q - 1) + \sqrt{2(Erf^{-1}(2Q - 1))^2 + 4n_{obs}}}{2} \right]^2 - n_b \quad (\text{A.11})$$

This approximation should be weighted with the Poisson probability of its occurrence to get the new parametrization of *the average upper limit*:

$$\bar{\mu}_Q(n_b) = \sum_{n_{obs}}^{\infty} \tilde{\mu}_Q(n_{obs}, n_b) \frac{(n_b)^{n_{obs}}}{(n_{obs})!} exp(-n_b) \quad (\text{A.12})$$

note that this approximation is applied for large values of $n_{obs} > n_{obs}^{crit}$ such that $|FC_{ul} - n_s|/FC_{ul} \leq 10\%$, where FC_{ul} is FC upper limit. Thus for $n_{obs} > n_{crit}$ we redefine the ratio to be minimized, in section 5.4.1 as follow:

$$M\tilde{R}F(\text{cuts}) = \frac{\bar{\mu}_Q(n_b(\text{cuts}))}{n_s(\text{cuts})} \quad (\text{A.13})$$

DEMONSTRATION OF THE MRF APPROXIMATION

REFERENCES

- [1] W. J. METZGER, Statistical Methods in Data Analysis, HEN-343 (2002). [178](#)

REFERENCES

APPENDIX B

COHERENT WAVEBURST STATISTICS

We have discussed the coherent WaveBurst and the skymask-coherent WaveBurst pipelines in chapters 3 and 5 respectively. In this appendix we define the coherent statistics used in the identification of the GW triggers, i.e net_{cc} , net_{ED} and ρ .

We consider that we project the time-aligned data onto a complete wavelet basis. Let us denote $w[i, j]$ is the corresponding wavelet coefficients where i, j are the time-frequency indices. We do the same for the detector response $\xi[i, j] = F_+(\theta, \phi)w_+[i, j] + F_\times(\theta, \phi)w_\times[i, j]$ where $w_{+(\times)}[i, j]$ denotes the wavelet coefficients of the GW polarizations $h_{+(\times)}$. The antenna patterns $F_{+(\times)}$ are defined in Sec. 3.4. Let $\sigma[i, j]$ be the RMS noise in the time-frequency bin (i, j) .

The log-likelihood functional is obtained assuming a Gaussian quasi-stationary noise and can be expressed in the wavelet domain as

$$L_{noise} = \sum_{i,j \in \Omega_{TF}} \left[\frac{w^2[i, j]}{\sigma^2[i, j]} - \frac{(w[i, j] - \xi[i, j])^2}{\sigma^2[i, j]} \right] \quad (\text{B.1})$$

where Ω_{TF} is the time-frequency area selected for the analysis.

This expression in the case of a one-detector analysis. Eq. (B.1) can be generalized to K detectors

$$L_{noise} = \sum_{k=1}^K \sum_{i,j \in \Omega_{TF}} \left[\frac{w_k^2[i, j]}{\sigma_k^2[i, j]} - \frac{(w_k[i, j] - \xi_k[i, j])^2}{\sigma_k^2[i, j]} \right]. \quad (\text{B.2})$$

Coherent WaveBurst relies on the maximum likelihood ratio statistic i.e., maximizing Eq. (B.2) over all sky locations (θ, ϕ) . This quantity is a quadratic form of w , thus it can be expressed in a matrix form as follows

$$L_{noise}^{max}(\theta, \phi) = \sum_{n,m} L_{nm}, \quad (\text{B.3})$$

where $L_{nm} = \sum_{i,j \in \Omega_{TF}} w_n[i, j]w_m[i, j]P_{nm}[i, j]$ and P is the orthogonal projector onto the GW

COHERENT WAVEBURST STATISTICS

plane spanned by normalized antenna pattern vectors f_+ and f_\times defined as follows

$$f_{+(\times)} = \left\{ \frac{F_{1+(\times)}(\theta, \phi)}{\sigma_1[i, j]}, \dots, \frac{F_{K+(\times)}(\theta, \phi)}{\sigma_K[i, j]} \right\}. \quad (\text{B.4})$$

We refer to *coherent energy*

$$E_c = \sum_{m \neq n} L_{mn} \quad (\text{B.5})$$

as the sum of the off-diagonal terms of the log-likelihood matrix. E_c measures the correlation between the detector responses to a common GW signal. We also defined the *reduced coherent energy* $e_c = \sum_{n \neq m} L_{nm} |r_{nm}|$ where the terms are weighted by the Pearson's coefficients

$$r_{nm} = \frac{L_{nm}}{\sqrt{L_{nn}L_{mm}}}. \quad (\text{B.6})$$

By projecting the data onto the *null space* complementary to the GW plane, we define the null matrix $N_{nm} = E_{nm} - L_{nm}$ with $E_{nm} = w_n^2$ and the associated null energy

$$N_{null} = \sum_{n,m} N_{nm}. \quad (\text{B.7})$$

Instrumental glitches have a small E_c and large N_{null} .

Finally, given these ingredients we can define the *network correlation coefficient*

$$net_{cc} = \frac{E_c}{N_{null} + |E_c|}, \quad (\text{B.8})$$

the *coherent network amplitude*

$$\rho = \sqrt{\frac{e_c}{K} net_{cc}}, \quad (\text{B.9})$$

and the *network energy disbalance*

$$net_{ED} = \sum_k \frac{|\Delta_k|}{E_c}, \quad (\text{B.10})$$

where Δ_k is the energy disbalance for detector k .

While cuts on net_{cc} and net_{ED} are used to distinguish noise outliers from genuine GW signals, the final event selection is done through a cut over the statistic ρ which characterises the event significance (see chapter 5 for the application of these statistics).

APPENDIX C

LIST OF HIGH ENERGY NEUTRINO CANDIDATES FOR THE 2009-2010 DATA

| 1 | # | ID | JD | GPS | RA[deg.] | DEC[deg.] | radius[deg.] | location[deg.] | scale[deg.] | shape | normalization | nhit | ASW_90 |
|----|------|------------------|-----------|---------|----------|-------------|--------------|----------------|-------------|-------|---------------|------|--------|
| 2 | ## | start | S6A | | | | | | | | | | |
| 3 | 0001 | 2455021.06199646 | 931094971 | 317.666 | 4.358 | -1.1724e-01 | 4.7983e-01 | 5.2936e-01 | 3.8897e-02 | 51 | 0.9 | | |
| 4 | 0002 | 2455021.76038040 | 931155311 | 138.462 | 5.235 | -1.3370e-01 | 8.5313e-01 | 6.3102e-01 | 3.7539e-02 | 30 | 2.4 | | |
| 5 | 0003 | 2455021.95309485 | 931171962 | 205.006 | 3.064 | -9.2963e-02 | 5.6770e-01 | 6.3052e-01 | 3.8106e-02 | 44 | 1.4 | | |
| 6 | 0004 | 2455022.13148593 | 931187375 | 278.683 | 1.967 | -1.2873e-01 | 4.3155e-01 | 4.6595e-01 | 3.9162e-02 | 57 | 0.7 | | |
| 7 | 0005 | 2455022.31313315 | 931203069 | 255.984 | -46.786 | -9.2963e-02 | 5.6770e-01 | 6.3052e-01 | 3.8106e-02 | 67 | 1.4 | | |
| 8 | 0006 | 2455022.44211534 | 931214213 | 118.664 | 28.874 | -1.1909e-01 | 7.2127e-01 | 6.0423e-01 | 3.7507e-02 | 27 | 1.8 | | |
| 9 | 0007 | 2455022.45728516 | 931215524 | 157.294 | -39.769 | -9.2963e-02 | 5.6770e-01 | 6.3052e-01 | 3.8106e-02 | 53 | 1.4 | | |
| 10 | 0008 | 2455022.94472038 | 931257638 | 168.102 | -42.850 | -9.2963e-02 | 5.6770e-01 | 6.3052e-01 | 3.8106e-02 | 47 | 1.4 | | |
| 11 | 0009 | 2455023.18653782 | 931278531 | 272.997 | -21.999 | -9.2963e-02 | 5.6770e-01 | 6.3052e-01 | 3.8106e-02 | 50 | 1.4 | | |
| 12 | 0010 | 2455023.18998930 | 931278830 | 1.531 | -28.790 | -9.2963e-02 | 5.6770e-01 | 6.3052e-01 | 3.8106e-02 | 45 | 1.4 | | |
| 13 | 0011 | 2455023.37019701 | 931294400 | 334.105 | -10.712 | -9.2963e-02 | 5.6770e-01 | 6.3052e-01 | 3.8106e-02 | 48 | 1.4 | | |
| 14 | 0012 | 2455023.39396068 | 931296453 | 69.937 | -17.854 | -9.2963e-02 | 5.6770e-01 | 6.3052e-01 | 3.8106e-02 | 38 | 1.4 | | |
| 15 | 0013 | 2455023.40570083 | 931297467 | 32.350 | -40.431 | -9.2963e-02 | 5.6770e-01 | 6.3052e-01 | 3.8106e-02 | 45 | 1.4 | | |
| 16 | 0014 | 2455023.89575708 | 931339808 | 237.065 | 42.325 | -9.2963e-02 | 5.6770e-01 | 6.3052e-01 | 3.8106e-02 | 67 | 1.4 | | |
| 17 | 0015 | 2455024.96057196 | 931431808 | 206.881 | -5.697 | -1.3370e-01 | 8.5313e-01 | 6.3102e-01 | 3.7539e-02 | 27 | 2.4 | | |
| 18 | 0016 | 2455028.74935072 | 931759158 | 192.449 | -49.417 | -9.2963e-02 | 5.6770e-01 | 6.3052e-01 | 3.8106e-02 | 46 | 1.4 | | |
| 19 | 0017 | 2455029.82388645 | 931851998 | 45.763 | -56.811 | -9.2963e-02 | 5.6770e-01 | 6.3052e-01 | 3.8106e-02 | 42 | 1.4 | | |
| 20 | 0018 | 2455030.16800912 | 931881730 | 74.591 | 14.647 | -9.2963e-02 | 5.6770e-01 | 6.3052e-01 | 3.8106e-02 | 36 | 1.4 | | |
| 21 | 0019 | 2455030.27551389 | 931891019 | 29.548 | 7.599 | -1.1724e-01 | 4.7983e-01 | 5.2936e-01 | 3.8897e-02 | 41 | 0.9 | | |
| 22 | 0020 | 2455030.33532665 | 931896187 | 51.484 | -12.502 | -1.1724e-01 | 4.7983e-01 | 5.2936e-01 | 3.8897e-02 | 62 | 0.9 | | |
| 23 | 0021 | 2455030.38375704 | 931900371 | 70.987 | 39.204 | -1.1724e-01 | 4.7983e-01 | 5.2936e-01 | 3.8897e-02 | 31 | 0.9 | | |
| 24 | 0022 | 2455030.93817457 | 931948273 | 308.219 | -48.184 | -9.2963e-02 | 5.6770e-01 | 6.3052e-01 | 3.8106e-02 | 72 | 1.4 | | |
| 25 | 0023 | 2455031.60103568 | 932005544 | 206.992 | -38.656 | -9.2963e-02 | 5.6770e-01 | 6.3052e-01 | 3.8106e-02 | 38 | 1.4 | | |
| 26 | 0024 | 2455031.91920714 | 932033034 | 270.687 | -44.455 | -9.2963e-02 | 5.6770e-01 | 6.3052e-01 | 3.8106e-02 | 65 | 1.4 | | |
| 27 | 0025 | 2455032.08877353 | 932047685 | 2.736 | -63.554 | -9.2963e-02 | 5.6770e-01 | 6.3052e-01 | 3.8106e-02 | 57 | 1.4 | | |
| 28 | 0026 | 2455032.42253465 | 932076521 | 164.843 | 16.811 | -9.2963e-02 | 5.6770e-01 | 6.3052e-01 | 3.8106e-02 | 43 | 1.4 | | |
| 29 | 0027 | 2455033.33583128 | 932155430 | 351.912 | -40.016 | -9.2963e-02 | 5.6770e-01 | 6.3052e-01 | 3.8106e-02 | 58 | 1.4 | | |
| 30 | 0028 | 2455033.57360678 | 932175974 | 174.370 | 43.050 | -1.3370e-01 | 8.5313e-01 | 6.3102e-01 | 3.7539e-02 | 29 | 2.4 | | |
| 31 | 0029 | 2455033.61363238 | 932179432 | 227.699 | -29.385 | -9.2963e-02 | 5.6770e-01 | 6.3052e-01 | 3.8106e-02 | 38 | 1.4 | | |
| 32 | 0030 | 2455033.66610532 | 932183966 | 101.450 | -43.373 | -9.2963e-02 | 5.6770e-01 | 6.3052e-01 | 3.8106e-02 | 53 | 1.4 | | |
| 33 | 0031 | 2455034.45436583 | 932252072 | 109.591 | -13.022 | -9.2963e-02 | 5.6770e-01 | 6.3052e-01 | 3.8106e-02 | 87 | 1.4 | | |
| 34 | 0032 | 2455035.07953033 | 932306086 | 281.293 | 23.853 | -1.1909e-01 | 7.2127e-01 | 6.0423e-01 | 3.7507e-02 | 22 | 1.8 | | |
| 35 | 0033 | 2455035.18161884 | 932314906 | 29.890 | -63.436 | -1.1724e-01 | 4.7983e-01 | 5.2936e-01 | 3.8897e-02 | 56 | 0.9 | | |

LIST OF HIGH ENERGY NEUTRINO CANDIDATES FOR THE 2009-2010 DATA

| | | | | | | | | | | | |
|----|------|------------------|-----------|---------|---------|-------------|------------|------------|------------|-----|-----|
| 36 | 0034 | 2455035.40957799 | 932334602 | 101.450 | 32.177 | -1.7861e+00 | 6.7827e+00 | 8.6368e-01 | 3.8440e-01 | 30 | 1.4 |
| 37 | 0035 | 2455035.64492418 | 932354936 | 247.231 | -26.876 | -9.2963e-02 | 5.6770e-01 | 6.3052e-01 | 3.8106e-02 | 35 | 1.4 |
| 38 | 0036 | 2455035.70030035 | 932359720 | 227.842 | 42.919 | -9.2963e-02 | 5.6770e-01 | 6.3052e-01 | 3.8106e-02 | 46 | 1.4 |
| 39 | 0037 | 2455035.97026079 | 932383045 | 211.009 | -59.338 | -9.2963e-02 | 5.6770e-01 | 6.3052e-01 | 3.8106e-02 | 34 | 1.4 |
| 40 | 0038 | 2455036.00870766 | 932386367 | 242.953 | -39.003 | -9.2963e-02 | 5.6770e-01 | 6.3052e-01 | 3.8106e-02 | 67 | 1.4 |
| 41 | 0039 | 2455036.60298826 | 932437713 | 62.518 | -47.951 | -1.1724e-01 | 4.7983e-01 | 5.2936e-01 | 3.8897e-02 | 53 | 0.9 |
| 42 | 0040 | 2455036.60985464 | 932438306 | 102.326 | 15.432 | -9.2963e-02 | 5.6770e-01 | 6.3052e-01 | 3.8106e-02 | 44 | 1.4 |
| 43 | 0041 | 2455036.63224016 | 932440240 | 272.965 | -8.272 | -9.2963e-02 | 5.6770e-01 | 6.3052e-01 | 3.8106e-02 | 59 | 1.4 |
| 44 | 0042 | 2455036.70911771 | 932446882 | 140.991 | -37.795 | -9.2963e-02 | 5.6770e-01 | 6.3052e-01 | 3.8106e-02 | 45 | 1.4 |
| 45 | 0043 | 2455036.71386641 | 932447293 | 197.929 | -9.068 | -1.1724e-01 | 4.7983e-01 | 5.2936e-01 | 3.8897e-02 | 72 | 0.9 |
| 46 | 0044 | 2455036.97629850 | 932469967 | 49.100 | -45.947 | -1.1724e-01 | 4.7983e-01 | 5.2936e-01 | 3.8897e-02 | 26 | 0.9 |
| 47 | 0045 | 2455036.99191191 | 932471316 | 260.728 | 1.668 | -1.1724e-01 | 4.7983e-01 | 5.2936e-01 | 3.8897e-02 | 42 | 0.9 |
| 48 | 0046 | 2455037.07504211 | 932478498 | 181.562 | -44.687 | -5.8944e-02 | 2.9333e-01 | 5.7306e-01 | 3.8834e-02 | 110 | 0.6 |
| 49 | 0047 | 2455037.09645452 | 932480348 | 266.521 | -55.111 | -9.2963e-02 | 5.6770e-01 | 6.3052e-01 | 3.8106e-02 | 79 | 1.4 |
| 50 | 0048 | 2455037.42636007 | 932508852 | 135.162 | -42.375 | -1.1724e-01 | 4.7983e-01 | 5.2936e-01 | 3.8897e-02 | 45 | 0.9 |
| 51 | 0049 | 2455037.54148144 | 932518798 | 166.903 | 36.240 | -9.2963e-02 | 5.6770e-01 | 6.3052e-01 | 3.8106e-02 | 38 | 1.4 |
| 52 | 0050 | 2455037.85645194 | 932546012 | 210.049 | -5.290 | -9.2963e-02 | 5.6770e-01 | 6.3052e-01 | 3.8106e-02 | 44 | 1.4 |
| 53 | 0051 | 2455038.44163643 | 932596572 | 120.888 | 13.742 | -9.2963e-02 | 5.6770e-01 | 6.3052e-01 | 3.8106e-02 | 47 | 1.4 |
| 54 | 0052 | 2455038.95829055 | 932641211 | 278.848 | 31.341 | -9.2963e-02 | 5.6770e-01 | 6.3052e-01 | 3.8106e-02 | 50 | 1.4 |
| 55 | 0053 | 2455038.97211600 | 932642405 | 163.861 | -45.126 | -9.2963e-02 | 5.6770e-01 | 6.3052e-01 | 3.8106e-02 | 37 | 1.4 |
| 56 | 0054 | 2455039.30290420 | 932670985 | 138.019 | -66.930 | -9.2963e-02 | 5.6770e-01 | 6.3052e-01 | 3.8106e-02 | 64 | 1.4 |
| 57 | 0055 | 2455041.87228627 | 932892980 | 323.880 | -62.866 | -9.2963e-02 | 5.6770e-01 | 6.3052e-01 | 3.8106e-02 | 53 | 1.4 |
| 58 | 0056 | 2455041.97123183 | 932901529 | 333.888 | 17.928 | -1.3370e-01 | 8.5313e-01 | 6.3102e-01 | 3.7539e-02 | 29 | 2.4 |
| 59 | 0057 | 2455042.17163841 | 932918844 | 349.430 | -6.478 | -9.2963e-02 | 5.6770e-01 | 6.3052e-01 | 3.8106e-02 | 46 | 1.4 |
| 60 | 0058 | 2455042.35897386 | 932935030 | 124.059 | 6.046 | -9.2963e-02 | 5.6770e-01 | 6.3052e-01 | 3.8106e-02 | 33 | 1.4 |
| 61 | 0059 | 2455042.45033082 | 932942923 | 3.545 | -71.453 | -1.3370e-01 | 8.5313e-01 | 6.3102e-01 | 3.7539e-02 | 30 | 2.4 |
| 62 | 0060 | 2455042.87758885 | 932979838 | 303.584 | -28.374 | -1.1724e-01 | 4.7983e-01 | 5.2936e-01 | 3.8897e-02 | 40 | 0.9 |
| 63 | 0061 | 2455042.89936669 | 932981720 | 250.252 | -30.276 | -9.2963e-02 | 5.6770e-01 | 6.3052e-01 | 3.8106e-02 | 37 | 1.4 |
| 64 | 0062 | 2455043.89864128 | 933068057 | 316.089 | 4.421 | -9.2963e-02 | 5.6770e-01 | 6.3052e-01 | 3.8106e-02 | 36 | 1.4 |
| 65 | 0063 | 2455050.32408157 | 933623215 | 72.132 | 1.396 | -5.8944e-02 | 2.9333e-01 | 5.7306e-01 | 3.8834e-02 | 114 | 0.6 |
| 66 | 0064 | 2455050.38858959 | 933628789 | 356.053 | -31.259 | -9.2963e-02 | 5.6770e-01 | 6.3052e-01 | 3.8106e-02 | 42 | 1.4 |
| 67 | 0065 | 2455050.40529145 | 933630232 | 313.438 | -51.861 | -9.2963e-02 | 5.6770e-01 | 6.3052e-01 | 3.8106e-02 | 55 | 1.4 |
| 68 | 0066 | 2455050.44870235 | 933633982 | 38.167 | -55.362 | -1.3370e-01 | 8.5313e-01 | 6.3102e-01 | 3.7539e-02 | 23 | 2.4 |
| 69 | 0067 | 2455052.47328426 | 933808906 | 115.206 | -18.798 | -1.1724e-01 | 4.7983e-01 | 5.2936e-01 | 3.8897e-02 | 47 | 0.9 |
| 70 | 0068 | 2455052.58433722 | 933818501 | 206.041 | -45.213 | -1.2873e-01 | 4.3155e-01 | 4.6595e-01 | 3.9162e-02 | 42 | 0.7 |
| 71 | 0069 | 2455052.85057939 | 933841505 | 166.502 | -25.475 | -1.2873e-01 | 4.3155e-01 | 4.6595e-01 | 3.9162e-02 | 60 | 0.7 |
| 72 | 0070 | 2455052.95932832 | 933850900 | 253.817 | -75.759 | -9.2963e-02 | 5.6770e-01 | 6.3052e-01 | 3.8106e-02 | 60 | 1.4 |
| 73 | 0071 | 2455052.97455143 | 933852216 | 286.417 | 37.666 | -9.2963e-02 | 5.6770e-01 | 6.3052e-01 | 3.8106e-02 | 65 | 1.4 |
| 74 | 0072 | 2455053.41821454 | 933890548 | 20.185 | -23.592 | -9.2963e-02 | 5.6770e-01 | 6.3052e-01 | 3.8106e-02 | 59 | 1.4 |
| 75 | 0073 | 2455053.48363661 | 933896201 | 49.990 | -19.411 | -9.2963e-02 | 5.6770e-01 | 6.3052e-01 | 3.8106e-02 | 40 | 1.4 |
| 76 | 0074 | 2455053.53529934 | 933900664 | 187.949 | -6.248 | -1.1724e-01 | 4.7983e-01 | 5.2936e-01 | 3.8897e-02 | 52 | 0.9 |
| 77 | 0075 | 2455053.53684889 | 933900798 | 44.865 | -25.779 | -9.2963e-02 | 5.6770e-01 | 6.3052e-01 | 3.8106e-02 | 67 | 1.4 |
| 78 | 0076 | 2455053.74347266 | 933918651 | 163.514 | 13.204 | -9.2963e-02 | 5.6770e-01 | 6.3052e-01 | 3.8106e-02 | 37 | 1.4 |
| 79 | 0077 | 2455053.74875280 | 933919107 | 78.440 | -60.862 | -9.2963e-02 | 5.6770e-01 | 6.3052e-01 | 3.8106e-02 | 34 | 1.4 |
| 80 | 0078 | 2455053.81557582 | 933924880 | 276.507 | 28.587 | -9.2963e-02 | 5.6770e-01 | 6.3052e-01 | 3.8106e-02 | 85 | 1.4 |
| 81 | 0079 | 2455053.83153518 | 933926259 | 186.604 | -39.316 | -9.2963e-02 | 5.6770e-01 | 6.3052e-01 | 3.8106e-02 | 32 | 1.4 |
| 82 | 0080 | 2455054.19238734 | 933957437 | 79.365 | -26.764 | -9.2963e-02 | 5.6770e-01 | 6.3052e-01 | 3.8106e-02 | 29 | 1.4 |
| 83 | 0081 | 2455054.30248002 | 933966949 | 211.712 | -45.529 | -1.3370e-01 | 8.5313e-01 | 6.3102e-01 | 3.7539e-02 | 29 | 2.4 |
| 84 | 0082 | 2455054.32037523 | 933968495 | 41.278 | 31.473 | -9.2963e-02 | 5.6770e-01 | 6.3052e-01 | 3.8106e-02 | 52 | 1.4 |
| 85 | 0083 | 2455054.65740359 | 933997614 | 289.824 | -23.322 | -9.2963e-02 | 5.6770e-01 | 6.3052e-01 | 3.8106e-02 | 34 | 1.4 |
| 86 | 0084 | 2455055.01582708 | 934028582 | 273.787 | -44.754 | -9.2963e-02 | 5.6770e-01 | 6.3052e-01 | 3.8106e-02 | 38 | 1.4 |
| 87 | 0085 | 2455057.10660147 | 934209225 | 355.481 | -47.229 | -1.1724e-01 | 4.7983e-01 | 5.2936e-01 | 3.8897e-02 | 40 | 0.9 |

88 0086 2455057.72174617 934262373 197.766 37.641 -9.2963e-02 5.6770e-01 6.3052e-01 3.8106e-02 32 1.4
89 0087 2455057.73197650 934263257 343.302 -21.717 -9.2963e-02 5.6770e-01 6.3052e-01 3.8106e-02 62 1.4
90 0088 2455057.77638293 934267094 18.317 -71.965 -1.1724e-01 4.7983e-01 5.2936e-01 3.8897e-02 36 0.9
91 0089 2455057.99678427 934286137 338.646 -57.019 -1.1724e-01 4.7983e-01 5.2936e-01 3.8897e-02 36 0.9
92 0090 2455058.10416152 934295414 25.851 14.336 -1.3370e-01 8.5313e-01 6.3102e-01 3.7539e-02 26 2.4
93 0091 2455058.18834888 934302688 178.236 -41.215 -9.2963e-02 5.6770e-01 6.3052e-01 3.8106e-02 46 1.4
94 0092 2455058.76158587 934352216 246.087 -39.107 -1.1724e-01 4.7983e-01 5.2936e-01 3.8897e-02 42 0.9
95 0093 2455058.86341465 934361014 3.491 -27.687 -9.2963e-02 5.6770e-01 6.3052e-01 3.8106e-02 72 1.4
96 0094 2455058.91450708 934365428 288.617 39.340 -9.2963e-02 5.6770e-01 6.3052e-01 3.8106e-02 30 1.4
97 0095 2455059.05793775 934377820 78.537 -81.132 -1.1724e-01 4.7983e-01 5.2936e-01 3.8897e-02 36 0.9
98 0096 2455059.14860678 934385654 296.207 -56.333 -1.1724e-01 4.7983e-01 5.2936e-01 3.8897e-02 35 0.9
99 0097 2455059.39256684 934406732 86.229 -5.943 -9.2963e-02 5.6770e-01 6.3052e-01 3.8106e-02 42 1.4
100 0098 2455059.55834199 934421055 110.022 -52.160 -1.2873e-01 4.3155e-01 4.6595e-01 3.9162e-02 41 0.7
101 0099 2455059.60484498 934425073 348.050 -74.294 -1.3370e-01 8.5313e-01 6.3102e-01 3.7539e-02 29 2.4
102 0100 2455059.72044919 934435061 88.907 -77.196 -1.2873e-01 4.3155e-01 4.6595e-01 3.9162e-02 59 0.7
103 0101 2455059.87421622 934448347 259.574 7.695 -1.3370e-01 8.5313e-01 6.3102e-01 3.7539e-02 25 2.4
104 0102 2455059.91445785 934451824 224.493 10.941 -9.2963e-02 5.6770e-01 6.3052e-01 3.8106e-02 49 1.4
105 0103 2455059.98885820 934458252 241.941 -37.187 -9.2963e-02 5.6770e-01 6.3052e-01 3.8106e-02 35 1.4
106 0104 2455060.09424206 934467357 323.311 -40.725 -9.2963e-02 5.6770e-01 6.3052e-01 3.8106e-02 42 1.4
107 0105 2455060.18410076 934475121 205.068 -72.845 -9.2963e-02 5.6770e-01 6.3052e-01 3.8106e-02 38 1.4
108 0106 2455060.25954351 934481639 9.288 -7.403 -9.2963e-02 5.6770e-01 6.3052e-01 3.8106e-02 42 1.4
109 0107 2455060.35331136 934489741 179.878 -53.666 -9.2963e-02 5.6770e-01 6.3052e-01 3.8106e-02 57 1.4
110 0108 2455060.52726260 934504770 47.437 -33.261 -9.2963e-02 5.6770e-01 6.3052e-01 3.8106e-02 55 1.4
111 0109 2455061.31263711 934572626 192.544 -55.694 -9.2963e-02 5.6770e-01 6.3052e-01 3.8106e-02 50 1.4
112 0110 2455061.44684815 934584222 72.470 -28.046 -9.2963e-02 5.6770e-01 6.3052e-01 3.8106e-02 42 1.4
113 0111 2455061.51759585 934590335 237.226 -9.551 -9.2963e-02 5.6770e-01 6.3052e-01 3.8106e-02 37 1.4
114 0112 2455061.55946493 934593952 202.888 33.499 -9.2963e-02 5.6770e-01 6.3052e-01 3.8106e-02 37 1.4
115 0113 2455061.73849454 934609420 19.756 -50.560 -9.2963e-02 5.6770e-01 6.3052e-01 3.8106e-02 51 1.4
116 0114 2455061.74870241 934610302 152.932 -6.469 -9.2963e-02 5.6770e-01 6.3052e-01 3.8106e-02 34 1.4
117 0115 2455061.83503097 934617761 298.604 -42.499 -9.2963e-02 5.6770e-01 6.3052e-01 3.8106e-02 25 1.4
118 0116 2455061.88976534 934622490 214.252 -34.716 -9.2963e-02 5.6770e-01 6.3052e-01 3.8106e-02 41 1.4
119 0117 2455061.94754236 934627482 357.669 13.929 -9.2963e-02 5.6770e-01 6.3052e-01 3.8106e-02 43 1.4
120 0118 2455062.02194877 934633911 172.194 -63.516 -9.2963e-02 5.6770e-01 6.3052e-01 3.8106e-02 32 1.4
121 0119 2455062.08912358 934639715 101.379 -14.331 -9.2963e-02 5.6770e-01 6.3052e-01 3.8106e-02 40 1.4
122 0120 2455062.21500284 934650591 295.537 -40.361 -9.2963e-02 5.6770e-01 6.3052e-01 3.8106e-02 33 1.4
123 0121 2455062.82701440 934703469 300.123 35.695 -9.2963e-02 5.6770e-01 6.3052e-01 3.8106e-02 34 1.4
124 0122 2455062.85720530 934706077 323.861 -6.029 -1.1909e-01 7.2127e-01 6.0423e-01 3.7507e-02 20 1.8
125 0123 2455062.88545185 934708518 263.884 8.358 -1.1909e-01 7.2127e-01 6.0423e-01 3.7507e-02 66 1.8
126 0124 2455062.89821627 934709620 245.558 16.387 -9.2963e-02 5.6770e-01 6.3052e-01 3.8106e-02 32 1.4
127 0125 2455062.97267542 934716054 285.690 27.039 -1.3370e-01 8.5313e-01 6.3102e-01 3.7539e-02 26 2.4
128 0126 2455063.17559712 934733586 25.934 -60.307 -1.1724e-01 4.7983e-01 5.2936e-01 3.8897e-02 43 0.9
129 0127 2455063.48054315 934759933 162.308 -30.704 -9.2963e-02 5.6770e-01 6.3052e-01 3.8106e-02 37 1.4
130 0128 2455063.57841217 934768389 314.799 -37.629 -9.2963e-02 5.6770e-01 6.3052e-01 3.8106e-02 35 1.4
131 0129 2455063.60847560 934770987 173.670 45.183 -1.1724e-01 4.7983e-01 5.2936e-01 3.8897e-02 57 0.9
132 0130 2455063.63467694 934773251 170.213 -13.859 -1.1724e-01 4.7983e-01 5.2936e-01 3.8897e-02 31 0.9
133 0131 2455063.68940751 934777979 233.357 -1.269 -1.1724e-01 4.7983e-01 5.2936e-01 3.8897e-02 37 0.9
134 0132 2455063.77603876 934785464 260.557 -19.652 -1.1724e-01 4.7983e-01 5.2936e-01 3.8897e-02 80 0.9
135 0133 2455063.78605218 934786329 138.906 -50.654 -9.2963e-02 5.6770e-01 6.3052e-01 3.8106e-02 58 1.4
136 0134 2455063.88720217 934795069 212.069 -22.876 -9.2963e-02 5.6770e-01 6.3052e-01 3.8106e-02 35 1.4
137 0135 2455064.04774615 934808940 335.759 44.453 -9.2963e-02 5.6770e-01 6.3052e-01 3.8106e-02 39 1.4
138 0136 2455064.14454310 934817303 288.283 -49.621 -9.2963e-02 5.6770e-01 6.3052e-01 3.8106e-02 36 1.4
139 0137 2455064.26502570 934827713 161.003 -8.728 -9.2963e-02 5.6770e-01 6.3052e-01 3.8106e-02 46 1.4

LIST OF HIGH ENERGY NEUTRINO CANDIDATES FOR THE 2009-2010 DATA

| | | | | | | | | | | | |
|-----|------|------------------|-----------|---------|---------|-------------|------------|------------|------------|----|-----|
| 140 | 0138 | 2455064.56062293 | 934853252 | 38.039 | -52.296 | -9.2963e-02 | 5.6770e-01 | 6.3052e-01 | 3.8106e-02 | 74 | 1.4 |
| 141 | 0139 | 2455064.65752250 | 934861624 | 281.452 | -16.760 | -9.2963e-02 | 5.6770e-01 | 6.3052e-01 | 3.8106e-02 | 39 | 1.4 |
| 142 | 0140 | 2455064.78114668 | 934872306 | 257.829 | -0.921 | -9.2963e-02 | 5.6770e-01 | 6.3052e-01 | 3.8106e-02 | 35 | 1.4 |
| 143 | 0141 | 2455064.88179257 | 934881001 | 22.451 | -15.508 | -9.2963e-02 | 5.6770e-01 | 6.3052e-01 | 3.8106e-02 | 47 | 1.4 |
| 144 | 0142 | 2455064.95292887 | 934887148 | 146.216 | -65.464 | -9.2963e-02 | 5.6770e-01 | 6.3052e-01 | 3.8106e-02 | 40 | 1.4 |
| 145 | 0143 | 2455064.99601715 | 934890870 | 11.022 | 8.344 | -9.2963e-02 | 5.6770e-01 | 6.3052e-01 | 3.8106e-02 | 41 | 1.4 |
| 146 | 0144 | 2455065.36133282 | 934922434 | 169.335 | -47.674 | -1.1724e-01 | 4.7983e-01 | 5.2936e-01 | 3.8897e-02 | 40 | 0.9 |
| 147 | 0145 | 2455065.60217816 | 934943243 | 165.957 | -25.904 | -1.1724e-01 | 4.7983e-01 | 5.2936e-01 | 3.8897e-02 | 56 | 0.9 |
| 148 | 0146 | 2455065.93864074 | 934972313 | 62.855 | -28.983 | -9.2963e-02 | 5.6770e-01 | 6.3052e-01 | 3.8106e-02 | 59 | 1.4 |
| 149 | 0147 | 2455066.39089495 | 935011388 | 176.976 | -11.310 | -1.1724e-01 | 4.7983e-01 | 5.2936e-01 | 3.8897e-02 | 36 | 0.9 |
| 150 | 0148 | 2455066.57591951 | 935027374 | 193.704 | -21.759 | -9.2963e-02 | 5.6770e-01 | 6.3052e-01 | 3.8106e-02 | 49 | 1.4 |
| 151 | 0149 | 2455066.61269078 | 935030551 | 3.471 | -59.062 | -9.2963e-02 | 5.6770e-01 | 6.3052e-01 | 3.8106e-02 | 71 | 1.4 |
| 152 | 0150 | 2455066.75797386 | 935043103 | 211.403 | -49.385 | -9.2963e-02 | 5.6770e-01 | 6.3052e-01 | 3.8106e-02 | 45 | 1.4 |
| 153 | 0151 | 2455066.77956388 | 935044969 | 235.841 | 17.491 | -9.2963e-02 | 5.6770e-01 | 6.3052e-01 | 3.8106e-02 | 40 | 1.4 |
| 154 | 0152 | 2455067.01314266 | 935065150 | 289.079 | -74.713 | -9.2963e-02 | 5.6770e-01 | 6.3052e-01 | 3.8106e-02 | 44 | 1.4 |
| 155 | 0153 | 2455067.08142308 | 935071049 | 54.618 | -13.711 | -9.2963e-02 | 5.6770e-01 | 6.3052e-01 | 3.8106e-02 | 35 | 1.4 |
| 156 | 0154 | 2455067.11560343 | 935074003 | 234.943 | -63.137 | -1.3370e-01 | 8.5313e-01 | 6.3102e-01 | 3.7539e-02 | 29 | 2.4 |
| 157 | 0155 | 2455067.12042047 | 935074419 | 304.395 | -12.814 | -1.1909e-01 | 7.2127e-01 | 6.0423e-01 | 3.7507e-02 | 27 | 1.8 |
| 158 | 0156 | 2455067.15376586 | 935077300 | 21.271 | -27.720 | -1.2873e-01 | 4.3155e-01 | 4.6595e-01 | 3.9162e-02 | 45 | 0.7 |
| 159 | 0157 | 2455067.30991995 | 935090792 | 105.702 | -6.759 | -1.2873e-01 | 4.3155e-01 | 4.6595e-01 | 3.9162e-02 | 52 | 0.7 |
| 160 | 0158 | 2455070.47703972 | 935364431 | 265.930 | -75.124 | -9.2963e-02 | 5.6770e-01 | 6.3052e-01 | 3.8106e-02 | 41 | 1.4 |
| 161 | 0159 | 2455070.94445264 | 935404815 | 296.500 | 12.771 | -1.1724e-01 | 4.7983e-01 | 5.2936e-01 | 3.8897e-02 | 39 | 0.9 |
| 162 | 0160 | 2455070.96791834 | 935406843 | 329.554 | 17.101 | -1.1724e-01 | 4.7983e-01 | 5.2936e-01 | 3.8897e-02 | 45 | 0.9 |
| 163 | 0161 | 2455070.99781936 | 935409426 | 35.999 | -50.428 | -9.2963e-02 | 5.6770e-01 | 6.3052e-01 | 3.8106e-02 | 67 | 1.4 |
| 164 | 0162 | 2455071.13297930 | 935421104 | 91.198 | -60.854 | -1.3370e-01 | 8.5313e-01 | 6.3102e-01 | 3.7539e-02 | 25 | 2.4 |
| 165 | 0163 | 2455071.26768616 | 935432743 | 60.807 | 27.094 | -9.2963e-02 | 5.6770e-01 | 6.3052e-01 | 3.8106e-02 | 51 | 1.4 |
| 166 | 0164 | 2455071.29632968 | 935435217 | 294.982 | -48.854 | -1.3370e-01 | 8.5313e-01 | 6.3102e-01 | 3.7539e-02 | 25 | 2.4 |
| 167 | 0165 | 2455071.32881274 | 935438024 | 197.670 | -19.309 | -1.1909e-01 | 7.2127e-01 | 6.0423e-01 | 3.7507e-02 | 28 | 1.8 |
| 168 | 0166 | 2455071.39038574 | 935443344 | 110.555 | -56.593 | -9.2963e-02 | 5.6770e-01 | 6.3052e-01 | 3.8106e-02 | 37 | 1.4 |
| 169 | 0167 | 2455071.40315053 | 935444447 | 60.000 | 19.101 | -9.2963e-02 | 5.6770e-01 | 6.3052e-01 | 3.8106e-02 | 47 | 1.4 |
| 170 | 0168 | 2455071.76877458 | 935476037 | 285.997 | 1.892 | -1.1724e-01 | 4.7983e-01 | 5.2936e-01 | 3.8897e-02 | 42 | 0.9 |
| 171 | 0169 | 2455071.82952120 | 935481285 | 6.548 | -1.611 | -9.2963e-02 | 5.6770e-01 | 6.3052e-01 | 3.8106e-02 | 32 | 1.4 |
| 172 | 0170 | 2455072.02111240 | 935497839 | 332.166 | -27.354 | -1.3370e-01 | 8.5313e-01 | 6.3102e-01 | 3.7539e-02 | 26 | 2.4 |
| 173 | 0171 | 2455072.08589852 | 935503436 | 267.489 | -18.082 | -9.2963e-02 | 5.6770e-01 | 6.3052e-01 | 3.8106e-02 | 53 | 1.4 |
| 174 | 0172 | 2455072.10148270 | 935504783 | 71.396 | -42.301 | -1.3370e-01 | 8.5313e-01 | 6.3102e-01 | 3.7539e-02 | 28 | 2.4 |
| 175 | 0173 | 2455072.42031869 | 935532330 | 42.345 | -50.906 | -9.2963e-02 | 5.6770e-01 | 6.3052e-01 | 3.8106e-02 | 50 | 1.4 |
| 176 | 0174 | 2455072.85751870 | 935570104 | 151.015 | -64.369 | -9.2963e-02 | 5.6770e-01 | 6.3052e-01 | 3.8106e-02 | 81 | 1.4 |
| 177 | 0175 | 2455072.87929551 | 935571986 | 302.403 | -2.080 | -1.1724e-01 | 4.7983e-01 | 5.2936e-01 | 3.8897e-02 | 38 | 0.9 |
| 178 | 0176 | 2455073.03755802 | 935585660 | 341.378 | 26.213 | -1.2873e-01 | 4.3155e-01 | 4.6595e-01 | 3.9162e-02 | 38 | 0.7 |
| 179 | 0177 | 2455073.04830593 | 935586588 | 333.750 | 6.568 | -9.2963e-02 | 5.6770e-01 | 6.3052e-01 | 3.8106e-02 | 73 | 1.4 |
| 180 | 0178 | 2455073.21274276 | 935600795 | 28.475 | 20.486 | -1.1909e-01 | 7.2127e-01 | 6.0423e-01 | 3.7507e-02 | 28 | 1.8 |
| 181 | 0179 | 2455073.43171108 | 935619714 | 191.985 | 29.561 | -9.2963e-02 | 5.6770e-01 | 6.3052e-01 | 3.8106e-02 | 34 | 1.4 |
| 182 | 0180 | 2455073.44068156 | 935620489 | 148.114 | -0.467 | -9.2963e-02 | 5.6770e-01 | 6.3052e-01 | 3.8106e-02 | 70 | 1.4 |
| 183 | 0181 | 2455073.46909432 | 935622944 | 195.280 | -21.809 | -9.2963e-02 | 5.6770e-01 | 6.3052e-01 | 3.8106e-02 | 32 | 1.4 |
| 184 | 0182 | 2455073.64250209 | 935637927 | 98.395 | -50.232 | -9.2963e-02 | 5.6770e-01 | 6.3052e-01 | 3.8106e-02 | 69 | 1.4 |
| 185 | 0183 | 2455073.64388251 | 935638046 | 264.339 | 28.544 | -9.2963e-02 | 5.6770e-01 | 6.3052e-01 | 3.8106e-02 | 47 | 1.4 |
| 186 | 0184 | 2455073.69052558 | 935642076 | 180.486 | -21.394 | -9.2963e-02 | 5.6770e-01 | 6.3052e-01 | 3.8106e-02 | 38 | 1.4 |
| 187 | 0185 | 2455073.76116355 | 935648179 | 298.854 | 36.684 | -9.2963e-02 | 5.6770e-01 | 6.3052e-01 | 3.8106e-02 | 48 | 1.4 |
| 188 | 0186 | 2455073.97565402 | 935666711 | 283.507 | -12.569 | -1.3370e-01 | 8.5313e-01 | 6.3102e-01 | 3.7539e-02 | 26 | 2.4 |
| 189 | 0187 | 2455074.16081558 | 935682709 | 1.175 | -18.999 | -9.2963e-02 | 5.6770e-01 | 6.3052e-01 | 3.8106e-02 | 34 | 1.4 |
| 190 | 0188 | 2455074.21222119 | 935687150 | 108.559 | -53.956 | -9.2963e-02 | 5.6770e-01 | 6.3052e-01 | 3.8106e-02 | 71 | 1.4 |
| 191 | 0189 | 2455074.32623248 | 935697001 | 298.966 | -58.654 | -9.2963e-02 | 5.6770e-01 | 6.3052e-01 | 3.8106e-02 | 37 | 1.4 |

192 0190 2455074.56496007 935717627 84.393 -37.166 -9.2963e-02 5.6770e-01 6.3052e-01 3.8106e-02 62 1.4
193 0191 2455074.57640119 935718616 79.034 -30.771 -9.2963e-02 5.6770e-01 6.3052e-01 3.8106e-02 38 1.4
194 0192 2455074.60422679 935721020 272.659 4.576 -9.2963e-02 5.6770e-01 6.3052e-01 3.8106e-02 75 1.4
195 0193 2455074.79432343 935737444 67.313 -48.050 -1.1724e-01 4.7983e-01 5.2936e-01 3.8897e-02 51 0.9
196 0194 2455075.10189846 935764019 8.468 1.425 -1.3370e-01 8.5313e-01 6.3102e-01 3.7539e-02 15 2.4
197 0195 2455075.17740608 935770542 14.325 29.555 -1.1724e-01 4.7983e-01 5.2936e-01 3.8897e-02 46 0.9
198 0196 2455075.21724744 935773985 348.538 -50.641 -1.3370e-01 8.5313e-01 6.3102e-01 3.7539e-02 29 2.4
199 0197 2455075.28702876 935780014 150.807 0.342 -1.3370e-01 8.5313e-01 6.3102e-01 3.7539e-02 30 2.4
200 0198 2455075.36731093 935786950 159.178 -34.961 -9.2963e-02 5.6770e-01 6.3052e-01 3.8106e-02 36 1.4
201 0199 2455075.38729420 935788677 26.551 -9.824 -9.2963e-02 5.6770e-01 6.3052e-01 3.8106e-02 66 1.4
202 0200 2455075.41695957 935791240 50.676 -64.237 -1.1909e-01 7.2127e-01 6.0423e-01 3.7507e-02 30 1.8
203 ## stop S6A -- start
204 0201 2455075.56390515 935803936 186.645 -78.234 -9.2963e-02 5.6770e-01 6.3052e-01 3.8106e-02 39 1.4
205 0202 2455075.77641224 935822297 26.229 -51.325 -9.2963e-02 5.6770e-01 6.3052e-01 3.8106e-02 35 1.4
206 0203 2455075.99417841 935841112 42.364 11.601 -1.1909e-01 7.2127e-01 6.0423e-01 3.7507e-02 22 1.8
207 0204 2455075.99462135 935841150 292.792 -26.328 -9.2963e-02 5.6770e-01 6.3052e-01 3.8106e-02 35 1.4
208 0205 2455076.01741383 935843119 315.405 34.672 -9.2963e-02 5.6770e-01 6.3052e-01 3.8106e-02 44 1.4
209 0206 2455076.15557493 935855056 253.920 -64.226 -1.1724e-01 4.7983e-01 5.2936e-01 3.8897e-02 46 0.9
210 0207 2455076.18136926 935857285 160.419 -29.016 -1.1724e-01 4.7983e-01 5.2936e-01 3.8897e-02 34 0.9
211 0208 2455076.23681134 935862075 113.337 -57.305 -1.3370e-01 8.5313e-01 6.3102e-01 3.7539e-02 25 2.4
212 0209 2455076.27127798 935865053 307.233 -60.805 -9.2963e-02 5.6770e-01 6.3052e-01 3.8106e-02 72 1.4
213 0210 2455076.32513939 935869707 134.496 38.062 -9.2963e-02 5.6770e-01 6.3052e-01 3.8106e-02 51 1.4
214 0211 2455076.33399198 935870471 208.913 -12.640 -9.2963e-02 5.6770e-01 6.3052e-01 3.8106e-02 32 1.4
215 0212 2455076.35855125 935872593 147.308 -15.700 -9.2963e-02 5.6770e-01 6.3052e-01 3.8106e-02 32 1.4
216 0213 2455076.57486298 935891283 251.261 -16.281 -1.1724e-01 4.7983e-01 5.2936e-01 3.8897e-02 34 0.9
217 0214 2455076.58392926 935892066 118.896 2.822 -1.3370e-01 8.5313e-01 6.3102e-01 3.7539e-02 24 2.4
218 0215 2455076.77056074 935908191 274.193 -63.643 -9.2963e-02 5.6770e-01 6.3052e-01 3.8106e-02 47 1.4
219 0216 2455077.08998965 935935790 232.891 -61.107 -1.3370e-01 8.5313e-01 6.3102e-01 3.7539e-02 28 2.4
220 0217 2455077.29565244 935953559 99.410 -5.291 -1.3370e-01 8.5313e-01 6.3102e-01 3.7539e-02 32 2.4
221 0218 2455077.76187250 935993840 342.896 -9.615 -9.2963e-02 5.6770e-01 6.3052e-01 3.8106e-02 37 1.4
222 0219 2455077.79683288 935996861 196.981 -12.760 -9.2963e-02 5.6770e-01 6.3052e-01 3.8106e-02 38 1.4
223 0220 2455077.91146154 936006765 342.016 -46.411 -9.2963e-02 5.6770e-01 6.3052e-01 3.8106e-02 37 1.4
224 0221 2455078.11485758 936024338 41.640 46.071 -9.2963e-02 5.6770e-01 6.3052e-01 3.8106e-02 32 1.4
225 0222 2455078.14156621 936026646 282.452 -45.117 -9.2963e-02 5.6770e-01 6.3052e-01 3.8106e-02 54 1.4
226 0223 2455078.24965750 936035985 337.977 -49.741 -9.2963e-02 5.6770e-01 6.3052e-01 3.8106e-02 73 1.4
227 0224 2455078.31163506 936041340 182.403 -12.568 -9.2963e-02 5.6770e-01 6.3052e-01 3.8106e-02 28 1.4
228 0225 2455078.66255429 936071659 224.546 14.682 -9.2963e-02 5.6770e-01 6.3052e-01 3.8106e-02 53 1.4
229 0226 2455079.09997850 936109453 220.691 -78.436 -9.2963e-02 5.6770e-01 6.3052e-01 3.8106e-02 67 1.4
230 0227 2455079.14743735 936113553 235.278 -66.087 -1.3370e-01 8.5313e-01 6.3102e-01 3.7539e-02 24 2.4
231 0228 2455079.23722766 936121311 183.940 -49.505 -9.2963e-02 5.6770e-01 6.3052e-01 3.8106e-02 42 1.4
232 0229 2455079.30866599 936127483 21.285 -38.030 -9.2963e-02 5.6770e-01 6.3052e-01 3.8106e-02 53 1.4
233 0230 2455079.40743016 936136016 170.021 -12.730 -9.2963e-02 5.6770e-01 6.3052e-01 3.8106e-02 59 1.4
234 0231 2455079.47519614 936141871 63.018 -27.148 -1.1909e-01 7.2127e-01 6.0423e-01 3.7507e-02 25 1.8
235 0232 2455079.47590578 936141933 109.353 -43.789 -9.2963e-02 5.6770e-01 6.3052e-01 3.8106e-02 48 1.4
236 0233 2455079.56121105 936149303 132.409 1.719 -9.2963e-02 5.6770e-01 6.3052e-01 3.8106e-02 34 1.4
237 0234 2455079.57961689 936150893 219.567 44.493 -1.1724e-01 4.7983e-01 5.2936e-01 3.8897e-02 32 0.9
238 0235 2455079.60719435 936153276 105.653 -38.931 -9.2963e-02 5.6770e-01 6.3052e-01 3.8106e-02 37 1.4
239 0236 2455079.63811721 936155948 243.927 -85.337 -1.3370e-01 8.5313e-01 6.3102e-01 3.7539e-02 30 2.4
240 0237 2455079.78572540 936168701 340.634 -31.464 -9.2963e-02 5.6770e-01 6.3052e-01 3.8106e-02 49 1.4
241 0238 2455079.86039597 936175153 16.488 -32.619 -9.2963e-02 5.6770e-01 6.3052e-01 3.8106e-02 36 1.4
242 0239 2455079.91700502 936180044 241.291 -33.317 -1.1909e-01 7.2127e-01 6.0423e-01 3.7507e-02 20 1.8
243 0240 2455079.96408156 936184111 53.170 -4.564 -9.2963e-02 5.6770e-01 6.3052e-01 3.8106e-02 33 1.4

LIST OF HIGH ENERGY NEUTRINO CANDIDATES FOR THE 2009-2010 DATA

| | | | | | | | | | | | |
|-----|------|------------------|-----------|---------|---------|-------------|------------|------------|------------|----|-----|
| 244 | 0241 | 2455079.99178393 | 936186505 | 53.833 | -46.456 | -1.3370e-01 | 8.5313e-01 | 6.3102e-01 | 3.7539e-02 | 23 | 2.4 |
| 245 | 0242 | 2455080.26754240 | 936210330 | 304.848 | -63.157 | -1.3370e-01 | 8.5313e-01 | 6.3102e-01 | 3.7539e-02 | 65 | 2.4 |
| 246 | 0243 | 2455080.30098932 | 936213220 | 200.562 | -14.125 | -9.2963e-02 | 5.6770e-01 | 6.3052e-01 | 3.8106e-02 | 33 | 1.4 |
| 247 | 0244 | 2455080.50745682 | 936231059 | 131.300 | -53.602 | -1.1724e-01 | 4.7983e-01 | 5.2936e-01 | 3.8897e-02 | 47 | 0.9 |
| 248 | 0245 | 2455080.61428536 | 936240289 | 171.795 | 19.682 | -9.2963e-02 | 5.6770e-01 | 6.3052e-01 | 3.8106e-02 | 79 | 1.4 |
| 249 | 0246 | 2455080.65172297 | 936243523 | 346.127 | -38.193 | -1.3370e-01 | 8.5313e-01 | 6.3102e-01 | 3.7539e-02 | 25 | 2.4 |
| 250 | 0247 | 2455080.78975878 | 936255450 | 140.283 | -42.237 | -9.2963e-02 | 5.6770e-01 | 6.3052e-01 | 3.8106e-02 | 37 | 1.4 |
| 251 | 0248 | 2455080.81326229 | 936257480 | 153.269 | -48.309 | -9.2963e-02 | 5.6770e-01 | 6.3052e-01 | 3.8106e-02 | 56 | 1.4 |
| 252 | 0249 | 2455080.86532787 | 936261979 | 239.266 | 22.131 | -9.2963e-02 | 5.6770e-01 | 6.3052e-01 | 3.8106e-02 | 32 | 1.4 |
| 253 | 0250 | 2455081.03265593 | 936276436 | 316.385 | -27.710 | -9.2963e-02 | 5.6770e-01 | 6.3052e-01 | 3.8106e-02 | 36 | 1.4 |
| 254 | 0251 | 2455081.17430312 | 936288674 | 145.492 | -65.358 | -1.3370e-01 | 8.5313e-01 | 6.3102e-01 | 3.7539e-02 | 29 | 2.4 |
| 255 | 0252 | 2455081.17518076 | 936288750 | 310.872 | -35.986 | -1.3370e-01 | 8.5313e-01 | 6.3102e-01 | 3.7539e-02 | 28 | 2.4 |
| 256 | 0253 | 2455081.27522467 | 936297394 | 33.006 | -20.002 | -9.2963e-02 | 5.6770e-01 | 6.3052e-01 | 3.8106e-02 | 51 | 1.4 |
| 257 | 0254 | 2455081.36548723 | 936305193 | 352.796 | -38.440 | -9.2963e-02 | 5.6770e-01 | 6.3052e-01 | 3.8106e-02 | 55 | 1.4 |
| 258 | 0255 | 2455081.42963220 | 936310735 | 172.399 | -46.444 | -1.1724e-01 | 4.7983e-01 | 5.2936e-01 | 3.8897e-02 | 44 | 0.9 |
| 259 | 0256 | 2455081.43810186 | 936311467 | 119.039 | 16.706 | -1.1724e-01 | 4.7983e-01 | 5.2936e-01 | 3.8897e-02 | 42 | 0.9 |
| 260 | 0257 | 2455081.46934234 | 936314166 | 141.511 | 43.768 | -9.2963e-02 | 5.6770e-01 | 6.3052e-01 | 3.8106e-02 | 41 | 1.4 |
| 261 | 0258 | 2455081.75732313 | 936339047 | 350.102 | -7.725 | -1.3370e-01 | 8.5313e-01 | 6.3102e-01 | 3.7539e-02 | 30 | 2.4 |
| 262 | 0259 | 2455081.87184067 | 936348942 | 2.549 | 24.156 | -1.3370e-01 | 8.5313e-01 | 6.3102e-01 | 3.7539e-02 | 59 | 2.4 |
| 263 | 0260 | 2455082.03341998 | 936362902 | 8.738 | -11.288 | -9.2963e-02 | 5.6770e-01 | 6.3052e-01 | 3.8106e-02 | 37 | 1.4 |
| 264 | 0261 | 2455082.23583768 | 936380391 | 122.853 | 10.639 | -9.2963e-02 | 5.6770e-01 | 6.3052e-01 | 3.8106e-02 | 37 | 1.4 |
| 265 | 0262 | 2455082.28760713 | 936384864 | 21.450 | -56.564 | -1.1724e-01 | 4.7983e-01 | 5.2936e-01 | 3.8897e-02 | 63 | 0.9 |
| 266 | 0263 | 2455082.53515656 | 936406252 | 197.978 | -64.291 | -1.2873e-01 | 4.3155e-01 | 4.6595e-01 | 3.9162e-02 | 44 | 0.7 |
| 267 | 0264 | 2455082.61202671 | 936412894 | 250.676 | -9.426 | -9.2963e-02 | 5.6770e-01 | 6.3052e-01 | 3.8106e-02 | 35 | 1.4 |
| 268 | 0265 | 2455082.63848570 | 936415180 | 187.983 | 16.341 | -1.1724e-01 | 4.7983e-01 | 5.2936e-01 | 3.8897e-02 | 32 | 0.9 |
| 269 | 0266 | 2455082.67468045 | 936418307 | 274.678 | -8.183 | -9.2963e-02 | 5.6770e-01 | 6.3052e-01 | 3.8106e-02 | 38 | 1.4 |
| 270 | 0267 | 2455082.76755631 | 936426331 | 283.751 | -21.164 | -9.2963e-02 | 5.6770e-01 | 6.3052e-01 | 3.8106e-02 | 34 | 1.4 |
| 271 | 0268 | 2455082.92962440 | 936440334 | 316.109 | -67.492 | -9.2963e-02 | 5.6770e-01 | 6.3052e-01 | 3.8106e-02 | 42 | 1.4 |
| 272 | 0269 | 2455083.03701931 | 936449613 | 37.804 | -45.552 | -1.1724e-01 | 4.7983e-01 | 5.2936e-01 | 3.8897e-02 | 83 | 0.9 |
| 273 | 0270 | 2455083.05275481 | 936450973 | 5.566 | -53.262 | -1.2873e-01 | 4.3155e-01 | 4.6595e-01 | 3.9162e-02 | 60 | 0.7 |
| 274 | 0271 | 2455083.06745450 | 936452243 | 312.436 | -15.372 | -9.2963e-02 | 5.6770e-01 | 6.3052e-01 | 3.8106e-02 | 41 | 1.4 |
| 275 | 0272 | 2455083.18404952 | 936462316 | 355.395 | -3.458 | -9.2963e-02 | 5.6770e-01 | 6.3052e-01 | 3.8106e-02 | 62 | 1.4 |
| 276 | 0273 | 2455083.42293132 | 936482956 | 103.993 | 28.368 | -1.1724e-01 | 4.7983e-01 | 5.2936e-01 | 3.8897e-02 | 44 | 0.9 |
| 277 | 0274 | 2455083.50672955 | 936490196 | 196.316 | 36.018 | -1.3370e-01 | 8.5313e-01 | 6.3102e-01 | 3.7539e-02 | 29 | 2.4 |
| 278 | 0275 | 2455083.73577995 | 936509986 | 320.376 | -43.986 | -1.1724e-01 | 4.7983e-01 | 5.2936e-01 | 3.8897e-02 | 36 | 0.9 |
| 279 | 0276 | 2455083.73592252 | 936509998 | 195.708 | 8.432 | -1.1724e-01 | 4.7983e-01 | 5.2936e-01 | 3.8897e-02 | 56 | 0.9 |
| 280 | 0277 | 2455083.73668266 | 936510064 | 314.963 | 23.670 | -9.2963e-02 | 5.6770e-01 | 6.3052e-01 | 3.8106e-02 | 36 | 1.4 |
| 281 | 0278 | 2455083.80856309 | 936516274 | 220.616 | -58.925 | -1.1909e-01 | 7.2127e-01 | 6.0423e-01 | 3.7507e-02 | 31 | 1.8 |
| 282 | 0279 | 2455084.13393384 | 936544386 | 359.862 | -42.770 | -9.2963e-02 | 5.6770e-01 | 6.3052e-01 | 3.8106e-02 | 45 | 1.4 |
| 283 | 0280 | 2455084.29535617 | 936558333 | 149.835 | -40.793 | -1.1909e-01 | 7.2127e-01 | 6.0423e-01 | 3.7507e-02 | 29 | 1.8 |
| 284 | 0281 | 2455084.47954483 | 936574247 | 250.232 | -29.542 | -9.2963e-02 | 5.6770e-01 | 6.3052e-01 | 3.8106e-02 | 98 | 1.4 |
| 285 | 0282 | 2455084.52238013 | 936577948 | 86.300 | -15.433 | -9.2963e-02 | 5.6770e-01 | 6.3052e-01 | 3.8106e-02 | 50 | 1.4 |
| 286 | 0283 | 2455084.70065469 | 936593351 | 193.669 | 16.403 | -9.2963e-02 | 5.6770e-01 | 6.3052e-01 | 3.8106e-02 | 36 | 1.4 |
| 287 | 0284 | 2455084.73734402 | 936596521 | 272.373 | -12.385 | -9.2963e-02 | 5.6770e-01 | 6.3052e-01 | 3.8106e-02 | 46 | 1.4 |
| 288 | 0285 | 2455084.93151646 | 936613298 | 11.085 | -31.666 | -9.2963e-02 | 5.6770e-01 | 6.3052e-01 | 3.8106e-02 | 44 | 1.4 |
| 289 | 0286 | 2455085.02272638 | 936621178 | 284.122 | -4.322 | -9.2963e-02 | 5.6770e-01 | 6.3052e-01 | 3.8106e-02 | 80 | 1.4 |
| 290 | 0287 | 2455085.17644877 | 936634460 | 39.562 | 4.080 | -9.2963e-02 | 5.6770e-01 | 6.3052e-01 | 3.8106e-02 | 36 | 1.4 |
| 291 | 0288 | 2455085.39207416 | 936653090 | 149.682 | -9.064 | -9.2963e-02 | 5.6770e-01 | 6.3052e-01 | 3.8106e-02 | 33 | 1.4 |
| 292 | 0289 | 2455085.53667003 | 936665583 | 238.313 | 3.530 | -9.2963e-02 | 5.6770e-01 | 6.3052e-01 | 3.8106e-02 | 42 | 1.4 |
| 293 | 0290 | 2455085.63388097 | 936673982 | 223.456 | -13.145 | -9.2963e-02 | 5.6770e-01 | 6.3052e-01 | 3.8106e-02 | 68 | 1.4 |
| 294 | 0291 | 2455085.81000029 | 936689199 | 258.033 | 28.657 | -1.1724e-01 | 4.7983e-01 | 5.2936e-01 | 3.8897e-02 | 63 | 0.9 |
| 295 | 0292 | 2455085.81627549 | 936689741 | 181.333 | -81.504 | -9.2963e-02 | 5.6770e-01 | 6.3052e-01 | 3.8106e-02 | 44 | 1.4 |

| | | | | | | | | | | | |
|-----|------|------------------|-----------|---------|---------|-------------|------------|------------|------------|-----|-----|
| 296 | 0293 | 2455085.94696772 | 936701033 | 355.609 | 12.623 | -9.2963e-02 | 5.6770e-01 | 6.3052e-01 | 3.8106e-02 | 37 | 1.4 |
| 297 | 0294 | 2455085.99814372 | 936705454 | 334.364 | -73.035 | -9.2963e-02 | 5.6770e-01 | 6.3052e-01 | 3.8106e-02 | 46 | 1.4 |
| 298 | 0295 | 2455086.33772210 | 936734794 | 51.412 | -50.081 | -9.2963e-02 | 5.6770e-01 | 6.3052e-01 | 3.8106e-02 | 41 | 1.4 |
| 299 | 0296 | 2455086.35776611 | 936736525 | 115.358 | -1.712 | -9.2963e-02 | 5.6770e-01 | 6.3052e-01 | 3.8106e-02 | 43 | 1.4 |
| 300 | 0297 | 2455086.40197481 | 936740345 | 212.435 | -52.563 | -5.8944e-02 | 2.9333e-01 | 5.7306e-01 | 3.8834e-02 | 101 | 0.6 |
| 301 | 0298 | 2455086.40866353 | 936740923 | 112.413 | -1.239 | -5.8944e-02 | 2.9333e-01 | 5.7306e-01 | 3.8834e-02 | 47 | 0.6 |
| 302 | 0299 | 2455086.48541717 | 936747555 | 131.185 | -55.889 | -1.3370e-01 | 8.5313e-01 | 6.3102e-01 | 3.7539e-02 | 28 | 2.4 |
| 303 | 0300 | 2455086.51202936 | 936749854 | 91.114 | -85.172 | -1.1724e-01 | 4.7983e-01 | 5.2936e-01 | 3.8897e-02 | 61 | 0.9 |
| 304 | 0301 | 2455086.81907830 | 936776383 | 272.525 | -6.543 | -9.2963e-02 | 5.6770e-01 | 6.3052e-01 | 3.8106e-02 | 56 | 1.4 |
| 305 | 0302 | 2455087.24479815 | 936813165 | 63.225 | -16.889 | -9.2963e-02 | 5.6770e-01 | 6.3052e-01 | 3.8106e-02 | 56 | 1.4 |
| 306 | 0303 | 2455087.38036137 | 936824878 | 215.603 | -52.496 | -1.1724e-01 | 4.7983e-01 | 5.2936e-01 | 3.8897e-02 | 33 | 0.9 |
| 307 | 0304 | 2455088.42721201 | 936915326 | 91.969 | -36.275 | -9.2963e-02 | 5.6770e-01 | 6.3052e-01 | 3.8106e-02 | 40 | 1.4 |
| 308 | 0305 | 2455088.46528086 | 936918615 | 132.251 | -56.236 | -9.2963e-02 | 5.6770e-01 | 6.3052e-01 | 3.8106e-02 | 66 | 1.4 |
| 309 | 0306 | 2455088.57025334 | 936927684 | 168.350 | -16.421 | -9.2963e-02 | 5.6770e-01 | 6.3052e-01 | 3.8106e-02 | 79 | 1.4 |
| 310 | 0307 | 2455089.41468143 | 937000643 | 245.913 | -65.604 | -9.2963e-02 | 5.6770e-01 | 6.3052e-01 | 3.8106e-02 | 45 | 1.4 |
| 311 | 0308 | 2455090.05202632 | 937055710 | 343.455 | 24.853 | -9.2963e-02 | 5.6770e-01 | 6.3052e-01 | 3.8106e-02 | 38 | 1.4 |
| 312 | 0309 | 2455090.07066954 | 937057320 | 330.588 | -13.538 | -9.2963e-02 | 5.6770e-01 | 6.3052e-01 | 3.8106e-02 | 44 | 1.4 |
| 313 | 0310 | 2455090.07539159 | 937057728 | 2.778 | 6.638 | -9.2963e-02 | 5.6770e-01 | 6.3052e-01 | 3.8106e-02 | 33 | 1.4 |
| 314 | 0311 | 2455090.08057983 | 937058177 | 328.174 | 16.945 | -9.2963e-02 | 5.6770e-01 | 6.3052e-01 | 3.8106e-02 | 37 | 1.4 |
| 315 | 0312 | 2455090.11482057 | 937061135 | 307.431 | -35.535 | -9.2963e-02 | 5.6770e-01 | 6.3052e-01 | 3.8106e-02 | 42 | 1.4 |
| 316 | 0313 | 2455090.17635614 | 937066452 | 129.887 | -15.388 | -9.2963e-02 | 5.6770e-01 | 6.3052e-01 | 3.8106e-02 | 80 | 1.4 |
| 317 | 0314 | 2455090.26020686 | 937073696 | 99.595 | -63.557 | -9.2963e-02 | 5.6770e-01 | 6.3052e-01 | 3.8106e-02 | 50 | 1.4 |
| 318 | 0315 | 2455090.32316510 | 937079136 | 159.295 | 34.297 | -9.2963e-02 | 5.6770e-01 | 6.3052e-01 | 3.8106e-02 | 47 | 1.4 |
| 319 | 0316 | 2455090.41727628 | 937087267 | 202.391 | 7.376 | -9.2963e-02 | 5.6770e-01 | 6.3052e-01 | 3.8106e-02 | 45 | 1.4 |
| 320 | 0317 | 2455090.44945331 | 937090047 | 18.880 | -41.386 | -9.2963e-02 | 5.6770e-01 | 6.3052e-01 | 3.8106e-02 | 80 | 1.4 |
| 321 | 0318 | 2455090.46335818 | 937091249 | 271.916 | -31.743 | -9.2963e-02 | 5.6770e-01 | 6.3052e-01 | 3.8106e-02 | 58 | 1.4 |
| 322 | 0319 | 2455090.50333907 | 937094703 | 159.524 | -15.889 | -9.2963e-02 | 5.6770e-01 | 6.3052e-01 | 3.8106e-02 | 46 | 1.4 |
| 323 | 0320 | 2455091.11569909 | 937147611 | 181.766 | -46.886 | -9.2963e-02 | 5.6770e-01 | 6.3052e-01 | 3.8106e-02 | 39 | 1.4 |
| 324 | 0321 | 2455091.22797368 | 937157311 | 189.470 | -64.559 | -1.3370e-01 | 8.5313e-01 | 6.3102e-01 | 3.7539e-02 | 28 | 2.4 |
| 325 | 0322 | 2455091.24194602 | 937158519 | 93.087 | -30.725 | -9.2963e-02 | 5.6770e-01 | 6.3052e-01 | 3.8106e-02 | 45 | 1.4 |
| 326 | 0323 | 2455091.28544568 | 937162277 | 48.500 | 19.241 | -1.3370e-01 | 8.5313e-01 | 6.3102e-01 | 3.7539e-02 | 31 | 2.4 |
| 327 | 0324 | 2455091.41615599 | 937173570 | 324.521 | -48.735 | -1.3370e-01 | 8.5313e-01 | 6.3102e-01 | 3.7539e-02 | 24 | 2.4 |
| 328 | 0325 | 2455091.44493275 | 937176057 | 229.094 | -26.141 | -9.2963e-02 | 5.6770e-01 | 6.3052e-01 | 3.8106e-02 | 42 | 1.4 |
| 329 | 0326 | 2455091.46355564 | 937177666 | 197.124 | 6.631 | -1.3370e-01 | 8.5313e-01 | 6.3102e-01 | 3.7539e-02 | 23 | 2.4 |
| 330 | 0327 | 2455091.64030714 | 937192937 | 91.279 | -40.405 | -1.3370e-01 | 8.5313e-01 | 6.3102e-01 | 3.7539e-02 | 40 | 2.4 |
| 331 | 0328 | 2455091.76433502 | 937203653 | 187.982 | -38.231 | -1.1724e-01 | 4.7983e-01 | 5.2936e-01 | 3.8897e-02 | 36 | 0.9 |
| 332 | 0329 | 2455091.77363468 | 937204457 | 287.123 | 43.801 | -9.2963e-02 | 5.6770e-01 | 6.3052e-01 | 3.8106e-02 | 42 | 1.4 |
| 333 | 0330 | 2455092.26310601 | 937246747 | 312.379 | -64.703 | -1.3370e-01 | 8.5313e-01 | 6.3102e-01 | 3.7539e-02 | 29 | 2.4 |
| 334 | 0331 | 2455092.38553911 | 937257325 | 43.981 | -23.647 | -1.3370e-01 | 8.5313e-01 | 6.3102e-01 | 3.7539e-02 | 55 | 2.4 |
| 335 | 0332 | 2455092.57538687 | 937273728 | 293.416 | -31.917 | -9.2963e-02 | 5.6770e-01 | 6.3052e-01 | 3.8106e-02 | 57 | 1.4 |
| 336 | 0333 | 2455092.63911316 | 937279234 | 260.435 | 27.843 | -9.2963e-02 | 5.6770e-01 | 6.3052e-01 | 3.8106e-02 | 42 | 1.4 |
| 337 | 0334 | 2455092.81691255 | 937294596 | 353.786 | 12.035 | -1.3370e-01 | 8.5313e-01 | 6.3102e-01 | 3.7539e-02 | 30 | 2.4 |
| 338 | 0335 | 2455092.82023761 | 937294883 | 186.894 | -32.649 | -9.2963e-02 | 5.6770e-01 | 6.3052e-01 | 3.8106e-02 | 33 | 1.4 |
| 339 | 0336 | 2455092.90980427 | 937302622 | 315.280 | -0.447 | -1.1724e-01 | 4.7983e-01 | 5.2936e-01 | 3.8897e-02 | 46 | 0.9 |
| 340 | 0337 | 2455092.94552705 | 937305708 | 298.898 | -61.532 | -9.2963e-02 | 5.6770e-01 | 6.3052e-01 | 3.8106e-02 | 88 | 1.4 |
| 341 | 0338 | 2455093.05334004 | 937315023 | 3.893 | -7.564 | -1.2873e-01 | 4.3155e-01 | 4.6595e-01 | 3.9162e-02 | 55 | 0.7 |
| 342 | 0339 | 2455093.29306832 | 937335736 | 193.268 | -17.158 | -1.3370e-01 | 8.5313e-01 | 6.3102e-01 | 3.7539e-02 | 22 | 2.4 |
| 343 | 0340 | 2455093.32564608 | 937338550 | 90.124 | -5.205 | -9.2963e-02 | 5.6770e-01 | 6.3052e-01 | 3.8106e-02 | 44 | 1.4 |
| 344 | 0341 | 2455093.40926251 | 937345775 | 317.116 | -75.871 | -9.2963e-02 | 5.6770e-01 | 6.3052e-01 | 3.8106e-02 | 33 | 1.4 |
| 345 | 0342 | 2455093.47608774 | 937351548 | 118.676 | 19.345 | -1.1724e-01 | 4.7983e-01 | 5.2936e-01 | 3.8897e-02 | 57 | 0.9 |
| 346 | 0343 | 2455093.48161499 | 937352026 | 172.275 | 24.961 | -9.2963e-02 | 5.6770e-01 | 6.3052e-01 | 3.8106e-02 | 70 | 1.4 |
| 347 | 0344 | 2455093.72319728 | 937372899 | 210.676 | -15.984 | -9.2963e-02 | 5.6770e-01 | 6.3052e-01 | 3.8106e-02 | 42 | 1.4 |

LIST OF HIGH ENERGY NEUTRINO CANDIDATES FOR THE 2009-2010 DATA

| | | | | | | | | | | | |
|-----|------|------------------|-----------|---------|---------|-------------|------------|------------|------------|----|-----|
| 348 | 0345 | 2455093.85862360 | 937384600 | 289.632 | 28.662 | -9.2963e-02 | 5.6770e-01 | 6.3052e-01 | 3.8106e-02 | 63 | 1.4 |
| 349 | 0346 | 2455094.04037710 | 937400303 | 45.899 | 30.911 | -1.3370e-01 | 8.5313e-01 | 6.3102e-01 | 3.7539e-02 | 26 | 2.4 |
| 350 | 0347 | 2455094.09017880 | 937404606 | 73.479 | -7.003 | -1.1724e-01 | 4.7983e-01 | 5.2936e-01 | 3.8897e-02 | 40 | 0.9 |
| 351 | 0348 | 2455094.29038023 | 937421903 | 25.237 | -8.833 | -9.2963e-02 | 5.6770e-01 | 6.3052e-01 | 3.8106e-02 | 42 | 1.4 |
| 352 | 0349 | 2455094.43607690 | 937434492 | 210.009 | -52.230 | -9.2963e-02 | 5.6770e-01 | 6.3052e-01 | 3.8106e-02 | 54 | 1.4 |
| 353 | 0350 | 2455094.78884488 | 937464971 | 3.674 | -48.582 | -9.2963e-02 | 5.6770e-01 | 6.3052e-01 | 3.8106e-02 | 34 | 1.4 |
| 354 | 0351 | 2455094.92212449 | 937476486 | 353.805 | -48.761 | -1.1724e-01 | 4.7983e-01 | 5.2936e-01 | 3.8897e-02 | 51 | 0.9 |
| 355 | 0352 | 2455094.96444620 | 937480143 | 268.251 | -11.069 | -9.2963e-02 | 5.6770e-01 | 6.3052e-01 | 3.8106e-02 | 35 | 1.4 |
| 356 | 0353 | 2455095.02124958 | 937485050 | 21.663 | 1.555 | -9.2963e-02 | 5.6770e-01 | 6.3052e-01 | 3.8106e-02 | 73 | 1.4 |
| 357 | 0354 | 2455095.08594664 | 937490640 | 95.314 | -40.052 | -9.2963e-02 | 5.6770e-01 | 6.3052e-01 | 3.8106e-02 | 37 | 1.4 |
| 358 | 0355 | 2455095.31074892 | 937510063 | 5.839 | -69.210 | -9.2963e-02 | 5.6770e-01 | 6.3052e-01 | 3.8106e-02 | 44 | 1.4 |
| 359 | 0356 | 2455095.40141202 | 937517896 | 51.941 | -13.238 | -9.2963e-02 | 5.6770e-01 | 6.3052e-01 | 3.8106e-02 | 58 | 1.4 |
| 360 | 0357 | 2455096.24040858 | 937590386 | 136.272 | -47.028 | -9.2963e-02 | 5.6770e-01 | 6.3052e-01 | 3.8106e-02 | 64 | 1.4 |
| 361 | 0358 | 2455096.29589030 | 937595179 | 146.780 | -9.331 | -9.2963e-02 | 5.6770e-01 | 6.3052e-01 | 3.8106e-02 | 40 | 1.4 |
| 362 | 0359 | 2455096.41449365 | 937605427 | 104.963 | -33.021 | -9.2963e-02 | 5.6770e-01 | 6.3052e-01 | 3.8106e-02 | 55 | 1.4 |
| 363 | 0360 | 2455096.52800333 | 937615234 | 128.593 | -29.992 | -9.2963e-02 | 5.6770e-01 | 6.3052e-01 | 3.8106e-02 | 32 | 1.4 |
| 364 | 0361 | 2455096.68391567 | 937628705 | 141.312 | -39.629 | -9.2963e-02 | 5.6770e-01 | 6.3052e-01 | 3.8106e-02 | 70 | 1.4 |
| 365 | 0362 | 2455097.45008271 | 937694902 | 228.978 | -38.159 | -9.2963e-02 | 5.6770e-01 | 6.3052e-01 | 3.8106e-02 | 32 | 1.4 |
| 366 | 0363 | 2455097.56872116 | 937705152 | 193.538 | -2.264 | -9.2963e-02 | 5.6770e-01 | 6.3052e-01 | 3.8106e-02 | 56 | 1.4 |
| 367 | 0364 | 2455098.16288293 | 937756488 | 148.194 | -4.399 | -9.2963e-02 | 5.6770e-01 | 6.3052e-01 | 3.8106e-02 | 35 | 1.4 |
| 368 | 0365 | 2455098.54092366 | 937789150 | 192.691 | 14.963 | -9.2963e-02 | 5.6770e-01 | 6.3052e-01 | 3.8106e-02 | 40 | 1.4 |
| 369 | 0366 | 2455098.68646128 | 937801725 | 240.770 | 35.351 | -9.2963e-02 | 5.6770e-01 | 6.3052e-01 | 3.8106e-02 | 48 | 1.4 |
| 370 | 0367 | 2455098.91636730 | 937821589 | 351.543 | 3.824 | -9.2963e-02 | 5.6770e-01 | 6.3052e-01 | 3.8106e-02 | 36 | 1.4 |
| 371 | 0368 | 2455099.24073472 | 937849614 | 18.588 | -14.617 | -1.3370e-01 | 8.5313e-01 | 6.3102e-01 | 3.7539e-02 | 30 | 2.4 |
| 372 | 0369 | 2455099.59653242 | 937880355 | 296.078 | 0.247 | -9.2963e-02 | 5.6770e-01 | 6.3052e-01 | 3.8106e-02 | 52 | 1.4 |
| 373 | 0370 | 2455099.63512643 | 937883689 | 175.922 | 0.378 | -9.2963e-02 | 5.6770e-01 | 6.3052e-01 | 3.8106e-02 | 45 | 1.4 |
| 374 | 0371 | 2455099.79334823 | 937897360 | 93.697 | -49.992 | -1.1724e-01 | 4.7983e-01 | 5.2936e-01 | 3.8897e-02 | 40 | 0.9 |
| 375 | 0372 | 2455102.27178044 | 938111496 | 200.139 | -27.965 | -9.2963e-02 | 5.6770e-01 | 6.3052e-01 | 3.8106e-02 | 75 | 1.4 |
| 376 | 0373 | 2455102.27805785 | 938112039 | 67.798 | 22.646 | -9.2963e-02 | 5.6770e-01 | 6.3052e-01 | 3.8106e-02 | 37 | 1.4 |
| 377 | 0374 | 2455102.35356275 | 938118562 | 132.628 | -14.614 | -9.2963e-02 | 5.6770e-01 | 6.3052e-01 | 3.8106e-02 | 40 | 1.4 |
| 378 | 0375 | 2455102.39752847 | 938122361 | 175.148 | 35.082 | -9.2963e-02 | 5.6770e-01 | 6.3052e-01 | 3.8106e-02 | 41 | 1.4 |
| 379 | 0376 | 2455103.04918244 | 938178664 | 356.482 | -3.559 | -9.2963e-02 | 5.6770e-01 | 6.3052e-01 | 3.8106e-02 | 32 | 1.4 |
| 380 | 0377 | 2455103.40413438 | 938209332 | 278.252 | -36.117 | -9.2963e-02 | 5.6770e-01 | 6.3052e-01 | 3.8106e-02 | 38 | 1.4 |
| 381 | 0378 | 2455103.58586945 | 938225034 | 282.729 | -79.220 | -1.3370e-01 | 8.5313e-01 | 6.3102e-01 | 3.7539e-02 | 29 | 2.4 |
| 382 | 0379 | 2455103.78034553 | 938241836 | 204.419 | -18.149 | -9.2963e-02 | 5.6770e-01 | 6.3052e-01 | 3.8106e-02 | 36 | 1.4 |
| 383 | 0380 | 2455103.88545957 | 938250918 | 15.509 | 1.608 | -9.2963e-02 | 5.6770e-01 | 6.3052e-01 | 3.8106e-02 | 52 | 1.4 |
| 384 | 0381 | 2455103.94084063 | 938255703 | 45.803 | 30.019 | -9.2963e-02 | 5.6770e-01 | 6.3052e-01 | 3.8106e-02 | 47 | 1.4 |
| 385 | 0382 | 2455104.04120529 | 938264375 | 53.910 | -56.310 | -1.2873e-01 | 4.3155e-01 | 4.6595e-01 | 3.9162e-02 | 60 | 0.7 |
| 386 | 0383 | 2455104.16566846 | 938275128 | 288.279 | -56.157 | -9.2963e-02 | 5.6770e-01 | 6.3052e-01 | 3.8106e-02 | 74 | 1.4 |
| 387 | 0384 | 2455104.20894439 | 938278867 | 210.871 | -51.328 | -1.1724e-01 | 4.7983e-01 | 5.2936e-01 | 3.8897e-02 | 59 | 0.9 |
| 388 | 0385 | 2455104.23098445 | 938280772 | 63.085 | -23.178 | -9.2963e-02 | 5.6770e-01 | 6.3052e-01 | 3.8106e-02 | 33 | 1.4 |
| 389 | 0386 | 2455104.48051724 | 938302331 | 226.405 | -28.934 | -9.2963e-02 | 5.6770e-01 | 6.3052e-01 | 3.8106e-02 | 38 | 1.4 |
| 390 | 0387 | 2455104.68229967 | 938319765 | 288.159 | -42.235 | -1.1724e-01 | 4.7983e-01 | 5.2936e-01 | 3.8897e-02 | 75 | 0.9 |
| 391 | 0388 | 2455104.70328215 | 938321578 | 307.095 | -6.614 | -1.1724e-01 | 4.7983e-01 | 5.2936e-01 | 3.8897e-02 | 37 | 0.9 |
| 392 | 0389 | 2455104.90458370 | 938338971 | 8.751 | -29.573 | -9.2963e-02 | 5.6770e-01 | 6.3052e-01 | 3.8106e-02 | 51 | 1.4 |
| 393 | 0390 | 2455105.26904169 | 938370460 | 135.057 | -0.240 | -9.2963e-02 | 5.6770e-01 | 6.3052e-01 | 3.8106e-02 | 52 | 1.4 |
| 394 | 0391 | 2455105.47162534 | 938387963 | 76.853 | -23.921 | -1.3370e-01 | 8.5313e-01 | 6.3102e-01 | 3.7539e-02 | 24 | 2.4 |
| 395 | 0392 | 2455105.47359406 | 938388133 | 169.350 | 6.763 | -1.1724e-01 | 4.7983e-01 | 5.2936e-01 | 3.8897e-02 | 37 | 0.9 |
| 396 | 0393 | 2455105.69289356 | 938407081 | 331.632 | -21.688 | -9.2963e-02 | 5.6770e-01 | 6.3052e-01 | 3.8106e-02 | 62 | 1.4 |
| 397 | 0394 | 2455106.09898691 | 938442167 | 349.394 | -64.148 | -1.3370e-01 | 8.5313e-01 | 6.3102e-01 | 3.7539e-02 | 30 | 2.4 |
| 398 | 0395 | 2455106.10501045 | 938442687 | 97.016 | -14.779 | -1.3370e-01 | 8.5313e-01 | 6.3102e-01 | 3.7539e-02 | 17 | 2.4 |
| 399 | 0396 | 2455106.13841955 | 938445574 | 20.880 | -34.063 | -1.3370e-01 | 8.5313e-01 | 6.3102e-01 | 3.7539e-02 | 18 | 2.4 |

| | | | | | | | | | | | |
|-----|------|------------------|-----------|---------|---------|-------------|------------|------------|------------|----|-----|
| 400 | 0397 | 2455106.15760056 | 938447231 | 111.651 | -66.684 | -9.2963e-02 | 5.6770e-01 | 6.3052e-01 | 3.8106e-02 | 33 | 1.4 |
| 401 | 0398 | 2455106.15804839 | 938447270 | 308.309 | -35.751 | -1.1724e-01 | 4.7983e-01 | 5.2936e-01 | 3.8897e-02 | 55 | 0.9 |
| 402 | 0399 | 2455106.33725387 | 938462753 | 69.956 | 18.560 | -1.3370e-01 | 8.5313e-01 | 6.3102e-01 | 3.7539e-02 | 29 | 2.4 |
| 403 | 0400 | 2455106.33770698 | 938462792 | 35.802 | -64.301 | -9.2963e-02 | 5.6770e-01 | 6.3052e-01 | 3.8106e-02 | 57 | 1.4 |
| 404 | 0401 | 2455106.38053544 | 938466493 | 230.019 | -43.933 | -1.1724e-01 | 4.7983e-01 | 5.2936e-01 | 3.8897e-02 | 35 | 0.9 |
| 405 | 0402 | 2455106.41301495 | 938469299 | 303.756 | -66.111 | -9.2963e-02 | 5.6770e-01 | 6.3052e-01 | 3.8106e-02 | 67 | 1.4 |
| 406 | 0403 | 2455106.43796736 | 938471455 | 173.146 | 22.524 | -9.2963e-02 | 5.6770e-01 | 6.3052e-01 | 3.8106e-02 | 35 | 1.4 |
| 407 | 0404 | 2455106.59420504 | 938484954 | 267.949 | 15.123 | -1.3370e-01 | 8.5313e-01 | 6.3102e-01 | 3.7539e-02 | 30 | 2.4 |
| 408 | 0405 | 2455106.59899067 | 938485367 | 186.962 | -13.071 | -1.3370e-01 | 8.5313e-01 | 6.3102e-01 | 3.7539e-02 | 20 | 2.4 |
| 409 | 0406 | 2455106.67855854 | 938492242 | 28.342 | -53.398 | -1.3370e-01 | 8.5313e-01 | 6.3102e-01 | 3.7539e-02 | 24 | 2.4 |
| 410 | 0407 | 2455106.68526612 | 938492821 | 183.389 | -35.410 | -1.3370e-01 | 8.5313e-01 | 6.3102e-01 | 3.7539e-02 | 27 | 2.4 |
| 411 | 0408 | 2455106.75716598 | 938499034 | 204.453 | -8.382 | -1.3370e-01 | 8.5313e-01 | 6.3102e-01 | 3.7539e-02 | 27 | 2.4 |
| 412 | 0409 | 2455106.93284884 | 938514213 | 6.804 | 17.120 | -9.2963e-02 | 5.6770e-01 | 6.3052e-01 | 3.8106e-02 | 41 | 1.4 |
| 413 | 0410 | 2455106.94926794 | 938515631 | 275.171 | -49.706 | -1.3370e-01 | 8.5313e-01 | 6.3102e-01 | 3.7539e-02 | 31 | 2.4 |
| 414 | 0411 | 2455107.06586108 | 938525705 | 200.162 | -51.684 | -9.2963e-02 | 5.6770e-01 | 6.3052e-01 | 3.8106e-02 | 50 | 1.4 |
| 415 | 0412 | 2455107.06993162 | 938526057 | 89.805 | -19.215 | -1.3370e-01 | 8.5313e-01 | 6.3102e-01 | 3.7539e-02 | 26 | 2.4 |
| 416 | 0413 | 2455107.16309664 | 938534106 | 113.966 | -2.746 | -1.3370e-01 | 8.5313e-01 | 6.3102e-01 | 3.7539e-02 | 29 | 2.4 |
| 417 | 0414 | 2455107.22904195 | 938539804 | 47.678 | -1.816 | -9.2963e-02 | 5.6770e-01 | 6.3052e-01 | 3.8106e-02 | 33 | 1.4 |
| 418 | 0415 | 2455107.24446919 | 938541137 | 29.501 | 5.593 | -9.2963e-02 | 5.6770e-01 | 6.3052e-01 | 3.8106e-02 | 52 | 1.4 |
| 419 | 0416 | 2455107.73067877 | 938583145 | 163.598 | -27.937 | -1.3370e-01 | 8.5313e-01 | 6.3102e-01 | 3.7539e-02 | 30 | 2.4 |
| 420 | 0417 | 2455107.74286200 | 938584198 | 15.701 | -15.867 | -9.2963e-02 | 5.6770e-01 | 6.3052e-01 | 3.8106e-02 | 52 | 1.4 |
| 421 | 0418 | 2455108.09088190 | 938614267 | 210.184 | -75.982 | -1.1909e-01 | 7.2127e-01 | 6.0423e-01 | 3.7507e-02 | 26 | 1.8 |
| 422 | 0419 | 2455108.13113839 | 938617745 | 76.988 | -27.793 | -1.1909e-01 | 7.2127e-01 | 6.0423e-01 | 3.7507e-02 | 27 | 1.8 |
| 423 | 0420 | 2455108.65188488 | 938662737 | 302.757 | 8.166 | -9.2963e-02 | 5.6770e-01 | 6.3052e-01 | 3.8106e-02 | 34 | 1.4 |
| 424 | 0421 | 2455108.72213116 | 938668807 | 254.230 | -49.669 | -1.1724e-01 | 4.7983e-01 | 5.2936e-01 | 3.8897e-02 | 69 | 0.9 |
| 425 | 0422 | 2455108.77672014 | 938673523 | 233.790 | 16.947 | -1.3370e-01 | 8.5313e-01 | 6.3102e-01 | 3.7539e-02 | 19 | 2.4 |
| 426 | 0423 | 2455108.93658872 | 938687336 | 88.782 | -11.029 | -9.2963e-02 | 5.6770e-01 | 6.3052e-01 | 3.8106e-02 | 38 | 1.4 |
| 427 | 0424 | 2455108.94028716 | 938687655 | 302.904 | 11.418 | -1.3370e-01 | 8.5313e-01 | 6.3102e-01 | 3.7539e-02 | 30 | 2.4 |
| 428 | 0425 | 2455109.04694551 | 938696871 | 277.608 | -35.585 | -9.2963e-02 | 5.6770e-01 | 6.3052e-01 | 3.8106e-02 | 34 | 1.4 |
| 429 | 0426 | 2455109.27708373 | 938716755 | 42.313 | 12.270 | -9.2963e-02 | 5.6770e-01 | 6.3052e-01 | 3.8106e-02 | 63 | 1.4 |
| 430 | 0427 | 2455109.27978510 | 938716988 | 81.125 | 24.193 | -1.1724e-01 | 4.7983e-01 | 5.2936e-01 | 3.8897e-02 | 60 | 0.9 |
| 431 | 0428 | 2455109.30529717 | 938719192 | 245.768 | -54.777 | -9.2963e-02 | 5.6770e-01 | 6.3052e-01 | 3.8106e-02 | 48 | 1.4 |
| 432 | 0429 | 2455109.32126382 | 938720572 | 111.881 | 7.221 | -1.1724e-01 | 4.7983e-01 | 5.2936e-01 | 3.8897e-02 | 46 | 0.9 |
| 433 | 0430 | 2455109.50827962 | 938736730 | 97.654 | -76.296 | -9.2963e-02 | 5.6770e-01 | 6.3052e-01 | 3.8106e-02 | 37 | 1.4 |
| 434 | 0431 | 2455109.64102689 | 938748199 | 150.037 | -53.125 | -9.2963e-02 | 5.6770e-01 | 6.3052e-01 | 3.8106e-02 | 28 | 1.4 |
| 435 | 0432 | 2455109.70997371 | 938754156 | 240.039 | -55.760 | -1.3370e-01 | 8.5313e-01 | 6.3102e-01 | 3.7539e-02 | 28 | 2.4 |
| 436 | 0433 | 2455109.78012252 | 938760217 | 191.092 | -76.308 | -9.2963e-02 | 5.6770e-01 | 6.3052e-01 | 3.8106e-02 | 48 | 1.4 |
| 437 | 0434 | 2455109.95262540 | 938775121 | 307.876 | 27.691 | -9.2963e-02 | 5.6770e-01 | 6.3052e-01 | 3.8106e-02 | 38 | 1.4 |
| 438 | 0435 | 2455110.35278849 | 938809695 | 0.831 | -83.787 | -9.2963e-02 | 5.6770e-01 | 6.3052e-01 | 3.8106e-02 | 36 | 1.4 |
| 439 | 0436 | 2455110.39121065 | 938813015 | 231.918 | -15.213 | -9.2963e-02 | 5.6770e-01 | 6.3052e-01 | 3.8106e-02 | 70 | 1.4 |
| 440 | 0437 | 2455110.75548297 | 938844488 | 15.339 | -17.305 | -1.3370e-01 | 8.5313e-01 | 6.3102e-01 | 3.7539e-02 | 24 | 2.4 |
| 441 | 0438 | 2455110.76066198 | 938844936 | 77.634 | -68.946 | -1.1724e-01 | 4.7983e-01 | 5.2936e-01 | 3.8897e-02 | 58 | 0.9 |
| 442 | 0439 | 2455110.80497928 | 938848765 | 314.592 | -2.379 | -1.1724e-01 | 4.7983e-01 | 5.2936e-01 | 3.8897e-02 | 85 | 0.9 |
| 443 | 0440 | 2455110.91119889 | 938857942 | 262.753 | 2.770 | -1.3370e-01 | 8.5313e-01 | 6.3102e-01 | 3.7539e-02 | 25 | 2.4 |
| 444 | 0441 | 2455110.99633956 | 938865298 | 78.485 | 25.500 | -1.3370e-01 | 8.5313e-01 | 6.3102e-01 | 3.7539e-02 | 45 | 2.4 |
| 445 | 0442 | 2455111.07609910 | 938872189 | 62.979 | -7.400 | -1.1724e-01 | 4.7983e-01 | 5.2936e-01 | 3.8897e-02 | 42 | 0.9 |
| 446 | 0443 | 2455111.29796803 | 938891359 | 209.033 | -50.034 | -1.3370e-01 | 8.5313e-01 | 6.3102e-01 | 3.7539e-02 | 25 | 2.4 |
| 447 | 0444 | 2455111.31306605 | 938892663 | 224.628 | -12.990 | -1.3370e-01 | 8.5313e-01 | 6.3102e-01 | 3.7539e-02 | 26 | 2.4 |
| 448 | 0445 | 2455111.34094428 | 938895072 | 177.023 | -21.854 | -1.1724e-01 | 4.7983e-01 | 5.2936e-01 | 3.8897e-02 | 43 | 0.9 |
| 449 | 0446 | 2455111.52696723 | 938911144 | 221.214 | -20.684 | -1.2873e-01 | 4.3155e-01 | 4.6595e-01 | 3.9162e-02 | 77 | 0.7 |
| 450 | 0447 | 2455112.40857237 | 938987315 | 233.452 | -14.584 | -1.2873e-01 | 4.3155e-01 | 4.6595e-01 | 3.9162e-02 | 45 | 0.7 |
| 451 | 0448 | 2455112.49756440 | 938995004 | 126.204 | -2.166 | -9.2963e-02 | 5.6770e-01 | 6.3052e-01 | 3.8106e-02 | 35 | 1.4 |

LIST OF HIGH ENERGY NEUTRINO CANDIDATES FOR THE 2009-2010 DATA

| | | | | | | | | | | | |
|-----|------|------------------|-----------|---------|---------|-------------|------------|------------|------------|----|-----|
| 452 | 0449 | 2455112.67848511 | 939010636 | 173.150 | -48.876 | -9.2963e-02 | 5.6770e-01 | 6.3052e-01 | 3.8106e-02 | 54 | 1.4 |
| 453 | 0450 | 2455112.80672018 | 939021715 | 200.152 | -36.498 | -9.2963e-02 | 5.6770e-01 | 6.3052e-01 | 3.8106e-02 | 54 | 1.4 |
| 454 | 0451 | 2455112.94746167 | 939033875 | 107.088 | -34.198 | -9.2963e-02 | 5.6770e-01 | 6.3052e-01 | 3.8106e-02 | 42 | 1.4 |
| 455 | 0452 | 2455113.29913474 | 939064260 | 146.416 | 39.410 | -9.2963e-02 | 5.6770e-01 | 6.3052e-01 | 3.8106e-02 | 49 | 1.4 |
| 456 | 0453 | 2455113.52092373 | 939083422 | 170.341 | 6.919 | -9.2963e-02 | 5.6770e-01 | 6.3052e-01 | 3.8106e-02 | 46 | 1.4 |
| 457 | 0454 | 2455113.66173084 | 939095588 | 356.420 | -35.023 | -9.2963e-02 | 5.6770e-01 | 6.3052e-01 | 3.8106e-02 | 40 | 1.4 |
| 458 | 0455 | 2455113.74950718 | 939103172 | 24.051 | -14.475 | -9.2963e-02 | 5.6770e-01 | 6.3052e-01 | 3.8106e-02 | 25 | 1.4 |
| 459 | 0456 | 2455113.87727032 | 939114211 | 72.400 | -22.222 | -1.1909e-01 | 7.2127e-01 | 6.0423e-01 | 3.7507e-02 | 29 | 1.8 |
| 460 | 0457 | 2455114.02079491 | 939126611 | 14.529 | -34.800 | -9.2963e-02 | 5.6770e-01 | 6.3052e-01 | 3.8106e-02 | 41 | 1.4 |
| 461 | 0458 | 2455114.08210711 | 939131909 | 131.171 | -56.990 | -9.2963e-02 | 5.6770e-01 | 6.3052e-01 | 3.8106e-02 | 39 | 1.4 |
| 462 | 0459 | 2455114.10003122 | 939133457 | 149.562 | -23.916 | -9.2963e-02 | 5.6770e-01 | 6.3052e-01 | 3.8106e-02 | 46 | 1.4 |
| 463 | 0460 | 2455114.47014329 | 939165435 | 171.940 | -58.800 | -1.1724e-01 | 4.7983e-01 | 5.2936e-01 | 3.8897e-02 | 72 | 0.9 |
| 464 | 0461 | 2455114.48221273 | 939166478 | 330.533 | -41.798 | -1.3370e-01 | 8.5313e-01 | 6.3102e-01 | 3.7539e-02 | 23 | 2.4 |
| 465 | 0462 | 2455114.61945104 | 939178335 | 299.100 | -24.130 | -1.1724e-01 | 4.7983e-01 | 5.2936e-01 | 3.8897e-02 | 46 | 0.9 |
| 466 | 0463 | 2455114.96373037 | 939208081 | 23.482 | -38.374 | -9.2963e-02 | 5.6770e-01 | 6.3052e-01 | 3.8106e-02 | 56 | 1.4 |
| 467 | 0464 | 2455115.20252461 | 939228713 | 7.009 | -12.443 | -9.2963e-02 | 5.6770e-01 | 6.3052e-01 | 3.8106e-02 | 33 | 1.4 |
| 468 | 0465 | 2455115.25815626 | 939233519 | 122.012 | 5.774 | -9.2963e-02 | 5.6770e-01 | 6.3052e-01 | 3.8106e-02 | 40 | 1.4 |
| 469 | 0466 | 2455115.69694165 | 939271430 | 243.642 | -31.468 | -9.2963e-02 | 5.6770e-01 | 6.3052e-01 | 3.8106e-02 | 45 | 1.4 |
| 470 | 0467 | 2455115.73724370 | 939274912 | 339.596 | 30.885 | -9.2963e-02 | 5.6770e-01 | 6.3052e-01 | 3.8106e-02 | 34 | 1.4 |
| 471 | 0468 | 2455115.77108010 | 939277836 | 251.583 | -16.284 | -1.3370e-01 | 8.5313e-01 | 6.3102e-01 | 3.7539e-02 | 29 | 2.4 |
| 472 | 0469 | 2455115.85696732 | 939285256 | 14.422 | 1.130 | -9.2963e-02 | 5.6770e-01 | 6.3052e-01 | 3.8106e-02 | 34 | 1.4 |
| 473 | 0470 | 2455115.96788788 | 939294840 | 278.270 | -83.675 | -9.2963e-02 | 5.6770e-01 | 6.3052e-01 | 3.8106e-02 | 41 | 1.4 |
| 474 | 0471 | 2455115.96792188 | 939294843 | 237.923 | -69.630 | -1.3370e-01 | 8.5313e-01 | 6.3102e-01 | 3.7539e-02 | 30 | 2.4 |
| 475 | 0472 | 2455116.24429123 | 939318721 | 194.052 | -28.568 | -9.2963e-02 | 5.6770e-01 | 6.3052e-01 | 3.8106e-02 | 40 | 1.4 |
| 476 | 0473 | 2455116.42582425 | 939334406 | 351.379 | -55.731 | -9.2963e-02 | 5.6770e-01 | 6.3052e-01 | 3.8106e-02 | 56 | 1.4 |
| 477 | 0474 | 2455116.42960646 | 939334732 | 209.405 | -17.414 | -9.2963e-02 | 5.6770e-01 | 6.3052e-01 | 3.8106e-02 | 57 | 1.4 |
| 478 | 0475 | 2455116.59190139 | 939348755 | 164.209 | -70.024 | -9.2963e-02 | 5.6770e-01 | 6.3052e-01 | 3.8106e-02 | 53 | 1.4 |
| 479 | 0476 | 2455116.66839094 | 939355363 | 205.711 | -67.549 | -9.2963e-02 | 5.6770e-01 | 6.3052e-01 | 3.8106e-02 | 46 | 1.4 |
| 480 | 0477 | 2455116.72638818 | 939360374 | 89.399 | -46.879 | -9.2963e-02 | 5.6770e-01 | 6.3052e-01 | 3.8106e-02 | 41 | 1.4 |
| 481 | 0478 | 2455116.75696082 | 939363016 | 217.008 | -18.117 | -9.2963e-02 | 5.6770e-01 | 6.3052e-01 | 3.8106e-02 | 87 | 1.4 |
| 482 | 0479 | 2455116.91970536 | 939377077 | 299.273 | -34.680 | -9.2963e-02 | 5.6770e-01 | 6.3052e-01 | 3.8106e-02 | 40 | 1.4 |
| 483 | 0480 | 2455116.96917723 | 939381351 | 297.645 | -0.251 | -9.2963e-02 | 5.6770e-01 | 6.3052e-01 | 3.8106e-02 | 54 | 1.4 |
| 484 | 0481 | 2455117.11302713 | 939393780 | 58.528 | -35.957 | -1.1724e-01 | 4.7983e-01 | 5.2936e-01 | 3.8897e-02 | 44 | 0.9 |
| 485 | 0482 | 2455117.13440548 | 939395627 | 220.053 | -52.071 | -1.1724e-01 | 4.7983e-01 | 5.2936e-01 | 3.8897e-02 | 37 | 0.9 |
| 486 | 0483 | 2455117.30518671 | 939410383 | 87.764 | -69.789 | -9.2963e-02 | 5.6770e-01 | 6.3052e-01 | 3.8106e-02 | 42 | 1.4 |
| 487 | 0484 | 2455117.39428554 | 939418081 | 51.843 | -27.383 | -1.3370e-01 | 8.5313e-01 | 6.3102e-01 | 3.7539e-02 | 23 | 2.4 |
| 488 | 0485 | 2455117.41056783 | 939419488 | 62.812 | -23.353 | -9.2963e-02 | 5.6770e-01 | 6.3052e-01 | 3.8106e-02 | 42 | 1.4 |
| 489 | 0486 | 2455117.43264564 | 939421395 | 86.844 | -31.075 | -9.2963e-02 | 5.6770e-01 | 6.3052e-01 | 3.8106e-02 | 36 | 1.4 |
| 490 | 0487 | 2455117.44347119 | 939422330 | 222.113 | -20.451 | -1.2873e-01 | 4.3155e-01 | 4.6595e-01 | 3.9162e-02 | 46 | 0.7 |
| 491 | 0488 | 2455117.47784299 | 939425300 | 147.514 | 33.030 | -9.2963e-02 | 5.6770e-01 | 6.3052e-01 | 3.8106e-02 | 58 | 1.4 |
| 492 | 0489 | 2455117.58490281 | 939434550 | 301.777 | 10.870 | -9.2963e-02 | 5.6770e-01 | 6.3052e-01 | 3.8106e-02 | 37 | 1.4 |
| 493 | 0490 | 2455117.99339341 | 939469844 | 291.060 | -38.797 | -9.2963e-02 | 5.6770e-01 | 6.3052e-01 | 3.8106e-02 | 32 | 1.4 |
| 494 | 0491 | 2455118.09652087 | 939478754 | 339.369 | -46.066 | -9.2963e-02 | 5.6770e-01 | 6.3052e-01 | 3.8106e-02 | 37 | 1.4 |
| 495 | 0492 | 2455118.18926273 | 939486767 | 89.990 | -53.063 | -9.2963e-02 | 5.6770e-01 | 6.3052e-01 | 3.8106e-02 | 53 | 1.4 |
| 496 | 0493 | 2455118.71224171 | 939531952 | 10.798 | -7.637 | -9.2963e-02 | 5.6770e-01 | 6.3052e-01 | 3.8106e-02 | 40 | 1.4 |
| 497 | 0494 | 2455118.78390243 | 939538144 | 353.904 | 15.452 | -9.2963e-02 | 5.6770e-01 | 6.3052e-01 | 3.8106e-02 | 61 | 1.4 |
| 498 | 0495 | 2455118.82267344 | 939541493 | 283.496 | -49.890 | -1.1909e-01 | 7.2127e-01 | 6.0423e-01 | 3.7507e-02 | 27 | 1.8 |
| 499 | 0496 | 2455118.83480135 | 939542541 | 31.539 | -29.662 | -1.1724e-01 | 4.7983e-01 | 5.2936e-01 | 3.8897e-02 | 69 | 0.9 |
| 500 | 0497 | 2455118.93664650 | 939551341 | 345.681 | -26.193 | -1.1724e-01 | 4.7983e-01 | 5.2936e-01 | 3.8897e-02 | 56 | 0.9 |
| 501 | 0498 | 2455118.95626420 | 939553036 | 0.772 | 26.750 | -9.2963e-02 | 5.6770e-01 | 6.3052e-01 | 3.8106e-02 | 44 | 1.4 |
| 502 | 0499 | 2455118.98722376 | 939555711 | 31.086 | 44.150 | -1.3370e-01 | 8.5313e-01 | 6.3102e-01 | 3.7539e-02 | 28 | 2.4 |
| 503 | 0500 | 2455119.06038976 | 939562032 | 107.194 | -46.814 | -1.1724e-01 | 4.7983e-01 | 5.2936e-01 | 3.8897e-02 | 43 | 0.9 |

| | | | | | | | | | | | |
|-----|------|------------------|-----------|---------|---------|-------------|------------|------------|------------|-----|-----|
| 504 | 0501 | 2455119.10381960 | 939565785 | 111.700 | -29.431 | -1.1724e-01 | 4.7983e-01 | 5.2936e-01 | 3.8897e-02 | 52 | 0.9 |
| 505 | 0502 | 2455119.23430143 | 939577058 | 98.321 | 19.419 | -9.2963e-02 | 5.6770e-01 | 6.3052e-01 | 3.8106e-02 | 79 | 1.4 |
| 506 | 0503 | 2455119.50723823 | 939600640 | 117.050 | -25.781 | -9.2963e-02 | 5.6770e-01 | 6.3052e-01 | 3.8106e-02 | 36 | 1.4 |
| 507 | 0504 | 2455119.54814882 | 939604175 | 128.668 | -73.127 | -1.3370e-01 | 8.5313e-01 | 6.3102e-01 | 3.7539e-02 | 31 | 2.4 |
| 508 | 0505 | 2455119.60944940 | 939609471 | 103.082 | -79.016 | -1.3370e-01 | 8.5313e-01 | 6.3102e-01 | 3.7539e-02 | 26 | 2.4 |
| 509 | 0506 | 2455119.66618321 | 939614373 | 288.891 | 10.154 | -1.3370e-01 | 8.5313e-01 | 6.3102e-01 | 3.7539e-02 | 27 | 2.4 |
| 510 | 0507 | 2455119.80532641 | 939626395 | 339.224 | -13.088 | -9.2963e-02 | 5.6770e-01 | 6.3052e-01 | 3.8106e-02 | 55 | 1.4 |
| 511 | 0508 | 2455119.85847406 | 939630987 | 13.254 | -22.584 | -9.2963e-02 | 5.6770e-01 | 6.3052e-01 | 3.8106e-02 | 32 | 1.4 |
| 512 | 0509 | 2455119.87126979 | 939632092 | 301.247 | -15.812 | -9.2963e-02 | 5.6770e-01 | 6.3052e-01 | 3.8106e-02 | 100 | 1.4 |
| 513 | 0510 | 2455120.14462516 | 939655710 | 38.322 | 27.279 | -9.2963e-02 | 5.6770e-01 | 6.3052e-01 | 3.8106e-02 | 73 | 1.4 |
| 514 | 0511 | 2455120.43275522 | 939680605 | 214.461 | -53.564 | -1.1724e-01 | 4.7983e-01 | 5.2936e-01 | 3.8897e-02 | 53 | 0.9 |
| 515 | 0512 | 2455120.47931155 | 939684627 | 333.194 | -46.537 | -1.1724e-01 | 4.7983e-01 | 5.2936e-01 | 3.8897e-02 | 77 | 0.9 |
| 516 | 0513 | 2455120.49385715 | 939685884 | 227.452 | 45.373 | -9.2963e-02 | 5.6770e-01 | 6.3052e-01 | 3.8106e-02 | 39 | 1.4 |
| 517 | 0514 | 2455120.69817599 | 939703537 | 6.947 | -61.248 | -9.2963e-02 | 5.6770e-01 | 6.3052e-01 | 3.8106e-02 | 35 | 1.4 |
| 518 | 0515 | 2455120.73808635 | 939706985 | 234.113 | -47.606 | -9.2963e-02 | 5.6770e-01 | 6.3052e-01 | 3.8106e-02 | 38 | 1.4 |
| 519 | 0516 | 2455120.81641992 | 939713753 | 294.394 | 24.516 | -9.2963e-02 | 5.6770e-01 | 6.3052e-01 | 3.8106e-02 | 35 | 1.4 |
| 520 | 0517 | 2455120.89703852 | 939720719 | 256.611 | -70.079 | -1.1724e-01 | 4.7983e-01 | 5.2936e-01 | 3.8897e-02 | 33 | 0.9 |
| 521 | 0518 | 2455120.98134161 | 939728002 | 90.085 | 22.423 | -1.1724e-01 | 4.7983e-01 | 5.2936e-01 | 3.8897e-02 | 50 | 0.9 |
| 522 | 0519 | 2455121.18227442 | 939745363 | 162.392 | -43.568 | -1.3370e-01 | 8.5313e-01 | 6.3102e-01 | 3.7539e-02 | 31 | 2.4 |
| 523 | 0520 | 2455121.33633591 | 939758674 | 90.349 | 5.215 | -1.1724e-01 | 4.7983e-01 | 5.2936e-01 | 3.8897e-02 | 34 | 0.9 |
| 524 | 0521 | 2455121.77626935 | 939796684 | 280.168 | -57.413 | -1.1724e-01 | 4.7983e-01 | 5.2936e-01 | 3.8897e-02 | 72 | 0.9 |
| 525 | 0522 | 2455121.92770574 | 939809768 | 46.175 | -18.464 | -9.2963e-02 | 5.6770e-01 | 6.3052e-01 | 3.8106e-02 | 41 | 1.4 |
| 526 | 0523 | 2455122.35754073 | 939846906 | 121.636 | 5.775 | -9.2963e-02 | 5.6770e-01 | 6.3052e-01 | 3.8106e-02 | 36 | 1.4 |
| 527 | 0524 | 2455122.53895372 | 939862580 | 233.077 | -7.957 | -1.1724e-01 | 4.7983e-01 | 5.2936e-01 | 3.8897e-02 | 37 | 0.9 |
| 528 | 0525 | 2455122.88976745 | 939892890 | 21.355 | -24.817 | -1.1724e-01 | 4.7983e-01 | 5.2936e-01 | 3.8897e-02 | 26 | 0.9 |
| 529 | 0526 | 2455122.96905831 | 939899741 | 349.006 | 31.298 | -9.2963e-02 | 5.6770e-01 | 6.3052e-01 | 3.8106e-02 | 64 | 1.4 |
| 530 | 0527 | 2455123.17154615 | 939917236 | 250.627 | -48.299 | -9.2963e-02 | 5.6770e-01 | 6.3052e-01 | 3.8106e-02 | 68 | 1.4 |
| 531 | 0528 | 2455123.31624400 | 939929738 | 165.563 | -5.823 | -1.1909e-01 | 7.2127e-01 | 6.0423e-01 | 3.7507e-02 | 30 | 1.8 |
| 532 | 0529 | 2455123.43635652 | 939940116 | 273.038 | -58.888 | -9.2963e-02 | 5.6770e-01 | 6.3052e-01 | 3.8106e-02 | 53 | 1.4 |
| 533 | 0530 | 2455123.50894756 | 939946388 | 121.026 | -53.723 | -9.2963e-02 | 5.6770e-01 | 6.3052e-01 | 3.8106e-02 | 34 | 1.4 |
| 534 | 0531 | 2455123.77341984 | 939969238 | 242.247 | -78.692 | -9.2963e-02 | 5.6770e-01 | 6.3052e-01 | 3.8106e-02 | 42 | 1.4 |
| 535 | 0532 | 2455123.81395575 | 939972740 | 0.505 | -50.354 | -1.1724e-01 | 4.7983e-01 | 5.2936e-01 | 3.8897e-02 | 58 | 0.9 |
| 536 | 0533 | 2455123.84153899 | 939975123 | 3.414 | 14.939 | -9.2963e-02 | 5.6770e-01 | 6.3052e-01 | 3.8106e-02 | 34 | 1.4 |
| 537 | 0534 | 2455124.41617295 | 940024772 | 218.431 | 17.849 | -9.2963e-02 | 5.6770e-01 | 6.3052e-01 | 3.8106e-02 | 53 | 1.4 |
| 538 | 0535 | 2455124.42550676 | 940025578 | 278.630 | -23.522 | -9.2963e-02 | 5.6770e-01 | 6.3052e-01 | 3.8106e-02 | 80 | 1.4 |
| 539 | 0536 | 2455124.66281391 | 940046082 | 246.738 | -75.528 | -1.1724e-01 | 4.7983e-01 | 5.2936e-01 | 3.8897e-02 | 55 | 0.9 |
| 540 | 0537 | 2455124.73301856 | 940052147 | 308.761 | -75.284 | -9.2963e-02 | 5.6770e-01 | 6.3052e-01 | 3.8106e-02 | 78 | 1.4 |
| 541 | 0538 | 2455124.89469364 | 940066116 | 320.685 | -33.509 | -9.2963e-02 | 5.6770e-01 | 6.3052e-01 | 3.8106e-02 | 39 | 1.4 |
| 542 | 0539 | 2455124.99847915 | 940075083 | 51.269 | -66.319 | -1.3370e-01 | 8.5313e-01 | 6.3102e-01 | 3.7539e-02 | 21 | 2.4 |
| 543 | 0540 | 2455125.05026863 | 940079558 | 3.031 | -9.007 | -9.2963e-02 | 5.6770e-01 | 6.3052e-01 | 3.8106e-02 | 32 | 1.4 |
| 544 | 0541 | 2455125.13125508 | 940086555 | 31.563 | 8.618 | -9.2963e-02 | 5.6770e-01 | 6.3052e-01 | 3.8106e-02 | 34 | 1.4 |
| 545 | 0542 | 2455125.17651380 | 940090465 | 346.590 | -53.355 | -1.1909e-01 | 7.2127e-01 | 6.0423e-01 | 3.7507e-02 | 31 | 1.8 |
| 546 | 0543 | 2455125.54695083 | 940122471 | 210.268 | -65.801 | -1.3370e-01 | 8.5313e-01 | 6.3102e-01 | 3.7539e-02 | 23 | 2.4 |
| 547 | 0544 | 2455125.67692770 | 940133701 | 243.164 | 16.606 | -9.2963e-02 | 5.6770e-01 | 6.3052e-01 | 3.8106e-02 | 39 | 1.4 |
| 548 | 0545 | 2455125.78264708 | 940142835 | 9.373 | -49.397 | -1.1724e-01 | 4.7983e-01 | 5.2936e-01 | 3.8897e-02 | 58 | 0.9 |
| 549 | 0546 | 2455125.82050078 | 940146106 | 271.614 | -68.371 | -9.2963e-02 | 5.6770e-01 | 6.3052e-01 | 3.8106e-02 | 36 | 1.4 |
| 550 | 0547 | 2455125.86797558 | 940150208 | 26.170 | 39.099 | -9.2963e-02 | 5.6770e-01 | 6.3052e-01 | 3.8106e-02 | 40 | 1.4 |
| 551 | 0548 | 2455126.16958920 | 940176267 | 26.159 | -3.051 | -9.2963e-02 | 5.6770e-01 | 6.3052e-01 | 3.8106e-02 | 44 | 1.4 |
| 552 | 0549 | 2455126.57395115 | 940211204 | 277.858 | 31.085 | -1.1724e-01 | 4.7983e-01 | 5.2936e-01 | 3.8897e-02 | 45 | 0.9 |
| 553 | 0550 | 2455126.84745015 | 940234834 | 42.955 | 21.035 | -1.1909e-01 | 7.2127e-01 | 6.0423e-01 | 3.7507e-02 | 26 | 1.8 |
| 554 | 0551 | 2455126.89342438 | 940238806 | 104.686 | -34.039 | -1.1724e-01 | 4.7983e-01 | 5.2936e-01 | 3.8897e-02 | 53 | 0.9 |
| 555 | 0552 | 2455126.90883151 | 940240138 | 40.048 | -63.297 | -9.2963e-02 | 5.6770e-01 | 6.3052e-01 | 3.8106e-02 | 41 | 1.4 |

LIST OF HIGH ENERGY NEUTRINO CANDIDATES FOR THE 2009-2010 DATA

| | | | | | | | | | | | |
|-----|------|------------------|-----------|---------|---------|-------------|------------|------------|------------|----|-----|
| 556 | 0553 | 2455127.62431524 | 940301955 | 276.272 | 9.594 | -1.2873e-01 | 4.3155e-01 | 4.6595e-01 | 3.9162e-02 | 64 | 0.7 |
| 557 | 0554 | 2455127.70146982 | 940308621 | 40.170 | -42.834 | -1.1724e-01 | 4.7983e-01 | 5.2936e-01 | 3.8897e-02 | 37 | 0.9 |
| 558 | 0555 | 2455127.78941914 | 940316220 | 317.629 | 37.671 | -1.1724e-01 | 4.7983e-01 | 5.2936e-01 | 3.8897e-02 | 47 | 0.9 |
| 559 | 0556 | 2455128.37791950 | 940367067 | 226.634 | -67.325 | -9.2963e-02 | 5.6770e-01 | 6.3052e-01 | 3.8106e-02 | 41 | 1.4 |
| 560 | 0557 | 2455128.48421007 | 940376250 | 332.441 | -29.655 | -9.2963e-02 | 5.6770e-01 | 6.3052e-01 | 3.8106e-02 | 45 | 1.4 |
| 561 | 0558 | 2455128.49604244 | 940377273 | 222.078 | 42.240 | -9.2963e-02 | 5.6770e-01 | 6.3052e-01 | 3.8106e-02 | 57 | 1.4 |
| 562 | 0559 | 2455128.87890660 | 940410352 | 33.977 | -13.513 | -9.2963e-02 | 5.6770e-01 | 6.3052e-01 | 3.8106e-02 | 34 | 1.4 |
| 563 | 0560 | 2455128.94782299 | 940416306 | 82.861 | -28.278 | -1.1724e-01 | 4.7983e-01 | 5.2936e-01 | 3.8897e-02 | 45 | 0.9 |
| 564 | 0561 | 2455128.99911445 | 940420738 | 28.863 | 39.702 | -9.2963e-02 | 5.6770e-01 | 6.3052e-01 | 3.8106e-02 | 48 | 1.4 |
| 565 | 0562 | 2455129.23151505 | 940440817 | 63.399 | -53.583 | -9.2963e-02 | 5.6770e-01 | 6.3052e-01 | 3.8106e-02 | 36 | 1.4 |
| 566 | 0563 | 2455129.24410961 | 940441906 | 6.151 | -58.770 | -1.3370e-01 | 8.5313e-01 | 6.3102e-01 | 3.7539e-02 | 21 | 2.4 |
| 567 | 0564 | 2455129.42888012 | 940457870 | 165.708 | -58.167 | -1.3370e-01 | 8.5313e-01 | 6.3102e-01 | 3.7539e-02 | 25 | 2.4 |
| 568 | 0565 | 2455129.46803809 | 940461253 | 26.096 | -57.126 | -1.3370e-01 | 8.5313e-01 | 6.3102e-01 | 3.7539e-02 | 47 | 2.4 |
| 569 | 0566 | 2455129.63331953 | 940475533 | 260.848 | -32.698 | -1.3370e-01 | 8.5313e-01 | 6.3102e-01 | 3.7539e-02 | 36 | 2.4 |
| 570 | 0567 | 2455129.74693742 | 940485350 | 166.756 | -58.293 | -9.2963e-02 | 5.6770e-01 | 6.3052e-01 | 3.8106e-02 | 52 | 1.4 |
| 571 | 0568 | 2455129.85060141 | 940494306 | 65.732 | -60.227 | -9.2963e-02 | 5.6770e-01 | 6.3052e-01 | 3.8106e-02 | 43 | 1.4 |
| 572 | 0569 | 2455129.97996590 | 940505484 | 212.346 | -48.187 | -1.1724e-01 | 4.7983e-01 | 5.2936e-01 | 3.8897e-02 | 34 | 0.9 |
| 573 | 0570 | 2455130.04261403 | 940510896 | 313.204 | -18.608 | -1.3370e-01 | 8.5313e-01 | 6.3102e-01 | 3.7539e-02 | 21 | 2.4 |
| 574 | 0571 | 2455130.71697979 | 940569162 | 276.164 | 0.823 | -1.1724e-01 | 4.7983e-01 | 5.2936e-01 | 3.8897e-02 | 44 | 0.9 |
| 575 | 0572 | 2455130.73928354 | 940571089 | 342.991 | -32.316 | -1.1724e-01 | 4.7983e-01 | 5.2936e-01 | 3.8897e-02 | 42 | 0.9 |
| 576 | 0573 | 2455130.90883162 | 940585738 | 90.482 | -23.827 | -9.2963e-02 | 5.6770e-01 | 6.3052e-01 | 3.8106e-02 | 94 | 1.4 |
| 577 | 0574 | 2455131.04302858 | 940597332 | 149.284 | -3.053 | -1.3370e-01 | 8.5313e-01 | 6.3102e-01 | 3.7539e-02 | 26 | 2.4 |
| 578 | 0575 | 2455131.09322920 | 940601670 | 25.112 | 15.380 | -9.2963e-02 | 5.6770e-01 | 6.3052e-01 | 3.8106e-02 | 46 | 1.4 |
| 579 | 0576 | 2455131.09736405 | 940602027 | 330.097 | -22.425 | -1.3370e-01 | 8.5313e-01 | 6.3102e-01 | 3.7539e-02 | 26 | 2.4 |
| 580 | 0577 | 2455131.10132227 | 940602369 | 70.967 | 24.886 | -9.2963e-02 | 5.6770e-01 | 6.3052e-01 | 3.8106e-02 | 40 | 1.4 |
| 581 | 0578 | 2455131.13305411 | 940605110 | 21.637 | -26.976 | -1.1724e-01 | 4.7983e-01 | 5.2936e-01 | 3.8897e-02 | 61 | 0.9 |
| 582 | 0579 | 2455131.46665416 | 940633933 | 27.225 | -51.185 | -1.1724e-01 | 4.7983e-01 | 5.2936e-01 | 3.8897e-02 | 84 | 0.9 |
| 583 | 0580 | 2455131.50656328 | 940637382 | 218.474 | 32.134 | -9.2963e-02 | 5.6770e-01 | 6.3052e-01 | 3.8106e-02 | 45 | 1.4 |
| 584 | 0581 | 2455131.73572846 | 940657181 | 268.470 | 29.503 | -9.2963e-02 | 5.6770e-01 | 6.3052e-01 | 3.8106e-02 | 67 | 1.4 |
| 585 | 0582 | 2455132.41269022 | 940715671 | 91.722 | -16.046 | -9.2963e-02 | 5.6770e-01 | 6.3052e-01 | 3.8106e-02 | 52 | 1.4 |
| 586 | 0583 | 2455132.71350595 | 940741661 | 230.084 | -2.542 | -9.2963e-02 | 5.6770e-01 | 6.3052e-01 | 3.8106e-02 | 40 | 1.4 |
| 587 | 0584 | 2455133.24511799 | 940787593 | 34.831 | -10.815 | -9.2963e-02 | 5.6770e-01 | 6.3052e-01 | 3.8106e-02 | 36 | 1.4 |
| 588 | 0585 | 2455133.86701904 | 940841325 | 181.531 | -53.320 | -1.3370e-01 | 8.5313e-01 | 6.3102e-01 | 3.7539e-02 | 29 | 2.4 |
| 589 | 0586 | 2455133.87178621 | 940841737 | 346.348 | -25.473 | -1.1724e-01 | 4.7983e-01 | 5.2936e-01 | 3.8897e-02 | 79 | 0.9 |
| 590 | 0587 | 2455133.93840643 | 940847493 | 359.884 | -8.175 | -9.2963e-02 | 5.6770e-01 | 6.3052e-01 | 3.8106e-02 | 66 | 1.4 |
| 591 | 0588 | 2455133.94025409 | 940847652 | 217.462 | -56.767 | -9.2963e-02 | 5.6770e-01 | 6.3052e-01 | 3.8106e-02 | 70 | 1.4 |
| 592 | 0589 | 2455133.94301469 | 940847891 | 317.600 | -33.199 | -9.2963e-02 | 5.6770e-01 | 6.3052e-01 | 3.8106e-02 | 66 | 1.4 |
| 593 | 0590 | 2455134.88193759 | 940929014 | 334.006 | 10.852 | -9.2963e-02 | 5.6770e-01 | 6.3052e-01 | 3.8106e-02 | 42 | 1.4 |
| 594 | 0591 | 2455135.17944633 | 940954719 | 171.056 | -40.090 | -1.3370e-01 | 8.5313e-01 | 6.3102e-01 | 3.7539e-02 | 29 | 2.4 |
| 595 | 0592 | 2455135.27592074 | 940963054 | 136.558 | 34.198 | -9.2963e-02 | 5.6770e-01 | 6.3052e-01 | 3.8106e-02 | 39 | 1.4 |
| 596 | 0593 | 2455135.30288916 | 940965384 | 134.181 | -41.672 | -1.1724e-01 | 4.7983e-01 | 5.2936e-01 | 3.8897e-02 | 51 | 0.9 |
| 597 | 0594 | 2455136.66749813 | 941083286 | 251.830 | 22.254 | -9.2963e-02 | 5.6770e-01 | 6.3052e-01 | 3.8106e-02 | 42 | 1.4 |
| 598 | 0595 | 2455136.73338158 | 941088979 | 267.951 | -18.728 | -9.2963e-02 | 5.6770e-01 | 6.3052e-01 | 3.8106e-02 | 43 | 1.4 |
| 599 | 0596 | 2455136.90881518 | 941104136 | 325.566 | 29.975 | -9.2963e-02 | 5.6770e-01 | 6.3052e-01 | 3.8106e-02 | 39 | 1.4 |
| 600 | 0597 | 2455137.01383289 | 941113210 | 107.265 | -21.099 | -1.1724e-01 | 4.7983e-01 | 5.2936e-01 | 3.8897e-02 | 89 | 0.9 |
| 601 | 0598 | 2455137.05125840 | 941116443 | 356.996 | 18.432 | -1.3370e-01 | 8.5313e-01 | 6.3102e-01 | 3.7539e-02 | 14 | 2.4 |
| 602 | 0599 | 2455137.40940642 | 941147387 | 194.166 | 38.150 | -1.1724e-01 | 4.7983e-01 | 5.2936e-01 | 3.8897e-02 | 53 | 0.9 |
| 603 | 0600 | 2455138.07224381 | 941204656 | 45.023 | -73.484 | -1.1724e-01 | 4.7983e-01 | 5.2936e-01 | 3.8897e-02 | 29 | 0.9 |
| 604 | 0601 | 2455138.22964691 | 941218256 | 187.377 | 22.481 | -9.2963e-02 | 5.6770e-01 | 6.3052e-01 | 3.8106e-02 | 54 | 1.4 |
| 605 | 0602 | 2455138.49297261 | 941241007 | 319.308 | -68.022 | -9.2963e-02 | 5.6770e-01 | 6.3052e-01 | 3.8106e-02 | 41 | 1.4 |
| 606 | 0603 | 2455138.66407874 | 941255791 | 259.420 | 15.133 | -9.2963e-02 | 5.6770e-01 | 6.3052e-01 | 3.8106e-02 | 32 | 1.4 |
| 607 | 0604 | 2455138.70878856 | 941259654 | 305.961 | -56.371 | -9.2963e-02 | 5.6770e-01 | 6.3052e-01 | 3.8106e-02 | 53 | 1.4 |

| | | | | | | | | | | | |
|-----|------|------------------|-----------|---------|---------|-------------|------------|------------|------------|----|-----|
| 608 | 0605 | 2455138.80484908 | 941267953 | 267.146 | 6.146 | -9.2963e-02 | 5.6770e-01 | 6.3052e-01 | 3.8106e-02 | 44 | 1.4 |
| 609 | 0606 | 2455139.17659348 | 941300072 | 188.397 | -18.520 | -9.2963e-02 | 5.6770e-01 | 6.3052e-01 | 3.8106e-02 | 33 | 1.4 |
| 610 | 0607 | 2455139.38663643 | 941318220 | 301.403 | -39.883 | -9.2963e-02 | 5.6770e-01 | 6.3052e-01 | 3.8106e-02 | 33 | 1.4 |
| 611 | 0608 | 2455139.55354005 | 941332640 | 120.588 | -45.707 | -9.2963e-02 | 5.6770e-01 | 6.3052e-01 | 3.8106e-02 | 32 | 1.4 |
| 612 | 0609 | 2455139.67658649 | 941343272 | 288.496 | -10.161 | -9.2963e-02 | 5.6770e-01 | 6.3052e-01 | 3.8106e-02 | 48 | 1.4 |
| 613 | 0610 | 2455139.84273192 | 941357627 | 30.147 | 4.845 | -9.2963e-02 | 5.6770e-01 | 6.3052e-01 | 3.8106e-02 | 37 | 1.4 |
| 614 | 0611 | 2455139.93447511 | 941365553 | 288.410 | -34.817 | -1.2873e-01 | 4.3155e-01 | 4.6595e-01 | 3.9162e-02 | 38 | 0.7 |
| 615 | 0612 | 2455139.97019810 | 941368640 | 65.107 | 37.544 | -9.2963e-02 | 5.6770e-01 | 6.3052e-01 | 3.8106e-02 | 54 | 1.4 |
| 616 | 0613 | 2455140.06783770 | 941377076 | 11.931 | 19.418 | -9.2963e-02 | 5.6770e-01 | 6.3052e-01 | 3.8106e-02 | 39 | 1.4 |
| 617 | 0614 | 2455140.20084105 | 941388567 | 10.769 | -43.905 | -9.2963e-02 | 5.6770e-01 | 6.3052e-01 | 3.8106e-02 | 56 | 1.4 |
| 618 | 0615 | 2455140.23956732 | 941391913 | 108.903 | -17.148 | -9.2963e-02 | 5.6770e-01 | 6.3052e-01 | 3.8106e-02 | 38 | 1.4 |
| 619 | 0616 | 2455140.25011695 | 941392825 | 200.972 | -60.354 | -1.1724e-01 | 4.7983e-01 | 5.2936e-01 | 3.8897e-02 | 36 | 0.9 |
| 620 | 0617 | 2455140.56937111 | 941420408 | 289.436 | -42.581 | -1.1724e-01 | 4.7983e-01 | 5.2936e-01 | 3.8897e-02 | 48 | 0.9 |
| 621 | 0618 | 2455140.62746823 | 941425428 | 348.550 | -19.841 | -9.2963e-02 | 5.6770e-01 | 6.3052e-01 | 3.8106e-02 | 38 | 1.4 |
| 622 | 0619 | 2455140.99363963 | 941457065 | 38.911 | 23.479 | -1.3370e-01 | 8.5313e-01 | 6.3102e-01 | 3.7539e-02 | 24 | 2.4 |
| 623 | 0620 | 2455176.36060023 | 944512770 | 195.011 | -32.392 | -9.2963e-02 | 5.6770e-01 | 6.3052e-01 | 3.8106e-02 | 46 | 1.4 |
| 624 | 0621 | 2455176.40237466 | 944516380 | 359.823 | -65.837 | -9.2963e-02 | 5.6770e-01 | 6.3052e-01 | 3.8106e-02 | 46 | 1.4 |
| 625 | 0622 | 2455176.46654245 | 944521924 | 257.082 | 4.281 | -1.1724e-01 | 4.7983e-01 | 5.2936e-01 | 3.8897e-02 | 46 | 0.9 |
| 626 | 0623 | 2455176.60589619 | 944533964 | 303.881 | -8.242 | -1.1724e-01 | 4.7983e-01 | 5.2936e-01 | 3.8897e-02 | 49 | 0.9 |
| 627 | 0624 | 2455177.03758351 | 944571262 | 72.237 | 24.741 | -9.2963e-02 | 5.6770e-01 | 6.3052e-01 | 3.8106e-02 | 44 | 1.4 |
| 628 | 0625 | 2455177.29581319 | 944593573 | 250.629 | -28.328 | -9.2963e-02 | 5.6770e-01 | 6.3052e-01 | 3.8106e-02 | 36 | 1.4 |
| 629 | 0626 | 2455177.37983646 | 944600832 | 264.444 | 2.125 | -9.2963e-02 | 5.6770e-01 | 6.3052e-01 | 3.8106e-02 | 31 | 1.4 |
| 630 | 0627 | 2455177.47043999 | 944608661 | 185.947 | 16.929 | -1.3370e-01 | 8.5313e-01 | 6.3102e-01 | 3.7539e-02 | 25 | 2.4 |
| 631 | 0628 | 2455177.49870100 | 944611102 | 257.049 | -46.286 | -1.1724e-01 | 4.7983e-01 | 5.2936e-01 | 3.8897e-02 | 42 | 0.9 |
| 632 | 0629 | 2455177.68067624 | 944626825 | 328.826 | 1.137 | -9.2963e-02 | 5.6770e-01 | 6.3052e-01 | 3.8106e-02 | 49 | 1.4 |
| 633 | 0630 | 2455177.73889666 | 944631855 | 48.550 | -8.711 | -1.3370e-01 | 8.5313e-01 | 6.3102e-01 | 3.7539e-02 | 26 | 2.4 |
| 634 | 0631 | 2455177.96495108 | 944651386 | 250.890 | -56.828 | -1.1724e-01 | 4.7983e-01 | 5.2936e-01 | 3.8897e-02 | 36 | 0.9 |
| 635 | 0632 | 2455178.07888863 | 944661230 | 162.809 | 0.994 | -1.1724e-01 | 4.7983e-01 | 5.2936e-01 | 3.8897e-02 | 42 | 0.9 |
| 636 | 0633 | 2455178.08458527 | 944661723 | 104.357 | 21.695 | -9.2963e-02 | 5.6770e-01 | 6.3052e-01 | 3.8106e-02 | 33 | 1.4 |
| 637 | 0634 | 2455178.65448253 | 944710962 | 285.130 | -27.855 | -1.1724e-01 | 4.7983e-01 | 5.2936e-01 | 3.8897e-02 | 67 | 0.9 |
| 638 | 0635 | 2455178.66430116 | 944711810 | 301.419 | -0.560 | -1.1724e-01 | 4.7983e-01 | 5.2936e-01 | 3.8897e-02 | 68 | 0.9 |
| 639 | 0636 | 2455178.76675491 | 944720662 | 318.784 | -31.718 | -9.2963e-02 | 5.6770e-01 | 6.3052e-01 | 3.8106e-02 | 32 | 1.4 |
| 640 | 0637 | 2455178.87802147 | 944730276 | 13.866 | 32.173 | -9.2963e-02 | 5.6770e-01 | 6.3052e-01 | 3.8106e-02 | 53 | 1.4 |
| 641 | 0638 | 2455179.05028598 | 944745159 | 10.291 | -78.284 | -9.2963e-02 | 5.6770e-01 | 6.3052e-01 | 3.8106e-02 | 42 | 1.4 |
| 642 | 0639 | 2455179.40395461 | 944775716 | 93.361 | -46.081 | -9.2963e-02 | 5.6770e-01 | 6.3052e-01 | 3.8106e-02 | 39 | 1.4 |
| 643 | 0640 | 2455179.40550306 | 944775850 | 97.663 | -46.538 | -9.2963e-02 | 5.6770e-01 | 6.3052e-01 | 3.8106e-02 | 40 | 1.4 |
| 644 | 0641 | 2455179.56627066 | 944789740 | 301.081 | 32.891 | -9.2963e-02 | 5.6770e-01 | 6.3052e-01 | 3.8106e-02 | 48 | 1.4 |
| 645 | 0642 | 2455179.58936774 | 944791736 | 212.966 | -3.599 | -1.3370e-01 | 8.5313e-01 | 6.3102e-01 | 3.7539e-02 | 27 | 2.4 |
| 646 | 0643 | 2455179.73058975 | 944803937 | 87.161 | -14.830 | -9.2963e-02 | 5.6770e-01 | 6.3052e-01 | 3.8106e-02 | 45 | 1.4 |
| 647 | 0644 | 2455179.84496806 | 944813820 | 310.268 | -36.443 | -9.2963e-02 | 5.6770e-01 | 6.3052e-01 | 3.8106e-02 | 34 | 1.4 |
| 648 | 0645 | 2455179.85397646 | 944814598 | 207.057 | -49.995 | -9.2963e-02 | 5.6770e-01 | 6.3052e-01 | 3.8106e-02 | 73 | 1.4 |
| 649 | 0646 | 2455180.06707255 | 944833010 | 74.832 | 19.767 | -1.3370e-01 | 8.5313e-01 | 6.3102e-01 | 3.7539e-02 | 31 | 2.4 |
| 650 | 0647 | 2455180.27510587 | 944850984 | 30.776 | -51.459 | -1.2873e-01 | 4.3155e-01 | 4.6595e-01 | 3.9162e-02 | 66 | 0.7 |
| 651 | 0648 | 2455180.32389121 | 944855199 | 175.448 | 18.109 | -1.1724e-01 | 4.7983e-01 | 5.2936e-01 | 3.8897e-02 | 46 | 0.9 |
| 652 | 0649 | 2455180.64733940 | 944883145 | 128.707 | -53.534 | -1.1724e-01 | 4.7983e-01 | 5.2936e-01 | 3.8897e-02 | 35 | 0.9 |
| 653 | 0650 | 2455180.87835807 | 944903105 | 127.231 | -43.494 | -9.2963e-02 | 5.6770e-01 | 6.3052e-01 | 3.8106e-02 | 56 | 1.4 |
| 654 | 0651 | 2455180.88672615 | 944903828 | 334.541 | -32.892 | -9.2963e-02 | 5.6770e-01 | 6.3052e-01 | 3.8106e-02 | 37 | 1.4 |
| 655 | 0652 | 2455180.98455891 | 944912280 | 53.371 | -21.714 | -1.1724e-01 | 4.7983e-01 | 5.2936e-01 | 3.8897e-02 | 36 | 0.9 |
| 656 | 0653 | 2455181.06941845 | 944919612 | 169.837 | -35.463 | -9.2963e-02 | 5.6770e-01 | 6.3052e-01 | 3.8106e-02 | 33 | 1.4 |
| 657 | 0654 | 2455181.10539858 | 944922721 | 98.553 | 14.371 | -9.2963e-02 | 5.6770e-01 | 6.3052e-01 | 3.8106e-02 | 37 | 1.4 |
| 658 | 0655 | 2455181.11092318 | 944923198 | 197.227 | -62.747 | -9.2963e-02 | 5.6770e-01 | 6.3052e-01 | 3.8106e-02 | 42 | 1.4 |
| 659 | 0656 | 2455181.25572826 | 944935709 | 54.726 | -75.030 | -9.2963e-02 | 5.6770e-01 | 6.3052e-01 | 3.8106e-02 | 43 | 1.4 |

LIST OF HIGH ENERGY NEUTRINO CANDIDATES FOR THE 2009-2010 DATA

| | | | | | | | | | | | |
|-----|------|------------------|-----------|---------|---------|-------------|------------|------------|------------|-----|-----|
| 660 | 0657 | 2455181.26114534 | 944936177 | 224.202 | 15.433 | -1.1724e-01 | 4.7983e-01 | 5.2936e-01 | 3.8897e-02 | 35 | 0.9 |
| 661 | 0658 | 2455181.27213487 | 944937127 | 221.375 | -39.836 | -9.2963e-02 | 5.6770e-01 | 6.3052e-01 | 3.8106e-02 | 39 | 1.4 |
| 662 | 0659 | 2455181.39615310 | 944947842 | 331.913 | -18.848 | -9.2963e-02 | 5.6770e-01 | 6.3052e-01 | 3.8106e-02 | 63 | 1.4 |
| 663 | 0660 | 2455181.43261759 | 944950993 | 249.079 | -9.585 | -9.2963e-02 | 5.6770e-01 | 6.3052e-01 | 3.8106e-02 | 42 | 1.4 |
| 664 | 0661 | 2455181.52212712 | 944958726 | 203.664 | 4.713 | -9.2963e-02 | 5.6770e-01 | 6.3052e-01 | 3.8106e-02 | 35 | 1.4 |
| 665 | 0662 | 2455181.52726115 | 944959170 | 303.200 | 15.620 | -1.3370e-01 | 8.5313e-01 | 6.3102e-01 | 3.7539e-02 | 29 | 2.4 |
| 666 | 0663 | 2455181.68452047 | 944972757 | 66.048 | -55.284 | -9.2963e-02 | 5.6770e-01 | 6.3052e-01 | 3.8106e-02 | 44 | 1.4 |
| 667 | 0664 | 2455181.80611859 | 944983263 | 93.140 | -38.941 | -9.2963e-02 | 5.6770e-01 | 6.3052e-01 | 3.8106e-02 | 46 | 1.4 |
| 668 | 0665 | 2455181.81130490 | 944983711 | 278.108 | -41.385 | -9.2963e-02 | 5.6770e-01 | 6.3052e-01 | 3.8106e-02 | 49 | 1.4 |
| 669 | 0666 | 2455181.88721786 | 944990270 | 50.770 | 1.863 | -1.1909e-01 | 7.2127e-01 | 6.0423e-01 | 3.7507e-02 | 27 | 1.8 |
| 670 | 0667 | 2455181.96213342 | 944996743 | 256.497 | -62.777 | -1.1909e-01 | 7.2127e-01 | 6.0423e-01 | 3.7507e-02 | 52 | 1.8 |
| 671 | 0668 | 2455182.25901530 | 945022393 | 280.095 | -52.426 | -9.2963e-02 | 5.6770e-01 | 6.3052e-01 | 3.8106e-02 | 41 | 1.4 |
| 672 | 0669 | 2455182.37235249 | 945032186 | 280.887 | -0.198 | -9.2963e-02 | 5.6770e-01 | 6.3052e-01 | 3.8106e-02 | 46 | 1.4 |
| 673 | 0670 | 2455182.42272247 | 945036538 | 180.013 | -86.062 | -1.3370e-01 | 8.5313e-01 | 6.3102e-01 | 3.7539e-02 | 21 | 2.4 |
| 674 | 0671 | 2455182.55033348 | 945047563 | 359.212 | -53.044 | -1.1724e-01 | 4.7983e-01 | 5.2936e-01 | 3.8897e-02 | 53 | 0.9 |
| 675 | 0672 | 2455182.88636941 | 945076597 | 20.025 | 14.276 | -1.3370e-01 | 8.5313e-01 | 6.3102e-01 | 3.7539e-02 | 30 | 2.4 |
| 676 | 0673 | 2455182.91177126 | 945078792 | 340.218 | -37.075 | -9.2963e-02 | 5.6770e-01 | 6.3052e-01 | 3.8106e-02 | 32 | 1.4 |
| 677 | 0674 | 2455182.92972610 | 945080343 | 175.828 | -26.912 | -9.2963e-02 | 5.6770e-01 | 6.3052e-01 | 3.8106e-02 | 42 | 1.4 |
| 678 | 0675 | 2455182.95503343 | 945082529 | 27.317 | 28.658 | -9.2963e-02 | 5.6770e-01 | 6.3052e-01 | 3.8106e-02 | 52 | 1.4 |
| 679 | 0676 | 2455182.99577626 | 945086050 | 163.523 | 3.164 | -9.2963e-02 | 5.6770e-01 | 6.3052e-01 | 3.8106e-02 | 46 | 1.4 |
| 680 | 0677 | 2455183.31495369 | 945113626 | 107.294 | -16.030 | -9.2963e-02 | 5.6770e-01 | 6.3052e-01 | 3.8106e-02 | 27 | 1.4 |
| 681 | 0678 | 2455183.60883661 | 945139018 | 198.168 | -27.954 | -9.2963e-02 | 5.6770e-01 | 6.3052e-01 | 3.8106e-02 | 46 | 1.4 |
| 682 | 0679 | 2455183.72978068 | 945149468 | 293.436 | -33.187 | -9.2963e-02 | 5.6770e-01 | 6.3052e-01 | 3.8106e-02 | 39 | 1.4 |
| 683 | 0680 | 2455183.75057692 | 945151264 | 295.289 | -49.467 | -9.2963e-02 | 5.6770e-01 | 6.3052e-01 | 3.8106e-02 | 35 | 1.4 |
| 684 | 0681 | 2455184.30304891 | 945198998 | 131.205 | 1.572 | -5.8944e-02 | 2.9333e-01 | 5.7306e-01 | 3.8834e-02 | 101 | 0.6 |
| 685 | 0682 | 2455184.30656651 | 945199302 | 155.365 | -12.477 | -1.3370e-01 | 8.5313e-01 | 6.3102e-01 | 3.7539e-02 | 19 | 2.4 |
| 686 | 0683 | 2455184.44487798 | 945211252 | 175.855 | -48.298 | -9.2963e-02 | 5.6770e-01 | 6.3052e-01 | 3.8106e-02 | 33 | 1.4 |
| 687 | 0684 | 2455184.47752719 | 945214073 | 225.544 | 35.043 | -9.2963e-02 | 5.6770e-01 | 6.3052e-01 | 3.8106e-02 | 51 | 1.4 |
| 688 | 0685 | 2455184.48765474 | 945214948 | 119.704 | -52.224 | -9.2963e-02 | 5.6770e-01 | 6.3052e-01 | 3.8106e-02 | 46 | 1.4 |
| 689 | 0686 | 2455184.53726252 | 945219234 | 323.409 | -52.930 | -1.2873e-01 | 4.3155e-01 | 4.6595e-01 | 3.9162e-02 | 54 | 0.7 |
| 690 | 0687 | 2455184.69114048 | 945232529 | 333.907 | -3.422 | -1.1724e-01 | 4.7983e-01 | 5.2936e-01 | 3.8897e-02 | 50 | 0.9 |
| 691 | 0688 | 2455184.73246867 | 945236100 | 307.564 | 17.928 | -9.2963e-02 | 5.6770e-01 | 6.3052e-01 | 3.8106e-02 | 55 | 1.4 |
| 692 | 0689 | 2455184.99949594 | 945259171 | 267.437 | -73.667 | -9.2963e-02 | 5.6770e-01 | 6.3052e-01 | 3.8106e-02 | 44 | 1.4 |
| 693 | 0690 | 2455185.01604326 | 945260601 | 37.022 | 6.420 | -9.2963e-02 | 5.6770e-01 | 6.3052e-01 | 3.8106e-02 | 39 | 1.4 |
| 694 | 0691 | 2455185.02234563 | 945261145 | 176.017 | 16.588 | -1.3370e-01 | 8.5313e-01 | 6.3102e-01 | 3.7539e-02 | 22 | 2.4 |
| 695 | 0692 | 2455185.05988826 | 945264389 | 130.558 | 33.827 | -1.3370e-01 | 8.5313e-01 | 6.3102e-01 | 3.7539e-02 | 31 | 2.4 |
| 696 | 0693 | 2455185.07594380 | 945265776 | 212.062 | -44.087 | -9.2963e-02 | 5.6770e-01 | 6.3052e-01 | 3.8106e-02 | 37 | 1.4 |
| 697 | 0694 | 2455185.16263358 | 945273266 | 334.567 | -52.112 | -9.2963e-02 | 5.6770e-01 | 6.3052e-01 | 3.8106e-02 | 54 | 1.4 |
| 698 | 0695 | 2455185.19185599 | 945275791 | 357.646 | -51.206 | -1.3370e-01 | 8.5313e-01 | 6.3102e-01 | 3.7539e-02 | 29 | 2.4 |
| 699 | 0696 | 2455185.19297753 | 945275888 | 92.645 | -35.479 | -9.2963e-02 | 5.6770e-01 | 6.3052e-01 | 3.8106e-02 | 33 | 1.4 |
| 700 | 0697 | 2455185.25821923 | 945281525 | 215.916 | -2.103 | -9.2963e-02 | 5.6770e-01 | 6.3052e-01 | 3.8106e-02 | 31 | 1.4 |
| 701 | 0698 | 2455185.31207878 | 945286178 | 218.766 | 11.076 | -1.1724e-01 | 4.7983e-01 | 5.2936e-01 | 3.8897e-02 | 97 | 0.9 |
| 702 | 0699 | 2455185.32505852 | 945287300 | 307.682 | -27.176 | -9.2963e-02 | 5.6770e-01 | 6.3052e-01 | 3.8106e-02 | 35 | 1.4 |
| 703 | 0700 | 2455185.70732004 | 945320327 | 302.210 | -34.967 | -9.2963e-02 | 5.6770e-01 | 6.3052e-01 | 3.8106e-02 | 40 | 1.4 |
| 704 | 0701 | 2455185.77454881 | 945326136 | 281.345 | -11.892 | -9.2963e-02 | 5.6770e-01 | 6.3052e-01 | 3.8106e-02 | 43 | 1.4 |
| 705 | 0702 | 2455185.92937998 | 945339513 | 332.200 | -25.898 | -9.2963e-02 | 5.6770e-01 | 6.3052e-01 | 3.8106e-02 | 34 | 1.4 |
| 706 | 0703 | 2455186.02294166 | 945347597 | 85.141 | 10.661 | -1.2873e-01 | 4.3155e-01 | 4.6595e-01 | 3.9162e-02 | 65 | 0.7 |
| 707 | 0704 | 2455186.02409992 | 945347697 | 174.475 | -21.966 | -1.3370e-01 | 8.5313e-01 | 6.3102e-01 | 3.7539e-02 | 31 | 2.4 |
| 708 | 0705 | 2455186.05520124 | 945350384 | 216.031 | -58.688 | -9.2963e-02 | 5.6770e-01 | 6.3052e-01 | 3.8106e-02 | 49 | 1.4 |
| 709 | 0706 | 2455186.22819540 | 945365331 | 193.511 | -23.269 | -1.1724e-01 | 4.7983e-01 | 5.2936e-01 | 3.8897e-02 | 56 | 0.9 |
| 710 | 0707 | 2455186.30411782 | 945371890 | 225.989 | 13.623 | -1.1724e-01 | 4.7983e-01 | 5.2936e-01 | 3.8897e-02 | 48 | 0.9 |
| 711 | 0708 | 2455186.30578811 | 945372035 | 55.800 | -61.690 | -9.2963e-02 | 5.6770e-01 | 6.3052e-01 | 3.8106e-02 | 38 | 1.4 |

| | | | | | | | | | | | |
|-----|------|------------------|-----------|---------|---------|-------------|------------|------------|------------|----|-----|
| 712 | 0709 | 2455186.31640317 | 945372952 | 232.495 | 3.022 | -9.2963e-02 | 5.6770e-01 | 6.3052e-01 | 3.8106e-02 | 48 | 1.4 |
| 713 | 0710 | 2455186.31770412 | 945373064 | 111.159 | -45.507 | -9.2963e-02 | 5.6770e-01 | 6.3052e-01 | 3.8106e-02 | 51 | 1.4 |
| 714 | 0711 | 2455186.41036246 | 945381070 | 269.648 | -24.735 | -9.2963e-02 | 5.6770e-01 | 6.3052e-01 | 3.8106e-02 | 42 | 1.4 |
| 715 | 0712 | 2455186.45940630 | 945385307 | 209.129 | -64.340 | -9.2963e-02 | 5.6770e-01 | 6.3052e-01 | 3.8106e-02 | 35 | 1.4 |
| 716 | 0713 | 2455186.49715197 | 945388568 | 264.619 | 3.712 | -1.1724e-01 | 4.7983e-01 | 5.2936e-01 | 3.8897e-02 | 68 | 0.9 |
| 717 | 0714 | 2455186.56137737 | 945394118 | 157.661 | -49.228 | -9.2963e-02 | 5.6770e-01 | 6.3052e-01 | 3.8106e-02 | 39 | 1.4 |
| 718 | 0715 | 2455186.57689280 | 945395458 | 117.489 | -49.812 | -9.2963e-02 | 5.6770e-01 | 6.3052e-01 | 3.8106e-02 | 54 | 1.4 |
| 719 | 0716 | 2455186.59625851 | 945397131 | 55.495 | -22.319 | -9.2963e-02 | 5.6770e-01 | 6.3052e-01 | 3.8106e-02 | 41 | 1.4 |
| 720 | 0717 | 2455186.66107419 | 945402731 | 51.556 | -41.455 | -1.1909e-01 | 7.2127e-01 | 6.0423e-01 | 3.7507e-02 | 27 | 1.8 |
| 721 | 0718 | 2455186.69145344 | 945405356 | 86.896 | -59.383 | -1.3370e-01 | 8.5313e-01 | 6.3102e-01 | 3.7539e-02 | 24 | 2.4 |
| 722 | 0719 | 2455186.69459665 | 945405628 | 75.712 | -43.954 | -1.2873e-01 | 4.3155e-01 | 4.6595e-01 | 3.9162e-02 | 34 | 0.7 |
| 723 | 0720 | 2455186.75393546 | 945410755 | 297.910 | 15.664 | -1.3370e-01 | 8.5313e-01 | 6.3102e-01 | 3.7539e-02 | 26 | 2.4 |
| 724 | 0721 | 2455186.78126233 | 945413116 | 313.747 | -52.164 | -1.3370e-01 | 8.5313e-01 | 6.3102e-01 | 3.7539e-02 | 31 | 2.4 |
| 725 | 0722 | 2455186.81286299 | 945415846 | 150.491 | -45.271 | -1.1724e-01 | 4.7983e-01 | 5.2936e-01 | 3.8897e-02 | 40 | 0.9 |
| 726 | 0723 | 2455186.81826188 | 945416312 | 358.520 | 12.668 | -1.1724e-01 | 4.7983e-01 | 5.2936e-01 | 3.8897e-02 | 49 | 0.9 |
| 727 | 0724 | 2455186.86866401 | 945420667 | 75.767 | -57.310 | -9.2963e-02 | 5.6770e-01 | 6.3052e-01 | 3.8106e-02 | 39 | 1.4 |
| 728 | 0725 | 2455188.19673582 | 945535412 | 89.244 | -42.022 | -1.1909e-01 | 7.2127e-01 | 6.0423e-01 | 3.7507e-02 | 29 | 1.8 |
| 729 | 0726 | 2455188.22021508 | 945537441 | 245.781 | -69.885 | -9.2963e-02 | 5.6770e-01 | 6.3052e-01 | 3.8106e-02 | 37 | 1.4 |
| 730 | 0727 | 2455188.23699775 | 945538891 | 110.626 | -36.628 | -1.3370e-01 | 8.5313e-01 | 6.3102e-01 | 3.7539e-02 | 18 | 2.4 |
| 731 | 0728 | 2455188.26880437 | 945541639 | 163.605 | -65.409 | -1.1724e-01 | 4.7983e-01 | 5.2936e-01 | 3.8897e-02 | 66 | 0.9 |
| 732 | 0729 | 2455188.31900133 | 945545976 | 186.434 | 37.369 | -1.3370e-01 | 8.5313e-01 | 6.3102e-01 | 3.7539e-02 | 18 | 2.4 |
| 733 | 0730 | 2455188.43355275 | 945555873 | 216.759 | 20.508 | -1.3370e-01 | 8.5313e-01 | 6.3102e-01 | 3.7539e-02 | 53 | 2.4 |
| 734 | 0731 | 2455188.60491998 | 945570680 | 313.066 | -6.654 | -9.2963e-02 | 5.6770e-01 | 6.3052e-01 | 3.8106e-02 | 58 | 1.4 |
| 735 | 0732 | 2455188.62120062 | 945572086 | 293.448 | -2.703 | -9.2963e-02 | 5.6770e-01 | 6.3052e-01 | 3.8106e-02 | 43 | 1.4 |
| 736 | 0733 | 2455188.71726245 | 945580386 | 295.426 | -16.357 | -1.1909e-01 | 7.2127e-01 | 6.0423e-01 | 3.7507e-02 | 23 | 1.8 |
| 737 | 0734 | 2455189.17977206 | 945620347 | 135.221 | 8.397 | -1.3370e-01 | 8.5313e-01 | 6.3102e-01 | 3.7539e-02 | 27 | 2.4 |
| 738 | 0735 | 2455189.19309817 | 945621498 | 154.937 | 4.552 | -9.2963e-02 | 5.6770e-01 | 6.3052e-01 | 3.8106e-02 | 58 | 1.4 |
| 739 | 0736 | 2455189.21772394 | 945623626 | 240.573 | -12.974 | -9.2963e-02 | 5.6770e-01 | 6.3052e-01 | 3.8106e-02 | 71 | 1.4 |
| 740 | 0737 | 2455189.30541555 | 945631202 | 109.819 | -50.505 | -9.2963e-02 | 5.6770e-01 | 6.3052e-01 | 3.8106e-02 | 52 | 1.4 |
| 741 | 0738 | 2455189.33156785 | 945633462 | 98.313 | -55.134 | -9.2963e-02 | 5.6770e-01 | 6.3052e-01 | 3.8106e-02 | 41 | 1.4 |
| 742 | 0739 | 2455189.34552145 | 945634668 | 291.811 | -13.060 | -9.2963e-02 | 5.6770e-01 | 6.3052e-01 | 3.8106e-02 | 58 | 1.4 |
| 743 | 0740 | 2455189.43989452 | 945642821 | 261.356 | 4.773 | -9.2963e-02 | 5.6770e-01 | 6.3052e-01 | 3.8106e-02 | 75 | 1.4 |
| 744 | 0741 | 2455189.50517487 | 945648462 | 318.110 | 0.333 | -1.1909e-01 | 7.2127e-01 | 6.0423e-01 | 3.7507e-02 | 22 | 1.8 |
| 745 | 0742 | 2455189.53259519 | 945650831 | 292.638 | -28.398 | -1.1724e-01 | 4.7983e-01 | 5.2936e-01 | 3.8897e-02 | 56 | 0.9 |
| 746 | 0743 | 2455189.54650895 | 945652033 | 227.451 | 18.216 | -1.3370e-01 | 8.5313e-01 | 6.3102e-01 | 3.7539e-02 | 28 | 2.4 |
| 747 | 0744 | 2455189.56117206 | 945653300 | 241.954 | -34.181 | -9.2963e-02 | 5.6770e-01 | 6.3052e-01 | 3.8106e-02 | 33 | 1.4 |
| 748 | 0745 | 2455189.56900697 | 945653977 | 12.139 | -26.821 | -9.2963e-02 | 5.6770e-01 | 6.3052e-01 | 3.8106e-02 | 38 | 1.4 |
| 749 | 0746 | 2455189.58712903 | 945655542 | 84.859 | -41.621 | -9.2963e-02 | 5.6770e-01 | 6.3052e-01 | 3.8106e-02 | 41 | 1.4 |
| 750 | 0747 | 2455189.61079032 | 945657587 | 23.576 | 11.120 | -9.2963e-02 | 5.6770e-01 | 6.3052e-01 | 3.8106e-02 | 32 | 1.4 |
| 751 | 0748 | 2455189.67531367 | 945663162 | 260.686 | 3.375 | -9.2963e-02 | 5.6770e-01 | 6.3052e-01 | 3.8106e-02 | 40 | 1.4 |
| 752 | 0749 | 2455189.76234013 | 945670681 | 333.358 | 24.397 | -9.2963e-02 | 5.6770e-01 | 6.3052e-01 | 3.8106e-02 | 62 | 1.4 |
| 753 | 0750 | 2455189.84112265 | 945677487 | 295.226 | -24.967 | -9.2963e-02 | 5.6770e-01 | 6.3052e-01 | 3.8106e-02 | 48 | 1.4 |
| 754 | 0751 | 2455189.86724503 | 945679744 | 28.891 | 3.611 | -1.2873e-01 | 4.3155e-01 | 4.6595e-01 | 3.9162e-02 | 43 | 0.7 |
| 755 | 0752 | 2455189.88137404 | 945680965 | 30.357 | -60.141 | -1.1724e-01 | 4.7983e-01 | 5.2936e-01 | 3.8897e-02 | 32 | 0.9 |
| 756 | 0753 | 2455190.06489370 | 945696821 | 105.702 | 4.303 | -9.2963e-02 | 5.6770e-01 | 6.3052e-01 | 3.8106e-02 | 41 | 1.4 |
| 757 | 0754 | 2455190.23295942 | 945711342 | 271.920 | -16.015 | -9.2963e-02 | 5.6770e-01 | 6.3052e-01 | 3.8106e-02 | 86 | 1.4 |
| 758 | 0755 | 2455190.26165361 | 945713821 | 113.719 | -33.912 | -1.3370e-01 | 8.5313e-01 | 6.3102e-01 | 3.7539e-02 | 24 | 2.4 |
| 759 | 0756 | 2455190.30101956 | 945717223 | 253.703 | -20.745 | -9.2963e-02 | 5.6770e-01 | 6.3052e-01 | 3.8106e-02 | 57 | 1.4 |
| 760 | 0757 | 2455190.36577198 | 945722817 | 280.345 | 14.397 | -1.1909e-01 | 7.2127e-01 | 6.0423e-01 | 3.7507e-02 | 27 | 1.8 |
| 761 | 0758 | 2455190.43494695 | 945728794 | 173.296 | 3.863 | -1.1909e-01 | 7.2127e-01 | 6.0423e-01 | 3.7507e-02 | 50 | 1.8 |
| 762 | 0759 | 2455190.43802490 | 945729060 | 15.382 | -37.340 | -1.3370e-01 | 8.5313e-01 | 6.3102e-01 | 3.7539e-02 | 28 | 2.4 |
| 763 | 0760 | 2455190.58809914 | 945742026 | 230.744 | -67.190 | -9.2963e-02 | 5.6770e-01 | 6.3052e-01 | 3.8106e-02 | 44 | 1.4 |

LIST OF HIGH ENERGY NEUTRINO CANDIDATES FOR THE 2009-2010 DATA

| | | | | | | | | | | | |
|-----|------|------------------|-----------|---------|---------|-------------|------------|------------|------------|-----|-----|
| 764 | 0761 | 2455190.64852638 | 945747247 | 257.281 | -43.345 | -1.1724e-01 | 4.7983e-01 | 5.2936e-01 | 3.8897e-02 | 35 | 0.9 |
| 765 | 0762 | 2455190.75656885 | 945756582 | 26.679 | 39.333 | -9.2963e-02 | 5.6770e-01 | 6.3052e-01 | 3.8106e-02 | 41 | 1.4 |
| 766 | 0763 | 2455190.77666783 | 945758319 | 346.528 | -55.446 | -1.3370e-01 | 8.5313e-01 | 6.3102e-01 | 3.7539e-02 | 31 | 2.4 |
| 767 | 0764 | 2455190.90073477 | 945769038 | 353.761 | -10.056 | -1.3370e-01 | 8.5313e-01 | 6.3102e-01 | 3.7539e-02 | 22 | 2.4 |
| 768 | 0765 | 2455191.07954270 | 945784487 | 94.727 | -59.338 | -9.2963e-02 | 5.6770e-01 | 6.3052e-01 | 3.8106e-02 | 47 | 1.4 |
| 769 | 0766 | 2455191.09109280 | 945785485 | 169.178 | -26.613 | -1.1724e-01 | 4.7983e-01 | 5.2936e-01 | 3.8897e-02 | 45 | 0.9 |
| 770 | 0767 | 2455191.13633636 | 945789394 | 239.339 | -47.795 | -9.2963e-02 | 5.6770e-01 | 6.3052e-01 | 3.8106e-02 | 33 | 1.4 |
| 771 | 0768 | 2455191.15140879 | 945790696 | 228.930 | 15.437 | -1.3370e-01 | 8.5313e-01 | 6.3102e-01 | 3.7539e-02 | 30 | 2.4 |
| 772 | 0769 | 2455191.20783708 | 945795572 | 138.246 | -37.687 | -1.1724e-01 | 4.7983e-01 | 5.2936e-01 | 3.8897e-02 | 80 | 0.9 |
| 773 | 0770 | 2455191.21603047 | 945796280 | 285.247 | -19.755 | -1.3370e-01 | 8.5313e-01 | 6.3102e-01 | 3.7539e-02 | 30 | 2.4 |
| 774 | 0771 | 2455191.24990460 | 945799206 | 85.087 | -27.823 | -9.2963e-02 | 5.6770e-01 | 6.3052e-01 | 3.8106e-02 | 59 | 1.4 |
| 775 | 0772 | 2455191.27287725 | 945801191 | 132.431 | 16.119 | -9.2963e-02 | 5.6770e-01 | 6.3052e-01 | 3.8106e-02 | 38 | 1.4 |
| 776 | 0773 | 2455191.43364389 | 945815081 | 301.206 | -3.407 | -1.3370e-01 | 8.5313e-01 | 6.3102e-01 | 3.7539e-02 | 31 | 2.4 |
| 777 | 0774 | 2455191.49072895 | 945820013 | 241.216 | -50.228 | -9.2963e-02 | 5.6770e-01 | 6.3052e-01 | 3.8106e-02 | 36 | 1.4 |
| 778 | 0775 | 2455191.52547335 | 945823015 | 217.600 | -3.941 | -9.2963e-02 | 5.6770e-01 | 6.3052e-01 | 3.8106e-02 | 42 | 1.4 |
| 779 | 0776 | 2455191.53177773 | 945823560 | 330.378 | 27.810 | -9.2963e-02 | 5.6770e-01 | 6.3052e-01 | 3.8106e-02 | 39 | 1.4 |
| 780 | 0777 | 2455192.15463775 | 945877375 | 289.784 | -45.262 | -1.1724e-01 | 4.7983e-01 | 5.2936e-01 | 3.8897e-02 | 42 | 0.9 |
| 781 | 0778 | 2455192.24410402 | 945885105 | 105.900 | -41.732 | -1.1724e-01 | 4.7983e-01 | 5.2936e-01 | 3.8897e-02 | 45 | 0.9 |
| 782 | 0779 | 2455192.26786255 | 945887158 | 121.622 | -0.163 | -9.2963e-02 | 5.6770e-01 | 6.3052e-01 | 3.8106e-02 | 60 | 1.4 |
| 783 | 0780 | 2455192.38032764 | 945896875 | 42.982 | -52.148 | -9.2963e-02 | 5.6770e-01 | 6.3052e-01 | 3.8106e-02 | 37 | 1.4 |
| 784 | 0781 | 2455192.49069143 | 945906410 | 210.878 | -11.458 | -1.1909e-01 | 7.2127e-01 | 6.0423e-01 | 3.7507e-02 | 22 | 1.8 |
| 785 | 0782 | 2455192.55556949 | 945912016 | 209.560 | -39.589 | -9.2963e-02 | 5.6770e-01 | 6.3052e-01 | 3.8106e-02 | 42 | 1.4 |
| 786 | 0783 | 2455192.61748737 | 945917365 | 339.288 | -0.221 | -9.2963e-02 | 5.6770e-01 | 6.3052e-01 | 3.8106e-02 | 47 | 1.4 |
| 787 | 0784 | 2455192.74176696 | 945928103 | 120.755 | -39.027 | -1.3370e-01 | 8.5313e-01 | 6.3102e-01 | 3.7539e-02 | 29 | 2.4 |
| 788 | 0785 | 2455192.77533777 | 945931004 | 22.964 | 6.706 | -9.2963e-02 | 5.6770e-01 | 6.3052e-01 | 3.8106e-02 | 46 | 1.4 |
| 789 | 0786 | 2455192.79055565 | 945932319 | 214.877 | -62.088 | -9.2963e-02 | 5.6770e-01 | 6.3052e-01 | 3.8106e-02 | 34 | 1.4 |
| 790 | 0787 | 2455192.85197386 | 945937625 | 45.151 | -14.234 | -9.2963e-02 | 5.6770e-01 | 6.3052e-01 | 3.8106e-02 | 50 | 1.4 |
| 791 | 0788 | 2455192.86945414 | 945939135 | 217.271 | -71.745 | -9.2963e-02 | 5.6770e-01 | 6.3052e-01 | 3.8106e-02 | 41 | 1.4 |
| 792 | 0789 | 2455192.93074785 | 945944431 | 18.933 | 28.914 | -5.8944e-02 | 2.9333e-01 | 5.7306e-01 | 3.8834e-02 | 214 | 0.6 |
| 793 | 0790 | 2455193.12625274 | 945961323 | 117.358 | 42.733 | -9.2963e-02 | 5.6770e-01 | 6.3052e-01 | 3.8106e-02 | 32 | 1.4 |
| 794 | 0791 | 2455193.23920794 | 945971082 | 157.049 | -11.993 | -1.3370e-01 | 8.5313e-01 | 6.3102e-01 | 3.7539e-02 | 30 | 2.4 |
| 795 | 0792 | 2455193.25177703 | 945972168 | 177.245 | -38.820 | -9.2963e-02 | 5.6770e-01 | 6.3052e-01 | 3.8106e-02 | 49 | 1.4 |
| 796 | 0793 | 2455193.49933465 | 945993557 | 169.553 | -26.928 | -9.2963e-02 | 5.6770e-01 | 6.3052e-01 | 3.8106e-02 | 66 | 1.4 |
| 797 | 0794 | 2455193.76033573 | 946016108 | 299.098 | 7.281 | -9.2963e-02 | 5.6770e-01 | 6.3052e-01 | 3.8106e-02 | 56 | 1.4 |
| 798 | 0795 | 2455193.77183890 | 946017101 | 175.039 | -73.664 | -1.3370e-01 | 8.5313e-01 | 6.3102e-01 | 3.7539e-02 | 27 | 2.4 |
| 799 | 0796 | 2455193.88955972 | 946027272 | 2.766 | -58.139 | -9.2963e-02 | 5.6770e-01 | 6.3052e-01 | 3.8106e-02 | 61 | 1.4 |
| 800 | 0797 | 2455194.21847979 | 946055691 | 154.212 | 24.974 | -9.2963e-02 | 5.6770e-01 | 6.3052e-01 | 3.8106e-02 | 40 | 1.4 |
| 801 | 0798 | 2455194.24334194 | 946057839 | 207.659 | -3.927 | -9.2963e-02 | 5.6770e-01 | 6.3052e-01 | 3.8106e-02 | 38 | 1.4 |
| 802 | 0799 | 2455194.34810904 | 946066891 | 224.203 | 9.163 | -9.2963e-02 | 5.6770e-01 | 6.3052e-01 | 3.8106e-02 | 44 | 1.4 |
| 803 | 0800 | 2455194.43836779 | 946074689 | 253.304 | -36.764 | -1.2873e-01 | 4.3155e-01 | 4.6595e-01 | 3.9162e-02 | 48 | 0.7 |
| 804 | 0801 | 2455194.68717315 | 946096186 | 42.081 | 28.673 | -9.2963e-02 | 5.6770e-01 | 6.3052e-01 | 3.8106e-02 | 45 | 1.4 |
| 805 | 0802 | 2455194.68736318 | 946096203 | 250.934 | -16.820 | -9.2963e-02 | 5.6770e-01 | 6.3052e-01 | 3.8106e-02 | 51 | 1.4 |
| 806 | 0803 | 2455194.83326808 | 946108809 | 81.804 | 7.745 | -9.2963e-02 | 5.6770e-01 | 6.3052e-01 | 3.8106e-02 | 85 | 1.4 |
| 807 | 0804 | 2455194.94157086 | 946118166 | 342.996 | -41.451 | -1.3370e-01 | 8.5313e-01 | 6.3102e-01 | 3.7539e-02 | 31 | 2.4 |
| 808 | 0805 | 2455195.04014714 | 946126683 | 11.335 | -32.386 | -9.2963e-02 | 5.6770e-01 | 6.3052e-01 | 3.8106e-02 | 42 | 1.4 |
| 809 | 0806 | 2455195.05106900 | 946127627 | 81.040 | 28.972 | -1.3370e-01 | 8.5313e-01 | 6.3102e-01 | 3.7539e-02 | 26 | 2.4 |
| 810 | 0807 | 2455195.33607486 | 946152251 | 205.709 | -74.502 | -5.3660e-02 | 3.7117e-01 | 6.4893e-01 | 3.6677e-02 | 72 | 1.2 |
| 811 | 0808 | 2455195.49918680 | 946166344 | 60.392 | -84.483 | -1.1724e-01 | 4.7983e-01 | 5.2936e-01 | 3.8897e-02 | 71 | 0.9 |
| 812 | 0809 | 2455195.65716034 | 946179993 | 233.724 | -33.022 | -9.2963e-02 | 5.6770e-01 | 6.3052e-01 | 3.8106e-02 | 42 | 1.4 |
| 813 | 0810 | 2455195.86609631 | 946198045 | 195.789 | -87.647 | -1.2873e-01 | 4.3155e-01 | 4.6595e-01 | 3.9162e-02 | 60 | 0.7 |
| 814 | 0811 | 2455195.87305563 | 946198647 | 359.106 | 7.661 | -1.1724e-01 | 4.7983e-01 | 5.2936e-01 | 3.8897e-02 | 64 | 0.9 |
| 815 | 0812 | 2455196.03698362 | 946212810 | 36.351 | 7.189 | -9.2963e-02 | 5.6770e-01 | 6.3052e-01 | 3.8106e-02 | 36 | 1.4 |

| | | | | | | | | | | | |
|-----|------|------------------|-----------|---------|---------|-------------|------------|------------|------------|-----|-----|
| 816 | 0813 | 2455196.09357134 | 946217699 | 128.368 | 1.391 | -9.2963e-02 | 5.6770e-01 | 6.3052e-01 | 3.8106e-02 | 35 | 1.4 |
| 817 | 0814 | 2455196.10573781 | 946218750 | 133.970 | 36.838 | -1.1909e-01 | 7.2127e-01 | 6.0423e-01 | 3.7507e-02 | 27 | 1.8 |
| 818 | 0815 | 2455196.20104784 | 946226985 | 112.585 | 21.455 | -9.2963e-02 | 5.6770e-01 | 6.3052e-01 | 3.8106e-02 | 76 | 1.4 |
| 819 | 0816 | 2455196.20195120 | 946227063 | 229.146 | -35.530 | -9.2963e-02 | 5.6770e-01 | 6.3052e-01 | 3.8106e-02 | 34 | 1.4 |
| 820 | 0817 | 2455196.32910411 | 946238049 | 270.230 | -1.033 | -1.1724e-01 | 4.7983e-01 | 5.2936e-01 | 3.8897e-02 | 34 | 0.9 |
| 821 | 0818 | 2455196.34582890 | 946239494 | 355.325 | -42.724 | -1.3370e-01 | 8.5313e-01 | 6.3102e-01 | 3.7539e-02 | 27 | 2.4 |
| 822 | 0819 | 2455196.51730728 | 946254310 | 347.485 | 31.268 | -9.2963e-02 | 5.6770e-01 | 6.3052e-01 | 3.8106e-02 | 49 | 1.4 |
| 823 | 0820 | 2455196.68476378 | 946268778 | 276.091 | 12.169 | -9.2963e-02 | 5.6770e-01 | 6.3052e-01 | 3.8106e-02 | 45 | 1.4 |
| 824 | 0821 | 2455196.77623850 | 946276682 | 153.640 | -70.377 | -9.2963e-02 | 5.6770e-01 | 6.3052e-01 | 3.8106e-02 | 34 | 1.4 |
| 825 | 0822 | 2455196.81660113 | 946280169 | 310.156 | -69.503 | -9.2963e-02 | 5.6770e-01 | 6.3052e-01 | 3.8106e-02 | 47 | 1.4 |
| 826 | 0823 | 2455197.01356936 | 946297187 | 14.566 | -9.847 | -9.2963e-02 | 5.6770e-01 | 6.3052e-01 | 3.8106e-02 | 68 | 1.4 |
| 827 | 0824 | 2455197.11318555 | 946305794 | 66.453 | -0.840 | -1.3370e-01 | 8.5313e-01 | 6.3102e-01 | 3.7539e-02 | 27 | 2.4 |
| 828 | 0825 | 2455197.22022673 | 946315042 | 139.423 | -23.609 | -1.3370e-01 | 8.5313e-01 | 6.3102e-01 | 3.7539e-02 | 21 | 2.4 |
| 829 | 0826 | 2455197.22654436 | 946315588 | 160.856 | -0.828 | -1.1724e-01 | 4.7983e-01 | 5.2936e-01 | 3.8897e-02 | 50 | 0.9 |
| 830 | 0827 | 2455197.62020656 | 946349600 | 54.788 | -44.624 | -1.1724e-01 | 4.7983e-01 | 5.2936e-01 | 3.8897e-02 | 37 | 0.9 |
| 831 | 0828 | 2455197.72030308 | 946358249 | 213.686 | -52.286 | -9.2963e-02 | 5.6770e-01 | 6.3052e-01 | 3.8106e-02 | 39 | 1.4 |
| 832 | 0829 | 2455197.73813817 | 946359790 | 51.332 | 25.007 | -9.2963e-02 | 5.6770e-01 | 6.3052e-01 | 3.8106e-02 | 45 | 1.4 |
| 833 | 0830 | 2455197.90974396 | 946374616 | 90.680 | -0.331 | -9.2963e-02 | 5.6770e-01 | 6.3052e-01 | 3.8106e-02 | 43 | 1.4 |
| 834 | 0831 | 2455198.20461957 | 946400094 | 115.214 | 6.246 | -9.2963e-02 | 5.6770e-01 | 6.3052e-01 | 3.8106e-02 | 47 | 1.4 |
| 835 | 0832 | 2455198.48822306 | 946424597 | 299.902 | 18.907 | -9.2963e-02 | 5.6770e-01 | 6.3052e-01 | 3.8106e-02 | 40 | 1.4 |
| 836 | 0833 | 2455198.49936446 | 946425560 | 214.464 | -38.282 | -9.2963e-02 | 5.6770e-01 | 6.3052e-01 | 3.8106e-02 | 45 | 1.4 |
| 837 | 0834 | 2455198.75505946 | 946447652 | 20.804 | 3.496 | -1.1724e-01 | 4.7983e-01 | 5.2936e-01 | 3.8897e-02 | 39 | 0.9 |
| 838 | 0835 | 2455198.80386155 | 946451868 | 29.893 | 36.624 | -9.2963e-02 | 5.6770e-01 | 6.3052e-01 | 3.8106e-02 | 42 | 1.4 |
| 839 | 0836 | 2455198.84553438 | 946455469 | 325.184 | -17.620 | -9.2963e-02 | 5.6770e-01 | 6.3052e-01 | 3.8106e-02 | 35 | 1.4 |
| 840 | 0837 | 2455199.11695812 | 946478920 | 60.294 | -46.073 | -9.2963e-02 | 5.6770e-01 | 6.3052e-01 | 3.8106e-02 | 35 | 1.4 |
| 841 | 0838 | 2455199.32165197 | 946496605 | 177.612 | -43.608 | -1.1724e-01 | 4.7983e-01 | 5.2936e-01 | 3.8897e-02 | 61 | 0.9 |
| 842 | 0839 | 2455199.50425473 | 946512382 | 174.596 | -26.646 | -1.3370e-01 | 8.5313e-01 | 6.3102e-01 | 3.7539e-02 | 29 | 2.4 |
| 843 | 0840 | 2455199.65344042 | 946525272 | 315.545 | -14.142 | -1.1909e-01 | 7.2127e-01 | 6.0423e-01 | 3.7507e-02 | 30 | 1.8 |
| 844 | 0841 | 2455199.67326995 | 946526985 | 342.880 | 11.294 | -1.3370e-01 | 8.5313e-01 | 6.3102e-01 | 3.7539e-02 | 22 | 2.4 |
| 845 | 0842 | 2455199.73837464 | 946532610 | 300.436 | -17.084 | -1.3370e-01 | 8.5313e-01 | 6.3102e-01 | 3.7539e-02 | 22 | 2.4 |
| 846 | 0843 | 2455199.80482370 | 946538351 | 346.532 | -9.574 | -1.3370e-01 | 8.5313e-01 | 6.3102e-01 | 3.7539e-02 | 23 | 2.4 |
| 847 | 0844 | 2455199.97867064 | 946553372 | 118.522 | 5.126 | -9.2963e-02 | 5.6770e-01 | 6.3052e-01 | 3.8106e-02 | 43 | 1.4 |
| 848 | 0845 | 2455200.19836435 | 946572353 | 156.136 | 17.143 | -1.1724e-01 | 4.7983e-01 | 5.2936e-01 | 3.8897e-02 | 41 | 0.9 |
| 849 | 0846 | 2455200.21128236 | 946573469 | 281.206 | -27.685 | -5.8944e-02 | 2.9333e-01 | 5.7306e-01 | 3.8834e-02 | 111 | 0.6 |
| 850 | 0847 | 2455200.24253147 | 946576169 | 158.037 | -30.857 | -9.2963e-02 | 5.6770e-01 | 6.3052e-01 | 3.8106e-02 | 34 | 1.4 |
| 851 | 0848 | 2455200.39128406 | 946589021 | 233.851 | -18.053 | -9.2963e-02 | 5.6770e-01 | 6.3052e-01 | 3.8106e-02 | 40 | 1.4 |
| 852 | 0849 | 2455200.40955362 | 946590600 | 333.699 | -33.135 | -9.2963e-02 | 5.6770e-01 | 6.3052e-01 | 3.8106e-02 | 42 | 1.4 |
| 853 | 0850 | 2455200.49801000 | 946598243 | 115.394 | -61.523 | -1.3370e-01 | 8.5313e-01 | 6.3102e-01 | 3.7539e-02 | 29 | 2.4 |
| 854 | 0851 | 2455200.50295737 | 946598670 | 118.432 | -73.416 | -1.1909e-01 | 7.2127e-01 | 6.0423e-01 | 3.7507e-02 | 24 | 1.8 |
| 855 | 0852 | 2455200.63914878 | 946610437 | 257.750 | -18.706 | -1.1724e-01 | 4.7983e-01 | 5.2936e-01 | 3.8897e-02 | 36 | 0.9 |
| 856 | 0853 | 2455200.73664624 | 946618861 | 68.630 | -46.294 | -5.8944e-02 | 2.9333e-01 | 5.7306e-01 | 3.8834e-02 | 114 | 0.6 |
| 857 | 0854 | 2455200.82720896 | 946626685 | 43.219 | -18.838 | -1.1724e-01 | 4.7983e-01 | 5.2936e-01 | 3.8897e-02 | 52 | 0.9 |
| 858 | 0855 | 2455200.85383520 | 946628986 | 4.746 | -61.413 | -1.1724e-01 | 4.7983e-01 | 5.2936e-01 | 3.8897e-02 | 42 | 0.9 |
| 859 | 0856 | 2455200.86111443 | 946629615 | 351.922 | -8.619 | -9.2963e-02 | 5.6770e-01 | 6.3052e-01 | 3.8106e-02 | 53 | 1.4 |
| 860 | 0857 | 2455200.91682470 | 946634428 | 155.629 | 2.871 | -9.2963e-02 | 5.6770e-01 | 6.3052e-01 | 3.8106e-02 | 39 | 1.4 |
| 861 | 0858 | 2455201.27852597 | 946665679 | 135.621 | 15.304 | -9.2963e-02 | 5.6770e-01 | 6.3052e-01 | 3.8106e-02 | 52 | 1.4 |
| 862 | 0859 | 2455201.50119943 | 946684918 | 272.419 | -5.337 | -9.2963e-02 | 5.6770e-01 | 6.3052e-01 | 3.8106e-02 | 46 | 1.4 |
| 863 | 0860 | 2455201.51964677 | 946686512 | 182.276 | -25.628 | -1.3370e-01 | 8.5313e-01 | 6.3102e-01 | 3.7539e-02 | 25 | 2.4 |
| 864 | 0861 | 2455201.57071479 | 946690924 | 118.513 | -77.902 | -1.3370e-01 | 8.5313e-01 | 6.3102e-01 | 3.7539e-02 | 53 | 2.4 |
| 865 | 0862 | 2455201.62218506 | 946695371 | 300.067 | 18.551 | -1.1724e-01 | 4.7983e-01 | 5.2936e-01 | 3.8897e-02 | 32 | 0.9 |
| 866 | 0863 | 2455201.71330061 | 946703244 | 310.037 | -9.823 | -1.1724e-01 | 4.7983e-01 | 5.2936e-01 | 3.8897e-02 | 46 | 0.9 |
| 867 | 0864 | 2455201.90501365 | 946719808 | 56.506 | 15.541 | -1.1909e-01 | 7.2127e-01 | 6.0423e-01 | 3.7507e-02 | 31 | 1.8 |

LIST OF HIGH ENERGY NEUTRINO CANDIDATES FOR THE 2009-2010 DATA

| | | | | | | | | | | | |
|-----|----------------------|------------------|-----------|---------|---------|-------------|------------|------------|------------|-----|-----|
| 868 | 0865 | 2455202.56619047 | 946776933 | 226.425 | -26.198 | -9.2963e-02 | 5.6770e-01 | 6.3052e-01 | 3.8106e-02 | 43 | 1.4 |
| 869 | 0866 | 2455202.57824478 | 946777975 | 48.026 | -3.908 | -9.2963e-02 | 5.6770e-01 | 6.3052e-01 | 3.8106e-02 | 48 | 1.4 |
| 870 | 0867 | 2455202.89990655 | 946805766 | 32.564 | -22.498 | -9.2963e-02 | 5.6770e-01 | 6.3052e-01 | 3.8106e-02 | 54 | 1.4 |
| 871 | 0868 | 2455203.00614741 | 946814946 | 9.277 | -20.964 | -1.3370e-01 | 8.5313e-01 | 6.3102e-01 | 3.7539e-02 | 25 | 2.4 |
| 872 | 0869 | 2455203.13391412 | 946825985 | 89.082 | -11.646 | -1.1724e-01 | 4.7983e-01 | 5.2936e-01 | 3.8897e-02 | 52 | 0.9 |
| 873 | 0870 | 2455203.28664686 | 946839181 | 214.259 | -0.251 | -1.1724e-01 | 4.7983e-01 | 5.2936e-01 | 3.8897e-02 | 44 | 0.9 |
| 874 | 0871 | 2455203.64317126 | 946869984 | 311.290 | -22.788 | -1.1724e-01 | 4.7983e-01 | 5.2936e-01 | 3.8897e-02 | 63 | 0.9 |
| 875 | 0872 | 2455203.79039468 | 946882705 | 76.056 | 12.364 | -9.2963e-02 | 5.6770e-01 | 6.3052e-01 | 3.8106e-02 | 32 | 1.4 |
| 876 | 0873 | 2455203.95790065 | 946897177 | 186.720 | -16.253 | -1.3370e-01 | 8.5313e-01 | 6.3102e-01 | 3.7539e-02 | 24 | 2.4 |
| 877 | 0874 | 2455204.07717164 | 946907482 | 44.618 | -23.035 | -9.2963e-02 | 5.6770e-01 | 6.3052e-01 | 3.8106e-02 | 49 | 1.4 |
| 878 | 0875 | 2455204.08132679 | 946907841 | 167.712 | 33.081 | -1.1724e-01 | 4.7983e-01 | 5.2936e-01 | 3.8897e-02 | 34 | 0.9 |
| 879 | 0876 | 2455204.16160983 | 946914778 | 177.142 | -20.882 | -1.1210e-01 | 3.5816e-01 | 4.5437e-01 | 4.0298e-02 | 130 | 0.5 |
| 880 | 0877 | 2455204.24444168 | 946921934 | 73.211 | -55.726 | -9.2963e-02 | 5.6770e-01 | 6.3052e-01 | 3.8106e-02 | 54 | 1.4 |
| 881 | 0878 | 2455204.91856534 | 946980179 | 101.313 | 27.139 | -9.2963e-02 | 5.6770e-01 | 6.3052e-01 | 3.8106e-02 | 42 | 1.4 |
| 882 | 0879 | 2455205.34927857 | 947017392 | 334.347 | -45.866 | -9.2963e-02 | 5.6770e-01 | 6.3052e-01 | 3.8106e-02 | 63 | 1.4 |
| 883 | 0880 | 2455205.37763531 | 947019842 | 103.421 | -58.168 | -8.8598e-02 | 3.3283e-01 | 5.3278e-01 | 3.9884e-02 | 126 | 0.6 |
| 884 | ## stop S6B -- start | | | | | | | | | | |
| 885 | 0881 | 2455205.59201854 | 947038365 | 267.264 | -51.054 | -1.1724e-01 | 4.7983e-01 | 5.2936e-01 | 3.8897e-02 | 48 | 0.9 |
| 886 | 0882 | 2455205.75899046 | 947052791 | 118.043 | -18.373 | -1.1909e-01 | 7.2127e-01 | 6.0423e-01 | 3.7507e-02 | 30 | 1.8 |
| 887 | 0883 | 2455205.97940864 | 947071835 | 115.109 | 16.753 | -1.1724e-01 | 4.7983e-01 | 5.2936e-01 | 3.8897e-02 | 37 | 0.9 |
| 888 | 0884 | 2455206.00180145 | 947073770 | 130.615 | -21.946 | -9.2963e-02 | 5.6770e-01 | 6.3052e-01 | 3.8106e-02 | 51 | 1.4 |
| 889 | 0885 | 2455206.26931457 | 947096883 | 332.136 | -37.905 | -1.3370e-01 | 8.5313e-01 | 6.3102e-01 | 3.7539e-02 | 27 | 2.4 |
| 890 | 0886 | 2455206.36533759 | 947105180 | 237.271 | -52.013 | -9.2963e-02 | 5.6770e-01 | 6.3052e-01 | 3.8106e-02 | 56 | 1.4 |
| 891 | 0887 | 2455206.40668835 | 947108752 | 345.728 | -52.192 | -1.3370e-01 | 8.5313e-01 | 6.3102e-01 | 3.7539e-02 | 29 | 2.4 |
| 892 | 0888 | 2455206.52609776 | 947119069 | 80.905 | -44.259 | -1.3370e-01 | 8.5313e-01 | 6.3102e-01 | 3.7539e-02 | 23 | 2.4 |
| 893 | 0889 | 2455206.63121873 | 947128152 | 325.758 | -9.835 | -1.1724e-01 | 4.7983e-01 | 5.2936e-01 | 3.8897e-02 | 41 | 0.9 |
| 894 | 0890 | 2455206.66747144 | 947131284 | 1.693 | 19.163 | -1.1724e-01 | 4.7983e-01 | 5.2936e-01 | 3.8897e-02 | 41 | 0.9 |
| 895 | 0891 | 2455206.67259082 | 947131726 | 329.613 | -44.847 | -1.1724e-01 | 4.7983e-01 | 5.2936e-01 | 3.8897e-02 | 33 | 0.9 |
| 896 | 0892 | 2455206.73749282 | 947137334 | 67.664 | 7.449 | -1.1724e-01 | 4.7983e-01 | 5.2936e-01 | 3.8897e-02 | 55 | 0.9 |
| 897 | 0893 | 2455206.74643766 | 947138107 | 203.141 | -64.683 | -1.1724e-01 | 4.7983e-01 | 5.2936e-01 | 3.8897e-02 | 56 | 0.9 |
| 898 | 0894 | 2455206.74980613 | 947138398 | 87.173 | 26.354 | -9.2963e-02 | 5.6770e-01 | 6.3052e-01 | 3.8106e-02 | 50 | 1.4 |
| 899 | 0895 | 2455206.75151176 | 947138545 | 26.082 | -22.605 | -1.1724e-01 | 4.7983e-01 | 5.2936e-01 | 3.8897e-02 | 56 | 0.9 |
| 900 | 0896 | 2455206.87608301 | 947149308 | 7.058 | -47.541 | -9.2963e-02 | 5.6770e-01 | 6.3052e-01 | 3.8106e-02 | 32 | 1.4 |
| 901 | 0897 | 2455206.91583704 | 947152743 | 212.966 | -38.042 | -9.2963e-02 | 5.6770e-01 | 6.3052e-01 | 3.8106e-02 | 48 | 1.4 |
| 902 | 0898 | 2455207.01591151 | 947161389 | 152.202 | 15.928 | -1.1724e-01 | 4.7983e-01 | 5.2936e-01 | 3.8897e-02 | 58 | 0.9 |
| 903 | 0899 | 2455207.08166584 | 947167070 | 86.772 | 14.539 | -1.1724e-01 | 4.7983e-01 | 5.2936e-01 | 3.8897e-02 | 32 | 0.9 |
| 904 | 0900 | 2455207.20778341 | 947177967 | 117.999 | 14.092 | -1.1724e-01 | 4.7983e-01 | 5.2936e-01 | 3.8897e-02 | 37 | 0.9 |
| 905 | 0901 | 2455207.22579561 | 947179523 | 129.025 | 19.866 | -1.1909e-01 | 7.2127e-01 | 6.0423e-01 | 3.7507e-02 | 31 | 1.8 |
| 906 | 0902 | 2455207.33615105 | 947189058 | 139.241 | -22.835 | -1.3370e-01 | 8.5313e-01 | 6.3102e-01 | 3.7539e-02 | 26 | 2.4 |
| 907 | 0903 | 2455207.47513383 | 947201066 | 227.609 | -3.938 | -1.3370e-01 | 8.5313e-01 | 6.3102e-01 | 3.7539e-02 | 28 | 2.4 |
| 908 | 0904 | 2455207.64567817 | 947215801 | 4.079 | 4.212 | -9.2963e-02 | 5.6770e-01 | 6.3052e-01 | 3.8106e-02 | 42 | 1.4 |
| 909 | 0905 | 2455207.79742100 | 947228912 | 81.020 | 17.226 | -1.2873e-01 | 4.3155e-01 | 4.6595e-01 | 3.9162e-02 | 42 | 0.7 |
| 910 | 0906 | 2455208.19976877 | 947263675 | 241.253 | -47.750 | -1.2873e-01 | 4.3155e-01 | 4.6595e-01 | 3.9162e-02 | 48 | 0.7 |
| 911 | 0907 | 2455208.24828695 | 947267866 | 94.459 | -22.668 | -1.2873e-01 | 4.3155e-01 | 4.6595e-01 | 3.9162e-02 | 73 | 0.7 |
| 912 | 0908 | 2455208.27795336 | 947270430 | 183.964 | 31.182 | -1.1724e-01 | 4.7983e-01 | 5.2936e-01 | 3.8897e-02 | 46 | 0.9 |
| 913 | 0909 | 2455208.46690315 | 947286755 | 11.208 | -2.795 | -9.2963e-02 | 5.6770e-01 | 6.3052e-01 | 3.8106e-02 | 43 | 1.4 |
| 914 | 0910 | 2455208.65447656 | 947302961 | 240.837 | -83.941 | -9.2963e-02 | 5.6770e-01 | 6.3052e-01 | 3.8106e-02 | 38 | 1.4 |
| 915 | 0911 | 2455208.82690760 | 947317859 | 45.053 | -35.434 | -1.1724e-01 | 4.7983e-01 | 5.2936e-01 | 3.8897e-02 | 58 | 0.9 |
| 916 | 0912 | 2455208.94043913 | 947327668 | 74.696 | 1.665 | -1.3370e-01 | 8.5313e-01 | 6.3102e-01 | 3.7539e-02 | 21 | 2.4 |
| 917 | 0913 | 2455208.95740231 | 947329134 | 33.176 | 7.278 | -9.2963e-02 | 5.6770e-01 | 6.3052e-01 | 3.8106e-02 | 43 | 1.4 |
| 918 | 0914 | 2455208.95959556 | 947329324 | 310.556 | -56.006 | -1.3370e-01 | 8.5313e-01 | 6.3102e-01 | 3.7539e-02 | 26 | 2.4 |
| 919 | 0915 | 2455209.13629385 | 947344590 | 230.622 | -33.109 | -1.3370e-01 | 8.5313e-01 | 6.3102e-01 | 3.7539e-02 | 23 | 2.4 |

| | | | | | | | | | | | |
|-----|------|------------------|-----------|---------|---------|-------------|------------|------------|------------|----|-----|
| 920 | 0916 | 2455209.22185271 | 947351983 | 277.762 | -52.548 | -9.2963e-02 | 5.6770e-01 | 6.3052e-01 | 3.8106e-02 | 39 | 1.4 |
| 921 | 0917 | 2455209.30528449 | 947359191 | 14.398 | -54.989 | -9.2963e-02 | 5.6770e-01 | 6.3052e-01 | 3.8106e-02 | 56 | 1.4 |
| 922 | 0918 | 2455209.33191709 | 947361492 | 149.062 | -29.658 | -1.3370e-01 | 8.5313e-01 | 6.3102e-01 | 3.7539e-02 | 25 | 2.4 |
| 923 | 0919 | 2455209.35135004 | 947363171 | 253.749 | -52.798 | -1.1724e-01 | 4.7983e-01 | 5.2936e-01 | 3.8897e-02 | 50 | 0.9 |
| 924 | 0920 | 2455209.38793623 | 947366332 | 311.044 | 32.084 | -9.2963e-02 | 5.6770e-01 | 6.3052e-01 | 3.8106e-02 | 56 | 1.4 |
| 925 | 0921 | 2455209.44853596 | 947371568 | 339.721 | -27.964 | -1.1724e-01 | 4.7983e-01 | 5.2936e-01 | 3.8897e-02 | 37 | 0.9 |
| 926 | 0922 | 2455209.47386163 | 947373756 | 263.659 | 13.193 | -9.2963e-02 | 5.6770e-01 | 6.3052e-01 | 3.8106e-02 | 52 | 1.4 |
| 927 | 0923 | 2455209.77249363 | 947399558 | 131.683 | -28.552 | -1.1724e-01 | 4.7983e-01 | 5.2936e-01 | 3.8897e-02 | 76 | 0.9 |
| 928 | 0924 | 2455209.79083373 | 947401143 | 44.297 | 27.973 | -1.1724e-01 | 4.7983e-01 | 5.2936e-01 | 3.8897e-02 | 80 | 0.9 |
| 929 | 0925 | 2455209.83807158 | 947405224 | 28.661 | -36.461 | -1.3370e-01 | 8.5313e-01 | 6.3102e-01 | 3.7539e-02 | 23 | 2.4 |
| 930 | 0926 | 2455209.86684556 | 947407710 | 205.102 | -56.088 | -9.2963e-02 | 5.6770e-01 | 6.3052e-01 | 3.8106e-02 | 81 | 1.4 |
| 931 | 0927 | 2455209.96111612 | 947415855 | 108.564 | -16.082 | -9.2963e-02 | 5.6770e-01 | 6.3052e-01 | 3.8106e-02 | 43 | 1.4 |
| 932 | 0928 | 2455210.05777507 | 947424206 | 23.435 | -36.751 | -1.3370e-01 | 8.5313e-01 | 6.3102e-01 | 3.7539e-02 | 31 | 2.4 |
| 933 | 0929 | 2455210.16938478 | 947433849 | 219.044 | 34.427 | -1.3370e-01 | 8.5313e-01 | 6.3102e-01 | 3.7539e-02 | 26 | 2.4 |
| 934 | 0930 | 2455210.18549947 | 947435242 | 173.028 | 36.944 | -9.2963e-02 | 5.6770e-01 | 6.3052e-01 | 3.8106e-02 | 37 | 1.4 |
| 935 | 0931 | 2455210.21484370 | 947437777 | 123.166 | -37.100 | -9.2963e-02 | 5.6770e-01 | 6.3052e-01 | 3.8106e-02 | 59 | 1.4 |
| 936 | 0932 | 2455210.21804241 | 947438053 | 264.968 | -49.697 | -1.2873e-01 | 4.3155e-01 | 4.6595e-01 | 3.9162e-02 | 50 | 0.7 |
| 937 | 0933 | 2455210.43937220 | 947457176 | 270.955 | -6.792 | -1.3370e-01 | 8.5313e-01 | 6.3102e-01 | 3.7539e-02 | 29 | 2.4 |
| 938 | 0934 | 2455210.50426152 | 947462783 | 228.357 | 7.854 | -9.2963e-02 | 5.6770e-01 | 6.3052e-01 | 3.8106e-02 | 45 | 1.4 |
| 939 | 0935 | 2455210.58498972 | 947469758 | 267.813 | 22.353 | -9.2963e-02 | 5.6770e-01 | 6.3052e-01 | 3.8106e-02 | 32 | 1.4 |
| 940 | 0936 | 2455210.63097229 | 947473731 | 305.927 | 26.076 | -9.2963e-02 | 5.6770e-01 | 6.3052e-01 | 3.8106e-02 | 19 | 1.4 |
| 941 | 0937 | 2455210.67885656 | 947477868 | 6.182 | -25.268 | -1.1724e-01 | 4.7983e-01 | 5.2936e-01 | 3.8897e-02 | 36 | 0.9 |
| 942 | 0938 | 2455210.75309901 | 947484282 | 336.174 | -26.774 | -1.7861e+00 | 6.7827e+00 | 8.6368e-01 | 3.8440e-01 | 28 | 1.4 |
| 943 | 0939 | 2455210.78665557 | 947487182 | 32.647 | -50.787 | -1.3370e-01 | 8.5313e-01 | 6.3102e-01 | 3.7539e-02 | 14 | 2.4 |
| 944 | 0940 | 2455210.81492192 | 947489624 | 53.093 | 6.017 | -1.1724e-01 | 4.7983e-01 | 5.2936e-01 | 3.8897e-02 | 36 | 0.9 |
| 945 | 0941 | 2455210.88302667 | 947495508 | 159.777 | -43.026 | -1.3370e-01 | 8.5313e-01 | 6.3102e-01 | 3.7539e-02 | 21 | 2.4 |
| 946 | 0942 | 2455210.95532939 | 947501755 | 121.446 | 21.508 | -1.3370e-01 | 8.5313e-01 | 6.3102e-01 | 3.7539e-02 | 47 | 2.4 |
| 947 | 0943 | 2455210.96064258 | 947502214 | 17.852 | -5.590 | -9.2963e-02 | 5.6770e-01 | 6.3052e-01 | 3.8106e-02 | 59 | 1.4 |
| 948 | 0944 | 2455211.02021087 | 947507361 | 117.161 | -30.028 | -1.7861e+00 | 6.7827e+00 | 8.6368e-01 | 3.8440e-01 | 31 | 1.4 |
| 949 | 0945 | 2455211.17875483 | 947521059 | 152.515 | 23.840 | -1.7861e+00 | 6.7827e+00 | 8.6368e-01 | 3.8440e-01 | 37 | 1.4 |
| 950 | 0946 | 2455211.19979930 | 947522877 | 263.441 | -47.207 | -1.7861e+00 | 6.7827e+00 | 8.6368e-01 | 3.8440e-01 | 50 | 1.4 |
| 951 | 0947 | 2455211.23356536 | 947525795 | 177.446 | -20.883 | -1.1724e-01 | 4.7983e-01 | 5.2936e-01 | 3.8897e-02 | 49 | 0.9 |
| 952 | 0948 | 2455211.23625788 | 947526027 | 179.400 | -5.439 | -1.3370e-01 | 8.5313e-01 | 6.3102e-01 | 3.7539e-02 | 30 | 2.4 |
| 953 | 0949 | 2455211.35794080 | 947536541 | 225.210 | -32.172 | -1.3370e-01 | 8.5313e-01 | 6.3102e-01 | 3.7539e-02 | 30 | 2.4 |
| 954 | 0950 | 2455211.39414760 | 947539669 | 158.473 | -15.134 | -9.2963e-02 | 5.6770e-01 | 6.3052e-01 | 3.8106e-02 | 75 | 1.4 |
| 955 | 0951 | 2455211.49668203 | 947548528 | 62.133 | -47.866 | -9.2963e-02 | 5.6770e-01 | 6.3052e-01 | 3.8106e-02 | 33 | 1.4 |
| 956 | 0952 | 2455211.53471177 | 947551814 | 292.684 | 34.166 | -9.2963e-02 | 5.6770e-01 | 6.3052e-01 | 3.8106e-02 | 61 | 1.4 |
| 957 | 0953 | 2455211.55099228 | 947553220 | 353.837 | 14.121 | -9.2963e-02 | 5.6770e-01 | 6.3052e-01 | 3.8106e-02 | 39 | 1.4 |
| 958 | 0954 | 2455211.57554351 | 947555341 | 32.428 | -57.857 | -1.1724e-01 | 4.7983e-01 | 5.2936e-01 | 3.8897e-02 | 37 | 0.9 |
| 959 | 0955 | 2455211.59760908 | 947557248 | 197.748 | -54.015 | -1.1724e-01 | 4.7983e-01 | 5.2936e-01 | 3.8897e-02 | 39 | 0.9 |
| 960 | 0956 | 2455211.65511459 | 947562216 | 100.629 | -24.442 | -9.2963e-02 | 5.6770e-01 | 6.3052e-01 | 3.8106e-02 | 57 | 1.4 |
| 961 | 0957 | 2455211.76506830 | 947571716 | 32.353 | 40.097 | -1.1724e-01 | 4.7983e-01 | 5.2936e-01 | 3.8897e-02 | 40 | 0.9 |
| 962 | 0958 | 2455212.20425262 | 947609662 | 183.042 | 45.535 | -9.2963e-02 | 5.6770e-01 | 6.3052e-01 | 3.8106e-02 | 41 | 1.4 |
| 963 | 0959 | 2455212.27313993 | 947615614 | 49.168 | -51.723 | -1.1724e-01 | 4.7983e-01 | 5.2936e-01 | 3.8897e-02 | 93 | 0.9 |
| 964 | 0960 | 2455212.28904463 | 947616988 | 148.081 | 2.273 | -1.1724e-01 | 4.7983e-01 | 5.2936e-01 | 3.8897e-02 | 33 | 0.9 |
| 965 | 0961 | 2455212.37899045 | 947624759 | 350.098 | -69.949 | -9.2963e-02 | 5.6770e-01 | 6.3052e-01 | 3.8106e-02 | 63 | 1.4 |
| 966 | 0962 | 2455212.41061837 | 947627492 | 298.791 | -28.302 | -9.2963e-02 | 5.6770e-01 | 6.3052e-01 | 3.8106e-02 | 42 | 1.4 |
| 967 | 0963 | 2455212.46859616 | 947632501 | 36.526 | -67.883 | -1.1724e-01 | 4.7983e-01 | 5.2936e-01 | 3.8897e-02 | 32 | 0.9 |
| 968 | 0964 | 2455212.56806648 | 947641095 | 359.404 | -60.557 | -1.2873e-01 | 4.3155e-01 | 4.6595e-01 | 3.9162e-02 | 53 | 0.7 |
| 969 | 0965 | 2455212.58355032 | 947642433 | 32.563 | 3.851 | -1.1909e-01 | 7.2127e-01 | 6.0423e-01 | 3.7507e-02 | 30 | 1.8 |
| 970 | 0966 | 2455212.59013134 | 947643002 | 203.433 | -45.794 | -9.2963e-02 | 5.6770e-01 | 6.3052e-01 | 3.8106e-02 | 58 | 1.4 |
| 971 | 0967 | 2455212.77125714 | 947658651 | 50.658 | -59.275 | -1.1724e-01 | 4.7983e-01 | 5.2936e-01 | 3.8897e-02 | 49 | 0.9 |

LIST OF HIGH ENERGY NEUTRINO CANDIDATES FOR THE 2009-2010 DATA

| | | | | | | | | | | | |
|------|------|------------------|-----------|---------|---------|-------------|------------|------------|------------|----|-----|
| 972 | 0968 | 2455212.79352479 | 947660575 | 69.802 | -16.268 | -1.1724e-01 | 4.7983e-01 | 5.2936e-01 | 3.8897e-02 | 50 | 0.9 |
| 973 | 0969 | 2455212.81448302 | 947662386 | 124.386 | 17.047 | -9.2963e-02 | 5.6770e-01 | 6.3052e-01 | 3.8106e-02 | 34 | 1.4 |
| 974 | 0970 | 2455212.88081398 | 947668117 | 166.762 | -22.996 | -1.3370e-01 | 8.5313e-01 | 6.3102e-01 | 3.7539e-02 | 23 | 2.4 |
| 975 | 0971 | 2455212.88892148 | 947668817 | 166.939 | -31.081 | -1.1909e-01 | 7.2127e-01 | 6.0423e-01 | 3.7507e-02 | 28 | 1.8 |
| 976 | 0972 | 2455212.92046770 | 947671543 | 122.686 | 4.647 | -1.3370e-01 | 8.5313e-01 | 6.3102e-01 | 3.7539e-02 | 19 | 2.4 |
| 977 | 0973 | 2455212.92471797 | 947671910 | 74.808 | -75.830 | -9.2963e-02 | 5.6770e-01 | 6.3052e-01 | 3.8106e-02 | 61 | 1.4 |
| 978 | 0974 | 2455213.15414407 | 947691733 | 238.454 | 25.548 | -1.3370e-01 | 8.5313e-01 | 6.3102e-01 | 3.7539e-02 | 14 | 2.4 |
| 979 | 0975 | 2455213.19806784 | 947695528 | 160.430 | -1.371 | -9.2963e-02 | 5.6770e-01 | 6.3052e-01 | 3.8106e-02 | 32 | 1.4 |
| 980 | 0976 | 2455213.21381213 | 947696888 | 200.820 | -38.225 | -1.2873e-01 | 4.3155e-01 | 4.6595e-01 | 3.9162e-02 | 77 | 0.7 |
| 981 | 0977 | 2455213.35664608 | 947709229 | 276.946 | -23.016 | -9.2963e-02 | 5.6770e-01 | 6.3052e-01 | 3.8106e-02 | 34 | 1.4 |
| 982 | 0978 | 2455213.39821696 | 947712820 | 234.501 | 34.173 | -9.2963e-02 | 5.6770e-01 | 6.3052e-01 | 3.8106e-02 | 36 | 1.4 |
| 983 | 0979 | 2455213.40174958 | 947713126 | 67.726 | -53.436 | -1.3370e-01 | 8.5313e-01 | 6.3102e-01 | 3.7539e-02 | 24 | 2.4 |
| 984 | 0980 | 2455213.43431247 | 947715939 | 211.552 | 13.112 | -9.2963e-02 | 5.6770e-01 | 6.3052e-01 | 3.8106e-02 | 56 | 1.4 |
| 985 | 0981 | 2455213.48770472 | 947720552 | 250.051 | -5.168 | -1.1724e-01 | 4.7983e-01 | 5.2936e-01 | 3.8897e-02 | 64 | 0.9 |
| 986 | 0982 | 2455213.49114798 | 947720850 | 261.905 | -20.117 | -1.3370e-01 | 8.5313e-01 | 6.3102e-01 | 3.7539e-02 | 20 | 2.4 |
| 987 | 0983 | 2455213.50139438 | 947721735 | 299.654 | 33.847 | -9.2963e-02 | 5.6770e-01 | 6.3052e-01 | 3.8106e-02 | 46 | 1.4 |
| 988 | 0984 | 2455213.51991054 | 947723335 | 209.996 | -14.521 | -1.1724e-01 | 4.7983e-01 | 5.2936e-01 | 3.8897e-02 | 39 | 0.9 |
| 989 | 0985 | 2455213.53946560 | 947725024 | 200.485 | -29.139 | -1.1724e-01 | 4.7983e-01 | 5.2936e-01 | 3.8897e-02 | 27 | 0.9 |
| 990 | 0986 | 2455213.53971454 | 947725046 | 109.252 | -46.437 | -9.2963e-02 | 5.6770e-01 | 6.3052e-01 | 3.8106e-02 | 37 | 1.4 |
| 991 | 0987 | 2455213.54156747 | 947725206 | 320.335 | -68.918 | -9.2963e-02 | 5.6770e-01 | 6.3052e-01 | 3.8106e-02 | 55 | 1.4 |
| 992 | 0988 | 2455214.01182564 | 947765836 | 175.032 | -4.417 | -9.2963e-02 | 5.6770e-01 | 6.3052e-01 | 3.8106e-02 | 34 | 1.4 |
| 993 | 0989 | 2455214.11136989 | 947774437 | 114.048 | -11.184 | -1.3370e-01 | 8.5313e-01 | 6.3102e-01 | 3.7539e-02 | 29 | 2.4 |
| 994 | 0990 | 2455214.28131093 | 947789120 | 223.097 | -28.813 | -9.2963e-02 | 5.6770e-01 | 6.3052e-01 | 3.8106e-02 | 40 | 1.4 |
| 995 | 0991 | 2455214.30593188 | 947791247 | 277.461 | -9.760 | -9.2963e-02 | 5.6770e-01 | 6.3052e-01 | 3.8106e-02 | 61 | 1.4 |
| 996 | 0992 | 2455214.36089245 | 947795996 | 178.073 | -27.653 | -1.3370e-01 | 8.5313e-01 | 6.3102e-01 | 3.7539e-02 | 30 | 2.4 |
| 997 | 0993 | 2455214.42798763 | 947801793 | 301.777 | 24.406 | -1.1909e-01 | 7.2127e-01 | 6.0423e-01 | 3.7507e-02 | 30 | 1.8 |
| 998 | 0994 | 2455214.87267737 | 947840214 | 299.101 | -41.611 | -9.2963e-02 | 5.6770e-01 | 6.3052e-01 | 3.8106e-02 | 51 | 1.4 |
| 999 | 0995 | 2455214.89370262 | 947842030 | 35.968 | 5.427 | -9.2963e-02 | 5.6770e-01 | 6.3052e-01 | 3.8106e-02 | 69 | 1.4 |
| 1000 | 0996 | 2455215.50331896 | 947894701 | 283.750 | -77.656 | -1.3370e-01 | 8.5313e-01 | 6.3102e-01 | 3.7539e-02 | 25 | 2.4 |
| 1001 | 0997 | 2455215.56109982 | 947899694 | 276.305 | -55.215 | -1.1724e-01 | 4.7983e-01 | 5.2936e-01 | 3.8897e-02 | 35 | 0.9 |
| 1002 | 0998 | 2455215.65139634 | 947907495 | 357.315 | 13.840 | -1.3370e-01 | 8.5313e-01 | 6.3102e-01 | 3.7539e-02 | 28 | 2.4 |
| 1003 | 0999 | 2455215.78045199 | 947918646 | 349.378 | 16.011 | -1.2873e-01 | 4.3155e-01 | 4.6595e-01 | 3.9162e-02 | 47 | 0.7 |
| 1004 | 1000 | 2455215.90226208 | 947929170 | 8.882 | -52.036 | -1.3370e-01 | 8.5313e-01 | 6.3102e-01 | 3.7539e-02 | 29 | 2.4 |
| 1005 | 1001 | 2455216.01085793 | 947938553 | 41.373 | -84.886 | -1.3370e-01 | 8.5313e-01 | 6.3102e-01 | 3.7539e-02 | 27 | 2.4 |
| 1006 | 1002 | 2455216.34873897 | 947967746 | 203.507 | 30.062 | -9.2963e-02 | 5.6770e-01 | 6.3052e-01 | 3.8106e-02 | 47 | 1.4 |
| 1007 | 1003 | 2455216.36133052 | 947968833 | 201.399 | -26.520 | -1.3370e-01 | 8.5313e-01 | 6.3102e-01 | 3.7539e-02 | 31 | 2.4 |
| 1008 | 1004 | 2455216.45310313 | 947976763 | 249.040 | 10.568 | -9.2963e-02 | 5.6770e-01 | 6.3052e-01 | 3.8106e-02 | 32 | 1.4 |
| 1009 | 1005 | 2455216.59292969 | 947988844 | 98.494 | -30.628 | -1.3370e-01 | 8.5313e-01 | 6.3102e-01 | 3.7539e-02 | 30 | 2.4 |
| 1010 | 1006 | 2455216.72955620 | 948000648 | 333.831 | 7.730 | -9.2963e-02 | 5.6770e-01 | 6.3052e-01 | 3.8106e-02 | 32 | 1.4 |
| 1011 | 1007 | 2455216.86105434 | 948012010 | 341.944 | -11.576 | -9.2963e-02 | 5.6770e-01 | 6.3052e-01 | 3.8106e-02 | 47 | 1.4 |
| 1012 | 1008 | 2455216.88993180 | 948014505 | 26.279 | -39.408 | -9.2963e-02 | 5.6770e-01 | 6.3052e-01 | 3.8106e-02 | 42 | 1.4 |
| 1013 | 1009 | 2455216.89107169 | 948014603 | 31.229 | -15.565 | -9.2963e-02 | 5.6770e-01 | 6.3052e-01 | 3.8106e-02 | 62 | 1.4 |
| 1014 | 1010 | 2455216.89991008 | 948015367 | 208.509 | -31.749 | -9.2963e-02 | 5.6770e-01 | 6.3052e-01 | 3.8106e-02 | 20 | 1.4 |
| 1015 | 1011 | 2455216.91641982 | 948016793 | 76.145 | -33.772 | -9.2963e-02 | 5.6770e-01 | 6.3052e-01 | 3.8106e-02 | 41 | 1.4 |
| 1016 | 1012 | 2455217.20964166 | 948042128 | 197.893 | 16.200 | -9.2963e-02 | 5.6770e-01 | 6.3052e-01 | 3.8106e-02 | 26 | 1.4 |
| 1017 | 1013 | 2455217.30659437 | 948050504 | 140.939 | -33.050 | -9.2963e-02 | 5.6770e-01 | 6.3052e-01 | 3.8106e-02 | 78 | 1.4 |
| 1018 | 1014 | 2455217.37064803 | 948056038 | 153.145 | -27.790 | -9.2963e-02 | 5.6770e-01 | 6.3052e-01 | 3.8106e-02 | 79 | 1.4 |
| 1019 | 1015 | 2455217.38352752 | 948057151 | 267.267 | -3.638 | -1.1724e-01 | 4.7983e-01 | 5.2936e-01 | 3.8897e-02 | 53 | 0.9 |
| 1020 | 1016 | 2455217.43662342 | 948061739 | 70.824 | -44.897 | -9.2963e-02 | 5.6770e-01 | 6.3052e-01 | 3.8106e-02 | 44 | 1.4 |
| 1021 | 1017 | 2455217.48114018 | 948065585 | 35.632 | -14.867 | -9.2963e-02 | 5.6770e-01 | 6.3052e-01 | 3.8106e-02 | 44 | 1.4 |
| 1022 | 1018 | 2455217.63457306 | 948078842 | 318.290 | 1.948 | -1.3370e-01 | 8.5313e-01 | 6.3102e-01 | 3.7539e-02 | 28 | 2.4 |
| 1023 | 1019 | 2455217.68534775 | 948083229 | 73.186 | -66.497 | -9.2963e-02 | 5.6770e-01 | 6.3052e-01 | 3.8106e-02 | 45 | 1.4 |

| | | | | | | | | | | | |
|------|------|------------------|-----------|---------|---------|-------------|------------|------------|------------|-----|-----|
| 1024 | 1020 | 2455217.69372588 | 948083952 | 76.056 | -24.998 | -9.2963e-02 | 5.6770e-01 | 6.3052e-01 | 3.8106e-02 | 37 | 1.4 |
| 1025 | 1021 | 2455217.72233598 | 948086424 | 22.124 | -41.139 | -9.2963e-02 | 5.6770e-01 | 6.3052e-01 | 3.8106e-02 | 58 | 1.4 |
| 1026 | 1022 | 2455217.77375757 | 948090867 | 258.509 | -50.920 | -9.2963e-02 | 5.6770e-01 | 6.3052e-01 | 3.8106e-02 | 34 | 1.4 |
| 1027 | 1023 | 2455217.79942390 | 948093085 | 79.440 | -10.827 | -9.2963e-02 | 5.6770e-01 | 6.3052e-01 | 3.8106e-02 | 40 | 1.4 |
| 1028 | 1024 | 2455217.93751951 | 948105016 | 209.026 | -29.980 | -1.1724e-01 | 4.7983e-01 | 5.2936e-01 | 3.8897e-02 | 32 | 0.9 |
| 1029 | 1025 | 2455217.96018590 | 948106975 | 158.933 | -9.470 | -9.2963e-02 | 5.6770e-01 | 6.3052e-01 | 3.8106e-02 | 37 | 1.4 |
| 1030 | 1026 | 2455218.00320179 | 948110691 | 297.851 | -71.415 | -9.2963e-02 | 5.6770e-01 | 6.3052e-01 | 3.8106e-02 | 36 | 1.4 |
| 1031 | 1027 | 2455218.04921834 | 948114667 | 66.443 | -9.481 | -9.2963e-02 | 5.6770e-01 | 6.3052e-01 | 3.8106e-02 | 33 | 1.4 |
| 1032 | 1028 | 2455218.06026285 | 948115621 | 136.881 | -48.062 | -9.2963e-02 | 5.6770e-01 | 6.3052e-01 | 3.8106e-02 | 45 | 1.4 |
| 1033 | 1029 | 2455218.12468535 | 948121187 | 212.250 | -21.730 | -1.3370e-01 | 8.5313e-01 | 6.3102e-01 | 3.7539e-02 | 30 | 2.4 |
| 1034 | 1030 | 2455218.14745146 | 948123154 | 207.128 | 3.288 | -9.2963e-02 | 5.6770e-01 | 6.3052e-01 | 3.8106e-02 | 52 | 1.4 |
| 1035 | 1031 | 2455218.16159433 | 948124376 | 306.424 | -76.348 | -1.1724e-01 | 4.7983e-01 | 5.2936e-01 | 3.8897e-02 | 40 | 0.9 |
| 1036 | 1032 | 2455218.23743555 | 948130929 | 203.209 | 4.090 | -1.1724e-01 | 4.7983e-01 | 5.2936e-01 | 3.8897e-02 | 37 | 0.9 |
| 1037 | 1033 | 2455218.28351038 | 948134910 | 146.554 | 6.006 | -9.2963e-02 | 5.6770e-01 | 6.3052e-01 | 3.8106e-02 | 36 | 1.4 |
| 1038 | 1034 | 2455218.37466473 | 948142786 | 246.216 | -25.287 | -9.2963e-02 | 5.6770e-01 | 6.3052e-01 | 3.8106e-02 | 53 | 1.4 |
| 1039 | 1035 | 2455218.52024679 | 948155364 | 263.409 | 0.566 | -1.3370e-01 | 8.5313e-01 | 6.3102e-01 | 3.7539e-02 | 26 | 2.4 |
| 1040 | 1036 | 2455218.71965313 | 948172593 | 54.200 | -18.294 | -1.1909e-01 | 7.2127e-01 | 6.0423e-01 | 3.7507e-02 | 28 | 1.8 |
| 1041 | 1037 | 2455218.80594342 | 948180048 | 113.978 | -7.262 | -1.3370e-01 | 8.5313e-01 | 6.3102e-01 | 3.7539e-02 | 21 | 2.4 |
| 1042 | 1038 | 2455219.09213103 | 948204775 | 244.287 | 5.275 | -1.3370e-01 | 8.5313e-01 | 6.3102e-01 | 3.7539e-02 | 23 | 2.4 |
| 1043 | 1039 | 2455219.14023248 | 948208931 | 246.829 | -84.491 | -1.3370e-01 | 8.5313e-01 | 6.3102e-01 | 3.7539e-02 | 22 | 2.4 |
| 1044 | 1040 | 2455219.15124774 | 948209882 | 122.980 | 23.331 | -9.2963e-02 | 5.6770e-01 | 6.3052e-01 | 3.8106e-02 | 51 | 1.4 |
| 1045 | 1041 | 2455219.18000458 | 948212367 | 117.554 | -7.495 | -9.2963e-02 | 5.6770e-01 | 6.3052e-01 | 3.8106e-02 | 74 | 1.4 |
| 1046 | 1042 | 2455219.22247143 | 948216036 | 186.590 | -6.019 | -1.2873e-01 | 4.3155e-01 | 4.6595e-01 | 3.9162e-02 | 50 | 0.7 |
| 1047 | 1043 | 2455219.23366936 | 948217004 | 223.687 | -36.116 | -9.2963e-02 | 5.6770e-01 | 6.3052e-01 | 3.8106e-02 | 38 | 1.4 |
| 1048 | 1044 | 2455219.25388962 | 948218751 | 255.211 | -29.602 | -1.3370e-01 | 8.5313e-01 | 6.3102e-01 | 3.7539e-02 | 28 | 2.4 |
| 1049 | 1045 | 2455219.33250068 | 948225543 | 306.654 | -6.792 | -9.2963e-02 | 5.6770e-01 | 6.3052e-01 | 3.8106e-02 | 41 | 1.4 |
| 1050 | 1046 | 2455219.33472768 | 948225735 | 350.803 | -62.116 | -9.2963e-02 | 5.6770e-01 | 6.3052e-01 | 3.8106e-02 | 41 | 1.4 |
| 1051 | 1047 | 2455219.48966383 | 948239121 | 250.112 | -13.580 | -1.3370e-01 | 8.5313e-01 | 6.3102e-01 | 3.7539e-02 | 21 | 2.4 |
| 1052 | 1048 | 2455219.63133488 | 948251362 | 286.211 | 10.829 | -9.2963e-02 | 5.6770e-01 | 6.3052e-01 | 3.8106e-02 | 36 | 1.4 |
| 1053 | 1049 | 2455219.75108672 | 948261708 | 324.316 | -55.637 | -1.1724e-01 | 4.7983e-01 | 5.2936e-01 | 3.8897e-02 | 36 | 0.9 |
| 1054 | 1050 | 2455219.75716941 | 948262234 | 4.511 | 9.788 | -1.3370e-01 | 8.5313e-01 | 6.3102e-01 | 3.7539e-02 | 31 | 2.4 |
| 1055 | 1051 | 2455219.78046755 | 948264247 | 85.081 | 24.757 | -1.3370e-01 | 8.5313e-01 | 6.3102e-01 | 3.7539e-02 | 95 | 2.4 |
| 1056 | 1052 | 2455219.80331319 | 948266221 | 72.520 | -3.493 | -1.1210e-01 | 3.5816e-01 | 4.5437e-01 | 4.0298e-02 | 108 | 0.5 |
| 1057 | 1053 | 2455219.96904028 | 948280540 | 194.174 | -73.655 | -1.3370e-01 | 8.5313e-01 | 6.3102e-01 | 3.7539e-02 | 24 | 2.4 |
| 1058 | 1054 | 2455220.04206527 | 948286849 | 162.689 | -53.608 | -8.8598e-02 | 3.3283e-01 | 5.3278e-01 | 3.9884e-02 | 150 | 0.6 |
| 1059 | 1055 | 2455220.36821775 | 948315029 | 335.818 | 12.849 | -9.2963e-02 | 5.6770e-01 | 6.3052e-01 | 3.8106e-02 | 37 | 1.4 |
| 1060 | 1056 | 2455220.44918721 | 948322024 | 305.047 | 22.556 | -1.3370e-01 | 8.5313e-01 | 6.3102e-01 | 3.7539e-02 | 23 | 2.4 |
| 1061 | 1057 | 2455220.49848040 | 948326283 | 289.880 | 32.873 | -1.3370e-01 | 8.5313e-01 | 6.3102e-01 | 3.7539e-02 | 55 | 2.4 |
| 1062 | 1058 | 2455220.57302099 | 948332724 | 246.263 | -8.464 | -9.2963e-02 | 5.6770e-01 | 6.3052e-01 | 3.8106e-02 | 56 | 1.4 |
| 1063 | 1059 | 2455220.66813892 | 948340942 | 39.348 | 38.839 | -9.2963e-02 | 5.6770e-01 | 6.3052e-01 | 3.8106e-02 | 44 | 1.4 |
| 1064 | 1060 | 2455220.74677507 | 948347736 | 107.446 | -65.438 | -1.1724e-01 | 4.7983e-01 | 5.2936e-01 | 3.8897e-02 | 61 | 0.9 |
| 1065 | 1061 | 2455220.77984676 | 948350593 | 183.238 | -45.749 | -1.3370e-01 | 8.5313e-01 | 6.3102e-01 | 3.7539e-02 | 28 | 2.4 |
| 1066 | 1062 | 2455220.81694154 | 948353798 | 99.911 | -60.413 | -1.1724e-01 | 4.7983e-01 | 5.2936e-01 | 3.8897e-02 | 42 | 0.9 |
| 1067 | 1063 | 2455220.99541059 | 948369218 | 51.487 | 13.658 | -1.3370e-01 | 8.5313e-01 | 6.3102e-01 | 3.7539e-02 | 24 | 2.4 |
| 1068 | 1064 | 2455221.06080764 | 948374868 | 38.067 | -24.461 | -1.3370e-01 | 8.5313e-01 | 6.3102e-01 | 3.7539e-02 | 39 | 2.4 |
| 1069 | 1065 | 2455221.13791954 | 948381531 | 294.711 | -29.451 | -5.8944e-02 | 2.9333e-01 | 5.7306e-01 | 3.8834e-02 | 119 | 0.6 |
| 1070 | 1066 | 2455221.27910554 | 948393729 | 158.171 | -2.711 | -9.2963e-02 | 5.6770e-01 | 6.3052e-01 | 3.8106e-02 | 36 | 1.4 |
| 1071 | 1067 | 2455221.30351473 | 948395838 | 129.469 | -24.215 | -1.3370e-01 | 8.5313e-01 | 6.3102e-01 | 3.7539e-02 | 23 | 2.4 |
| 1072 | 1068 | 2455221.33926419 | 948398927 | 124.093 | -72.093 | -9.2963e-02 | 5.6770e-01 | 6.3052e-01 | 3.8106e-02 | 35 | 1.4 |
| 1073 | 1069 | 2455221.50481393 | 948413230 | 347.248 | 37.295 | -1.3370e-01 | 8.5313e-01 | 6.3102e-01 | 3.7539e-02 | 27 | 2.4 |
| 1074 | 1070 | 2455221.54215549 | 948416457 | 52.033 | -5.111 | -9.2963e-02 | 5.6770e-01 | 6.3052e-01 | 3.8106e-02 | 63 | 1.4 |
| 1075 | 1071 | 2455221.57922778 | 948419660 | 137.678 | -78.180 | -1.1724e-01 | 4.7983e-01 | 5.2936e-01 | 3.8897e-02 | 33 | 0.9 |

LIST OF HIGH ENERGY NEUTRINO CANDIDATES FOR THE 2009-2010 DATA

| | | | | | | | | | | | |
|------|------|------------------|-----------|---------|---------|-------------|------------|------------|------------|----|-----|
| 1076 | 1072 | 2455221.64028048 | 948424935 | 357.852 | 47.000 | -1.1724e-01 | 4.7983e-01 | 5.2936e-01 | 3.8897e-02 | 41 | 0.9 |
| 1077 | 1073 | 2455221.75557236 | 948434896 | 279.748 | -56.149 | -9.2963e-02 | 5.6770e-01 | 6.3052e-01 | 3.8106e-02 | 42 | 1.4 |
| 1078 | 1074 | 2455222.32131253 | 948483776 | 165.999 | 5.048 | -9.2963e-02 | 5.6770e-01 | 6.3052e-01 | 3.8106e-02 | 37 | 1.4 |
| 1079 | 1075 | 2455222.62123264 | 948509689 | 286.165 | 18.345 | -9.2963e-02 | 5.6770e-01 | 6.3052e-01 | 3.8106e-02 | 33 | 1.4 |
| 1080 | 1076 | 2455222.69290437 | 948515881 | 118.419 | -13.132 | -9.2963e-02 | 5.6770e-01 | 6.3052e-01 | 3.8106e-02 | 48 | 1.4 |
| 1081 | 1077 | 2455222.74576054 | 948520448 | 266.505 | -62.370 | -1.1724e-01 | 4.7983e-01 | 5.2936e-01 | 3.8897e-02 | 84 | 0.9 |
| 1082 | 1078 | 2455222.75772050 | 948521482 | 112.018 | 1.505 | -1.1724e-01 | 4.7983e-01 | 5.2936e-01 | 3.8897e-02 | 32 | 0.9 |
| 1083 | 1079 | 2455222.91335717 | 948534929 | 270.682 | -56.529 | -1.1724e-01 | 4.7983e-01 | 5.2936e-01 | 3.8897e-02 | 33 | 0.9 |
| 1084 | 1080 | 2455223.16058157 | 948556289 | 148.651 | -61.979 | -1.3370e-01 | 8.5313e-01 | 6.3102e-01 | 3.7539e-02 | 25 | 2.4 |
| 1085 | 1081 | 2455223.29012699 | 948567481 | 234.251 | -28.644 | -1.1724e-01 | 4.7983e-01 | 5.2936e-01 | 3.8897e-02 | 58 | 0.9 |
| 1086 | 1082 | 2455223.31370597 | 948569519 | 207.332 | -25.654 | -9.2963e-02 | 5.6770e-01 | 6.3052e-01 | 3.8106e-02 | 39 | 1.4 |
| 1087 | 1083 | 2455223.34636204 | 948572340 | 204.991 | -24.691 | -9.2963e-02 | 5.6770e-01 | 6.3052e-01 | 3.8106e-02 | 33 | 1.4 |
| 1088 | 1084 | 2455223.62032678 | 948596011 | 322.678 | -0.872 | -9.2963e-02 | 5.6770e-01 | 6.3052e-01 | 3.8106e-02 | 47 | 1.4 |
| 1089 | 1085 | 2455223.95972438 | 948625335 | 65.928 | 3.770 | -1.1724e-01 | 4.7983e-01 | 5.2936e-01 | 3.8897e-02 | 33 | 0.9 |
| 1090 | 1086 | 2455224.01295691 | 948629934 | 137.206 | -14.028 | -9.2963e-02 | 5.6770e-01 | 6.3052e-01 | 3.8106e-02 | 32 | 1.4 |
| 1091 | 1087 | 2455224.05723229 | 948633759 | 243.915 | -18.892 | -1.3370e-01 | 8.5313e-01 | 6.3102e-01 | 3.7539e-02 | 27 | 2.4 |
| 1092 | 1088 | 2455224.37403218 | 948661131 | 196.278 | -23.099 | -9.2963e-02 | 5.6770e-01 | 6.3052e-01 | 3.8106e-02 | 74 | 1.4 |
| 1093 | 1089 | 2455224.46085038 | 948668632 | 235.820 | 19.710 | -9.2963e-02 | 5.6770e-01 | 6.3052e-01 | 3.8106e-02 | 34 | 1.4 |
| 1094 | 1090 | 2455224.66861514 | 948686583 | 346.007 | -26.315 | -9.2963e-02 | 5.6770e-01 | 6.3052e-01 | 3.8106e-02 | 28 | 1.4 |
| 1095 | 1091 | 2455224.79992182 | 948697928 | 156.004 | -64.575 | -9.2963e-02 | 5.6770e-01 | 6.3052e-01 | 3.8106e-02 | 89 | 1.4 |
| 1096 | 1092 | 2455224.89850966 | 948706446 | 21.848 | 5.295 | -9.2963e-02 | 5.6770e-01 | 6.3052e-01 | 3.8106e-02 | 38 | 1.4 |
| 1097 | 1093 | 2455225.09116564 | 948723091 | 251.221 | -41.631 | -1.3370e-01 | 8.5313e-01 | 6.3102e-01 | 3.7539e-02 | 23 | 2.4 |
| 1098 | 1094 | 2455225.11815454 | 948725423 | 190.873 | -1.819 | -1.3370e-01 | 8.5313e-01 | 6.3102e-01 | 3.7539e-02 | 92 | 2.4 |
| 1099 | 1095 | 2455225.19082410 | 948731702 | 192.131 | 11.316 | -9.2963e-02 | 5.6770e-01 | 6.3052e-01 | 3.8106e-02 | 34 | 1.4 |
| 1100 | 1096 | 2455225.30049046 | 948741177 | 91.608 | -48.254 | -1.1724e-01 | 4.7983e-01 | 5.2936e-01 | 3.8897e-02 | 84 | 0.9 |
| 1101 | 1097 | 2455225.33291445 | 948743978 | 229.733 | -75.828 | -1.1724e-01 | 4.7983e-01 | 5.2936e-01 | 3.8897e-02 | 60 | 0.9 |
| 1102 | 1098 | 2455225.55116786 | 948762835 | 342.094 | 35.552 | -9.2963e-02 | 5.6770e-01 | 6.3052e-01 | 3.8106e-02 | 43 | 1.4 |
| 1103 | 1099 | 2455225.55806497 | 948763431 | 262.072 | 11.086 | -9.2963e-02 | 5.6770e-01 | 6.3052e-01 | 3.8106e-02 | 32 | 1.4 |
| 1104 | 1100 | 2455225.65571585 | 948771868 | 37.747 | 18.739 | -9.2963e-02 | 5.6770e-01 | 6.3052e-01 | 3.8106e-02 | 33 | 1.4 |
| 1105 | 1101 | 2455225.78345525 | 948782905 | 77.575 | -0.047 | -9.2963e-02 | 5.6770e-01 | 6.3052e-01 | 3.8106e-02 | 36 | 1.4 |
| 1106 | 1102 | 2455225.86544796 | 948789989 | 162.560 | -38.927 | -9.2963e-02 | 5.6770e-01 | 6.3052e-01 | 3.8106e-02 | 35 | 1.4 |
| 1107 | 1103 | 2455225.98945937 | 948800704 | 208.863 | -42.351 | -1.3370e-01 | 8.5313e-01 | 6.3102e-01 | 3.7539e-02 | 23 | 2.4 |
| 1108 | 1104 | 2455226.49592804 | 948844463 | 12.922 | -67.977 | -1.1724e-01 | 4.7983e-01 | 5.2936e-01 | 3.8897e-02 | 52 | 0.9 |
| 1109 | 1105 | 2455226.62185065 | 948855342 | 244.096 | -32.250 | -9.2963e-02 | 5.6770e-01 | 6.3052e-01 | 3.8106e-02 | 48 | 1.4 |
| 1110 | 1106 | 2455226.62876391 | 948855940 | 30.090 | -24.777 | -9.2963e-02 | 5.6770e-01 | 6.3052e-01 | 3.8106e-02 | 57 | 1.4 |
| 1111 | 1107 | 2455226.63261844 | 948856273 | 326.561 | -9.564 | -1.3370e-01 | 8.5313e-01 | 6.3102e-01 | 3.7539e-02 | 29 | 2.4 |
| 1112 | 1108 | 2455226.69199090 | 948861403 | 317.119 | -29.785 | -9.2963e-02 | 5.6770e-01 | 6.3052e-01 | 3.8106e-02 | 32 | 1.4 |
| 1113 | 1109 | 2455227.38304052 | 948921109 | 274.256 | -10.089 | -9.2963e-02 | 5.6770e-01 | 6.3052e-01 | 3.8106e-02 | 43 | 1.4 |
| 1114 | 1110 | 2455227.58180827 | 948938283 | 88.182 | -36.395 | -9.2963e-02 | 5.6770e-01 | 6.3052e-01 | 3.8106e-02 | 33 | 1.4 |
| 1115 | 1111 | 2455227.71621039 | 948949895 | 65.838 | -38.510 | -9.2963e-02 | 5.6770e-01 | 6.3052e-01 | 3.8106e-02 | 39 | 1.4 |
| 1116 | 1112 | 2455228.22342598 | 948993719 | 230.812 | 27.397 | -9.2963e-02 | 5.6770e-01 | 6.3052e-01 | 3.8106e-02 | 32 | 1.4 |
| 1117 | 1113 | 2455228.55535479 | 949022397 | 136.282 | -49.505 | -9.2963e-02 | 5.6770e-01 | 6.3052e-01 | 3.8106e-02 | 63 | 1.4 |
| 1118 | 1114 | 2455231.82649058 | 949305023 | 44.587 | -9.319 | -9.2963e-02 | 5.6770e-01 | 6.3052e-01 | 3.8106e-02 | 32 | 1.4 |
| 1119 | 1115 | 2455231.96039399 | 949316593 | 89.812 | -31.333 | -1.3370e-01 | 8.5313e-01 | 6.3102e-01 | 3.7539e-02 | 29 | 2.4 |
| 1120 | 1116 | 2455232.01008270 | 949320886 | 208.901 | 6.636 | -9.2963e-02 | 5.6770e-01 | 6.3052e-01 | 3.8106e-02 | 40 | 1.4 |
| 1121 | 1117 | 2455232.04375434 | 949323795 | 187.660 | -66.270 | -9.2963e-02 | 5.6770e-01 | 6.3052e-01 | 3.8106e-02 | 52 | 1.4 |
| 1122 | 1118 | 2455232.15063248 | 949333029 | 180.283 | 15.690 | -1.2873e-01 | 4.3155e-01 | 4.6595e-01 | 3.9162e-02 | 59 | 0.7 |
| 1123 | 1119 | 2455232.20247236 | 949337508 | 1.888 | -46.375 | -1.3370e-01 | 8.5313e-01 | 6.3102e-01 | 3.7539e-02 | 26 | 2.4 |
| 1124 | 1120 | 2455232.23740823 | 949340527 | 221.282 | -35.734 | -1.1724e-01 | 4.7983e-01 | 5.2936e-01 | 3.8897e-02 | 80 | 0.9 |
| 1125 | 1121 | 2455232.36926152 | 949351919 | 195.137 | -1.809 | -9.2963e-02 | 5.6770e-01 | 6.3052e-01 | 3.8106e-02 | 43 | 1.4 |
| 1126 | 1122 | 2455232.38524317 | 949353300 | 167.865 | -28.090 | -1.3370e-01 | 8.5313e-01 | 6.3102e-01 | 3.7539e-02 | 24 | 2.4 |
| 1127 | 1123 | 2455232.40058797 | 949354625 | 9.860 | -56.106 | -9.2963e-02 | 5.6770e-01 | 6.3052e-01 | 3.8106e-02 | 40 | 1.4 |

| | | | | | | | | | | | |
|------|------|------------------|-----------|---------|---------|-------------|------------|------------|------------|----|-----|
| 1128 | 1124 | 2455232.59851963 | 949371727 | 0.104 | -46.954 | -1.1724e-01 | 4.7983e-01 | 5.2936e-01 | 3.8897e-02 | 40 | 0.9 |
| 1129 | 1125 | 2455232.60584214 | 949372359 | 65.585 | -33.839 | -1.2873e-01 | 4.3155e-01 | 4.6595e-01 | 3.9162e-02 | 34 | 0.7 |
| 1130 | 1126 | 2455232.63352183 | 949374751 | 345.528 | 17.806 | -9.2963e-02 | 5.6770e-01 | 6.3052e-01 | 3.8106e-02 | 68 | 1.4 |
| 1131 | 1127 | 2455232.77243470 | 949386753 | 89.698 | 37.040 | -9.2963e-02 | 5.6770e-01 | 6.3052e-01 | 3.8106e-02 | 72 | 1.4 |
| 1132 | 1128 | 2455232.79390368 | 949388608 | 125.976 | 22.166 | -9.2963e-02 | 5.6770e-01 | 6.3052e-01 | 3.8106e-02 | 35 | 1.4 |
| 1133 | 1129 | 2455232.89347699 | 949397211 | 82.098 | -83.428 | -9.2963e-02 | 5.6770e-01 | 6.3052e-01 | 3.8106e-02 | 33 | 1.4 |
| 1134 | 1130 | 2455232.96587954 | 949403466 | 102.746 | 1.604 | -9.2963e-02 | 5.6770e-01 | 6.3052e-01 | 3.8106e-02 | 42 | 1.4 |
| 1135 | 1131 | 2455233.27333710 | 949430031 | 294.057 | -0.258 | -9.2963e-02 | 5.6770e-01 | 6.3052e-01 | 3.8106e-02 | 88 | 1.4 |
| 1136 | 1132 | 2455233.37104961 | 949438473 | 294.315 | -12.876 | -9.2963e-02 | 5.6770e-01 | 6.3052e-01 | 3.8106e-02 | 57 | 1.4 |
| 1137 | 1133 | 2455233.38794543 | 949439933 | 38.527 | -41.127 | -1.1724e-01 | 4.7983e-01 | 5.2936e-01 | 3.8897e-02 | 38 | 0.9 |
| 1138 | 1134 | 2455233.49782838 | 949449427 | 358.312 | 31.742 | -1.1724e-01 | 4.7983e-01 | 5.2936e-01 | 3.8897e-02 | 34 | 0.9 |
| 1139 | 1135 | 2455233.60557642 | 949458736 | 116.915 | -41.156 | -9.2963e-02 | 5.6770e-01 | 6.3052e-01 | 3.8106e-02 | 64 | 1.4 |
| 1140 | 1136 | 2455233.78372019 | 949474128 | 264.184 | -56.082 | -9.2963e-02 | 5.6770e-01 | 6.3052e-01 | 3.8106e-02 | 31 | 1.4 |
| 1141 | 1137 | 2455233.79082307 | 949474742 | 81.396 | -8.198 | -1.2873e-01 | 4.3155e-01 | 4.6595e-01 | 3.9162e-02 | 60 | 0.7 |
| 1142 | 1138 | 2455233.99792775 | 949492635 | 178.429 | -8.704 | -1.2873e-01 | 4.3155e-01 | 4.6595e-01 | 3.9162e-02 | 47 | 0.7 |
| 1143 | 1139 | 2455234.05581226 | 949497637 | 304.342 | -55.041 | -1.1724e-01 | 4.7983e-01 | 5.2936e-01 | 3.8897e-02 | 32 | 0.9 |
| 1144 | 1140 | 2455234.06206055 | 949498177 | 203.235 | -24.044 | -1.1724e-01 | 4.7983e-01 | 5.2936e-01 | 3.8897e-02 | 50 | 0.9 |
| 1145 | 1141 | 2455234.10329669 | 949501739 | 203.033 | 42.253 | -1.1724e-01 | 4.7983e-01 | 5.2936e-01 | 3.8897e-02 | 88 | 0.9 |
| 1146 | 1142 | 2455234.11349118 | 949502620 | 144.672 | -25.741 | -9.2963e-02 | 5.6770e-01 | 6.3052e-01 | 3.8106e-02 | 37 | 1.4 |
| 1147 | 1143 | 2455234.17226805 | 949507698 | 116.168 | -36.173 | -1.1909e-01 | 7.2127e-01 | 6.0423e-01 | 3.7507e-02 | 31 | 1.8 |
| 1148 | 1144 | 2455234.17458007 | 949507898 | 232.149 | -73.066 | -9.2963e-02 | 5.6770e-01 | 6.3052e-01 | 3.8106e-02 | 32 | 1.4 |
| 1149 | 1145 | 2455234.20308039 | 949510361 | 288.287 | 17.564 | -9.2963e-02 | 5.6770e-01 | 6.3052e-01 | 3.8106e-02 | 44 | 1.4 |
| 1150 | 1146 | 2455234.23349760 | 949512989 | 274.625 | -85.271 | -9.2963e-02 | 5.6770e-01 | 6.3052e-01 | 3.8106e-02 | 62 | 1.4 |
| 1151 | 1147 | 2455234.27105166 | 949516233 | 338.716 | -11.411 | -9.2963e-02 | 5.6770e-01 | 6.3052e-01 | 3.8106e-02 | 35 | 1.4 |
| 1152 | 1148 | 2455234.28405659 | 949517357 | 206.358 | 5.535 | -1.3370e-01 | 8.5313e-01 | 6.3102e-01 | 3.7539e-02 | 22 | 2.4 |
| 1153 | 1149 | 2455234.35606033 | 949523578 | 291.066 | 32.423 | -1.3370e-01 | 8.5313e-01 | 6.3102e-01 | 3.7539e-02 | 41 | 2.4 |
| 1154 | 1150 | 2455234.43237098 | 949530171 | 255.404 | -22.884 | -9.2963e-02 | 5.6770e-01 | 6.3052e-01 | 3.8106e-02 | 38 | 1.4 |
| 1155 | 1151 | 2455234.43997151 | 949530828 | 250.749 | -82.903 | -9.2963e-02 | 5.6770e-01 | 6.3052e-01 | 3.8106e-02 | 46 | 1.4 |
| 1156 | 1152 | 2455234.46632278 | 949533105 | 161.252 | -56.190 | -9.2963e-02 | 5.6770e-01 | 6.3052e-01 | 3.8106e-02 | 34 | 1.4 |
| 1157 | 1153 | 2455234.50218369 | 949536203 | 178.883 | -51.967 | -9.2963e-02 | 5.6770e-01 | 6.3052e-01 | 3.8106e-02 | 36 | 1.4 |
| 1158 | 1154 | 2455235.00724824 | 949579841 | 101.607 | -74.960 | -9.2963e-02 | 5.6770e-01 | 6.3052e-01 | 3.8106e-02 | 30 | 1.4 |
| 1159 | 1155 | 2455235.48053110 | 949620732 | 255.276 | 21.010 | -1.3370e-01 | 8.5313e-01 | 6.3102e-01 | 3.7539e-02 | 31 | 2.4 |
| 1160 | 1156 | 2455235.60015703 | 949631068 | 344.160 | 35.564 | -1.3370e-01 | 8.5313e-01 | 6.3102e-01 | 3.7539e-02 | 54 | 2.4 |
| 1161 | 1157 | 2455235.66886048 | 949637004 | 91.296 | 14.301 | -1.3370e-01 | 8.5313e-01 | 6.3102e-01 | 3.7539e-02 | 45 | 2.4 |
| 1162 | 1158 | 2455235.90736161 | 949657611 | 346.345 | -35.238 | -9.2963e-02 | 5.6770e-01 | 6.3052e-01 | 3.8106e-02 | 41 | 1.4 |
| 1163 | 1159 | 2455236.09782212 | 949674066 | 216.286 | -28.671 | -1.1724e-01 | 4.7983e-01 | 5.2936e-01 | 3.8897e-02 | 43 | 0.9 |
| 1164 | 1160 | 2455236.51118661 | 949709781 | 21.396 | -58.381 | -1.3370e-01 | 8.5313e-01 | 6.3102e-01 | 3.7539e-02 | 22 | 2.4 |
| 1165 | 1161 | 2455236.65832392 | 949722494 | 311.032 | -37.363 | -1.1909e-01 | 7.2127e-01 | 6.0423e-01 | 3.7507e-02 | 29 | 1.8 |
| 1166 | 1162 | 2455236.69194154 | 949725398 | 151.987 | -57.454 | -1.1724e-01 | 4.7983e-01 | 5.2936e-01 | 3.8897e-02 | 38 | 0.9 |
| 1167 | 1163 | 2455236.79559207 | 949734354 | 0.681 | -37.195 | -1.1909e-01 | 7.2127e-01 | 6.0423e-01 | 3.7507e-02 | 29 | 1.8 |
| 1168 | 1164 | 2455237.05170999 | 949756482 | 330.298 | -50.913 | -1.1724e-01 | 4.7983e-01 | 5.2936e-01 | 3.8897e-02 | 37 | 0.9 |
| 1169 | 1165 | 2455237.05319009 | 949756610 | 278.469 | -23.573 | -1.3370e-01 | 8.5313e-01 | 6.3102e-01 | 3.7539e-02 | 31 | 2.4 |
| 1170 | 1166 | 2455237.05822559 | 949757045 | 54.677 | -31.165 | -9.2963e-02 | 5.6770e-01 | 6.3052e-01 | 3.8106e-02 | 63 | 1.4 |
| 1171 | 1167 | 2455237.27419539 | 949775705 | 250.101 | 1.844 | -9.2963e-02 | 5.6770e-01 | 6.3052e-01 | 3.8106e-02 | 37 | 1.4 |
| 1172 | 1168 | 2455237.67022373 | 949809922 | 87.573 | 27.633 | -9.2963e-02 | 5.6770e-01 | 6.3052e-01 | 3.8106e-02 | 37 | 1.4 |
| 1173 | 1169 | 2455237.90749359 | 949830422 | 194.588 | -80.618 | -9.2963e-02 | 5.6770e-01 | 6.3052e-01 | 3.8106e-02 | 40 | 1.4 |
| 1174 | 1170 | 2455238.04709435 | 949842483 | 129.891 | -10.447 | -1.2873e-01 | 4.3155e-01 | 4.6595e-01 | 3.9162e-02 | 41 | 0.7 |
| 1175 | 1171 | 2455238.29850840 | 949864206 | 268.915 | -41.544 | -1.1724e-01 | 4.7983e-01 | 5.2936e-01 | 3.8897e-02 | 48 | 0.9 |
| 1176 | 1172 | 2455238.54279775 | 949885312 | 233.262 | -22.124 | -1.3370e-01 | 8.5313e-01 | 6.3102e-01 | 3.7539e-02 | 22 | 2.4 |
| 1177 | 1173 | 2455238.80680592 | 949908123 | 318.764 | -52.914 | -1.3370e-01 | 8.5313e-01 | 6.3102e-01 | 3.7539e-02 | 30 | 2.4 |
| 1178 | 1174 | 2455238.83067321 | 949910185 | 16.152 | 8.161 | -9.2963e-02 | 5.6770e-01 | 6.3052e-01 | 3.8106e-02 | 49 | 1.4 |
| 1179 | 1175 | 2455238.84593511 | 949911503 | 35.966 | 17.808 | -9.2963e-02 | 5.6770e-01 | 6.3052e-01 | 3.8106e-02 | 51 | 1.4 |

LIST OF HIGH ENERGY NEUTRINO CANDIDATES FOR THE 2009-2010 DATA

| | | | | | | | | | | | |
|------|------|------------------|-----------|---------|---------|-------------|------------|------------|------------|----|-----|
| 1180 | 1176 | 2455238.86708216 | 949913330 | 308.956 | -60.607 | -9.2963e-02 | 5.6770e-01 | 6.3052e-01 | 3.8106e-02 | 42 | 1.4 |
| 1181 | 1177 | 2455239.15188527 | 949937937 | 133.415 | 2.981 | -9.2963e-02 | 5.6770e-01 | 6.3052e-01 | 3.8106e-02 | 59 | 1.4 |
| 1182 | 1178 | 2455239.42988479 | 949961957 | 338.995 | 5.574 | -9.2963e-02 | 5.6770e-01 | 6.3052e-01 | 3.8106e-02 | 44 | 1.4 |
| 1183 | 1179 | 2455239.67181225 | 949982859 | 67.722 | -54.693 | -9.2963e-02 | 5.6770e-01 | 6.3052e-01 | 3.8106e-02 | 56 | 1.4 |
| 1184 | 1180 | 2455239.96451713 | 950008149 | 172.860 | -14.823 | -9.2963e-02 | 5.6770e-01 | 6.3052e-01 | 3.8106e-02 | 52 | 1.4 |
| 1185 | 1181 | 2455240.18513263 | 950027210 | 284.347 | -23.086 | -9.2963e-02 | 5.6770e-01 | 6.3052e-01 | 3.8106e-02 | 49 | 1.4 |
| 1186 | 1182 | 2455240.21007501 | 950029365 | 242.480 | -3.892 | -9.2963e-02 | 5.6770e-01 | 6.3052e-01 | 3.8106e-02 | 34 | 1.4 |
| 1187 | 1183 | 2455240.21160765 | 950029497 | 211.312 | -45.305 | -9.2963e-02 | 5.6770e-01 | 6.3052e-01 | 3.8106e-02 | 36 | 1.4 |
| 1188 | 1184 | 2455240.23034532 | 950031116 | 185.137 | -73.085 | -1.1724e-01 | 4.7983e-01 | 5.2936e-01 | 3.8897e-02 | 58 | 0.9 |
| 1189 | 1185 | 2455240.34505034 | 950041027 | 272.662 | -37.470 | -1.1724e-01 | 4.7983e-01 | 5.2936e-01 | 3.8897e-02 | 63 | 0.9 |
| 1190 | 1186 | 2455240.41802997 | 950047332 | 351.348 | -19.590 | -9.2963e-02 | 5.6770e-01 | 6.3052e-01 | 3.8106e-02 | 55 | 1.4 |
| 1191 | 1187 | 2455240.66495751 | 950068667 | 21.024 | -3.372 | -9.2963e-02 | 5.6770e-01 | 6.3052e-01 | 3.8106e-02 | 35 | 1.4 |
| 1192 | 1188 | 2455240.80404601 | 950080684 | 130.577 | -17.357 | -9.2963e-02 | 5.6770e-01 | 6.3052e-01 | 3.8106e-02 | 43 | 1.4 |
| 1193 | 1189 | 2455240.91853798 | 950090576 | 91.702 | -67.632 | -1.1724e-01 | 4.7983e-01 | 5.2936e-01 | 3.8897e-02 | 39 | 0.9 |
| 1194 | 1190 | 2455240.93571007 | 950092060 | 44.912 | -12.529 | -1.3370e-01 | 8.5313e-01 | 6.3102e-01 | 3.7539e-02 | 29 | 2.4 |
| 1195 | 1191 | 2455241.09773842 | 950106059 | 266.207 | -53.110 | -1.3370e-01 | 8.5313e-01 | 6.3102e-01 | 3.7539e-02 | 34 | 2.4 |
| 1196 | 1192 | 2455241.13957804 | 950109674 | 196.043 | -4.553 | -1.1724e-01 | 4.7983e-01 | 5.2936e-01 | 3.8897e-02 | 50 | 0.9 |
| 1197 | 1193 | 2455241.65199051 | 950153946 | 69.486 | 30.920 | -9.2963e-02 | 5.6770e-01 | 6.3052e-01 | 3.8106e-02 | 32 | 1.4 |
| 1198 | 1194 | 2455241.72682003 | 950160412 | 212.961 | -69.030 | -1.1724e-01 | 4.7983e-01 | 5.2936e-01 | 3.8897e-02 | 36 | 0.9 |
| 1199 | 1195 | 2455241.96851666 | 950181294 | 58.341 | 8.207 | -1.3370e-01 | 8.5313e-01 | 6.3102e-01 | 3.7539e-02 | 22 | 2.4 |
| 1200 | 1196 | 2455242.14205350 | 950196288 | 159.121 | -46.988 | -1.1724e-01 | 4.7983e-01 | 5.2936e-01 | 3.8897e-02 | 54 | 0.9 |
| 1201 | 1197 | 2455242.21229851 | 950202357 | 331.966 | -59.103 | -1.1909e-01 | 7.2127e-01 | 6.0423e-01 | 3.7507e-02 | 30 | 1.8 |
| 1202 | 1198 | 2455242.39309355 | 950217978 | 232.213 | 0.320 | -1.3370e-01 | 8.5313e-01 | 6.3102e-01 | 3.7539e-02 | 27 | 2.4 |
| 1203 | 1199 | 2455242.50935854 | 950228023 | 216.341 | -30.679 | -9.2963e-02 | 5.6770e-01 | 6.3052e-01 | 3.8106e-02 | 58 | 1.4 |
| 1204 | 1200 | 2455242.53919763 | 950230601 | 248.625 | -35.295 | -1.3370e-01 | 8.5313e-01 | 6.3102e-01 | 3.7539e-02 | 29 | 2.4 |
| 1205 | 1201 | 2455242.62830058 | 950238300 | 267.614 | -27.172 | -1.3370e-01 | 8.5313e-01 | 6.3102e-01 | 3.7539e-02 | 50 | 2.4 |
| 1206 | 1202 | 2455242.64813353 | 950240013 | 304.941 | 5.364 | -9.2963e-02 | 5.6770e-01 | 6.3052e-01 | 3.8106e-02 | 46 | 1.4 |
| 1207 | 1203 | 2455242.69406945 | 950243982 | 101.511 | -44.945 | -9.2963e-02 | 5.6770e-01 | 6.3052e-01 | 3.8106e-02 | 41 | 1.4 |
| 1208 | 1204 | 2455242.74461460 | 950248349 | 331.102 | -37.505 | -9.2963e-02 | 5.6770e-01 | 6.3052e-01 | 3.8106e-02 | 54 | 1.4 |
| 1209 | 1205 | 2455242.98259308 | 950268911 | 166.229 | 9.696 | -9.2963e-02 | 5.6770e-01 | 6.3052e-01 | 3.8106e-02 | 38 | 1.4 |
| 1210 | 1206 | 2455242.98397481 | 950269030 | 266.530 | -63.085 | -1.1724e-01 | 4.7983e-01 | 5.2936e-01 | 3.8897e-02 | 43 | 0.9 |
| 1211 | 1207 | 2455243.02402614 | 950272490 | 153.353 | 17.113 | -9.2963e-02 | 5.6770e-01 | 6.3052e-01 | 3.8106e-02 | 44 | 1.4 |
| 1212 | 1208 | 2455243.26316068 | 950293152 | 273.627 | 13.975 | -1.3370e-01 | 8.5313e-01 | 6.3102e-01 | 3.7539e-02 | 31 | 2.4 |
| 1213 | 1209 | 2455244.04238785 | 950360477 | 105.430 | -19.063 | -1.3370e-01 | 8.5313e-01 | 6.3102e-01 | 3.7539e-02 | 25 | 2.4 |
| 1214 | 1210 | 2455244.11037502 | 950366351 | 309.510 | -35.744 | -1.1724e-01 | 4.7983e-01 | 5.2936e-01 | 3.8897e-02 | 57 | 0.9 |
| 1215 | 1211 | 2455244.18681015 | 950372955 | 110.253 | -58.106 | -1.1724e-01 | 4.7983e-01 | 5.2936e-01 | 3.8897e-02 | 42 | 0.9 |
| 1216 | 1212 | 2455244.34751617 | 950386840 | 49.400 | -46.820 | -9.2963e-02 | 5.6770e-01 | 6.3052e-01 | 3.8106e-02 | 65 | 1.4 |
| 1217 | 1213 | 2455244.70301797 | 950417555 | 49.645 | -6.026 | -9.2963e-02 | 5.6770e-01 | 6.3052e-01 | 3.8106e-02 | 56 | 1.4 |
| 1218 | 1214 | 2455245.06326866 | 950448681 | 206.368 | -49.273 | -9.2963e-02 | 5.6770e-01 | 6.3052e-01 | 3.8106e-02 | 46 | 1.4 |
| 1219 | 1215 | 2455245.08729539 | 950450757 | 144.462 | -25.738 | -1.3370e-01 | 8.5313e-01 | 6.3102e-01 | 3.7539e-02 | 21 | 2.4 |
| 1220 | 1216 | 2455245.11403893 | 950453067 | 159.365 | 32.917 | -1.1724e-01 | 4.7983e-01 | 5.2936e-01 | 3.8897e-02 | 52 | 0.9 |
| 1221 | 1217 | 2455245.27470075 | 950466949 | 164.540 | -60.394 | -1.1724e-01 | 4.7983e-01 | 5.2936e-01 | 3.8897e-02 | 59 | 0.9 |
| 1222 | 1218 | 2455245.44499140 | 950481662 | 231.172 | -85.484 | -1.3370e-01 | 8.5313e-01 | 6.3102e-01 | 3.7539e-02 | 24 | 2.4 |
| 1223 | 1219 | 2455245.44966551 | 950482066 | 244.638 | -4.769 | -9.2963e-02 | 5.6770e-01 | 6.3052e-01 | 3.8106e-02 | 83 | 1.4 |
| 1224 | 1220 | 2455245.45975074 | 950482937 | 300.302 | 14.171 | -9.2963e-02 | 5.6770e-01 | 6.3052e-01 | 3.8106e-02 | 33 | 1.4 |
| 1225 | 1221 | 2455245.60601843 | 950495574 | 106.127 | -65.269 | -9.2963e-02 | 5.6770e-01 | 6.3052e-01 | 3.8106e-02 | 38 | 1.4 |
| 1226 | 1222 | 2455245.71563288 | 950505045 | 53.773 | 13.446 | -9.2963e-02 | 5.6770e-01 | 6.3052e-01 | 3.8106e-02 | 54 | 1.4 |
| 1227 | 1223 | 2455246.02217481 | 950531530 | 97.378 | -16.582 | -9.2963e-02 | 5.6770e-01 | 6.3052e-01 | 3.8106e-02 | 57 | 1.4 |
| 1228 | 1224 | 2455246.03158917 | 950532344 | 233.263 | -46.073 | -9.2963e-02 | 5.6770e-01 | 6.3052e-01 | 3.8106e-02 | 35 | 1.4 |
| 1229 | 1225 | 2455246.09805670 | 950538087 | 174.332 | -1.822 | -1.3370e-01 | 8.5313e-01 | 6.3102e-01 | 3.7539e-02 | 25 | 2.4 |
| 1230 | 1226 | 2455246.11528234 | 950539575 | 214.466 | 17.640 | -9.2963e-02 | 5.6770e-01 | 6.3052e-01 | 3.8106e-02 | 70 | 1.4 |
| 1231 | 1227 | 2455246.28998500 | 950554669 | 197.475 | 9.682 | -9.2963e-02 | 5.6770e-01 | 6.3052e-01 | 3.8106e-02 | 64 | 1.4 |

| | | | | | | | | | | | |
|------|------|------------------|-----------|---------|---------|-------------|------------|------------|------------|----|-----|
| 1232 | 1228 | 2455246.33228058 | 950558324 | 312.487 | -16.123 | -9.2963e-02 | 5.6770e-01 | 6.3052e-01 | 3.8106e-02 | 50 | 1.4 |
| 1233 | 1229 | 2455246.42955897 | 950566728 | 165.777 | -50.785 | -9.2963e-02 | 5.6770e-01 | 6.3052e-01 | 3.8106e-02 | 33 | 1.4 |
| 1234 | 1230 | 2455246.75944578 | 950595231 | 25.761 | 15.246 | -9.2963e-02 | 5.6770e-01 | 6.3052e-01 | 3.8106e-02 | 99 | 1.4 |
| 1235 | 1231 | 2455246.88573043 | 950606142 | 159.477 | 36.232 | -9.2963e-02 | 5.6770e-01 | 6.3052e-01 | 3.8106e-02 | 65 | 1.4 |
| 1236 | 1232 | 2455246.91716358 | 950608857 | 111.797 | 21.931 | -9.2963e-02 | 5.6770e-01 | 6.3052e-01 | 3.8106e-02 | 58 | 1.4 |
| 1237 | 1233 | 2455247.21308151 | 950634425 | 209.838 | -49.177 | -1.1724e-01 | 4.7983e-01 | 5.2936e-01 | 3.8897e-02 | 50 | 0.9 |
| 1238 | 1234 | 2455247.24815218 | 950637455 | 349.328 | -72.661 | -1.3370e-01 | 8.5313e-01 | 6.3102e-01 | 3.7539e-02 | 24 | 2.4 |
| 1239 | 1235 | 2455247.38435043 | 950649222 | 300.730 | -81.634 | -1.1724e-01 | 4.7983e-01 | 5.2936e-01 | 3.8897e-02 | 58 | 0.9 |
| 1240 | 1236 | 2455247.64487348 | 950671732 | 333.654 | -35.879 | -1.1724e-01 | 4.7983e-01 | 5.2936e-01 | 3.8897e-02 | 38 | 0.9 |
| 1241 | 1237 | 2455248.12800971 | 950713475 | 244.347 | 6.203 | -1.3370e-01 | 8.5313e-01 | 6.3102e-01 | 3.7539e-02 | 30 | 2.4 |
| 1242 | 1238 | 2455248.15882571 | 950716137 | 189.658 | -63.631 | -1.2873e-01 | 4.3155e-01 | 4.6595e-01 | 3.9162e-02 | 83 | 0.7 |
| 1243 | 1239 | 2455248.37754314 | 950735034 | 216.336 | 5.409 | -1.2873e-01 | 4.3155e-01 | 4.6595e-01 | 3.9162e-02 | 53 | 0.7 |
| 1244 | 1240 | 2455248.70727778 | 950763523 | 298.895 | -33.968 | -9.2963e-02 | 5.6770e-01 | 6.3052e-01 | 3.8106e-02 | 52 | 1.4 |
| 1245 | 1241 | 2455248.87771300 | 950778249 | 99.719 | -15.781 | -1.1724e-01 | 4.7983e-01 | 5.2936e-01 | 3.8897e-02 | 51 | 0.9 |
| 1246 | 1242 | 2455248.91453510 | 950781430 | 239.154 | -23.460 | -1.1724e-01 | 4.7983e-01 | 5.2936e-01 | 3.8897e-02 | 32 | 0.9 |
| 1247 | 1243 | 2455249.05170480 | 950793282 | 109.860 | -2.231 | -1.3370e-01 | 8.5313e-01 | 6.3102e-01 | 3.7539e-02 | 31 | 2.4 |
| 1248 | 1244 | 2455249.07433209 | 950795237 | 288.527 | -70.925 | -9.2963e-02 | 5.6770e-01 | 6.3052e-01 | 3.8106e-02 | 65 | 1.4 |
| 1249 | 1245 | 2455249.32470947 | 950816869 | 352.745 | -11.411 | -9.2963e-02 | 5.6770e-01 | 6.3052e-01 | 3.8106e-02 | 50 | 1.4 |
| 1250 | 1246 | 2455249.48498370 | 950830717 | 331.292 | -45.173 | -9.2963e-02 | 5.6770e-01 | 6.3052e-01 | 3.8106e-02 | 48 | 1.4 |
| 1251 | 1247 | 2455249.53726233 | 950835234 | 104.269 | -29.206 | -9.2963e-02 | 5.6770e-01 | 6.3052e-01 | 3.8106e-02 | 36 | 1.4 |
| 1252 | 1248 | 2455249.90214154 | 950866760 | 88.128 | -32.685 | -1.1724e-01 | 4.7983e-01 | 5.2936e-01 | 3.8897e-02 | 61 | 0.9 |
| 1253 | 1249 | 2455249.94436753 | 950870408 | 133.525 | 39.457 | -1.1909e-01 | 7.2127e-01 | 6.0423e-01 | 3.7507e-02 | 31 | 1.8 |
| 1254 | 1250 | 2455250.04090446 | 950878749 | 147.859 | -28.125 | -1.1909e-01 | 7.2127e-01 | 6.0423e-01 | 3.7507e-02 | 28 | 1.8 |
| 1255 | 1251 | 2455250.04838391 | 950879395 | 147.227 | 22.454 | -9.2963e-02 | 5.6770e-01 | 6.3052e-01 | 3.8106e-02 | 39 | 1.4 |
| 1256 | 1252 | 2455250.47216235 | 950916009 | 223.921 | -39.904 | -9.2963e-02 | 5.6770e-01 | 6.3052e-01 | 3.8106e-02 | 54 | 1.4 |
| 1257 | 1253 | 2455250.50063640 | 950918469 | 316.257 | -3.098 | -1.3370e-01 | 8.5313e-01 | 6.3102e-01 | 3.7539e-02 | 28 | 2.4 |
| 1258 | 1254 | 2455250.54714032 | 950922487 | 246.636 | -32.686 | -1.1724e-01 | 4.7983e-01 | 5.2936e-01 | 3.8897e-02 | 35 | 0.9 |
| 1259 | 1255 | 2455250.70674558 | 950936277 | 25.209 | 21.320 | -9.2963e-02 | 5.6770e-01 | 6.3052e-01 | 3.8106e-02 | 36 | 1.4 |
| 1260 | 1256 | 2455251.06517422 | 950967246 | 171.914 | 42.818 | -9.2963e-02 | 5.6770e-01 | 6.3052e-01 | 3.8106e-02 | 60 | 1.4 |
| 1261 | 1257 | 2455251.11415422 | 950971477 | 183.872 | -24.055 | -9.2963e-02 | 5.6770e-01 | 6.3052e-01 | 3.8106e-02 | 55 | 1.4 |
| 1262 | 1258 | 2455251.13918401 | 950973640 | 354.176 | -81.250 | -1.1724e-01 | 4.7983e-01 | 5.2936e-01 | 3.8897e-02 | 43 | 0.9 |
| 1263 | 1259 | 2455251.19776064 | 950978701 | 280.767 | -6.270 | -1.1724e-01 | 4.7983e-01 | 5.2936e-01 | 3.8897e-02 | 58 | 0.9 |
| 1264 | 1260 | 2455251.28195543 | 950985975 | 355.240 | -7.914 | -9.2963e-02 | 5.6770e-01 | 6.3052e-01 | 3.8106e-02 | 33 | 1.4 |
| 1265 | 1261 | 2455251.37408099 | 950993935 | 257.172 | 25.183 | -9.2963e-02 | 5.6770e-01 | 6.3052e-01 | 3.8106e-02 | 44 | 1.4 |
| 1266 | 1262 | 2455251.43607378 | 950999291 | 273.004 | -26.267 | -1.1724e-01 | 4.7983e-01 | 5.2936e-01 | 3.8897e-02 | 44 | 0.9 |
| 1267 | 1263 | 2455251.45271221 | 951000729 | 242.559 | -48.993 | -1.3370e-01 | 8.5313e-01 | 6.3102e-01 | 3.7539e-02 | 27 | 2.4 |
| 1268 | 1264 | 2455251.53134595 | 951007523 | 120.158 | -52.530 | -1.3370e-01 | 8.5313e-01 | 6.3102e-01 | 3.7539e-02 | 31 | 2.4 |
| 1269 | 1265 | 2455254.56912428 | 951269987 | 300.560 | -22.486 | -1.1724e-01 | 4.7983e-01 | 5.2936e-01 | 3.8897e-02 | 38 | 0.9 |
| 1270 | 1266 | 2455254.83440150 | 951292907 | 113.376 | -39.305 | -9.2963e-02 | 5.6770e-01 | 6.3052e-01 | 3.8106e-02 | 50 | 1.4 |
| 1271 | 1267 | 2455255.15049270 | 951320217 | 334.300 | -27.545 | -1.3370e-01 | 8.5313e-01 | 6.3102e-01 | 3.7539e-02 | 30 | 2.4 |
| 1272 | 1268 | 2455255.19945811 | 951324448 | 305.669 | 8.883 | -9.2963e-02 | 5.6770e-01 | 6.3052e-01 | 3.8106e-02 | 54 | 1.4 |
| 1273 | 1269 | 2455255.21161200 | 951325498 | 299.542 | -66.919 | -1.1724e-01 | 4.7983e-01 | 5.2936e-01 | 3.8897e-02 | 52 | 0.9 |
| 1274 | 1270 | 2455255.27759747 | 951331199 | 239.712 | -50.950 | -1.1724e-01 | 4.7983e-01 | 5.2936e-01 | 3.8897e-02 | 76 | 0.9 |
| 1275 | 1271 | 2455255.28326351 | 951331688 | 341.809 | -38.533 | -1.3370e-01 | 8.5313e-01 | 6.3102e-01 | 3.7539e-02 | 29 | 2.4 |
| 1276 | 1272 | 2455255.43858706 | 951345108 | 104.708 | -49.112 | -1.3370e-01 | 8.5313e-01 | 6.3102e-01 | 3.7539e-02 | 34 | 2.4 |
| 1277 | 1273 | 2455255.75018716 | 951372031 | 32.381 | -24.453 | -1.3370e-01 | 8.5313e-01 | 6.3102e-01 | 3.7539e-02 | 27 | 2.4 |
| 1278 | 1274 | 2455255.83863293 | 951379672 | 198.367 | -22.289 | -9.2963e-02 | 5.6770e-01 | 6.3052e-01 | 3.8106e-02 | 45 | 1.4 |
| 1279 | 1275 | 2455255.90554189 | 951385453 | 95.598 | -57.626 | -1.3370e-01 | 8.5313e-01 | 6.3102e-01 | 3.7539e-02 | 30 | 2.4 |
| 1280 | 1276 | 2455256.15353235 | 951406880 | 265.867 | -14.570 | -1.1724e-01 | 4.7983e-01 | 5.2936e-01 | 3.8897e-02 | 33 | 0.9 |
| 1281 | 1277 | 2455256.29602770 | 951419191 | 153.135 | -27.213 | -9.2963e-02 | 5.6770e-01 | 6.3052e-01 | 3.8106e-02 | 62 | 1.4 |
| 1282 | 1278 | 2455256.40462749 | 951428574 | 272.305 | 34.817 | -1.1724e-01 | 4.7983e-01 | 5.2936e-01 | 3.8897e-02 | 47 | 0.9 |
| 1283 | 1279 | 2455256.60036258 | 951445486 | 113.578 | -58.128 | -1.3370e-01 | 8.5313e-01 | 6.3102e-01 | 3.7539e-02 | 27 | 2.4 |

LIST OF HIGH ENERGY NEUTRINO CANDIDATES FOR THE 2009-2010 DATA

| | | | | | | | | | | | |
|------|------|------------------|-----------|---------|---------|-------------|------------|------------|------------|----|-----|
| 1284 | 1280 | 2455256.60499258 | 951445886 | 40.650 | 28.305 | -9.2963e-02 | 5.6770e-01 | 6.3052e-01 | 3.8106e-02 | 50 | 1.4 |
| 1285 | 1281 | 2455256.71003407 | 951454961 | 68.124 | 16.054 | -9.2963e-02 | 5.6770e-01 | 6.3052e-01 | 3.8106e-02 | 47 | 1.4 |
| 1286 | 1282 | 2455256.79754508 | 951462522 | 122.853 | -74.560 | -1.1724e-01 | 4.7983e-01 | 5.2936e-01 | 3.8897e-02 | 42 | 0.9 |
| 1287 | 1283 | 2455256.89157759 | 951470647 | 137.086 | 37.464 | -1.1724e-01 | 4.7983e-01 | 5.2936e-01 | 3.8897e-02 | 47 | 0.9 |
| 1288 | 1284 | 2455256.91242316 | 951472448 | 92.657 | -35.438 | -1.1909e-01 | 7.2127e-01 | 6.0423e-01 | 3.7507e-02 | 31 | 1.8 |
| 1289 | 1285 | 2455256.93188579 | 951474129 | 186.059 | -27.492 | -1.1909e-01 | 7.2127e-01 | 6.0423e-01 | 3.7507e-02 | 29 | 1.8 |
| 1290 | 1286 | 2455257.31602508 | 951507319 | 247.774 | 28.999 | -9.2963e-02 | 5.6770e-01 | 6.3052e-01 | 3.8106e-02 | 57 | 1.4 |
| 1291 | 1287 | 2455257.47023293 | 951520643 | 251.381 | -6.165 | -9.2963e-02 | 5.6770e-01 | 6.3052e-01 | 3.8106e-02 | 66 | 1.4 |
| 1292 | 1288 | 2455257.66049793 | 951537082 | 152.998 | -27.867 | -1.2873e-01 | 4.3155e-01 | 4.6595e-01 | 3.9162e-02 | 58 | 0.7 |
| 1293 | 1289 | 2455257.70898795 | 951541271 | 137.758 | -63.620 | -1.2873e-01 | 4.3155e-01 | 4.6595e-01 | 3.9162e-02 | 59 | 0.7 |
| 1294 | 1290 | 2455257.73587488 | 951543594 | 29.546 | 27.063 | -1.3370e-01 | 8.5313e-01 | 6.3102e-01 | 3.7539e-02 | 31 | 2.4 |
| 1295 | 1291 | 2455257.79489538 | 951548693 | 61.982 | 2.317 | -1.3370e-01 | 8.5313e-01 | 6.3102e-01 | 3.7539e-02 | 88 | 2.4 |
| 1296 | 1292 | 2455258.03068668 | 951569066 | 244.968 | -5.899 | -1.1909e-01 | 7.2127e-01 | 6.0423e-01 | 3.7507e-02 | 30 | 1.8 |
| 1297 | 1293 | 2455258.06352406 | 951571903 | 252.012 | -74.408 | -1.1909e-01 | 7.2127e-01 | 6.0423e-01 | 3.7507e-02 | 32 | 1.8 |
| 1298 | 1294 | 2455258.08327040 | 951573609 | 224.081 | -12.926 | -1.1724e-01 | 4.7983e-01 | 5.2936e-01 | 3.8897e-02 | 80 | 0.9 |
| 1299 | 1295 | 2455258.10306321 | 951575319 | 112.776 | -2.369 | -9.2963e-02 | 5.6770e-01 | 6.3052e-01 | 3.8106e-02 | 97 | 1.4 |
| 1300 | 1296 | 2455258.16277478 | 951580478 | 311.195 | -16.847 | -9.2963e-02 | 5.6770e-01 | 6.3052e-01 | 3.8106e-02 | 43 | 1.4 |
| 1301 | 1297 | 2455258.25098552 | 951588100 | 199.424 | -68.796 | -9.2963e-02 | 5.6770e-01 | 6.3052e-01 | 3.8106e-02 | 45 | 1.4 |
| 1302 | 1298 | 2455259.94614591 | 951734562 | 147.978 | 14.078 | -9.2963e-02 | 5.6770e-01 | 6.3052e-01 | 3.8106e-02 | 52 | 1.4 |
| 1303 | 1299 | 2455259.96364018 | 951736073 | 32.567 | -41.438 | -1.3370e-01 | 8.5313e-01 | 6.3102e-01 | 3.7539e-02 | 28 | 2.4 |
| 1304 | 1300 | 2455260.02215769 | 951741129 | 189.316 | -66.285 | -9.2963e-02 | 5.6770e-01 | 6.3052e-01 | 3.8106e-02 | 35 | 1.4 |
| 1305 | 1301 | 2455260.12224479 | 951749776 | 157.221 | 30.385 | -9.2963e-02 | 5.6770e-01 | 6.3052e-01 | 3.8106e-02 | 46 | 1.4 |
| 1306 | 1302 | 2455260.18633076 | 951755313 | 232.560 | 18.338 | -1.3370e-01 | 8.5313e-01 | 6.3102e-01 | 3.7539e-02 | 30 | 2.4 |
| 1307 | 1303 | 2455260.32220811 | 951767053 | 288.229 | -11.089 | -1.3370e-01 | 8.5313e-01 | 6.3102e-01 | 3.7539e-02 | 30 | 2.4 |
| 1308 | 1304 | 2455260.43713780 | 951776983 | 38.091 | 14.978 | -9.2963e-02 | 5.6770e-01 | 6.3052e-01 | 3.8106e-02 | 71 | 1.4 |
| 1309 | 1305 | 2455260.44574146 | 951777727 | 252.298 | 5.147 | -9.2963e-02 | 5.6770e-01 | 6.3052e-01 | 3.8106e-02 | 46 | 1.4 |
| 1310 | 1306 | 2455260.53491109 | 951785431 | 322.231 | -40.597 | -1.1909e-01 | 7.2127e-01 | 6.0423e-01 | 3.7507e-02 | 31 | 1.8 |
| 1311 | 1307 | 2455260.60643335 | 951791610 | 137.134 | -63.994 | -1.3370e-01 | 8.5313e-01 | 6.3102e-01 | 3.7539e-02 | 31 | 2.4 |
| 1312 | 1308 | 2455260.75423916 | 951804381 | 38.562 | -31.526 | -9.2963e-02 | 5.6770e-01 | 6.3052e-01 | 3.8106e-02 | 40 | 1.4 |
| 1313 | 1309 | 2455261.19588286 | 951842539 | 315.265 | -7.455 | -9.2963e-02 | 5.6770e-01 | 6.3052e-01 | 3.8106e-02 | 35 | 1.4 |
| 1314 | 1310 | 2455261.31298374 | 951852656 | 230.839 | 16.296 | -9.2963e-02 | 5.6770e-01 | 6.3052e-01 | 3.8106e-02 | 35 | 1.4 |
| 1315 | 1311 | 2455261.34274907 | 951855228 | 286.390 | -75.079 | -9.2963e-02 | 5.6770e-01 | 6.3052e-01 | 3.8106e-02 | 35 | 1.4 |
| 1316 | 1312 | 2455261.76379208 | 951891606 | 339.817 | -33.331 | -9.2963e-02 | 5.6770e-01 | 6.3052e-01 | 3.8106e-02 | 60 | 1.4 |
| 1317 | 1313 | 2455261.78229491 | 951893205 | 154.027 | 10.076 | -1.3370e-01 | 8.5313e-01 | 6.3102e-01 | 3.7539e-02 | 30 | 2.4 |
| 1318 | 1314 | 2455261.80862669 | 951895480 | 138.568 | -13.318 | -1.3370e-01 | 8.5313e-01 | 6.3102e-01 | 3.7539e-02 | 31 | 2.4 |
| 1319 | 1315 | 2455261.89353787 | 951902816 | 33.102 | -15.791 | -1.3370e-01 | 8.5313e-01 | 6.3102e-01 | 3.7539e-02 | 35 | 2.4 |
| 1320 | 1316 | 2455261.93239698 | 951906174 | 95.193 | 11.129 | -9.2963e-02 | 5.6770e-01 | 6.3052e-01 | 3.8106e-02 | 35 | 1.4 |
| 1321 | 1317 | 2455263.29721293 | 952024094 | 210.043 | 3.714 | -9.2963e-02 | 5.6770e-01 | 6.3052e-01 | 3.8106e-02 | 82 | 1.4 |
| 1322 | 1318 | 2455267.62379628 | 952397910 | 83.137 | -15.107 | -1.1724e-01 | 4.7983e-01 | 5.2936e-01 | 3.8897e-02 | 40 | 0.9 |
| 1323 | 1319 | 2455267.67307166 | 952402168 | 132.980 | -18.113 | -9.2963e-02 | 5.6770e-01 | 6.3052e-01 | 3.8106e-02 | 33 | 1.4 |
| 1324 | 1320 | 2455267.67338965 | 952402195 | 3.705 | -35.560 | -1.3370e-01 | 8.5313e-01 | 6.3102e-01 | 3.7539e-02 | 28 | 2.4 |
| 1325 | 1321 | 2455267.67367323 | 952402220 | 100.637 | 37.467 | -1.3370e-01 | 8.5313e-01 | 6.3102e-01 | 3.7539e-02 | 60 | 2.4 |
| 1326 | 1322 | 2455267.81031033 | 952414025 | 159.353 | 32.380 | -1.3370e-01 | 8.5313e-01 | 6.3102e-01 | 3.7539e-02 | 30 | 2.4 |
| 1327 | 1323 | 2455267.84146818 | 952416717 | 233.180 | -26.350 | -1.3370e-01 | 8.5313e-01 | 6.3102e-01 | 3.7539e-02 | 29 | 2.4 |
| 1328 | 1324 | 2455268.35150423 | 952460784 | 189.398 | -60.340 | -1.3370e-01 | 8.5313e-01 | 6.3102e-01 | 3.7539e-02 | 24 | 2.4 |
| 1329 | 1325 | 2455268.35481495 | 952461071 | 214.756 | -29.087 | -1.3370e-01 | 8.5313e-01 | 6.3102e-01 | 3.7539e-02 | 30 | 2.4 |
| 1330 | 1326 | 2455268.40013440 | 952464986 | 301.321 | -50.569 | -1.1724e-01 | 4.7983e-01 | 5.2936e-01 | 3.8897e-02 | 49 | 0.9 |
| 1331 | 1327 | 2455280.29903374 | 953493051 | 274.970 | -70.396 | -9.2963e-02 | 5.6770e-01 | 6.3052e-01 | 3.8106e-02 | 37 | 1.4 |
| 1332 | 1328 | 2455283.30609960 | 953752862 | 198.173 | -42.956 | -9.2963e-02 | 5.6770e-01 | 6.3052e-01 | 3.8106e-02 | 38 | 1.4 |
| 1333 | 1329 | 2455283.43377335 | 953763893 | 18.049 | -35.932 | -9.2963e-02 | 5.6770e-01 | 6.3052e-01 | 3.8106e-02 | 33 | 1.4 |
| 1334 | 1330 | 2455283.47959317 | 953767851 | 66.466 | -22.341 | -9.2963e-02 | 5.6770e-01 | 6.3052e-01 | 3.8106e-02 | 52 | 1.4 |
| 1335 | 1331 | 2455283.77032782 | 953792971 | 131.524 | -17.652 | -1.1724e-01 | 4.7983e-01 | 5.2936e-01 | 3.8897e-02 | 52 | 0.9 |

1336 1332 2455284.90541283 953891042 71.241 -33.435 -9.2963e-02 5.6770e-01 6.3052e-01 3.8106e-02 37 1.4
1337 1333 2455284.91821652 953892148 227.039 -65.340 -9.2963e-02 5.6770e-01 6.3052e-01 3.8106e-02 31 1.4
1338 1334 2455285.01907694 953900863 155.875 -29.601 -9.2963e-02 5.6770e-01 6.3052e-01 3.8106e-02 61 1.4
1339 1335 2455285.22608287 953918748 316.749 -64.999 -9.2963e-02 5.6770e-01 6.3052e-01 3.8106e-02 61 1.4
1340 1336 2455285.32338085 953927155 232.948 -29.647 -9.2963e-02 5.6770e-01 6.3052e-01 3.8106e-02 54 1.4
1341 1337 2455285.45588485 953938603 111.069 -50.826 -9.2963e-02 5.6770e-01 6.3052e-01 3.8106e-02 47 1.4
1342 1338 2455285.50638051 953942966 43.810 0.722 -9.2963e-02 5.6770e-01 6.3052e-01 3.8106e-02 35 1.4
1343 1339 2455285.63365691 953953962 342.064 -46.721 -9.2963e-02 5.6770e-01 6.3052e-01 3.8106e-02 42 1.4
1344 1340 2455285.78249703 953966822 78.165 30.326 -9.2963e-02 5.6770e-01 6.3052e-01 3.8106e-02 37 1.4
1345 1341 2455285.84646996 953972350 166.717 23.895 -1.1724e-01 4.7983e-01 5.2936e-01 3.8897e-02 52 0.9
1346 1342 2455286.05485091 953990354 76.126 -71.186 -5.8944e-02 2.9333e-01 5.7306e-01 3.8834e-02 106 0.6
1347 1343 2455286.12994036 953996841 272.941 33.026 -9.2963e-02 5.6770e-01 6.3052e-01 3.8106e-02 42 1.4
1348 1344 2455286.19644749 954002588 333.943 -54.377 -9.2963e-02 5.6770e-01 6.3052e-01 3.8106e-02 94 1.4
1349 1345 2455286.45788897 954025176 265.583 -7.233 -9.2963e-02 5.6770e-01 6.3052e-01 3.8106e-02 36 1.4
1350 1346 2455286.65496167 954042203 117.467 -31.204 -1.1724e-01 4.7983e-01 5.2936e-01 3.8897e-02 46 0.9
1351 1347 2455286.68027402 954044390 34.538 -83.079 -9.2963e-02 5.6770e-01 6.3052e-01 3.8106e-02 43 1.4
1352 1348 2455286.69960489 954046060 60.444 -40.071 -1.1724e-01 4.7983e-01 5.2936e-01 3.8897e-02 83 0.9
1353 1349 2455286.70877901 954046853 347.634 -31.890 -1.1724e-01 4.7983e-01 5.2936e-01 3.8897e-02 43 0.9
1354 1350 2455286.83997087 954058188 124.098 -20.895 -9.2963e-02 5.6770e-01 6.3052e-01 3.8106e-02 38 1.4
1355 1351 2455287.02338135 954074035 163.752 -62.606 -1.3370e-01 8.5313e-01 6.3102e-01 3.7539e-02 23 2.4
1356 1352 2455287.08176524 954079079 277.041 -13.477 -1.3370e-01 8.5313e-01 6.3102e-01 3.7539e-02 28 2.4
1357 1353 2455287.61673736 954125301 83.916 32.279 -1.1909e-01 7.2127e-01 6.0423e-01 3.7507e-02 31 1.8
1358 1354 2455287.86721703 954146942 104.179 -35.902 -5.8944e-02 2.9333e-01 5.7306e-01 3.8834e-02 107 0.6
1359 1355 2455287.88643340 954148602 105.853 32.275 -1.3370e-01 8.5313e-01 6.3102e-01 3.7539e-02 27 2.4
1360 1356 2455288.20731313 954176326 242.669 -7.154 -1.3370e-01 8.5313e-01 6.3102e-01 3.7539e-02 25 2.4
1361 1357 2455288.21580076 954177060 164.575 -21.435 -9.2963e-02 5.6770e-01 6.3052e-01 3.8106e-02 35 1.4
1362 1358 2455288.42881651 954195464 335.653 -1.559 -9.2963e-02 5.6770e-01 6.3052e-01 3.8106e-02 44 1.4
1363 1359 2455288.59563127 954209877 95.769 -49.679 -9.2963e-02 5.6770e-01 6.3052e-01 3.8106e-02 42 1.4
1364 1360 2455288.62424942 954212350 108.890 23.990 -9.2963e-02 5.6770e-01 6.3052e-01 3.8106e-02 36 1.4
1365 1361 2455288.68381763 954217496 165.791 -20.770 -1.1724e-01 4.7983e-01 5.2936e-01 3.8897e-02 65 0.9
1366 1362 2455289.15006982 954257781 270.689 -28.074 -9.2963e-02 5.6770e-01 6.3052e-01 3.8106e-02 36 1.4
1367 1363 2455291.12335500 954428272 262.101 20.130 -1.1724e-01 4.7983e-01 5.2936e-01 3.8897e-02 47 0.9
1368 1364 2455291.46249512 954457574 343.776 -15.150 -1.1724e-01 4.7983e-01 5.2936e-01 3.8897e-02 48 0.9
1369 1365 2455291.69763300 954477890 54.094 19.770 -9.2963e-02 5.6770e-01 6.3052e-01 3.8106e-02 37 1.4
1370 1366 2455292.22765110 954523684 247.471 -29.202 -1.3370e-01 8.5313e-01 6.3102e-01 3.7539e-02 31 2.4
1371 1367 2455292.24820815 954525460 234.509 21.605 -1.1724e-01 4.7983e-01 5.2936e-01 3.8897e-02 94 0.9
1372 1368 2455292.29463392 954529471 270.203 8.486 -9.2963e-02 5.6770e-01 6.3052e-01 3.8106e-02 39 1.4
1373 1369 2455292.49014666 954546363 359.652 -10.742 -1.3370e-01 8.5313e-01 6.3102e-01 3.7539e-02 29 2.4
1374 1370 2455292.52128847 954549054 33.260 14.021 -9.2963e-02 5.6770e-01 6.3052e-01 3.8106e-02 36 1.4
1375 1371 2455292.57108652 954553356 51.280 -35.735 -9.2963e-02 5.6770e-01 6.3052e-01 3.8106e-02 66 1.4
1376 1372 2455292.68902117 954563546 96.097 -32.419 -8.8598e-02 3.3283e-01 5.3278e-01 3.9884e-02 111 0.6
1377 1373 2455292.73629607 954567630 91.906 10.251 -1.3370e-01 8.5313e-01 6.3102e-01 3.7539e-02 30 2.4
1378 1374 2455292.75246910 954569028 203.231 -3.709 -9.2963e-02 5.6770e-01 6.3052e-01 3.8106e-02 36 1.4
1379 1375 2455292.81947784 954574817 127.065 12.601 -1.3370e-01 8.5313e-01 6.3102e-01 3.7539e-02 31 2.4
1380 1376 2455292.89357225 954581219 44.004 -29.827 -1.3370e-01 8.5313e-01 6.3102e-01 3.7539e-02 31 2.4
1381 1377 2455293.11053481 954599965 2.780 -40.146 -9.2963e-02 5.6770e-01 6.3052e-01 3.8106e-02 35 1.4
1382 1378 2455293.11912271 954600707 292.842 17.945 -9.2963e-02 5.6770e-01 6.3052e-01 3.8106e-02 43 1.4
1383 1379 2455293.17125132 954605211 262.566 -41.919 -9.2963e-02 5.6770e-01 6.3052e-01 3.8106e-02 41 1.4
1384 1380 2455293.27960597 954614572 256.933 0.180 -1.3370e-01 8.5313e-01 6.3102e-01 3.7539e-02 30 2.4
1385 1381 2455293.28418842 954614968 91.264 -78.875 -9.2963e-02 5.6770e-01 6.3052e-01 3.8106e-02 45 1.4
1386 1382 2455293.30188583 954616497 18.778 -34.856 -1.3370e-01 8.5313e-01 6.3102e-01 3.7539e-02 28 2.4
1387 1383 2455293.41606072 954626362 6.602 2.667 -1.1724e-01 4.7983e-01 5.2936e-01 3.8897e-02 32 0.9

LIST OF HIGH ENERGY NEUTRINO CANDIDATES FOR THE 2009-2010 DATA

| | | | | | | | | | | | |
|------|------|------------------|-----------|---------|---------|-------------|------------|------------|------------|----|-----|
| 1388 | 1384 | 2455293.41668533 | 954626416 | 325.188 | 37.603 | -9.2963e-02 | 5.6770e-01 | 6.3052e-01 | 3.8106e-02 | 61 | 1.4 |
| 1389 | 1385 | 2455293.44424809 | 954628798 | 77.478 | 11.282 | -9.2963e-02 | 5.6770e-01 | 6.3052e-01 | 3.8106e-02 | 43 | 1.4 |
| 1390 | 1386 | 2455293.45458253 | 954629690 | 31.232 | -9.580 | -1.1724e-01 | 4.7983e-01 | 5.2936e-01 | 3.8897e-02 | 44 | 0.9 |
| 1391 | 1387 | 2455293.49485037 | 954633170 | 101.306 | -2.677 | -1.1724e-01 | 4.7983e-01 | 5.2936e-01 | 3.8897e-02 | 37 | 0.9 |
| 1392 | 1388 | 2455293.57516357 | 954640109 | 4.230 | -29.401 | -9.2963e-02 | 5.6770e-01 | 6.3052e-01 | 3.8106e-02 | 40 | 1.4 |
| 1393 | 1389 | 2455293.60671236 | 954642834 | 255.412 | -46.157 | -9.2963e-02 | 5.6770e-01 | 6.3052e-01 | 3.8106e-02 | 41 | 1.4 |
| 1394 | 1390 | 2455293.63365788 | 954645163 | 103.551 | 19.820 | -1.3370e-01 | 8.5313e-01 | 6.3102e-01 | 3.7539e-02 | 31 | 2.4 |
| 1395 | 1391 | 2455293.69882299 | 954650793 | 41.047 | -30.233 | -1.2873e-01 | 4.3155e-01 | 4.6595e-01 | 3.9162e-02 | 80 | 0.7 |
| 1396 | 1392 | 2455293.75432706 | 954655588 | 292.463 | -47.971 | -1.1724e-01 | 4.7983e-01 | 5.2936e-01 | 3.8897e-02 | 47 | 0.9 |
| 1397 | 1393 | 2455293.76192011 | 954656244 | 219.685 | -27.691 | -1.3370e-01 | 8.5313e-01 | 6.3102e-01 | 3.7539e-02 | 25 | 2.4 |
| 1398 | 1394 | 2455293.92012988 | 954669914 | 164.733 | -37.380 | -9.2963e-02 | 5.6770e-01 | 6.3052e-01 | 3.8106e-02 | 41 | 1.4 |
| 1399 | 1395 | 2455294.13527096 | 954688502 | 140.999 | -32.182 | -9.2963e-02 | 5.6770e-01 | 6.3052e-01 | 3.8106e-02 | 29 | 1.4 |
| 1400 | 1396 | 2455294.38711661 | 954710261 | 316.658 | 8.995 | -9.2963e-02 | 5.6770e-01 | 6.3052e-01 | 3.8106e-02 | 33 | 1.4 |
| 1401 | 1397 | 2455295.03622396 | 954766344 | 25.019 | -57.540 | -9.2963e-02 | 5.6770e-01 | 6.3052e-01 | 3.8106e-02 | 41 | 1.4 |
| 1402 | 1398 | 2455297.80116550 | 955005235 | 232.497 | -15.102 | -9.2963e-02 | 5.6770e-01 | 6.3052e-01 | 3.8106e-02 | 48 | 1.4 |
| 1403 | 1399 | 2455298.00370654 | 955022735 | 31.428 | -47.200 | -9.2963e-02 | 5.6770e-01 | 6.3052e-01 | 3.8106e-02 | 68 | 1.4 |
| 1404 | 1400 | 2455298.18076100 | 955038032 | 300.351 | -16.365 | -9.2963e-02 | 5.6770e-01 | 6.3052e-01 | 3.8106e-02 | 81 | 1.4 |
| 1405 | 1401 | 2455299.04094349 | 955112352 | 209.653 | 29.951 | -9.2963e-02 | 5.6770e-01 | 6.3052e-01 | 3.8106e-02 | 85 | 1.4 |
| 1406 | 1402 | 2455299.89983036 | 955186560 | 231.575 | -24.476 | -9.2963e-02 | 5.6770e-01 | 6.3052e-01 | 3.8106e-02 | 37 | 1.4 |
| 1407 | 1403 | 2455300.09199446 | 955203163 | 313.716 | -61.118 | -1.3370e-01 | 8.5313e-01 | 6.3102e-01 | 3.7539e-02 | 23 | 2.4 |
| 1408 | 1404 | 2455300.10737209 | 955204491 | 323.104 | -32.401 | -1.1909e-01 | 7.2127e-01 | 6.0423e-01 | 3.7507e-02 | 30 | 1.8 |
| 1409 | 1405 | 2455300.11100524 | 955204805 | 312.823 | -44.083 | -9.2963e-02 | 5.6770e-01 | 6.3052e-01 | 3.8106e-02 | 36 | 1.4 |
| 1410 | 1406 | 2455300.13246019 | 955206659 | 225.520 | -44.910 | -1.1724e-01 | 4.7983e-01 | 5.2936e-01 | 3.8897e-02 | 62 | 0.9 |
| 1411 | 1407 | 2455316.80675897 | 956647318 | 231.896 | -23.457 | -9.2963e-02 | 5.6770e-01 | 6.3052e-01 | 3.8106e-02 | 42 | 1.4 |
| 1412 | 1408 | 2455316.85196370 | 956651224 | 122.597 | 15.279 | -9.2963e-02 | 5.6770e-01 | 6.3052e-01 | 3.8106e-02 | 48 | 1.4 |
| 1413 | 1409 | 2455316.94276806 | 956659070 | 254.038 | 26.451 | -9.2963e-02 | 5.6770e-01 | 6.3052e-01 | 3.8106e-02 | 67 | 1.4 |
| 1414 | 1410 | 2455317.02226984 | 956665939 | 232.771 | -44.501 | -1.2873e-01 | 4.3155e-01 | 4.6595e-01 | 3.9162e-02 | 50 | 0.7 |
| 1415 | 1411 | 2455317.08609056 | 956671453 | 352.206 | -74.182 | -1.1724e-01 | 4.7983e-01 | 5.2936e-01 | 3.8897e-02 | 51 | 0.9 |
| 1416 | 1412 | 2455317.11340286 | 956673813 | 1.290 | -25.203 | -9.2963e-02 | 5.6770e-01 | 6.3052e-01 | 3.8106e-02 | 36 | 1.4 |
| 1417 | 1413 | 2455317.73010541 | 956727096 | 280.399 | -79.105 | -1.1724e-01 | 4.7983e-01 | 5.2936e-01 | 3.8897e-02 | 34 | 0.9 |
| 1418 | 1414 | 2455317.76486827 | 956730099 | 152.380 | 7.549 | -9.2963e-02 | 5.6770e-01 | 6.3052e-01 | 3.8106e-02 | 32 | 1.4 |
| 1419 | 1415 | 2455320.27713519 | 956947159 | 33.757 | -0.495 | -9.2963e-02 | 5.6770e-01 | 6.3052e-01 | 3.8106e-02 | 48 | 1.4 |
| 1420 | 1416 | 2455322.80545293 | 957165606 | 174.047 | -55.550 | -9.2963e-02 | 5.6770e-01 | 6.3052e-01 | 3.8106e-02 | 41 | 1.4 |
| 1421 | 1417 | 2455322.84338650 | 957168883 | 158.385 | -71.000 | -9.2963e-02 | 5.6770e-01 | 6.3052e-01 | 3.8106e-02 | 59 | 1.4 |
| 1422 | 1418 | 2455322.91332532 | 957174926 | 249.189 | -28.790 | -9.2963e-02 | 5.6770e-01 | 6.3052e-01 | 3.8106e-02 | 46 | 1.4 |
| 1423 | 1419 | 2455322.91586188 | 957175145 | 181.247 | 5.545 | -9.2963e-02 | 5.6770e-01 | 6.3052e-01 | 3.8106e-02 | 46 | 1.4 |
| 1424 | 1420 | 2455344.35894043 | 959027827 | 63.679 | -65.365 | -1.3370e-01 | 8.5313e-01 | 6.3102e-01 | 3.7539e-02 | 28 | 2.4 |
| 1425 | 1421 | 2455344.42181101 | 959033259 | 47.194 | -38.129 | -9.2963e-02 | 5.6770e-01 | 6.3052e-01 | 3.8106e-02 | 62 | 1.4 |
| 1426 | 1422 | 2455345.19932765 | 959100436 | 259.712 | -78.579 | -9.2963e-02 | 5.6770e-01 | 6.3052e-01 | 3.8106e-02 | 67 | 1.4 |
| 1427 | 1423 | 2455358.21125349 | 960224667 | 234.974 | -37.476 | -9.2963e-02 | 5.6770e-01 | 6.3052e-01 | 3.8106e-02 | 50 | 1.4 |
| 1428 | 1424 | 2455358.35228472 | 960236852 | 17.868 | 8.193 | -9.2963e-02 | 5.6770e-01 | 6.3052e-01 | 3.8106e-02 | 42 | 1.4 |
| 1429 | 1425 | 2455358.37698580 | 960238986 | 120.692 | -7.779 | -9.2963e-02 | 5.6770e-01 | 6.3052e-01 | 3.8106e-02 | 60 | 1.4 |
| 1430 | 1426 | 2455358.41296782 | 960242095 | 73.628 | -61.822 | -9.2963e-02 | 5.6770e-01 | 6.3052e-01 | 3.8106e-02 | 48 | 1.4 |
| 1431 | 1427 | 2455358.47477294 | 960247435 | 109.298 | -53.125 | -9.2963e-02 | 5.6770e-01 | 6.3052e-01 | 3.8106e-02 | 42 | 1.4 |
| 1432 | 1428 | 2455358.95643379 | 960289050 | 202.414 | 28.594 | -9.2963e-02 | 5.6770e-01 | 6.3052e-01 | 3.8106e-02 | 42 | 1.4 |
| 1433 | 1429 | 2455359.00592964 | 960293327 | 129.586 | -41.588 | -9.2963e-02 | 5.6770e-01 | 6.3052e-01 | 3.8106e-02 | 32 | 1.4 |
| 1434 | 1430 | 2455359.19807954 | 960309929 | 56.894 | -74.614 | -9.2963e-02 | 5.6770e-01 | 6.3052e-01 | 3.8106e-02 | 80 | 1.4 |
| 1435 | 1431 | 2455359.26808122 | 960315977 | 10.652 | -49.793 | -9.2963e-02 | 5.6770e-01 | 6.3052e-01 | 3.8106e-02 | 53 | 1.4 |
| 1436 | 1432 | 2455361.23326367 | 960485768 | 274.802 | -67.332 | -1.3370e-01 | 8.5313e-01 | 6.3102e-01 | 3.7539e-02 | 22 | 2.4 |
| 1437 | 1433 | 2455363.94296776 | 960719887 | 180.786 | -46.451 | -1.1724e-01 | 4.7983e-01 | 5.2936e-01 | 3.8897e-02 | 47 | 0.9 |
| 1438 | 1434 | 2455364.48756816 | 960766940 | 127.780 | -27.446 | -1.1724e-01 | 4.7983e-01 | 5.2936e-01 | 3.8897e-02 | 47 | 0.9 |
| 1439 | 1435 | 2455364.82054339 | 960795709 | 56.488 | -75.717 | -9.2963e-02 | 5.6770e-01 | 6.3052e-01 | 3.8106e-02 | 45 | 1.4 |

```

1440 1436 2455364.82141812 960795785 189.450 -24.416 -9.2963e-02 5.6770e-01 6.3052e-01 3.8106e-02 47 1.4
1441 1437 2455365.38584119 960844551 115.391 23.256 -1.3370e-01 8.5313e-01 6.3102e-01 3.7539e-02 28 2.4
1442 1438 2455365.55524306 960859188 219.344 -31.908 -9.2963e-02 5.6770e-01 6.3052e-01 3.8106e-02 42 1.4
1443 1439 2455365.63625495 960866187 74.309 -9.347 -9.2963e-02 5.6770e-01 6.3052e-01 3.8106e-02 53 1.4
1444 1440 2455365.72809334 960874122 118.809 9.255 -9.2963e-02 5.6770e-01 6.3052e-01 3.8106e-02 43 1.4
1445 1441 2455366.08878634 960905286 7.788 25.082 -1.3370e-01 8.5313e-01 6.3102e-01 3.7539e-02 24 2.4
1446 1442 2455366.15344437 960910872 334.794 11.446 -1.3370e-01 8.5313e-01 6.3102e-01 3.7539e-02 43 2.4
1447 1443 2455366.17056137 960912351 118.883 -43.657 -9.2963e-02 5.6770e-01 6.3052e-01 3.8106e-02 71 1.4
1448 1444 2455366.26401931 960920426 137.585 -38.630 -9.2963e-02 5.6770e-01 6.3052e-01 3.8106e-02 33 1.4
1449 1445 2455366.32874271 960926018 63.457 -16.829 -9.2963e-02 5.6770e-01 6.3052e-01 3.8106e-02 54 1.4
1450 1446 2455366.67018804 960955519 221.094 -11.824 -9.2963e-02 5.6770e-01 6.3052e-01 3.8106e-02 48 1.4
1451 1447 2455366.68754250 960957018 242.556 -36.774 -8.8598e-02 3.3283e-01 5.3278e-01 3.9884e-02 148 0.6
1452 1448 2455366.78625159 960965547 29.983 -84.119 -8.8598e-02 3.3283e-01 5.3278e-01 3.9884e-02 29 0.6
1453 1449 2455366.86441567 960972300 341.787 -51.758 -1.1724e-01 4.7983e-01 5.2936e-01 3.8897e-02 65 0.9
1454 1450 2455366.94538879 960979296 334.229 -21.182 -5.8944e-02 2.9333e-01 5.7306e-01 3.8834e-02 115 0.6
1455 1451 2455366.96332096 960980845 55.272 -46.520 -9.2963e-02 5.6770e-01 6.3052e-01 3.8106e-02 41 1.4
1456 1452 2455367.37588935 961016491 71.926 -29.398 -9.2963e-02 5.6770e-01 6.3052e-01 3.8106e-02 48 1.4
1457 1453 2455367.99364515 961069865 284.757 -37.977 -9.2963e-02 5.6770e-01 6.3052e-01 3.8106e-02 41 1.4
1458 1454 2455368.26262811 961093106 38.030 -5.528 -9.2963e-02 5.6770e-01 6.3052e-01 3.8106e-02 48 1.4
1459 1455 2455368.36648407 961102079 6.572 -49.190 -9.2963e-02 5.6770e-01 6.3052e-01 3.8106e-02 60 1.4
1460 1456 2455368.70294318 961131149 113.119 -33.695 -9.2963e-02 5.6770e-01 6.3052e-01 3.8106e-02 44 1.4
1461 1457 2455368.89872659 961148064 248.170 -19.935 -9.2963e-02 5.6770e-01 6.3052e-01 3.8106e-02 43 1.4
1462 1458 2455368.99524298 961156403 291.187 -54.659 -9.2963e-02 5.6770e-01 6.3052e-01 3.8106e-02 56 1.4
1463 1459 2455369.10473938 961165864 300.718 -28.056 -1.2873e-01 4.3155e-01 4.6595e-01 3.9162e-02 60 0.7
1464 1460 2455369.18190296 961172531 59.854 4.334 -1.2873e-01 4.3155e-01 4.6595e-01 3.9162e-02 46 0.7
1465 1461 2455369.98898602 961242263 207.260 -35.786 -1.2873e-01 4.3155e-01 4.6595e-01 3.9162e-02 76 0.7
1466 1462 2455371.69582045 961389733 266.951 -9.712 -1.2873e-01 4.3155e-01 4.6595e-01 3.9162e-02 76 0.7
1467 1463 2455371.91391682 961408577 235.455 40.263 -9.2963e-02 5.6770e-01 6.3052e-01 3.8106e-02 54 1.4
1468 1464 2455371.91509862 961408679 203.451 11.810 -9.2963e-02 5.6770e-01 6.3052e-01 3.8106e-02 38 1.4
1469 1465 2455372.02870194 961418494 354.329 -2.969 -9.2963e-02 5.6770e-01 6.3052e-01 3.8106e-02 61 1.4
1470 1466 2455372.75174290 961480965 184.012 -22.011 -1.1724e-01 4.7983e-01 5.2936e-01 3.8897e-02 55 0.9
1471 1467 2455372.83658108 961488295 176.420 -1.942 -9.2963e-02 5.6770e-01 6.3052e-01 3.8106e-02 39 1.4
1472 # stop S6C -- start
1473 1468 2455373.90313579 961580445 5.989 -70.629 -9.2963e-02 5.6770e-01 6.3052e-01 3.8106e-02 63 1.4
1474 1469 2455374.49172512 961631300 123.617 4.409 -1.1724e-01 4.7983e-01 5.2936e-01 3.8897e-02 66 0.9
1475 1470 2455375.14686582 961687904 44.359 -3.731 -1.1724e-01 4.7983e-01 5.2936e-01 3.8897e-02 86 0.9
1476 1471 2455375.51446072 961719664 67.031 -6.509 -9.2963e-02 5.6770e-01 6.3052e-01 3.8106e-02 56 1.4
1477 1472 2455375.76383908 961741210 175.990 -2.733 -1.1724e-01 4.7983e-01 5.2936e-01 3.8897e-02 53 0.9
1478 1473 2455376.04986419 961765923 358.947 13.176 -9.2963e-02 5.6770e-01 6.3052e-01 3.8106e-02 40 1.4
1479 1474 2455376.07209754 961767844 306.986 -18.809 -9.2963e-02 5.6770e-01 6.3052e-01 3.8106e-02 60 1.4
1480 1475 2455376.60249931 961813670 358.852 -50.026 -9.2963e-02 5.6770e-01 6.3052e-01 3.8106e-02 33 1.4
1481 1476 2455379.12838555 962031907 288.827 35.383 -1.1724e-01 4.7983e-01 5.2936e-01 3.8897e-02 41 0.9
1482 1477 2455379.16635990 962035188 302.257 -19.197 -9.2963e-02 5.6770e-01 6.3052e-01 3.8106e-02 50 1.4
1483 1478 2455379.45978149 962060540 108.331 9.730 -9.2963e-02 5.6770e-01 6.3052e-01 3.8106e-02 35 1.4
1484 1479 2455379.73571086 962084380 281.294 -46.943 -9.2963e-02 5.6770e-01 6.3052e-01 3.8106e-02 51 1.4
1485 1480 2455380.12874386 962118338 265.592 -52.702 -1.1724e-01 4.7983e-01 5.2936e-01 3.8897e-02 34 0.9
1486 1481 2455380.21582264 962125862 41.444 2.236 -9.2963e-02 5.6770e-01 6.3052e-01 3.8106e-02 58 1.4
1487 1482 2455381.26283730 962216324 46.290 -22.895 -9.2963e-02 5.6770e-01 6.3052e-01 3.8106e-02 38 1.4
1488 1483 2455381.32268154 962221494 36.502 4.215 -9.2963e-02 5.6770e-01 6.3052e-01 3.8106e-02 39 1.4
1489 1484 2455381.52888911 962239311 170.937 16.473 -8.8598e-02 3.3283e-01 5.3278e-01 3.9884e-02 121 0.6
1490 1485 2455381.55279714 962241376 210.295 -3.444 -1.3370e-01 8.5313e-01 6.3102e-01 3.7539e-02 31 2.4
1491 1486 2455383.34716509 962396410 41.078 -1.939 -9.2963e-02 5.6770e-01 6.3052e-01 3.8106e-02 56 1.4

```

LIST OF HIGH ENERGY NEUTRINO CANDIDATES FOR THE 2009-2010 DATA

| | | | | | | | | | | | |
|------|------|------------------|-----------|---------|---------|-------------|------------|------------|------------|----|-----|
| 1492 | 1487 | 2455384.07014133 | 962458875 | 268.290 | 11.144 | -9.2963e-02 | 5.6770e-01 | 6.3052e-01 | 3.8106e-02 | 44 | 1.4 |
| 1493 | 1488 | 2455384.14838615 | 962465635 | 280.349 | -0.236 | -9.2963e-02 | 5.6770e-01 | 6.3052e-01 | 3.8106e-02 | 43 | 1.4 |
| 1494 | 1489 | 2455384.50147035 | 962496142 | 141.142 | -51.345 | -9.2963e-02 | 5.6770e-01 | 6.3052e-01 | 3.8106e-02 | 39 | 1.4 |
| 1495 | 1490 | 2455384.58535537 | 962503389 | 34.387 | -72.951 | -9.2963e-02 | 5.6770e-01 | 6.3052e-01 | 3.8106e-02 | 50 | 1.4 |
| 1496 | 1491 | 2455384.58735360 | 962503562 | 82.034 | -5.806 | -1.1724e-01 | 4.7983e-01 | 5.2936e-01 | 3.8897e-02 | 51 | 0.9 |
| 1497 | 1492 | 2455384.67206094 | 962510881 | 211.819 | -59.991 | -1.1724e-01 | 4.7983e-01 | 5.2936e-01 | 3.8897e-02 | 53 | 0.9 |
| 1498 | 1493 | 2455384.84454509 | 962525783 | 340.199 | -18.425 | -1.3370e-01 | 8.5313e-01 | 6.3102e-01 | 3.7539e-02 | 27 | 2.4 |
| 1499 | 1494 | 2455385.01038952 | 962540112 | 255.698 | -17.156 | -9.2963e-02 | 5.6770e-01 | 6.3052e-01 | 3.8106e-02 | 39 | 1.4 |
| 1500 | 1495 | 2455385.04728529 | 962543300 | 226.310 | -24.719 | -1.1909e-01 | 7.2127e-01 | 6.0423e-01 | 3.7507e-02 | 31 | 1.8 |
| 1501 | 1496 | 2455385.26635610 | 962562228 | 136.573 | -39.175 | -1.1909e-01 | 7.2127e-01 | 6.0423e-01 | 3.7507e-02 | 94 | 1.8 |
| 1502 | 1497 | 2455385.42705640 | 962576112 | 84.338 | 33.769 | -1.1724e-01 | 4.7983e-01 | 5.2936e-01 | 3.8897e-02 | 48 | 0.9 |
| 1503 | 1498 | 2455385.84846503 | 962612522 | 350.902 | -58.961 | -9.2963e-02 | 5.6770e-01 | 6.3052e-01 | 3.8106e-02 | 48 | 1.4 |
| 1504 | 1499 | 2455385.87065587 | 962614439 | 209.722 | -9.175 | -1.2873e-01 | 4.3155e-01 | 4.6595e-01 | 3.9162e-02 | 57 | 0.7 |
| 1505 | 1500 | 2455386.64829265 | 962681627 | 204.374 | 38.929 | -9.2963e-02 | 5.6770e-01 | 6.3052e-01 | 3.8106e-02 | 59 | 1.4 |
| 1506 | 1501 | 2455386.68276354 | 962684605 | 219.334 | 24.891 | -1.3370e-01 | 8.5313e-01 | 6.3102e-01 | 3.7539e-02 | 26 | 2.4 |
| 1507 | 1502 | 2455387.02261932 | 962713969 | 246.653 | -45.851 | -9.2963e-02 | 5.6770e-01 | 6.3052e-01 | 3.8106e-02 | 34 | 1.4 |
| 1508 | 1503 | 2455387.19454592 | 962728823 | 318.334 | -14.532 | -1.7861e+00 | 6.7827e+00 | 8.6368e-01 | 3.8440e-01 | 26 | 1.4 |
| 1509 | 1504 | 2455387.22718896 | 962731644 | 217.429 | -61.109 | -9.2963e-02 | 5.6770e-01 | 6.3052e-01 | 3.8106e-02 | 41 | 1.4 |
| 1510 | 1505 | 2455387.23182377 | 962732044 | 309.818 | -56.973 | -9.2963e-02 | 5.6770e-01 | 6.3052e-01 | 3.8106e-02 | 32 | 1.4 |
| 1511 | 1506 | 2455387.42003623 | 962748306 | 122.565 | -0.590 | -1.3370e-01 | 8.5313e-01 | 6.3102e-01 | 3.7539e-02 | 31 | 2.4 |
| 1512 | 1507 | 2455387.66092453 | 962769118 | 109.719 | 11.035 | -9.2963e-02 | 5.6770e-01 | 6.3052e-01 | 3.8106e-02 | 39 | 1.4 |
| 1513 | 1508 | 2455387.79549742 | 962780745 | 317.174 | -8.815 | -9.2963e-02 | 5.6770e-01 | 6.3052e-01 | 3.8106e-02 | 37 | 1.4 |
| 1514 | 1509 | 2455388.25188769 | 962820178 | 336.079 | -41.845 | -1.1724e-01 | 4.7983e-01 | 5.2936e-01 | 3.8897e-02 | 46 | 0.9 |
| 1515 | 1510 | 2455388.27647286 | 962822302 | 239.542 | -45.034 | -9.2963e-02 | 5.6770e-01 | 6.3052e-01 | 3.8106e-02 | 34 | 1.4 |
| 1516 | 1511 | 2455388.45725814 | 962837922 | 75.514 | -64.535 | -9.2963e-02 | 5.6770e-01 | 6.3052e-01 | 3.8106e-02 | 42 | 1.4 |
| 1517 | 1512 | 2455388.49139560 | 962840871 | 77.617 | -26.651 | -1.2873e-01 | 4.3155e-01 | 4.6595e-01 | 3.9162e-02 | 49 | 0.7 |
| 1518 | 1513 | 2455388.64444318 | 962854094 | 147.968 | 14.852 | -9.2963e-02 | 5.6770e-01 | 6.3052e-01 | 3.8106e-02 | 82 | 1.4 |
| 1519 | 1514 | 2455388.76476178 | 962864490 | 185.579 | 8.436 | -9.2963e-02 | 5.6770e-01 | 6.3052e-01 | 3.8106e-02 | 41 | 1.4 |
| 1520 | 1515 | 2455388.76672677 | 962864660 | 94.380 | -61.145 | -9.2963e-02 | 5.6770e-01 | 6.3052e-01 | 3.8106e-02 | 53 | 1.4 |
| 1521 | 1516 | 2455388.85713631 | 962872471 | 208.389 | -14.968 | -9.2963e-02 | 5.6770e-01 | 6.3052e-01 | 3.8106e-02 | 40 | 1.4 |
| 1522 | 1517 | 2455388.88175389 | 962874598 | 305.962 | -51.989 | -1.1724e-01 | 4.7983e-01 | 5.2936e-01 | 3.8897e-02 | 38 | 0.9 |
| 1523 | 1518 | 2455389.18574832 | 962900863 | 286.138 | -18.429 | -1.1724e-01 | 4.7983e-01 | 5.2936e-01 | 3.8897e-02 | 48 | 0.9 |
| 1524 | 1519 | 2455389.49712053 | 962927766 | 130.908 | 11.714 | -9.2963e-02 | 5.6770e-01 | 6.3052e-01 | 3.8106e-02 | 45 | 1.4 |
| 1525 | 1520 | 2455389.52152963 | 962929875 | 160.448 | -42.283 | -1.1724e-01 | 4.7983e-01 | 5.2936e-01 | 3.8897e-02 | 52 | 0.9 |
| 1526 | 1521 | 2455389.53943972 | 962931422 | 165.847 | 29.750 | -9.2963e-02 | 5.6770e-01 | 6.3052e-01 | 3.8106e-02 | 69 | 1.4 |
| 1527 | 1522 | 2455389.63683500 | 962939837 | 179.316 | -20.342 | -1.3370e-01 | 8.5313e-01 | 6.3102e-01 | 3.7539e-02 | 31 | 2.4 |
| 1528 | 1523 | 2455389.87726054 | 962960610 | 336.881 | -38.636 | -9.2963e-02 | 5.6770e-01 | 6.3052e-01 | 3.8106e-02 | 32 | 1.4 |
| 1529 | 1524 | 2455390.02402431 | 962973290 | 151.515 | -62.033 | -9.2963e-02 | 5.6770e-01 | 6.3052e-01 | 3.8106e-02 | 52 | 1.4 |
| 1530 | 1525 | 2455390.54528381 | 963018327 | 27.766 | -41.501 | -9.2963e-02 | 5.6770e-01 | 6.3052e-01 | 3.8106e-02 | 41 | 1.4 |
| 1531 | 1526 | 2455390.68555944 | 963030447 | 222.228 | 8.629 | -1.3370e-01 | 8.5313e-01 | 6.3102e-01 | 3.7539e-02 | 28 | 2.4 |
| 1532 | 1527 | 2455390.69935538 | 963031639 | 254.640 | -10.566 | -1.3370e-01 | 8.5313e-01 | 6.3102e-01 | 3.7539e-02 | 29 | 2.4 |
| 1533 | 1528 | 2455390.93820683 | 963052276 | 210.622 | 3.885 | -9.2963e-02 | 5.6770e-01 | 6.3052e-01 | 3.8106e-02 | 41 | 1.4 |
| 1534 | 1529 | 2455391.26882551 | 963080841 | 332.910 | -13.269 | -9.2963e-02 | 5.6770e-01 | 6.3052e-01 | 3.8106e-02 | 32 | 1.4 |
| 1535 | 1530 | 2455391.29238911 | 963082877 | 150.464 | -48.353 | -1.1724e-01 | 4.7983e-01 | 5.2936e-01 | 3.8897e-02 | 48 | 0.9 |
| 1536 | 1531 | 2455391.29684010 | 963083261 | 33.686 | -80.121 | -9.2963e-02 | 5.6770e-01 | 6.3052e-01 | 3.8106e-02 | 41 | 1.4 |
| 1537 | 1532 | 2455391.44676429 | 963096215 | 346.265 | -23.497 | -9.2963e-02 | 5.6770e-01 | 6.3052e-01 | 3.8106e-02 | 62 | 1.4 |
| 1538 | 1533 | 2455391.51726329 | 963102306 | 101.889 | -71.360 | -9.2963e-02 | 5.6770e-01 | 6.3052e-01 | 3.8106e-02 | 54 | 1.4 |
| 1539 | 1534 | 2455391.98485833 | 963142706 | 312.346 | 7.081 | -9.2963e-02 | 5.6770e-01 | 6.3052e-01 | 3.8106e-02 | 85 | 1.4 |
| 1540 | 1535 | 2455392.09837487 | 963152514 | 313.628 | -65.214 | -1.1724e-01 | 4.7983e-01 | 5.2936e-01 | 3.8897e-02 | 48 | 0.9 |
| 1541 | 1536 | 2455392.11320869 | 963153796 | 105.445 | -41.411 | -9.2963e-02 | 5.6770e-01 | 6.3052e-01 | 3.8106e-02 | 38 | 1.4 |
| 1542 | 1537 | 2455392.19615406 | 963160962 | 7.207 | 46.000 | -1.3370e-01 | 8.5313e-01 | 6.3102e-01 | 3.7539e-02 | 19 | 2.4 |
| 1543 | 1538 | 2455392.48761505 | 963186144 | 93.162 | -11.278 | -9.2963e-02 | 5.6770e-01 | 6.3052e-01 | 3.8106e-02 | 88 | 1.4 |

| | | | | | | | | | | | |
|------|------|------------------|-----------|---------|---------|-------------|------------|------------|------------|-----|-----|
| 1544 | 1539 | 2455392.51090710 | 963188157 | 96.435 | 36.323 | -9.2963e-02 | 5.6770e-01 | 6.3052e-01 | 3.8106e-02 | 44 | 1.4 |
| 1545 | 1540 | 2455392.68417985 | 963203128 | 239.970 | -0.784 | -1.3370e-01 | 8.5313e-01 | 6.3102e-01 | 3.7539e-02 | 29 | 2.4 |
| 1546 | 1541 | 2455396.07159846 | 963495801 | 296.094 | 17.169 | -9.2963e-02 | 5.6770e-01 | 6.3052e-01 | 3.8106e-02 | 40 | 1.4 |
| 1547 | 1542 | 2455396.29105526 | 963514762 | 57.010 | 6.188 | -9.2963e-02 | 5.6770e-01 | 6.3052e-01 | 3.8106e-02 | 54 | 1.4 |
| 1548 | 1543 | 2455396.42950057 | 963526723 | 133.517 | 8.850 | -1.3370e-01 | 8.5313e-01 | 6.3102e-01 | 3.7539e-02 | 24 | 2.4 |
| 1549 | 1544 | 2455396.44622235 | 963528168 | 59.009 | -3.628 | -5.8944e-02 | 2.9333e-01 | 5.7306e-01 | 3.8834e-02 | 101 | 0.6 |
| 1550 | 1545 | 2455396.53987868 | 963536260 | 75.075 | 3.888 | -1.3370e-01 | 8.5313e-01 | 6.3102e-01 | 3.7539e-02 | 25 | 2.4 |
| 1551 | 1546 | 2455396.59061666 | 963540644 | 112.253 | 2.542 | -1.3370e-01 | 8.5313e-01 | 6.3102e-01 | 3.7539e-02 | 38 | 2.4 |
| 1552 | 1547 | 2455396.69411137 | 963549586 | 256.047 | 20.499 | -1.3370e-01 | 8.5313e-01 | 6.3102e-01 | 3.7539e-02 | 23 | 2.4 |
| 1553 | 1548 | 2455397.05813910 | 963581038 | 78.141 | -60.199 | -1.1724e-01 | 4.7983e-01 | 5.2936e-01 | 3.8897e-02 | 38 | 0.9 |
| 1554 | 1549 | 2455397.06047488 | 963581240 | 215.015 | -42.034 | -1.3370e-01 | 8.5313e-01 | 6.3102e-01 | 3.7539e-02 | 23 | 2.4 |
| 1555 | 1550 | 2455397.19554695 | 963592910 | 329.391 | -16.566 | -1.1724e-01 | 4.7983e-01 | 5.2936e-01 | 3.8897e-02 | 47 | 0.9 |
| 1556 | 1551 | 2455397.64009648 | 963631319 | 48.756 | -64.158 | -9.2963e-02 | 5.6770e-01 | 6.3052e-01 | 3.8106e-02 | 76 | 1.4 |
| 1557 | 1552 | 2455397.69566175 | 963636120 | 54.397 | -41.147 | -9.2963e-02 | 5.6770e-01 | 6.3052e-01 | 3.8106e-02 | 33 | 1.4 |
| 1558 | 1553 | 2455397.95582273 | 963658598 | 19.932 | -21.140 | -1.3370e-01 | 8.5313e-01 | 6.3102e-01 | 3.7539e-02 | 30 | 2.4 |
| 1559 | 1554 | 2455398.07279179 | 963668704 | 30.381 | 15.265 | -1.3370e-01 | 8.5313e-01 | 6.3102e-01 | 3.7539e-02 | 23 | 2.4 |
| 1560 | 1555 | 2455398.16670441 | 963676818 | 47.179 | -59.568 | -1.3370e-01 | 8.5313e-01 | 6.3102e-01 | 3.7539e-02 | 28 | 2.4 |
| 1561 | 1556 | 2455398.20316353 | 963679968 | 28.490 | -4.236 | -9.2963e-02 | 5.6770e-01 | 6.3052e-01 | 3.8106e-02 | 41 | 1.4 |
| 1562 | 1557 | 2455398.36393923 | 963693859 | 54.360 | 4.932 | -1.1724e-01 | 4.7983e-01 | 5.2936e-01 | 3.8897e-02 | 48 | 0.9 |
| 1563 | 1558 | 2455398.44059353 | 963700482 | 77.734 | -21.196 | -9.2963e-02 | 5.6770e-01 | 6.3052e-01 | 3.8106e-02 | 44 | 1.4 |
| 1564 | 1559 | 2455398.46876191 | 963702916 | 63.192 | 10.778 | -1.1724e-01 | 4.7983e-01 | 5.2936e-01 | 3.8897e-02 | 52 | 0.9 |
| 1565 | 1560 | 2455398.54297531 | 963709328 | 145.348 | -51.806 | -9.2963e-02 | 5.6770e-01 | 6.3052e-01 | 3.8106e-02 | 56 | 1.4 |
| 1566 | 1561 | 2455398.73030620 | 963725513 | 263.267 | 0.649 | -1.3370e-01 | 8.5313e-01 | 6.3102e-01 | 3.7539e-02 | 25 | 2.4 |
| 1567 | 1562 | 2455398.82056218 | 963733311 | 65.161 | -49.828 | -9.2963e-02 | 5.6770e-01 | 6.3052e-01 | 3.8106e-02 | 41 | 1.4 |
| 1568 | 1563 | 2455398.90865081 | 963740922 | 165.275 | -61.816 | -1.3370e-01 | 8.5313e-01 | 6.3102e-01 | 3.7539e-02 | 29 | 2.4 |
| 1569 | 1564 | 2455399.07744975 | 963755506 | 326.980 | 12.709 | -9.2963e-02 | 5.6770e-01 | 6.3052e-01 | 3.8106e-02 | 49 | 1.4 |
| 1570 | 1565 | 2455399.17494927 | 963763930 | 277.281 | -57.701 | -9.2963e-02 | 5.6770e-01 | 6.3052e-01 | 3.8106e-02 | 35 | 1.4 |
| 1571 | 1566 | 2455399.75873374 | 963814369 | 157.299 | -40.395 | -9.2963e-02 | 5.6770e-01 | 6.3052e-01 | 3.8106e-02 | 33 | 1.4 |
| 1572 | 1567 | 2455405.34960546 | 964297420 | 50.755 | -62.232 | -9.2963e-02 | 5.6770e-01 | 6.3052e-01 | 3.8106e-02 | 92 | 1.4 |
| 1573 | 1568 | 2455405.53609605 | 964313533 | 97.317 | -35.782 | -9.2963e-02 | 5.6770e-01 | 6.3052e-01 | 3.8106e-02 | 37 | 1.4 |
| 1574 | 1569 | 2455405.98854355 | 964352625 | 328.322 | -77.202 | -9.2963e-02 | 5.6770e-01 | 6.3052e-01 | 3.8106e-02 | 42 | 1.4 |
| 1575 | 1570 | 2455406.26117066 | 964376180 | 89.769 | -36.885 | -9.2963e-02 | 5.6770e-01 | 6.3052e-01 | 3.8106e-02 | 34 | 1.4 |
| 1576 | 1571 | 2455406.63367816 | 964408364 | 187.842 | 17.240 | -9.2963e-02 | 5.6770e-01 | 6.3052e-01 | 3.8106e-02 | 44 | 1.4 |
| 1577 | 1572 | 2455406.79152398 | 964422002 | 54.867 | -61.780 | -9.2963e-02 | 5.6770e-01 | 6.3052e-01 | 3.8106e-02 | 48 | 1.4 |
| 1578 | 1573 | 2455407.00565888 | 964440503 | 286.714 | -13.592 | -1.1724e-01 | 4.7983e-01 | 5.2936e-01 | 3.8897e-02 | 55 | 0.9 |
| 1579 | 1574 | 2455407.11088480 | 964449595 | 285.558 | -53.702 | -9.2963e-02 | 5.6770e-01 | 6.3052e-01 | 3.8106e-02 | 44 | 1.4 |
| 1580 | 1575 | 2455407.25114877 | 964461714 | 354.543 | -33.245 | -9.2963e-02 | 5.6770e-01 | 6.3052e-01 | 3.8106e-02 | 47 | 1.4 |
| 1581 | 1576 | 2455407.40058597 | 964474625 | 140.357 | -29.592 | -9.2963e-02 | 5.6770e-01 | 6.3052e-01 | 3.8106e-02 | 35 | 1.4 |
| 1582 | 1577 | 2455407.58625397 | 964490667 | 138.391 | -19.949 | -9.2963e-02 | 5.6770e-01 | 6.3052e-01 | 3.8106e-02 | 64 | 1.4 |
| 1583 | 1578 | 2455407.79421643 | 964508635 | 171.837 | 7.523 | -9.2963e-02 | 5.6770e-01 | 6.3052e-01 | 3.8106e-02 | 44 | 1.4 |
| 1584 | 1579 | 2455407.89173694 | 964517061 | 235.571 | 27.482 | -1.3370e-01 | 8.5313e-01 | 6.3102e-01 | 3.7539e-02 | 24 | 2.4 |
| 1585 | 1580 | 2455408.60103370 | 964578344 | 165.047 | 26.423 | -9.2963e-02 | 5.6770e-01 | 6.3052e-01 | 3.8106e-02 | 34 | 1.4 |
| 1586 | 1581 | 2455409.54893676 | 964660243 | 122.521 | -8.117 | -9.2963e-02 | 5.6770e-01 | 6.3052e-01 | 3.8106e-02 | 53 | 1.4 |
| 1587 | 1582 | 2455409.71998793 | 964675021 | 213.815 | -14.903 | -9.2963e-02 | 5.6770e-01 | 6.3052e-01 | 3.8106e-02 | 50 | 1.4 |
| 1588 | 1583 | 2455410.34271102 | 964728825 | 118.803 | -21.503 | -9.2963e-02 | 5.6770e-01 | 6.3052e-01 | 3.8106e-02 | 36 | 1.4 |
| 1589 | 1584 | 2455410.65032080 | 964755402 | 189.118 | 27.898 | -9.2963e-02 | 5.6770e-01 | 6.3052e-01 | 3.8106e-02 | 77 | 1.4 |
| 1590 | 1585 | 2455410.72016895 | 964761437 | 186.235 | 42.879 | -9.2963e-02 | 5.6770e-01 | 6.3052e-01 | 3.8106e-02 | 47 | 1.4 |
| 1591 | 1586 | 2455410.95517517 | 964781742 | 278.609 | 20.398 | -9.2963e-02 | 5.6770e-01 | 6.3052e-01 | 3.8106e-02 | 99 | 1.4 |
| 1592 | 1587 | 2455410.98121297 | 964783991 | 278.015 | -0.243 | -9.2963e-02 | 5.6770e-01 | 6.3052e-01 | 3.8106e-02 | 49 | 1.4 |
| 1593 | 1588 | 2455411.20149212 | 964803023 | 328.739 | 22.200 | -9.2963e-02 | 5.6770e-01 | 6.3052e-01 | 3.8106e-02 | 47 | 1.4 |
| 1594 | 1589 | 2455411.29430793 | 964811043 | 131.155 | -41.499 | -9.2963e-02 | 5.6770e-01 | 6.3052e-01 | 3.8106e-02 | 58 | 1.4 |
| 1595 | 1590 | 2455411.40650879 | 964820737 | 240.098 | -49.745 | -9.2963e-02 | 5.6770e-01 | 6.3052e-01 | 3.8106e-02 | 50 | 1.4 |

LIST OF HIGH ENERGY NEUTRINO CANDIDATES FOR THE 2009-2010 DATA

| | | | | | | | | | | | |
|------|------|------------------|-----------|---------|---------|-------------|------------|------------|------------|----|-----|
| 1596 | 1591 | 2455411.44335445 | 964823920 | 150.859 | 21.608 | -9.2963e-02 | 5.6770e-01 | 6.3052e-01 | 3.8106e-02 | 39 | 1.4 |
| 1597 | 1592 | 2455411.68580267 | 964844868 | 138.110 | -3.563 | -1.1724e-01 | 4.7983e-01 | 5.2936e-01 | 3.8897e-02 | 35 | 0.9 |
| 1598 | 1593 | 2455411.72122069 | 964847928 | 201.585 | 43.448 | -1.1724e-01 | 4.7983e-01 | 5.2936e-01 | 3.8897e-02 | 40 | 0.9 |
| 1599 | 1594 | 2455411.82257757 | 964856685 | 1.722 | -59.887 | -1.1724e-01 | 4.7983e-01 | 5.2936e-01 | 3.8897e-02 | 52 | 0.9 |
| 1600 | 1595 | 2455411.89406440 | 964862862 | 54.756 | -49.620 | -1.1724e-01 | 4.7983e-01 | 5.2936e-01 | 3.8897e-02 | 74 | 0.9 |
| 1601 | 1596 | 2455411.94043781 | 964866868 | 182.167 | -30.453 | -9.2963e-02 | 5.6770e-01 | 6.3052e-01 | 3.8106e-02 | 57 | 1.4 |
| 1602 | 1597 | 2455412.05739074 | 964876973 | 340.269 | 24.848 | -9.2963e-02 | 5.6770e-01 | 6.3052e-01 | 3.8106e-02 | 44 | 1.4 |
| 1603 | 1598 | 2455412.06133395 | 964877314 | 231.903 | -26.820 | -9.2963e-02 | 5.6770e-01 | 6.3052e-01 | 3.8106e-02 | 40 | 1.4 |
| 1604 | 1599 | 2455412.06920058 | 964877993 | 25.985 | 26.147 | -9.2963e-02 | 5.6770e-01 | 6.3052e-01 | 3.8106e-02 | 42 | 1.4 |
| 1605 | 1600 | 2455412.09714234 | 964880408 | 82.909 | -74.640 | -9.2963e-02 | 5.6770e-01 | 6.3052e-01 | 3.8106e-02 | 47 | 1.4 |
| 1606 | 1601 | 2455412.23159644 | 964892024 | 81.573 | -54.420 | -1.2873e-01 | 4.3155e-01 | 4.6595e-01 | 3.9162e-02 | 47 | 0.7 |
| 1607 | 1602 | 2455412.31984813 | 964899649 | 355.591 | 5.232 | -9.2963e-02 | 5.6770e-01 | 6.3052e-01 | 3.8106e-02 | 38 | 1.4 |
| 1608 | 1603 | 2455412.45190219 | 964911059 | 219.013 | -20.328 | -9.2963e-02 | 5.6770e-01 | 6.3052e-01 | 3.8106e-02 | 77 | 1.4 |
| 1609 | 1604 | 2455412.47150470 | 964912753 | 5.474 | -43.144 | -9.2963e-02 | 5.6770e-01 | 6.3052e-01 | 3.8106e-02 | 40 | 1.4 |
| 1610 | 1605 | 2455412.67484742 | 964930321 | 121.704 | 5.153 | -9.2963e-02 | 5.6770e-01 | 6.3052e-01 | 3.8106e-02 | 49 | 1.4 |
| 1611 | 1606 | 2455413.24667944 | 964979728 | 126.881 | -30.190 | -1.3370e-01 | 8.5313e-01 | 6.3102e-01 | 3.7539e-02 | 23 | 2.4 |
| 1612 | 1607 | 2455413.26990541 | 964981734 | 100.996 | 7.694 | -9.2963e-02 | 5.6770e-01 | 6.3052e-01 | 3.8106e-02 | 48 | 1.4 |
| 1613 | 1608 | 2455413.62293001 | 965012236 | 202.157 | 9.644 | -9.2963e-02 | 5.6770e-01 | 6.3052e-01 | 3.8106e-02 | 45 | 1.4 |
| 1614 | 1609 | 2455413.62309067 | 965012250 | 197.447 | -53.627 | -9.2963e-02 | 5.6770e-01 | 6.3052e-01 | 3.8106e-02 | 46 | 1.4 |
| 1615 | 1610 | 2455413.65482573 | 965014991 | 65.591 | -47.281 | -9.2963e-02 | 5.6770e-01 | 6.3052e-01 | 3.8106e-02 | 37 | 1.4 |
| 1616 | 1611 | 2455413.84677035 | 965031575 | 238.036 | -8.435 | -9.2963e-02 | 5.6770e-01 | 6.3052e-01 | 3.8106e-02 | 55 | 1.4 |
| 1617 | 1612 | 2455413.86081947 | 965032789 | 304.777 | 14.607 | -9.2963e-02 | 5.6770e-01 | 6.3052e-01 | 3.8106e-02 | 45 | 1.4 |
| 1618 | 1613 | 2455413.88250034 | 965034663 | 2.283 | -62.468 | -9.2963e-02 | 5.6770e-01 | 6.3052e-01 | 3.8106e-02 | 43 | 1.4 |
| 1619 | 1614 | 2455414.06564428 | 965050486 | 34.480 | -19.110 | -9.2963e-02 | 5.6770e-01 | 6.3052e-01 | 3.8106e-02 | 54 | 1.4 |
| 1620 | 1615 | 2455414.19301958 | 965061491 | 51.291 | 13.925 | -1.3370e-01 | 8.5313e-01 | 6.3102e-01 | 3.7539e-02 | 26 | 2.4 |
| 1621 | 1616 | 2455414.20250958 | 965062311 | 124.313 | -3.286 | -9.2963e-02 | 5.6770e-01 | 6.3052e-01 | 3.8106e-02 | 51 | 1.4 |
| 1622 | 1617 | 2455414.81650328 | 965115360 | 189.228 | 5.082 | -9.2963e-02 | 5.6770e-01 | 6.3052e-01 | 3.8106e-02 | 45 | 1.4 |
| 1623 | 1618 | 2455414.88050599 | 965120890 | 313.700 | -33.401 | -9.2963e-02 | 5.6770e-01 | 6.3052e-01 | 3.8106e-02 | 38 | 1.4 |
| 1624 | 1619 | 2455415.32265675 | 965159092 | 127.642 | 5.416 | -1.3370e-01 | 8.5313e-01 | 6.3102e-01 | 3.7539e-02 | 28 | 2.4 |
| 1625 | 1620 | 2455415.79980090 | 965200317 | 230.472 | -23.253 | -9.2963e-02 | 5.6770e-01 | 6.3052e-01 | 3.8106e-02 | 55 | 1.4 |
| 1626 | 1621 | 2455416.24052251 | 965238396 | 32.097 | 9.841 | -9.2963e-02 | 5.6770e-01 | 6.3052e-01 | 3.8106e-02 | 45 | 1.4 |
| 1627 | 1622 | 2455416.39728093 | 965251940 | 93.417 | -2.898 | -9.2963e-02 | 5.6770e-01 | 6.3052e-01 | 3.8106e-02 | 64 | 1.4 |
| 1628 | 1623 | 2455416.41189513 | 965253202 | 39.306 | -51.194 | -9.2963e-02 | 5.6770e-01 | 6.3052e-01 | 3.8106e-02 | 58 | 1.4 |
| 1629 | 1624 | 2455416.85135381 | 965291171 | 228.601 | 27.528 | -9.2963e-02 | 5.6770e-01 | 6.3052e-01 | 3.8106e-02 | 31 | 1.4 |
| 1630 | 1625 | 2455416.99133890 | 965303266 | 325.211 | 18.155 | -9.2963e-02 | 5.6770e-01 | 6.3052e-01 | 3.8106e-02 | 48 | 1.4 |
| 1631 | 1626 | 2455418.11804856 | 965400614 | 51.357 | -38.619 | -9.2963e-02 | 5.6770e-01 | 6.3052e-01 | 3.8106e-02 | 65 | 1.4 |
| 1632 | 1627 | 2455419.17279374 | 965491744 | 334.367 | -19.407 | -9.2963e-02 | 5.6770e-01 | 6.3052e-01 | 3.8106e-02 | 47 | 1.4 |
| 1633 | 1628 | 2455419.66193775 | 965534006 | 274.301 | -2.131 | -9.2963e-02 | 5.6770e-01 | 6.3052e-01 | 3.8106e-02 | 40 | 1.4 |
| 1634 | 1629 | 2455420.58188819 | 965613490 | 134.184 | -9.965 | -9.2963e-02 | 5.6770e-01 | 6.3052e-01 | 3.8106e-02 | 50 | 1.4 |
| 1635 | 1630 | 2455420.64478845 | 965618924 | 140.585 | 25.252 | -9.2963e-02 | 5.6770e-01 | 6.3052e-01 | 3.8106e-02 | 37 | 1.4 |
| 1636 | 1631 | 2455421.01842883 | 965651207 | 52.057 | -20.234 | -1.3370e-01 | 8.5313e-01 | 6.3102e-01 | 3.7539e-02 | 24 | 2.4 |
| 1637 | 1632 | 2455421.13481522 | 965661263 | 47.267 | -17.304 | -9.2963e-02 | 5.6770e-01 | 6.3052e-01 | 3.8106e-02 | 41 | 1.4 |
| 1638 | 1633 | 2455421.17550090 | 965664778 | 341.923 | -30.664 | -1.3370e-01 | 8.5313e-01 | 6.3102e-01 | 3.7539e-02 | 28 | 2.4 |
| 1639 | 1634 | 2455421.18388006 | 965665502 | 356.147 | -54.737 | -9.2963e-02 | 5.6770e-01 | 6.3052e-01 | 3.8106e-02 | 44 | 1.4 |
| 1640 | 1635 | 2455421.20734816 | 965667529 | 193.559 | -59.953 | -9.2963e-02 | 5.6770e-01 | 6.3052e-01 | 3.8106e-02 | 49 | 1.4 |
| 1641 | 1636 | 2455421.26966946 | 965672914 | 33.709 | -8.258 | -1.1724e-01 | 4.7983e-01 | 5.2936e-01 | 3.8897e-02 | 55 | 0.9 |
| 1642 | 1637 | 2455421.31489924 | 965676822 | 145.228 | -6.521 | -9.2963e-02 | 5.6770e-01 | 6.3052e-01 | 3.8106e-02 | 32 | 1.4 |
| 1643 | 1638 | 2455421.50370376 | 965693135 | 61.422 | -22.894 | -9.2963e-02 | 5.6770e-01 | 6.3052e-01 | 3.8106e-02 | 71 | 1.4 |
| 1644 | 1639 | 2455421.64049105 | 965704953 | 162.548 | 38.503 | -9.2963e-02 | 5.6770e-01 | 6.3052e-01 | 3.8106e-02 | 33 | 1.4 |
| 1645 | 1640 | 2455421.64943180 | 965705725 | 305.359 | -28.389 | -9.2963e-02 | 5.6770e-01 | 6.3052e-01 | 3.8106e-02 | 40 | 1.4 |
| 1646 | 1641 | 2455421.70295410 | 965710350 | 121.166 | -24.871 | -9.2963e-02 | 5.6770e-01 | 6.3052e-01 | 3.8106e-02 | 34 | 1.4 |
| 1647 | 1642 | 2455421.97428930 | 965733793 | 290.181 | -41.123 | -9.2963e-02 | 5.6770e-01 | 6.3052e-01 | 3.8106e-02 | 44 | 1.4 |

| | | | | | | | | | | | |
|------|------|------------------|-----------|---------|---------|-------------|------------|------------|------------|----|-----|
| 1648 | 1643 | 2455422.01567384 | 965737369 | 285.616 | -20.758 | -9.2963e-02 | 5.6770e-01 | 6.3052e-01 | 3.8106e-02 | 65 | 1.4 |
| 1649 | 1644 | 2455422.10703200 | 965745262 | 325.751 | -38.644 | -1.3370e-01 | 8.5313e-01 | 6.3102e-01 | 3.7539e-02 | 28 | 2.4 |
| 1650 | 1645 | 2455422.19272734 | 965752666 | 322.679 | -41.813 | -1.3370e-01 | 8.5313e-01 | 6.3102e-01 | 3.7539e-02 | 38 | 2.4 |
| 1651 | 1646 | 2455422.20932694 | 965754100 | 63.902 | 17.355 | -1.3370e-01 | 8.5313e-01 | 6.3102e-01 | 3.7539e-02 | 31 | 2.4 |
| 1652 | 1647 | 2455422.34728654 | 965766020 | 61.990 | -29.209 | -1.3370e-01 | 8.5313e-01 | 6.3102e-01 | 3.7539e-02 | 26 | 2.4 |
| 1653 | 1648 | 2455422.37016411 | 965767997 | 168.206 | -14.173 | -1.1724e-01 | 4.7983e-01 | 5.2936e-01 | 3.8897e-02 | 46 | 0.9 |
| 1654 | 1649 | 2455422.54721552 | 965783294 | 0.807 | -50.504 | -1.3370e-01 | 8.5313e-01 | 6.3102e-01 | 3.7539e-02 | 23 | 2.4 |
| 1655 | 1650 | 2455422.70648059 | 965797054 | 300.507 | 7.048 | -9.2963e-02 | 5.6770e-01 | 6.3052e-01 | 3.8106e-02 | 49 | 1.4 |
| 1656 | 1651 | 2455422.93377367 | 965816693 | 300.421 | 17.063 | -9.2963e-02 | 5.6770e-01 | 6.3052e-01 | 3.8106e-02 | 35 | 1.4 |
| 1657 | 1652 | 2455423.07352596 | 965828767 | 320.854 | -18.990 | -9.2963e-02 | 5.6770e-01 | 6.3052e-01 | 3.8106e-02 | 34 | 1.4 |
| 1658 | 1653 | 2455423.09972906 | 965831031 | 294.205 | 15.139 | -1.2873e-01 | 4.3155e-01 | 4.6595e-01 | 3.9162e-02 | 59 | 0.7 |
| 1659 | 1654 | 2455423.10299524 | 965831313 | 50.049 | -47.905 | -1.2873e-01 | 4.3155e-01 | 4.6595e-01 | 3.9162e-02 | 60 | 0.7 |
| 1660 | 1655 | 2455423.61643567 | 965875675 | 309.142 | -28.397 | -9.2963e-02 | 5.6770e-01 | 6.3052e-01 | 3.8106e-02 | 50 | 1.4 |
| 1661 | 1656 | 2455423.80698012 | 965892138 | 350.920 | -31.017 | -9.2963e-02 | 5.6770e-01 | 6.3052e-01 | 3.8106e-02 | 51 | 1.4 |
| 1662 | 1657 | 2455423.83849925 | 965894861 | 199.005 | -61.231 | -1.2873e-01 | 4.3155e-01 | 4.6595e-01 | 3.9162e-02 | 57 | 0.7 |
| 1663 | 1658 | 2455423.84040886 | 965895026 | 190.940 | -61.557 | -9.2963e-02 | 5.6770e-01 | 6.3052e-01 | 3.8106e-02 | 37 | 1.4 |
| 1664 | 1659 | 2455423.87209296 | 965897763 | 196.226 | -0.480 | -9.2963e-02 | 5.6770e-01 | 6.3052e-01 | 3.8106e-02 | 25 | 1.4 |
| 1665 | 1660 | 2455424.21539309 | 965927424 | 73.948 | -35.590 | -1.1724e-01 | 4.7983e-01 | 5.2936e-01 | 3.8897e-02 | 39 | 0.9 |
| 1666 | 1661 | 2455424.23310282 | 965928955 | 164.980 | -22.524 | -9.2963e-02 | 5.6770e-01 | 6.3052e-01 | 3.8106e-02 | 33 | 1.4 |
| 1667 | 1662 | 2455424.52232128 | 965953943 | 272.523 | -67.829 | -9.2963e-02 | 5.6770e-01 | 6.3052e-01 | 3.8106e-02 | 33 | 1.4 |
| 1668 | 1663 | 2455425.06198192 | 966000570 | 23.139 | -42.407 | -1.1909e-01 | 7.2127e-01 | 6.0423e-01 | 3.7507e-02 | 31 | 1.8 |
| 1669 | 1664 | 2455425.56386018 | 966043932 | 177.165 | -45.668 | -1.2873e-01 | 4.3155e-01 | 4.6595e-01 | 3.9162e-02 | 92 | 0.7 |
| 1670 | 1665 | 2455425.95365897 | 966077611 | 10.359 | 24.096 | -9.2963e-02 | 5.6770e-01 | 6.3052e-01 | 3.8106e-02 | 45 | 1.4 |
| 1671 | 1666 | 2455426.00529824 | 966082072 | 260.094 | 9.219 | -9.2963e-02 | 5.6770e-01 | 6.3052e-01 | 3.8106e-02 | 32 | 1.4 |
| 1672 | 1667 | 2455426.02304114 | 966083605 | 267.758 | -16.403 | -1.3370e-01 | 8.5313e-01 | 6.3102e-01 | 3.7539e-02 | 30 | 2.4 |
| 1673 | 1668 | 2455426.02816909 | 966084048 | 2.878 | 12.071 | -1.3370e-01 | 8.5313e-01 | 6.3102e-01 | 3.7539e-02 | 31 | 2.4 |
| 1674 | 1669 | 2455426.18466108 | 966097569 | 300.647 | -74.729 | -1.3370e-01 | 8.5313e-01 | 6.3102e-01 | 3.7539e-02 | 24 | 2.4 |
| 1675 | 1670 | 2455426.27978837 | 966105788 | 104.893 | -46.328 | -9.2963e-02 | 5.6770e-01 | 6.3052e-01 | 3.8106e-02 | 33 | 1.4 |
| 1676 | 1671 | 2455426.68160543 | 966140505 | 284.851 | -81.391 | -9.2963e-02 | 5.6770e-01 | 6.3052e-01 | 3.8106e-02 | 60 | 1.4 |
| 1677 | 1672 | 2455427.03499794 | 966171038 | 316.091 | 22.544 | -9.2963e-02 | 5.6770e-01 | 6.3052e-01 | 3.8106e-02 | 39 | 1.4 |
| 1678 | 1673 | 2455427.07843445 | 966174791 | 62.896 | -45.680 | -9.2963e-02 | 5.6770e-01 | 6.3052e-01 | 3.8106e-02 | 41 | 1.4 |
| 1679 | 1674 | 2455427.21933358 | 966186965 | 85.067 | -51.409 | -9.2963e-02 | 5.6770e-01 | 6.3052e-01 | 3.8106e-02 | 44 | 1.4 |
| 1680 | 1675 | 2455427.40387959 | 966202910 | 158.621 | -34.187 | -9.2963e-02 | 5.6770e-01 | 6.3052e-01 | 3.8106e-02 | 53 | 1.4 |
| 1681 | 1676 | 2455427.44496192 | 966206459 | 298.221 | -50.612 | -1.3370e-01 | 8.5313e-01 | 6.3102e-01 | 3.7539e-02 | 29 | 2.4 |
| 1682 | 1677 | 2455427.65459995 | 966224572 | 293.625 | -51.197 | -1.1724e-01 | 4.7983e-01 | 5.2936e-01 | 3.8897e-02 | 36 | 0.9 |
| 1683 | 1678 | 2455427.66846274 | 966225770 | 30.561 | -59.887 | -9.2963e-02 | 5.6770e-01 | 6.3052e-01 | 3.8106e-02 | 32 | 1.4 |
| 1684 | 1679 | 2455428.08346722 | 966261626 | 341.423 | -26.854 | -9.2963e-02 | 5.6770e-01 | 6.3052e-01 | 3.8106e-02 | 51 | 1.4 |
| 1685 | 1680 | 2455428.11037461 | 966263951 | 109.837 | -10.540 | -9.2963e-02 | 5.6770e-01 | 6.3052e-01 | 3.8106e-02 | 34 | 1.4 |
| 1686 | 1681 | 2455428.21922358 | 966273355 | 332.675 | 5.883 | -1.3370e-01 | 8.5313e-01 | 6.3102e-01 | 3.7539e-02 | 27 | 2.4 |
| 1687 | 1682 | 2455428.23824451 | 966274999 | 122.614 | -42.221 | -9.2963e-02 | 5.6770e-01 | 6.3052e-01 | 3.8106e-02 | 34 | 1.4 |
| 1688 | 1683 | 2455441.45374207 | 967416818 | 94.562 | -25.760 | -1.1724e-01 | 4.7983e-01 | 5.2936e-01 | 3.8897e-02 | 41 | 0.9 |
| 1689 | 1684 | 2455441.48969199 | 967419924 | 67.477 | -35.895 | -9.2963e-02 | 5.6770e-01 | 6.3052e-01 | 3.8106e-02 | 58 | 1.4 |
| 1690 | 1685 | 2455441.56147618 | 967426126 | 104.308 | -48.963 | -1.3370e-01 | 8.5313e-01 | 6.3102e-01 | 3.7539e-02 | 27 | 2.4 |
| 1691 | 1686 | 2455441.56792120 | 967426683 | 158.748 | -35.408 | -9.2963e-02 | 5.6770e-01 | 6.3052e-01 | 3.8106e-02 | 54 | 1.4 |
| 1692 | 1687 | 2455442.03270271 | 967466840 | 295.604 | -58.742 | -9.2963e-02 | 5.6770e-01 | 6.3052e-01 | 3.8106e-02 | 50 | 1.4 |
| 1693 | 1688 | 2455442.21609640 | 967482685 | 9.822 | 12.791 | -1.1724e-01 | 4.7983e-01 | 5.2936e-01 | 3.8897e-02 | 46 | 0.9 |
| 1694 | 1689 | 2455442.31723545 | 967491424 | 192.412 | -78.016 | -1.1909e-01 | 7.2127e-01 | 6.0423e-01 | 3.7507e-02 | 29 | 1.8 |
| 1695 | 1690 | 2455442.36213883 | 967495303 | 155.833 | 17.577 | -9.2963e-02 | 5.6770e-01 | 6.3052e-01 | 3.8106e-02 | 58 | 1.4 |
| 1696 | 1691 | 2455442.70921974 | 967525291 | 27.780 | -81.366 | -9.2963e-02 | 5.6770e-01 | 6.3052e-01 | 3.8106e-02 | 43 | 1.4 |
| 1697 | 1692 | 2455442.71087246 | 967525434 | 327.359 | -45.899 | -9.2963e-02 | 5.6770e-01 | 6.3052e-01 | 3.8106e-02 | 31 | 1.4 |
| 1698 | 1693 | 2455442.87448866 | 967539570 | 294.521 | 40.132 | -9.2963e-02 | 5.6770e-01 | 6.3052e-01 | 3.8106e-02 | 64 | 1.4 |
| 1699 | 1694 | 2455442.89214633 | 967541096 | 230.263 | -66.383 | -1.1724e-01 | 4.7983e-01 | 5.2936e-01 | 3.8897e-02 | 54 | 0.9 |

LIST OF HIGH ENERGY NEUTRINO CANDIDATES FOR THE 2009-2010 DATA

| | | | | | | | | | | | |
|------|------|------------------|-----------|---------|---------|-------------|------------|------------|------------|-----|-----|
| 1700 | 1695 | 2455443.02464581 | 967552544 | 1.238 | 44.416 | -9.2963e-02 | 5.6770e-01 | 6.3052e-01 | 3.8106e-02 | 35 | 1.4 |
| 1701 | 1696 | 2455443.20190358 | 967567859 | 191.607 | -49.942 | -1.1724e-01 | 4.7983e-01 | 5.2936e-01 | 3.8897e-02 | 61 | 0.9 |
| 1702 | 1697 | 2455443.20944823 | 967568511 | 28.412 | -57.455 | -9.2963e-02 | 5.6770e-01 | 6.3052e-01 | 3.8106e-02 | 52 | 1.4 |
| 1703 | 1698 | 2455443.28496185 | 967575035 | 22.892 | -15.778 | -9.2963e-02 | 5.6770e-01 | 6.3052e-01 | 3.8106e-02 | 36 | 1.4 |
| 1704 | 1699 | 2455443.28555079 | 967575086 | 89.108 | 13.049 | -1.3370e-01 | 8.5313e-01 | 6.3102e-01 | 3.7539e-02 | 21 | 2.4 |
| 1705 | 1700 | 2455443.78091011 | 967617885 | 99.606 | -55.991 | -1.3370e-01 | 8.5313e-01 | 6.3102e-01 | 3.7539e-02 | 29 | 2.4 |
| 1706 | 1701 | 2455444.11103544 | 967646408 | 28.467 | 8.555 | -9.2963e-02 | 5.6770e-01 | 6.3052e-01 | 3.8106e-02 | 42 | 1.4 |
| 1707 | 1702 | 2455444.81675966 | 967707383 | 338.543 | 2.164 | -9.2963e-02 | 5.6770e-01 | 6.3052e-01 | 3.8106e-02 | 34 | 1.4 |
| 1708 | 1703 | 2455444.89938478 | 967714521 | 17.411 | 9.451 | -1.3370e-01 | 8.5313e-01 | 6.3102e-01 | 3.7539e-02 | 30 | 2.4 |
| 1709 | 1704 | 2455444.98906271 | 967722270 | 7.528 | -20.007 | -9.2963e-02 | 5.6770e-01 | 6.3052e-01 | 3.8106e-02 | 36 | 1.4 |
| 1710 | 1705 | 2455445.24470879 | 967744357 | 86.630 | 33.205 | -9.2963e-02 | 5.6770e-01 | 6.3052e-01 | 3.8106e-02 | 44 | 1.4 |
| 1711 | 1706 | 2455445.26592067 | 967746190 | 22.609 | -71.529 | -9.2963e-02 | 5.6770e-01 | 6.3052e-01 | 3.8106e-02 | 52 | 1.4 |
| 1712 | 1707 | 2455445.28335692 | 967747697 | 160.296 | -69.197 | -9.2963e-02 | 5.6770e-01 | 6.3052e-01 | 3.8106e-02 | 53 | 1.4 |
| 1713 | 1708 | 2455445.85291538 | 967796906 | 358.180 | -31.748 | -1.3370e-01 | 8.5313e-01 | 6.3102e-01 | 3.7539e-02 | 25 | 2.4 |
| 1714 | 1709 | 2455445.87460896 | 967798781 | 230.756 | 6.897 | -9.2963e-02 | 5.6770e-01 | 6.3052e-01 | 3.8106e-02 | 44 | 1.4 |
| 1715 | 1710 | 2455446.05589751 | 967814444 | 314.241 | -32.061 | -9.2963e-02 | 5.6770e-01 | 6.3052e-01 | 3.8106e-02 | 40 | 1.4 |
| 1716 | 1711 | 2455446.46786945 | 967850038 | 117.580 | -46.652 | -1.1724e-01 | 4.7983e-01 | 5.2936e-01 | 3.8897e-02 | 70 | 0.9 |
| 1717 | 1712 | 2455446.54708421 | 967856883 | 279.306 | -11.358 | -9.2963e-02 | 5.6770e-01 | 6.3052e-01 | 3.8106e-02 | 35 | 1.4 |
| 1718 | 1713 | 2455446.75667797 | 967874991 | 140.782 | -63.664 | -1.1909e-01 | 7.2127e-01 | 6.0423e-01 | 3.7507e-02 | 30 | 1.8 |
| 1719 | 1714 | 2455446.80403547 | 967879083 | 1.952 | -23.709 | -9.2963e-02 | 5.6770e-01 | 6.3052e-01 | 3.8106e-02 | 63 | 1.4 |
| 1720 | 1715 | 2455446.94695755 | 967891432 | 59.918 | -8.642 | -9.2963e-02 | 5.6770e-01 | 6.3052e-01 | 3.8106e-02 | 49 | 1.4 |
| 1721 | 1716 | 2455446.99029482 | 967895176 | 59.824 | 14.294 | -9.2963e-02 | 5.6770e-01 | 6.3052e-01 | 3.8106e-02 | 68 | 1.4 |
| 1722 | 1717 | 2455447.03362027 | 967898919 | 308.926 | -22.196 | -9.2963e-02 | 5.6770e-01 | 6.3052e-01 | 3.8106e-02 | 105 | 1.4 |
| 1723 | 1718 | 2455447.26917945 | 967919272 | 52.097 | -41.938 | -9.2963e-02 | 5.6770e-01 | 6.3052e-01 | 3.8106e-02 | 40 | 1.4 |
| 1724 | 1719 | 2455447.27743756 | 967919985 | 134.272 | 2.371 | -9.2963e-02 | 5.6770e-01 | 6.3052e-01 | 3.8106e-02 | 54 | 1.4 |
| 1725 | 1720 | 2455447.83084432 | 967967799 | 350.188 | 23.967 | -9.2963e-02 | 5.6770e-01 | 6.3052e-01 | 3.8106e-02 | 51 | 1.4 |
| 1726 | 1721 | 2455447.97088409 | 967979899 | 61.608 | -35.476 | -9.2963e-02 | 5.6770e-01 | 6.3052e-01 | 3.8106e-02 | 40 | 1.4 |
| 1727 | 1722 | 2455448.08618777 | 967989861 | 49.698 | -3.116 | -9.2963e-02 | 5.6770e-01 | 6.3052e-01 | 3.8106e-02 | 35 | 1.4 |
| 1728 | 1723 | 2455448.31741339 | 968009839 | 179.983 | -35.432 | -9.2963e-02 | 5.6770e-01 | 6.3052e-01 | 3.8106e-02 | 30 | 1.4 |
| 1729 | 1724 | 2455448.39402879 | 968016459 | 200.622 | 12.571 | -9.2963e-02 | 5.6770e-01 | 6.3052e-01 | 3.8106e-02 | 67 | 1.4 |
| 1730 | 1725 | 2455448.42772426 | 968019370 | 217.913 | 2.598 | -1.3370e-01 | 8.5313e-01 | 6.3102e-01 | 3.7539e-02 | 29 | 2.4 |
| 1731 | 1726 | 2455448.68787973 | 968041847 | 282.067 | -29.940 | -9.2963e-02 | 5.6770e-01 | 6.3052e-01 | 3.8106e-02 | 36 | 1.4 |
| 1732 | 1727 | 2455448.77399536 | 968049288 | 24.896 | -48.870 | -9.2963e-02 | 5.6770e-01 | 6.3052e-01 | 3.8106e-02 | 49 | 1.4 |
| 1733 | 1728 | 2455448.79541924 | 968051139 | 219.211 | -0.092 | -9.2963e-02 | 5.6770e-01 | 6.3052e-01 | 3.8106e-02 | 20 | 1.4 |
| 1734 | 1729 | 2455448.83752018 | 968054776 | 193.173 | -35.721 | -1.1909e-01 | 7.2127e-01 | 6.0423e-01 | 3.7507e-02 | 30 | 1.8 |
| 1735 | 1730 | 2455448.87335538 | 968057872 | 43.387 | -84.199 | -1.1724e-01 | 4.7983e-01 | 5.2936e-01 | 3.8897e-02 | 42 | 0.9 |
| 1736 | 1731 | 2455449.00031679 | 968068842 | 44.362 | 2.314 | -9.2963e-02 | 5.6770e-01 | 6.3052e-01 | 3.8106e-02 | 39 | 1.4 |
| 1737 | 1732 | 2455449.38702265 | 968102253 | 98.425 | -39.494 | -9.2963e-02 | 5.6770e-01 | 6.3052e-01 | 3.8106e-02 | 46 | 1.4 |
| 1738 | 1733 | 2455449.54458668 | 968115867 | 117.406 | -59.687 | -9.2963e-02 | 5.6770e-01 | 6.3052e-01 | 3.8106e-02 | 34 | 1.4 |
| 1739 | 1734 | 2455449.78084109 | 968136279 | 252.108 | 43.031 | -9.2963e-02 | 5.6770e-01 | 6.3052e-01 | 3.8106e-02 | 32 | 1.4 |
| 1740 | 1735 | 2455449.78381254 | 968136536 | 280.903 | -39.117 | -1.2873e-01 | 4.3155e-01 | 4.6595e-01 | 3.9162e-02 | 37 | 0.7 |
| 1741 | 1736 | 2455449.84177884 | 968141544 | 262.672 | -48.550 | -9.2963e-02 | 5.6770e-01 | 6.3052e-01 | 3.8106e-02 | 40 | 1.4 |
| 1742 | 1737 | 2455449.98687581 | 968154081 | 285.448 | -51.109 | -9.2963e-02 | 5.6770e-01 | 6.3052e-01 | 3.8106e-02 | 33 | 1.4 |
| 1743 | 1738 | 2455450.08299150 | 968162385 | 33.874 | 6.552 | -9.2963e-02 | 5.6770e-01 | 6.3052e-01 | 3.8106e-02 | 39 | 1.4 |
| 1744 | 1739 | 2455450.08345315 | 968162425 | 313.492 | -21.837 | -1.1909e-01 | 7.2127e-01 | 6.0423e-01 | 3.7507e-02 | 29 | 1.8 |
| 1745 | 1740 | 2455450.13989163 | 968167301 | 258.531 | -67.610 | -1.1909e-01 | 7.2127e-01 | 6.0423e-01 | 3.7507e-02 | 45 | 1.8 |
| 1746 | 1741 | 2455450.29677551 | 968180856 | 285.437 | -87.541 | -1.3370e-01 | 8.5313e-01 | 6.3102e-01 | 3.7539e-02 | 21 | 2.4 |
| 1747 | 1742 | 2455450.83399792 | 968227272 | 238.619 | 23.875 | -9.2963e-02 | 5.6770e-01 | 6.3052e-01 | 3.8106e-02 | 94 | 1.4 |
| 1748 | 1743 | 2455450.86255113 | 968229739 | 266.493 | -69.117 | -1.1724e-01 | 4.7983e-01 | 5.2936e-01 | 3.8897e-02 | 75 | 0.9 |
| 1749 | 1744 | 2455450.87407838 | 968230735 | 67.154 | -33.516 | -1.1724e-01 | 4.7983e-01 | 5.2936e-01 | 3.8897e-02 | 43 | 0.9 |
| 1750 | 1745 | 2455451.07600479 | 968248181 | 339.338 | 18.516 | -9.2963e-02 | 5.6770e-01 | 6.3052e-01 | 3.8106e-02 | 79 | 1.4 |
| 1751 | 1746 | 2455451.23133647 | 968261602 | 53.617 | -31.862 | -1.1909e-01 | 7.2127e-01 | 6.0423e-01 | 3.7507e-02 | 25 | 1.8 |

| | | | | | | | | | | | |
|------|------|------------------|-----------|---------|---------|-------------|------------|------------|------------|-----|-----|
| 1752 | 1747 | 2455451.28454823 | 968266199 | 67.115 | 33.041 | -9.2963e-02 | 5.6770e-01 | 6.3052e-01 | 3.8106e-02 | 48 | 1.4 |
| 1753 | 1748 | 2455451.50674469 | 968285397 | 115.947 | -2.447 | -9.2963e-02 | 5.6770e-01 | 6.3052e-01 | 3.8106e-02 | 48 | 1.4 |
| 1754 | 1749 | 2455451.78208613 | 968309187 | 184.436 | -52.226 | -1.1724e-01 | 4.7983e-01 | 5.2936e-01 | 3.8897e-02 | 41 | 0.9 |
| 1755 | 1750 | 2455451.80424182 | 968311101 | 197.555 | 0.462 | -1.3370e-01 | 8.5313e-01 | 6.3102e-01 | 3.7539e-02 | 27 | 2.4 |
| 1756 | 1751 | 2455452.07326191 | 968334344 | 65.706 | -4.102 | -1.1909e-01 | 7.2127e-01 | 6.0423e-01 | 3.7507e-02 | 29 | 1.8 |
| 1757 | 1752 | 2455452.08551482 | 968335403 | 28.354 | -49.227 | -9.2963e-02 | 5.6770e-01 | 6.3052e-01 | 3.8106e-02 | 52 | 1.4 |
| 1758 | 1753 | 2455452.10731938 | 968337287 | 343.683 | -79.519 | -1.3370e-01 | 8.5313e-01 | 6.3102e-01 | 3.7539e-02 | 24 | 2.4 |
| 1759 | 1754 | 2455452.20449255 | 968345683 | 57.043 | -1.560 | -1.1724e-01 | 4.7983e-01 | 5.2936e-01 | 3.8897e-02 | 38 | 0.9 |
| 1760 | 1755 | 2455452.22965164 | 968347856 | 250.902 | -83.167 | -9.2963e-02 | 5.6770e-01 | 6.3052e-01 | 3.8106e-02 | 42 | 1.4 |
| 1761 | 1756 | 2455452.23154252 | 968348020 | 151.291 | -35.510 | -1.3370e-01 | 8.5313e-01 | 6.3102e-01 | 3.7539e-02 | 30 | 2.4 |
| 1762 | 1757 | 2455452.36088703 | 968359195 | 162.197 | 12.472 | -1.1724e-01 | 4.7983e-01 | 5.2936e-01 | 3.8897e-02 | 49 | 0.9 |
| 1763 | 1758 | 2455452.36702477 | 968359725 | 176.041 | 29.863 | -1.3370e-01 | 8.5313e-01 | 6.3102e-01 | 3.7539e-02 | 24 | 2.4 |
| 1764 | 1759 | 2455452.57756140 | 968377916 | 294.351 | -54.310 | -1.1724e-01 | 4.7983e-01 | 5.2936e-01 | 3.8897e-02 | 57 | 0.9 |
| 1765 | 1760 | 2455453.24560289 | 968435635 | 90.253 | -58.855 | -1.1724e-01 | 4.7983e-01 | 5.2936e-01 | 3.8897e-02 | 63 | 0.9 |
| 1766 | 1761 | 2455453.25190889 | 968436179 | 211.328 | -67.028 | -9.2963e-02 | 5.6770e-01 | 6.3052e-01 | 3.8106e-02 | 33 | 1.4 |
| 1767 | 1762 | 2455453.25259588 | 968436239 | 35.524 | -70.161 | -9.2963e-02 | 5.6770e-01 | 6.3052e-01 | 3.8106e-02 | 34 | 1.4 |
| 1768 | 1763 | 2455453.36087261 | 968445594 | 53.510 | -16.938 | -1.3370e-01 | 8.5313e-01 | 6.3102e-01 | 3.7539e-02 | 28 | 2.4 |
| 1769 | 1764 | 2455453.41293734 | 968450092 | 206.813 | 15.460 | -9.2963e-02 | 5.6770e-01 | 6.3052e-01 | 3.8106e-02 | 45 | 1.4 |
| 1770 | 1765 | 2455453.41348776 | 968450140 | 162.361 | 42.798 | -1.1210e-01 | 3.5816e-01 | 4.5437e-01 | 4.0298e-02 | 114 | 0.5 |
| 1771 | 1766 | 2455453.42685768 | 968451295 | 143.073 | 25.880 | -1.1724e-01 | 4.7983e-01 | 5.2936e-01 | 3.8897e-02 | 40 | 0.9 |
| 1772 | 1767 | 2455453.86968999 | 968489556 | 320.407 | 24.216 | -9.2963e-02 | 5.6770e-01 | 6.3052e-01 | 3.8106e-02 | 34 | 1.4 |
| 1773 | 1768 | 2455453.93808666 | 968495465 | 265.853 | 3.678 | -9.2963e-02 | 5.6770e-01 | 6.3052e-01 | 3.8106e-02 | 46 | 1.4 |
| 1774 | 1769 | 2455454.30271870 | 968526969 | 282.908 | -51.377 | -1.7861e+00 | 6.7827e+00 | 8.6368e-01 | 3.8440e-01 | 26 | 1.4 |
| 1775 | 1770 | 2455454.37953530 | 968533606 | 72.904 | -37.762 | -1.1724e-01 | 4.7983e-01 | 5.2936e-01 | 3.8897e-02 | 48 | 0.9 |
| 1776 | 1771 | 2455454.43112392 | 968538064 | 204.179 | -38.790 | -1.3370e-01 | 8.5313e-01 | 6.3102e-01 | 3.7539e-02 | 30 | 2.4 |
| 1777 | 1772 | 2455454.46976008 | 968541402 | 82.501 | -53.496 | -9.2963e-02 | 5.6770e-01 | 6.3052e-01 | 3.8106e-02 | 38 | 1.4 |
| 1778 | 1773 | 2455454.48323023 | 968542566 | 133.147 | -46.521 | -1.3370e-01 | 8.5313e-01 | 6.3102e-01 | 3.7539e-02 | 30 | 2.4 |
| 1779 | 1774 | 2455454.50385255 | 968544347 | 124.003 | -30.084 | -1.1724e-01 | 4.7983e-01 | 5.2936e-01 | 3.8897e-02 | 89 | 0.9 |
| 1780 | 1775 | 2455454.77093044 | 968567423 | 249.674 | -4.856 | -9.2963e-02 | 5.6770e-01 | 6.3052e-01 | 3.8106e-02 | 57 | 1.4 |
| 1781 | 1776 | 2455454.91359343 | 968579749 | 89.688 | -42.864 | -9.2963e-02 | 5.6770e-01 | 6.3052e-01 | 3.8106e-02 | 33 | 1.4 |
| 1782 | 1777 | 2455454.96372225 | 968584080 | 52.293 | 4.365 | -1.3370e-01 | 8.5313e-01 | 6.3102e-01 | 3.7539e-02 | 28 | 2.4 |
| 1783 | 1778 | 2455454.98309502 | 968585754 | 253.150 | -27.544 | -1.1909e-01 | 7.2127e-01 | 6.0423e-01 | 3.7507e-02 | 23 | 1.8 |
| 1784 | 1779 | 2455455.20882833 | 968605257 | 0.276 | 8.491 | -1.3370e-01 | 8.5313e-01 | 6.3102e-01 | 3.7539e-02 | 28 | 2.4 |
| 1785 | 1780 | 2455455.51356785 | 968631587 | 102.524 | -7.292 | -9.2963e-02 | 5.6770e-01 | 6.3052e-01 | 3.8106e-02 | 51 | 1.4 |
| 1786 | 1781 | 2455455.80973056 | 968657175 | 20.353 | -55.592 | -1.7861e+00 | 6.7827e+00 | 8.6368e-01 | 3.8440e-01 | 29 | 1.4 |
| 1787 | 1782 | 2455455.90317996 | 968665249 | 225.192 | -52.217 | -1.1909e-01 | 7.2127e-01 | 6.0423e-01 | 3.7507e-02 | 28 | 1.8 |
| 1788 | 1783 | 2455455.99218813 | 968672940 | 77.351 | -4.361 | -9.2963e-02 | 5.6770e-01 | 6.3052e-01 | 3.8106e-02 | 45 | 1.4 |
| 1789 | 1784 | 2455456.15787180 | 968687255 | 129.863 | -65.277 | -1.1724e-01 | 4.7983e-01 | 5.2936e-01 | 3.8897e-02 | 34 | 0.9 |
| 1790 | 1785 | 2455456.20172689 | 968691044 | 44.735 | 5.830 | -1.3370e-01 | 8.5313e-01 | 6.3102e-01 | 3.7539e-02 | 27 | 2.4 |
| 1791 | 1786 | 2455456.20605460 | 968691418 | 191.833 | -57.155 | -9.2963e-02 | 5.6770e-01 | 6.3052e-01 | 3.8106e-02 | 44 | 1.4 |
| 1792 | 1787 | 2455456.59749667 | 968725238 | 172.467 | 9.421 | -9.2963e-02 | 5.6770e-01 | 6.3052e-01 | 3.8106e-02 | 42 | 1.4 |
| 1793 | 1788 | 2455456.61395583 | 968726660 | 223.122 | -33.374 | -1.1724e-01 | 4.7983e-01 | 5.2936e-01 | 3.8897e-02 | 72 | 0.9 |
| 1794 | 1789 | 2455457.12617472 | 968770916 | 62.516 | 30.053 | -1.1724e-01 | 4.7983e-01 | 5.2936e-01 | 3.8897e-02 | 46 | 0.9 |
| 1795 | 1790 | 2455457.27603636 | 968783864 | 149.913 | -57.385 | -9.2963e-02 | 5.6770e-01 | 6.3052e-01 | 3.8106e-02 | 44 | 1.4 |
| 1796 | 1791 | 2455457.70004021 | 968820498 | 311.329 | -24.458 | -9.2963e-02 | 5.6770e-01 | 6.3052e-01 | 3.8106e-02 | 30 | 1.4 |
| 1797 | 1792 | 2455457.74421786 | 968824315 | 315.362 | -83.810 | -9.2963e-02 | 5.6770e-01 | 6.3052e-01 | 3.8106e-02 | 34 | 1.4 |
| 1798 | 1793 | 2455457.76773135 | 968826346 | 261.090 | -43.762 | -9.2963e-02 | 5.6770e-01 | 6.3052e-01 | 3.8106e-02 | 47 | 1.4 |
| 1799 | 1794 | 2455457.81715868 | 968830617 | 216.741 | -3.327 | -9.2963e-02 | 5.6770e-01 | 6.3052e-01 | 3.8106e-02 | 44 | 1.4 |
| 1800 | 1795 | 2455458.27230883 | 968869942 | 13.094 | -10.294 | -9.2963e-02 | 5.6770e-01 | 6.3052e-01 | 3.8106e-02 | 69 | 1.4 |
| 1801 | 1796 | 2455458.32611694 | 968874591 | 7.234 | -62.816 | -9.2963e-02 | 5.6770e-01 | 6.3052e-01 | 3.8106e-02 | 32 | 1.4 |
| 1802 | 1797 | 2455458.45893698 | 968886067 | 182.219 | 39.801 | -1.1724e-01 | 4.7983e-01 | 5.2936e-01 | 3.8897e-02 | 36 | 0.9 |
| 1803 | 1798 | 2455458.61452063 | 968899509 | 246.751 | 12.499 | -9.2963e-02 | 5.6770e-01 | 6.3052e-01 | 3.8106e-02 | 36 | 1.4 |

LIST OF HIGH ENERGY NEUTRINO CANDIDATES FOR THE 2009-2010 DATA

| | | | | | | | | | | | |
|------|------|------------------|-----------|---------|---------|-------------|------------|------------|------------|-----|-----|
| 1804 | 1799 | 2455458.81424959 | 968916766 | 118.206 | -48.445 | -1.3370e-01 | 8.5313e-01 | 6.3102e-01 | 3.7539e-02 | 31 | 2.4 |
| 1805 | 1800 | 2455458.86849402 | 968921452 | 189.228 | -35.980 | -9.2963e-02 | 5.6770e-01 | 6.3052e-01 | 3.8106e-02 | 40 | 1.4 |
| 1806 | 1801 | 2455458.94910179 | 968928417 | 264.027 | -44.981 | -1.3370e-01 | 8.5313e-01 | 6.3102e-01 | 3.7539e-02 | 30 | 2.4 |
| 1807 | 1802 | 2455459.05437309 | 968937512 | 42.274 | 30.380 | -9.2963e-02 | 5.6770e-01 | 6.3052e-01 | 3.8106e-02 | 45 | 1.4 |
| 1808 | 1803 | 2455459.13172550 | 968944196 | 340.949 | 13.071 | -9.2963e-02 | 5.6770e-01 | 6.3052e-01 | 3.8106e-02 | 40 | 1.4 |
| 1809 | 1804 | 2455459.18837762 | 968949090 | 122.851 | 5.024 | -9.2963e-02 | 5.6770e-01 | 6.3052e-01 | 3.8106e-02 | 48 | 1.4 |
| 1810 | 1805 | 2455459.35471725 | 968963462 | 124.037 | 45.249 | -1.3370e-01 | 8.5313e-01 | 6.3102e-01 | 3.7539e-02 | 25 | 2.4 |
| 1811 | 1806 | 2455459.52773436 | 968978411 | 319.930 | -54.225 | -9.2963e-02 | 5.6770e-01 | 6.3052e-01 | 3.8106e-02 | 54 | 1.4 |
| 1812 | 1807 | 2455459.70348314 | 968993595 | 271.569 | 44.217 | -9.2963e-02 | 5.6770e-01 | 6.3052e-01 | 3.8106e-02 | 42 | 1.4 |
| 1813 | 1808 | 2455459.70862106 | 968994039 | 2.090 | -36.578 | -1.1724e-01 | 4.7983e-01 | 5.2936e-01 | 3.8897e-02 | 39 | 0.9 |
| 1814 | 1809 | 2455459.93289750 | 969013417 | 315.066 | -64.835 | -8.8598e-02 | 3.3283e-01 | 5.3278e-01 | 3.9884e-02 | 125 | 0.6 |
| 1815 | 1810 | 2455460.12238082 | 969029788 | 215.906 | -49.693 | -1.3370e-01 | 8.5313e-01 | 6.3102e-01 | 3.7539e-02 | 18 | 2.4 |
| 1816 | 1811 | 2455460.34336759 | 969048881 | 155.483 | -5.338 | -9.2963e-02 | 5.6770e-01 | 6.3052e-01 | 3.8106e-02 | 49 | 1.4 |
| 1817 | 1812 | 2455460.35634849 | 969050003 | 135.241 | 0.318 | -9.2963e-02 | 5.6770e-01 | 6.3052e-01 | 3.8106e-02 | 44 | 1.4 |
| 1818 | 1813 | 2455460.37567663 | 969051673 | 101.999 | -1.694 | -9.2963e-02 | 5.6770e-01 | 6.3052e-01 | 3.8106e-02 | 58 | 1.4 |
| 1819 | 1814 | 2455461.16192720 | 969119605 | 152.141 | -9.531 | -9.2963e-02 | 5.6770e-01 | 6.3052e-01 | 3.8106e-02 | 57 | 1.4 |
| 1820 | 1815 | 2455461.87336644 | 969181073 | 287.104 | -2.908 | -9.2963e-02 | 5.6770e-01 | 6.3052e-01 | 3.8106e-02 | 40 | 1.4 |
| 1821 | 1816 | 2455461.89217576 | 969182698 | 43.941 | 13.215 | -1.1724e-01 | 4.7983e-01 | 5.2936e-01 | 3.8897e-02 | 53 | 0.9 |
| 1822 | 1817 | 2455461.98280990 | 969190529 | 6.948 | 34.909 | -9.2963e-02 | 5.6770e-01 | 6.3052e-01 | 3.8106e-02 | 39 | 1.4 |
| 1823 | 1818 | 2455462.02469139 | 969194148 | 337.255 | 25.388 | -9.2963e-02 | 5.6770e-01 | 6.3052e-01 | 3.8106e-02 | 36 | 1.4 |
| 1824 | 1819 | 2455462.31736533 | 969219435 | 105.227 | -43.216 | -9.2963e-02 | 5.6770e-01 | 6.3052e-01 | 3.8106e-02 | 40 | 1.4 |
| 1825 | 1820 | 2455462.38022886 | 969224866 | 35.947 | -54.463 | -9.2963e-02 | 5.6770e-01 | 6.3052e-01 | 3.8106e-02 | 42 | 1.4 |
| 1826 | 1821 | 2455462.40710516 | 969227188 | 152.609 | 16.647 | -1.1724e-01 | 4.7983e-01 | 5.2936e-01 | 3.8897e-02 | 87 | 0.9 |
| 1827 | 1822 | 2455462.52875500 | 969237699 | 124.849 | -24.464 | -9.2963e-02 | 5.6770e-01 | 6.3052e-01 | 3.8106e-02 | 39 | 1.4 |
| 1828 | 1823 | 2455462.58753144 | 969242777 | 173.333 | -7.415 | -9.2963e-02 | 5.6770e-01 | 6.3052e-01 | 3.8106e-02 | 48 | 1.4 |
| 1829 | 1824 | 2455462.65078916 | 969248243 | 174.637 | -45.211 | -9.2963e-02 | 5.6770e-01 | 6.3052e-01 | 3.8106e-02 | 33 | 1.4 |
| 1830 | 1825 | 2455462.91259969 | 969270863 | 63.928 | 2.929 | -9.2963e-02 | 5.6770e-01 | 6.3052e-01 | 3.8106e-02 | 41 | 1.4 |
| 1831 | 1826 | 2455462.95610410 | 969274622 | 125.749 | -65.055 | -9.2963e-02 | 5.6770e-01 | 6.3052e-01 | 3.8106e-02 | 35 | 1.4 |
| 1832 | 1827 | 2455463.78877374 | 969346565 | 277.962 | -0.582 | -1.1724e-01 | 4.7983e-01 | 5.2936e-01 | 3.8897e-02 | 48 | 0.9 |
| 1833 | 1828 | 2455463.92620325 | 969358438 | 3.320 | 24.990 | -9.2963e-02 | 5.6770e-01 | 6.3052e-01 | 3.8106e-02 | 36 | 1.4 |
| 1834 | 1829 | 2455463.94571679 | 969360124 | 355.573 | 4.437 | -1.1724e-01 | 4.7983e-01 | 5.2936e-01 | 3.8897e-02 | 37 | 0.9 |
| 1835 | 1830 | 2455464.18784837 | 969381045 | 342.251 | -38.295 | -1.1724e-01 | 4.7983e-01 | 5.2936e-01 | 3.8897e-02 | 64 | 0.9 |
| 1836 | 1831 | 2455464.24919048 | 969386345 | 102.662 | -29.369 | -1.1724e-01 | 4.7983e-01 | 5.2936e-01 | 3.8897e-02 | 48 | 0.9 |
| 1837 | 1832 | 2455464.25432507 | 969386788 | 63.376 | -33.042 | -1.3370e-01 | 8.5313e-01 | 6.3102e-01 | 3.7539e-02 | 22 | 2.4 |
| 1838 | 1833 | 2455464.47117015 | 969405524 | 117.889 | -12.746 | -1.3370e-01 | 8.5313e-01 | 6.3102e-01 | 3.7539e-02 | 40 | 2.4 |
| 1839 | 1834 | 2455464.52591589 | 969410254 | 149.584 | 29.662 | -9.2963e-02 | 5.6770e-01 | 6.3052e-01 | 3.8106e-02 | 60 | 1.4 |
| 1840 | 1835 | 2455464.59014824 | 969415803 | 329.730 | -41.640 | -9.2963e-02 | 5.6770e-01 | 6.3052e-01 | 3.8106e-02 | 43 | 1.4 |
| 1841 | 1836 | 2455464.76883134 | 969431242 | 286.862 | 28.859 | -1.3370e-01 | 8.5313e-01 | 6.3102e-01 | 3.7539e-02 | 31 | 2.4 |
| 1842 | 1837 | 2455464.98477664 | 969449899 | 336.140 | -53.616 | -9.2963e-02 | 5.6770e-01 | 6.3052e-01 | 3.8106e-02 | 68 | 1.4 |
| 1843 | 1838 | 2455465.20217247 | 969468682 | 300.366 | -64.441 | -1.3370e-01 | 8.5313e-01 | 6.3102e-01 | 3.7539e-02 | 24 | 2.4 |
| 1844 | 1839 | 2455465.22110820 | 969470318 | 9.733 | -66.005 | -1.2873e-01 | 4.3155e-01 | 4.6595e-01 | 3.9162e-02 | 45 | 0.7 |
| 1845 | 1840 | 2455465.26766302 | 969474341 | 3.905 | -54.082 | -1.2873e-01 | 4.3155e-01 | 4.6595e-01 | 3.9162e-02 | 50 | 0.7 |
| 1846 | 1841 | 2455465.34250419 | 969480807 | 61.534 | -9.946 | -1.3370e-01 | 8.5313e-01 | 6.3102e-01 | 3.7539e-02 | 23 | 2.4 |
| 1847 | 1842 | 2455465.71727566 | 969513187 | 163.475 | -77.000 | -1.3370e-01 | 8.5313e-01 | 6.3102e-01 | 3.7539e-02 | 25 | 2.4 |
| 1848 | 1843 | 2455465.81941184 | 969522012 | 336.446 | -10.660 | -9.2963e-02 | 5.6770e-01 | 6.3052e-01 | 3.8106e-02 | 41 | 1.4 |
| 1849 | 1844 | 2455465.98171801 | 969536035 | 264.668 | -15.524 | -1.3370e-01 | 8.5313e-01 | 6.3102e-01 | 3.7539e-02 | 21 | 2.4 |
| 1850 | 1845 | 2455466.06624986 | 969543338 | 15.199 | -68.529 | -1.1724e-01 | 4.7983e-01 | 5.2936e-01 | 3.8897e-02 | 44 | 0.9 |
| 1851 | 1846 | 2455466.18644652 | 969553723 | 16.764 | 26.422 | -9.2963e-02 | 5.6770e-01 | 6.3052e-01 | 3.8106e-02 | 36 | 1.4 |
| 1852 | 1847 | 2455466.21055843 | 969555807 | 40.706 | -3.228 | -9.2963e-02 | 5.6770e-01 | 6.3052e-01 | 3.8106e-02 | 34 | 1.4 |
| 1853 | 1848 | 2455466.42180381 | 969574058 | 181.618 | 15.791 | -9.2963e-02 | 5.6770e-01 | 6.3052e-01 | 3.8106e-02 | 67 | 1.4 |
| 1854 | 1849 | 2455466.51320002 | 969581955 | 234.615 | -47.282 | -1.1724e-01 | 4.7983e-01 | 5.2936e-01 | 3.8897e-02 | 41 | 0.9 |
| 1855 | 1850 | 2455466.51323532 | 969581958 | 31.811 | -47.983 | -9.2963e-02 | 5.6770e-01 | 6.3052e-01 | 3.8106e-02 | 55 | 1.4 |

| | | | | | | | | | | | |
|------|------|------------------|-----------|---------|---------|-------------|------------|------------|------------|----|-----|
| 1856 | 1851 | 2455466.73762422 | 969601345 | 295.242 | 19.950 | -9.2963e-02 | 5.6770e-01 | 6.3052e-01 | 3.8106e-02 | 44 | 1.4 |
| 1857 | 1852 | 2455466.76198870 | 969603450 | 90.070 | -54.647 | -9.2963e-02 | 5.6770e-01 | 6.3052e-01 | 3.8106e-02 | 32 | 1.4 |
| 1858 | 1853 | 2455466.78865597 | 969605754 | 335.481 | 17.898 | -1.1909e-01 | 7.2127e-01 | 6.0423e-01 | 3.7507e-02 | 29 | 1.8 |
| 1859 | 1854 | 2455466.88795078 | 969614333 | 302.620 | -83.652 | -9.2963e-02 | 5.6770e-01 | 6.3052e-01 | 3.8106e-02 | 51 | 1.4 |
| 1860 | 1855 | 2455466.93633213 | 969618514 | 39.241 | -67.012 | -1.1724e-01 | 4.7983e-01 | 5.2936e-01 | 3.8897e-02 | 37 | 0.9 |
| 1861 | 1856 | 2455466.98716546 | 969622906 | 100.356 | -3.848 | -9.2963e-02 | 5.6770e-01 | 6.3052e-01 | 3.8106e-02 | 60 | 1.4 |
| 1862 | 1857 | 2455467.42747723 | 969660949 | 49.092 | -81.461 | -9.2963e-02 | 5.6770e-01 | 6.3052e-01 | 3.8106e-02 | 49 | 1.4 |
| 1863 | 1858 | 2455467.43249122 | 969661382 | 224.770 | 6.317 | -9.2963e-02 | 5.6770e-01 | 6.3052e-01 | 3.8106e-02 | 75 | 1.4 |
| 1864 | 1859 | 2455467.76027688 | 969689702 | 299.915 | 19.464 | -9.2963e-02 | 5.6770e-01 | 6.3052e-01 | 3.8106e-02 | 34 | 1.4 |
| 1865 | 1860 | 2455467.80525130 | 969693588 | 267.331 | -54.250 | -1.2873e-01 | 4.3155e-01 | 4.6595e-01 | 3.9162e-02 | 46 | 0.7 |
| 1866 | 1861 | 2455468.01548934 | 969711753 | 57.472 | -1.745 | -9.2963e-02 | 5.6770e-01 | 6.3052e-01 | 3.8106e-02 | 37 | 1.4 |
| 1867 | 1862 | 2455468.12238422 | 969720988 | 47.996 | -10.893 | -1.1909e-01 | 7.2127e-01 | 6.0423e-01 | 3.7507e-02 | 19 | 1.8 |
| 1868 | 1863 | 2455468.40786635 | 969745654 | 54.319 | -58.179 | -1.3370e-01 | 8.5313e-01 | 6.3102e-01 | 3.7539e-02 | 27 | 2.4 |
| 1869 | 1864 | 2455468.51448225 | 969754866 | 180.319 | -5.392 | -1.1724e-01 | 4.7983e-01 | 5.2936e-01 | 3.8897e-02 | 56 | 0.9 |
| 1870 | 1865 | 2455468.52250588 | 969755559 | 264.080 | 20.810 | -9.2963e-02 | 5.6770e-01 | 6.3052e-01 | 3.8106e-02 | 36 | 1.4 |
| 1871 | 1866 | 2455468.53763206 | 969756866 | 91.030 | -50.021 | -1.3370e-01 | 8.5313e-01 | 6.3102e-01 | 3.7539e-02 | 31 | 2.4 |
| 1872 | 1867 | 2455468.57377213 | 969759988 | 267.644 | -10.242 | -1.1724e-01 | 4.7983e-01 | 5.2936e-01 | 3.8897e-02 | 39 | 0.9 |
| 1873 | 1868 | 2455468.76184332 | 969776238 | 189.447 | -36.529 | -9.2963e-02 | 5.6770e-01 | 6.3052e-01 | 3.8106e-02 | 38 | 1.4 |
| 1874 | 1869 | 2455468.89205756 | 969787488 | 0.389 | -16.059 | -9.2963e-02 | 5.6770e-01 | 6.3052e-01 | 3.8106e-02 | 75 | 1.4 |
| 1875 | 1870 | 2455470.45784087 | 969922772 | 180.031 | -11.653 | -1.3370e-01 | 8.5313e-01 | 6.3102e-01 | 3.7539e-02 | 22 | 2.4 |
| 1876 | 1871 | 2455470.55339879 | 969931028 | 222.317 | 38.197 | -9.2963e-02 | 5.6770e-01 | 6.3052e-01 | 3.8106e-02 | 44 | 1.4 |
| 1877 | 1872 | 2455470.60049885 | 969935098 | 144.127 | -39.135 | -9.2963e-02 | 5.6770e-01 | 6.3052e-01 | 3.8106e-02 | 37 | 1.4 |
| 1878 | 1873 | 2455470.61300779 | 969936178 | 54.832 | -48.685 | -9.2963e-02 | 5.6770e-01 | 6.3052e-01 | 3.8106e-02 | 68 | 1.4 |
| 1879 | 1874 | 2455471.09057801 | 969977440 | 301.358 | -26.443 | -9.2963e-02 | 5.6770e-01 | 6.3052e-01 | 3.8106e-02 | 26 | 1.4 |
| 1880 | 1875 | 2455471.12168407 | 969980128 | 21.267 | 20.121 | -1.3370e-01 | 8.5313e-01 | 6.3102e-01 | 3.7539e-02 | 28 | 2.4 |
| 1881 | 1876 | 2455471.19216048 | 969986217 | 348.237 | -17.299 | -1.3370e-01 | 8.5313e-01 | 6.3102e-01 | 3.7539e-02 | 23 | 2.4 |
| 1882 | 1877 | 2455471.27659978 | 969993513 | 56.015 | -18.756 | -1.3370e-01 | 8.5313e-01 | 6.3102e-01 | 3.7539e-02 | 31 | 2.4 |
| 1883 | 1878 | 2455471.44108016 | 970007724 | 141.301 | 27.161 | -9.2963e-02 | 5.6770e-01 | 6.3052e-01 | 3.8106e-02 | 43 | 1.4 |
| 1884 | 1879 | 2455471.44284181 | 970007876 | 103.697 | 13.652 | -9.2963e-02 | 5.6770e-01 | 6.3052e-01 | 3.8106e-02 | 38 | 1.4 |
| 1885 | 1880 | 2455471.48984280 | 970011937 | 75.428 | -34.192 | -9.2963e-02 | 5.6770e-01 | 6.3052e-01 | 3.8106e-02 | 35 | 1.4 |
| 1886 | 1881 | 2455472.15431079 | 970069347 | 47.518 | -15.983 | -9.2963e-02 | 5.6770e-01 | 6.3052e-01 | 3.8106e-02 | 37 | 1.4 |
| 1887 | 1882 | 2455472.22932264 | 970075828 | 108.595 | 1.605 | -9.2963e-02 | 5.6770e-01 | 6.3052e-01 | 3.8106e-02 | 63 | 1.4 |
| 1888 | 1883 | 2455472.29622119 | 970081608 | 61.476 | -26.025 | -1.3370e-01 | 8.5313e-01 | 6.3102e-01 | 3.7539e-02 | 22 | 2.4 |
| 1889 | 1884 | 2455472.32062918 | 970083717 | 145.591 | -6.634 | -9.2963e-02 | 5.6770e-01 | 6.3052e-01 | 3.8106e-02 | 47 | 1.4 |
| 1890 | 1885 | 2455472.41634610 | 970091987 | 138.004 | 11.225 | -1.3370e-01 | 8.5313e-01 | 6.3102e-01 | 3.7539e-02 | 23 | 2.4 |
| 1891 | 1886 | 2455472.57447945 | 970105650 | 136.947 | -81.216 | -9.2963e-02 | 5.6770e-01 | 6.3052e-01 | 3.8106e-02 | 40 | 1.4 |
| 1892 | 1887 | 2455472.70844984 | 970117225 | 204.603 | 10.738 | -9.2963e-02 | 5.6770e-01 | 6.3052e-01 | 3.8106e-02 | 66 | 1.4 |
| 1893 | 1888 | 2455472.88317258 | 970132321 | 248.890 | 0.717 | -9.2963e-02 | 5.6770e-01 | 6.3052e-01 | 3.8106e-02 | 42 | 1.4 |
| 1894 | 1889 | 2455473.04086075 | 970145945 | 284.629 | -24.863 | -1.3370e-01 | 8.5313e-01 | 6.3102e-01 | 3.7539e-02 | 27 | 2.4 |
| 1895 | 1890 | 2455473.30473971 | 970168744 | 106.459 | -24.086 | -1.3370e-01 | 8.5313e-01 | 6.3102e-01 | 3.7539e-02 | 24 | 2.4 |
| 1896 | 1891 | 2455474.02785861 | 970231221 | 10.296 | 6.186 | -1.3370e-01 | 8.5313e-01 | 6.3102e-01 | 3.7539e-02 | 28 | 2.4 |
| 1897 | 1892 | 2455474.41903012 | 970265019 | 114.811 | 23.813 | -9.2963e-02 | 5.6770e-01 | 6.3052e-01 | 3.8106e-02 | 71 | 1.4 |
| 1898 | 1893 | 2455474.46438909 | 970268938 | 130.208 | 13.199 | -1.3370e-01 | 8.5313e-01 | 6.3102e-01 | 3.7539e-02 | 28 | 2.4 |
| 1899 | 1894 | 2455474.52924379 | 970274541 | 209.702 | -19.198 | -1.3370e-01 | 8.5313e-01 | 6.3102e-01 | 3.7539e-02 | 22 | 2.4 |
| 1900 | 1895 | 2455474.85116494 | 970302355 | 2.157 | 20.246 | -9.2963e-02 | 5.6770e-01 | 6.3052e-01 | 3.8106e-02 | 57 | 1.4 |
| 1901 | 1896 | 2455474.95486273 | 970311315 | 41.393 | 6.314 | -9.2963e-02 | 5.6770e-01 | 6.3052e-01 | 3.8106e-02 | 41 | 1.4 |
| 1902 | 1897 | 2455475.03581629 | 970318309 | 48.341 | 25.042 | -9.2963e-02 | 5.6770e-01 | 6.3052e-01 | 3.8106e-02 | 81 | 1.4 |
| 1903 | 1898 | 2455475.05119788 | 970319638 | 303.291 | -10.743 | -9.2963e-02 | 5.6770e-01 | 6.3052e-01 | 3.8106e-02 | 41 | 1.4 |
| 1904 | 1899 | 2455475.25459109 | 970337211 | 103.881 | 18.048 | -9.2963e-02 | 5.6770e-01 | 6.3052e-01 | 3.8106e-02 | 41 | 1.4 |
| 1905 | 1900 | 2455475.33083298 | 970343798 | 95.339 | -23.100 | -9.2963e-02 | 5.6770e-01 | 6.3052e-01 | 3.8106e-02 | 64 | 1.4 |
| 1906 | 1901 | 2455475.69275791 | 970375069 | 357.122 | -22.579 | -9.2963e-02 | 5.6770e-01 | 6.3052e-01 | 3.8106e-02 | 48 | 1.4 |
| 1907 | 1902 | 2455475.83398988 | 970387271 | 330.954 | -55.084 | -1.1724e-01 | 4.7983e-01 | 5.2936e-01 | 3.8897e-02 | 46 | 0.9 |

LIST OF HIGH ENERGY NEUTRINO CANDIDATES FOR THE 2009-2010 DATA

| | | | | | | | | | | | |
|------|------|------------------|-----------|---------|---------|-------------|------------|------------|------------|----|-----|
| 1908 | 1903 | 2455476.17378727 | 970416630 | 90.707 | 19.135 | -1.3370e-01 | 8.5313e-01 | 6.3102e-01 | 3.7539e-02 | 25 | 2.4 |
| 1909 | 1904 | 2455476.61735227 | 970454954 | 311.182 | -11.663 | -1.1909e-01 | 7.2127e-01 | 6.0423e-01 | 3.7507e-02 | 26 | 1.8 |
| 1910 | 1905 | 2455476.69835011 | 970461952 | 324.323 | -55.779 | -1.1724e-01 | 4.7983e-01 | 5.2936e-01 | 3.8897e-02 | 47 | 0.9 |
| 1911 | 1906 | 2455476.84185180 | 970474350 | 169.516 | -51.599 | -1.1724e-01 | 4.7983e-01 | 5.2936e-01 | 3.8897e-02 | 42 | 0.9 |
| 1912 | 1907 | 2455476.86915061 | 970476709 | 67.844 | -9.655 | -1.3370e-01 | 8.5313e-01 | 6.3102e-01 | 3.7539e-02 | 26 | 2.4 |
| 1913 | 1908 | 2455476.87110898 | 970476878 | 114.738 | -54.099 | -9.2963e-02 | 5.6770e-01 | 6.3052e-01 | 3.8106e-02 | 33 | 1.4 |
| 1914 | 1909 | 2455477.13119858 | 970499350 | 107.767 | -5.724 | -9.2963e-02 | 5.6770e-01 | 6.3052e-01 | 3.8106e-02 | 77 | 1.4 |
| 1915 | 1910 | 2455477.26743633 | 970511121 | 269.986 | -48.508 | -9.2963e-02 | 5.6770e-01 | 6.3052e-01 | 3.8106e-02 | 49 | 1.4 |
| 1916 | 1911 | 2455478.54320654 | 970621348 | 339.811 | -49.212 | -9.2963e-02 | 5.6770e-01 | 6.3052e-01 | 3.8106e-02 | 33 | 1.4 |
| 1917 | 1912 | 2455478.66409797 | 970631793 | 276.690 | -0.243 | -1.1724e-01 | 4.7983e-01 | 5.2936e-01 | 3.8897e-02 | 52 | 0.9 |
| 1918 | 1913 | 2455478.69726989 | 970634659 | 13.426 | -79.916 | -1.3370e-01 | 8.5313e-01 | 6.3102e-01 | 3.7539e-02 | 27 | 2.4 |
| 1919 | 1914 | 2455478.95793565 | 970657180 | 271.367 | -68.747 | -9.2963e-02 | 5.6770e-01 | 6.3052e-01 | 3.8106e-02 | 34 | 1.4 |
| 1920 | 1915 | 2455478.98190327 | 970659251 | 332.564 | 2.512 | -9.2963e-02 | 5.6770e-01 | 6.3052e-01 | 3.8106e-02 | 46 | 1.4 |
| 1921 | 1916 | 2455479.00982090 | 970661663 | 263.958 | -46.564 | -9.2963e-02 | 5.6770e-01 | 6.3052e-01 | 3.8106e-02 | 38 | 1.4 |
| 1922 | 1917 | 2455479.02115066 | 970662642 | 44.158 | -9.799 | -1.2873e-01 | 4.3155e-01 | 4.6595e-01 | 3.9162e-02 | 59 | 0.7 |
| 1923 | 1918 | 2455479.03418574 | 970663768 | 10.564 | -15.409 | -9.2963e-02 | 5.6770e-01 | 6.3052e-01 | 3.8106e-02 | 44 | 1.4 |
| 1924 | 1919 | 2455479.03642127 | 970663961 | 110.156 | -44.611 | -9.2963e-02 | 5.6770e-01 | 6.3052e-01 | 3.8106e-02 | 25 | 1.4 |
| 1925 | 1920 | 2455479.06134852 | 970666115 | 311.090 | -26.609 | -1.3370e-01 | 8.5313e-01 | 6.3102e-01 | 3.7539e-02 | 29 | 2.4 |
| 1926 | 1921 | 2455479.10224807 | 970669649 | 345.468 | -10.674 | -9.2963e-02 | 5.6770e-01 | 6.3052e-01 | 3.8106e-02 | 75 | 1.4 |
| 1927 | 1922 | 2455479.34993596 | 970691049 | 65.110 | -22.549 | -1.3370e-01 | 8.5313e-01 | 6.3102e-01 | 3.7539e-02 | 23 | 2.4 |
| 1928 | 1923 | 2455479.95994526 | 970743754 | 6.694 | -59.147 | -1.1724e-01 | 4.7983e-01 | 5.2936e-01 | 3.8897e-02 | 33 | 0.9 |
| 1929 | 1924 | 2455479.97126507 | 970744732 | 18.951 | 18.034 | -9.2963e-02 | 5.6770e-01 | 6.3052e-01 | 3.8106e-02 | 33 | 1.4 |
| 1930 | 1925 | 2455480.00556085 | 970747695 | 129.718 | -33.692 | -9.2963e-02 | 5.6770e-01 | 6.3052e-01 | 3.8106e-02 | 26 | 1.4 |
| 1931 | 1926 | 2455480.04324654 | 970750951 | 145.303 | -17.009 | -9.2963e-02 | 5.6770e-01 | 6.3052e-01 | 3.8106e-02 | 75 | 1.4 |
| 1932 | 1927 | 2455480.08674619 | 970754709 | 181.854 | -49.848 | -1.1724e-01 | 4.7983e-01 | 5.2936e-01 | 3.8897e-02 | 43 | 0.9 |
| 1933 | 1928 | 2455480.12686491 | 970758176 | 158.766 | -22.579 | -1.1724e-01 | 4.7983e-01 | 5.2936e-01 | 3.8897e-02 | 25 | 0.9 |
| 1934 | 1929 | 2455480.19020144 | 970763648 | 258.119 | -61.760 | -9.2963e-02 | 5.6770e-01 | 6.3052e-01 | 3.8106e-02 | 62 | 1.4 |
| 1935 | 1930 | 2455480.31483632 | 970774416 | 215.226 | -53.528 | -1.3370e-01 | 8.5313e-01 | 6.3102e-01 | 3.7539e-02 | 29 | 2.4 |
| 1936 | 1931 | 2455480.38875956 | 970780803 | 119.721 | -24.317 | -9.2963e-02 | 5.6770e-01 | 6.3052e-01 | 3.8106e-02 | 38 | 1.4 |
| 1937 | 1932 | 2455480.43083866 | 970784439 | 119.501 | -71.390 | -9.2963e-02 | 5.6770e-01 | 6.3052e-01 | 3.8106e-02 | 36 | 1.4 |
| 1938 | 1933 | 2455480.49024313 | 970789572 | 96.431 | -37.780 | -9.2963e-02 | 5.6770e-01 | 6.3052e-01 | 3.8106e-02 | 38 | 1.4 |
| 1939 | 1934 | 2455480.52861682 | 970792887 | 228.597 | 27.745 | -9.2963e-02 | 5.6770e-01 | 6.3052e-01 | 3.8106e-02 | 56 | 1.4 |
| 1940 | 1935 | 2455480.53011919 | 970793017 | 120.579 | -18.015 | -9.2963e-02 | 5.6770e-01 | 6.3052e-01 | 3.8106e-02 | 38 | 1.4 |
| 1941 | 1936 | 2455480.75810719 | 970812715 | 222.309 | 6.494 | -9.2963e-02 | 5.6770e-01 | 6.3052e-01 | 3.8106e-02 | 43 | 1.4 |
| 1942 | 1937 | 2455481.15369736 | 970846894 | 36.564 | 26.380 | -9.2963e-02 | 5.6770e-01 | 6.3052e-01 | 3.8106e-02 | 58 | 1.4 |
| 1943 | 1938 | 2455481.49201310 | 970876124 | 223.065 | 7.969 | -9.2963e-02 | 5.6770e-01 | 6.3052e-01 | 3.8106e-02 | 35 | 1.4 |
| 1944 | 1939 | 2455481.49501402 | 970876384 | 216.875 | -33.004 | -9.2963e-02 | 5.6770e-01 | 6.3052e-01 | 3.8106e-02 | 32 | 1.4 |
| 1945 | 1940 | 2455481.69228371 | 970893428 | 341.109 | -71.517 | -1.2873e-01 | 4.3155e-01 | 4.6595e-01 | 3.9162e-02 | 65 | 0.7 |
| 1946 | 1941 | 2455481.76719164 | 970899900 | 244.308 | 10.344 | -1.3370e-01 | 8.5313e-01 | 6.3102e-01 | 3.7539e-02 | 30 | 2.4 |
| 1947 | 1942 | 2455481.90847431 | 970912107 | 64.283 | 18.936 | -1.3370e-01 | 8.5313e-01 | 6.3102e-01 | 3.7539e-02 | 49 | 2.4 |
| 1948 | 1943 | 2455482.06437262 | 970925576 | 79.706 | -31.700 | -9.2963e-02 | 5.6770e-01 | 6.3052e-01 | 3.8106e-02 | 35 | 1.4 |
| 1949 | 1944 | 2455482.06639273 | 970925751 | 19.136 | -66.978 | -9.2963e-02 | 5.6770e-01 | 6.3052e-01 | 3.8106e-02 | 57 | 1.4 |
| 1950 | 1945 | 2455482.36233079 | 970951320 | 190.485 | 26.391 | -1.1909e-01 | 7.2127e-01 | 6.0423e-01 | 3.7507e-02 | 26 | 1.8 |
| 1951 | 1946 | 2455482.38583820 | 970953351 | 172.135 | -6.447 | -9.2963e-02 | 5.6770e-01 | 6.3052e-01 | 3.8106e-02 | 47 | 1.4 |
| 1952 | 1947 | 2455482.55774061 | 970968203 | 160.126 | -41.528 | -9.2963e-02 | 5.6770e-01 | 6.3052e-01 | 3.8106e-02 | 37 | 1.4 |
| 1953 | 1948 | 2455482.62741040 | 970974223 | 150.044 | -38.405 | -9.2963e-02 | 5.6770e-01 | 6.3052e-01 | 3.8106e-02 | 34 | 1.4 |
| 1954 | 1949 | 2455483.09039424 | 971014225 | 274.654 | -44.501 | -9.2963e-02 | 5.6770e-01 | 6.3052e-01 | 3.8106e-02 | 93 | 1.4 |
| 1955 | 1950 | 2455483.11543480 | 971016388 | 308.764 | -47.814 | -9.2963e-02 | 5.6770e-01 | 6.3052e-01 | 3.8106e-02 | 47 | 1.4 |
| 1956 | 1951 | 2455483.16705295 | 971020848 | 135.085 | -17.001 | -9.2963e-02 | 5.6770e-01 | 6.3052e-01 | 3.8106e-02 | 44 | 1.4 |
| 1957 | 1952 | 2455483.55215420 | 971054121 | 189.108 | -29.403 | -1.3370e-01 | 8.5313e-01 | 6.3102e-01 | 3.7539e-02 | 29 | 2.4 |
| 1958 | 1953 | 2455483.58125118 | 971056635 | 252.514 | -8.394 | -9.2963e-02 | 5.6770e-01 | 6.3052e-01 | 3.8106e-02 | 43 | 1.4 |
| 1959 | 1954 | 2455483.75950707 | 971072036 | 171.680 | -44.441 | -9.2963e-02 | 5.6770e-01 | 6.3052e-01 | 3.8106e-02 | 38 | 1.4 |

1960 1955 2455483.76670481 971072658 75.469 -40.554 -1.1724e-01 4.7983e-01 5.2936e-01 3.8897e-02 35 0.9
1961 1956 2455484.10195056 971101623 43.278 -74.754 -9.2963e-02 5.6770e-01 6.3052e-01 3.8106e-02 42 1.4
1962 1957 2455484.13545589 971104518 38.247 -41.413 -9.2963e-02 5.6770e-01 6.3052e-01 3.8106e-02 38 1.4
1963 1958 2455484.14975944 971105754 2.375 -8.639 -1.1724e-01 4.7983e-01 5.2936e-01 3.8897e-02 43 0.9
1964 1959 2455484.41203071 971128414 280.092 -62.120 -1.3370e-01 8.5313e-01 6.3102e-01 3.7539e-02 17 2.4
1965 1960 2455484.48576566 971134785 334.616 -50.421 -1.3370e-01 8.5313e-01 6.3102e-01 3.7539e-02 29 2.4
1966 1961 2455485.04007020 971182677 343.340 -6.544 -9.2963e-02 5.6770e-01 6.3052e-01 3.8106e-02 35 1.4
1967 1962 2455485.51717531 971223898 190.861 12.885 -9.2963e-02 5.6770e-01 6.3052e-01 3.8106e-02 44 1.4
1968 1963 2455485.73196050 971242456 298.942 18.580 -1.3370e-01 8.5313e-01 6.3102e-01 3.7539e-02 27 2.4
1969 1964 2455485.75650172 971244576 221.307 -5.957 -9.2963e-02 5.6770e-01 6.3052e-01 3.8106e-02 38 1.4
1970 1965 2455485.99184515 971264910 25.740 -3.819 -1.3370e-01 8.5313e-01 6.3102e-01 3.7539e-02 31 2.4
1971 1966 2455486.09282488 971273635 135.081 -32.208 -1.1724e-01 4.7983e-01 5.2936e-01 3.8897e-02 35 0.9
1972 1967 2455486.17871571 971281056 111.959 22.295 -9.2963e-02 5.6770e-01 6.3052e-01 3.8106e-02 38 1.4
1973 1968 2455486.33948603 971294946 130.302 10.915 -9.2963e-02 5.6770e-01 6.3052e-01 3.8106e-02 44 1.4
1974 1969 2455486.55353586 971313440 227.097 -18.404 -9.2963e-02 5.6770e-01 6.3052e-01 3.8106e-02 33 1.4
1975 1970 2455486.80741430 971335375 271.299 -36.165 -9.2963e-02 5.6770e-01 6.3052e-01 3.8106e-02 46 1.4
1976 1971 2455487.20057691 971369344 193.583 -24.483 -9.2963e-02 5.6770e-01 6.3052e-01 3.8106e-02 50 1.4
1977 1972 2455487.50511508 971395656 143.687 -13.520 -1.3370e-01 8.5313e-01 6.3102e-01 3.7539e-02 26 2.4
1978 1973 2455487.55444858 971399919 28.339 -47.858 -1.1724e-01 4.7983e-01 5.2936e-01 3.8897e-02 46 0.9
1979 1974 2455487.66057022 971409088 163.845 -20.206 -1.1724e-01 4.7983e-01 5.2936e-01 3.8897e-02 46 0.9
1980 1975 2455487.69682804 971412220 5.155 -25.859 -1.1724e-01 4.7983e-01 5.2936e-01 3.8897e-02 41 0.9
1981 1976 2455487.79404768 971420620 19.083 -11.251 -9.2963e-02 5.6770e-01 6.3052e-01 3.8106e-02 51 1.4
1982 1977 2455487.83337128 971424018 333.221 -85.966 -1.1724e-01 4.7983e-01 5.2936e-01 3.8897e-02 49 0.9
1983 1978 2455488.50990453 971482470 182.515 -31.720 -9.2963e-02 5.6770e-01 6.3052e-01 3.8106e-02 43 1.4
1984 1979 2455488.91902069 971517818 279.349 -8.999 -9.2963e-02 5.6770e-01 6.3052e-01 3.8106e-02 37 1.4
1985 1980 2455489.35628250 971555597 83.036 -56.437 -9.2963e-02 5.6770e-01 6.3052e-01 3.8106e-02 43 1.4
1986 1981 2455489.37466819 971557186 277.268 -62.564 -9.2963e-02 5.6770e-01 6.3052e-01 3.8106e-02 75 1.4
1987 1982 2455489.50905998 971568797 263.016 -6.010 -1.3370e-01 8.5313e-01 6.3102e-01 3.7539e-02 25 2.4
1988 1983 2455489.62683338 971578973 190.642 7.864 -1.3370e-01 8.5313e-01 6.3102e-01 3.7539e-02 26 2.4
1989 1984 2455489.72343844 971587320 248.142 -20.239 -1.3370e-01 8.5313e-01 6.3102e-01 3.7539e-02 17 2.4
1990 1985 2455489.72775112 971587692 216.433 -0.482 -9.2963e-02 5.6770e-01 6.3052e-01 3.8106e-02 37 1.4
1991 1986 2455489.87829766 971600699 26.194 -11.058 -1.2873e-01 4.3155e-01 4.6595e-01 3.9162e-02 58 0.7
1992 ## stop S6D

**LIST OF HIGH ENERGY NEUTRINO CANDIDATES FOR THE 2009-2010
DATA**
